ORIGIN AND DISTRIBUTION OF CORUNDUM FROM AN INTRAPLATE ALKALI BASALTIC PROVINCE IN THAILAND: EVIDENCE FROM FIELD AND INCLUSION STUDIES

by

Phisit Limtrakun

BSc. (Chiang Mai University)

Submitted in fulfilment of the requirements for the degree of Doctor of Philosophy

UNIVERSITY OF TASMANIA

March, 2003

This work is dedicated to my father, Phichai Limtrakul, for a lifetime of love, hope and understanding

Statement

This thesis contains the results of research done at the School of Earth Sciences, University of Tasmania, Hobart, Tasmania, Australia between 1998 and 2002. Part of the material presented in this thesis has been published as:

P. Limtrakun, Khin Zaw, C. G. Ryan and T. P. Mernagh (2001).
Formation of the Denchai gem sapphires, northern Thailand: Evidence from mineral chemistry and fluid/melt inclusion characteristics.
Mineralogical Magazine, **65(6)**, 725-735.

This thesis contains no material which has been accepted for the award of any other higher degree or graduate diploma in any tertiary institution and to the best of the author's knowledge and belief. This thesis contains no material previously published or written by another person, except where due reference is made in the text of the thesis.

This thesis may be available for loan and limited copying in accordance with the ***Copyright Act 1968.***

Phisit Limtrakun
Department of Geology,
School of Earth Sciences
University of Tasmania,
Hobart, Tasmania, Australia
March, 2003

Abstract

It has long been recognised that gem-quality corundums (sapphires and rubies) are commonly found in close proximity to intraplate alkali basalts. On this basis, a general consensus has developed that the gem-quality corundums were the products of weathering of "nearby" alkali basalts. However, despite this association, gem-quality corundums are rarely found hosted within fresh basalts.

Through the detail study of their mineralogy and inclusion compositions, this study derives new evidence on the origin of sapphires. All sapphires examined in this thesis were recovered from alluvial placer deposits in the Denchai gem fields of Phrae Province, Northern Thailand and are interpreted to have been derived from the late Cenozoic alkali Denchai basalts. The basalts have olivine + clinopyroxene + plagioclase phenocryst and microphenocryst assemblages, are alkali in character and have compositions varying from basanites, basalts, basaltic trachyandesites to trachybasalts. They have abundant mantle-derived xenoliths, mostly spinel-lherzolites, and rare crustal xenoliths. The equilibration *P-T* estimates of spinel-lherzolite xenoliths are 1030°C at 8 to 20 kbars. The basalts themselves show evidence of fractionation at mantle depths (> 10 kbars) and no evidence of low-pressure crystal fractionation prior to eruption. Isotopic data suggest that the basalts have not experienced crustal contamination and that mixing of three mantle components was involved; (1) an "A" component (Depleted Mantle, HIMU and a component lying somewhere between DM and HIMU line), (2) "A"-EM1 mixing component and (3) EM2-enriched subcontinental lithospheric mantle.

Most Denchai sapphires are blue in colour, having very low Cr contents and high Ti/Ga ratios. Their oxygen isotope compositions (+4.7 to +8.4‰) suggest a mixed source composition (crust and mantle) for sapphire crystallisation. Four types of inclusions were identified in the sapphires; CO_2-rich inclusions (Type-I), polyphase (V+L+S) inclusions (Type-II), silicate-melt inclusions (Type-III) and mineral inclusions. Type-I, CO_2-rich fluid inclusions have wide ranges of CO_2 density, up to about 0.87 g/cm^3. Type-II inclusions contain ~60 wt% NaCl equivalent, H_2O and anhydrite daughter crystals. Glass compositions of Type-III are silica-rich (~61 wt% SiO_2) 15-30 wt% Al_2O_3, ~10 wt% K_2O + Na_2O and high volatiles (S, Cl and H_2O). Critical assessment of the data suggests that the Denchai sapphires originated at pressure of in the range of 6-15 kbars, at a temperature between 700 and 900°C.

The source composition had low Si activity, high NaCl and was highly oxidised (hematite stable).

New evidence from this study suggests that the Denchai sapphires crystallised from melts that formed in the continental lithosphere. The crystallisation of these sapphires requires hybrid melts dominated by a mantle $\delta^{18}O$ signature, with high salinity, fO_2, CO_2 and low in Ca, Mg, Fe contents. It is also concluded that the role of the associated alkali basalts is to provide (1) a heat source, (2) possibly to act as a low $aSiO_2$ buffer that reacts with the contaminant, and (3) to provide an effective method of rapid transport to the surface.

This inclusion-based study emphasises the large variability of source compositions that can account for the genesis of corundum. Many sapphire provinces have a strong association with Nb-Ta oxides and have mantle $\delta^{18}O$. These features suggest carbonatites are a very important component. However the Thai sapphire provinces lack these feature. The Denchai sapphires were derived from highly oxidised Ca-poor parental melts which have variable $\delta^{18}O$. Partial melts of seafloor weathered MORB basalts are the most likely source for this composition.

Acknowledgements

Throughout the duration of this study the author greatly benefited from the knowledge, advice, help and friendship of many people. To all of them the author is indebted and extends his appreciation. An enormous thanks go to Dr. Ron F. Berry, the amounted of time and energy Ron has dedicated throughout the final year of this project would probably never been repaid. The author would like to thank for his invaluable supervision, patient guidance, expert advice, encouragement, stimulation, critical reading and comments on all chapters.

The author would like to express his gratitude to Dr. Trevor J. Falloon and Dr. Khin Zaw for their support and guidance. The author is also grateful to Prof. Anthony J. Crawford and Dr. Clive F. Burrett for offering an opportunity to do research at the Department of Geology, School of Earth Sciences, University of Tasmania.

Financial support for this project was provided by the Royal Thai Government and generously supplemented by research grants to his supervisors for which the author is very much grateful.

Fieldwork in Thailand was carried out with the assistance with Dr.Yuenyong Panjasawatwong, Dr. Apichet Boonsoong and Weerapan Sricharn, which the author appreciates very much. The author would like to thank Drs. Theerapongs Thanasuthipitak, Panjawan Thanasuthipitak and Boontarika Srithai for their advice and support.

Dr. David A. Steele (Central Science Laboratory, University of Tasmania) is very much appreciated for his expert advice on Electron Microprobe analysis (EMP).

Drs. Leonid Danyushevsky and Vadim Kamenetsky are acknowledged for their instruction and helpful discussions during the experimental course of melt inclusion work. Dr. Lin Sutherland and John L. Everard are also thanked for their advice during the early stages of this study.

Thanks are extended to Dr. Terry Mernagh (Australian Geological Survey Organisation) for Laser Raman Spectroscopy (LRS) analysis, Dr. Chris Ryan (CSIRO Exploration and Mining, Sydney) for Proton Induced X-Ray Emission (PIXE) analysis and Dr. Tzen-Fu Yui (Institute of Earth Science, Academia Sinica, Taiwan) for Oxygen Isotope analysis.

The author would like to acknowledge Phil Robinson, Nilar Hlaing, Katie McGoldrick and Dr. Zongshou Yu for their suggestions and helps in X-Ray Fluorescence (XRF) and Inductively Coupled Plasma Mass Spectrometer (ICP-MS) analyses. Drs. John Foden and David Bruce (Geology and Geophysics Department, Adelaide University) are thanked for Radiogenic Isotope analysis.

Simons Stephens (UTAS), Pipop Roppairee (CMU) and Chantip Punthusa (CMU) are thanked for their masterful preparation of thin sections and polished sections.

Thanks are also extended to other fellow students and staffs at the Geology Department and CODES (UTAS); Dr. Fernando Della-Pasqua, David Dedenczuk, Lyn Starr, Di Stevens, Christine Higgins, Peter Cornish and many others. June Pongratz is very much appreciated for her willingness to help and solve numerous unexpected computer problems.

All students, with whom the author shared Room 326A (Peter Winefield, David Rawlings, Holger Paulick, Tony Webster, Christian Schardt, Alan Wilson, Keiran Howards, Frank Smith and Jubo Liu) as well as Oliver Holm, Owen Hatton, Rick Squire and Dene Carroll are thanked for their friendship and great tolerance.

All friends from Thai Student Society (UTAS) are thanked for their hospitality, friendship and warm parties on many occasions; Surat, Pathompong, Wilasinee, Tapida, Prasert, Jongkolnee, Parichat, Fonthong, Jaruwong, Siriporn, Valerat, Tossapol and many others.
Mark Gardner and his fiancée (Anny-Kanokwan) are deeply appreciated for accommodating the author during this study as well as warm hospitality and friendship.

All staffs and students at the Department of Geological Sciences, Faculty of Science, Chiang Mai University (CMU), Thailand, are thanked for their support and friendship.
Surake Kongjai, Siraprapa Chatprasert and Pudhi Densompornpun are thanked for their friendship and support. The author also would like to thank to Dr. W.W.S, Yim, Dr. Pornsawat Wathanakul, Somruedee Sakkaravej and Mananya Suchaya for providing some of the sapphire samples and photographic collections.

The author also thanks to many friends and colleagues, who have not been earlier mentioned.

Finally, to his parents, his brother and his sister, and to Nhungrutai Dakamgad, without them none of this would have been possible. The author is indebted to them for all the love and cares that they always offer.

Table of Contents

List of Figures

Chapter 1

Chapter 2

Chapter 3

Chapter 4

Chapter 5

List of Tables

Chapter 1

Chapter 2

Chapter 3

Chapter 4

Chapter 5

Thai Geographical Terms

Amphoe	=	town, district
Ban	=	village, small community
Changwat	=	province, city
Doi	=	mountain (peak)
Huai	=	gully, creek
Khao	=	isolated hill or mountain
Khlong	=	stream, canal
Mae	=	small river
Mae Nam	=	large river
Phu	=	hill or mountain (particularly in NE-Thailand)
Phu Khao	=	mountain range
Phra That	=	pagoda
Wat	=	temple

Chapter 1

Introduction

Minerals are defined as solid crystalline natural substances and are mostly formed from inorganic processes. A mineral is characterised by homogeneous physical properties and has a distinctive chemical composition that may vary within certain clearly defined limits. Corundum (Al_2O_3) belongs to the trigonal crystallographic system. Although more than one polymorph of aluminium oxide can be produced in the laboratory (e.g., hexagonal β-Al_2O_3, cubic γ- Al_2O_3), only corundum (α-Al_2O_3) is found in nature (Deer *et al.*, 1992). The striking physical properties of corundum include its extreme hardness (9), high specific gravity (3.98-4.02) and distinctive basal parting {0001}. Corundum, although not a major rock forming mineral, is a common accessory mineral in a wide variety of rocks such as undersaturated igneous rocks, high-grade metamorphic rocks (poor in silica and rich in aluminium) and is also found in sedimentary rocks, frequently in alluvial deposits (Mottana *et al.*, 1978).

Natural substances that are beautiful, rare and are regarded as valuable gemstones have always caught the attention of mankind. Corundum ranks second only to diamond on Moh's hardness scale. The gem-quality varieties of corundum are sapphire (all colours except red) and ruby (red). Modern faceting techniques greatly enhance the value of sapphire and ruby. Sapphire production is among the fastest growing areas of the gemstone industry. The discoveries of new sources and the introduction of large-scale modern mining methods nearly a half-century ago, particularly in eastern Australia and Southeast Asia have been very important in this growth. Middle and Southeast Asian countries such as India, Sri Lanka, Burma and Thailand are the marketing centres of sapphire and ruby. Sri Lanka in particular has provided the world finest sapphires and rubies since the 18^{th} century. The largest ruby yet found, 6 cm long, came from the Mogok deposit of Northern Burma (Hughes, 1997). A large volume of gem-quality corundum has also been mined in east Africa and Madagascar (e.g., Hamid *et al.*, 1996; Milisenda and Henn, 1996; Schmetzer, 1999; Shida, 2002).

At present, gemstones are the leading export of Thailand. These gemstones mainly come from the Kanchanaburi deposit, western Thailand and the Chanthaburi-Trat deposit, southeastern Thailand (Vichit, 1992). However, the fast growing mining industry of

Thailand is dramatically depleting the existing gemstone fields of sapphire and ruby. New areas need to be explored in order to satisfy the future demand for gem-quality corundum.

1.1 Models of corundum occurrence

Most gem-quality corundum deposits are found as alluvial, eluvial and/or residual soils deposits. The main exceptions are Kashmir in India and Yogo Gulch in Montana, USA, which were mined for sapphires from pegmatites and an ultramafic dyke respectively. Searching for the parental source rocks is a challenging task in gem-quality corundum prospecting. Such attempts, however, are often compromised by the lack of understanding of corundum genesis and of petrogenesis of the corundum-bearing source rocks. Most gem-quality corundum deposits are specifically explained for one place and are not comparable to the other places. However, these studies on gem-quality-corundums have set up a useful background for further investigation.

After eliminating corundums found as detrital grains, a literature review indicated that corundum occurrences can be divided into seven groups on the basis of their host rocks setting. This classification is summarised in Table 1.1. Group 1 and 2 represent cases where the host rocks are metamorphic whereas Group 3, 4, 5 and 6 represent corundums found as accessory phase in igneous rocks. Group 7 represents corundums found as discrete crystals or simple intergrowths with other minerals in mafic/ultramafic dykes and basaltic rocks. The sapphires investigated in this study belong to Group 7.

Gem-quality corundums, both sapphire and ruby, mostly come from the Group 7. They have mainly come from forty basaltic fields, in six continental regions within fifteen countries (Table 1.2). These basaltic fields discharge both magmatic and metamorphic origin corundums from underlying sources. The corundums commonly include "magmatic" blue, green, yellow and coloured-zoned sapphires and less commonly "metamorphic" various coloured sapphires and rubies. Magmatic suites (60% of basaltic fields) dominate over 25% of mixed magmatic/metamorphic suites and 15% of metamorphic suites (Sutherland and Schwarz, 2001).

The unequivocal association that exists between gem-quality corundum and their parental rocks, to date, has not been satisfactorily explained in terms of their petrogenesis. Current models of corundum genesis that involve magmatic processes can be divided into those involving (1) plutonic crystallisation at high pressures and (2) magma mixing at mid-crustal depths. These two models are briefly described as follow.

Table 1.1 Major occurrence of corundum in different rock types (modified from Guo, 1993)

Group	Sub-group	Host rocks and occurrences
1	1.1	Si-poor hornfels within the aureole of igneous intrusions (e.g., Evans, 1964; Smith, 1965; Ferguson and Al-Ameen, 1985)
	1.2	Various types of gneisses, schists and granulites in metamorphic terrains as porphyroblasts (e.g., Clabaugh, 1952; Wells, 1956; Cooray and Kumarapeli, 1960; Lawrence *et al.*, 1987) or as corundum-rich bands within normal metasediments (e.g., Coetzee, 1940; Golani, 1989)
	1.3	Al-rich xenoliths enclosed in mafic and granitic intrusive rocks (Thomas, 1922; Hall and Nel, 1926; Read, 1931; Murdoch and Webb, 1942)
2	2.1	Marbles interbedded with other metasediments (Okrusch *et al.*, 1976; Gubelin, 1982; Bender, 1983; Keller, 1983; Bowersox, 1985)
	2.2	Skarns developed between limestones and granitic intrusion (Silva and Siriwandena, 1988)
3		Syenites, nepheline syenites and associated pegmatites (e.g., Du Toit; 1918; Wells, 1956; Carlson, 1957; Kerr, 1977)
4		Plagioclase pegmatite (Sokolov, 1931; Tomlinson, 1939; Rose, 1957; Solesbury, 1967; Petrussenko, 1981; Atkinson and Kothavala, 1983), oligoclase pegmatite (Lawson, 1904; Oftedal, 1963) and albitite veins (Larsen, 1928)
5		Altered igneous rocks in association with mineralization (e.g., Schwartz, 1982; Steefel and Atkinson, 1984; Wojdak and Sinclair, 1984)
6		Alkremite xenoliths (Exley *et al.*, 1983) and ecologitic xenoliths in kimberlites (e.g., Sobolov *et al.*, 1968; Dawson, 1980; Kornprobst *et al.*, 1982; Hill and Haggerty, 1989)
7	7.1	Ultramafic dyke as discrete crystals (Clabaugh, 1952; Brownlow and Komorowski, 1988; Meyer and Mitchell, 1988)
	7.2	Basaltic rocks as large discrete crystals or simple intergrowths with other phases (e.g., MacNevin, 1972; Stephenson, 1976; Upton *et al.*, 1983)

Table 1.2 Corundum-bearing basaltic fields (modified from Sutherland and Schwarz, 2001)

Continents	Country/State	Area	Type	Sources
Africa	Kenya	Garba Tula	Magmatic	Keller *et al.*, 1985;
		Turkana	Magmatic	Mychaluk, 1995;
	Madagascar	Antsiranana	Magmatic	Aspen *et al.*, 1990;
	Nigeria	Kaduna	Magmatic	Guo *et al.*, 1996a;
	Rwanda	Kamemba	Magmatic	Sutherland, 1996;
Asia	Cambodia	Pailin	Mixed	Hughes, 1997;
	China	Hainan	Magmatic	Sutherland *et al.*, 1998a, b;
		Fujian	Magmatic	Malinkova, 1999;
		Jiangsu	Magmatic	Upton *et al.*, 1999
		Shandong	Magmatic	
	Laos	Ban Huai Sai	Mixed	
	Thailand	Kanchanaburi	Mixed	
		Phrae	Magmatic	
		Si Sa Ket	Metamorphic	
		Chanthaburi-Trat	Mixed	
		Nam Yuen	Mixed	
	Vietnam	Di Linh	Magmatic	
		Phan Thiet	Magmatic	
		Gai Kiem	Magmatic	
Australia	New South Wales	New England	Mixed	
		Wellington	Mixed	
		Barrington	Mixed	
		Oberon	Magmatic	
		Tumbarumba	Mixed	
	Queensland	McLean	Magmatic	
		McBride	Magmatic	
		Anakie-Rubyvale	Magmatic	
		Boyne	Magmatic	
	Tasmania	Weldborough	Magmatic	
	Victoria	Myrniong	Mixed	
Europe	Czech Republic	Trebivlice	Metamorphic?	
	France	Jizerska Louka	Magmatic	
	Scotland	Outer Hebrides	Magmatic	
		Midland Valley	Magmatic	
		Velay	Magmatic?	
North America	United States	Idaho	Metamorphic?	
		Montana	Metamorphic?	
South America	Brazil	Mato Grosso	Magmatic	
	Colombia	Mercaderes	Metamorphic?	

Note: types of origin (magmatic, metamorphic and mixed) are either defined or recognised using the criteria outlined by the authors as listed.

1.1.1 Plutonic crystallisation of corundum at high pressures

Four models are currently proposed that involve plutonic crystallisation as the origin of corundum.

i. Plutonic crystallisation of corundum from highly evolved alkali melts formed by the fractional crystallisation of intraplate magmas (e.g., nephelinites, basanites) at mantle and lower crustal pressures (Irving, 1986).

ii. Plutonic crystallisation of corundum from syenitic melts that are the result from high temperature crystallisation of anhydrous trachytic magmas at deep crustal levels or in the upper mantle (Aspen *et al.*, 1990).

iii. Plutonic crystallisation from primary alkali melts which are produced by low-moderate degrees of partial melting of amphibole-metasomatised mantle, or alternatively by partial melting of a lower crustal amphibole-bearing assemblage (e.g., amphibole pyroxenite; Sutherland *et al.*, 1998a). This model also suggests that corundum can crystallise directly from volatile-rich saturated felsic melts that are generated and fractionated largely under mantle/lower crust conditions.

iv. Plutonic crystallisation from syenitic melts possibly originating from partial melting of metasomatised mantle, but with aluminous character developed by loss of alkalis and carbonatitic fractions (Upton *et al.*, 1999).

The plutonic crystallisation models of corundum genesis described above are all similar in that they require a highly aluminous volatile and trace element rich alkali parental magma. The three models simply differ in how such a parental magma was produced.

Sutherland *et al.* (1998a) argued that the absence of significant europium (Eu) anomalies in many zircons associated with corundum argued against significant crystal fractionation, as plagioclase fractionation should remove most of the Eu from the magma before corundum crystallisation. However, the high-pressure liquid line of descent of alkali magmas is poorly known (Irving, 1986). For normal basanite magma, under H_2O-undersaturated conditions, the liquidus phases in the pressure range 1-2 GPa are olivine and clinopyroxene. At lower temperatures, amphibole will be a major crystallising phase (Green, 1989). Thus it is not necessarily correct to infer that plagioclase will be a major fractionating phase for alkali magmas at high-pressures.

1.1.2 Generation of corundum by magma mixing at mid-crustal levels

This model suggests that at least two melt components (carbonatitic and felsic melts) are involved as the parental melt-source of corundum. The model is based on the occurrence of mineral inclusions (e.g., zircon and Nb-Ta oxides) in corundums. Guo (1993) suggested that at mid-crustal depth the interaction between host pegmatite body and intruding carbonatitic magma causes some Al-rich phase to crystallise in the hybrid zone, triggering corundum crystallisation. Subsequent episodes of basaltic magmatism, enriched in alkalis and volatiles, are able to carry fragments of corundum-bearing wall rocks rapidly to the surface.

On the basis of mineral inclusion relationships within corundum, Guo *et al.* (1996a) suggested that the age of corundum-growth is given by the age of zircon inclusions within corundum. This is identical to the age of associated basalt. However such timing can be reset during magma eruption. The *P-T* conditions of corundum formation were also estimated to be at mid-crustal levels (~5 kbar and 300-600°C) based on perthitic feldspar inclusions within corundum.

The data summarised above indicates that the genesis of all corundum is unlikely to be explained by a single model. The information provided by solid and fluid inclusions within magmatic corundum has resulted in considerable controversy over their interpretation, and hence this has resulted in significantly different models of origin. The controversy over the corundum solid inclusions centres on three main points.

i. The relationship between solid inclusions such as zircon and zircon found as rare megacrysts in the associated alkali magmas. Guo *et al.* (1996a) argued that the zircon inclusions found in corundum are far too enriched in rare earth elements (REE) compared to megacryst zircon and are therefore unrelated. Sutherland *et al.* (1998a) however, argued that there is some overlap in REE contents between zircon inclusions and megacrysts and also argued that both the corundum and zircon megacrysts must be explained by the same genetic model. Sutherland *et al.* (1998a) in particular used U-Pb dating of zircons to constrain the timing of corundum formation, as occurring both before and immediately after the main phase of basaltic volcanism. According to Sutherland *et al.* (1998a) the zircon age relationships can be best explained by the passing of a mantle plume beneath amphibole-metasomatised mantle sources.

ii. The significance of inclusions of Nb-Ta oxides, in particular, whether they demand the presence of exotic melt components such as carbonatites (Guo *et al.*, 1996a) or

can be explained by "normal" silicate pegmatitic crystallisation from highly evolved alkali melts (Sutherland *et al.*, 1998a).

iii. The interpretation of feldspar exsolution textures, whether they represent low-mid crustal temperatures (300-600°C; Guo *et al.*, 1996a) or alternatively higher temperatures (> 900°C) appropriate for the upper mantle conditions (Sutherland *et al.*, 1998a).

However, despite the controversy there is a general consensus that corundum genesis must involve at least two main stages. A first stage, in which corundum is produced by a magmatic phase at mantle/crustal depths and a second stage in which corundum is incorporated and transported to the surface via alkali within-plate magmatism in a subsequent magmatic event.

1.1.3 Generation of corundum by metamorphic recrystallisation

The generation of corundum by metamorphic recrystallisation of aluminous lower crustal rocks has also been documented. Metamorphic corundum is formed by recrystallisation of Al-rich Si-poor host rocks by either subduction of such rocks on the ocean floor (Levinson and Cook, 1994) or by contact metamorphism (Sutherland and Coenraads, 1996). Sutthirat *et al.* (2001) proposed that high-pressure metamorphism of Al-rich mafic rocks could also lead to crystallisation of corundum. The model proposed by Oakes *et al.* (1996) suggested that corundum was derived by reworking of clay-altered volcaniclastic host rocks. Barron *et al.* (1996) included corundum as an additional aspect of the subduction model. The model noted that corundum could be produced by prograde metamorphism in the descending slab which was claimed to explain the association of sapphire with alluvial diamond found in eastern Australia (Oakes *et al.*, 1996).

1.2 Overview of corundum-bearing intraplate basalts

Extensive studies on the characteristics and origin of different basaltic rocks have distinguished basalts from different environments such as the ocean floor (MORB), the ocean islands (OIB), the island arcs (IAB) and the continental regions. Gem-quality corundums are most often recovered from continental environments, and appear to have a close spatial relationship with intraplate alkali basaltic provinces rather than with large-scale intraplate volcanism such as continental flood basalts. Corundum deposits in intraplate environments are found throughout the world (Fig.1) but the majority of gem-quality corundum comes from alluvial deposits.

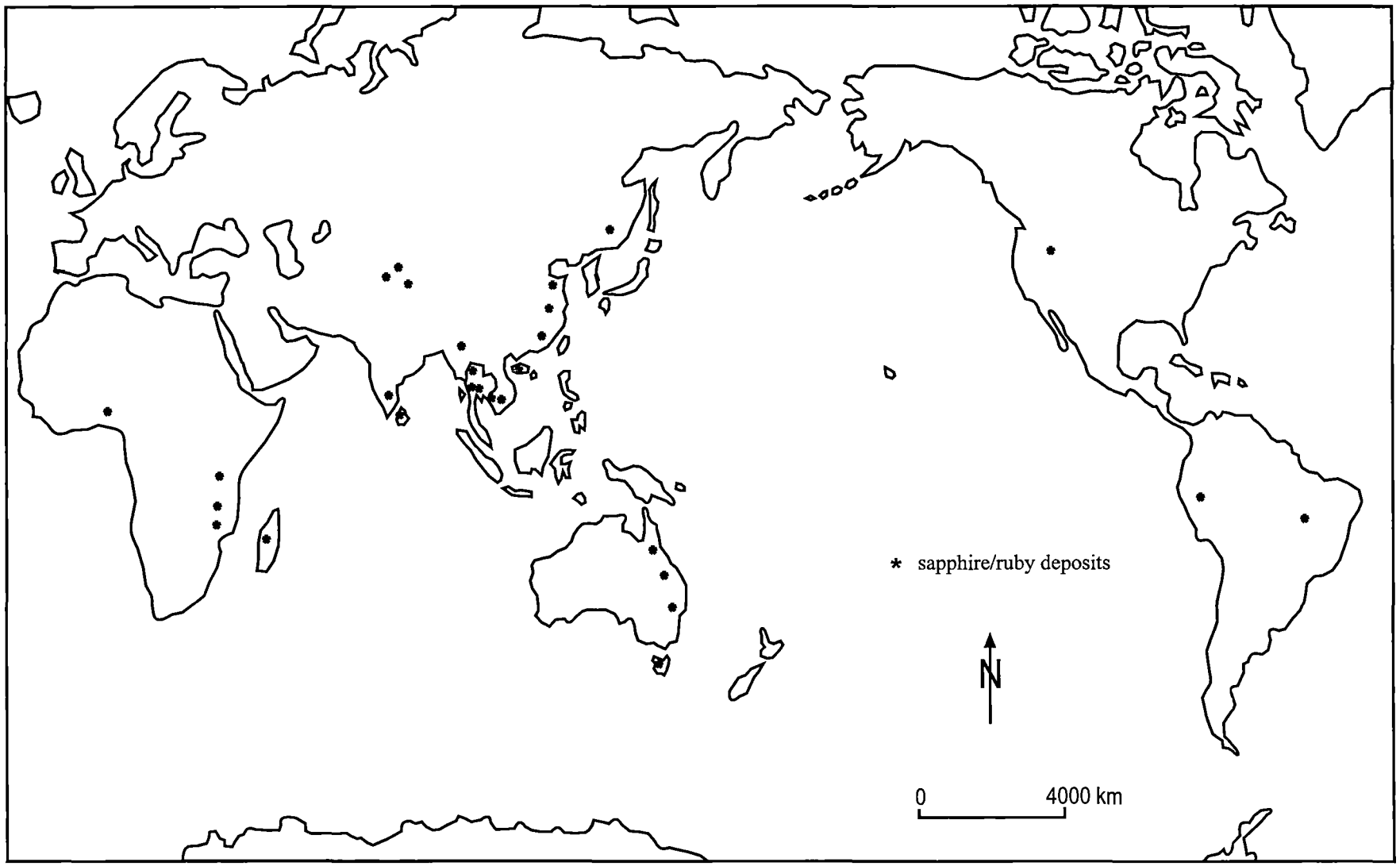

Figure 1 The localities of significant sapphire/ruby deposits in the world (modified from Guo, 1993)

These geological observations lead to the general assumption that the detrital corundum mined in these alluvial deposits was derived from the weathering and erosion of nearby basaltic lavas, plugs and diatremes (Guo, 1993).

Two good examples of intraplate corundum occurrences are eastern Australia and Thailand. In both places, corundums are concentrated within alluvium and in palaeo-channels, where they form economic deposits (e.g., Irving, 1974; Barr and Dostal, 1986; O'Reilly *et al.*, 1989; Vichit, 1992; Coenraads *et al.*, 1995; Guo *et al.*, 1996a; Sutherland *et al.*, 1998a).

A review of corundum occurrences associated with alkali volcanics in eastern Australia and Thailand reveals that the predominant igneous lithologies are basanite and alkali basalt (Table 1.3). These alkali volcanics overlie basement rocks, which mostly consist of folded and metamorphosed Palaeozoic fold belt rocks that have been extensively intruded by large volume granite batholiths. In the cases examined with good exposures, the alkali basaltic volcanics have intruded through granite batholiths, especially in the eastern Australian deposits. However, possibly due to the poor exposure in some of the Thai deposits, it has not been possible to establish this association with granite intrusions. The geochemistry of the granite batholiths in most cases is also poorly known. However, both I- and S-type granites are spatially associated with the sapphire-bearing alkali basaltic volcanics in Thailand.

In most of the alkali basaltic provinces, numerous upper mantle xenoliths, rare crustal xenoliths and megacryst assemblages are found in the basaltic successions. Mantle xenoliths include mainly Cr-diopside suite (lherzolites and pyroxenites) and less common Al-augite suite rocks (Wilshire and Shervais, 1975; Frey and Prinz, 1978; O'Reilly *et al.*, 1989). Crustal xenoliths are either mafic granulites or eclogitic rocks, which have been interpreted as having a lower crustal origin (O'Reilly *et al.*, 1989). These represent xenoliths accidentally enclosed in magma during ascent at different depths from the upper mantle to the surface. The associated mantle/crustal xenolith suites from eastern Australian and Thai deposits indicate that the most abundant mantle xenolith in these basalts is spinel-lherzolite, followed by pyroxenite and Al-augite suite rocks, whereas the lower crustal xenoliths are granulites/eclogitic rocks (Table 1.4).

The megacryst assemblages from eastern Australian and Thai deposits consist of a wide range of minerals, divided into common and rare megacrysts (Table 1.5). The common megacrysts are pyroxene (Al-augite), feldspar (mainly anorthoclase and less common plagioclase), spinel (mainly hercynite and less common chromite), amphibole (pargasite-kaersutite series) and mica (biotite and phlogopite).

Table 1.3 Gem-related basaltic rocks from Eastern Australian and Thai deposits

Localities	nephelinite	ne-hawaiite	hawaiite	ne-mugearite	mugearite	alkali basalt	basanite	phonolite	tholeiitic basalt	Sources
Eastern Australian deposits										
Lava Plains (QLD)	x	x	x	x	x	x	x	x	-	Stephenson *et al.*, 1980; Rudnick *et al.*, 1986
Anakie-Rubyvale (QLD)	x	x	x	-	-	x	x	-	-	Stephenson, 1990
Inverell-Glen Innes (NSW)	x	-	x	-	x	x	x	x	-	Wilkinson, 1966, 1969, Duggan, 1972
Barrington (NSW)	x	-	-	-	-	x	x	-	x	Sutherland and Coenraads, 1996, O'Reilly and Zhang, 1995, Sutherland and Fanning, 1996
Weldborough/Ringarooma (TAS)	x	-	x	-	-	x	x	-	-	McClenaghan *et al.*, 1982
Thai deposits										
Chiang Khong (North)	-	-	-	-	-	-	x	-	-	Barr and MacDonald, 1981
Phrae-Sukhothai (North)	-	-	-	-	-	x	x	-	-	Vichit *et al*, 1978; Barr and MacDonald, 1978, 1981
Wichianburi (Central)	-	x	x	-	-	x	x	-	-	Vichit *et al.*, 1988
Ubon Ratchathani-Si Sa Ket (East)	*	*	*	x	*	*	*	*	*	Barr and MacDonald, 1981
Kanchanabun (West)	x	x	-	-	-	x	x	-	-	Charaljavanaphet, 1951, Bunopas and Bunjitadulya, 1975; Vichit *et al.*, 1978; Yaemniyom, 1982
Chanthaburi-Trat (Southeast)	x	x	x	-	-	-	x	-	-	Barr and MacDonald, 1978, Barr and MacDonald, 1978, 1981, Vichit, 1987, 1992; Vichit *et al*, 1978; Yaemniyom, 1982

Notes (x) present, (-) absent, (*) not reported, ne = nepheline

Table 1.4 Associated mantle and crustal xenoliths from Eastern Australian and Thai deposits

Localities	Mantle xenoliths							Crustal xenoliths	Sources
	Cr-diopside / Fe rich Cr-diopside suite#				Al-augite suite			granulites/eclogitic rocks	
	lherzolite	harzburgite	pyroxenite	dunite	wehrlite series	metapyroxenite series	apatite/amphibole series		
Eastern Australian deposits									
Lava Plains (QLD)	x	-	x	-	-	-	-	x	O'Reilly *et al* , 1989
Anakie-Rubyvale (QLD)	*	*	*	*	*	*	*	x	Wass and Irving, 1976,
Inverell-Glen Innes (NSW)	-	-	x	-	x	x	x	-	Wilkinson, 1969, Duggan, 1972
Barrington (NSW)	x	x	x	x	-	-	x	-	Wilkinson, 1974; Wilkinson and Binns, 1977; Wilkinson and Hensel, 1991; Sutherland and Coenraads, 1996
Weldborough (TAS)	x	x	x	x	-	-	-	-	J Everard, (pers comm)
Thai deposits									
Chiang Khong (North)	x	-	-	-	-	-	-	-	Barr and MacDonald, 1981
Phrae-Sukhothai (North)	x	-	-	-	-	-	-	-	Vichit *et al* , 1978, Barr and MacDonald, 1978, 1981
Wichianburi (Central)	x	-	-	-	-	-	-	-	Vichit *et al* , 1988
Ubon Ratchathani-Si Sa Ket (East)	*	*	*	*	*	*	*	*	
Kanchanaburi (West)	x	-	-	-	-	-	-	-	Vichit, 1987, 1992
Chanthaburi-Trat (Southeast)	x	-	-	x	-	-	-	-	Barr and MacDonald, 1978, 1981, Vichit, 1987, 1992, Vichit *et al*., 1978; Yaemniyom, 1982

Notes (x) present, (-) absent, (*) not reported, (#) it not possible to distinguish xenolith type on the basis of published description

Table 1.5 Associated megacryst assemblages from Eastern Australian and Thai deposits

Localities	Common megacrysts						Rare megacrysts					Sources
	pyroxene[1]	plagioclase	anorthoclase	spinel[2]	amphibole[3]	mica[4]	ilmenite	apatite	zircon	garnet[5]	corundum	
Eastern Australian deposits												
Lava Plains (QLD)	x	x	x	x	x	x	x	x	x	x	x	Stephenson *et al* , 1980
Anakie-Rubyvale (QLD)	x	x	x	x	-	-	-	-	x	-	x	Stephenson *et al*., 1989
Inverell-Glen Innes (NSW)	-	-	x	x	x	x	x	-	x	x	x	Binns, 1969; Binns *et al* , 1970, MacNevin, 1972, Coenraads and Der Graaf, 1991
Barrington (NSW)	x	x	x	x	x	-	x	x	x	-	x	Wilkinson, 1974; Wilkinson and Binns, 1977, Wilkinson and Hensel, 1991, Sutherland and Coenraads, 1996
Weldborough (TAS)	-	-	-	x	-	-	x	-	x	-	x	Yim, 1990
Thai deposits												
Chiang Khong (North)	x	-	-	x	-	-	-	-	x	-	x	Barr and MacDonald, 1981
Phrae-Sukhothai (North)	x	-	x	x	-	-	x	-	x	x	x	Vichit, 1987, 1992; Barr and MacDonald, 1979, 1981; Barr and Dostal, 1986
Wichianburi (Central)	x	x	x	x	x	-	-	-	x	x	x	Vichit *et al*., 1988
Ubon Ratchathani-Si Sa Ket (East)	-	-	-	-	-	-	x	-	x	x	x	Vichit, 1987, 1992
Kanchanabun (West)	x	x	x	x	-	-	-	-	x	x	x	Vichit, 1992; Guo, 1993, Barr and Dostal, 1986
Chanthabun-Trat (Southeast)	x	-	x	x	-	x	x	-	x	x	x	Barr and MacDonald, 1978, 1981; Barr and Dostal, 1986; Vichit, 1987, 1992; Vichit *et al*., 1978; Yaemniyom, 1982 Sutthirat *et al*., 2001

Notes (x) present, (-) absent, (1) Al-augite, (2) mainly hercynite and less common chromite, (3) pargasite-kaersutite, (4) biotite and phlogopite, (5) pyrope

Rare megacrysts include zircon, corundum, garnet (mainly pyrope), ilmenite and apatite (Barr and McDonald, 1981; O'Reilly *et al.*, 1989; Vichit, 1992). The scenario for the crystallisation of these megacrysts may be complex, as they have been separated from their parent rocks. They could be either cognate high-pressure phases crystallised from magmas compositionally similar to their hosts or they may be accidentally entrained as xenocrysts representing the disaggregated wall rocks from different depths and completely exotic to the host magma.

The origin of these megacrysts together with the genesis of gem-quality corundum from intraplate environments, remains controversial in terms of genetic relationship with their host rocks. The nature of corundum and associated solid and fluid/melt inclusions, indicates that it might not be possible for one single petrogenetic model to explain corundum genesis worldwide. However, specific case studies put forward several corundum genesis models (e.g., Guo *et al.*, 1996a; Sutherland *et al.*, 1998a). The ultimate source of corundum as well as how and when it is formed remains questionable. Answers to these questions will assist the exploration for economic sapphire deposits. The understanding of these processes is the primary objective of this thesis.

1.3 Thesis aims

Large numbers of sapphire samples from different localities worldwide have been studied to address their original source (e.g., Guo *et al.*, 1996a; Sutherland *et al.*, 1998a; Upton *et al.*, 1999). In particular, the concentration of commercial sapphires is closely related to the basaltic rocks from several basaltic provinces (e.g., Eastern Australia and Thailand). This suggests that the basaltic rocks are among the best sources for commercial sapphires.

This thesis focuses on sapphires recovered from alluvial placer deposits that occur in close spatial association with late Cenozoic alkali basaltic rocks of Thailand. An attempt is made in this thesis to establish a genetic link between corundum occurrences and basalt geochemistry. This investigation is based on carefully selected alkali basaltic rocks, their petrogenesis and their relationship to the alluvial sapphires. This is further supplemented by fluid, solid and melt inclusion studies within sapphires, to constrain the interpretation of corundum genesis. Sapphire samples used in this study were collected from alluvial placer and palaeo-channel deposits at shallow depths during the field studies carried out in Amphoe Denchai, Changwat Phrae of northern Thailand. The alluvial sapphires are equivalent to the megacrysts that occur within the host basalt.

1.4 Thesis outline

The thesis structure develops a data set to address problems of sapphire genesis.

- Chapter 1 is an introductory review of competing models for corundum genesis associated with intraplate alkali basaltic volcanism.
- Chapter 2 is review of late Cenozoic basalts in mainland Southeast Asia as well as an overview of the major gem-related basalts in Thailand. This also includes the regional geology and settings of the study area (Denchai basalts, northern Thailand).
- Chapter 3 describes the petrography and mineral chemistry of the Denchai basalts and the associated xenoliths.
- Chapter 4 presents whole rock geochemistry of the Denchai basalts. This includes the major, trace and rare earth elements of the basalts. It assesses the role of crystal fractionation, and crustal contamination in the chemistry of these basalts and identifies the nature of the underlying lithosphere. An isotopic study of the Denchai basalts is also presented to constraint the nature of magmatic processes and sources.
- Chapter 5 describes general characteristics, trace element chemistry, oxygen isotopes and nature of inclusions in the Denchai sapphires. Attempts are made in this chapter to establish the relationship between the fluid, solid and melt inclusions of the studied gem sapphires. This is used to constraint the temperature, pressure and nature of corundum formation.
- Finally, Chapter 6 summarises the main conclusion presented in each of the previous chapters. Genetic models for corundum genesis are discussed and compared.

Chapter 2

Geological setting of gem-related basalts in Thailand

2.1 Late Cenozoic basalt provinces in southeast Asia

Late Cenozoic basalts in mainland southeast Asia range in age from 24 Ma to less than 1 Ma and form a large continental volcanic province. In Thailand and western Cambodia, exposures of late Cenozoic basalts are generally small and scattered, whereas those in eastern Cambodia and southern Laos as well as central and southern Vietnam tend to be larger and more extensive. Late Cenozoic basalts also occur in other parts of Asia including southeastern China, central Burma and Malaysia Peninsula (Fig.2.1). Several occurrences of late Cenozoic basalts in southeast Asia are regarded as a major source of gem-quality corundum, particularly in Thailand, western Cambodia and northern Burma. The Southeast Asian basalts have a diverse geochemistry ranging from tholeiitic to strongly alkalic affinities, including mugearites, hawaiites, alkali olivine basalts, basanites and nephelinites (Barr and MacDonald, 1978, 1981; Bender, 1983; Stephenson and Marshall, 1984). Late Cenozoic basalt occurrences of mainland Southeast Asia are briefly described below, according to their geographical localities.

2.1.1 Southeastern China

Late Cenozoic basalts of southeastern China are part of the eastern China volcanic belt and are closely associated with NNE-trending fracture zones. It is generally accepted that Cenozoic basaltic volcanism in southeastern China was related to lithospheric extension as a result of subduction of the Pacific plate beneath the Eurasian plate (Wu, 1984; Zhang and Cong, 1987). This subduction generated hot asthenosphere upwelling that led to back arc extensional rifting and the generation of fault basins and associated deep fracture zones. It is believed that the Cenozoic basaltic magmas of southeastern China were erupted along these deep fracture zones (Qu-Qi *et al.*, 1995).

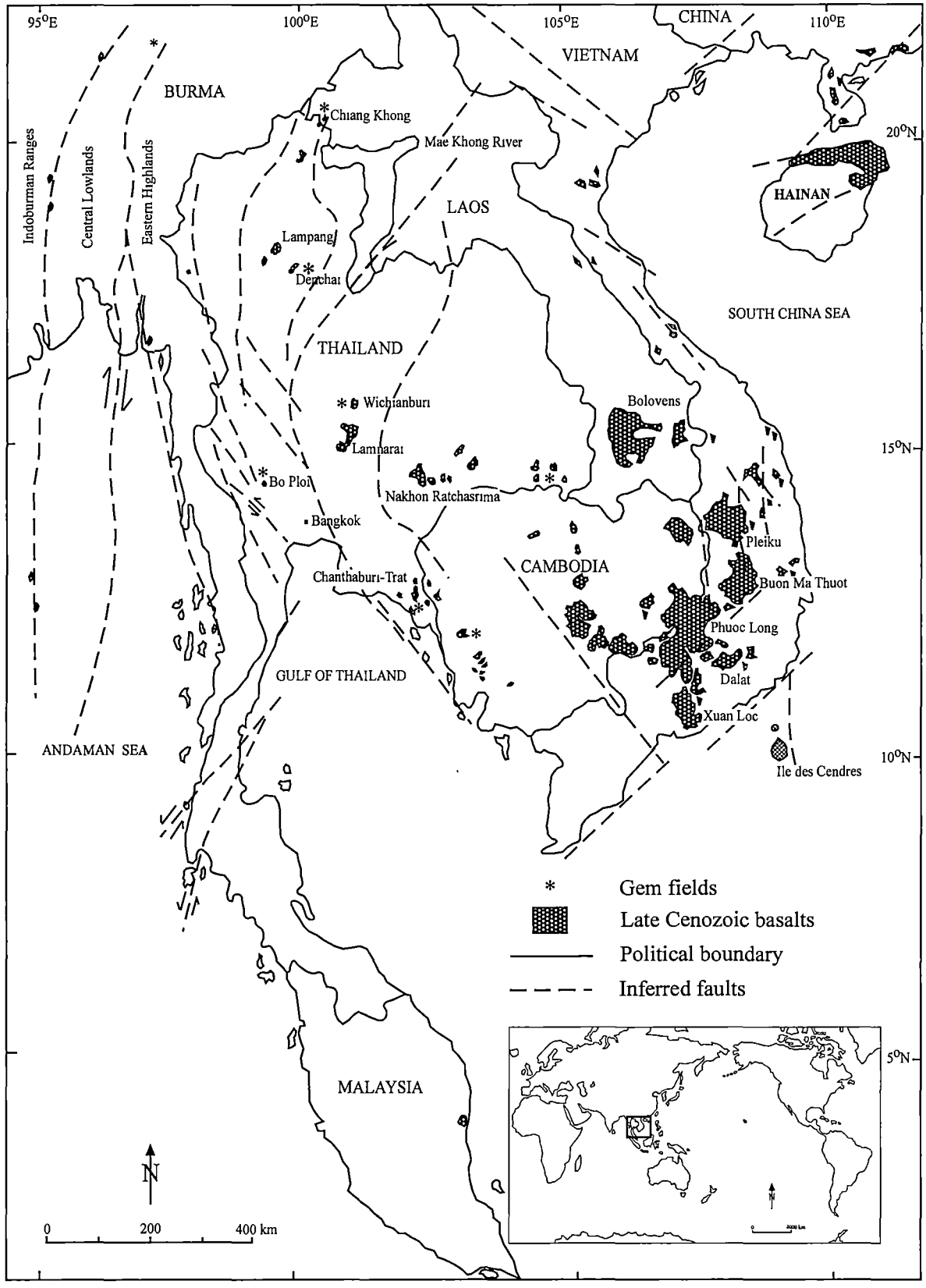

Figure 2.1 Map showing the distribution of late Cenozoic basalts in Southeast Asia (modified from Barr and MacDonald, 1981; Stephenson and Marshall, 1984; Hoang and Flower, 1998)

Numerous geochemical studies on basaltic rocks of eastern China have been reported but most are concentrated on the northern part because of the spectacular thick sequences exposed in that area. Several detailed studies from southeastern China showed that the basalts occur as relatively small, widely distributed volcanoes/flows showing marked spatial variation in chemical compositions (Fan and Hooper, 1991; Liu *et al.*, 1994). The southeastern China basalts are not major gem sources but sapphires have been reported from the Hainan Province (Guo, 1993).

2.1.2 Vietnam

Most Vietnamese exposures of Cenozoic basalts occur as plateaus in central and southern part of Vietnam (Fig.2.1). Basalt plateaus often exceed 100 km in diameter and are up to several hundred metres in thickness (Carbonnel *et al.*, 1973; Hoang and Han, 1990) and include primary volcanic landforms such as cones, crater lakes and lava flows.

Hoang and Flower (1998) suggested that at least two eruptive episodes have been recorded in the Vietnamese basalts. Quartz and olivine tholeiite lavas and rare alkali basalts are the products of early volcanic episodes, whereas the later episodes usually produced olivine tholeiites, alkali basalts, basanites and rarely nephelinites. However, most recent whole rock K-Ar and Ar-Ar ages of Vietnamese basalts (Lee *et al.*, 1998) suggest that they were erupted over an extended interval: Dalat (17.6-7.9 Ma), Phuoc Long (< 8-3.4 Ma), Buon Ma Thuot (5.8-1.67 Ma), Pleiku (4.3-0.8 Ma), Xuan Loc (0.83-0.44 Ma) and Ile des Cendres (0.8-0 Ma). There is no evidence from this dating of two discrete Vietnam-wide events. Gem-quality corundums have been found in southern Vietnam (Smith *et al.*, 1995).

2.1.3 Cambodia

Cenozoic basalts occur in eastern and western Cambodia. The eastern Cambodian basalts form low plateaus composed of the Kompong Cham basalts, which range in composition from tholeiitic to strongly alkalic (Carbonnel *et al.*, 1973). Basalts in western Cambodia occur as small, scattered volcanic bodies known as the Pailin basalts. They are also known as a major source of gem-quality corundum in Cambodia. The Pailin basalts are largely covered by reddish-brown residual soils but remnant craters are easily recognised. Compositionally, they include tholeiites and alkali basalts. Geochronological studies of the Pailin basalts (fission track and K-Ar dating) have demonstrated ages of 2.42 (±0.18) Ma at Phnum Yat,

1.43 (±0.10) Ma at Phnum Ko Ngoap and 1.09 (±0.13) Ma at Phnum O Tang (Carbonnel *et al.*, 1973).

2.1.4 Laos

Basaltic rocks from the Bolovens plateau in the southern part of Laos occur at an elevation of 1000 to 1200 m and occupy valleys descending radially from the center of the plateau towards sea level. These basalts are not well understood, due to the limited data available. However, they are considered to be Quaternary in age despite a zircon age of 1.36 ± 0.09 Ma (Hoffett, 1933). The gem-quality corundums have been recovered from alluvial deposits at Ban Huai Sai in northern Laos (Intasopa *et al.*, 1998).

2.1.5 Malaysia Peninsula

Cenozoic basalts occur in the Segamat and Kuantan areas in the east of the Malaysian Peninsula (Fitch, 1952; Hutchison, 1973). Chemically, the Segamat basalts are highly potassic whereas the Kuantan basalts include an older "alkali olivine basalt series" and a younger "nephelinite series" (Chakraborty, 1977). Bignell and Snelling (1977) reported K-Ar ages for the Segamat and the Kuantan basalts, of at least 62 Ma and 1.6 ± 0.2 Ma respectively. No gem-quality corundums have been reported in this area.

2.1.6 Burma

Burma can be divided into three major areas based on tectonic settings: the Indoburman Ranges, the Central Lowlands and the Eastern Highlands (Stephenson and Marshall, 1984). Igneous rocks in these three areas range in age from Lower Jurassic to Pleistocene and occur sparsely throughout a 1500 km long "volcanic arc" along the Central Lowlands (Chhibber, 1934). Late Cenozoic volcanics occur along the central volcanic line as well as at the recent active volcanoes of Barren and Narcondam Islands in the Andaman Sea (Fig.2.1). The central volcanic line also raises the possibility that they are associated with world-class ruby-sapphire deposits (Mogok) in northern Burma (Mitchell, 1993).

2.1.7 Thailand

Late Cenozoic basalts in Thailand occur in scattered small volcanic areas. Each occurrence is named after the local district or city where it occurs. They are exposed in northern, central,

western, eastern and southeastern parts of Thailand. Several localities of these basalts are regarded as the sources of gem-quality corundum, which are usually found in alluvial deposits adjacent to basalt outcrops (Fig.2.2). Gem-quality corundum is most commonly associated with strongly alkali basalt that contains abundant peridotitic mantle xenoliths. Many geochemical studies have been published on Thai basalts over the last two decades. Late Cenozoic basalts in Thailand are predominantly alkalic to tholeiitic in character (Barr and MacDonald, 1978, 1979, 1981; Boonsoong, 1997; Charusiri *et al.*, 1995; Intasopa, 1993; Panjasawatwong, 1995; Sriprasert, 1997; Sutthirat, 1995; Yaemniyom, 1982; Yamamoto, 1991). However, the Thoeng basalts of northern Thailand are tholeiitic in composition. Late Cenozoic basalts in Thailand have ages ranging from 24 Ma to less than 0.5 Ma (Table 2.1).

2.1.8 Summary

Late Cenozoic volcanism in Southeast Asia began at least 25 Ma ago and has continued to the present time. No systematic relationship appears to exist between age and geographic location, and volcanic activity seems to be randomly distributed throughout the region. Southeast Asia is also a region of complex tectonics. Several synchronous events may have influenced the tectonics of the area, including opening of the South China Sea (Ben-Avraham and Uyeda, 1973), opening of the Andaman Sea (Lawver *et al.*, 1976) and the collision between the Indian and Eurasia plates (Tapponnier *et al.*, 1986). The Late Cenozoic basalts in mainland Southeast Asia may, therefore, be a surface expression of these complex regional tectonic events in this region, mostly driven by escape tectonics related to the collision of India with Asia. Escape tectonics was a major influence in the gem areas of Southeast Asia from about 35 Ma to present (Morley *et al.*, 2001). The dominant deformation during this period was strike slip faulting. The structure was grossly compressional initially, but crustal extension started in Thailand during the Miocene (Dunning *et al.*, 1995), and most of the basalts date from this extensional period (Table 2.1).

2.2 Review of gem-related basalts in Thailand

Gemstones in Thailand are generally found as secondary alluvial deposits that form economic placer deposits (Table 2.2). Sapphires and rubies in particular are found in a great abundance compared to other gemstones such as garnet (pyrope), zircon, spinel (hercynite), quartz (rock crystal and amethyst), agate and chalcedony. Each occurrence is named after the local district or city where it is found (Fig.2.3). More than 90% of sapphire and ruby comes from the Kanchanaburi (western) and Chanthaburi and Trat (southeastern) deposits (Vichit, 1992).

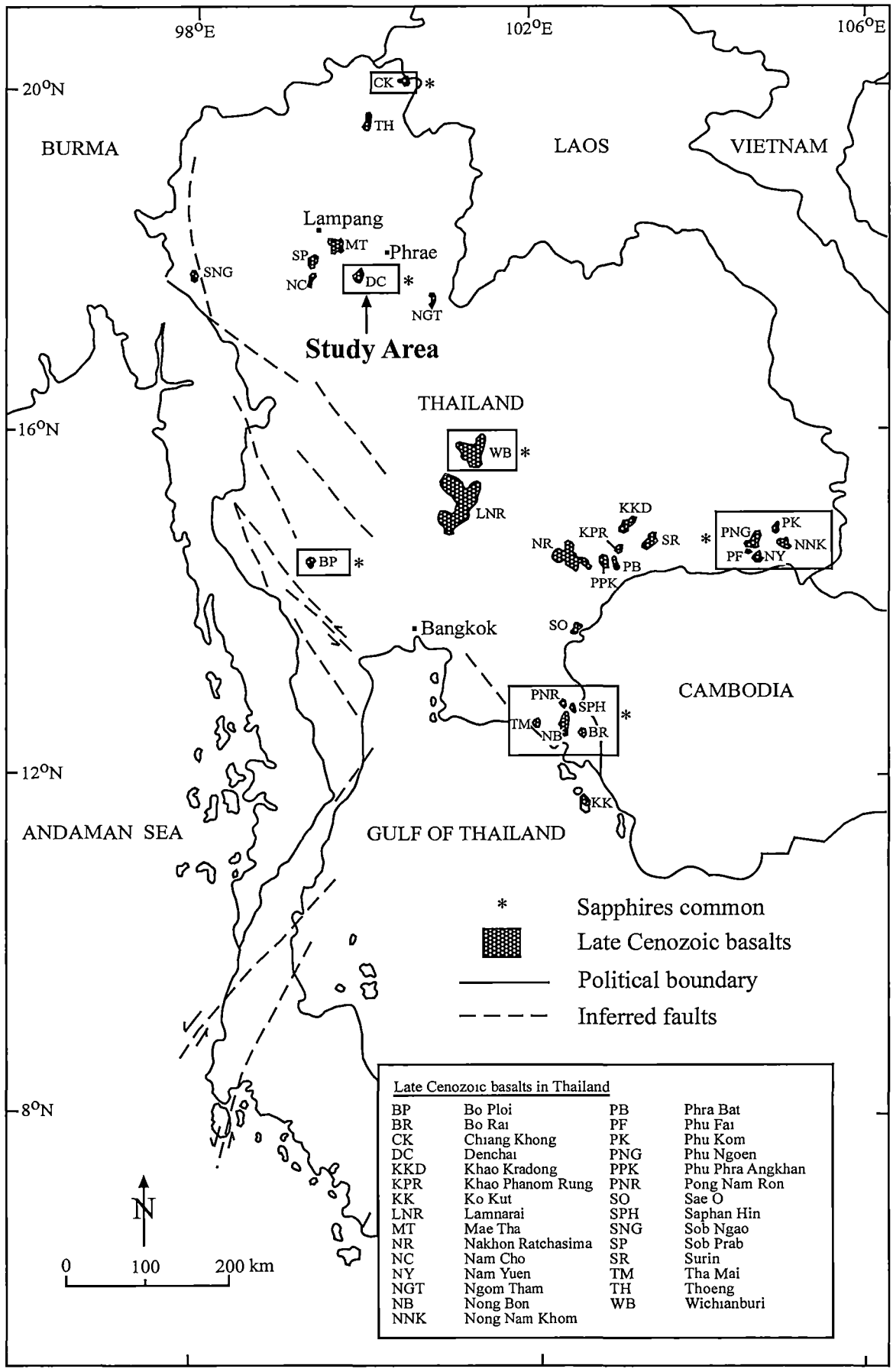

Figure 2.2 Map showing the distribution of late Cenozoic basalts in Thailand (modified from Jungyusuk and Khositanont, 1992; Boonsoong, 1997)

Table 2.1 Absolute whole rock ages of late Cenozoic basalts in Thailand (modified from Boonsoong, 1997)

Localities	Age (Ma)	Age Dating Methods	Rock type	Sources
Thoeng Basalt (TH)	1.69 ± 1.25	K-Ar (whole rock)	tholeiite	Barr and MacDonald, 1981
Chiang Khong Basalt (CK)	1.74 ± 0.18	K-Ar (whole rock)	basanite	Barr and MacDonald, 1981
Mae Tha Basalt (MT)	0.80 ± 0.30	K-Ar (whole rock)	basanite	Sasada *et al.*, 1987
	0.60 ± 0.20	K-Ar (whole rock)	basanite	Sasada *et al.*, 1987
	0.50 ± 0.05	Ar-Ar (whole rock)	basanite	Sutthirat *et al.*, 1994
	0.69 - 0.95	Paleomagnetic (whole rock)	basanite	Barr *et al.*, 1976
Sop Prab Basalt (SP)	2.30 ± 0.13	Ar-Ar (whole rock)	alkali basalt	Sutthirat, 1995
				Sutthirat *et al.*, 1995
	2.36 ± 0.13	Ar-Ar (whole rock)	alkali basalt	Sutthirat, 1995
				Sutthirat *et al.*, 1995
	2.38 ± 0.17	Ar-Ar (whole rock)	alkali basalt	Sutthirat, 1995
				Sutthirat *et al.*, 1995
	2.41 ± 0.17	Ar-Ar (whole rock)	alkali basalt	Sutthirat, 1995
				Sutthirat *et al.*, 1995
Nam Cho Basalt (NC)	2.02 ± 0.10	Ar-Ar (whole rock)	alkali basalt	Sutthirat, 1995
				Sutthirat *et al.*, 1995
Denchai Basalt (DC)	5.64 ± 0.28	K-Ar (whole rock)	basanite	Barr and MacDonald, 1981
Bo Ploi Basalt (BP)	3.14 ± 0.17	K-Ar (whole rock)	ne-hawaiite	Barr and MacDonald, 1981
Lamnarai Basalt (LNR)	11.29 ± 0.64	K-Ar (whole rock)	basalt	Barr and MacDonald, 1981
	18.1 ± 0.70	Ar-Ar (whole rock)	alkali basalt	Intasopa, 1993
	24.1 ± 1.0	Ar-Ar (whole rock)	alkali basalt	Intasopa, 1993
Wichianburi Basalt (WB)	9.7 - 11.6	Ar-Ar (whole rock)	basalt	Charusiri, 1989
	9 10 ± 0.03	Ar-Ar (whole rock)	basalt	Intasopa, 1993
Khao Kradong Basalt (KKD)	0.92 ± 0.30	K-Ar (whole rock)	basalt	Barr and MacDonald, 1981
Phu Fai Basalt (PF)	3.28 ± 0.48	K-Ar (whole rock)	ne-hawiite	Barr and MacDonald, 1981
Tha Mai Basalt (TM)	2.57 ± 0.20	Fission Track (whole rock)	basalt	Carbonnel *et al.*, 1973
	0.44 ± 0.11	K-Ar (whole rock)	basalt	Barr and MacDonald, 1981
Trat Basalt (TR)	1.13 ± 0.17	K-Ar (whole rock)	basalt	Barr and MacDonald, 1981
Ko Kut Basalt (KK)	8.5 ± 1.0	K-Ar (whole rock)	basalt	Bignell and Snelling, 1977

Note: ne = nepheline, basalt localities are shown in Figure 2.2

Table 2.2 Summary of major gem-related basalt deposits in Thailand

Localities	Gem-related basalts	Gemstones	Basement rocks	Xenoliths
Phrae-Sukhothai deposit (Denchai)	basanite	corundum, clinopyroxene, spinel, zircon	Permo-Triassic sedimentary rocks	spinel-lherzolites
Chiang Khong deposit (Chiang Khong)	basanite	corundum, clinopyroxene, spinel, zircon	Permo-Triassic tuff	ultramafic xenoliths
Wichianburi deposit (Wichianburi)	basanite and alkali basalt	corundum, zircon, garnet, spinel, feldspar, amphibole	Permian sedimentary and Triassic volcanic rocks	ultramafic xenoliths
Ubon Ratchathani-Si Sa Ket deposit (Phu Fai, Phu Kom, Phu Ngoen, Nam Yuen and Nong Nam Khom)	hawaiite	corundum, zircon, garnet, ilmenite, magnetite	Mesozoic sedimentary rocks	ultramafic xenoliths
Kanchanaburi deposit (Bo Ploi)	basanite and alkali basalt	corundum, clinopyroxene, sanidine, spinel	Precambrian metamorphic and Palaeozoic sedimentary rocks	spinel-lherzolites
Chanthaburi-Trat deposit (Tha Mai, Nong Bon, Pong Nam Ron, Bo Rai and Saphan Hin)	nephelinite	corundum, clinopyroxene, zircon, garnet, spinel	Carboniferous-Permian meatamorphic and volcanic rocks	ultramafic xenoliths

Note: all gem-related basalts in Thailand are shown in Figure 2.2

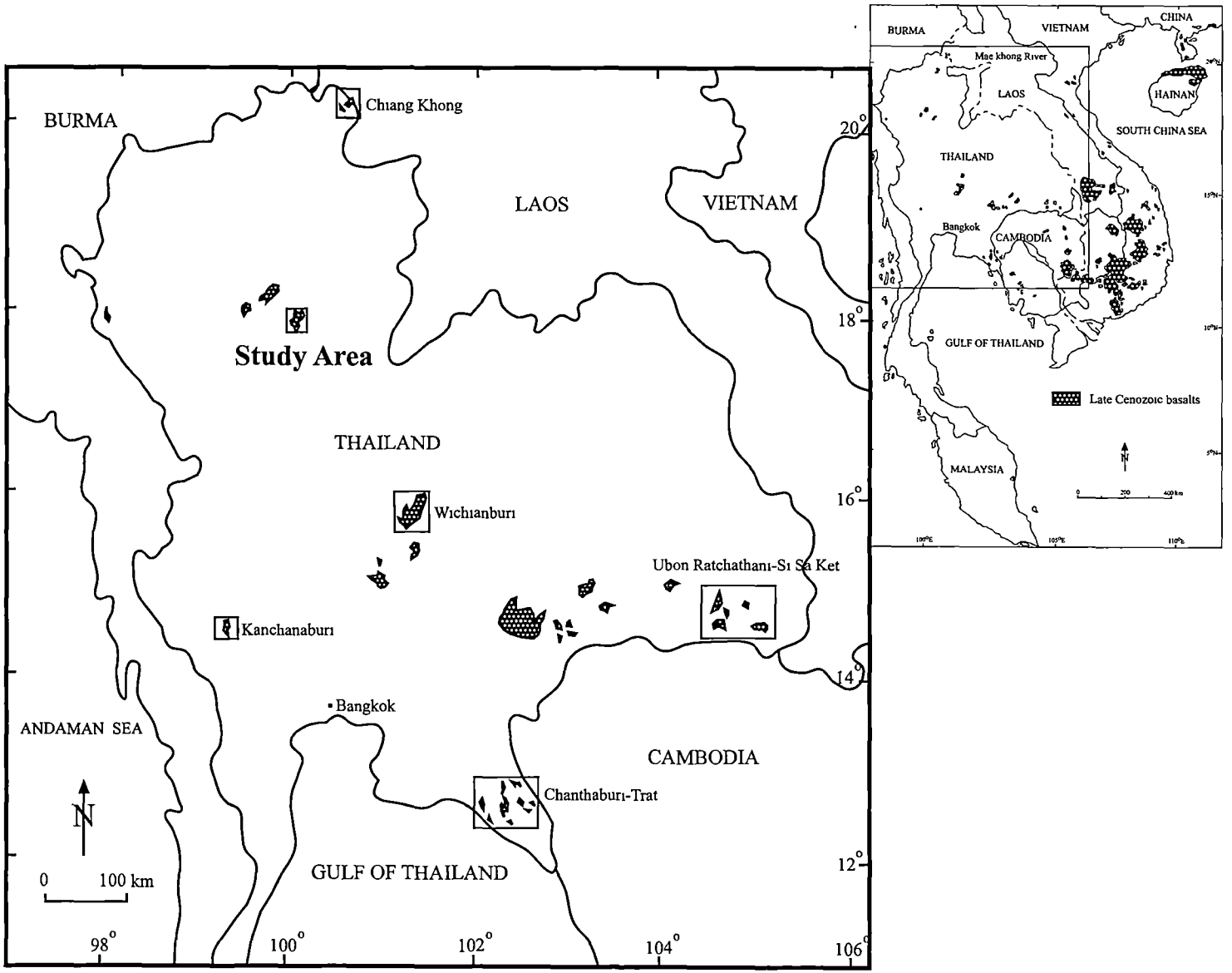

Figure 2.3 Map showing the distribution of the gem-related basalt deposits in Thailand (modified from Vichit, 1992)

The conventional view is that sapphires are found as a product of weathered and eroded basalts nearby; however sapphires are rarely found hosted within fresh basalts (Aranyakanon *et al.*, 1970; Vichit *et al.*, 1978). It is necessary to review the distribution and the geological settings of the well-known gem-related basalt deposits to establish a geological background for the understanding of sapphire origin. Detailed studies of gem-related basalts in Thailand have been reported in terms of their general geology and petrochemistry (Barr and Macdonald, 1981; Vichit, 1992). The geological setting of well-known gem deposits is briefly presented below.

2.2.1 Chiang Khong deposit, northern Thailand

The Chiang Khong basalt has long been regarded as corundum-bearing. Gem-quality corundum has only been mined from the alluvial and residual soils in nearby Laos. The Chiang Khong basalt is located on the bank of Mae Khong River at Changwat Chiang Rai and it can be traced across the Mae Khong River into Laos, where the main 50 m in diameter basaltic body crops out (Sukvattananunt and Assavapatchara, 1989). These basalts consist of two basanite flows (Panjasawatwong and Youngsanong, 1996) with K-Ar age of 1.74 ± 0.12 Ma (Barr and Macdonald, 1981).

2.2.2 Wichianburi deposit, central Thailand

The Wichianburi gem deposit is located at Ban Khok Samran and Ban Marp Samo, Amphoe Wichianburi, Changwat Phetchabun (Fig.2.4). The Wichianburi basalt occurs as volcanic plugs in a hilly area, covering an area of ~30 km long and 20 km wide. The basalt overlies Permian sedimentary rocks and Triassic volcanic rocks (Nakornsri, 1981). The Wichianburi basalt is predominantly alkali olivine basalt, hawaiite and basanite. It locally contains lherzolite nodules (Vichit, 1992). Gem-quality corundums are found in residual basaltic soils and in the streams dissecting the basalts. Gemstones from this deposit are poor in quality with only a small proportion of sapphires having commercial value.

2.2.3 Ubon Ratchathani-Si Sa Ket deposit, eastern Thailand

The Ubon Ratchathani-Si Sa Ket gem deposit is located in the southeast of the Khorat Plateau near the border of Thailand and Cambodia (Fig.2.5). The gem-related basalts in this area have been heavily weathered and can be found at Amphoe Nam Yuen of Changwat Ubon Ratchathani and Amphoe Khun Harn and Amphoe Kantharaluk of Changwat Si Sa Ket, covering an area of ~70 km long and 50 km wide.

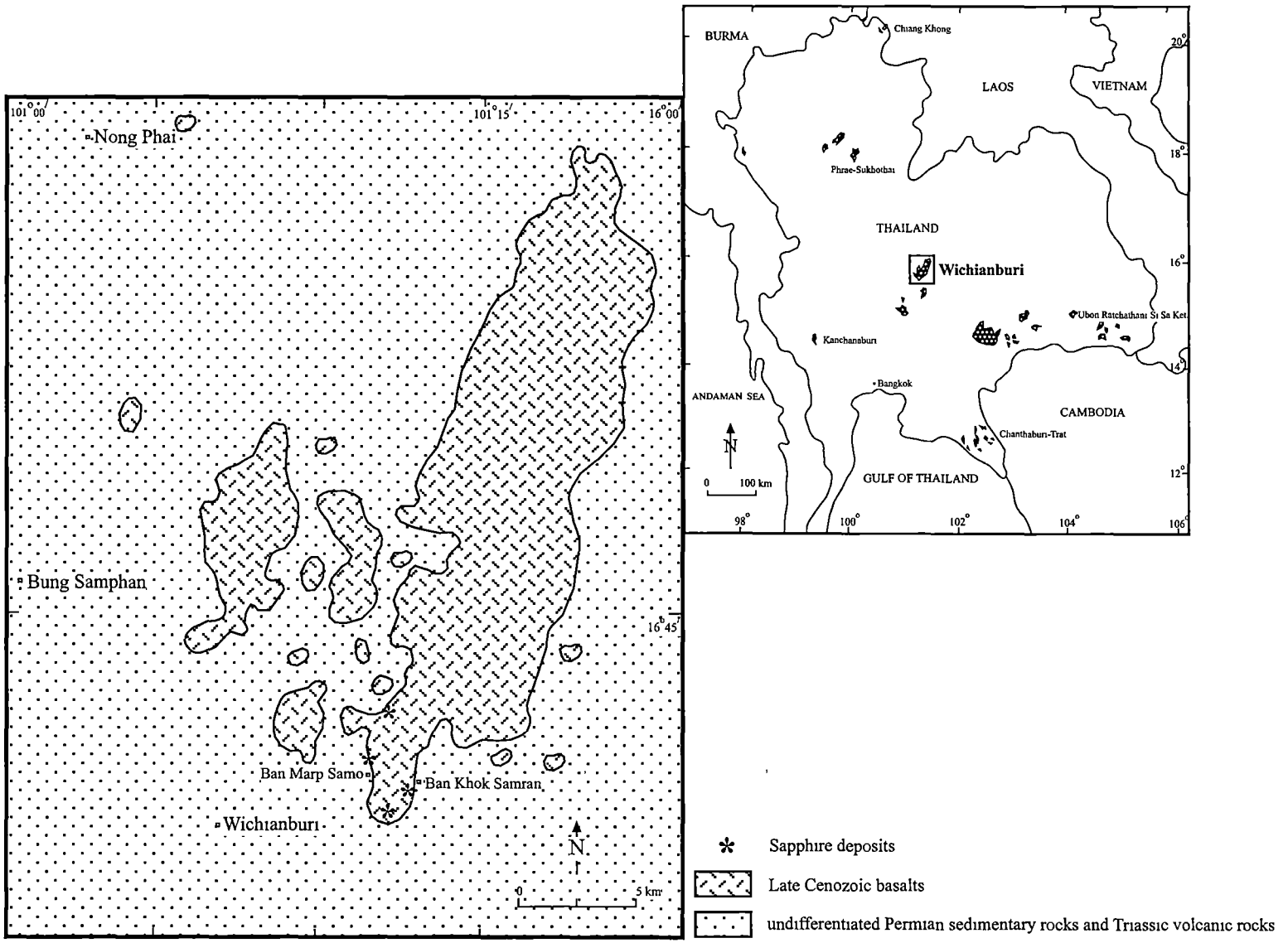

Figure 2.4 Map showing the distribution of the Wichianburi gem-related basalt deposit, central Thailand (modified from Vichit, 1992)

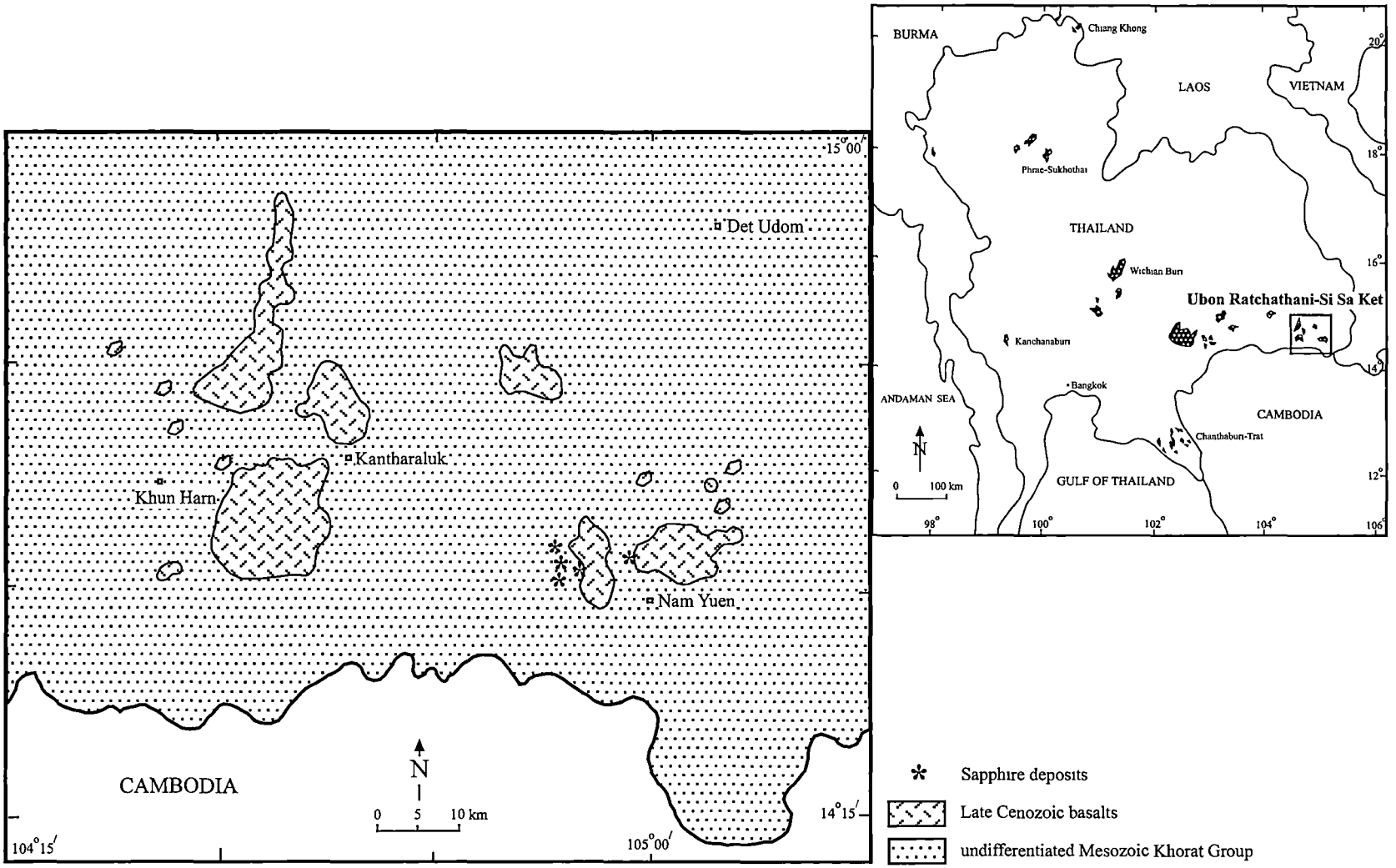

Figure 2.5 Map showing the distribution of the Ubon Ratchathani-Si Sa Ket gem-related basalt deposit, eastern Thailand (modified from Vichit, 1992)

They overlie the Khok Kruat and Phu Phan Formations (Cretaceous) and Sao Khua Formation (Jurassic) of the Mesozoic Khorat Group (Aranyakanon *et al.*, 1970). These basalts contain ultramafic nodules. They are geochemically classified as hawaiites (Jungyusuk and Khositanont, 1992). All gemstones in this deposit are recovered from alluvial deposits (Vichit, 1992).

2.2.4 Kanchanaburi deposit, western Thailand

The Kanchanaburi gem deposit is located in Amphoe Bo Ploi of Changwat Kanchanaburi (Fig.2.6). Basaltic rocks at Bo Ploi form a small, plug-like body covering ~1 km^2, in a fault zone within Silurian-Devonian quartzite. The basement rocks of Bo Ploi area range from Precambrian marble and gneiss complexes to Palaeozoic sedimentary succession intruded by granitic bodies of Cretaceous to Triassic age (Bunopas and Bunjitadulya, 1975). Bo Ploi basalt is classified as basanite by Vichit *et al.* (1978) with K-Ar age dating yielding ages of 3.14 ± 0.17 Ma (Barr and Macdonald, 1981) and 4.17 ± 0.11 Ma (Sutthirat *et al.*, 1994). This basalt contains numerous spinel-lherzolite xenoliths, and megacrysts of clinopyroxene and spinel. Bo Ploi basalt is a gem-quality blue sapphire carrier. Sapphires are found from alluvial placer deposits near basaltic outcrops (Vichit *et al.*, 1978; Srithai *et al.*, 1999). Bunopas and Bunjitadulya (1975) reported that sapphires have been mined from residual soils overlying basaltic rocks.

2.2.5 Chanthaburi-Trat deposit, southeastern Thailand

Chanthaburi-Trat is the most significant gem supplier in Thailand. It is divided into three distinctive geographic zones; the Western Chanthaburi zone, the Chanthaburi-Trat zone and the Trat zone (Fig.2.7). The gem-related basalts broadly occur between Amphoe Tha Mai of Changwat Chanthaburi and Amphoe Bo Rai of Changwat Trat (Vichit, 1992; Boonsoong, 2001). They overlie Carboniferous-Permian sedimentary and volcanic rocks (Sivabovorn *et al.*, 1976; Salyaphongse and Jungyusuk, 1983; Sutthirat *et al.*, 2001). These basalts generally form low relief plains and have commonly been weathered to red soils, with the exception of Ban Khao Ploi Waen, where small hills dominate the volcanic landform. They are strongly alkali in character, with low silica and high titanium contents, and are classified as nephelinite (Vichit *et al.*, 1978; Barr and MacDonald, 1978). These basalts contain lherzolite nodules and megacrysts of clinopyroxene, garnet and spinel. K-Ar age is 0.44 ± 0.11 Ma for a basalt from Khao Ploi Waen (Barr and Macdonald, 1981).

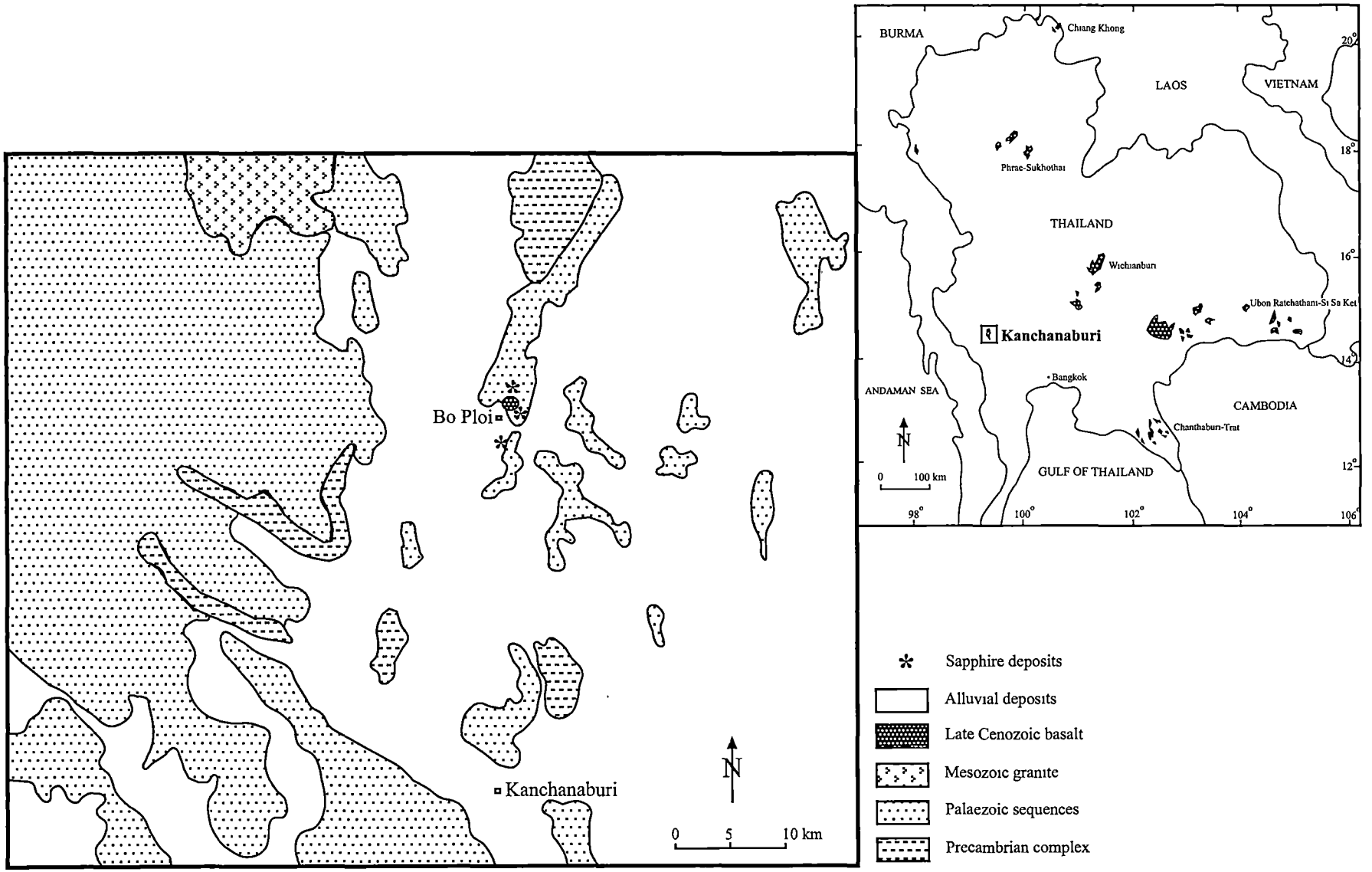

Figure 2.6 Map showing the distribution of the Kanchanaburi gem-related basalt deposit, western Thailand (modified from Vichit, 1992; Guo, 1993)

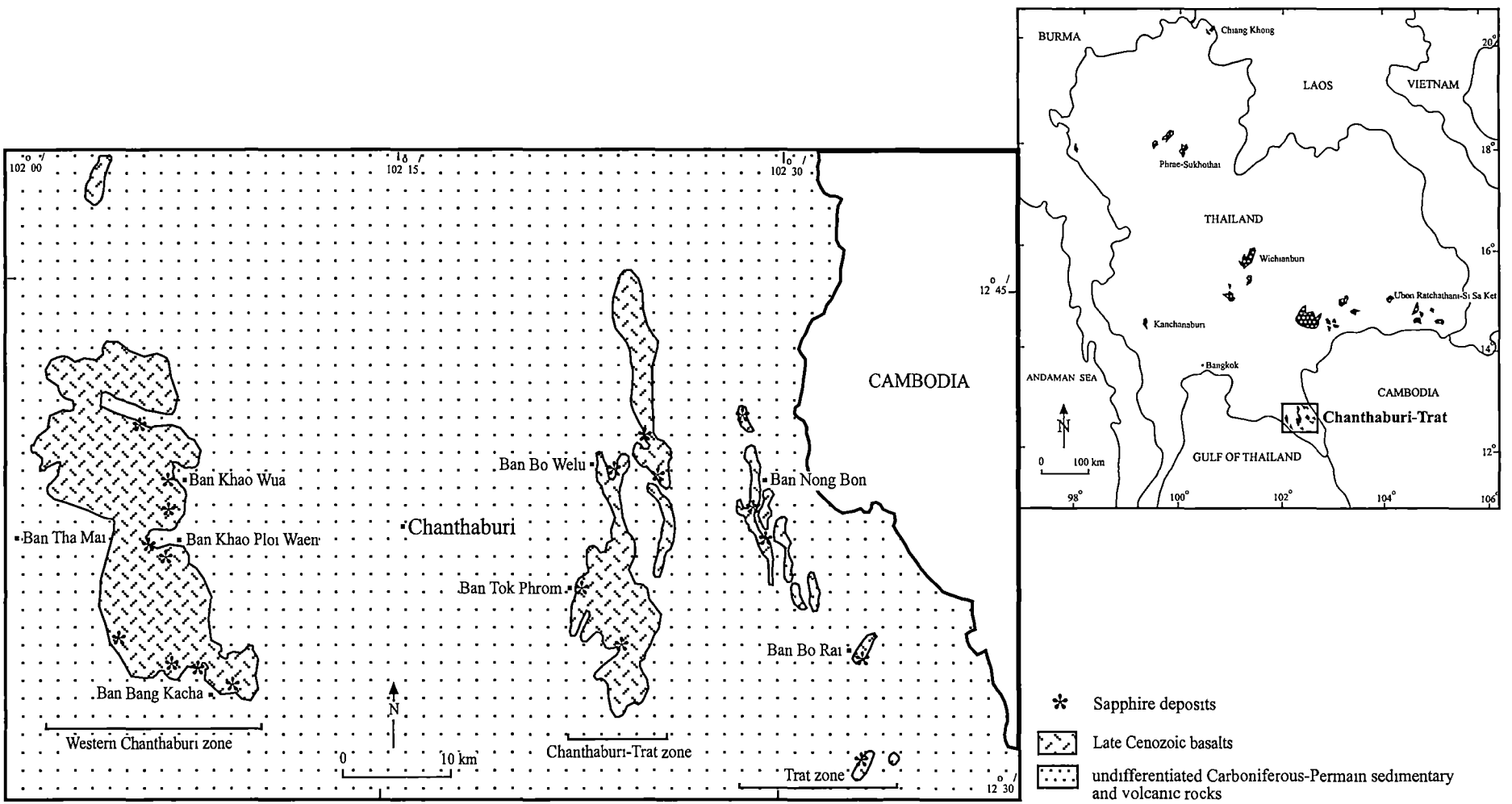

Figure 2.7 Map showing the distribution of the Chanthaburi-Trat gem-related basalt deposit, southeastern Thailand (modified from Vichit, 1992)

Sapphires and rubies are found at Ban Khao Wua, Ban Khao Ploi Waen, Ban Bang Kacha, Ban Bo Welu, Ban Tok Phrom, Ban Nong Bon and Ban Bo Rai (Fig.2.7). They have been recovered from highly weathered basaltic rocks at relatively shallow depths and in the stream gravels nearby.

2.3 Gem-sapphire and host basalt relationships

From a review of gem-related basalt in Thailand, it appears that gem-sapphires occur in close spatial association with late Cenozoic alkali basaltic rocks. Several key observations can be made for some striking similarities. (i) The basement rocks consist of Palaeozoic sedimentary and metamorphic rocks. (ii) In all gem-quality corundum deposits, the predominant igneous lithologies are basanites and alkali basalts. (iii) The most abundant mantle xenoliths are spinel-lherzolite, and crustal xenoliths are extremely rare, and (iv) the associated megacryst assemblages include clinopyroxene and spinel. This indicates that Cenozoic basaltic volcanism in Thailand may be responsible for much of sapphire reserves. The study area is one of the gem-related basalt deposits in Thailand.

2.4 The study area

The studied basalts are known as "the Denchai basalts", and are located in Changwat Phrae, northern Thailand. They cover an area ~25 km southwest of Amphoe Denchai and 40 km west of Amphoe Wang Chin (Fig.2.8), ~700 km north of Bangkok. Sealed roads provide convenient access to these basalts. The Denchai basalts and overlying residual reddish-brown soils form flat plains and small hills, and cover an area of ~70 km^2 lying along a northeast-trending lineament. They unconformably overlie basement rocks consisting of Permian sedimentary sequences and Triassic sandstone, siltstone, shale, limestone and conglomerate (Piyasin, 1975; Charoenprawat *et al.*, 1987; Chuaviroj *et al.*, 1992).

The Denchai basalts mostly consist of subaerial lava flows and show common internal features such as flow structures (Pahoe-hoe), volcanic bombs and scoria (Jungyusuk, 1971). The basalt shows similar internal structures to those typical worldwide subaerial basaltic flows (vesicular at the top and the base and massive with platy and columnar joints in the middle). The platy and columnar joints display variable attitudes, possibly due to paleotopography. The axes of columnar joints and dip angles of platy joints are, however, almost vertical and horizontal respectively.

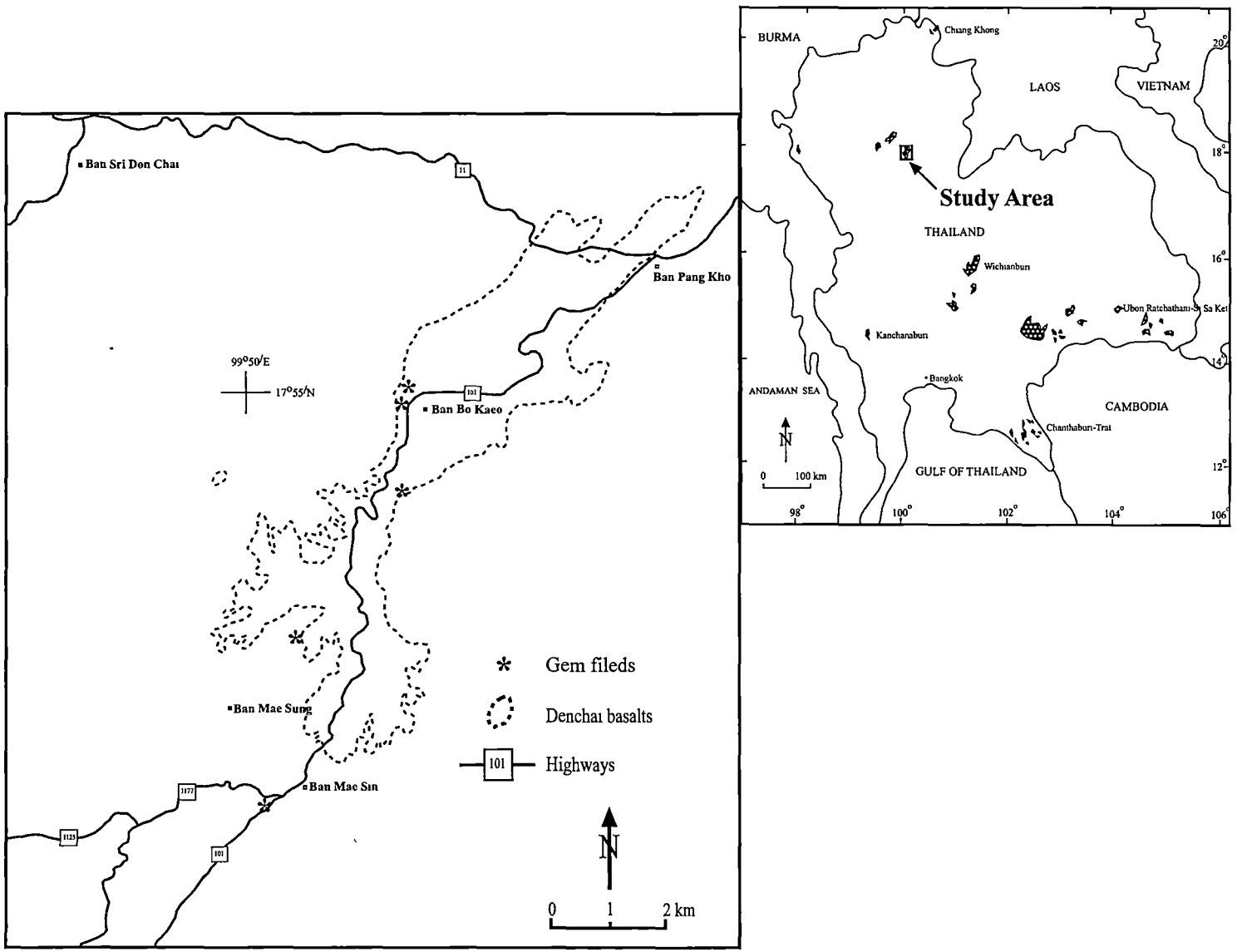

Figure 2.8 The study area map showing the distribution of the Denchai basalts and the Denchai gem fields (modified from Vichit, 1992)

The Denchai basalts are highly weathered to brownish red soil containing basaltic cobbles. Fresh exposures are usually along cliffs and slopes of hills and roadcuts.

Due to the highly weathered and decomposed nature of the Denchai basalts, it proved difficult to identify the total number of basaltic flows present in the area. Barr and MacDonald (1979) reported that the Denchai basalts consist of seven flows with individual thickness varying from 1-5 m, and that the uppermost flow has a K-Ar whole rock age of 5.64 ± 0.28 Ma. The Denchai basalts range in composition from hawaiite to basanite (Barr and MacDonald, 1979). They contain spinel-lherzolite mantle xenoliths and a megacryst assemblage of pyroxene, feldspar, spinel, ilmenite, magnetite, garnet, zircon and corundum (Vichit, 1987, 1992; Coenraads *et al.*, 1995). Gem-quality corundums are mostly found as alluvial materials and an *in situ* sapphire crystal has been observed within the basaltic rocks (Vichit, 1992). Occurrences of these gem-quality corundums are considered to be related to the uppermost flow of the Denchai basalts, which is exposed nearby (Vichit *et al.*, 1978; Barr and Macdonald, 1979; Vichit; 1992).

2.4.1 Regional geology

Geological information has been provided by the geological map of the area (Series L7017, sheet 4944 I, Ban Bo Kaeo 1:50000) by Charoenprawat *et al.* (1987) and Chuaviroj *et al.* (1992). The area consists of 20% plains and terraces, 30% small hills, and 50% highlands. The northwestern and southeastern parts of the area form the highlands, and have elevations ranging from 200 to 600 m above mean sea level. Small hills and plains predominate in the southwestern and northeastern sections. Rock units underlying the study area range in age from Permian to Quaternary (Fig.2.9). Individual rock units are briefly presented below.

Permian rocks

Permian rocks in this study area can be stratigraphically divided into two units. The lowermost unit outcrops at elevations of 200 to 400 m above mean sea level in the northern and middle parts of the area. The lower unit includes massive limestone, shale and calcareous shale and sandstone with corals and crinoid stems. The upper unit conformably overlies this lower unit. The upper unit consists of interbedded sandstone, tuff, quartz-schist, quartzite and shale. This unit is thinly to thickly bedded and is characteristically light to dark grey. The ages of both units are considered middle to upper Permian (Charoenprawat *et al.*, 1987; Chuaviroj *et al.*, 1992).

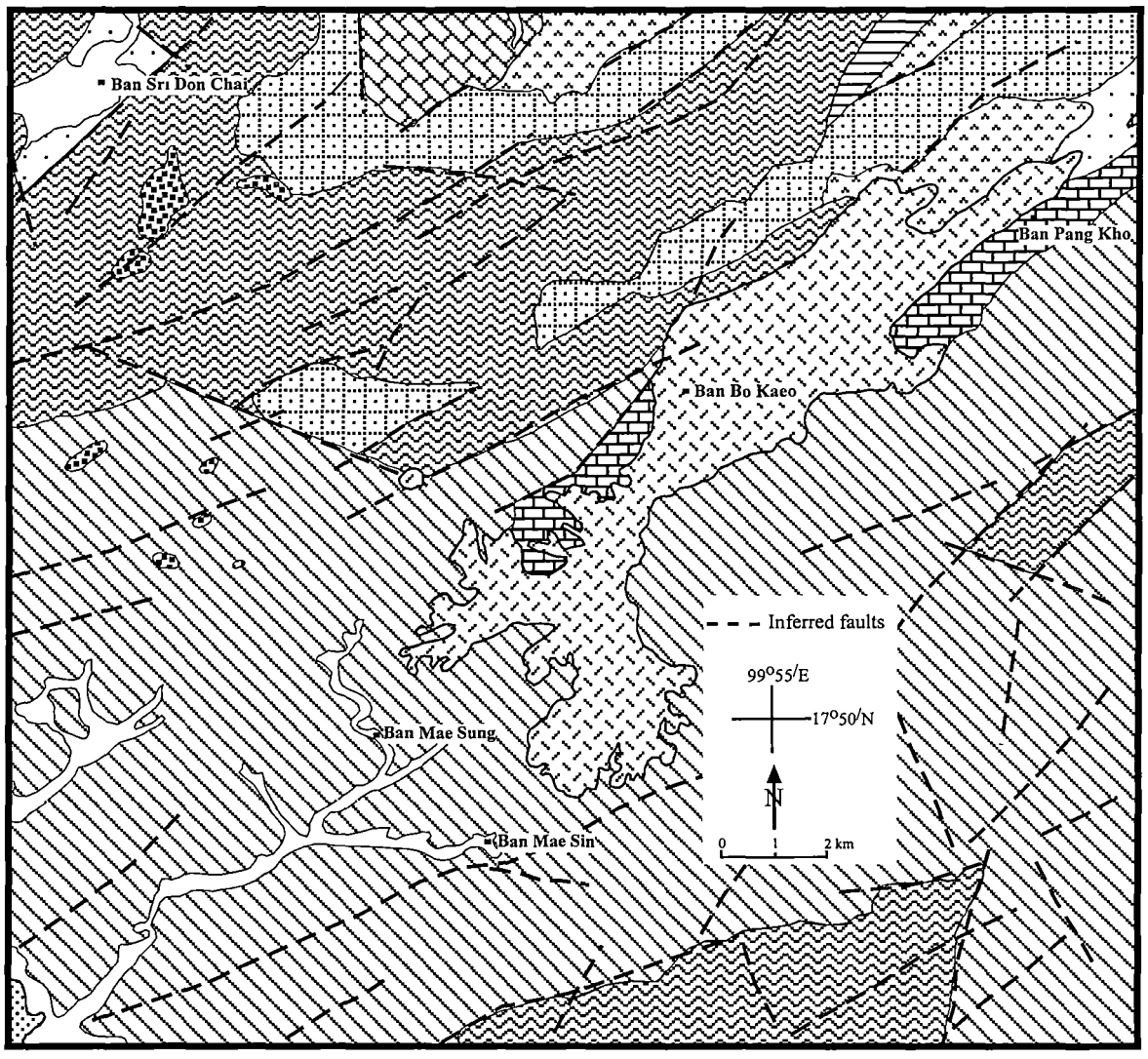

Explanation

- Quaternary alluvial deposits
- Quaternary terrace deposits
- Triassic sandstone and shale
- Triassic interbedded conglomerate, sandstone, siltstone, shale and limestone
- Triassic limestone, siltstone and agglomerate
- Triassic sandstone, siltstone, shale and conglomerate
- Permian interbedded sandstone, shale, tuff, quartz-schist and quartzite
- Permian massive limestone with thinly bedded shale and sandstone

Igneous rocks

- Late Cenozoic basalts
- Post Triassic gabbro and diabase
- Permo-Triassic rhyolite, andesite, dacite, tuff and agglomerate

Figure 2.9 Regional geology map of the study area showing distribution of the Denchai basalts (modified from Charoenprawat *et al.*, 1987; Chauviroj *et al.*, 1992)

Permo-Triassic rocks

Permo-Triassic volcanic rocks comprise the highlands in the northern part. These volcanic rocks consist of rhyolite, andesite, dacite, tuff and agglomerate. They conformably overlie middle to upper Permian formations and these outcrops generally trend northeast-southwest (Charoenprawat *et al.*, 1987; Chuaviroj *et al.*, 1992).

Triassic rocks

Triassic rocks cover about 70% of the study area, and can be divided into four units. Unit 1, the lowermost unit, unconformably overlies the Permo-Triassic volcanic formation. This unit is composed of thin to thickly bedded sandstone, siltstone, shale, limestone and conglomerate.

Unit 2, a light to dark grey, partly recrystallised fossiliferous limestone. Fossils include corals and crinoid stems. The limestone is massive to thinly bedded, and is sometimes interbedded shale, siltstone and conglomerate. This unit is conformably overlain by clastic Unit 3.

Unit 3 can be divided into three sub-units: The lower part consists of interbedded conglomerate, fine-grained sandstone, siltstone, black shale and tuff. The middle part comprises interbedded shale, sandstone, siltstone and grey to dark grey limestone. The clastic unit's upper part consists of thickly bedded, grey to dark grey shale, itself interbedded sandstone, siltstone and mudstone. Clastic units are also fossiliferous and contain Halobia, Daonella and Posidonia. They are conformably overlain by the uppermost Triassic unit.

Unit 4, is uppermost Triassic unit comprises grey to yellowish-brown sandstone and shale, intercalated with thinly bedded chert, sandstone, phyllitic sandstone, conglomerate and phyllite. It is unconformably overlain by Tertiary basaltic rocks and Quaternary sediments (Charoenprawat *et al.*, 1987; Chuaviroj *et al.*, 1992).

Quaternary sediments

The youngest rocks found in the study area can be divided into (i) terrace deposits and (ii) alluvial deposits. The terrace deposits are mainly semiconsolidated sediments of gravel, sand, silt, clay and lateritic soil. The alluvial deposits are composed of sand and gravel formed by recent streams and rivers. Most are unconsolidated and compositionally similar to those of the terrace deposits (Charoenprawat *et al.*, 1987; Chuaviroj *et al.*, 1992).

Intrusive igneous rocks

Intrusive igneous rocks are locally exposed in the western part of the study area. These rocks consist of green to dark green gabbro and diabase, intruded as dykes and sills. These

intrusions are probably post-Triassic in age (Charoenprawat *et al.*, 1987; Chauviroj *et al.*, 1992; Jungyusuk, 1971).

2.4.2 The gem fields

Field studies at the Denchai sapphire deposits have been previously undertaken by the Economic Division, Department of Mineral Resources of Thailand (Tonthongchai *et al.*, 1996). These authors noted that 50% of sapphire ranges in size between 3 to 5 mm across, 40% are less than 2mm across and 10% ranges in size between 5 to 10 mm across. Gem-quality corundums, mostly sapphires, were reported from several localities in this gem field. They were found as alluvial material in palaeo-channel deposits at depths between < 1 to 12 m below surface. The sapphires are blue, light blue and blue-green-yellow in colour. The associated minerals include black spinel (mainly hercynite and less common chromite), with less abundant black pyroxene, garnet (pyrope), feldspar, zircon, quartz (rock crystal) and peridot (olivine). The physical and optical properties of the Denchai sapphires have been documented by Hughes (1997). Inclusions in sapphires in this gem field include feldspar, garnet, rutile, hematite, boehmite and columbite.

The sapphires used in this study are all alluvial sapphires, recovered from alluvial placer and shallow palaeo-channel deposits, but are probably equivalent to corundum megacrysts that occur in host basalts. The studied sapphires were collected from two main areas; Ban Bo Kaeo (BK) and Ban Mae Sin (MS) in the Denchai gem fields (Fig.2.10). The majority (~90%) of sapphires show various shades of blue, ranging from light blue to dark blue and less common blue-green-yellow, and are up to 0.9 cm across. The associated mineral assemblages in the study area have been reported by Vichit (1992) and Tonthongchai *et al.* (1996), and include spinel, ilmenite, pyroxene, garnet, feldspar, zircon, quartz and olivine (peridot). They are described in Chapter 5.

2.5 Summary

Gem-quality corundums are found among heavy-mineral concentrations in many alluvial deposits, which occupy drainage descending from intraplate basaltic terrains, particularly in eastern Australia and Southeast Asia. Corundums are seldom observed within the basaltic rocks but they are considered to be genetically associated with the basaltic rocks nearby. In Thailand, gem-quality corundums are found in weathered residual soils or gravels in close spatial association with intraplate basaltics (basanite and alkali basalt) that contain numerous mantle xenoliths (mostly spinel-lherzolite); crustal xenoliths are rare.

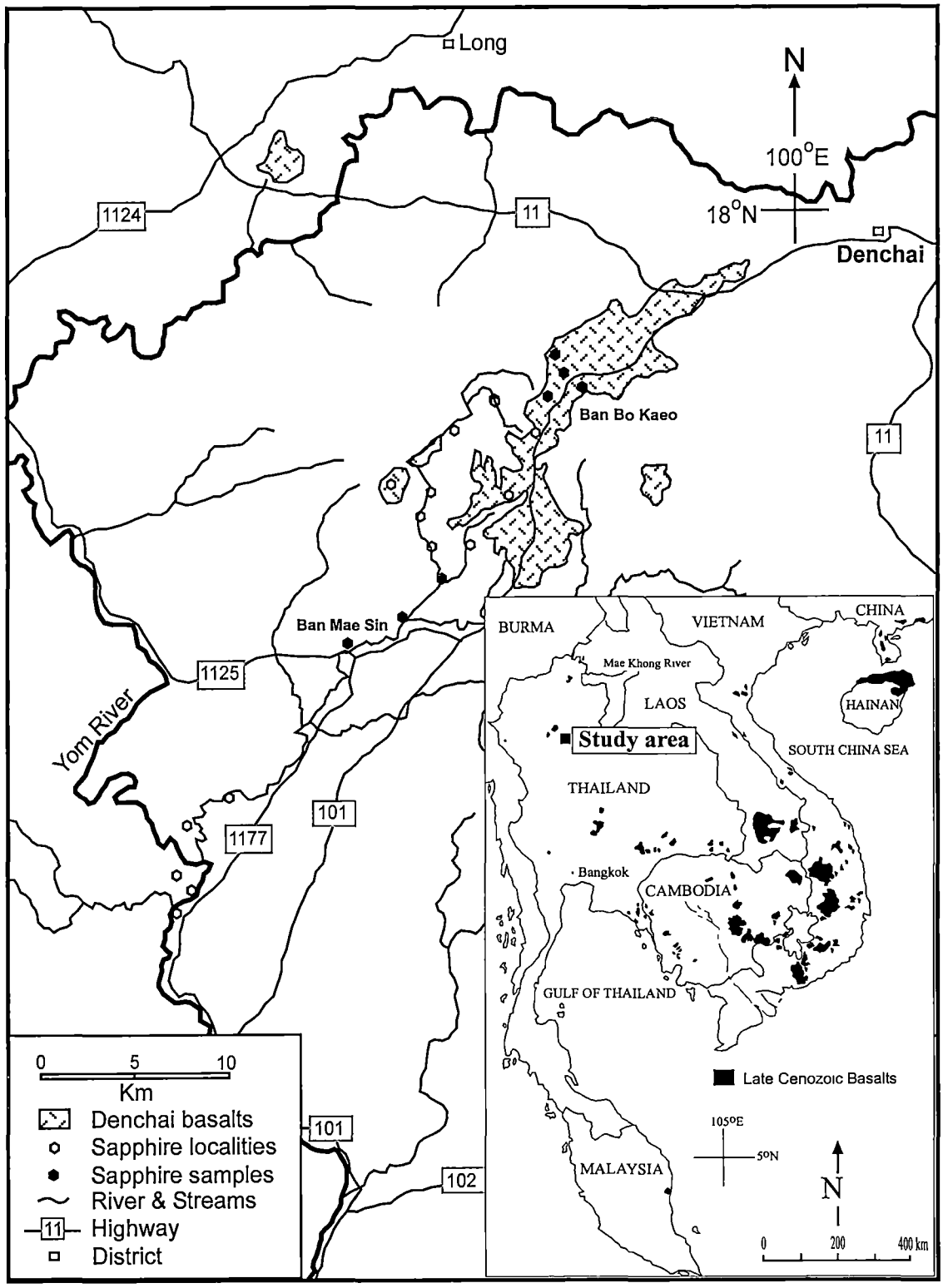

Figure 2.10 Map showing the distribution of the basalt outcrops, drainage pattern and sapphire localities in the Denchai area, northern Thailand

The most common minerals found together with gem-quality corundums are zircon and spinel (mainly hercynite). This supports the view that late Cenozoic basalts in Thailand are the source for much of sapphire reserves. The alluvial gem-quality corundums can be regarded as the equivalent of the corundum megacrysts that are rarely found in the basaltic rocks.

The field area studied here is known as "the Denchai basalts". These Cenozoic basalts are exposed as scattered masses, unconformably overlying Permo-Triassic sedimentary and volcanic rocks. The Denchai basalts contain mantle xenoliths, are highly weathered and decompose to brownish red soil. The gem sapphires, found in alluvial materials at shallow depths, are interpreted to have been derived from the Denchai basalts.

Detailed studies of the Denchai basalts in terms of petrography and mineral chemistry will be presented in Chapter 3.

Chapter 3

Petrography and mineralogy of the Denchai basalts and associated xenoliths

3.1 Introduction

Studies of the Denchai basalts have been previously undertaken by Barr and MacDonald (1979) in terms of their age, petrography and geochemistry. They reported that the basalts comprise seven flows cover a total area of 70 km^2. The uppermost flow has a K-Ar whole-rock age of 5.64 ± 0.28 Ma. The flows are fine- to medium-grained hawaiites to basanites with abundant ultramafic (spinel-lherzolite) xenoliths, phenocrysts and microphenocrysts of olivine (Fo_{82-65}), with minor plagioclase and rare clinopyroxene. However, much of this data was collected over a period of several years and there was little detail on the petrography and mineralogy of the basalts and associated xenolith suites.

This chapter provides a more detailed account of the petrography and mineralogical characteristics of the Denchai basalts and their associated xenolith suites. Sixty-six least-altered basalts were carefully selected for this study: a sample location map is shown in Figure 3.1. Due to the highly weathered and discontinuous nature of the outcrops, recognition of individual flow units was difficult (Fig.3.2). The petrological study was carried out on the least-altered basalt samples without regard to flow sequence. The Denchai basalts vary from medium grey to dark grey and are fine to medium grained. Xenoliths up to 5 cm across were observed in several samples. Vesicles and fractures are present, mainly infilled by carbonate, zeolite and iron oxide/hydroxide minerals. Lithological features and sample locations are briefly presented in Appendix A.

Petrographically, the Denchai basalts range from aphyric to weakly porphyritic with variable amounts of phenocrysts and microphenocrysts. Olivine is present as both phenocrysts and in the groundmass of all samples whereas clinopyroxene and plagioclase also occur as microphenocryst and groundmass phases in many samples. Clinopyroxene and plagioclase are commonly subhedral and weakly zoned. Opaque minerals occur as a groundmass phase and are mainly titanomagnetite. The suite of basalts collected for this study have been subdivided into four groups (A, B, C and D) based on their dominant phenocryst and

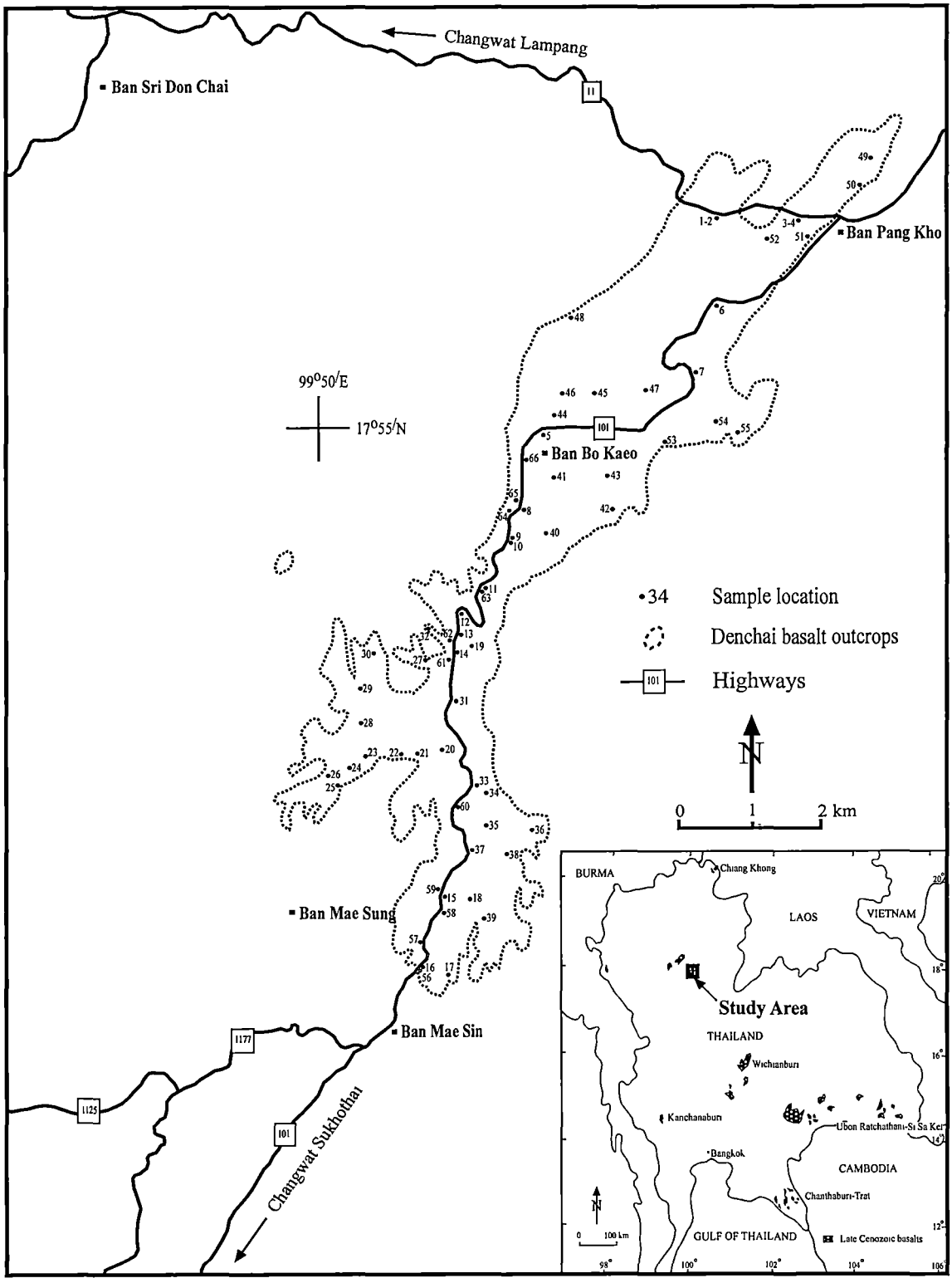

Figure 3.1 The sample location map showing the boundary of the Denchai basalt outcrops

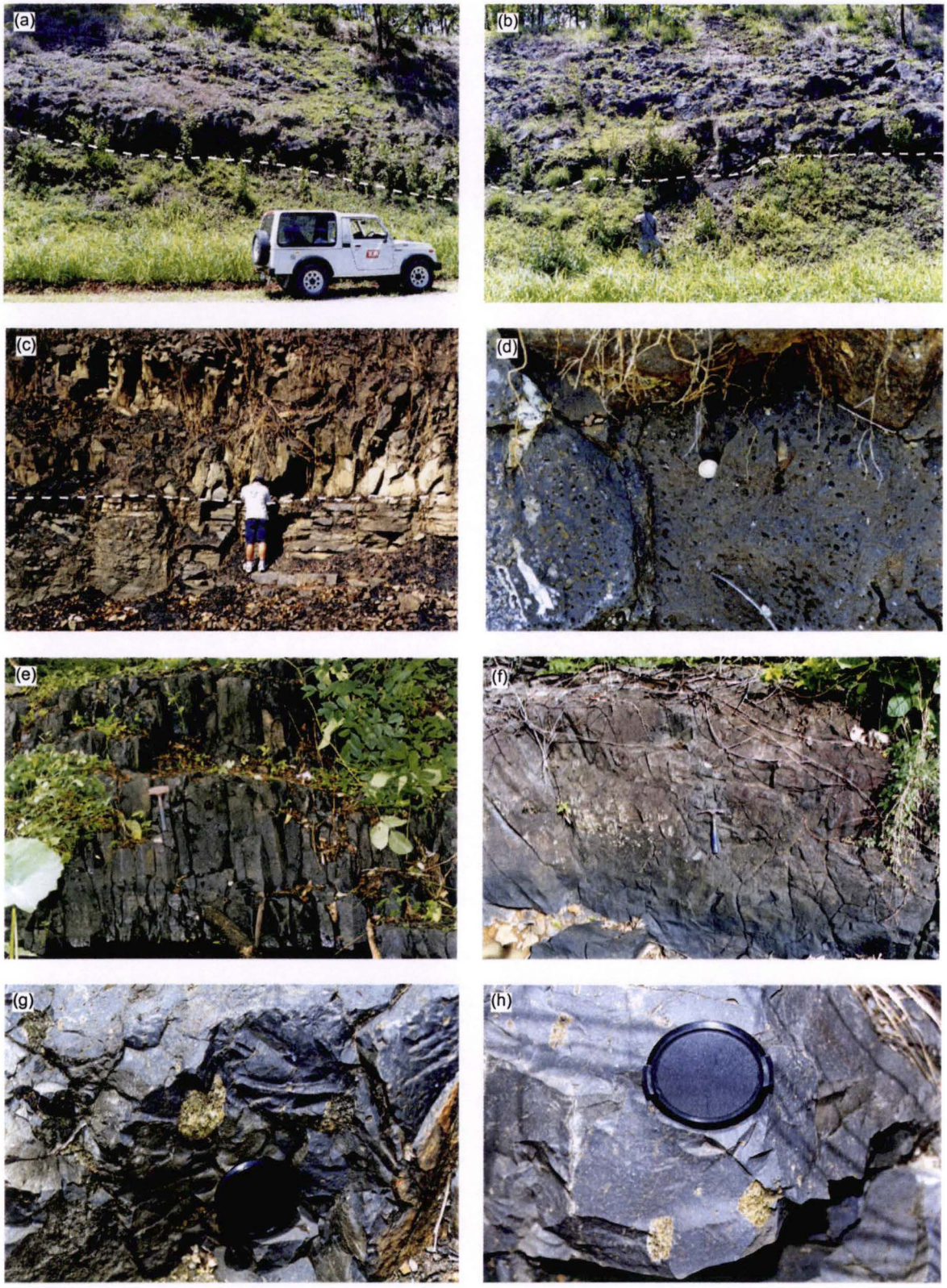

Figure 3.2 Photographs of the Denchai basalt exposures; (a) and (b) road cut outcrop along the Highway No.11 (Km.73); (c) columnar and platy jointings; (d) vesicular and amydaloidal texture; (e) columnar joints at Ban Bo Kaeo; (f) basalt exposure showing massive texture and (g), (h) xenoliths enclosed in the Denchai basalts

microphenocryst assemblages and groundmass texture (Table 3.1). These groups are also used in the discussion of geochemical compositions in the following chapter (Chapter 4). The whole rock geochemistry of each group is distinct and consistent with the subdivision made on the basis of petrography.

3.2 The Denchai basalts

3.2.1 Petrography

The four distinct groups of basalts based on the dominant phenocryst and microphenocryst assemblages and their groundmass texture are:

(1) Ol + Cpx, phyric (Group A),
(2) Ol ± Cpx, aphyric to microphyric (Group B),
(3) Ol + Cpx +Plag, aphyric to microphyric (Group C),
(4) Ol + Plag, aphyric to microphyric (Group D).

Petrographic features of each Denchai basalt group are summarised below, with particular emphasis on phenocryst and microphenocryst assemblages and their relationship to groundmass. A detailed petrographic description of individual samples is presented in Appendix B. Almost all samples show vesicles and fractures that are partly infilled with carbonate, zeolite and iron oxide/hydroxide minerals. Xenoliths and disaggregated nodule materials are described in Section 3.3.

Group A

Group A is represented by three samples, all of which have the phenocryst assemblage olivine + clinopyroxene (Figs.3.3a, b): these occur as isolated crystals and show resorption features. Olivine phenocrysts are subhedral, up to 1.5 mm across. Clinopyroxene phenocrysts are pale green subhedra up to 1.2 mm across. The groundmass is fine-grained holocrystalline to hypocrystalline, consisting of subhedral plagioclase laths with subordinate anhedral olivine, subhedral purplish clinopyroxene, Fe-Ti oxides and brown glass. Xenoliths were only found in Sample DC42, and are of crustal-derived origin.

Group B

Group B is represented by twelve samples, ranging in texture from aphyric to microphyric (Figs.3.3c, d). Olivine is a ubiquitous microphenocryst phase whereas clinopyroxene is a rare

Table 3.1 Summary of petrographic characteristics of the Denchai basalts

Group	Sample Nos.	Texture	Main phenocryst and microphenocryst assemblage	Groundmass	Remarks
A	DC- 25, 28, 42	Phyric	Ol + Cpx	Fine-grained holocrystallinc to hypocrystalline	Xenoliths (Cpx + Plag + Qtz) only in Sample DC42.
B	DC- 5, 13, 14, 19, 23, 27, 32, 43, 55, 56, 61, 62	Aphyric to microphyric	Ol ± Cpx	Fine-grained holocrystalline to hypocrystalline	Xenoliths (Ol + Cpx + Opx + Sp) and disaggregated nodule materials are common. Cpx is a rare microphenocryst phase.
C	DC- 15, 16, 17, 20, 21, 22, 29, 30, 31, 33, 34, 35, 36, 37, 38, 39, 40, 44, 47, 57, 58, 59, 60	Aphyric to microphyric	Ol + Cpx + Plag	Fine to coarse-grained holocrystalline	Xenoliths (Cpx + Plag) and disaggregated nodule materials are rare. Quartz xenocryst is found in Sample DC15.
D	DC- 1, 2, 3, 4, 6, 7, 8, 10, 11, 12, 41, 45, 46, 48, 49, 50, 51, 52, 53, 54, 63, 64, 65, 66	Aphyric to microphyric	Ol + Plag	Fine-grained holocrystalline to hypocrystalline	Xenoliths (Ol + Cpx + Sp) and disaggregated nodule materials only in Sample DC3. Cpx is a rare microphenocryst phase.

Ol = olivine, Cpx = clinopyroxene, Opx = orthopyroxene, Plag = plagioclase, Sp = spinel, Qtz = quartz

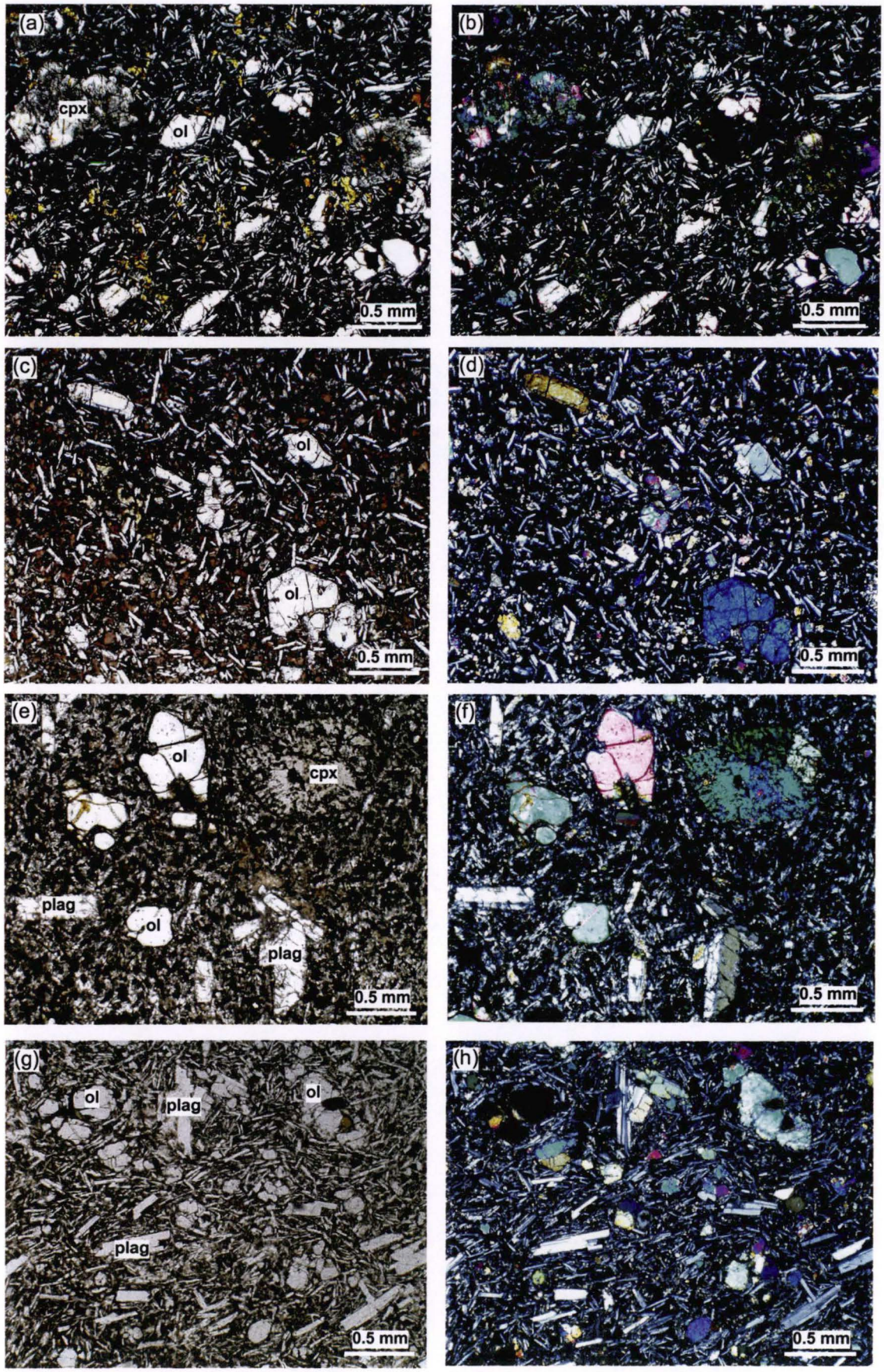

Figure 3.3 Photomicrographs of phenocryst/microphenocryst phases in the Denchai basalts (a) and (b) Group A; (c) and (d) Group B; (e) and (f) Group C and (g) and (h) Group D
Note: (a), (c), (e) and (g) are plane polarised lights; (b), (d), (f) and (h) are crossed polars

microphenocryst phase and appears only in Sample DC61. Subhedral olivine microphenocrysts to 0.8mm across occur as isolated crystals set in a fine-grained holocrystalline to hypocrystalline groundmass. Clinopyroxene is subhedral, purplish and up to 0.4 mm across. The groundmass is mainly composed of plagioclase laths with subordinate anhedral olivine, purplish clinopyroxene, Fe-Ti oxides and devitrified brown glass. Xenoliths and disaggregated nodule materials are common in this group.

Group C

Twenty-three samples of Group C basalt range in texture from aphyric to microphyric (Figs.3.3e, f). They contain the microphenocryst assemblage olivine + clinopyroxene + plagioclase set in holocrystalline groundmass. The microphenocryst assemblage commonly forms as isolated crystals, but rare glomerocrystic textures were observed. Olivine microphenocrysts are anhedral to euhedral, and up to 1 mm across with corroded outlines. Clinopyroxene mostly occurs as subhedral purplish microphenocrysts from 0.3 to 1 mm across. Plagioclase microphenocrysts are subhedral, locally zoned and are up to 0.5 mm across. The groundmass is fine- to coarse-grained holocrystalline with occasional trachytic textures. It mainly comprises subhedral felted plagioclase laths with subhedral olivine, purplish clinopyroxene plates, and Fe-Ti oxides. Xenoliths and disaggregated nodule materials are rare in this group. A quartz xenocryst 3 mm across was found in Sample DC15.

Group D

Group D is represented by twenty-four samples. These show petrographic texture ranging from aphyric to microphyric (Figs.3.3g, h) and have an olivine + plagioclase microphenocryst assemblage. Clinopyroxene also occurs as microphenocrysts but is rare. The microphenocryst phases mostly form as isolated crystals and are set in holocrystalline to hypocrystalline groundmass. Olivine mostly occurs as euhedral to anhedra microphenocrysts up to 1.2 mm across. Plagioclase microphenocrysts are subhedral crystals up to 0.5 mm across. The groundmass is fine-grained, holocrystalline to hypocrystalline, and consists of subhedral plagioclase laths, olivine, purplish clinopyroxene, Fe-Ti oxides and brown glass. Xenoliths and disaggregated nodule materials were found only in Sample DC3.

3.2.2 Mineral chemistry

Mineral analyses were carried out using a CAMECA SX-50 electron microprobe at the Central Science Laboratory (CSL), University of Tasmania. Microprobe analytical conditions are described in Appendix C and the complete set of mineral analyses of the studied basalts are given in Appendix D. In the text below, Mg# = $100Mg/(Mg+Fe^{2+})$.

Mineral names are abbreviated as follows: Ol = olivine, Cpx = clinopyroxene, and Plag = plagioclase.

Olivine

Olivine is the most abundant phenocryst and microphenocryst phase in the Denchai basalts and ranges in composition (Table 3.2) from $Fo_{91.1}$ to $Fo_{69.9}$, with NiO contents varying from 0.01 to 0.55wt% and CaO contents from 0.03 to 0.41wt%.

Olivine phenocrysts of Group A range from $Fo_{86.1}$ down to $Fo_{73.8}$ (Fig.3.4a). Within this range, the NiO content in olivine varies from 0.01 to 0.33wt% with increasing Fo content (Fig.3.5a). The CaO content in olivine shows a small increase as olivine varies from Fo_{86} to Fo_{74} (Fig.3.6a). Olivine microphenocrysts of Group B range from $Fo_{91.1}$ down to $Fo_{76.0}$ (Fig.3.4b). Within this range of decreasing Fo content, the NiO content decreases rapidly from 0.55 to 0.11wt% (Fig.3.5b). The CaO content ranges between 0.03 to 0.41wt% and increases with decreasing Fo content (Fig.3.6b). The twelve high *mg*-number (Mg#) grains analysed in this group are probably xenocrysts of mantle origin (c.f. xenolith olivine compositions, Figs.3.5e, 3.6e). In Group C, olivine microphenocrysts range from $Fo_{88.4}$ to $Fo_{71.1}$ (Fig.3.4c). The NiO content decreases rapidly from 0.40wt% in Fo_{88} down to ~0.20wt% in Fo_{82} and more gradually in less magnesian olivines (Fig.3.5c). The CaO content increases steeply from 0.08wt% in Fo_{88} up to 0.25wt% in Fo_{82} and thereafter more gently with decreasing Fo content (Fig.3.6c). Olivine microphenocrysts of Group D show similar characteristics to those in Group C olivine microphenocrysts, with compositions from $Fo_{85.2}$ down to $Fo_{69.9}$ (Fig.3.4d). Within this range, olivine NiO content decreases from 0.30wt% in Fo_{85} down to ~0.15wt% in Fo_{80} and then decreases more gently from Fo_{80} to Fo_{70} (Fig.3.5d). With decreasing Fo content from Fo_{85} to Fo_{80}, olivine CaO content increases from 0.06wt% to ~0.27wt% and then more increases more gently to 0.29wt% in Fo_{74} (Fig.3.6d).

Comparatively, olivine phenocrysts and microphenocrysts of the four groups show similar characteristics in terms of their Fo, CaO and NiO contents and are consistent with their phenocryst/microphenocryst assemblages (Figs.3.4-3.6). For example, Group B olivine microphenocrysts show decreasing NiO and increasing of CaO with decreasing Fo, isuggesting that crystallisation was solely controlled by olivine. This is consistent with the rare appearance of clinopyroxene microphenocryst in this group. In contrast, Group A olivine CaO contents show only a subdued increase with decreasing Fo, indicating that olivine and clinopyroxene were both early co-crystallising phases. Olivine microphenocrysts of Groups C and D show decreasing NiO and increasing CaO from about Fo_{89} down to ~ Fo_{80} suggesting that olivine was the liquidus phase, and that it was joined by clinopyroxene from Fo_{80} down to less magnesian olivines. Thus the observed differences in olivine CaO

Table 3.2 Representative analyses of olivine phenocrysts/microphenocrysts in the Denchai basalts

Group A

Sample	dc25	dc25	dc25	dc28	dc28	dc28	dc42	dc42	dc42	dc42	dc42	dc42
Grain	1	2	3	1	2	3	1	2	3	4	5	6
SiO_2	38.41	39 12	39.42	38 24	38 85	39.20	37.94	38 02	38 45	38 64	39.12	39 94
FeO	21.59	18 29	17.79	21 23	19 62	17.72	23.67	22 58	22 91	23 76	17 17	13.37
MgO	39 75	42 56	42.90	39 87	41.11	42.76	37.44	38.58	38 83	38 67	43.10	46 28
CaO	0 12	0 24	0.24	0.26	0.20	0.25	0.35	0.29	0.21	0 25	0.23	0 23
NiO	0.15	0 16	0.22	0.14	0 24	0 15	0 16	0.09	nd	0 01	nd	0.33
Total	100 02	100.37	100.57	99.74	100.02	100 08	99 56	99 56	100.40	101 33	99 62	100 15
Fe^{2+}	0.47	0 39	0.38	0 46	0 42	0 38	0 52	0.49	0 50	0.51	0.37	0.28
Mg^{2+}	1 53	1 61	1.61	1 54	1.57	1 62	1.46	1.50	1 50	1.48	1 63	1 72
Fo	76.6	80.6	81 1	77.0	78 9	81.1	73 8	75 3	75 1	74.4	81 7	86.1

Group B

Sample	dc5	dc5	dc5	dc13	dc19	dc19	dc19	dc23	dc23	dc23	dc27	dc27
Grain	1	2	3	1	1	2	3	1	2	3	1	2
SiO_2	40.41	41.02	41 28	41 15	38.96	39 74	40 48	39 02	40.84	40 87	38.34	40.52
FeO	9.76	10.70	8 88	10.22	17 44	14.01	10 27	17 02	9 24	10 58	20.52	10.31
MgO	48.76	48.55	49 97	48.87	42 43	45 38	48 87	43.35	49 64	48.15	40 53	48.41
CaO	0.08	0.11	0.10	0 08	0.30	0 21	0.08	0 20	0.07	0 03	0.21	0.08
NiO	0 34	0.30	0 43	0.36	0 19	0.21	0 37	0.22	0.55	0 40	0.11	0 43
Total	99.35	100.68	100.66	100 68	99.32	99 55	100.07	99 81	100.34	100.03	99 71	99.75
Fe^{2+}	0.20	0.22	0.18	0 21	0.37	0 29	0.21	0 36	0.19	0 22	0.44	0.21
Mg^{2+}	1.79	1 77	1 81	1.77	1 61	1.70	1 79	1 64	1 80	1 76	1 56	1.78
Fo	89 9	89.0	90 9	89.5	81 3	85 2	89 5	81.9	90 5	89.0	77 9	89.3

Group B

Sample	dc55	dc55	dc61	dc61	dc61	dc61	dc62	dc62	dc62	dc62
Grain	1	2	1	2	3	4	1	2	3	4
SiO_2	38.10	40.74	39.30	39 52	41 17	41 19	39 37	39 85	41 05	41.08
FeO	22.04	8.64	18 72	16 76	10 43	10 56	17 46	14 82	9 07	9.90
MgO	39.08	49 85	41.72	43.45	48 83	48.52	42 18	44.42	49 46	48.58
CaO	0 41	0.08	0 31	0.09	0 08	0.07	0.26	0.15	0 11	0 06
NiO	0 13	0 41	0 22	0 31	0.39	0 37	0.15	0.38	0 33	0.37
Total	99.76	99 72	100 27	100.13	100 90	100.71	99 42	99 62	100.02	99 99
Fe^{2+}	0.48	0 18	0.40	0.35	0 21	0 22	0.37	0 31	0.19	0 20
Mg^{2+}	1 51	1 82	1.58	1 63	1.77	1 76	1 60	1.67	1.80	1.77
Fo	76.0	91.1	79 9	82.2	89 3	89.1	81.2	84 2	90.7	89 7

Group C

Sample	dc15	dc15	dc15	dc16	dc16	dc16	dc16	dc16	dc16	dc16	dc16
Grain	1	2	3	1	2	3	4	5	6	7	8
SiO_2	39.03	39.15	40 18	37.80	38 37	39 23	39.70	40.12	40.37	40.47	40.82
FeO	17.00	17.51	14.47	27 00	19.76	19 94	18 27	12.46	13 23	11 18	13.43
MgO	43.33	42.74	45.65	35 21	41 05	40.99	42 82	46 99	46.92	47 62	46 59
CaO	0 25	0.20	0.23	0.33	0.29	0.26	0.24	0 10	0 08	0 11	0 09
NiO	0 19	0.19	0 26	0.08	0.17	0 14	0.22	0 40	0 33	0.38	0 24
Total	99 80	99 79	100 79	100.42	99 64	100 56	101.25	100.07	100.93	99.76	101.17
Fe^{2+}	0.36	0 37	0 30	0 60	0.43	0 43	0.38	0.26	0.27	0 23	0 28
Mg^{2+}	1.64	1 62	1.69	1.39	1 58	1.56	1 60	1.74	1.72	1 75	1 71
Fo	82 0	81.3	84.9	69.9	78.7	78.6	80 7	87.1	86.3	88 4	86.1

nd = not detected

Table 3.2 (Continued)

Group C

Sample	dc17	dc17	dc17	dc30	dc30	dc36	dc36	dc36	dc59	dc59	dc59
Grain	1	2	3	1	2	1	2	3	1	2	3
SiO_2	38.79	39.50	40 23	38 99	39.98	37 83	37 92	38.64	39.07	39.10	39.19
FeO	22.04	16.54	13 54	16.95	11.63	26 03	25 40	23.53	18 02	17.65	18.78
MgO	38.58	43.82	46 16	43.18	47.89	36 01	36 62	38 79	41 86	42.25	41 75
CaO	0 27	0.16	0.17	0 27	0.08	0.30	0.28	0 24	0.25	0 17	0 30
NiO	0 14	0.27	0.27	0 15	0.40	0 17	0.15	0.09	0 13	0.19	0 16
Total	99.82	100 29	100 37	99.54	99.98	100 34	100 37	101 29	99 33	99.36	100 18
Fe^{2+}	0.48	0 35	0.28	0 36	0.24	0.57	0.56	0 51	0 39	0 38	0 40
Mg^{2+}	1 49	1 65	1.71	1.64	1 77	1.41	1.43	1 49	1 60	1 61	1.58
Fo	75 7	82 5	85 9	82 0	88 0	71 1	72 0	74.6	80 5	81 0	79 8

Group D

Sample	dc11	dc11	dc11	dc53	dc53	dc53	dc63	dc63	dc63	dc63
Grain	1	2	3	1	2	3	1	2	3	4
SiO_2	38 92	39 22	39.39	38 76	39 13	39.42	37 68	38 34	39 51	40 22
FeO	16.47	16 61	16 06	20.28	18 76	15.59	27.16	23 40	17 67	14.07
MgO	43 18	43.94	43 82	40 55	42.35	43 97	35.47	38.07	42 72	45 53
CaO	0.29	0 23	0.25	0.27	0 20	0.21	0 16	0.13	0.16	0.06
NiO	0.15	0.27	0 24	0 21	0.16	0.30	0 10	0.08	0.16	0.30
Total	99.01	100 27	99 76	100.07	100 60	99 49	100.57	100 02	100 22	100.18
Fe^{2+}	0.35	0.35	0 34	0.44	0.40	0 33	0.60	0.51	0 37	0 29
Mg^{2+}	1 64	1.65	1 65	1.55	1.60	1 66	1.39	1 48	1.61	1 69
Fo	82 4	82.5	82.9	78.1	80 1	83.4	69 9	74 4	81.2	85 2

Group D

Sample	dc66	dc66	dc66	dc66	dc66	dc66	dc66
Grain	1	2	3	4	5	6	7
SiO_2	38.21	38 46	38.98	39.04	39 12	39.14	39.14
FeO	23.35	20 36	18 27	19.12	19.22	17 56	16.80
MgO	37.36	40.48	41 57	41 40	41.51	43 22	42 87
CaO	0.29	0 27	0.22	0.28	0.20	0 22	0.19
NiO	0 14	0 13	0 19	0 15	0.24	0.26	0 25
Total	99.35	99 70	99.23	99.99	100 29	100.40	99.25
Fe^{2+}	0 51	0 44	0.39	0 41	0.41	0.37	0.36
Mg^{2+}	1 46	1 56	1 59	1.58	1 58	1 63	1.63
Fo	74.0	78 0	80 2	79 4	79.4	81.4	82 0

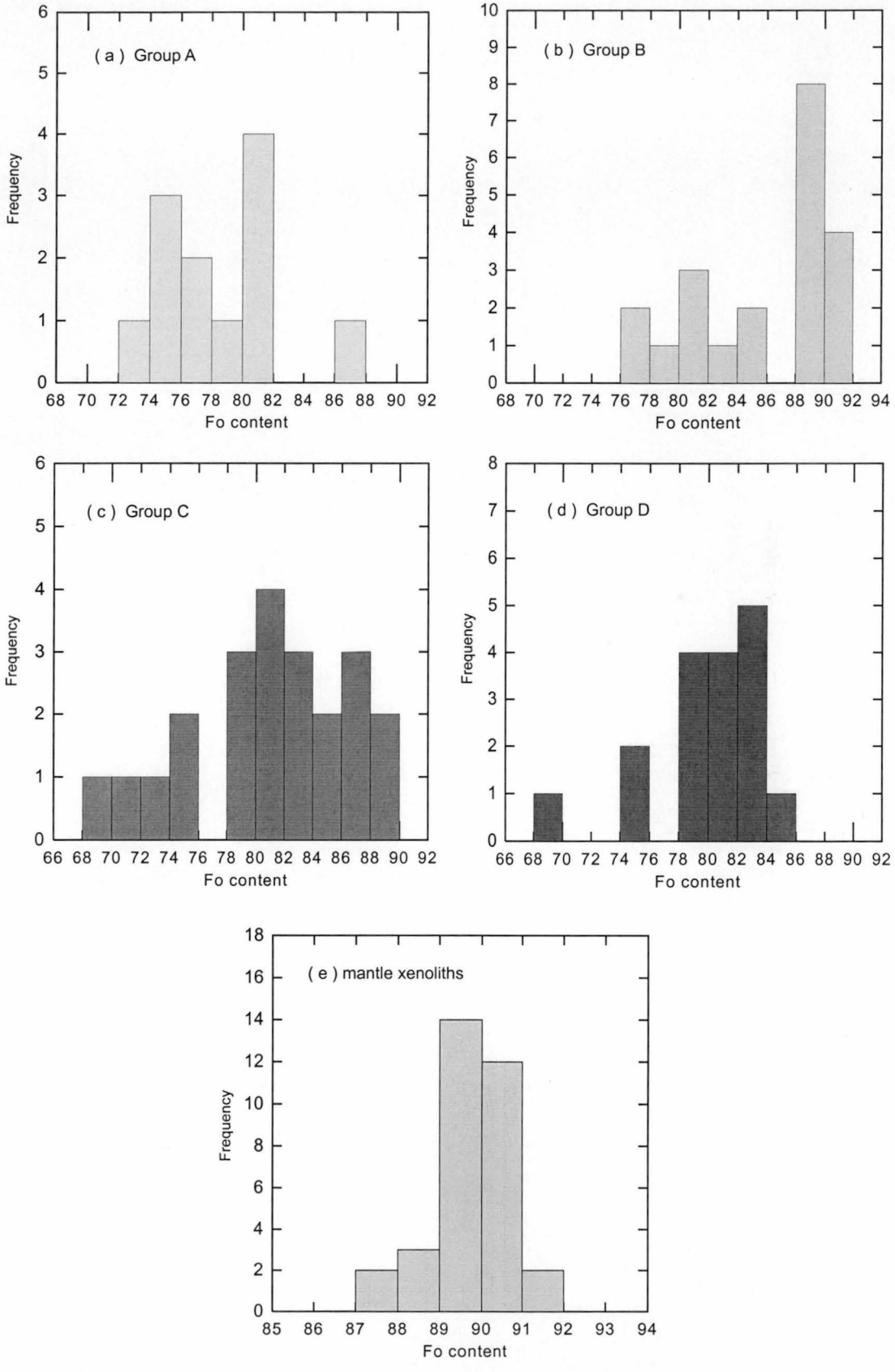

Figure 3.4 Histograms of olivine Fo content; (a), (b), (c) and (d) olivine phenocrysts and microphenocrysts of the Denchai basalts, (e) olivine in mantle xenoliths in the Denchai basalts

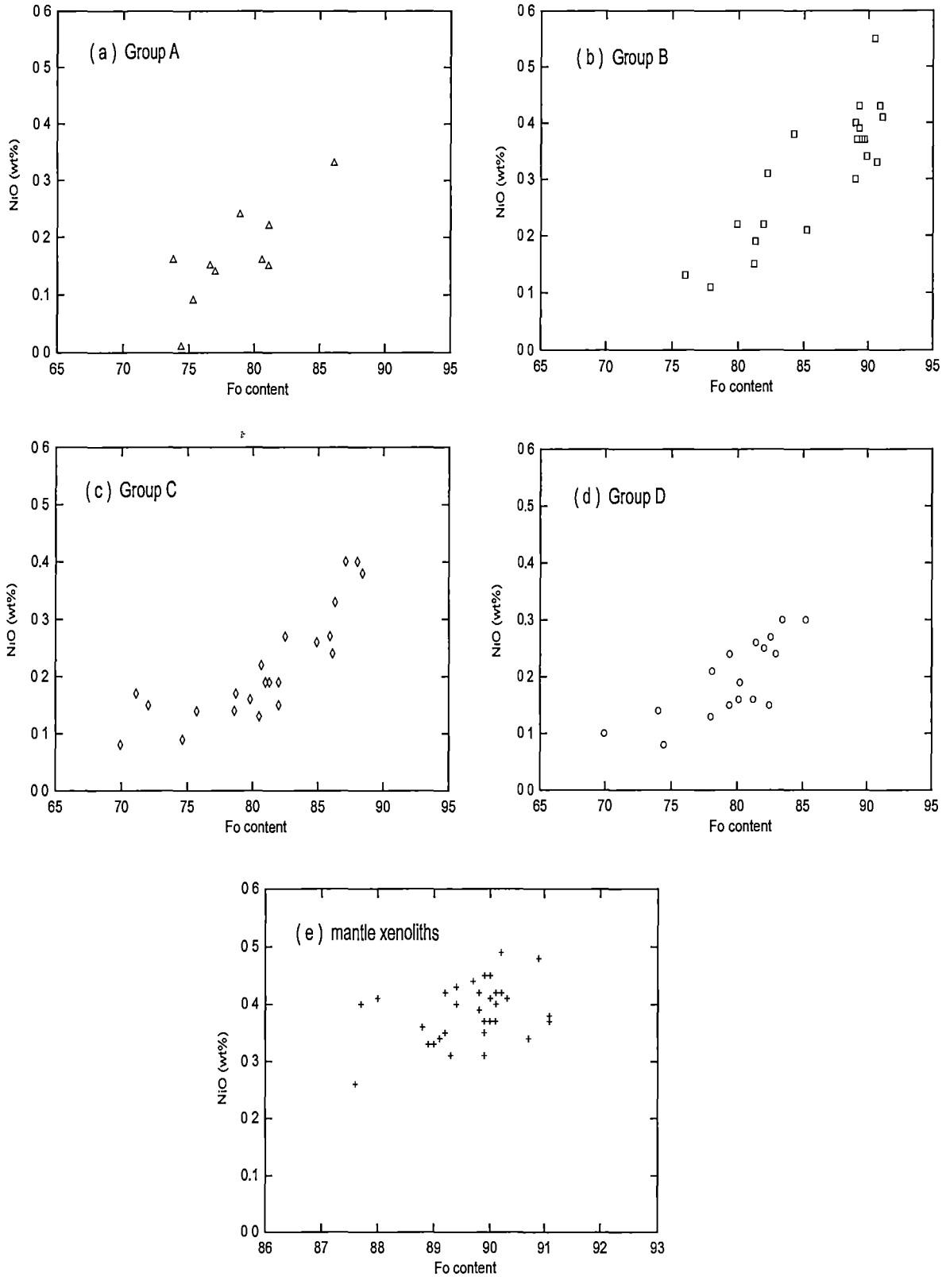

Figure 3.5 Concentration of NiO content (wt%) versus Fo content; (a), (b), (c) and (d) olivine phenocrysts and microphenocrysts of the Denchai basalts, (e) olivine in mantle xenoliths in the Denchai basalts

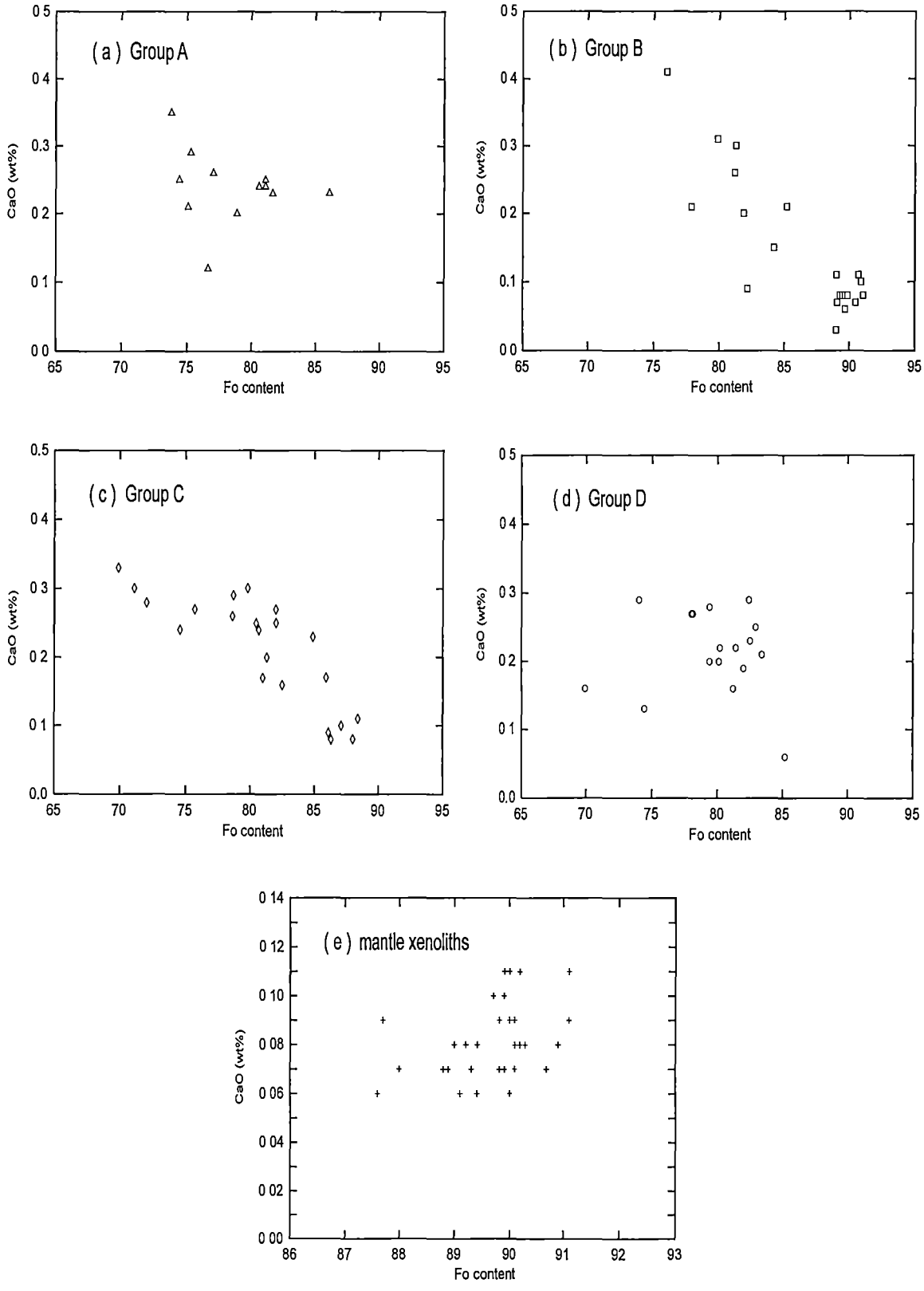

Figure 3.6 Concentration of CaO content (wt%) versus Fo content; (a), (b), (c) and (d) olivine phenocrysts and microphenocrysts of the Denchai basalts, (e) olivine in mantle xenoliths in the Denchai basalts

and NiO contents can be explained by variable crystal fractionation trends consistent with the observed phenocryst assemblages.

Clinopyroxene

Clinopyroxene occurs as both phenocryst and microphenocryst phases in the Denchai basalts. They are more abundant in Groups A and C compared to Groups B and D. Representative compositions of Denchai clinopyroxene phenocrysts and microphenocrysts (Table 3.3) show them to be mostly diopsidic ($Wo_{49\ 5\text{-}43.9}En_{45\ 9\text{-}37.9}Fs_{15\ 1\text{-}9.4}$; Figs.3.7a-d) with CaO contents range from 20.2-23.4wt%, with $Mg\#_{Cpx}$ values ranging from 71.8 to 83.0 (Figs.3.8a-d).

Clinopyroxene phenocrysts of Group A are mainly diopsidic compositions with some grains falling into augite field (Fig.3.7a). They have a maximum $Mg\#_{Cpx}$ of 82.9 (Fig.3.8a) and CaO contents varying between 20.2 to 23.2wt% whereas clinopyroxene microphenocrysts of Group B rarely occur and plot into diopside field (Fig.3.7b) with a maximum $Mg\#_{Cpx}$ of 75.6. In Group C, clinopyroxene microphenocrysts are mostly diopsidic compositions with few crystals have lower Ca contents and are plotted into augite field (Fig.3.7c). Their $Mg\#_{Cpx}$ values vary between 71.8 to 83.0 (Fig.3.8c). Clinopyroxene microphenocrysts of Group D are all diopsidic in composition (Fig.3.7d) with a maximum $Mg\#_{Cpx}$ values of 81.6 (Fig.3.8d).

Comparatively, clinopyroxene phenocrysts/microphenocrysts in the four Groups of Denchai basalts show no significant inter-group compositional variations. Most have diopsidic compositions with few grains extending into the augite field. $Mg\#_{Cpx}$ values range up to 83.0. Variations in clinopyroxene Al_2O_3 content versus $Mg\#_{Cpx}$ values show no effect of the commencement of plagioclase crystallisation. Occasional clinopyroxene analyses with high Al_2O_3 values (> 7wt%) represent disequilibrium quenched margins on phenocrysts, and crystallisation in the absence of plagioclase, rather than high-pressure crystallisation.

Plagioclase

Plagioclase occurs as microphenocrysts in Groups C and D basalts. They are commonly unzoned and the most calcic plagioclase microphenocrysts have compositions up to $An_{71\ 6}$. (Table 3.4). Plagioclase microphenocrysts in Group C basalts range from $An_{70.0}$ to $An_{42.6}$, whereas plagioclase microphenocrysts in Group D have An-content of $An_{71\ 6\text{-}50.9}$. The high values of Al_2O_3 in some clinopyroxene grains and the absence of plagioclase microphenocryst in Groups A and B indicates that plagioclase appears late in the crystallisation sequence.

Table 3.3 Representative analyses of clinopyroxene phenocrysts/microphenocrysts in the Denchai basalts

Group A

Sample	dc25	dc25	dc25	dc28	dc28	dc28	dc42	dc42	dc42	dc42	dc42	dc42
Grain	1	2	3	1	2	3	1	2	3	4	5	6
SiO_2	46.88	48 29	48.33	47 36	47.98	49 35	49.08	49.61	50 19	50.30	50.38	52 65
TiO_2	1.96	1.43	1 95	1.47	1 10	1 05	1.69	1 58	1.32	1.30	1.51	0.55
Al_2O_3	8 87	7 20	4 61	8.02	7 22	5 92	4.44	5 16	4.00	3.98	3 80	2.75
Cr_2O_3	0 60	0 24	0 52	0.49	0 83	0 49	0 22	0 54	0.39	0 38	0.26	0 56
FeO*	6 52	6 56	6 69	6.32	6 10	6 06	6.46	6 05	5 89	6 11	7 01	5.71
MnO	0.15	0 09	0.15	0 18	0 20	0.15	0 15	0.09	0 13	0 18	0 09	0.15
MgO	13 72	14.24	13 73	14.28	14.98	15 23	14.73	14.46	14 89	14.77	14 89	15 53
CaO	21 25	21 10	23 21	20.92	20 22	20 58	22.33	22 66	22.65	22.75	22 00	22 42
Na_2O	0.65	0 70	0.43	0.68	0 69	0.70	0 34	0 43	0.41	0 36	0.36	0 45
Total	101.01	100.22	100.05	100.14	99.74	99 87	99 77	100 83	100 14	100.37	100.51	100.89
Mg#	78 9	79.4	78 5	80 1	81 3	81 8	80.2	80.9	81 8	81 1	79 1	82.9
Ca#	46 6	45 8	48.7	45.6	44 0	44.2	46 5	47 6	47.1	47 2	45.6	46.1
Wo	46.6	45.8	48.7	45.6	44 0	44.2	46.5	47.6	47 1	47 2	45 6	46.1
En	41.9	43.0	40.1	43 3	45.3	45.4	42.7	42.3	43.1	42 6	42 9	44.4
Fs	11 5	11 3	11.2	11 1	10.7	10.4	10 8	10.1	9.8	10 2	11.5	9 4

Group A

Sample	dc42	dc42	dc42	dc42
Grain	7	8	9	10
SiO_2	52 69	52 95	53 05	53.24
TiO_2	0.60	0.56	0 28	0.49
Al_2O_3	2.42	2 58	1 60	2.17
Cr_2O_3	0.16	0 27	0 16	0 32
FeO*	7 45	6 69	6.64	6 13
MnO	0.20	0 19	0 18	0.13
MgO	15.49	15.85	15 92	15 57
CaO	21.48	21.61	22 05	22.40
Na_2O	0.38	0 40	0.34	0.39
Total	101.01	101.21	100.38	100.91
Mg#	78 7	80.9	81.0	81.9
Ca#	43 9	44.1	44.5	45 8
Wo	43.9	44 1	44 5	45 8
En	44.0	45 0	44 7	44.3
Fs	12.2	10.9	10.8	10.0

Group B

Sample	dc61
Grain	1
SiO_2	46.63
TiO_2	2 96
Al_2O_3	6 67
Cr_2O_3	0 00
FeO*	7.40
MnO	0 13
MgO	12 80
CaO	23 18
Na_2O	0.46
Total	100 23
Mg#	75 6
Ca#	49 5
Wo	49 5
En	38 0
Fs	12.5

Group C

Sample	dc15	dc15	dc15
Grain	1	2	3
SiO_2	47.82	48.00	50 44
TiO_2	1 82	1.65	1.16
Al_2O_3	6 80	7.07	3.84
Cr_2O_3	0 67	0 64	0.26
FeO*	5.92	5 89	6 39
MnO	0 14	0 15	0 18
MgO	13 88	14 22	15 67
CaO	22 41	21.58	21.41
Na_2O	0 51	0.60	0.41
Total	99.97	99 80	99 76
Mg#	80.7	81 2	81 4
Ca#	48.3	46 8	44 3
Wo	48 3	46 8	44 3
En	41 6	43 0	45.1
Fs	10 1	10.2	10 6

Total Fe as FeO*

Table 3.3 (Continued)

Group C

Sample	dc29	dc29	dc29	dc29	dc29	dc29	dc36	dc36	dc36	dc36	dc36	dc36
Grain	1	2	3	4	5	6	1	2	3	4	5	6
SiO_2	48.69	49 68	50.17	50 88	51 24	52.81	49.22	49.83	49 89	49.92	50.05	51 05
TiO_2	2 60	1.95	1 90	1 30	1 36	0.74	1 60	1.42	1 90	1 65	1 38	1 06
Al_2O_3	4 33	3.61	4 06	3.00	3.13	1.38	5.73	5 72	3 63	4 77	4 68	4 55
Cr_2O_3	0 09	0.09	0 29	0.23	0 51	0.09	0 47	0 48	0 27	0 39	0 58	0 21
FeO*	9 08	7.41	7 39	7 04	7 28	7.84	6.03	6 37	7 21	5 78	6 11	6 03
MnO	0 14	0.15	0 19	0.16	0 19	0.19	0 09	0.09	0 16	0.14	0 06	0 19
MgO	12.98	13 62	13.90	14.69	14 61	14.48	14 58	14.61	14 27	14.67	15 06	15.79
CaO	22 44	22 54	22.66	22 57	22.92	23.35	22.19	21.53	22.58	22 75	22.34	21 03
Na_2O	0 49	0.42	0 41	0 33	0 38	0.26	0.50	0.60	0 43	0 39	0.43	0.56
Total	100.84	99.47	100.97	100.20	101 62	101 14	100.41	100 65	100.34	100 46	100 69	100.47
Mg#	71.8	76.6	77 0	78 8	78 1	76.8	81 1	80.4	77.9	81 9	81 4	82 3
Ca#	47.0	47.5	47.3	46 4	46.7	46.9	47 0	45 9	46.8	47 6	46.4	43 9
Wo	47.0	47.5	47.3	46 4	46 7	46.9	47 0	45.9	46.8	47 6	46.4	43 9
En	37.9	40.0	40 3	42 0	41.4	40.5	42 9	43.4	41.2	42 7	43.5	45 9
Fs	15.1	12.5	12 4	11.5	11 9	12.6	10 1	10.7	12 0	9 6	10 0	10 2

Group C

Sample	dc59	dc59	dc59	dc59	dc59
Grain	1	2	3	4	6
SiO_2	48.88	50.12	50 36	50.47	51 57
TiO_2	1.61	1 17	1 08	1.06	0.92
Al_2O_3	5.72	5 06	4.55	4 89	3.39
Cr_2O_3	0 63	0 33	0 35	0.45	0 58
FeO*	6.03	6 01	5 71	5.51	5 70
MnO	0.07	0.12	0.11	0 12	0 15
MgO	14.27	15.04	15.49	15 17	15 61
CaO	22.10	21.45	21 40	21 36	21.26
Na_2O	0 47	0 59	0.47	0.56	0 70
Total	99 78	99.89	99 52	99 59	99.88
Mg#	80.9	81 7	82 8	83.0	82 9
Ca#	47.3	45.5	45.1	45 6	44 7
Wo	47.3	45.5	45.1	45.6	44 7
En	42 5	44 4	45 4	45.0	45 7
Fs	10 2	10 1	9 6	9.4	9.6

Group D

Sample	dc7	dc7	dc66
Grain	1	2	1
SiO_2	48 06	50 16	48 28
TiO_2	1.73	1.16	1 93
Al_2O_3	6.36	3 86	5.96
Cr_2O_3	0 86	0 45	0.50
FeO*	5 91	6.04	6 93
MnO	0.11	0 10	0.12
MgO	13.70	15.05	13 57
CaO	23 31	22 99	22 25
Na_2O	0.44	0.34	0 42
Total	100.48	100 15	99.96
Mg#	80.6	81 6	77 7
Ca#	49.5	47.2	47 7
Wo	49 5	47 2	47.7
En	40 5	43 0	40.5
Fs	10 0	9 8	11 8

Total Fe as FeO*

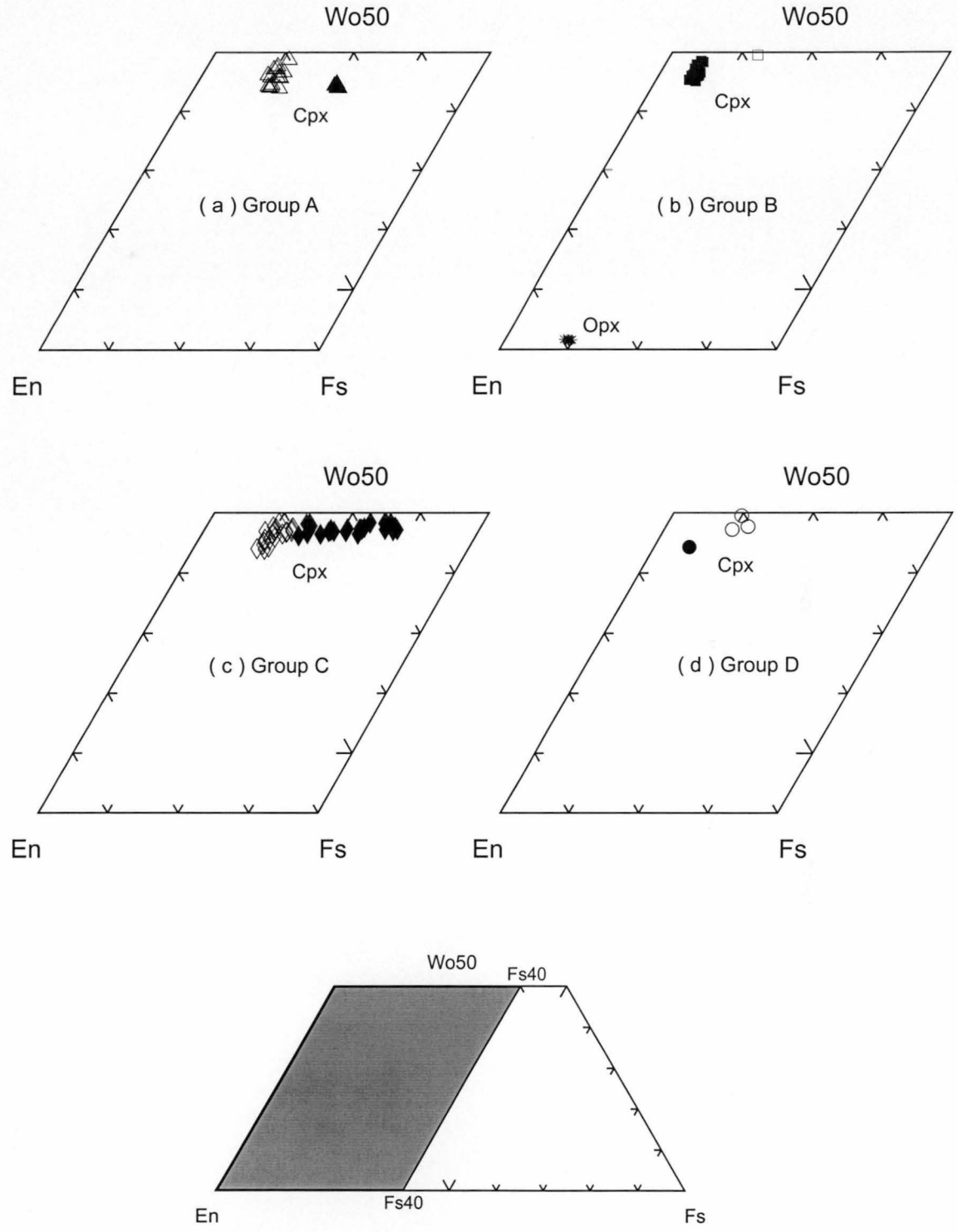

Figure 3.7 Composition of clinopyroxene (cpx) and orthopyroxene (opx) of the Denchai basalts and their associated xenoliths plotted on a pyroxene quadrilateral Wo-En-Fs after Moromito (1989);
(a) Group A, cpx phenocrysts/microphenocrysts (open triangle); cpx in crustal xenoliths (closed triangle),
(b) Group B, cpx microphenocrysts (open square), cpx in mantle xenoliths (closed square) and opx in mantle xenoliths (asterisk),
(c) Group C, cpx microphenocrysts (open diamond) and cpx in crustal xenoliths (closed diamond),
(d) Group D, cpx microphenocrysts (open circle) and cpx in mantle xenoliths (closed circle)

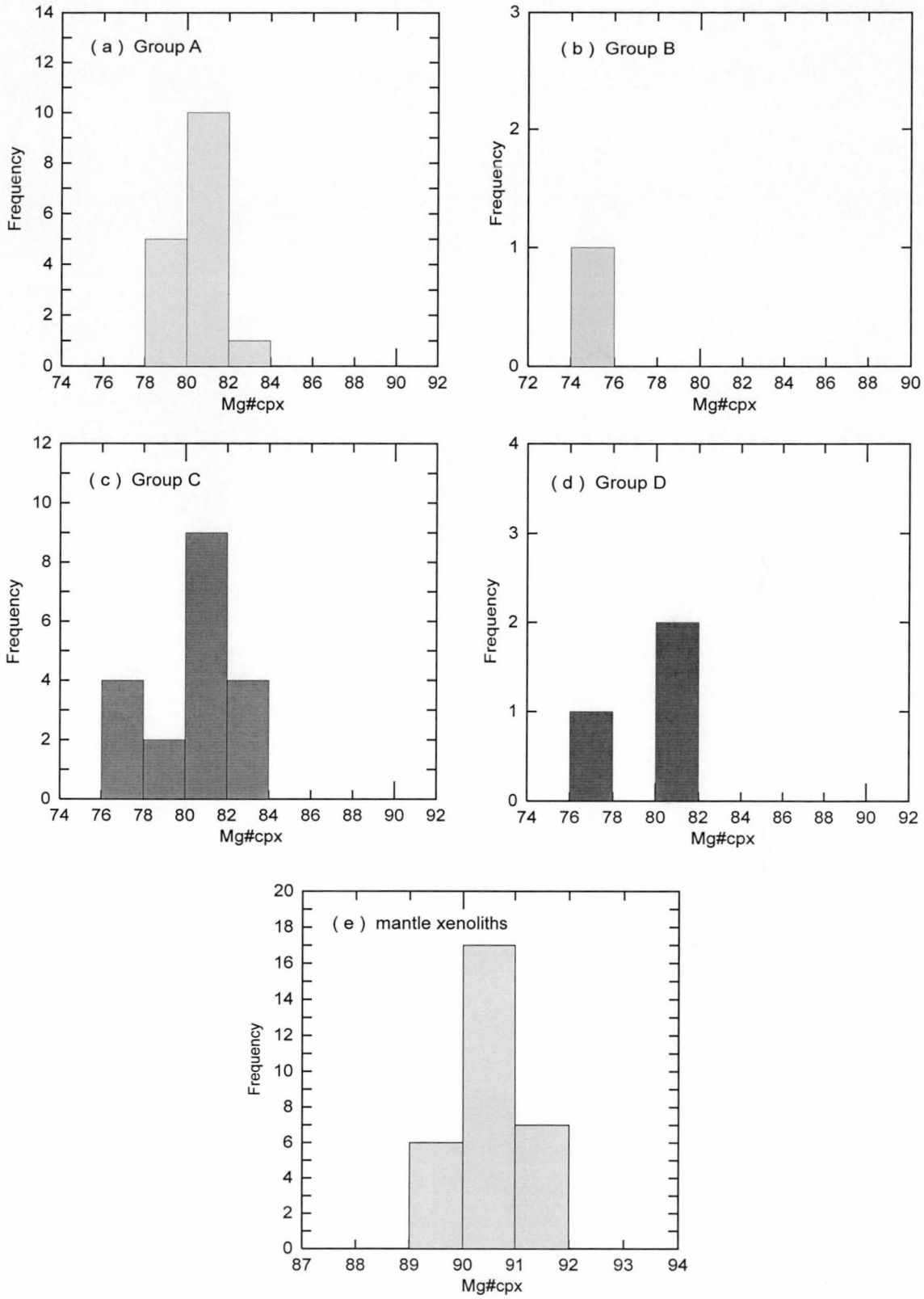

Figure 3.8 Histograms of $Mg\#_{Cpx}$ of clinopyroxene; (a), (b), (c) and (d) clinopyroxene phenocrysts and microphenocrysts of the Denchai basalts and (e) clinopyroxene in mantle xenoliths in the Denchai basalts

Table 3.4 Representative analyses of plagioclase microphenocrysts in the Denchai basalts

Group C

Sample	dc15	dc15	dc15	dc15	dc15	dc15	dc16	dc16	dc16	dc16	dc16	dc16
Grain	1	2	3	4	5	6	1	2	3	4	5	6
SiO_2	50 67	50.72	50.82	51.00	51 05	52.53	50 79	50 88	51 21	52 34	54.94	55 82
Al_2O_3	31.35	31 04	31 03	31 27	30 58	29 87	31.56	31 57	31 55	30 63	28 01	27.09
Fe_2O_3	0 42	0.43	0 48	0 43	0.55	0 45	0.44	0 55	0.45	0.47	0 72	0.64
CaO	14 02	13.91	13.82	13 66	13.56	12 35	14 65	14.52	14.23	13.33	10 71	8 84
Na_2O	3 54	3.43	3 51	3.71	3 53	4 12	3 29	3 23	3.38	3.90	5.22	5 98
K_2O	0.34	0 36	0.38	0 37	0 40	0.44	0.27	0 32	0.29	0 35	0.71	0 88
Total	100 34	99 89	100.07	100.44	99 67	99 76	101.00	101.07	101 11	101.02	100 31	99.25
An	67.0	67.7	66 8	65.4	66 4	60 7	70.0	69 9	68 7	64 1	51.0	42.6

Group C

Sample	dc17	dc17	dc29	dc29	dc29	dc29	dc29	dc30	dc30	dc30	dc36	dc36
Grain	1	2	1	2	3	4	5	1	2	3	1	2
SiO_2	51 10	51 57	52 65	52.65	52 47	53.05	55 1	50.02	50 69	51.05	52 64	53.40
Al_2O_3	31 64	30.88	29.94	30.23	30 31	29.42	28 59	31.78	31 10	31.16	30 29	30.15
Fe_2O_3	0 45	0.46	0 59	0.54	0 61	0.53	0 52	0.47	0 38	0 36	0.49	0.60
CaO	14 33	13 65	12.57	12.78	12.88	12 11	10.76	14.18	13.58	13 59	12.56	12.28
Na_2O	3.30	3 72	3.77	4.11	4 00	4 46	5 12	3.49	3.77	3 77	4 21	4.29
K_2O	0 35	0 36	0 63	0.44	0 44	0.52	0 65	0.27	0.37	0.37	0 38	0.47
Total	101 17	100 64	100.54	100.99	100.91	100.31	101.08	100 21	99 89	100.30	100.57	101 19
An	69.2	65 6	62.3	61.6	62.4	58 2	51.7	67 9	65 0	65 0	60 9	59.5

Group D

Sample	dc59	dc59	dc7	dc7	dc7	dc11	dc11	dc53	dc53	dc53	dc63
Grain	1	2	1	2	3	1	2	1	2	3	1
SiO_2	50.98	52.38	50 31	50.50	50 60	49 95	50.12	49 55	49.89	50 23	55 84
Al_2O_3	31.08	30.28	31.45	31.61	31.83	32 08	31.78	31 93	32.03	31.54	28 73
Fe_2O_3	0 43	0.39	0 56	0.46	0 39	0 55	0.51	0.47	0 36	0.46	0 08
CaO	13.84	12 83	14.37	14.38	14.43	15 04	14.63	14 91	14.78	14.43	10 54
Na_2O	3 51	4 02	3 43	3.46	3 41	3.08	3 28	3 21	3.22	3 36	5 26
K_2O	0.36	0 47	0.34	0.34	0.37	0.27	0 33	0.29	0.29	0 30	0 56
Total	100.20	100 37	100 46	100 75	101.03	100 97	100.65	100 36	100 57	100.32	101 01
An	67.0	62 0	68.3	68 0	68.5	71.6	69 6	70 4	70 0	68.9	50.9

Group D

Sample	dc66	dc66	dc66	dc66	dc66	dc66	dc66	dc66
Grain	1	2	3	4	5	6	7	8
SiO_2	50.82	50 83	50 91	51.06	51.07	51.13	51 38	51.72
Al_2O_3	31.14	31.11	31 01	30 81	31.03	31.06	30 90	30 77
Fe_2O_3	0.41	0 40	0.38	0.42	0 53	0.44	0.42	0 47
CaO	14 08	13 88	14 00	13 54	13.73	13 74	13.36	13.28
Na_2O	3 43	3.51	3 47	3.61	3 51	3 57	3.59	3.76
K_2O	0 32	0.33	0 29	0.30	0 36	0.31	0.31	0 32
Total	100.20	100 06	100.06	99.74	100.23	100 25	99 96	100.32
An	68.0	67.3	67.9	66 2	66.9	66.8	66 0	64.8

nd = not detected

3.3 The associated xenoliths

Ultramafic xenoliths of mantle-derivation are found in many alkali basaltic rocks worldwide (e.g., Frey and Green, 1974; Frey and Prinz, 1978; Press *et al.*, 1986; Qu Qi *et al.*, 1995). The most common types of mantle-derived xenoliths are assignable to either the Cr-Diopside series or the Al-Ti-augite series (e.g., Wilshire and Shervais, 1975; Wass and Irving, 1976; Irving, 1980; Frey and Prinz, 1978). The spinel-lherzolite suites are members of the Cr-diopside series and are the most abundant and widespread. Because of their direct mantle origin, these rocks provide valuable information about the petrology and geochemical composition of the upper mantle, enabling a better understanding of the major mantle processes and inferences about the thermal conditions of the mantle below the host basalt suite.

In Thailand, mantle-derived xenoliths are widespread throughout late Cenozoic basalts. In these basalts, the predominant mantle xenolith types are spinel-lherzolite with minor harzburgite and rare wehrlite, websterite, dunite and clinopyroxenite (Promprated *et al.*, 1999). Crustal-derived xenoliths have not been previously reported. The Denchai basalts are typical of intraplate late Cenozoic alkali basaltic volcanism, and they host common xenoliths. The petrography, mineral chemistry and *P-T* sensitive chemical partitioning relationships of these rocks are used here to determine the petrogenesis of the xenoliths.

3.3.1 Petrography

Xenoliths in the Denchai basalts are rounded or subangular, commonly less than 5 cm, and rarely up to 10 cm, across (Fig.3.2). Fresh xenoliths are commonly pale-green but are yellowish. No significant reaction zones between the xenoliths and the host basalts were recognised. From 66 sampling localities of the Denchai basalts, 14 xenoliths were selected for further examination. Among them, 3 are considered to be fragments of crustal-derived rocks on the basis of mineralogy and texture. Mantle xenoliths and disaggregated nodule materials are abundant in Group B and subordinate in Group D, whereas crustal-origin xenoliths were found in Group A and Group C. In general, these xenoliths have granoblastic texture and are medium- to coarse-grained (Figs.3.9e, f).

Mantle xenoliths

All the mantle-derived xenoliths are spinel-lherzolites with the mineral assemblage olivine, clinopyroxene, orthopyroxene and spinel (Figs.3.9a, e). The primary phases are all in mutual contact, suggesting attainment of equilibrium. Large olivine crystals (to 1.2 mm across)

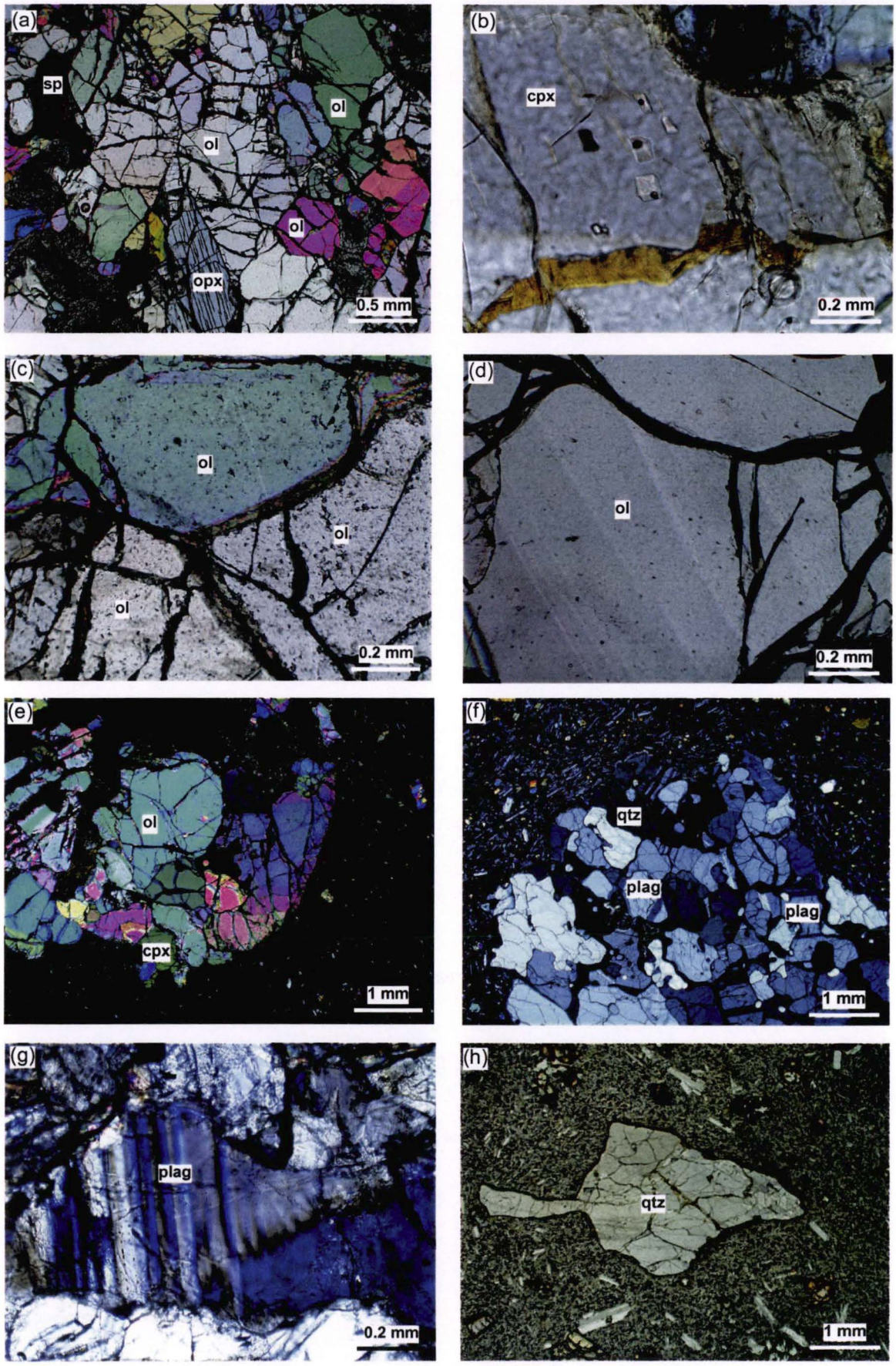

Figure 3.9 Photomicrographs of the associated xenoliths in the Denchai basalts
(a) coexisting minerals; (b) inclusions in cpx; (c) triple-junctions; (d) kink bands; (e) mantle xenolith; (f) crustal xenolith; (g) twinning of plagioclase and (h) quartz xenocryst (plane-polarised light)

display well-defined triple junctions (Fig.3.9c), weak kink bands (Fig.3.9d) and undulatory extinction. Both clinopyroxenes (to 0.5 mm across) and orthopyroxenes (to 0.4 mm across) are free from exsolution lamellae. Spinels form a common accessory phase in these mantle xenoliths, occurring as a dark brownish interstitial phase up to 0.3 mm across. Some clinopyroxene grains contain glassy inclusions (Fig.3.9b) suggesting that these xenoliths underwent very localised melting and/or reaction with infiltrated host magma. Naturally quenched glass inclusions in clinopyroxenes (Table 3.5, Fig.3.10) show a range in major element compositions very similar to glasses in mantle xenoliths from western Victoria, Australia (Yaxley *et al.*, 1997). The compositional variation of mantle-derived silicate glasses is notably different from the silicate-melt compositions of inclusions in the Denchai sapphires (see Section 5.6.3).

Table 3.5 Glass compositions in clinopyroxene of mantle xenolith

Sample	SiO_2	Ti_2O	Al_2O_3	FeO	MnO	MgO	CaO	Na_2O	K_2O	P_2O_5	Total
DC14	49.00	2 66	19 19	3.10	0.05	5.73	4 94	5.95	4.17	0.57	95.36
DC14	51.46	1.35	18 12	3.07	0.07	3.32	6.08	4.95	5.27	0.75	94.43
DC14	52.43	1 33	20.46	3.13	0.01	0 84	1.47	5.99	7.36	1.03	94.06
DC14	52.65	1.33	20.37	2.95	0.06	0 91	1.94	6.12	7.06	0 99	94.37
DC14	56.45	1.34	22.01	2 30	0.04	1.32	1.41	6.09	2.23	0.22	93.41
DC14	58.14	1 16	24.09	2.21	0.09	1 16	2.72	8.12	0 27	0 46	98 43

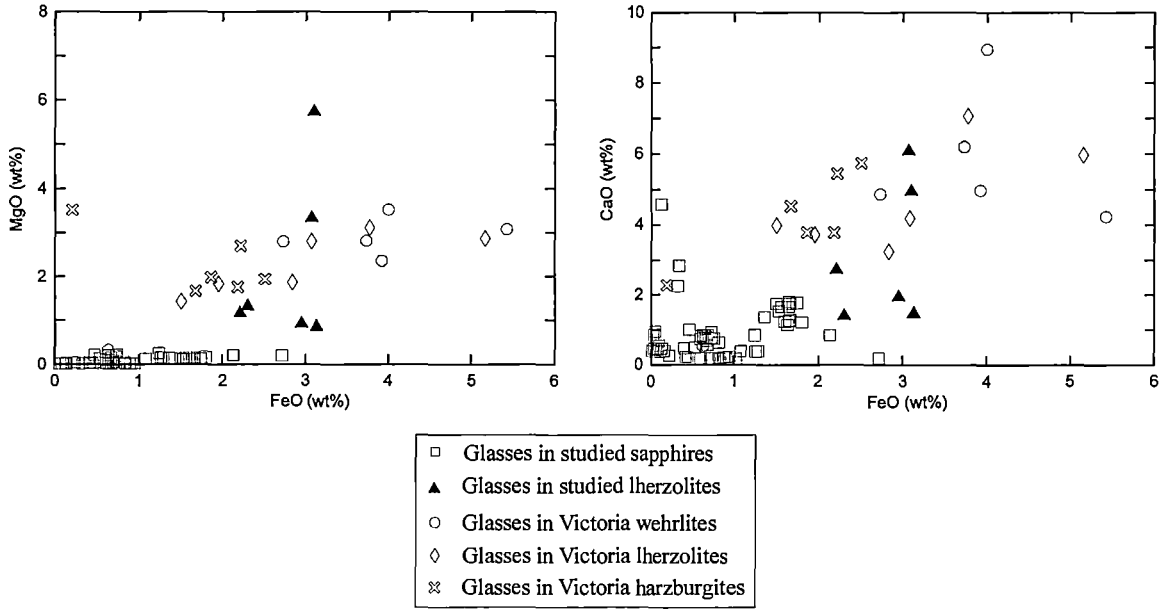

Figure 3.10 Geochemical plots comparing glass compositions from mantle peridotite xenoliths and glass compositions from the studied sapphires

Crustal xenoliths

Three crustal xenoliths were found in Group A (DC42) and Group C (DC16 and DC29). Sample DC42 contains a xenolith that has a unique character, consisting of clinopyroxene, plagioclase and quartz with all three phases in mutual contact (Fig.3.9f). Sample DC16 and DC29 contain xenoliths composed of clinopyroxene and plagioclase without quartz. The clinopyroxenes are green and display sieve textures, interpreted as evidence for disequilibrium between xenoliths and host basalts. Some plagioclase grains display deformation twinning (Fig.3.9g).

Quartz xenocryst

Besides the mantle- and crustal xenoliths, one quartz xenocryst was found in Group C rocks (DC15) with size of about 2 mm across. It has strong undulatory extinction (Fig.3.9h). Assuming this xenocryst comes from the deep crust, it also would be a sample from a fault zone.

3.3.2 Mineral chemistry

Major and minor element compositions of the coexisting minerals were analysed under the same analytical conditions as for phases in the host basalts. Microprobe analytical conditions are described in Appendix C and the complete sets of coexisting mineral analyses of the associated xenoliths are given in Appendix D. In the following Mg# = $100Mg/(Mg+Fe^{2+})$, and Cr# = $100Cr/(Al+Cr+Fe^{3+})$. Mineral names are abbreviated as follows: Ol = olivine, Cpx = clinopyroxene, Opx = orthopyroxene, Plag = plagioclase and Sp = spinel and their compositional variations within individual minerals are described below.

Mantle xenoliths

Olivine

Olivines in xenoliths have a restricted compositional range (Table 3.6) from $Fo_{87.6}$ to $Fo_{91.1}$ (Fig.3.4e). Olivine NiO contents range from 0.26 to 0.49wt% and CaO contents show a narrow range from 0.06 to 0.11wt% (Fig.3.6e). Apart from two grains that are less magnesian than Fo_{89}, there are no significant compositional differences among the olivines in these mantle xenoliths, which are similar to those of spinel lherzolite xenoliths worldwide (e.g., Frey and Prinz, 1978; Fan and Hooper, 1989).

Table 3.6 Representative analyses of olivine in mantle xenoliths in the Denchai basalts

Group B

Sample	dc5	dc5	dc5	dc5	dc5	dc5	dc5	dc13	dc13	dc14	dc14
Grain	1	2	3	4	5	6	7	1	2	1	2
SiO_2	40.73	40 78	40 83	40 87	40.95	41.04	41 13	41 24	41 36	40 49	40 67
FeO	9 43	10 54	10 52	9 80	9.79	9 55	9.67	9 68	9 87	10.55	10 74
MgO	48 95	47.85	48 13	49 21	49.35	48 82	48 90	49 12	48 77	47 51	47.75
CaO	0 08	0 08	0 06	0 10	0.09	0 07	0.09	0.06	0 07	0.07	0 07
NiO	0 49	0 33	0 34	0 37	0.41	0 37	0.41	0 45	0.39	0 33	0.36
Total	99.68	99.58	99 88	100.35	100.59	99.85	100 20	100 55	100 46	98.95	99 59
Fe^{2+}	0 19	0.22	0 22	0 20	0 20	0 20	0 20	0 20	0.20	0 22	0 22
Mg^{2+}	1 79	1 76	1.76	1 79	1.79	1 78	1.78	1 78	1.77	1 76	1 76
Fo	90.2	89.0	89.1	89 9	90.0	90 1	90 0	90 0	89.8	88.9	88 8

Group B

Sample	dc19	dc19	dc19	dc27	dc27	dc27	dc27	dc27	dc27	dc27
Grain	1	2	3	1	2	3	4	5	6	7
SiO_2	40.76	40 83	40.93	40 45	40.45	40 48	40.74	40 74	40.81	40.81
FeO	10.42	10.30	10 24	10.39	10 26	9.37	9 59	9.49	9.52	9.68
MgO	48 08	48.71	48.33	48 03	48.22	49 06	49.25	48 55	48.94	49.09
CaO	0 08	0.06	0.08	0 08	0.07	0 08	0 08	0.09	0 11	0.11
NiO	0.42	0.40	0.43	0 35	0 31	0.41	0 40	0.42	0 42	0.37
Total	99.76	100 30	100.01	99.30	99 31	99.40	100 06	99 29	99.80	100 06
Fe^{2+}	0 21	0.21	0.21	0 22	0.21	0 19	0 20	0.20	0 20	0.20
Mg^{2+}	1 76	1 78	1 77	1.77	1 78	1 80	1 80	1 78	1.79	1.79
Fo	89 2	89.4	89 4	89 2	89.3	90 3	90 1	90 1	90 2	90.0

Group B

Sample	dc43	dc43	dc43	dc55	dc55	dc55	dc55
Grain	1	2	3	1	2	3	4
SiO_2	40 19	40.25	40 40	40 83	40.88	40 99	41.00
FeO	11.48	11.94	11.70	8.65	9 09	8 65	8.76
MgO	47.29	47 24	46.93	49 69	49 73	49.92	49 29
CaO	0.07	0 06	0 09	0.11	0 07	0 09	0.08
NiO	0 41	0 26	0 40	0.38	0 34	0 37	0.48
Total	99 44	99.75	99 52	99 66	100 11	100 02	99.61
Fe^{2+}	0.24	0 25	0 24	0 18	0.19	0.18	0 18
Mg^{2+}	1.75	1.75	1 74	1 81	1 81	1.81	1 80
Fo	88.0	87 6	87.7	91.1	90 7	91.1	90.9

Group D

Sample	dc3	dc3	dc3	dc3	dc3
Grain	1	2	3	4	5
SiO_2	40.18	40.48	40.54	40 58	40.70
FeO	9 89	9.73	10.02	9 84	9 84
MgO	49 11	48 79	48.84	48 52	48 98
CaO	0 07	0 10	0.10	0.09	0 11
NiO	0 31	0.45	0.44	0 42	0 35
Total	99 56	99 55	99 94	99.45	99 98
Fe^{2+}	0 20	0.20	0.21	0 20	0 20
Mg^{2+}	1.80	1.79	1.79	1.78	1 79
Fo	89 9	89.9	89.7	89 8	89 9

Clinopyroxene

Clinopyroxenes in the mantle xenoliths are mainly diopsidic (Table 3.7; $Wo_{48.5-44.3}En_{50.6-46.4}Fs_{5.8-4.6}$; Figs.3.7b, d). The $Mg\#_{Cpx}$ values of clinopyroxenes show a narrow range from 89.2 to 91.3 (Fig.3.8e), CaO content ranges from 19.1 to 22.9wt%, and Al_2O_3 content varies from 3.3 to 7.9wt%. The most calcic clinopyroxenes have low Al contents, probably reflecting low temperature re-equilibration. Slight variation in clinopyroxene Al and Na contents is apparent, and Al_2O_3 contents of clinopyroxenes are weakly correlated with Al_2O_3 contents of coexisting spinel (Fig.3.11c). The Cr_2O_3 contents of clinopyroxenes show a stronger positive correlation with Cr_2O_3 contents of coexisting spinel. Compositions of Denchai spinel-lherzolite clinopyroxenes are Cr-rich and Ti-poor, similar to xenolithic spinel-lherzolite clinopyroxenes from most other localities globally (e.g., Frey and Prinz, 1978).

Orthopyroxene

Orthopyroxenes are all from xenoliths in Group B basalts and occupy the enstatite field in the pyroxene quadrilateral plot (Table 3.8; Fig.3.7b). Their $Mg\#_{opx}$ values cover a narrow range around 90, generally slightly higher values than those of coexisting olivine. The *Cr*-numbers ($Cr\#_{Opx}$) vary between 2.8 to 5.7 and a range of Ca/(Ca+Fe+Mg) varies from 1.4 to 1.7. Orthopyroxenes show little variation in terms of Mg, Fe, Ca, Ti and Al contents.

In comparison to global spinel lherzolites, orthopyroxene compositions from Denchai xenoliths are very similar to those of peridotites from eastern China (Fan and Hooper, 1989) but they have slightly higher Al and lower Cr than those from San Carlos, Arizona (Frey and Prinz, 1978) and the Massif Central, France (Brown *et al.*, 1980).

Spinel

Spinels are MgO- and Al_2O_3-rich with significant compositional variability in Cr_2O_3 (8.3 to 19.7wt% and Al_2O_3 (49.6-60.5wt%) contents (Table 3.9). They show a range of $100Cr/(Cr+Al+Fe^{3+})$; i.e., $Cr\#_{Sp}$) from 8.3 to 20.8 and the $Mg\#_{Sp}$ values range from 64.9 to 78.8. One grain from Sample DC5, with 40.4wt% of Al_2O_3 and 29.0wt% of Cr_2O_3 has a higher $Cr\#_{Sp}$ (32.1). There is a positive, albeit rather poor, correlation between both the Al_2O_3 and Cr_2O_3 concentrations of the two coexisting pyroxenes with spinel (Figs.3.11a-f), indicating control by bulk composition. The relatively Al-rich, Cr-poor compositions of spinels in the Denchai lherzolites indicate relatively fertile upper mantle compositions, and show no tendency to more depleted harzburgitic compositions (Fabries *et al.*, 1987; Fan and Hooper, 1989).

Table 3.7 Representative analyses of clinopyroxene in mantle xenoliths in the Denchai basalts

Group B

Sample	dc5	dc5	dc5	dc5	dc5	dc5	dc5	dc5	dc5
Grain	1	2	3	4	5	6	7	8	9
SiO_2	51.03	52.44	52.54	52.24	52.42	52.12	52.24	52 42	52.12
TiO_2	0 61	0.35	0.36	0 43	0.39	0 44	0.43	0 39	0.44
Al_2O_3	7.99	3.83	5.74	4 71	3.29	4 47	4.71	3 29	4 47
Cr_2O_3	0.84	1.35	1.20	1.47	1.38	1 26	1 47	1 38	1 26
FeO*	3.03	2.78	3 14	2.83	2.99	3.07	2.83	2 99	3 07
MnO	0 09	0.04	0 04	0.09	0.02	0.05	0.09	0.02	0.05
MgO	14 92	16 34	15.47	15 85	17 63	16.51	15 85	17.63	16 51
CaO	19 06	22 86	22.44	22.95	22.24	22 84	22 95	22.24	22 84
Na_2O	1 65	0 66	1 08	0.69	0.53	0.49	0.69	0 53	0.49
Total	99 30	100 80	102.01	101 39	100 89	101.41	101 26	100.89	101 41
Mg#	89.8	91 3	89 8	90 8	91.2	90.5	90 8	91.2	90 5
Ca#	45.1	47 9	48.3	48.5	45.3	47.3	48.5	45.3	47 3
Wo	45 1	47.9	48.3	48 5	45.3	47.3	48 5	45.3	47 3
En	49 1	47 5	46.4	46 6	49.9	47.6	46 6	49.9	47 6
Fs	5 8	4.6	5.3	4 9	4 8	5 1	4.9	4.8	5.1

Group B

Sample	dc13	dc13	dc13	dc13	dc13	dc13	dc14	dc14	dc14
Grain	1	2	3	4	5	6	1	2	3
SiO_2	51.81	51.99	52 28	52.40	51 87	52.47	50 63	51 20	51 23
TiO_2	0.45	0 43	0.48	0 48	0 43	0 51	0.65	0 61	0.63
Al_2O_3	7.16	7 08	7.08	7 05	6.88	7 00	5.31	4.99	5.27
Cr_2O_3	1.09	1 09	1 04	1 04	1 07	0.94	0 99	0.81	0 90
FeO*	2.79	2 69	2 71	3 01	2.83	2 90	3 06	3.03	2 95
MnO	0.04	0 06	0 12	0.10	0 09	0.05	0 09	0.08	0 13
MgO	15.08	15 15	15.33	15.10	14.97	15 28	16 00	16 68	16.32
CaO	20.36	20 21	20.31	20.25	19.94	20 15	21 75	21 28	21.46
Na_2O	1 67	1 66	1 68	1.68	1 69	1.66	0 58	0.54	0 51
Total	100.61	100 46	101.16	101.22	99.87	101.03	99.20	99 30	99.43
Mg#	90 5	90.9	91 0	89.9	90.5	90.3	90 3	90 8	90.8
Ca#	46.7	46 5	46.3	46 4	46.3	46.1	46 8	45 4	46.1
Wo	46.7	46 5	46.3	46 4	46.3	46.1	46.8	45 4	46.1
En	48 2	48.5	48.6	48.1	48.4	48.6	47.9	49 5	48.7
Fs	5.1	5.0	5.1	5 6	5.3	5.3	5.3	5 2	5.2

Group B

Sample	dc19	dc19	dc19	dc23	dc27	dc27	dc27	dc27	dc43
Grain	1	2	3	1	1	2	3	4	1
SiO_2	51 11	51 15	51 29	52 05	50 77	51.54	51.83	51.91	51.11
TiO_2	0.68	0.61	0 62	0.47	0 64	0.18	0.16	0 21	0.68
Al_2O_3	7.72	7 82	7.83	6 92	5.07	5.24	5 05	5.33	5.38
Cr_2O_3	0.75	0 71	0.82	1.02	1.02	0 97	0 96	0.94	0.92
FeO*	3 11	2.91	2 91	2.58	3.30	2.96	2.85	2.82	3.48
MnO	0.07	0.09	0 14	0 06	0.14	0 08	0 07	0.08	0 05
MgO	14 90	14.93	14 76	15.14	16 26	16.54	16.56	16 60	16.13
CaO	19.83	19 75	19.90	20 71	21.48	21 81	21 53	21.58	21.87
Na_2O	1.70	1.73	1.77	1.68	0 59	0.66	0.65	0.67	0.46
Total	100 06	99 86	100.19	100.79	99.45	100.17	99 77	100.24	100.15
Mg#	89 5	90.1	90 0	91.3	89 8	90.9	91 3	91.2	89 2
Ca#	46 1	46.1	46 5	47.2	45 9	46.2	46 0	46 0	46 5
Wo	46.1	46 1	46.5	47.2	45 9	46.2	46 0	46.0	46.5
En	48.2	48 4	47.9	48 1	48.4	48 8	49 2	49.2	47.7
Fs	5.8	5 5	5 6	4.7	5.7	5 0	4.8	4 8	5.8

Group D

Sample	dc3
Grain	1
SiO_2	52 05
TiO_2	0 16
Al_2O_3	4 63
Cr_2O_3	1.15
FeO*	2 97
MnO	0.07
MgO	16.86
CaO	20 57
Na_2O	0 73
Total	99.23
Mg#	91.0
Ca#	44.3
Wo	44.3
En	50.6
Fs	5.1

Total Fe as FeO*

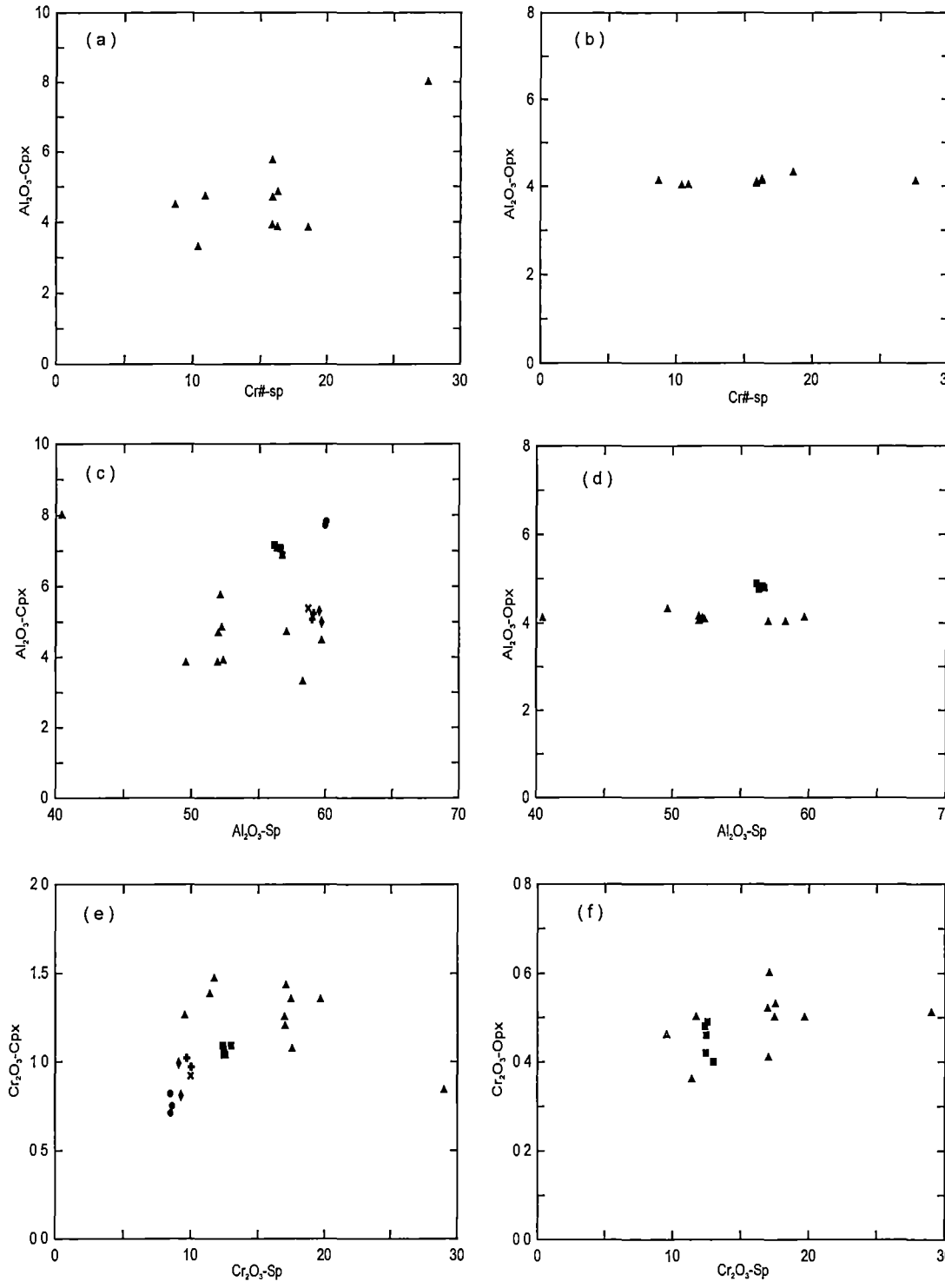

Figure 3.11 Oxide concentrations in coexisting minerals in various mantle xenoliths; Note: different symbols represent each xenolith

Table 3.8 Representative analyses of orthopyroxene in mantle xenoliths in the Denchai basalts

Group B

Sample	dc5	dc5	dc5	dc5	dc5	dc5	dc5	dc5	dc5	dc5	dc5	dc5
Grain	1	2	3	4	5	6	7	8	9	10	11	12
SiO2	55.32	55 55	55.55	55 65	55.70	55 74	55.82	55.98	55.64	56 06	56 04	55.83
TiO2	0 11	0 06	0.08	0 07	0.11	0.06	0 08	0.07	0 09	0 09	0 07	0.11
Al2O3	4.10	4.30	4.14	4 04	4.08	4.10	4.07	4 02	4 01	4 11	4 08	4 13
Cr2O3	0 51	0 50	0 53	0 52	0.41	0 50	0.60	0.50	0.36	0.46	0 42	0 59
FeO*	6.70	6 26	6.43	6 21	6.34	6.48	6.41	6.59	6 35	6.43	6.32	6 40
MnO	0.11	0 22	0.17	0.17	0.18	0 15	0 19	0.16	0 14	0.13	0.14	0.20
MgO	33.00	32 84	32 98	32.87	32 95	33.00	32.58	32.92	32.59	32 70	32 78	32 58
CaO	0 83	0.83	0 82	0 74	0.78	0 79	0.80	0.82	0.78	0 81	0 79	0.77
Total	100 90	100.71	100.89	100 38	100.75	100 97	100 67	101 14	100.08	100.89	100 76	100 73
Mg#	89.8	90 3	90.1	90 4	90.3	90 1	90.1	89 9	90.2	90 1	90 2	90.1
Ca#	1.6	1 6	1.6	1.4	1 5	1.5	1.6	1.6	1.5	1 6	1 5	1.5
Cr#	4.5	4.5	4 7	5.0	3.9	4 8	5.7	4.5	3.7	4 7	4.0	5.6
Wo	1.6	1.6	1 6	1.4	1 5	1 5	1.6	1.6	1 5	1 6	1.5	1.5
En	89 7	89.1	89 4	89.1	89.2	89 1	88.7	88 5	88 8	88.6	88.9	88.7
Fs	8.7	9.3	9 0	9 4	9.3	9 4	9.8	9 9	9.7	9 8	9.6	9.8

Group B

Sample	dc13	dc13	dc13	dc13	dc13	dc13	dc13	dc13	dc13	dc13	dc13
Grain	1	2	3	4	5	6	7	8	9	10	11
SiO2	55 16	55.72	55 82	55 42	55 78	55 88	55 46	55 39	55.65	55.76	55.59
TiO2	0.12	0 10	0.14	0 12	0.12	0 14	0.11	0 09	0 12	0 11	0.09
Al2O3	4 89	4 76	4.80	4 83	4.79	4 70	4.61	4 77	4.63	4 58	4.59
Cr2O3	0.40	0 48	0.42	0 49	0.46	0 40	0.48	0 43	0 44	0.45	0 43
FeO*	6.28	6 00	6.12	6 18	6.06	6 11	6 02	6 19	6 21	6 28	6.15
MnO	0 27	0.14	0.12	0.08	0 14	0.16	0 14	0.18	0.12	0.15	0.11
MgO	32 88	32.76	32 74	32.82	32 81	32.72	32 56	33 01	32.90	32 81	32 94
CaO	0 85	0 81	0.83	0 84	0.85	0 83	0 87	0 82	0 79	0.84	0.81
Total	101.04	100.90	101.13	100.89	101 13	101.08	100.39	101.07	100 99	101.11	100 82
Mg#	90.3	90 7	90 5	90.4	90 6	90.5	90.6	90.5	90.4	90 3	90 5
Ca#	1.7	1 6	1.6	1 6	1.7	1 6	1.7	1 6	1 5	1 6	1.6
Cr#	2 8	3 5	2 9	3 4	3 2	2 9	3 5	3.1	3 2	3.2	3 2
Wo	1.7	1.6	1.6	1 6	1.7	1.6	1.7	1.6	1 5	1.6	1 6
En	89.8	89.2	89.0	89.0	89.1	89 0	89 0	89.7	89.0	88.8	89.1
Fs	8 6	9.2	9.3	9 4	9 2	9.3	9 2	8.7	9.4	9.5	9 3

Total Fe as FeO*

Table 3 9 Representative analyses of spinel in mantle xenoliths in the Denchai basalts

Group B

Sample	dc5	dc5	dc5	dc5	dc5	dc5	dc5	dc5	dc5	dc5
Grain	1	2	3	4	5	6	7	8	9	10
Al_2O_3	40 45	49.62	51 94	51 95	52.11	52 20	52 35	57 01	58 28	59 67
Cr_2O_3	29 02	19.67	17 52	16 95	17.01	17 46	17.10	11 71	11 41	9.54
Fe_2O_3	1.31	1 27	1.41	1 57	1 37	0.21	1 06	1.09	nd	0 49
FeO	13.73	10 60	10.42	10 14	10 39	10.93	10 52	9.30	10.64	10 38
MnO	0.17	0.03	0 06	0.13	0 03	0.12	0 18	0.12	0.04	0 05
MgO	16 12	19.27	19 60	19.62	19 51	19.20	19 36	20 65	19.93	20 36
NiO	0 30	0.27	0.41	0.36	0.40	0.28	0 38	0.32	0.37	0 38
Total	101 49	101.00	101 66	101.09	101 28	100 80	101 40	100.54	100 88	101 06
Mg#	65.8	74 6	74 9	75 1	75 0	75.5	75 1	78.2	77.0	77.1
Cr#	32.1	20 8	18 2	17.7	17 7	18.3	17 8	12.0	11 6	9.6

Group B

Sample	dc13	dc13	dc13	dc13	dc13	dc14	dc14	dc19	dc19	dc19	dc19
Grain	1	2	3	4	5	1	2	1	2	3	4
Al_2O_3	56.13	56 31	56.55	56 59	56.71	59 51	59.69	59 95	59.99	60 04	60.49
Cr_2O_3	12 97	12 36	12.42	12 55	12 46	9.11	9.32	8.63	8.51	8 49	8.26
Fe_2O_3	1 10	1.48	1 19	1.01	1 01	0.31	0 66	0.92	0.56	0.65	0 82
FeO	9 51	8.91	9.36	9 50	9.45	10.71	10.33	9.66	9.43	9 88	9.60
MnO	0 03	0 06	0.12	0.11	0 09	0 10	0 15	0.05	0.05	0 09	0 09
MgO	20.50	20 73	20.53	20 51	20.47	19.90	20 20	20.71	20 79	20.48	20 92
NiO	0.36	0.41	0.33	0 41	0.41	0 39	0 42	0.45	0.37	0.36	0 34
Total	100 91	100 58	100.89	101 04	100.98	100 36	101 16	100 69	99 91	100 22	100.80
Mg#	77 7	78.3	77 8	77 8	77.9	76.4	76.7	77.8	78 8	77 7	78 2
Cr#	13 3	12 6	12.7	12.8	12.7	9 3	9 4	8.7	8.6	8.6	8 3

Group B

Sample	dc27	dc27	dc43	dc43	dc43	dc43	dc62
Grain	1	2	1	2	3	4	1
Al_2O_3	58 96	59 08	58.67	58.83	59 41	60.15	56 00
Cr_2O_3	9.68	10 00	10.01	10.44	9 58	8.42	8 87
Fe_2O_3	0 43	0 14	0.61	0 40	0 52	0.68	3.33
FeO	10.14	10.60	10 87	10.14	11 00	11 18	13.87
MnO	0.07	0.11	0 11	0.12	0 12	0 05	0.19
MgO	20.16	19.99	19.87	20 35	19 93	19 80	17.44
NiO	0 42	0.39	0.33	0.41	0.36	0.40	0 33
Total	100.22	100.79	100 79	100.99	101 13	101 06	100 49
Mg#	77.4	76.8	75.6	77.5	75.6	74.9	64 9
Cr#	9.9	10.2	10.2	10.6	9 7	8 5	9.3

nd = not detected

Crustal xenoliths

Clinopyroxene

Clinopyroxenes compositions in each crustal xenolith in the Denchai basaltsare slightly different (Table 3.10) In Sample DC42, xenolithic clinopyroxenes plot in the augite field with a maximum $Mg\#_{Cpx}$ values of 67.3 (Figs.3.7a, 3.12c). Clinopyroxenes in the xenolith from Sample DC16 are diopsidic with a large range of $Mg\#_{Cpx}$ values from 47.7 to 61.9 (Figs.3.7c, 3.12a). Most clinopyroxene grains have similar compositions in terms of Mg and Ca contents, but one grain has high TiO_2 (2.6wt%) and Al_2O_3 contents (4.5wt%), probably reflecting reaction with the host basalt magma. In Sample DC29, clinopyroxene compositions are all diopsidic with a large range of $Mg\#_{Cpx}$ values from 50.0 to 74.6 (Figs.3.7c, 3.12b).

Plagioclase

Plagioclase compositions in three crustal xenoliths are presented in Table 3.11. Plagioclases in each xenolith have homogeneous compositions with a uniform An content. In Sample DC42, plagioclases cluster around An_{38}, much lower than in Samples DC16 and DC29. Plagioclases from Sample DC29 are the most calcic compositions, around An_{80}. In Sample DC16, plagioclases range from An_{63} down to An_{48}.

3.4 Variations in mineral compositions

The systematic compositional variations of minerals in the Denchai basalts and various associated mantle- and crustal-derived xenoliths are shown in Figures 3.4-3.12. Mineral compositions were investigated to evaluate the possibility of intergranular and intragranular compositional variations, however only informative minerals were compared.

3.4.1 The Denchai basalts

The phenocryst and microphenocryst phases of the Denchai basalts particular olivine and clinopyroxene indicate the relationship to crystal fractionation. This is evident from the well-defined trend for Fo content versus NiO and CaO contents of olivine phenocrysts and microphenocrysts which could not be observed from olivine in the associated mantle xenoliths (Figs.3.5, 3.6). The $Mg\#_{Cpx}$ values of clinopyroxene phenocrysts and microphenocryst also show a large range (78-83) compared to the $Mg\#_{Cpx}$ values (89-91) of clinopyroxene in mantle xenoliths (Fig.3.8).

Table 3.10 Representative analyses of clinopyroxene in crustal xenoliths in the Denchai basalts

Group A

Sample	dc42	dc42	dc42	dc42	dc42
Grain	1	2	3	4	5
SiO_2	52 42	52.19	52 18	51 95	52.15
TiO_2	0.22	0 17	0 17	0.14	0 21
Al_2O_3	1.20	1 21	1.20	1.20	1 22
Cr_2O_3	nd	0.05	0.02	0.02	nd
FeO*	12 59	12.35	12 28	12.48	12.06
MnO	0.47	0.40	0.33	0.38	0.36
MgO	12.32	12.35	12 33	12.38	12.41
CaO	21 38	21.33	21.77	21.36	21.46
Na_2O	0.34	0.35	0 33	0.37	0.33
Total	101 05	100.56	100 80	100 46	100.31
Mg#	65.7	66 4	67 1	67.3	66.7
Ca#	43 9	44 0	44.6	43 9	44 3
Wo	43.9	44 0	44 6	43.9	44.3
En	35 2	35 5	35.1	35.4	35 6
Fs	20 9	20 5	20.2	20.7	20 0

Group C

Sample	dc16	dc16	dc16	dc16	dc16
Grain	1	2	3	4	5
SiO_2	47.57	50 22	50.52	50 61	51 05
TiO_2	2 64	0.11	0.07	0.09	0 37
Al_2O_3	4 50	1 06	0 92	0 92	1 36
Cr_2O_3	0 07	0 05	nd	0 03	0 03
FeO*	10 06	15 99	16 56	16 49	14 05
MnO	0.13	0.26	0.35	0 43	0 34
MgO	12 19	8.63	8.79	8 41	10.35
CaO	21 59	22 52	22 55	22.20	23 22
Na_2O	0.47	0.23	0.20	0 22	0.27
Total	99 50	99.23	100 20	99.51	101 30
Mg#	68.4	49 0	48.7	47.7	56 8
Ca#	46 4	47.7	47 0	47 1	47.5
Wo	46.4	47.7	47 0	47.1	47.5
En	36 5	25.4	25 5	24 8	29 5
Fs	17.1	26 9	27 5	28 0	23.0

Group C

Sample	dc16	dc16	dc16	dc16	dc16	dc16	dc16	dc16	dc16	dc16	dc16	dc16
Grain	6	7	8	9	10	11	12	13	14	15	16	17
SiO_2	51.18	51.20	51.21	51.30	51.41	51 42	51.43	51.54	51.63	51 75	51.86	52 15
TiO_2	0.09	0 09	0.16	0.08	0.11	0 34	0.10	0.06	0.19	0 25	0.25	0.19
Al_2O_3	0 82	0 88	1 14	0.86	0 93	1.27	0 86	0.83	0 90	0 90	0.90	0.96
Cr_2O_3	0.03	nd	0 04	0.05	0 03	0.05	0 01	nd	0.08	nd	0.02	0.09
FeO*	15.59	16 17	15 90	15.92	16.44	12.77	15 72	15.85	14.08	13 74	12.73	13.71
MnO	0.36	0.37	0 47	0 32	0.43	0.24	0 31	0 33	0 29	0.40	0.34	0.48
MgO	9 19	8.82	9.30	9 08	8 59	11.35	9.11	9.12	10.58	10 73	11.59	10.96
CaO	23 53	23.51	23 03	23 51	22 80	23.30	23.40	23.34	23.22	23 32	23 14	22.78
Na_2O	0.21	0 21	0.29	0 21	0.22	0 30	0 19	0 20	0.27	0 28	0 30	0.31
Total	101 24	101.48	101.85	101.58	101 07	101 37	101.32	101.47	101.51	101 63	101 43	101.85
Mg#	51.2	49.3	51.1	50 4	48.2	61.3	50.8	50 6	57 3	58 2	61.9	58 7
Ca#	48 2	48 3	47 2	48 1	47.6	47.3	48 2	48 0	47.2	47.3	46.8	46 4
Wo	48 2	48 3	47.2	48.1	47.6	47 3	48 2	48 0	47 2	47.3	46 8	46 4
En	26.2	25.2	26.6	25.9	24 9	32 1	26.1	26.1	30.0	30 3	32.6	31 0
Fs	25 6	26 5	26.2	26.0	27 5	20.6	25.8	26.0	22 8	22.4	20 6	22.6

Group C

Sample	dc29	dc29	dc29	dc29	dc29	dc29	dc29	dc29	dc29	dc29	dc29	dc29
Grain	1	2	3	4	5	6	7	8	10	11	12	13
SiO_2	50.66	51.17	51 48	51 61	51.65	51.84	52.19	52.33	52.46	52.55	52 72	53 26
TiO_2	0 06	0.09	0.18	0 11	1 07	0 22	0 13	0 12	0 23	0.14	0.37	0 20
Al_2O_3	0.70	1.07	0.78	1 02	4 41	0.91	2.01	1.67	0 83	2.04	1.24	0 46
Cr_2O_3	nd	0 05	0 01	0 04	0.11	nd	0.02	0.04	0 06	nd	0.01	0 03
FeO*	14.43	14.29	11 10	13.78	9 88	11.42	9.17	8 91	11.49	8.72	8.65	9 47
MnO	0 22	0 21	0.22	0.43	0.20	0 31	0.31	0.35	0 26	0 30	0.27	0.22
MgO	9.89	9 82	12 36	10 63	10 74	12.04	13 12	13.24	12.48	13.42	14.24	13.79
CaO	23.60	23 33	22.90	23.18	20.41	22 92	23.45	23 90	23 51	23 86	22 95	23.25
Na_2O	0 17	0.22	0.30	0 23	0.69	0.29	0.15	0.13	0.32	0 14	0 31	0.25
Total	100.03	100 45	99.58	101 28	100.00	100.13	100 68	100.87	101.95	101 31	100 97	101.11
Mg#	55 0	55 0	66.5	57 9	66 0	65.3	71.8	72 5	66 0	73.3	74 6	72.2
Ca#	48 4	48 3	46.8	47 3	47.2	46.9	47 8	48 2	47 0	48.1	46 1	46 5
Wo	48.4	48 3	46.8	47 3	47 2	46.9	47.8	48.2	47 0	48.1	46 1	46 5
En	28.2	28.3	35.1	30 1	34.6	34.3	37 2	37.2	34.7	37.7	39 8	38 4
Fs	23.5	23.5	18.1	22.6	18 2	18 8	15 1	14 6	18.3	14.2	14.0	15 1

nd = not detected; total Fe as FeO*

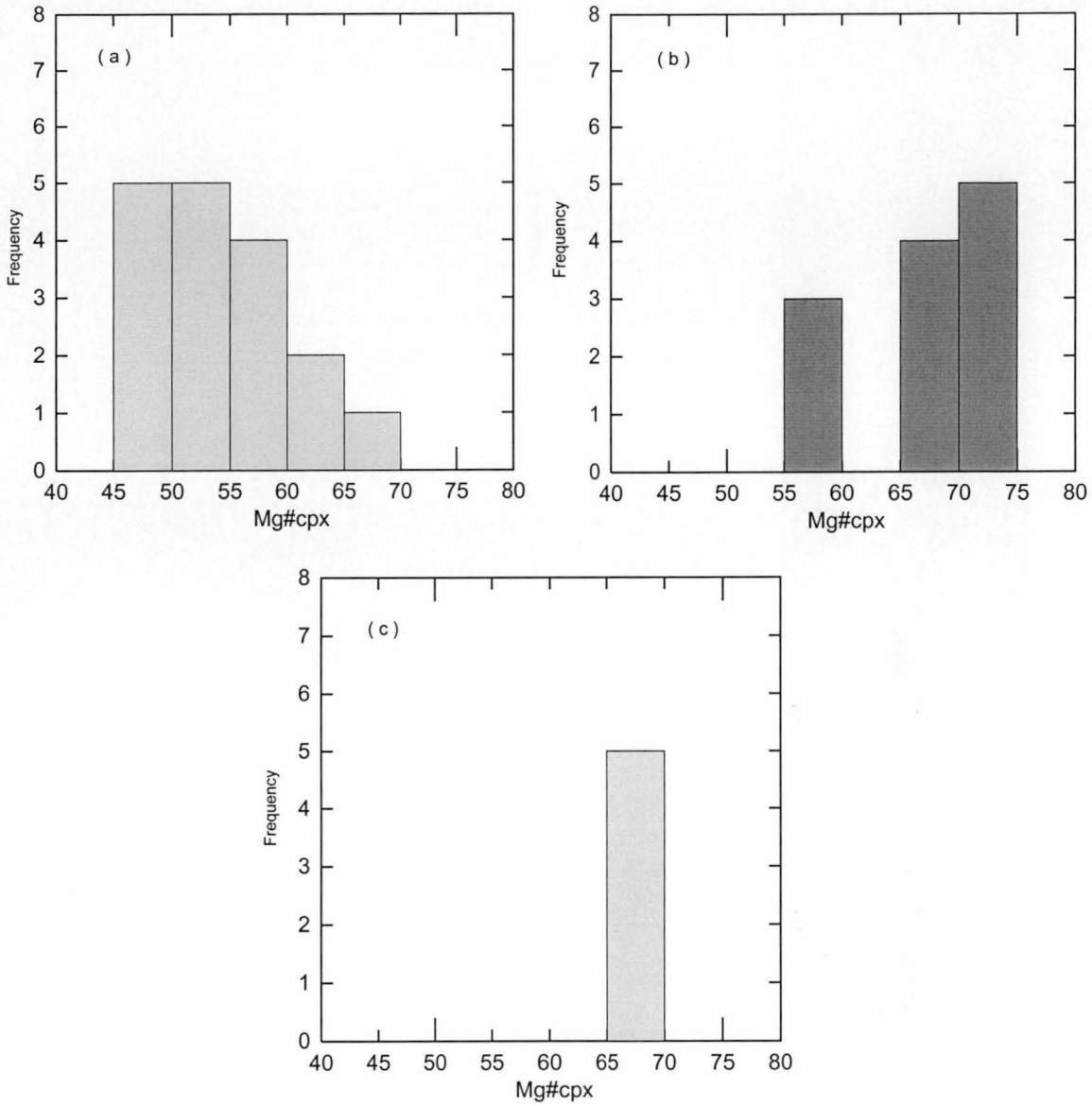

Figure 3.12 Histograms of $Mg\#_{Cpx}$ of clinopyroxene in crustal xenoliths; (a) Sample DC16; (b) Sample DC29 and (c) Sample DC42

Table 3.11 Representative analyses of plagioclase in crustal xenoliths in the Denchai basalts

Group A

Sample	dc42	dc42	dc42	dc42	dc42	dc42
Grain	1	2	3	4	5	6
SiO_2	58 23	58.42	58.45	58 52	58 73	58 98
Al_2O_3	26 24	26.24	26 17	26 34	26 20	26 79
Fe_2O_3	0 09	0.29	0.15	0 23	0 12	0 10
CaO	7 67	7 68	7 69	7 78	7 55	7.77
Na_2O	6.19	6 24	6.25	6 32	6 34	6 27
K_2O	0.77	0.83	1.00	0 76	0 79	0 80
Total	99 38	99.76	99 84	100.08	99 80	100 83
An	38.6	38.5	38.0	38 5	37 8	38 7

Group C

Sample	dc16	dc16	dc16	dc16	dc16	dc16	dc16	dc16	dc16	dc16
Grain	1	2	3	4	5	6	7	8	9	10
SiO_2	52.83	52 95	53 06	53.43	53.60	53.62	53.79	53.97	54.01	54.10
Al_2O_3	31.11	30 99	30 26	30 49	29 66	30.23	30.37	29 94	29 83	29 66
Fe_2O_3	0 07	0.07	0.25	0.18	0 08	0 13	0.11	0.26	0 22	0 35
CaO	13 15	12.94	12.01	12.63	11.48	12.40	12 29	12.11	12 15	11.92
Na_2O	4.06	4.13	4.38	4.36	4.52	4.56	4.46	4 63	4 67	4 68
K_2O	0.29	0.27	0.34	0.34	0 50	0.29	0 39	0.33	0.39	0 52
Total	101 60	101 47	100 46	101 50	99.94	101 30	101 47	101 40	101.33	101 38
An	63 0	62 3	59 0	60 3	56 7	59 0	59.0	57.9	57 6	56 8

Group C

Sample	dc16	dc16	dc16	dc16	dc16	dc16	dc16	dc16	dc16	dc16
Grain	11	12	13	14	15	16	17	18	19	20
SiO_2	54 46	54 56	55.38	55.38	55 49	55 54	55.58	55.95	55 97	56.38
Al_2O_3	29 72	29 22	28 18	28.99	28 93	28 79	28.78	28 21	28 78	28 31
Fe_2O_3	0 08	0 39	0.13	0 07	0.03	0 29	0 15	0 17	0.17	0.14
CaO	11.60	11 72	9.90	10.88	10 83	10.87	10 75	10 50	10 78	10 14
Na_2O	4 71	4 80	5 45	5 25	5 29	5 40	5.23	5.58	5.36	5 57
K_2O	0 40	0.42	0 52	0 44	0.50	0.46	0.52	0.48	0.55	0.60
Total	101.03	101.37	99.57	101.06	101 09	101.39	101.09	101 06	101 69	101 24
An	56.3	56 0	48 6	52.0	51.6	51.3	51.6	49.6	51 0	48 4

Group C

Sample	dc29	dc29	dc29	dc29	dc29	dc29	dc29	dc29	dc29	dc29
Grain	1	2	3	4	5	6	7	8	9	10
SiO_2	46.71	46.99	47.19	47.24	47.28	47.40	47.57	47.64	47.75	48.31
Al_2O_3	34.29	34.19	34.21	34 36	34.11	34.19	33.79	34.13	34.13	33 24
Fe_2O_3	0.09	0.15	0.12	0.11	0.15	0 16	0 24	0.10	0.19	0.26
CaO	17.31	17.29	17 10	17.35	17.26	17.15	16.34	17.14	17.10	16 53
Na_2O	1.87	1 81	1 86	1 86	1 96	2 01	2 20	2.07	2.00	2.28
K_2O	0.09	0.10	0.11	0.09	0.10	0 14	0 18	0.11	0.10	0.17
Total	100 47	100 59	100 73	101.09	100 97	101 10	100.40	101.32	101.42	100 83
An	83.2	83 6	82 9	83.3	82 4	81 9	79 5	81.5	82.0	79.2

The mineralogical variations within the phenocryst and microphenocryst assemblages of the Denchai basalts are consistent with normal fractionation trends. The study of crystallisation sequence of the Denchai basalts found no evidence for early crystallisation of clinopyroxene prior to olivine. Co-phenocrystic assemblages of olivine and clinopyroxene in Group A rocks is suggested by the near constant CaO contents of olivine, as their Fo contents decreased (Fig.3.6a). In Group B, the decreasing of NiO content and increasing of CaO content with decreasing of Fo content in olivines indicate that the crystallisation trend was entirely controlled by olivine (Fig.3.6b). This is consistent with a very rare appearance of clinopyroxene microphenocryst in Group B rocks. If the most magnesian olivines had crystallised before clinopyroxene, CaO contents of these olivines would firstly increase as their Fo content decreased, and then decreases when clinopyroxene joined olivine as a liquidus phase. Consequently, olivine phenocrysts and microphenocrysts of Group C and Group D show the decreasing of CaO contents from approximately ~Fo_{83} (Figs.3.6c, d), suggests that these suites crystallised olivine prior to clinopyroxene. No decline in the Al_2O_3 content was observed, as the $Mg\#_{Cpx}$ values decreased. This could be interpreted as evidence that plagioclase fractionation was not significant. However, in Group C and Group D samples clinopyroxene-plagioclase pairs occur as microphenocrysts throughout these lavas.

In summary, olivine is considered to be an early crystallising phase, which occurs throughout the crystallisation sequence in all groups. Clinopyroxene joins in the crystallisation sequence at about ~Fo_{83} in Group C and Group D basalts. Plagioclase appears late in the crystallisation sequence of Group C and Group D. In Group A, olivine and clinopyroxene are both early co-crystallised phases, whereas olivine is a major liquidus phase in Group B.

3.4.2 The associated xenoliths

Two types of xenoliths were found within the Denchai basalts, presumably mantle and crustal origins. The coexisting minerals in the associated xenoliths show equilibrium textures based on grain contact among mineral phases (Fig.3.9).

In mantle xenoliths, olivines have homogeneous compositions with a narrow range of Fo content from 87 to 91. Clinopyroxenes are mainly diopsidic with a $Mg\#_{Cpx}$ values ranges up to 91.3. The high Al_2O_3 contents of clinopyroxene (> 7wt%) is controlled by reactions with spinel and correlates with the the Cr/Al ratios in the coexisting spinel (Fig.3.11a). The same relationship is found with coexisting orthopyroxene (Fig.3.11b). Spinels are Mg- and Al-rich compositions with variations in Cr and Al contents. There is a positive correlation between both Cr_2O_3 and Al_2O_3 contents of spinel and clinopyroxene but little correlation of spinel and

orthopyroxene (Fig.3.11c-f). Mineral compositions of spinel lherzolites in the Denchai basalts compare with several typical occurrences of the other areas. The spinel lherzolites from the Denchai are similar to those of Group I spinel lherzolites from San Carlos, Arizona (Frey and Prinz, 1978) and of those spinel lherzolites from eastern China (Fan and Hooper, 1989).

For crustal xenoliths, clinopyroxene from three different xenoliths have a wide range of the $Mg\#_{Cpx}$ values from 49 to 79, but are very consistent in each xenolith. They are mainly diopsidic in composition with exception of clinopyroxene in Sample DC42, which are augitic in compositions. Plagioclases in each xenolith have a uniform anorthite (An) content.

3.5 Thermobarometry

Many experimentally calibrated thermodynamic models have been proposed either for calculation of phase diagrams, or as potential thermobarometers, for estimating the equilibration temperatures and pressures of natural rocks. The mineral chemistry of the xenoliths in the Denchai basalts was used to estimate their equilibration pressure-temperature conditions. The *P-T* evolution of peridotite xenoliths in late Cenozoic alkali basalts in Thailand has been previously studied by Promprated *et al.* (1999) who used six thermometers (Wood and Banno, 1973; Herzberg and Chapman, 1976; Bertrand and Mercier, 1985; Brey and Kohler, 1990; Ballhaus *et al.*, 1991; Witt-Eickschen and Seck, 1991) for mantle peridotite xenoliths using single minerals, mineral pairs and mineral assemblages. The equilibration temperatures and pressures of mantle peridotite xenoliths in late Cenozoic alkali basalts from Thailand are within a range of temperatures from 1000 to 1130°C within the spinel lherzolite field, at 8 to 20 kbars. The *P-T* conditions were interpreted as evidence of a heating event due to ascent of hot asthenosphere beneath Thailand.

3.5.1 Mantle xenoliths

In this study, equilibration temperatures of Denchai spinel lherzolite xenoliths were estimated from three geothermometers using single mineral and mineral pairs (Wood and Banno, 1973; Brey and Kohler, 1990; Witt-Eickschen and Seck, 1991). The PTMAFIC software (v.2.0) written by J.I. Sato (1993) and modified by J.I. Sato and V.M. Sato (1995) for IBM-compatible computers was used in thermometric and barometric calculations.

The mutual solubilities of diopside and enstatite components in clinopyroxene and orthopyroxene and the solubilities of Ca and Al in orthopyroxene in equilibrium with olivine, clinopyroxene and spinel, have been recognised as useful geothermometers of natural spinel peridotite (Wood and Banno, 1973; Brey and Kohler, 1990; Witt-Eickschen and Seck, 1991). There are no reliable geobarometers for spinel lherzolite and spinel harzburgite. However, experimental work on simple systems (CMAS; CaO-MgO-Al_2O_3-SiO_2) suggests that spinel peridotite is stable in a pressure range of approximately 8-16 kbars for temperatures of 900-1100°C (Herzberg, 1978; Gasparik, 1984). Applying Cr_2O_3 into the CMAS system increases the maximum pressure of spinel peridotite stability (O'Neill, 1981; Chatterjee and Terhart, 1985). An upper limit of 20 kbars is set by the absence of garnet (Green and Ringwood, 1970; O'Neill, 1981) and a lower limit of ~10 kbars by the absence of plagioclase in peridotite xenoliths (Green and Hibberson, 1970). Thus, temperatures were calculated assuming a pressure of 15 kbars, in the middle of the stability field for spinel lherzolite.

For the temperature calculations of three geothermometers (Wood and Banno, 1973; Brey and Kohler, 1990; Witt-Eickschen and Seck, 1991), spinel lherzolite from Samples DC5 and DC13 yield temperature estimates range between 990 and 1070°C (Table 3.12). The highest temperature estimates for all mineral pairs in these two spinel lherzolites are from Wood and Banno (1973) geothermometer, and the lowest temperature estimates are from the thermometer of Witt-Eickschen and Seck (1991). Using three geothermometers of Wood and Banno (1973), Brey and Kohler (1990) and Witt-Eickschen and Seck (1991), and an estimated pressure of 15 kbars, spinel-lherzolite from Sample DC5 yield temperature estimates range between 1000 and 1060°C with a mean value of 1030°C (6 values). Temperatures calculated from spinel lherzolite of Sample DC13 range from about 1000 to 1070°C with average values of 1040°C (6 values). The equilibration temperature of the Denchai spinel lherzolites is in the range from 1000 to 1070°C (Table 3.12).

3.5.2 Crustal xenoliths

The mineral association of clinopyroxene-plagioclase-quartz in the crustal xenoliths provides a useful geobarometer for crustal mafic granulites, proposed as an empirical geobarometer by Ellis (1980). This application requires consideration of the activity-composition relations for both coexisting clinopyroxene and plagioclase. The software THERMOCALC (v.2.7) written by Powell and Holland (1988) and modified by Powell *et al.* (1998) was applied for activity-composition calculations at P = 5 kbar and T = 550°C.

Table 3.12 Estimates temperature (°C) of spinel-lherzolites in the Denchai basalts (at 15 kbars)

Geothermometer	Minerals	Sample						Av Temp. (°C)
		DC5-1	DC5-2	DC5-3	DC5-4	DC5-5	DC5-6	
Wood & Banno (1973)	Cpx-Opx	1101	1034	1014	1033	1113	1052	1058
Brey & Kohler (1990)	Ca in Opx	977	1009	1001	1001	993	985	994
Witt-Eickschen & Seck (1991)	Al/Cr in Opx	1002	992	971	1002	973	1042	997

Geothermometer	Minerals	Sample						Av. Temp. (°C)
		DC13-1	DC13-2	DC13-3	DC13-4	DC13-5	DC13-6	
Wood & Banno (1973)	Cpx-Opx	1072	1069	1070	1064	1069	1078	1070
Brey & Kohler (1990)	Ca in Opx	1009	1001	1001	1009	1009	1001	1005
Witt-Eickschen & Seck (1991)	Al/Cr in Opx	971	1025	998	1017	1011	998	1003

Note: Av Temp. = averaged temperature

Table 3.13 Pressure (kbar) estimates of crustal xenoliths in the Denchai basalts

Geobarometer	Mineral assemblage	Assumed temperature (°C)	Mineral pairs					Averaged pressure (kbar)
			DC42-1	DC42-2	DC42-3	DC42-4	DC42-5	
Ellis (1980)	Cpx-Plag-Qtz	500	9.9	9 7	8.0	7.0	10 4	9.0
	Cpx-Plag-Qtz	600	9.3	9.1	7.1	6 0	9.8	8 3
	Cpx-Plag-Qtz	700	8 7	8.4	6.2	5 0	9.3	7.5
	Cpx-Plag-Qtz	800	8.1	7.7	5 3	4.0	8.7	6.8

In this study, only the crustal xenolith in Sample DC42 has plagioclase-clinopyroxene-quartz as coexisting phases, thus providing an opportunity to estimate pressure using Ellis (1980) geobarometer. Applying the possible range in temperature (500-800°C) appropriate to lower crustal metamorphic rocks gives an equilibration pressure for this xenolith of about 8 kbars (range 7-9 kbars; Table 3.13).

3.6 Summary

The Denchai basalts are mineralogically typical of intraplate alkali olivine basalt, with phenocrysts of olivine ± purplish clinopyroxene ± plagioclase. They often contain small xenoliths, mainly of spinel lherzolite, but including rare granulitic crustal xenoliths, as well as xenocrysts from disggregated peridotitic nodules. Olivine was the liquidus phase in all samples, joined by clinopyroxene around Fo_{83}, and plagioclase at lower temperatures. There is no evidence for high-pressure crystallisation of these phenocrysts.

Mineral compositions of spinel lherzolites in the Denchai basalts are similar to those of spinel lherzolite xenoliths worldwide, with Cr-poor, Al-rich spinels suggesting relatively fertile, not strongly depleted upper mantle peridotite compositions. The *P-T* estimates of the spinel lherzolites from three geothermometers are around 1030°C within the spinel lherzolite stability field at 8 to 20 kbars. This *P-T* condition corresponds to mantle conditions at depths of about 25 to 60 km.

The crustal-derived xenoliths consist mostly of clinopyroxene, plagioclase and rare quartz. Strain features in some plagioclases and in the single quartz xenocryst encountered indicate their origin from deep crustal fault zones. The clinopyroxene-plagioclase-quartz geobarometer suggests equilibration pressures of about 8 kbars, calculated assuming a crustal temperature of 700°C.

The whole rock compositions of the Denchai basalts is reviewed in the following chapter to determine the extent to which the composition of the parental magma has been modified by crystal fractionation, and the nature of the source mantle, including its isotopic characteristics.

Chapter 4

Geochemistry of the Denchai basalts

Basaltic magmas in continental intraplate settings are generally believed to form by decompression partial melting of an upwelling mantle plume or asthenospheric mantle. Interaction between the initial melts and the highly heterogeneous continental lithosphere is often considered to be the main cause of their compositional diversity (e.g., Arndt and Christensen, 1992; White and McKenzie, 1989). Small volumes of alkali mafic magmas may also be produced within the subcontinental lithospheric mantle (SCLM) through direct partial melting of metasomatised domains (McKenzie, 1989). Primitive continental basalts erupted within different crustal domains can record geochemical signatures of three major mantle sources (mantle plume, asthenosphere and SCLM). The extent to which the asthenospheric melts and continental lithospheric materials interact is at present controversial. The late Cenozoic lava-field provinces in Thailand (e.g., Denchai basalts) provide an opportunity to examine this debate. Detailed geochemical data for late Cenozoic intraplate basalts in the Denchai area, northern Thailand, are therefore presented in this chapter, to provide constraints on their petrogenesis and source regions, to compare their source mantle domains with those described from other parts of eastern Asia (Flower *et al.*, 1998), and to provide a framework for an evaluation of their role in the origin of the Denchai sapphires.

4.1 Sample selection and preparation

Sample locations are illustrated in Figure 3.1. Sixty least altered samples were carefully selected and prepared for whole-rock geochemical analysis. Special care was taken to avoid samples with:

(i) domains or veins of secondary alteration minerals such as quartz, carbonate, epidote and chlorite,

(ii) xenoliths,

(iii) abundant amygdales.

Samples were split into fragments and then crushed into pea-sized chips (~0.5cm across) using a Rocklabs hydraulic splitter/crusher. The small chips were then cleaned with compressed air to remove dusty materials. Approximately 30-50 g aliquots of the crushed

fragments showing no signs of weathered surfaces, vesicles, amygdale minerals, veinlets, megacrysts and steel from the crusher were ground for 1-2 minutes in a Rocklabs tungsten-carbide ring mill. All preparation procedures were carried out at the Department of Geological Sciences, Chiang Mai University, Chiang Mai, Thailand and at the School of Earth Sciences, University of Tasmania, Hobart, Tasmania, Australia.

4.2 Analytical techniques

Analytical work was carried out at the School of Earth Sciences, University of Tasmania. The samples were analysed for major elements (SiO_2, TiO_2, Al_2O_3, total Fe as FeO*, MnO, MgO, CaO, Na_2O, K_2O, P_2O_5 and loss on ignition) and a range of trace elements (Ba, Rb, Sr, Y, Zr, Nb, V, Ni, Cr and Sc). Fourteen of these samples were selected for rare earth element (REE) analysis.

Major and trace element analyses were obtained using an automated Philips PW1480 X-Ray Fluorescence (XRF) spectrometer with PW1510 sample changer. Major elements were measured from fusion discs prepared with 4.125 g Norrish flux, 0.055 g Lithium nitrate and 0.770 g sample powder. The loss on ignition (LOI) of the samples was determined by heating 1-2 g of sample at 1000°C for 12 hours.

Trace element analyses were performed on pellets made from pressed sample powder. These were manufactured using approximately 10 g of sample, which had been mixed with PVP-MC (Polyvinylpyrrolidone-Methylcellulose) binder solution prior to pressing. Trace elements were measured with a Sc-Mo tube and a Au-tube. Several local and international standard samples were measured during XRF analysis including TASBAS, TASGRAN, TASDOL, AGV1, BCR1, BHVO1, BIR1 and AW Quartz.

Rare earth elements (REE) were analysed using a HP4500 Inductively Coupled Plasma Mass Spectrometer (ICP-MS). Solutions for ICP-MS analysis were prepared using a Savillex Beaker (HF/HNO3) digestion technique. 100 mg aliquots of rock powder were weighed into 7 ml screw-top Savillex® Teflon beakers. After wetting with a few drops of ultra pure water, the sample was spiked with 0.1 ml 10 $\mu g\ g^{-1}$ Indium (In) solution. Then 2 ml HF and 0.5 ml HNO_3 were slowly added. After sealing, the beaker was placed on the hotplate at 130-150°C for 48 hours. The beaker was shaken occasionally during the digestion. During digestion, the sample beaker was removed from the hotplate twice (at the beginning and in the middle of the digestion) and placed in an ultrasonic bath for a couple of minutes to agitate the (HF +

HNO_3 + sample) mixture. The mixture was evaporated on a hotplate at 130-150°C to incipient dryness. The evaporation was repeated twice by adding 1 ml HNO_3 each time. The digestion residue was taken up using 2 ml HNO_3 and 3-5 ml ultra pure water on a hotplate. Finally, the solution was transferred into a polypropylene bottle and diluted to 100 ml with ultra pure water before ICP-MS analysis. Detection limits of ICP-MS analysis are listed in Appendix C.

Radiogenic isotope (Sr and Nd) ratios for seven representative basalts were analysed by thermal ionisation mass spectrometry (TIMS) at the Geology and Geophysics Department, Adelaide University, Australia. The analytical details have been described by O'Reilly and Zhang (1995). Averaged values of repeated standard analysis during the period of the analysis are $^{87}Sr/^{86}Sr$ = 0.710269 ±9 (2 SE, 14 analyses) for SRM 987 and $^{143}Nd/^{144}Nd$ = 0.511556 ±5 (2 SE, 10 analyses) for an internal Nd standard referred to La Jolla.

Pb isotope ratios of the seven basalts were also analysed by TIMS at the Geology and Geophysics Department, Adelaide University, Australia. All samples are handpicked rock chips leached by warm 6N HCl. A $^{207}Pb/^{204}Pb$ double-spiking technique was applied for Pb isotope analysis with precision (2 SD) on the corrected data for a rock sample $^{206}Pb/^{204}Pb$, $^{207}Pb/^{204}Pb$ and $^{208}Pb/^{204}Pb$ ratios of ±0.003, ±0.003 and ±0.001 respectively (Woodhead *et al.*, 1995). The double-spike was calibrated using SRM 981 standard values of $^{206}Pb/^{204}Pb$ = 16.937, $^{207}Pb/^{204}Pb$ = 15.492 and $^{208}Pb/^{204}Pb$ = 36.708 by Woodhead *et al.* (1995). Pb isotope ratios were corrected for mass fractionation by applying a correction factor of 0.12 %/a.m.u. to SRM 981 (Todt *et al.*, 1984).

4.3 Magmatic grouping

Petrographic classification in Chapter 3 suggested that the Denchai basalts may be assigned to four groups (A, B, C and D), each with a distinct phenocryst and microphenocryst assemblage (Table 3.1). Whole rock chemical compositions of each group are also distinct and consistent with the petrographic classification. On the basis of petrographic character (Chapter 3), and the new compositional data displayed in Figures 4.1-4.4, the Denchai basalts are subdivided into four compositional groups, termed Groups A, B, C and D. These groups are well defined by the SiO_2 versus P_2O_5 diagram (Fig.4.2), and other key diagnostic compositional features of each group are discussed below.

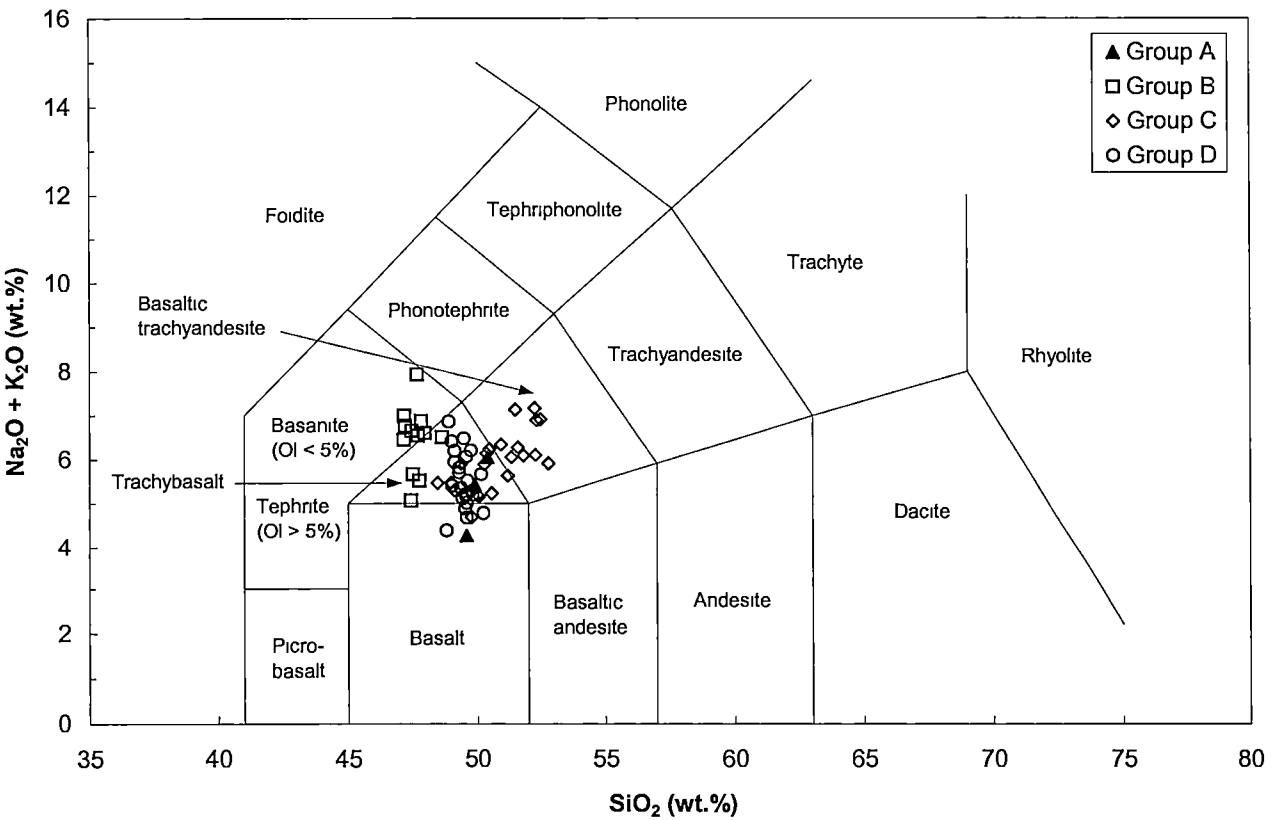

Figure 4.1 Chemical classification and nomenclature of the Denchai basalts using the total alkalis versus silica classification diagram (Le Bas *et al.*, 1986)

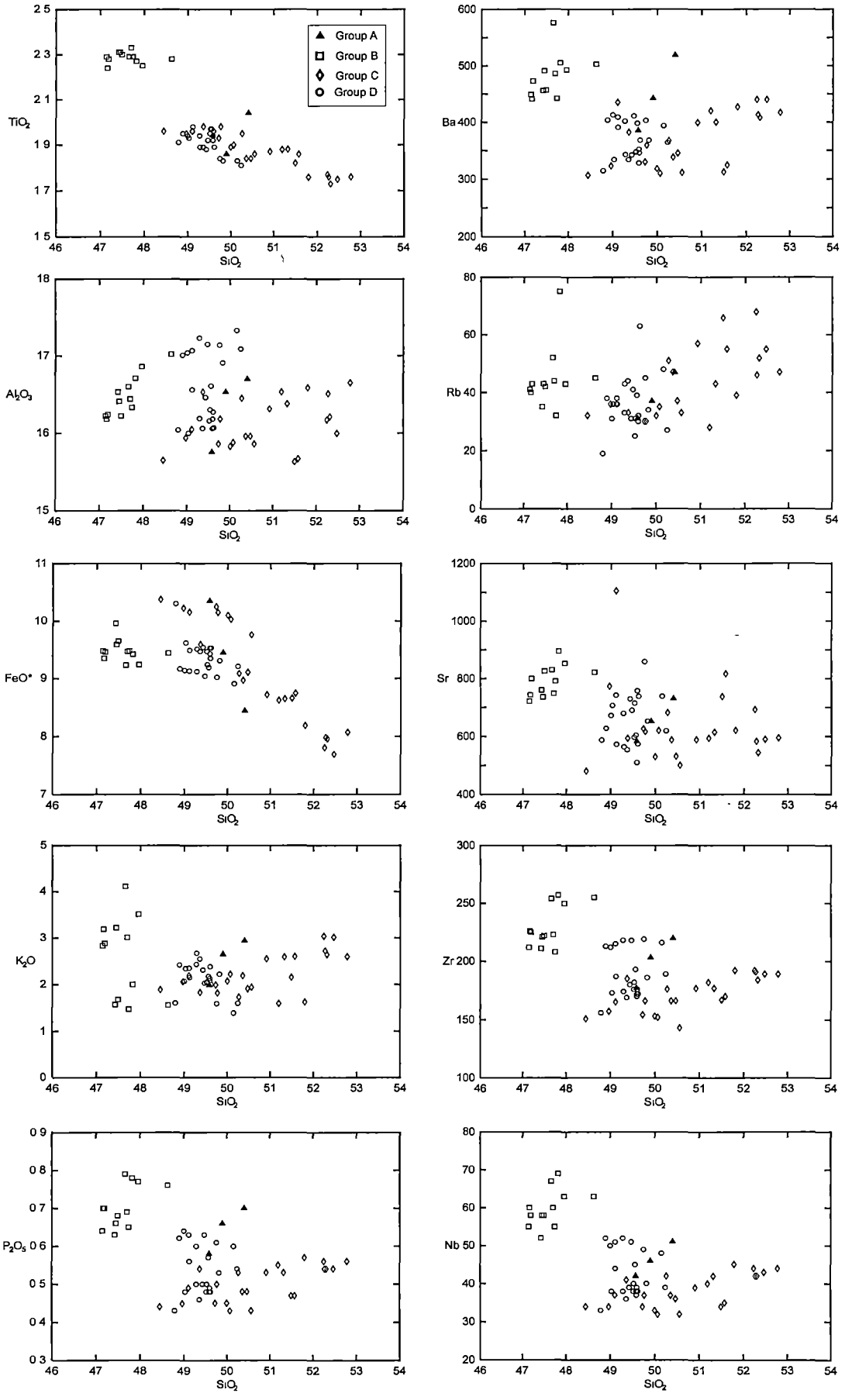

Figure 4.2 Variation diagrams of major (wt%), minor and trace (ppm) elements plotted against SiO_2 (wt%)

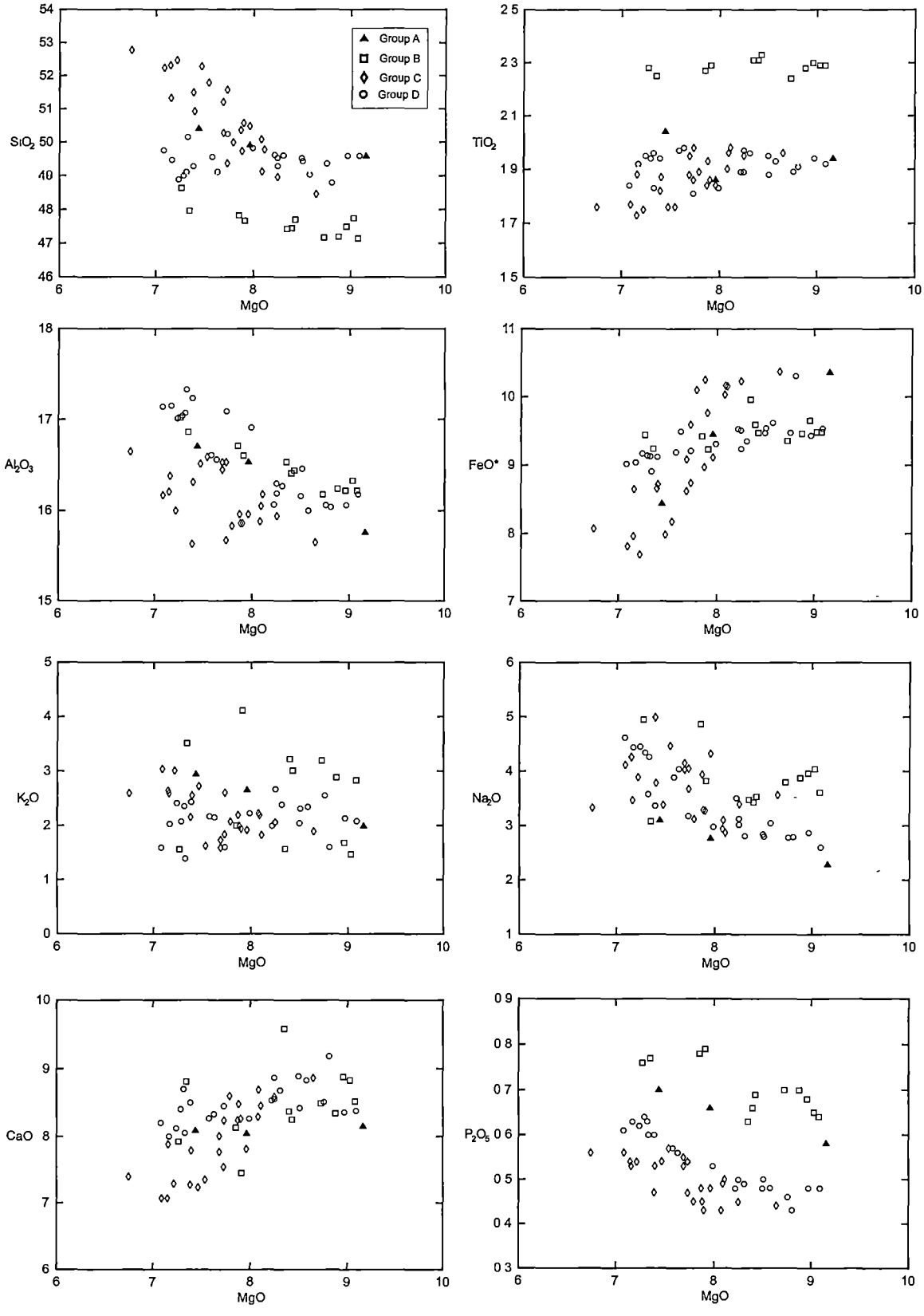

Figure 4.3 Variation diagrams of major (wt%), minor and trace (ppm) elements plotted against MgO (wt%)

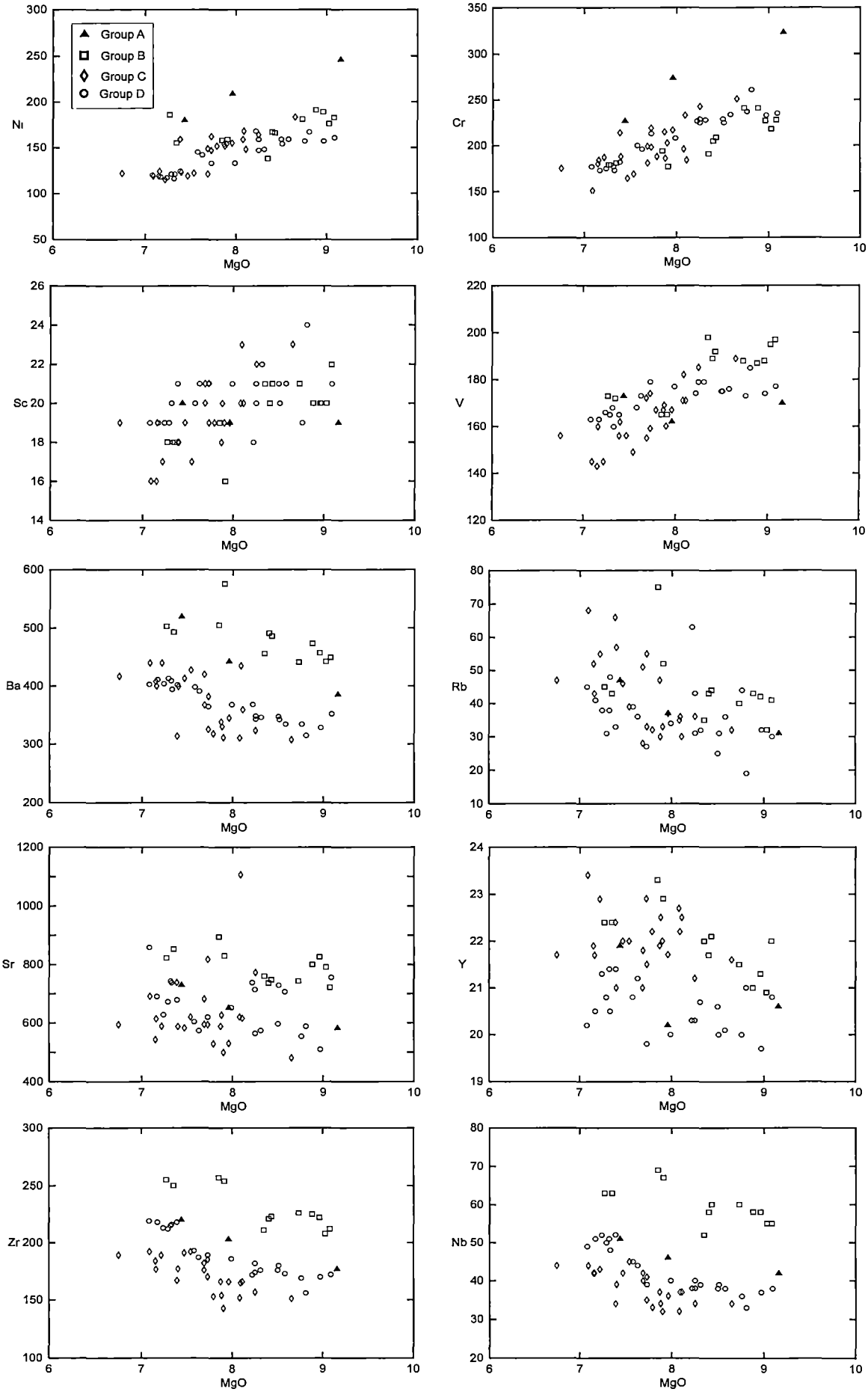

Figure 4.3 (Continued)

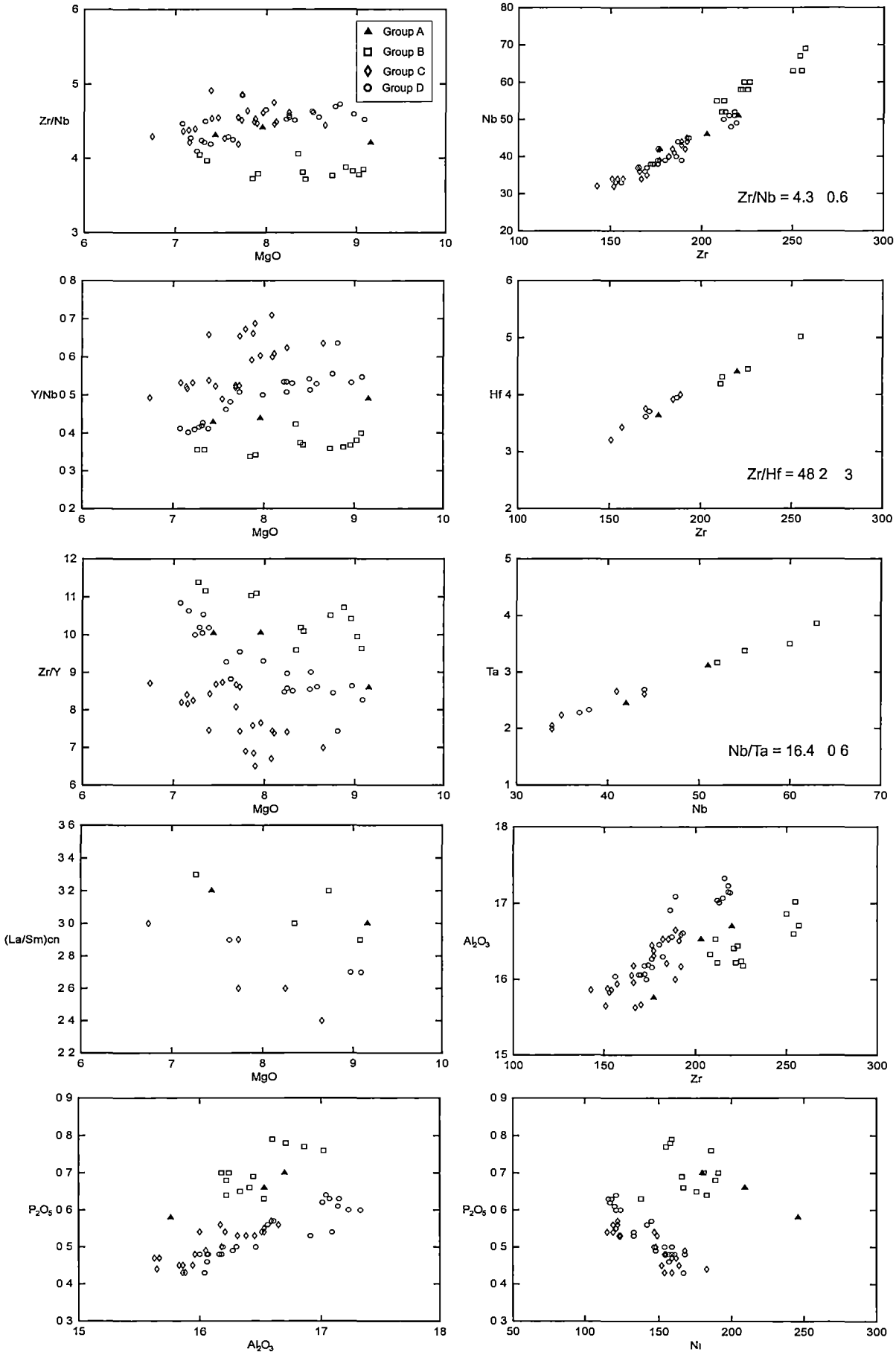

Figure 4.4 Variation diagrams of major (wt%), minor and trace (ppm) elements and element ratios (ppm) of the Denchai basalts

4.4 Geochemistry

4.4.1 Introduction

Although igneous rocks, particularly volcanic rocks, are susceptible to alteration, it is well documented that least altered samples can be informative with regards to their primary affinities if due care is taken with the selection of appropriate elements and element ratios used. The least altered (LOI < 4wt%) Denchai basalts (Tables 4.1-4.4) are all broadly basaltic with alkali affinities. Following recalculation of all analyses to 100% volatile (LOI)-free, the Denchai basalts are best classified as trachybasalts or basaltic trachyandesites on the basis of total alkalis (Na_2O+K_2O) versus SiO_2 classification diagram (Fig.4.1), although a few samples extend into the basalt or basanite compositional fields. Their SiO_2 contents range from 47.1 to 52.8wt%, MgO contents range between 6.8 and 9.2wt%, and *mg*-number [Mg# = $Mg/(Mg+Fe^{2+})$] values range between 0.58 and 0.63. Compositional variations for the Denchai basalts are shown in a series of variation diagrams in which major, minor and trace elements and element ratios are plotted against MgO and SiO_2 in Figures 4.2-4.3.

The geochemistry of the Denchai basalts presented in this study has been interpreted using major and trace elements (including large ion lithophile elements (LILE: Rb, Ba, K, Th and Sr), high field-strength elements (HFSE: Nb, Ta, P, Hf, Zr, Ti, Y, Yb) and rare earth elements (REE)), and Sr-Nd-Pb isotopic compositions. The first task was to examine the possible petrogenetic relationships between the four Groups. Then isotopic data are used to evaluate relationships proposed by major and trace element data. The four groups of studied basalt are described in the following sections.

4.4.2 Major, minor and trace elements

Group A

The three Group A basalts have distinctly higher Ni and Cr contents at a given MgO than most other Denchai basalts. Most major and trace elements increase with increasing fractionation, whereas FeO*, Ni, Cr decrease, and CaO, Sc and V show little change as MgO decreases from 9.2 to 7.4wt% (Fig.4.3).

Group B

Group B basalts have distinctly lower SiO_2 contents, and are more SiO_2 undersaturated than the other groups, with most plotting as basanites (Fig.4.1).

Table 4.1 Major and trace element compositions of Group A basalts

Sample	DC25	DC28	DC42
Major elements (wt%)			
SiO_2	49 90	49 58	50 40
TiO_2	1.86	1 94	2 04
Al_2O_3	16 53	15 76	16 70
FeO*	9 45	10.35	8.44
MnO	0 19	0.21	0 15
MgO	7.96	9.16	7.44
CaO	8.04	8.15	8.08
Na_2O	2 76	2.28	3.10
K_2O	2 65	1.99	2 94
P_2O_5	0.66	0.58	0.70
Total	100 00	100 00	100.00
LOI	2 95	2 79	1.98
Mg#	0 60	0.61	0.61
Trace elements (ppm)			
Ba	442	385	519
Rb	37	31	47
Nb	46.3	41.5	51.0
Sr	652	583	730
Zr	203	177	220
Y	20 2	20.6	21.9
Ni	209	246	180
Cr	274	323	227
V	162	170	173
Sc	18 7	19 2	20.0
Th		2.8	4 2
U		0 8	1.2
Pb		2.7	3 8
Hf		3.6	4 4
Ta		2.4	3.1
Li		2 6	5 2
Be		2 0	2.4
Co		55.5	40 7
Cu		55.3	48 7
Zn		86.3	73 4
Ga		18.1	18 1
Mo		3 4	4.2
Sn		2 1	2.2
Sb		0 1	0 1
Cs		0.5	1.7

Total Fe as FeO*, Mg# = $Mg/(Mg+Fe^{2+})$, LOI = Loss on Ignition

Analyses recalculated to 100% volatile free

Table 4.2 Major and trace element compositions of Group B basalts

Sample	DC5	DC13	DC14	DC19	DC23	DC27	DC32	DC43	DC55	DC56	DC61	DC62
Major elements (wt%)												
SiO_2	47.96	47 16	47.70	47 74	47.82	47.45	47.49	48.63	47.66	47.42	47.14	47.19
TiO_2	2 25	2.24	2 33	2 29	2 27	2.31	2 30	2 28	2 29	2.31	2 29	2.28
Al_2O_3	16 86	16.18	16 44	16 33	16.71	16 41	16.22	17.02	16.60	16.53	16 22	16 24
FeO*	9.24	9 35	9.47	9.48	9.42	9 59	9 65	9.44	9 23	9.96	9.48	9 46
MnO	0 17	0.16	0 16	0.16	0 17	0 15	0.16	0 16	0 16	0 17	0.17	0.17
MgO	7.35	8.73	8.43	9.03	7 85	8 40	8 96	7.27	7 91	8.35	9 08	8.88
CaO	8.81	8 49	8.25	8.83	8.13	8.37	8.88	7 92	7 45	9.58	8 52	8.34
Na_2O	3 08	3.80	3.53	4.04	4 86	3.43	3 96	4.95	3 82	3 48	3.61	3.88
K_2O	3.51	3.19	3.01	1.47	2.00	3.22	1.68	1 56	4 11	1.57	2 83	2.88
P_2O_5	0 77	0.70	0.69	0 65	0.78	0 66	0 68	0 76	0 79	0.63	0 64	0.7
Total	100 00	100 00	100 00	100.00	100 00	100.00	100 00	100.00	100.00	100 00	99 98	100 02
LOI	3.85	2.43	2 48	2.89	2 28	2.29	3 37	3.37	2.56	3 81	2.40	2 50
Mg#	0 59	0.62	0.61	0.63	0 60	0 61	0 62	0.58	0 60	0.60	0.63	0.63
Trace elements (ppm)												
Ba	493	441	486	442	505	491	457	503	576	456	449	473
Rb	43	40	44	32	75	43	42	45	52	35	41	43
Nb	62.6	59 7	59.5	55 0	68 9	57.9	58 1	62.8	66.6	52 1	55.1	57 9
Sr	853	743	748	791	895	736	826	822	830	760	721	800
Zr	250	226	223	208	257	221	222	255	254	211	212	225
Y	22.4	21 5	22.1	20.9	23 3	21 7	21.3	22.4	22.9	21.6	21 8	20.7
Ni	155	181	166	176	158	167	189	186	159	138	183	191
Cr	181	241	209	218	194	205	227	179	177	191	228	241
V	172	188	192	195	165	189	188	173	165	198	197	187
Sc	18.2	20 6	20 5	20.3	18 7	19.6	19.9	17.6	15.7	20.8	21.6	19.6
Th		4.4						4.7		4.1	4.1	
U		1.4						1.5		1.2	1.2	
Pb		3 0						3.2		2.9	2.9	
Hf		4 4						5 0		4 2	4.3	
Ta		3 5						3 9		3.2	3 4	
Li		6.9						7 7		6.6	5 6	
Be		2.6						2 9		2.2	2 4	
Co		38.4						37 0		38 7	41.0	
Cu		45.4						39.0		45.7	48 4	
Zn		76 7						75 4		77.6	77.3	
Ga		19 2						19.3		18.6	19.0	
Mo		4 9						3.8		2.5	4.3	
Sn		2.5						2.3		2.1	2.2	
Sb		0.2						0.1		0.1	0 1	
Cs		0.7						0 8		0 9	0.6	

Total Fe as FeO*, Mg# = $Mg/(Mg+Fe^{2+})$, LOI = Loss on Ignition; Analyses recalculated to 100% volatile free

Table 4.3 Major and trace element compositions of Group C basalts

Sample	DC15	DC16	DC17	DC20	DC21	DC22	DC29	DC30	DC31	DC33	DC34
Major elements (wt%)											
SiO_2	52.78	50 00	51 33	50.56	49.73	49.77	50.07	48.45	50.27	50 47	50 36
TiO_2	1.76	1 89	1 88	1 86	1.93	1 98	1 90	1.96	1.95	1.84	1.84
Al_2O_3	16.65	15 83	16.38	15 86	15.86	16.18	15 88	15.65	16 45	15.96	15 96
FeO*	8 07	10 10	8 65	9 76	10.25	10.15	10 03	10.37	9 09	9.11	8.97
MnO	0.14	0.16	0 13	0.15	0 16	0.16	0.16	0 16	0.14	0.14	0.15
MgO	6.75	7 79	7.16	7 90	7.88	8.11	8 08	8.65	7.69	7.96	7.87
CaO	7.39	8.60	7 88	8.26	8.48	8.45	8 29	8 86	8.00	7.81	8.24
Na_2O	3.33	3.12	3.47	3 28	3.29	2 87	2 94	3 56	4.15	4.32	3.94
K_2O	2.59	2.07	2 59	1 94	1.99	1 82	2.22	1.89	1 73	1.91	2.19
P_2O_5	0 56	0.45	0.53	0 43	0.45	0 50	0.43	0.44	0 53	0.48	0 48
Total	100 00	100 00	100.00	100.00	100 00	100.00	100.00	100 00	100.00	100.00	100 00
LOI	3 29	2.05	2.61	2.32	2.85	2.85	1.70	2.12	3.54	3.39	2.49
Mg#	0 60	0.58	0.60	0 59	0.58	0 59	0.59	0 60	0.60	0.61	0.61
Trace elements (ppm)											
Ba	417	318	400	311	330	359	310	307	367	345	338
Rb	47	32	43	33	30	30	35	32	51	37	47
Nb	44.4	33.2	41 5	31.9	33.7	37 2	31.7	33 5	42.0	35 7	36 8
Sr	595	529	614	500	627	616	620	481	681	530	588
Zr	189	153	177	143	154	166	152	151	176	166	166
Y	21.7	22 2	21.7	22.0	22.5	22 5	22 7	21.6	21.8	21 7	21 9
Ni	122	152	124	154	152	148	159	183	149	155	154
Cr	175	188	184	203	186	184	196	251	199	217	215
V	156	167	160	160	169	171	171	189	172	167	167
Sc	18.6	19.4	19 1	19.0	19 5	20.2	20.0	23 1	20.6	19.2	17.9
Th	5 0							2 7			
U	1 3							0.8			
Pb	4 3							2.5			
Hf	4.0							3 2			
Ta	2.6							2.0			
Li	5.4							7 5			
Be	2.2							1 6			
Co	33 3							44.1			
Cu	43 1							56.6			
Zn	71 6							88.8			
Ga	18.3							17.8			
Mo	2.9							2 2			
Sn	2.9							1.8			
Sb	0.1							0.1			
Cs	3.2							0.7			

Total Fe as FeO*, Mg# = $Mg/(Mg+Fe^{2+})$, LOI = Loss on Ignition; Analyses recalculated to 100% volatile free

Table 4.3 Continued

Sample	DC35	DC36	DC37	DC38	DC39	DC40	DC44	DC47	DC57	DC58	DC59	DC60
Major elements (wt%)												
SiO_2	51.58	52.47	51.50	52 24	52.31	48.97	49 11	49.37	50.92	51 20	52 27	51.80
TiO_2	1.86	1.75	1 82	1.77	1 73	1.95	1.96	1.98	1 87	1 88	1.76	1.76
Al_2O_3	15.67	16 00	15.63	16.17	16.21	15 94	16.05	16.53	16.31	16 53	16.51	16.59
FeO*	8 74	7 69	8.66	7 81	7 96	10 23	10.16	9.59	8 72	8.62	7.98	8.18
MnO	0.14	0.13	0 14	0 12	0.12	0.16	0.16	0.15	0.14	0 14	0 14	0 13
MgO	7.73	7 22	7.39	7.09	7 15	8 25	8.09	7 73	7.40	7.69	7.47	7.54
CaO	7.54	7 29	7 27	7.07	7.07	8 58	8 69	8.24	7.78	7.77	7 23	7.35
Na_2O	3.68	3.89	4.99	4.12	4 26	3.40	3.10	4 05	3.79	4.03	3 38	4.47
K_2O	2 60	3.01	2 15	3.04	2.64	2 06	2.19	1.83	2 55	1 59	2.72	1.62
P_2O_5	0 47	0 54	0.47	0 56	0.54	0.45	0.49	0.54	0.53	0.55	0.54	0 57
Total	100 00	100.00	100 00	100 00	100.00	100 00	100 00	100 00	100 01	100 00	100 00	100.01
LOI	2 05	2 20	2 26	2.44	2.92	2 44	1.31	2.28	2.66	2.70	2 94	3.29
Mg#	0.61	0 63	0.60	0.62	0 62	0.59	0.59	0 59	0.60	0.61	0 63	0.62
Trace elements (ppm)												
Ba	325	440	313	440	408	323	435	382	399	420	413	427
Rb	55	55	66	68	52	36	36	33	57	28	46	39
Nb	35.3	42.7	34.2	44 0	41.8	34.3	36 6	41 0	39.2	39.8	42.4	44 9
Sr	817	589	738	691	544	773	1106	593	588	594	582	620
Zr	170	189	167	192	184	157	165	185	177	182	191	192
Y	22 9	22.9	22.4	23 4	21 9	21.2	22 2	21.5	20.7	21 2	21 8	21 5
Ni	162	115	159	119	119	164	168	147	123	121	119	122
Cr	219	187	214	151	180	243	233	198	188	181	164	169
V	159	145	156	145	143	185	182	174	162	155	156	149
Sc	19 2	16.9	17 7	15.9	15 6	22.4	22.6	21 0	17.8	19.9	19.1	16 8
Th	4 1					3.0		3 9				
U	1.3					0.8		1.1				
Pb	4.2					2.7		3.2				
Hf	3.8					3.4		3.9				
Ta	2 2					2.1		2 7				
Li	7.1					7.4		8 2				
Be	2.0					1 7		2.0				
Co	37 7					43 9		39 3				
Cu	50 1					55.8		53.0				
Zn	78 3					89.8		82 5				
Ga	16.3					19.4		18.8				
Mo	2.0					2.5		3.2				
Sn	2.8					1.9		2.2				
Sb	0 1					0.1		0 1				
Cs	1 7					1.1		0 9				

Table 4.4 Major and trace element compositions of Group D basalts

Sample	DC1	DC2	DC3	DC4	DC6	DC8	DC10	DC11	DC12	DC41	DC45
Major elements (wt%)											
SiO_2	49.82	50 24	48 89	49 11	50.15	49 52	49.60	49 59	49.53	49 03	49 59
TiO_2	1 83	1.81	1.95	1 96	1 83	1.95	1 96	1.92	1 97	1.93	1.94
Al_2O_3	16.91	17 09	17.01	17 07	17 33	16 16	16.27	16 18	16.30	16 00	16 06
FeO*	9 31	9.21	9.17	9.13	8 91	9 47	9.35	9 53	9.24	9 62	9 43
MnO	0 16	0.15	0.15	0.16	0 15	0.15	0 15	0 15	0.15	0 15	0 16
MgO	7.99	7.73	7.24	7 32	7.33	8 50	8 31	9 09	8.25	8.58	8 97
CaO	8.26	8.45	8.12	8 70	8 05	8 89	8 68	8 38	8 87	8.83	8 36
Na_2O	2.98	3.18	4.45	3 58	4.26	2 84	2 81	2 60	3 13	3.05	2 87
K_2O	2.22	1.60	2.41	2.35	1.39	2 04	2.38	2 08	2 06	2.34	2.13
P_2O_5	0 53	0 54	0.62	0 63	0 60	0.48	0.49	0 48	0 50	0.48	0.48
Total	100.00	100 00	100 00	100 00	100.00	100 00	100 00	100.00	100 00	100.00	100 00
LOI	3.05	3 89	2.14	2 77	3.66	2.19	1 98	3.23	2.34	2 36	3 42
Mg#	0 60	0.60	0 58	0.59	0 59	0.62	0 61	0.63	0 61	0 61	0.63
Trace elements (ppm)											
Ba	368	364	404	409	394	347	346	352	348	334	328
Rb	34	27	38	38	48	25	32	30	31	36	32
Nb	39.8	39.1	51.5	51 1	48.2	38 3	38 8	37.5	39.5	37.6	37 0
Sr	652	619	628	743	738	597	574	757	714	707	510
Zr	186	189	213	215	216	176	176	172	182	173	170
Y	20.0	19.8	21.3	21.4	20 5	20 6	20.7	20 8	20.3	20.1	19.7
Ni	133	133	117	116	121	159	148	161	147	159	157
Cr	208	213	175	177	173	229	228	235	229	234	233
V	177	179	166	168	160	175	179	177	179	176	174
Sc	20 5	21.3	19 1	20.0	18 2	20.6	21.6	21 3	20.7	21.4	20 1
Th								3 5			3 5
U								1 0			1.0
Pb								3.2			3.1
Hf								3.7			3 6
Ta								2.3			2.3
Li								6.6			7.4
Be								1.9			1.9
Co								41 0			40.3
Cu								41 2			42 5
Zn								82.9			80.4
Ga								18 0			18 5
Mo								2 7			2 2
Sn								2.0			1.9
Sb								0.1			0 1
Cs								0.3			0.5

Total Fe as FeO*, Mg# = Mg/(Mg+Fe^{2+}), LOI = Loss on Ignition, Analyses recalculated to 100% volatile free

Table 4.4 Continued

Sample	DC46	DC48	DC49	DC50	DC51	DC52	DC53	DC54	DC64	DC65	DC66
Major elements (wt%)											
SiO_2	49.62	49.29	49.00	49.47	49 28	49.75	49.12	49.56	49 36	49.43	48 79
TiO_2	1.89	1.89	1.94	1.92	1.94	1 84	1.98	1.97	1.89	1.88	1.91
Al_2O_3	16 07	16.19	17.04	17 15	17 23	17.14	16.56	16.61	16 06	16 46	16.04
FeO*	9.53	9 51	9 14	9.04	9 12	9.02	9 49	9.19	9 47	9.54	10 30
MnO	0.15	0 14	0.16	0 14	0.15	0 17	0.16	0 20	0.15	0 16	0.16
MgO	8 22	8.25	7 29	7.17	7 39	7.08	7 63	7.58	8 76	8 51	8 81
CaO	8.53	8.55	8.40	8 00	8 50	8 20	8 33	8 27	8 51	8 42	9 18
Na_2O	3 51	3 02	4 34	4.44	3 37	4.62	4 04	3 89	2 78	2.80	2 79
K_2O	2.00	2 67	2.07	2.03	2 43	1.59	2 15	2.17	2.55	2 31	1 60
P_2O_5	0 48	0.50	0.64	0.63	0 60	0.61	0.56	0.57	0.46	0 50	0 43
Total	100.00	100.00	100 00	100.00	100.00	100 00	100.00	100.00	99.99	100 01	100.01
LOI	2 66	2 79	2.42	2.53	2 46	2.77	2 50	2.40	3.42	2.65	2 38
Mg#	0.61	0 61	0.59	0 59	0.59	0 58	0.59	0.60	0.62	0 61	0.60
Trace elements (ppm)											
Ba	368	343	413	411	402	403	391	398	334	342	315
Rb	63	43	31	41	33	45	36	39	44	31	19
Nb	37.7	38 2	50.1	51 2	51.6	49 1	43.6	44 8	36.0	38 9	33 0
Sr	738	564	672	690	679	859	573	604	554	729	588
Zr	172	174	212	218	218	219	187	193	169	180	156
Y	20 3	20 3	20.8	20 5	21.4	20 2	21.2	20 8	19.5	20 3	20.9
Ni	168	159	121	118	124	120	142	145	157	154	167
Cr	227	225	179	173	182	177	196	200	237	225	261
V	174	179	165	163	165	163	173	168	173	175	185
Sc	18.4	20.4	19 4	18 6	21.0	18.9	21 2	20.1	19.0	20.4	23 6
Th							3 9				
U							1.1				
Pb							3.1				
Hf							4 0				
Ta							2 7				
Li							8.0				
Be							2.1				
Co							38 6				
Cu							52.4				
Zn							81 1				
Ga							18 5				
Mo							3.2				
Sn							2.1				
Sb							0.1				
Cs							1.0				

Their MgO contents range between 7.3 and 9.1wt%, and Mg# values = 0.58-0.63. All twelve samples are distinctly enriched in TiO_2, P_2O_5 and other high field strength elements (HFSE) such as Zr and Nb, as well as consistently higher K-group elements (K_2O, Ba and Rb) and Sr contents (Table 4.2). Four of the five Group B basalts with highest LOI values also have significantly reduced K_2O contents, possibly due to slight but significant alteration of groundmass glass. This is supported by consideration of K_2O-REE plots further on.

Within Group B, the basalts show smooth fractionation trends of increasing SiO_2, Al_2O_3, P_2O_5 and probably K_2O and Na_2O, and slightly decreasing FeO* and CaO, with decreasing MgO, and no change apparent in TiO_2 across the MgO range (Fig.4.3). Ni, Cr, V and Sc show moderate decreases with diminishing MgO contents (Fig.4.3), whereas Ba, Sr, Zr, Nb and Y contents increase. K_2O and Rb contents show more dispersion than expected to result from simple fractionation, and this may be due to alteration. These compositional changes can be modelled by limited fractionation of ol + cpx phenocryst compositions, relating the least (DC19) and most fractionated (DC5) members of Group B basalts. A successful least squares model (GenMix; Le Maitre, 1993; Table 4.5) involves removal of 3.75% of olivine (Fo85) + 1.25% of clinopyroxene (Mg# 80) to fractionate from 9.0wt% MgO DC19 to produce 7.4wt% MgO DC5). However, the best fit least square calculation is inconsistent with cotectic proportions indicating that accumulation has occurred.

Group C

Group C basalts have the highest and largest range of SiO_2 contents (47.9-52.3wt%) with their MgO contents range between 6.8 to 8.6wt%, and Mg# values = 0.58-0.63 (Table 4.3). On many plots of major and minor elements against MgO or SiO_2 (Figs.4.2-4.3), the Group C basalts show well-defined fractionation trends. Unlike the other Groups, Group C basalts show a significant increase of SiO_2 as MgO decreases during fractionation from 8.6 to 6.8wt%, coupled with decreases in CaO, FeO*, TiO_2, Cr, Ni, V and Sc, and increases in K-group elements, Al_2O_3, P_2O_5 and HFSE (Fig.4.3). This trend of increasing SiO_2 paralleled by a sharp decrease in FeO*, TiO_2 and V is best accounted for Ti-magnetite joining the fractionation sequence involved in production of Group C basalts at an earlier stage than other basalt groups (in which Ti-magnetite fractionation never occurred; Figs.4.2-4.3). Increased levels of HFSE and P_2O_5 in the more SiO_2-rich Group C basalts would not be produced if this SiO_2-enrichment were the result of contamination by upper continental crust. Least square calculations show that these compositional changes can be modelled by limited fractionation of ol + cpx + plag + Ti-mt compositions, relating the least (DC30) and more fractionated (DC36) members of Group C basalts. The best least squares model (Table 4.6) using measured microphenocryst compositions involves removal of of 6.96% of olivine

Table 4.5 Results of Group B basalts from least square calculations

Reactants	% amounts	SiO_2	TiO_2	Al_2O_3	FeO	MgO	CaO	P_2O_5	Sum
DC5	95 00%	47.96	2 25	16 86	9.24	7 35	8 81	0.77	93 23
olivine	3 75%	39 74	0.03	0 06	14 01	45.38	0.21		99 43
cpx	1.25%	48 06	1.73	6 36	5.91	13 70	23.31		99 07
DC19	100.00%	47.74	2 29	16.33	9 48	9 03	8.83	0 65	94.34
Reactants		47 74	2 29	16 33	9.48	9 03	8.83	0 65	
Products		47 65	2.16	16 09	9 38	8 86	8 67	0.73	
Differences		0 09	0.12	0 23	0.10	0.17	0 16	-0.08	
Residual Sum Squares			0 15						
Distance			0.39						

Table 4.6 Results of Group C basalts from least square calculations

Reactants	% amounts	SiO_2	TiO_2	Al_2O_3	FeO	MgO	CaO	Na_2O	K_2O	P_2O_5	Sum
DC36	59 27%	52.47	1 75	16 00	7.69	7.22	7 29	3 89	3.01	0 54	99 87
olivine	6 96%	37.83	0.04	0 03	26.03	36.62	0 29				100 84
cpx	10 43%	51.05	1 06	4.55	6 03	15 79	21.03	0 56			100 07
plag	18 16%	52.64	0 07	30.29	0 49	0.05	12.58	4 21	0.38		100 71
mt	5 17%	0 07	21 17	5.39	64 40	4.35	0.08				95 46
DC30	100.00%	48 45	1 96	15 65	10.37	8 65	8.86	3 56	1.89	0.44	99.84
Reactants		48 45	1 96	15.65	10.37	8.65	8 86	3 56	1 89	0 44	
Products		48 63	2 26	15.74	10.41	8.71	8 83	3 13	1 86	0 32	99 89
Differences		-0.17	-0 30	-0 10	-0.04	-0.06	0 04	0.43	0 04	0 12	
Residual Sum Squares			0.34								
Distance			0.58								

Table 4.7 Results of Group D basalts from least square calculations

Reactants	% amounts	SiO_2	TiO_2	Al_2O_3	FeO	MgO	CaO	P_2O_5	Sum
DC52	92.66%	49.75	1.84	17.14	9 02	7 08	8.20	0.61	93.63
olivine	4 49%	39 22	0.04	0 06	16.61	43 94	0.23		100.10
cpx	2 85%	48.28	1 93	5.96	6.93	13.57	22 25		98.92
DC11	100 00%	49.59	1.92	16.18	9 53	9 09	8 38	0.48	95 17
Reactants		49 59	1.92	16 18	9.53	9.09	8.38	0 48	
Products		49.23	1 76	16.06	9 30	8.92	8 24	0.56	
Differences		0 36	0.16	0 12	0 23	0 17	0 14	-0 08	
Residual Sum Squares			0.28						
Distance			0 53						

Note cpx = clinopyroxene, plag = plagioclase, mt = Ti-magnetite

(Fo71) + 10.43% of clinopyroxene (Mg# 87) + 18.16% of plagioclase (An61) + 5.17% of Ti-magnetite to fractionate 8.6wt% MgO (DC30) to 7.2wt% MgO (DC36). The best fit least square calculation of Group C samples is inconsistent with cotectic proportions indicating accumulation has occurred.

Group D

Twenty-two Group D basalts have broadly similar compositions to those in Group C. In terms of SiO_2 contents, Group D basalts (48-50wt% SiO_2) fall largely between those of Group B and Group C. However, unlike Group C basalts, the Group D basalts show no increase in SiO_2 during fractionation from 9wt% to 7wt% MgO, but over this interval CaO, FeO*, Ni and Cr decrease, and Al_2O_3, Na_2O, P_2O_5, and both K-group elements and HFSE increase. The P_2O_5 contents of Group D basalts are consistently slightly higher than those of Group C and less than those of Groups A and B (Figs.4.2-4.3). The fractionation scheme relating the least (DC11) and most fractionated (DC52) members of Group D involves removal of ol + cpx. The best least squares model (Table 4.7) using measured microphenocryst compositions involves removal of of 4.25% of olivine (Fo82) + 2.85% of clinopyroxene (Mg# 89) to fractionate 9.1wt% MgO (DC11) to 7.1wt% MgO (DC52). Again, the best fit least square calculation is inconsistent with cotectic proportions indicating that accumulation has occurred.

4.4.3 REE and primitive mantle-normalised element variation patterns

The chondrite-normalised REE patterns of all Denchai basalts (Table 4.8) are remarkably similar shaped, smooth LREE-enriched patterns with moderate HREE depletions (Fig.4.5). Plots of relative LREE enrichment chondrite-normalised La/Sm $(La/Sm)_{cn}$ versus slope of the whole pattern of chondrite-normalised La/Yb $(La/Yb)_{cn}$ show that Groups A and B basalts have stronger LREE enrichment and slightly steeper slopes than Groups C and D basalts, and that the trend formed by all data extends through the origin (Fig.4.6). No patterns show any Eu anomaly, indicating that plagioclase was not fractionated during the generation and evolution of these magmas.

Plots of $(La/Yb)_{cn}$ versus typical HFSE (e.g., Zr), K-group elements (Ba) and P_2O_5 show linear trends for all Denchai basalts that extend to the origin (Fig.4.6), suggesting a control by partial melting, and source mantle composition, and precluding significant crustal contamination. However, two Group B basalts plot well away from this trend to low K_2O at a given (La/Yb_{cn}), suggesting K_2O loss by alteration, as argued earlier.

Table 4.8 Rare earth element (REE) compositions of representative Denchai basalts

Sample	DC28	DC42	DC13	DC43	DC56	DC61	DC15	DC30	DC35	DC40	DC47	DC11	DC45	DC53
Group	A	A	B	B	B	B	C	C	C	C	C	D	D	D
La	22.98	28 41	28.03	31 47	26.06	26.26	24 63	17.39	20 58	19.26	23.15	20 36	19.97	23.25
Ce	44.78	58 46	56.96	65 07	54 05	54.27	50 17	36.62	42 80	39 87	47.58	42.36	41 65	47.81
Pr	5.41	6.99	6 79	7 60	6.38	6.47	5.98	4.59	5 26	4 87	5.55	5 16	5.04	5.64
Nd	21.88	27 20	27.09	29 99	25 90	26.52	23 46	19.11	21 67	20.02	22.35	20.86	20 67	22.42
Sm	4 82	5 62	5.57	6 04	5 43	5 71	5.10	4 48	4.95	4 60	4.94	4 70	4 65	4 95
Eu	1.61	1 83	1 80	2.01	1 81	1.88	1 53	1 52	1.50	1 57	1.69	1 56	1.55	1.66
Gd	4 77	5.35	5 39	5.69	5 33	5.45	4.85	4 71	4.98	4 85	4.91	4 68	4.65	4 85
Tb	0.72	0 78	0 78	0.85	0 81	0.81	0 76	0.73	0.77	0 74	0.75	0.72	0.72	0 75
Dy	4.00	4 36	4 26	4.55	4.36	4.39	4 35	4.06	4.37	4 27	4.17	3 98	4.03	4 23
Ho	0.79	0 82	0 79	0.86	0 84	0.84	0 85	0.81	0.87	0 84	0.81	0 78	0.80	0 83
Er	2.08	2 24	2.17	2.29	2 26	2 20	2 30	2.18	2.34	2.27	2 20	2.08	2.11	2 17
Yb	1 72	1.89	1 80	1 96	1 88	1.85	1 94	1 83	1.99	1.92	1 85	1.83	1.77	1 88
Lu	0 26	0.28	0 25	0 28	0.27	0 27	0.29	0 26	0 29	0.28	0 28	0.26	0 26	0.27
$(La/Yb)_{cn}$	9 0	10.2	10.6	10.9	9 4	9 6	8.6	6 5	7 0	6.8	8.5	7.5	7 6	8.4
$(La/Sm)_{cn}$	3 0	3.2	3 2	3.3	3 0	2 9	3 0	2 4	2.6	2.6	2.9	2 7	2 7	2.9
$(Gd/Yb)_{cn}$	2 2	2.3	2 4	2 3	2.3	2 4	2.0	2.1	2 0	2.0	2.1	2.1	2 1	2.1

cn = chondrite-normalised

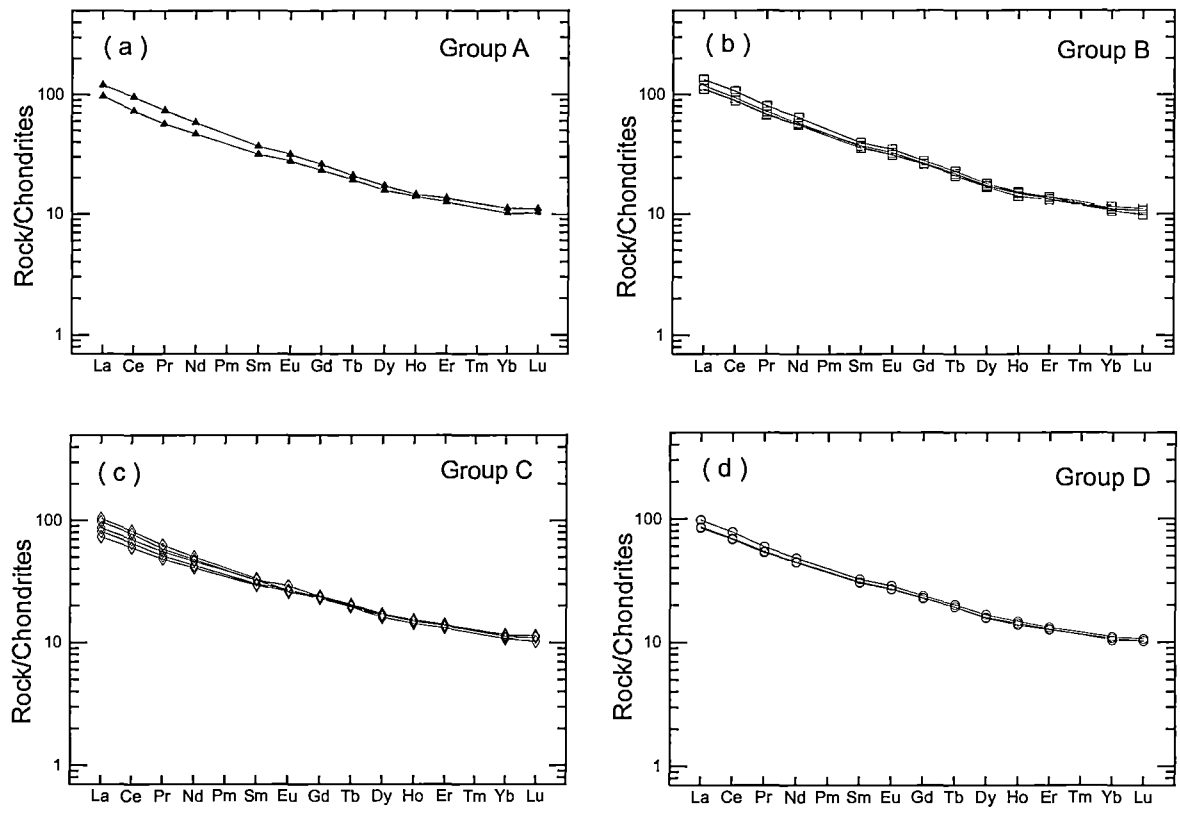

Figure 4.5 Chondrite normalised rare earth element (REE) patterns for the Denchai basalts; Chondrite normalised values are from Sun and McDonough (1989)

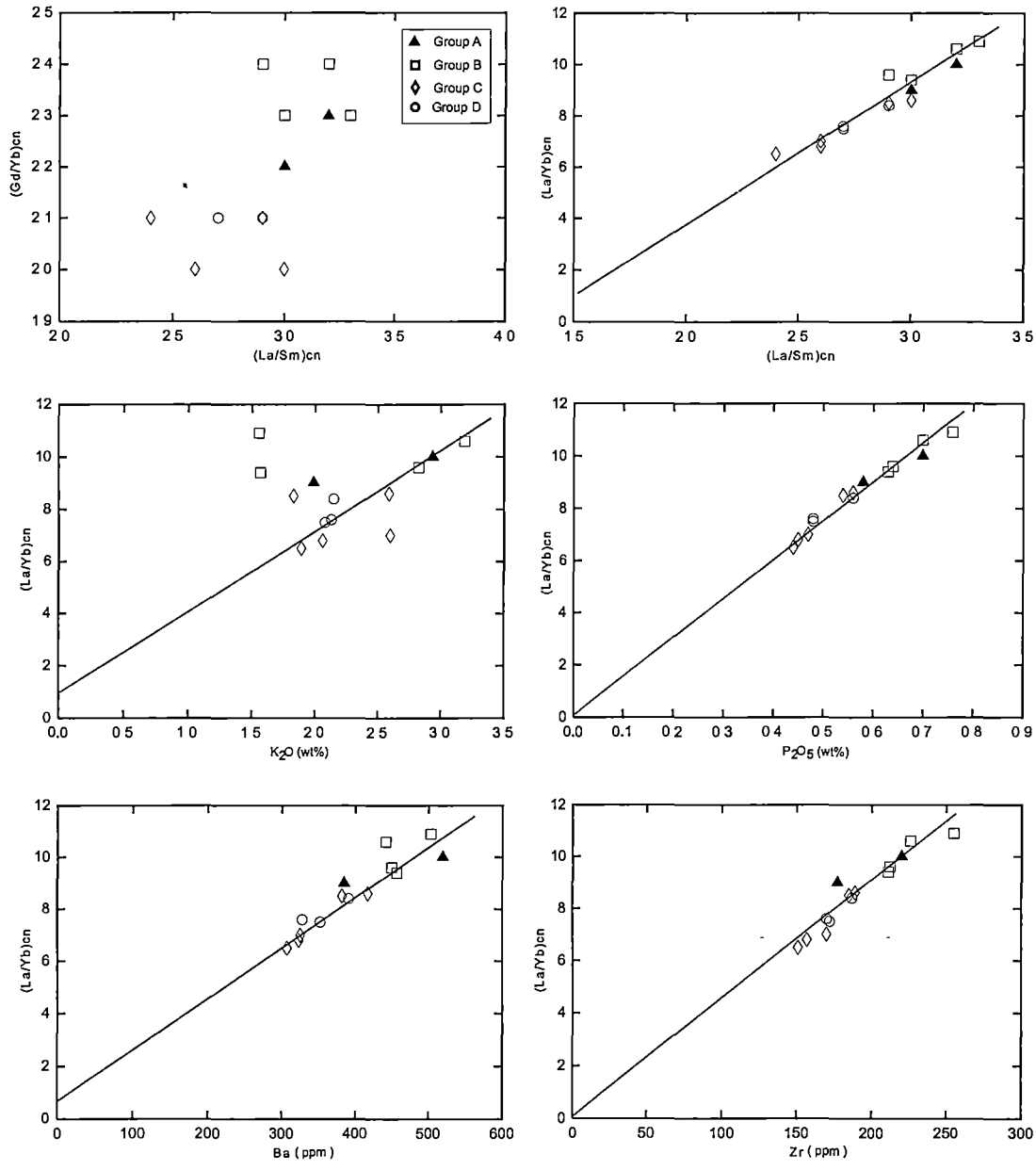

Figure 4.6 Variation diagrams of HFSE, K-group elements and P_2O_5 versus $(La/Yb)_{cn}$; Chondrite normalised values are from Sun and McDonough (1989)

Using primitive mantle normalisation factors from Sun and McDonough (1989), all Denchai basalts show near identical multi-element patterns (Fig.4.7), with the peak of the more incompatible elements always falling at K_2O for unaltered samples. Lesser peaks (weak to moderate positive anomalies) also occur for Pb and Sr.

All four groups of the Denchai basalts show significant enrichments in K relative to Nb, U, Th and LREE, and enrichments in Pb relative to Ce and Sr relative to P and Nd (Fig.4.7). The chondrite-normalised REE patterns of all four groups show significant LREE enrichment with little variation in HREE concentrations (Fig.4.5). Group B basalts show the strongest LREE enrichments and highest contents of TiO_2, P_2O_5, K_2O, Sr, Ba, HFSE than other groups (Figs.4.2-4.3).

The distinctly higher P_2O_5, TiO_2, HFSE and K-group element contents of Group B basalts compared to basalts from Groups A, C or D suggest that Group B basalts were formed by lower degrees of partial melting of the same (or very similar) source as yielded the other Denchai basalts. Coupled with the notably lower SiO_2 contents at any MgO level of the Group B basalts, and their higher FeO* contents, this probably reflects the fact that Group B basalts were produced by deeper (higher-P) partial melting, with consequent rather lower degrees of partial melting than that which produced Groups A, C and D basalts.

To evaluate whether the Denchai basalts were all derived from the same mantle source requires radiogenic isotopic data presented in Section 4.4.5.

4.4.4 Comparative geochemistry of Denchai basalts with other SE-Asian intraplate basalts

In Figure 4.8, the REE and muti-element primitive mantle-normalised patterns for representative Denchai basalts from each group are plotted together with other intraplate alkali basalts from North Queensland (Zhang *et al.*, 2001), Southeast China (SE-China; Zou *et al.*, 2000) and Vietnam (Hoang *et al.*, 1996; Hoang and Flower, 1998). Only basalts plotting in the basanite and basalt fields of Figure 4.1 are included, to ensure broad major element similarities with the Denchai basalts. The REE patterns of the North Queensland basalts are very similar to the Denchai basalts, but show slightly greater HREE depletion. Also, the multi-element patterns of these suites are similar apart from somewhat lower Rb and Ba, and aforementioned HREE depletion in the North Queensland basalts compared to those from Denchai.

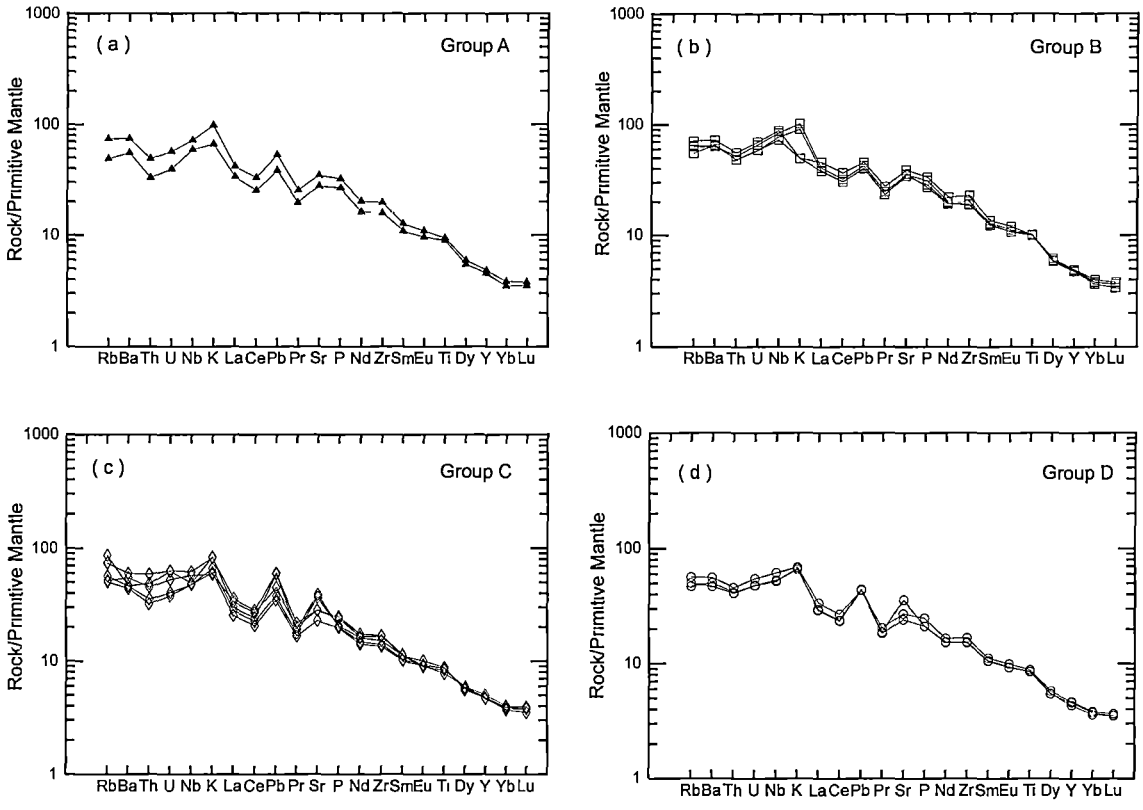

Figure 4.7 Spider diagrams showing primitive mantle normalised trace elements of the Denchai basalts. Normalisation values are from Sun and McDonough (1989)

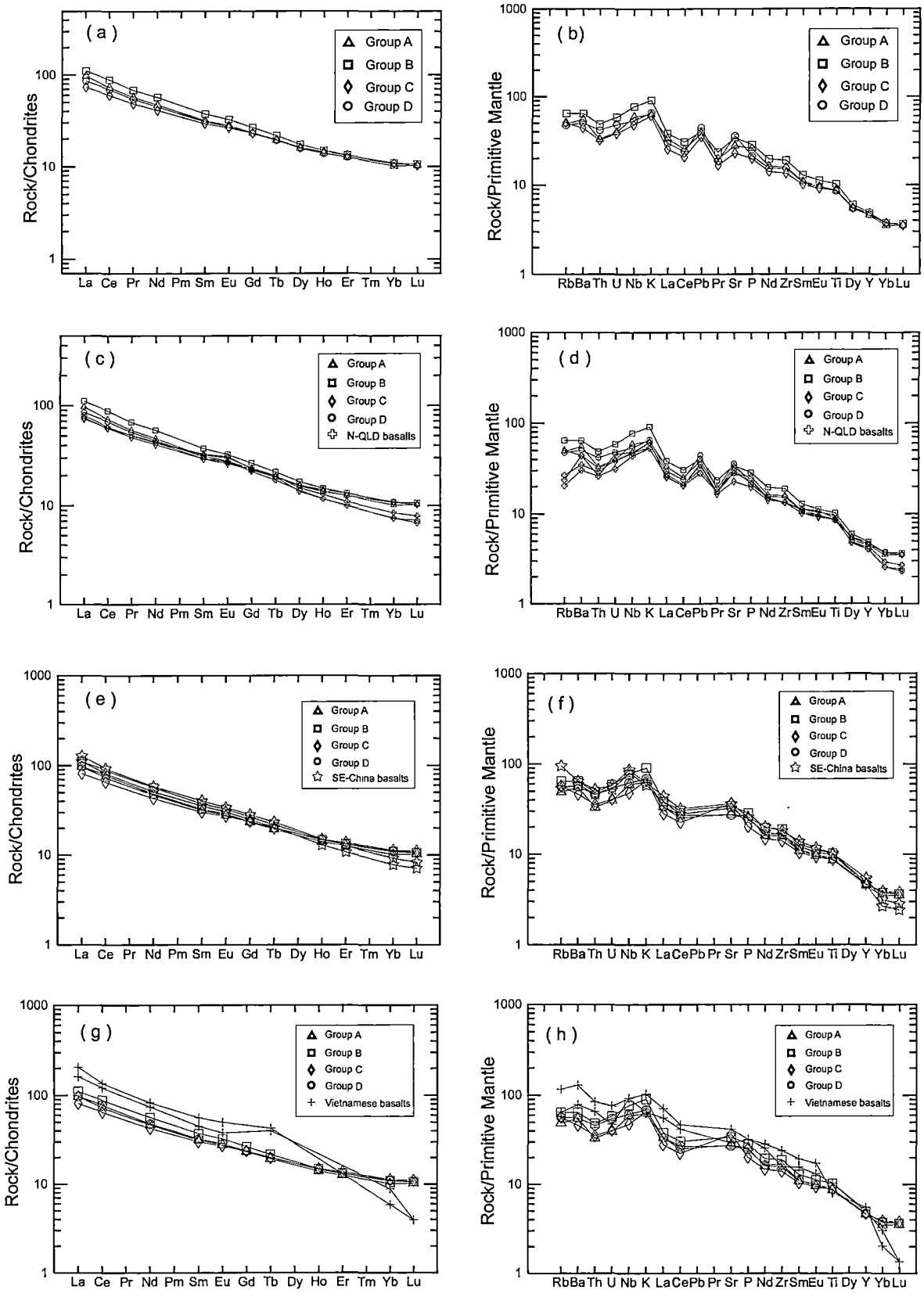

Figure 4.8 Representative Denchai basalts (Groups A, B, C and D), N-QLD = North Queensland, SE-China = Southeast China and Vietnamese basalts. Normalisation values are from Sun and McDonough (1989);
(a), (c), (e) and (g) Spider diagrams primitive mantle normalised trace elements
(b), (d), (f) and (h) Chondrite normalised rare earth element (REE) patterns

In comparison to the SE-China and Vietnamese basalts, the REE contents of the Denchai basalts are slightly lower in LREE and higher in HREE compared to those of intraplate basalts from SE-China, but much lower in LREE and greater in HREE than the Vietnamese basalts (Figs.4.8e, g). Again, incompatible element patterns of the SE-China basalts are similar to the Denchai basalts (Fig.4.8f). Unlike the SE-China basalts, multi-element patterns of those intraplate basalts from Vietnam are significantly different to the Denchai basalts (Fig.4.8h).

4.4.5 Sr-Nd-Pb isotopes

The reason for investigating the geochemistry of the Denchai basalts was to shed light on the source components (asthenosphere, plume, crust and SCLM) involved in the genesis of these lavas, and to test whether they were all derived from the same source. To this end, seven representative Denchai basalts were analysed for Sr-Nd-Pb isotope ratios (Table 4.9).

$^{87}Sr/^{86}Sr$ ratios of the Denchai basalts range from 0.70382 to 0.70429, $^{143}Nd/^{144}Nd$ ratios range from 0.512791 to 0.512903 and the ε_{Nd} values range from +5.2 to +3.0. These data are plotted on Figure 4.9 together with fields for intra-plate basalts from elsewhere in Thailand (Fig.4.9b) and basalts from SE-China, Vietnam and North Queensland (Fig.4.9a). Group B basalts show significantly higher $^{143}Nd/^{144}Nd$ ratios (0.512903; ε_{Nd} values = +5.2) and lower $^{87}Sr/^{86}Sr$ ratios (0.70383) than other Denchai basalts. Within Group C, the most evolved (52.3wt% SiO_2 and 6.75% MgO; DC15) basaltic trachyandesite has notably higher $^{87}Sr/^{86}Sr$ (0.704291) than the least evolved (48.5% SiO_2, 8.6% MgO; DC30) basalt (0.704122), suggesting that a limited amount of radiogenic Sr may have been added to the evolving magma during relatively prolonged residence time of this Group in an upper crustal reservoir.

4.4.6 Comparison with other Thai intraplate basalts

The array formed by the Denchai basalts in $^{143}Nd/^{144}Nd$ - $^{87}Sr/^{86}Sr$ space includes also three of four analysed sapphire-bearing basalts from Chantaburi (Mukasa *et al.*, 1996; Zhou and Mukasa, 1997), suggesting strong compositional links between the gem-bearing basalts. Most basalts from Bo Ploi are distinct from those from Denchai and Chantaburi in having lower $^{143}Nd/^{144}Nd$ values at given $^{87}Sr/^{86}Sr$ value. Basalts erupted through thicker crust of the Khorat Plateau fall into two distinct groups with markedly different $^{87}Sr/^{86}Sr$ values. One group, with $^{87}Sr/^{86}Sr > 0.7047$ and $^{143}Nd/^{144}Nd < 0.5128$ shows a linear trend with end

Table 4.9 Sr-Nd-Pb isotopic compositions of representative Denchai basalts

Sample	Group	$^{87}Sr/^{86}Sr$	2 SE	$^{143}Nd/^{144}Nd$	E_{Nd}	$^{206}Pb/^{204}Pb$	2 SE	$^{207}Pb/^{204}Pb$	2 SE	$^{208}Pb/^{204}Pb$	2 SE	$^{147}Sm/^{144}Nd$
DC28	A	0 70397	13	0 512849	4 2	18 26	14	15 55	12	38 30	30	0 13280
DC42	A	0 70402	13	0.512856	4 3	18.37	11	15 56	9	38 38	23	0 12500
DC43	B	0 70382	12	0 512888	4.9	18 26	11	15 54	10	38 23	26	0 12482
DC61	B	0 70383	13	0 512903	5 2	18 24	31	15 54	26	38.22	64	0 13005
DC15	C	0.70429	12	0 512793	3.1	18.71	50	15.61	42	38 74	102	0 13128
DC30	C	0.70412	12	0.512843	4.0	18.47	10	15 59	9	38.50	22	0 14511
DC11	D	0.70429	12	0 512791	3.0	18 60	15	15 60	12	38.61	30	0 13529

E_{Nd} = epsilon Nd, SE = standard deviations

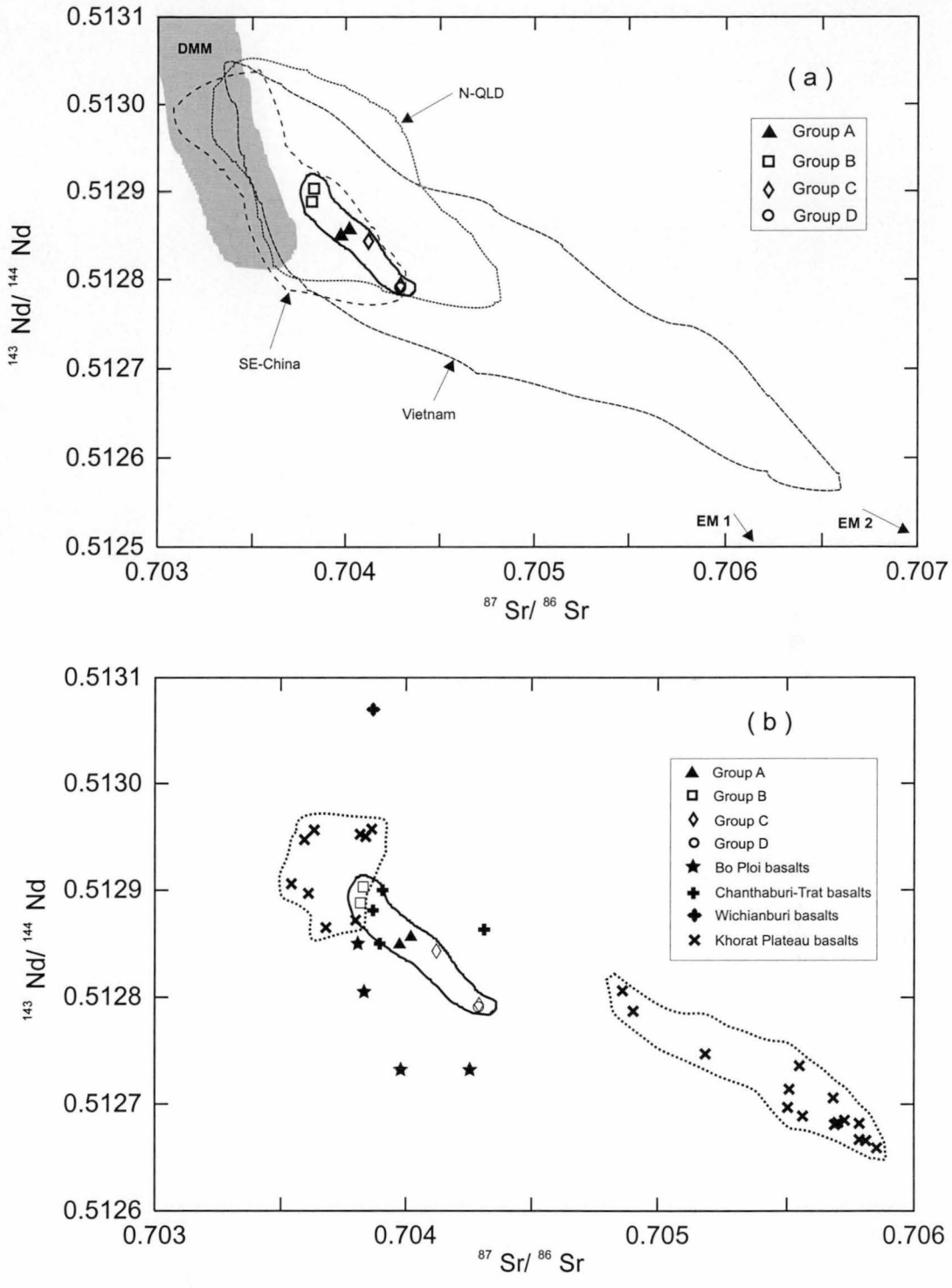

Figure 4.9 $^{87}Sr/^{86}Sr$ vs $^{143}Nd/^{144}Nd$ variation diagrams; (a) the Denchai basalts and (b) Compared with other intraplate alkali basalts in Thailand;
Fields for the North Queensland (N-QLD) lava-field basalts (Zhang *et al.*, 2001), Southeast China basalts (Zou *et al.*, 2000) and Vietnamese basalts (Hoang *et al.*, 1996), Field for DMM is from Hoftmann (1997),
Approximate localities for EM-1 and EM-2 are from Zindler and Hart (1986)

members that are Depleted Mantle and an enriched component with similarities to EM2 or a crustal component (Fig.4.9b). The second cluster of the Khorat basalts falls around the more primitive end of the Denchai array, extending to slightly less radiogenic Sr and more radiogenic Nd compositions.

Pb isotopic ratios for the Denchai basalts range in $^{206}Pb/^{204}Pb$ from 18.24 to 18.71, in $^{207}Pb/^{204}Pb$ from 15.54 to 15.61, and in $^{208}Pb/^{204}Pb$ from 38.22 to 38.74, and are plotted in Figure 4.10 together with intraplate basalts from North Queensland, SE-China and Vietnam, as well as Mid-Ocean Ridge basalts (MORB) from the Indian and Pacific Oceans. The Denchai basalts define linear arrays in both the $^{206}Pb/^{204}Pb$ - $^{207}Pb/^{204}Pb$ and $^{206}Pb/^{204}Pb$ - $^{208}Pb/^{204}Pb$ diagrams, parallel to the Northern Hemisphere Reference Line (Hart, 1984) but displaced to more radiogenic $^{208}Pb/^{204}Pb$ and $^{207}Pb/^{204}Pb$ values. The Group B basalts show the lowest $^{206}Pb/^{204}Pb$ and $^{207}Pb/^{204}Pb$ values, in keeping with their less radiogenic $^{87}Sr/^{86}Sr$ values.

The Denchai basalts show a near-perfect overlap with Indian Ocean MORB. Although $^{208}Pb/^{204}Pb$ values overlap with the field for basalts from SE-China, the Denchai basalts have higher $^{207}Pb/^{204}Pb$ values. Group C and Group D basalts are at the high end of $^{206}Pb/^{204}Pb$, whereas Groups A and B are plotted at the low $^{206}Pb/^{204}Pb$ end.

4.5 Isotopic variations and mixing models for sources of SE-Asian basalts

In this section, isotopic compositions of the Denchai basalts are compared with those for regional intraplate basalts to allow an assessment of their tectonic significance considered within the framework of mantle provinciality established by Flower *et al.* (1998).

Published data used for this regional comparison include Intasopa *et al.* (1995), Mukasa *et al.* (1996) and Zhou and Mukasa (1997) for late Cenozoic lava-field basalts in Thailand, Zou *et al.*, (2000) for the Cenozoic basalts in Southeast China, Hoang *et al.* (1996) and Hoang and Flower (1998) for Vietnamese basalts, and Zhang *et al.* (2001) for late Cenozoic intraplate basalts from North Queensland.

Figure 4.9 showed that in terms of Sr-Nd isotopic compositions, the Denchai and Chantaburi basalts plot towards the high $^{87}Sr/^{86}Sr$ and low $^{143}Nd/^{144}Nd$ end of the fields for the North Queensland and Southeast China basalts. The more isotopically primitive group of Khorat Plateau basalts also plot in the same general field. In contrast, basalts from Vietnam form a wide swath of compositions that overlap with the Thai, SE-China and North Queensland

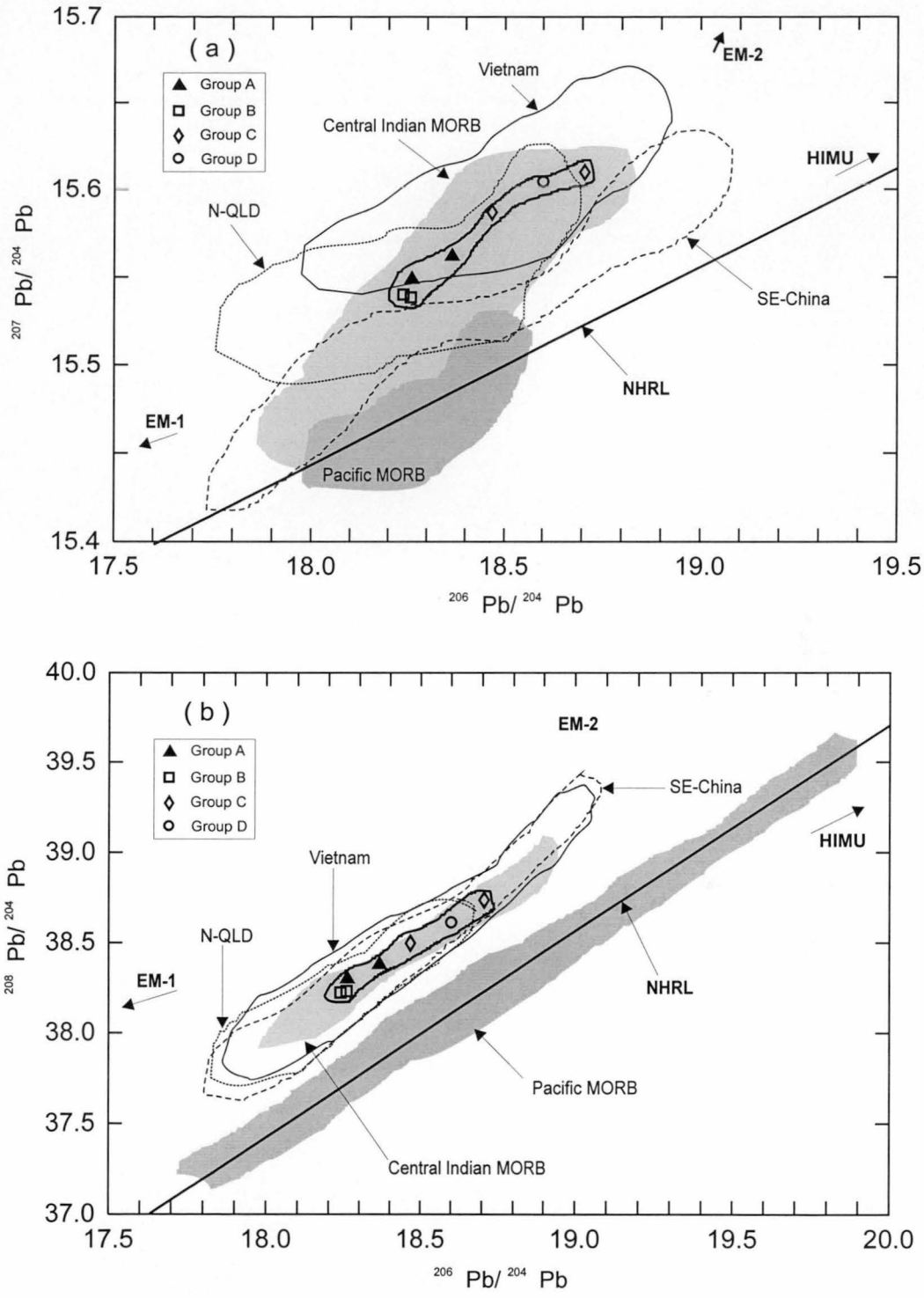

Figure 4.10 $^{206}Pb/^{204}Pb$ vs $^{207}Pb/^{204}Pb$ and $^{206}Pb/^{204}Pb$ vs $^{208}Pb/^{204}Pb$ diagrams for the Denchai basalts, Fields for the North Queensland (N-QLD) lava-field basalts (Zhang *et al.*, 2001), Southeast China basalts (Zou *et al.*, 2000) and Vietnamese basalts (Hoang *et al.*, 1996), Fields for the Pacific and Indian MORB are from Hoftmann (1997) and Mahoney *et al.* (1989), Approximate localities for EM-1, EM-2 and HIMU are from Zindler and Hart (1986),
NHRL = Northern Hemisphere Reference Line (Hart, 1984)

basalt fields, but extend to significantly higher $^{87}Sr/^{86}Sr$ and lower $^{143}Nd/^{144}Nd$. The latter part of the Vietnam basalt field overlaps the field for the radiogenic Khorat Plateau basalts, and demands significant contamination of the parental magmas by a lithospheric component with significant crustal modification (Zhou and Mukasa, 1997).

In the $^{206}Pb/^{204}Pb$ versus $^{87}Sr/^{86}Sr$ and $^{206}Pb/^{204}Pb$ versus $^{143}Nd/^{144}Nd$ diagrams (Fig.4.11), the Denchai basalts mostly lie within the North Queensland and Vietnamese basalt fields, but mostly plotted above the Southeast China basalts on the $^{206}Pb/^{204}Pb$ versus $^{87}Sr/^{86}Sr$ (Fig.4.11a), and mostly lie below the Southeast China basalt field on the $^{206}Pb/^{204}Pb$ versus $^{143}Nd/^{144}Nd$ (Fig.4.11b). On the $^{206}Pb/^{204}Pb$ versus $^{207}Pb/^{204}Pb$ (Fig.4.10a), basalts from North Queensland, SE-China and Vietnam show a well-defined positive trend lying slightly above the SE-China trend. On the $^{206}Pb/^{204}Pb$ versus $^{208}Pb/^{204}Pb$ (Fig.4.10b), all these basalt groups show a striking overlap in their compositional fields, paralleling the Indian Ocean MORB field at somewhat higher $^{208}Pb/^{204}Pb$ for any $^{206}Pb/^{204}Pb$ value. This parallelism with the Indian MORB field is interesting. The Denchai basalt field could be explained by derivation of these basalts from a mantle source that contained more of the 'enriched' component that is responsible for the 'separation' of the Indian MORB field from the Pacific MORB field. The nature of this component has been discussed by Mahoney *et al.* (1992), Douglass and Schilling (2000), Weis *et al.* (2001) and Kamenetsky *et al.* (2001). The latter authors demonstrated convincingly that it probably represents a Precambrian garnet-bearing mafic lithology related to crustal blocks stranded in the upper mantle during break-up of Gondwana.

Building on modelling of Flower *et al.* (2000), Figure 4.12 shows some modelling of mantle isotopic sources to attempt to account for the petrogenesis of the Denchai basalts in terms of mantle reservoirs. Figure 4.12a shows a $^{87}Sr/^{86}Sr$ versus $^{206}Pb/^{204}Pb$ diagram, with standard mantle sources (EM1, EM2 and Depleted Mantle (DM)) depicted. Also shown are the LOMU (LO) source implicated in Indian Ocean basalt genesis (Douglass and Schilling, 2000; Kamenetsky *et al.*, 2001), and a hybrid source (A) composed of 97% DM and 3% LOMU. Also shown are two mixing lines showing mixing between, respectively, source A and EM2, and DM and EM2. If both A and DM sources were involved in the production of the Denchai basalts, then the amount of contamination by EM2 is less than 1% for A, and < 2% for DM. However Figure 4.12b shows that a more satisfying fit can be obtained by contaminating source A with 15-25% HIMU mantle, implying little or no involvement of EM2 mantle. The Indian Ocean MORB spread could be similarly matched by contaminating a source lying between A and DM (that is, DM with only 1-2% contamination by LOMU) with 10-20% of HIMU mantle. Much of the Indian Ocean isotopic spread, and the Denchai

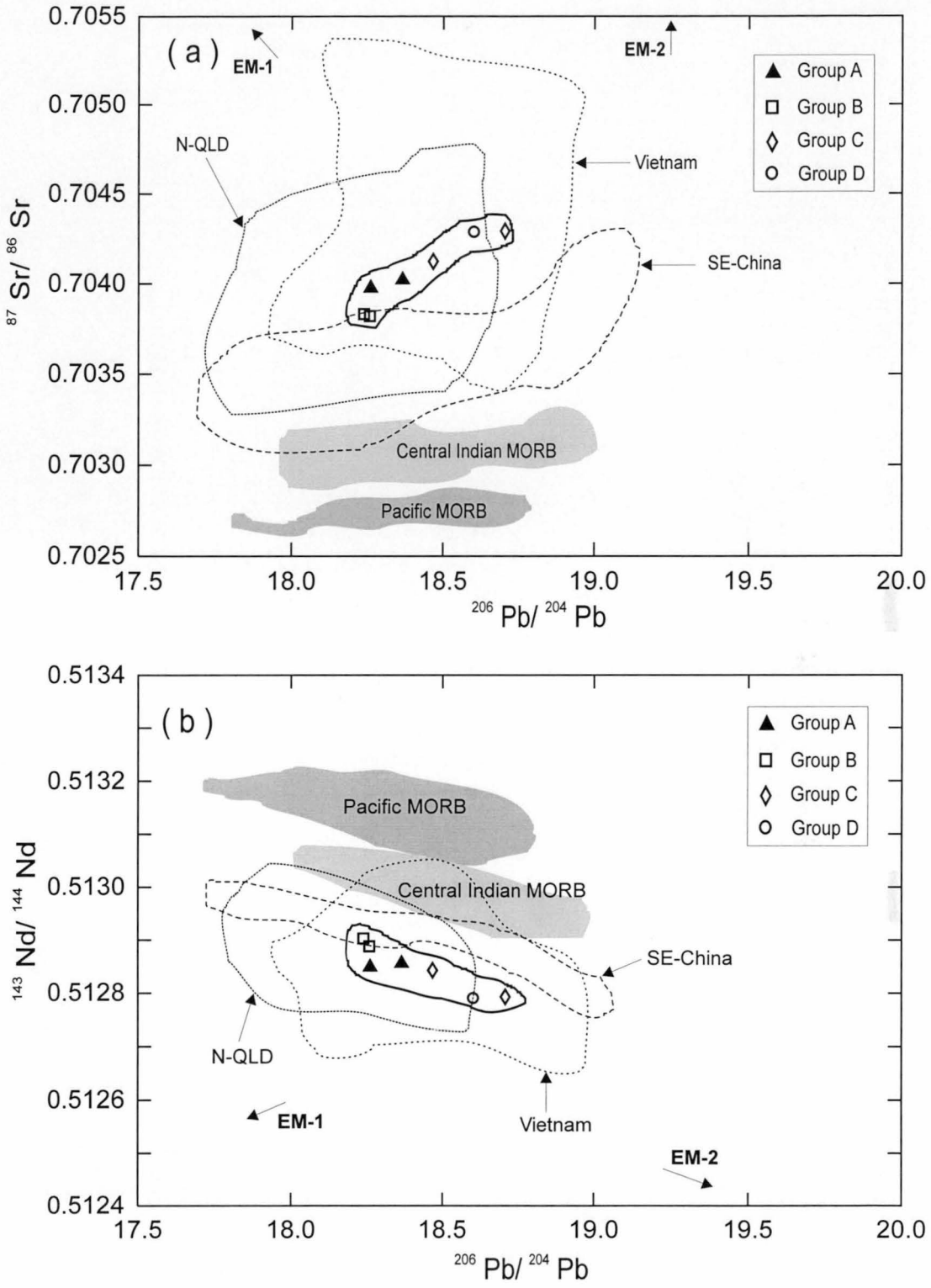

Figure 4.11 $^{206}Pb/^{204}Pb$ vs $^{87}Sr/^{86}Sr$ and $^{206}Pb/^{204}Pb$ vs $^{143}Nd/^{144}Nd$ diagrams for the Denchai basalts, Fields for the North Queensland (N-QLD) lava-field basalts (Zhang *et al.*, 2001), Southeast China basalts (Zou *et al.*, 2000) and Vietnam basalts (Hoang *et al.*, 1996). Fields for the Pacific and Indian MORB are from Hoftmann (1997) and Mahoney *et al.* (1989), Approximate localities for DMM, EM-1, EM-2 and HIMU are from Zindler and Hart (1986)

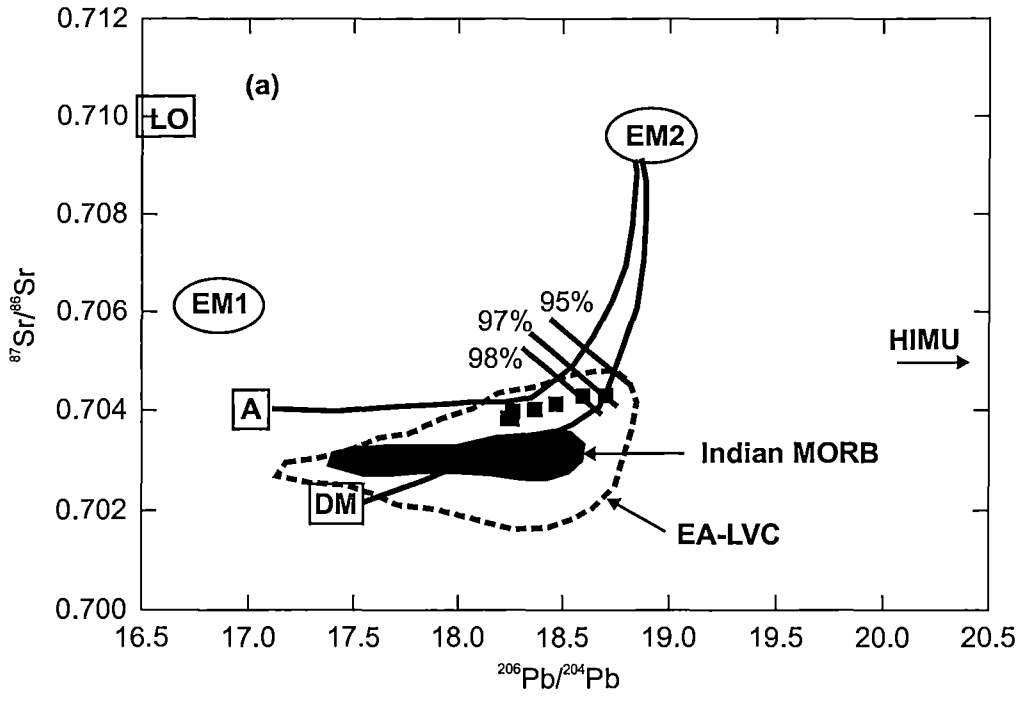

Figure 4.12a Mixing model accounting for isotopic variation of the Denchai basalts. [A] represents a mantle source composed of 97% Depleted Mantle (DM) contaminated by 3% of the LOMU component (LO) defined by Douglass and Schilling (2000) and Kamenetsky *et al.* (2001). Two mixing lines are shown representing contamination of source A and source DM by EM2 mantle. The Denchai basalts form a spread extending between a 99% mix of source A and 1% EM2, and an 97% Mixed of mix of DM and 3% EM2 (end-member data are taken from Flower *et al.* 1998). EA-LVC is East Asian Low Velocity Composition of Flower *et al.* (2000), taken to represent the ambient sub-East Asian, sub-West Pacific asthenospheric mantle.

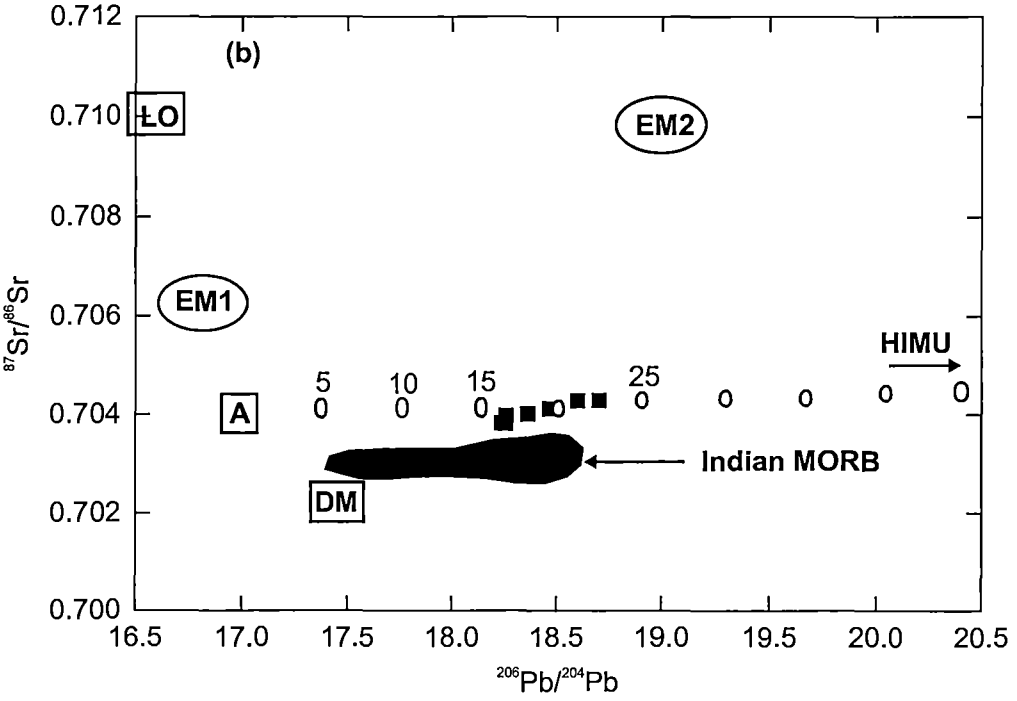

Figure 4.12b Isotopic mixing model showing that the Denchai basalts can be well modelled as derived from a source that consists of a mantle [A] (Depleted Mantle (DM) contaminated by 3% of LOMU (LO) contaminated by 15-25% of typical HIMU mantle (end-member data are taken from Flower *et al.*, (1998) and Kamenetsky *et al.*, (2001) for LOMU). Numbers from 5 to 25 show percentages of mixing of [A] with HIMU.

basalt field, are encompassed within the field defined by Flower *et al.* (2000) as the East Asian Low Velocity Composition (EA-LVC) that they argued was the ambient sub-East Asia, sub-West Pacific asthenospheric mantle.

4.6 Petrogenesis of the Denchai basalts

4.6.1 Major, minor and trace elements

Major element modelling shows that within each of the three groups for which more than five samples have been analysed (Groups B, C and D), fractionation of small amounts of ol + cpx can account for most of the intra-suite compositional variations; Ti-magnetite fractionation is also implied for driving the Group C basalts to higher SiO_2 contents than the other Groups. The late appearance of plagioclase and absence of a negative Eu anomaly in all samples (Fig.4.5) indicate that low pressure plagioclase fractionation has not been significant during the evolution of these magmas. However important differences in P_2O_5, TiO_2, HFSE element contents, and key element ratios such as Zr/Nb, Zr/Y and Y/Nb (Fig.4.4) show that fractionation cannot be responsible for generating the different suites from a single parental magma. Different parent magmas for each suite are indicated, with important differences due to either different sources, different degrees of partial melting, or different amounts of modification of a parental magma before arrival in upper crustal storage chambers where the modelled low-pressure fractionation occurred. In the following section, an attempt is made to account for these inter-suite differences.

A prime difference between Group B and the other three suites is the higher TiO_2, P_2O_5, and K-group and HFSE contents of Group B basalts. Group B basalts also have significantly lower SiO_2 contents than the other groups. The simplest explanation of this feature is that the parent magma of Group B was derived from partial melting at greater depths, and by a lower degree of partial melting, than parental magmas of the other groups. It is well known (e.g., Falloon and Green, 1987, 1988) that primary basalt SiO_2 contents are inversely proportional to the depth of magma generation in the upper mantle. Given that some degree (< 5wt%) of olivine fractionation occurred to drive the primary magma of Group B (Mg# > 0.66) to the composition of the least evolved Group B basalt (Mg# = 0.63), the primary magma of Group B may have had around 46.5-47.0wt% SiO_2. The amount of H_2O (and CO_2) in this primary magma is unconstrained, but Green *et al.* (1987) and Green and Falloon (1998) has shown that a typical Hawaiian alkali olivine basalt with similar SiO_2 contents can be derived by small degree partial melting of fertile peridotite at near 1 GPa. The parental magmas of Groups C and D were probably very similar, with perhaps only very small differences in

P_2O_5 and HFSE contents. These were probably generated at similar *P-T* conditions by similar amounts of partial melting. The parental basalt of Group C may have been more oxidised than for the other compositional groups, as it appears that this magma commenced crystallisation of Ti-magnetite at around 7.5% MgO, driving the magma to SiO_2 contents of 51-53% at 7.5-6.8% MgO.

Trace element ratios that are probably little modified from their source peridotite, including Zr/Nb, Zr/Hf and Nb/Ta (Fig.4.4) show coherent linear distributions suggesting that the Denchai basalts may have been derived from similar sources by variable degrees of partial melting. The more HFSE-enriched Group B basalts, with lowest Zr/Nb, represent the lowest degrees of partial melting, and slightly higher degrees of partial melting generated the Groups A, C and D basalts from otherwise very similar sources in terms of major and trace elements. Both (La/Sm)cn and (La/Yb)cn are higher, and (Gd/Yb)cn lower in Group B than other basalts, supporting the interpretation that Group B basalts derive via smaller degrees of partial melting, and thus show more enrichment in LREE and more depletion in HREE. The relative HREE depletion of all suites, coupled with their low Sc contents (17-22 ppm at 8wt% MgO) indicate that partial melting probably took place in the presence of residual garnet.

4.6.2 Isotopic signature

The limited variation of Sr, Nd and Pb isotopic compositions suggest very limited or no crustal contamination was involved during the generation of most Denchai basalts. Only the highest SiO_2 Group C trachyandesite has a suggestion of minor crustal contamination in its highest $^{87}Sr/^{86}Sr$ and $^{207}Pb/^{204}Pb$ among the analysed samples. Widespread ultramafic xenoliths in the Denchai basalts are further evidence that most were unlikely to have experienced any crustal contamination.

4.6.3 Pressure of crystallisation

As described above, most primitive samples from all four groups of the Denchai basalts contain olivine and clinopyroxene phenocrysts, and the chemical fractionation trends displayed by each group suggest cotectic olivine-clinopyroxene crystallisation. Co-saturation of the Denchai basalts with olivine and clinopyroxene throughout their fractionation history allows an estimate of crystallisation pressure to be made using the technique of Danyushevsky *et al.* (1996). This method is based on comparing calculated pseudo-liquidus temperatures of these two minerals. The temperatures are calculated from the composition of

the melt (approximated in this case by the compositions of the studied samples) using 1 atm mineral-melt geothermometers of Ford *et al.* (1983) for olivine and Danyushevsky (2001) for clinopyroxene. As demonstrated by Danyushevsky *et al.* (1996), the difference between calculated 1 atm temperatures of olivine and clinopyroxene is a linear function of the pressure of crystallisation (i.e., the higher is the pressure, the larger is the difference between calculated temperatures). The calculations have been performed using a computer program PETROLOG (v.2.1) written by L. V. Danyushevsky.

Crystallisation pressures calculated for samples from Group A range between 14.8 and 15.0 kbars. Group B samples are characterised by the highest calculated pressures, between 17.4 and 20.2 kbars. Group C samples have the lowest crystallisation pressure of 13.8 - 15.8 kbars, and Group D samples crystallised between 15.0 - 15.7 kbars. The results indicate that all suites of the Denchai basalts have fractionated at high pressures, > 10 kbars, and no low-pressure crystal fractionation was detected.

4.7 The Denchai basalts in the context of East Asian intraplate basalts and mantle sources

Miocene and younger intraplate basalts occur extensively but in patchy zones over large areas of eastern Asia. The undersaturated lavas often carry garnet- and spinel-lherzolite xenoliths, as well as megacrysts of sapphire, zircon, anorthoclase, garnet and pyroxenes all interpreted as products of high-pressure assimilation-fractional crystallisation processes (Flower *et al.*, 1992; Wickham and Flower, 1994).

There is no convincing evidence for the existence of any significant mantle plume beneath eastern Asia, but Flower *et al.* (1998) have drawn attention to swell-like zones of low velocity shown up by seismic topographic imagery, that are interpreted to be shallow perturbations of the asthenospheric mantle. Flower *et al.* (1998) discussed the tectonic evolution of eastern Asia (including the offshore arc-backarc basin systems) with respect to the development of mantle domains. They proposed the existence of a series of lobe-shaped mantle domains linked to both India-Asia collision and the collision of Australia into the Indonesian arcs. The intraplate basalts in Thailand, including those studied from Denchai, form part of the southern (Indochina) domain of their "inner" lobe.

Hickey-Vargas *et al.* (1995), Flower *et al.* (1998), and Chung *et al.* (2001) have addressed the origin of the mantle beneath eastern Asia, demonstrating that it has profound similarities

to typical Indian Ocean MORB, bearing the characteristic DUPAL isotopic signature of higher $^{208}Pb/^{204}Pb$, $^{207}Pb/^{204}Pb$, and $^{87}Sr/^{86}Sr$ at a given $^{206}Pb/^{204}Pb$ than Pacific or Atlantic MORB. Based on the presence of this DUPAL signature in eastern Asian basalts, and well shown by from the Sea of Japan (Cousens *et al.*, 1994) and South China Sea (Tu *et al.*, 1992; Chung and Sun, 1992), Chung *et al.* (2001) argued for the existence of a long-lasting, well-mixed reservoir of DUPAL- or Indian Ocean-type asthenospheric mantle beneath the entire region of eastern Asia. They proposed that this reservoir was produced by convective removal, and incorporation into the asthenosphere, of thickened Gondwanan subcontinental lithospheric mantle during recurrent northward transport of calved-off slices of Gondwana (since at least late Palaeozoic time) and the assembly of Asia.

Hoang *et al.* (1996) and Hoang and Flower (1998) argued that the DUPAL domain beneath eastern Asia, which Flower *et al.* (1998) termed the Eastern Asian Low Velocity Composition (EA-LVC), "appears to be a hybrid of Depleted Mantle (DM) and HIMU variably enriched by EM1, with small EM2 contributions from subducted slab-derived additions of Phanerozoic fluid/sediments". They argued that the high-pressure basalts, with more EM1 involvement, derived from the convecting asthenosphere. In contrast, the more EM2-rich east Asian tholeiites, not present among the Denchai basalts, derived from "converted lithospheric mantle" produced when lithospheric attenuation accompanied by mantle heating led to rheological conversion of refractory relatively EM2-rich mechanical boundary layer mantle into low velocity asthenosphere.

New isotopic data for Denchai basalts support the Flower *et al.* (1998) scheme. They are best modelled by mixing between three mantle source components:

(1) A component, herein called "A", lying somewhere along the DM-HIMU join, probably just beyond the Indian MORB field towards higher $^{206}Pb/^{204}Pb$. The reason for this component having higher $^{206}Pb/^{204}Pb$ compared with typical Indian Ocean MORB is that recent studies of MORB suites that include transitional alkali varieties best interpreted as low-degree melts show a stronger HIMU signature in the lower degree melts relative to the typical MORB (e.g., Kamenetsky *et al.*, 2001). As the alkali basalts from Denchai are best interpreted as relatively low degree melts of asthenospheric mantle, they might be expected to sample more of the (low melting?) HIMU component.
(2) An EM1 component, modelled above as making up only about 3% of the mixed source dominated by 97% of component "A". The primary magmas of the Denchai basalts are interpreted to have been derived from this "A"-EM1 source. On their passage through the upper mantle, they passed through the source of component.

(3) The EM2-enriched subcontinental lithospheric mantle mechanical boundary layer. Most Denchai basalts (Groups A, B and D) appear to have passed through the lithosphere with little or no interaction. However, Group C basalts appear to have reacted more extensively with the EM2-rich lithosphere, as they are both more oxidised, record lower pressures of equilibration, and show a trend towards higher EM2 than other Denchai basalt groups. Nevertheless, the extent of EM2 enrichment in these basalts is considerably less than in many other eastern Asian basalts (Flower *et al.*, 1998).

4.8 Summary

The Denchai basalts can be chemically divided into four groups (Groups A, B, C and D). They are alkali in character and have compositions that include basanites, basalts, basaltic trachyandesites and trachybasalts. Multi-element patterns show significant enrichments in K relative to Nb, U, Th and LREE, which are similar to those intraplate basalts from North Queensland and SE-China. The REE patterns show variable LREE enrichments, but identical HREE for all four groups. The REE patterns are also similar to those lava-field basalts from North Queensland and SE-China. The Denchai basalts have fractionated at high pressure, probably > 10 kbars, and no evidence for low-pressure crystal fractionation has been found.

The Sr-Nd-Pb isotopic compositions lie well above the Northern Hemisphere Reference Line (NHRL) line and are similar to the Indian Ocean MORB in terms of Pb-Pb isotopic ratios. However they have more radiogenic Sr and less radiogenic Nd than Indian Ocean MORB. The Sr-Nd-Pb isotopic ratios of the Denchai basalts most closely resemble those from the North Queensland lava-field basalts but an EM-2 mantle component was not observed. This indicative of less depleted parental source than the source of the Indian Ocean MORB and the North Queensland basalts. Isotopic data suggest that crustal contamination is minimal with three mantle components mixing; an "A" component (Depleted Mantle, HIMU and a component lying somewhere between DM and HIMU line), "A"-EM1 mixing component and EM2-enriched subcontinental lithospheric mantle.

Chapter 5

The Denchai sapphire and its inclusions

5.1 Introduction

As described in the introductory chapter, corundum (sapphire and ruby) is hosted in a variety of rocks. Most gem-quality corundums (sapphire and ruby) occur in intraplate basaltic provinces. However, the nature of its parental rock has remained unknown in comparison to other gems such as diamond (mantle-derived origin) and emerald (crustal-derived origin).

The strategy of this chapter is to employ different modern analytical techniques to investigate the mineral chemistry and oxygen isotope composition of the studied sapphires and their inclusions (fluid, solid and melt). The results are then used to critically evaluate plausible models of sapphire origin. Descriptions of the analytical facilities used in this study and sample preparation are described in the following sections. The detailed analytical conditions for particular techniques/experiments are given in later sections.

5.2 Analytical techniques

5.2.1 Electron Microprobe (EMP)

A CAMECA SX-50 electron microprobe at the Central Science Laboratory (CSL), University of Tasmania was used for the trace element analysis of sapphires and for the composition of glass and mineral inclusions. An accelerating voltage of 15 kV was used with a beam current of 25 nA. Analytical condition details are described in Appendix C. Clean areas without any visible inclusions in the sapphire grains were chosen for analysis. In order to analyse the minor and trace elements (Fe, Ti, Cr, Ga and V) of sapphires and F, Cl and S in glass inclusions at lower levels, the counting time for these elements was extended.

5.2.2 Heating/Freezing Stages

Fluid/melt inclusions in the sapphires were analysed at the Centre for Ore Deposit Research, University of Tasmania. Microthermometric measurements were carried out on an USGS Gas-Flow heating/freezing stage (Werre *et al.*, 1979; Wood *et al.*, 1981) manufactured by

Fluid Inc. and a Linkam MDS600 heating/freezing stage, manufactured by Linkam Scientific Instruments Ltd. Both stages have upper temperature limits of 600°C. They were calibrated using synthetic fluid inclusions supplied by Synflinc Inc. and the precision of measured temperatures are ±1.0°C for heating and ±0.3°C for freezing. The USGS heating/freezing stage is mounted on a Nikon microscope fitted with a long focal length 32x-objective lens. To avoid fog covering the sample during the freezing examinations, N_2 gas was blown over the sample chamber.

5.2.3 Laser Raman Spectroscopy (LRS)

Laser Raman Spectroscopic analysis was undertaken at the Australian Geological Survey Organisation (AGSO), Canberra using a Dilor® SuperLabram spectrometer equipped with a holographic notch filter, 600 and 1800 g/mm gratings, and a liquid N_2 cooled, 2000 x 450 pixel CCD detector. The inclusions were illuminated with 514.5 nm laser excitation from a Spectra Physics model 2017 argon ion laser, using 5mW power at the sample, and a single 30-second accumulation. A 100x Olympus microscope objective was used to focus the laser beam and collect the scattered light. The focused laser spot on the samples was approximately 1 μm in diameter. Wavenumbers are accurate to $\pm 1 cm^{-1}$ as determined by plasma and neon emission lines. For the analysis of CO_2, O_2, N_2, H_2S and CH_4 in the vapour phase, spectra were recorded from 1000 to 3800 cm^{-1} using a single 20-second integration time per spectrum. The detection limits are dependent upon the instrumental sensitivity, the partial pressure of each gas, and the optical quality of each fluid inclusion. Raman detection limits are estimated to be around 0.1 mole% for CO_2, O_2 and N_2, and 0.03 mole% for H_2S and CH_4 and errors in the calculated gas ratios are generally less than 1 mole%.

5.2.4 Proton Induced X-ray Emission (PIXE)

A Proton Induced X-ray Emission (PIXE) study was undertaken at the CSIRO Exploration and Mining, Sydney, Australia, using the CSIRO-GEMOC Nuclear Microprobe. PIXE analysis provides a non-destructive method for acquiring the chemical constituents of individual inclusions. Melt and fluid inclusions were imaged using a raster-scanned beam of 3 MeV protons, focused into a beam size of 1.3 μm for fluid inclusion analysis (Ryan *et al.*, 2001). The predictable nature of MeV proton trajectories enables the generation of PIXE X-rays from the inclusion volume to be calculated, which leads to a standardless measure of inclusion composition (Ryan *et al.*, 1995). This approach was used to determine the composition of the original trapped fluid and to image inclusion content.

5.3 Sample preparation

The sapphires collected from the two main gem fields in the Denchai area were separated into groups based on their colours (Fig.5.1). The selected rough sapphires were cleaned and mounted in epoxy resins, then cut, polished and optically examined under a petrographic microscope to locate and photograph all types of inclusions. For the sapphires containing fluid inclusions, they were prepared as doubly polished section approximately 0.1-0.3 mm in thickness. Those sapphires containing solid and melt inclusions were again carefully ground using a fine diamond wheel. When the inclusions neared the surface, 6μ, 3μ and 1μ diamond paste was used until they were exposed. This is a time-consuming process. Finally, the polished samples were coated with carbon for electron microprobe investigation.

5.4 General characteristics of corundum

5.4.1 Morphology

Corundum has two common morphological types; one is a flat, tabular crystal habit consisting of a hexagonal prism terminated at both ends by a basal plane with well-developed rhombohedral faces (Fig.5.2a), and the other shows a barrel shape comprising a hexagonal bipyramidal faces terminated at both ends by a basal plane (Fig.5.2b). The former crystal habit is characteristic of the Cr-rich variety (ruby) formed almost exclusively in metamorphic complexes (e.g., Oftedahl, 1963; Lawrence *et al.*, 1987). The latter type is restricted to the non-ruby corundum of either magmatic or metamorphic origin and found to be common for the corundum megacrysts derived from alkali basaltic rocks (e.g., MacNevin, 1972; Atkinson and Kothavala, 1983; Coldham, 1985).

5.4.2 Colour

Corundum contains minor amounts of elements such as Fe, Ti, V and Cr substituting for Al in its internal structures. Some of these elements are known to cause body colour, resulting in the wide variety of colour of the gem-quality corundum (Deer *et al.*, 1992). For instance, Cr is responsible for the red colour of ruby, Ti and Fe for the blue colour of sapphire (Nassau, 1983) and V, Cr, Ti and Fe for colour-changed sapphire (e.g., blue-green colour under fluorescence light; Schmetzer and Bank, 1980). Red corundums are called ruby whereas, all other gem-quality corundums are called sapphire. Rubies may be of various shades of red, but the deep red, known as pigeon-blood, is of greatest value, while gem

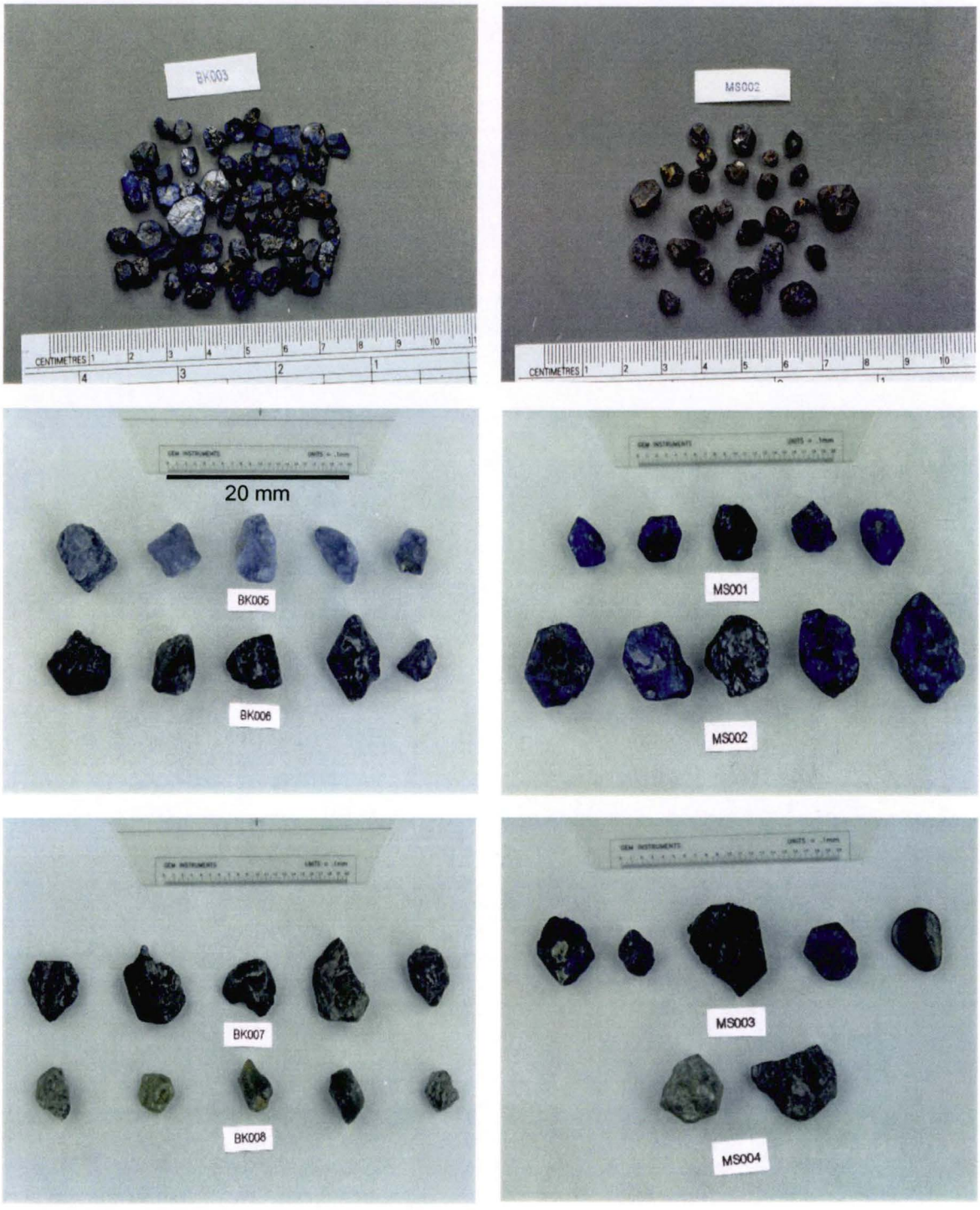

Figure 5.1 Photographs of the Denchai sapphires showing colours ranging from dark blue, blue and blue-green-yellow. BK = Ban Bo Kaeo and MS = Ban Mae Sin

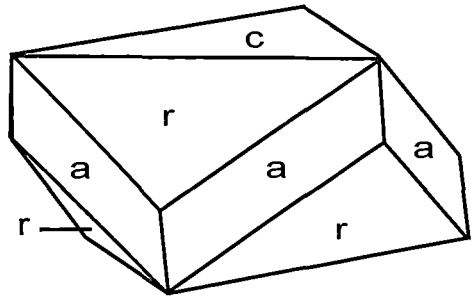

(a) Flat-shaped

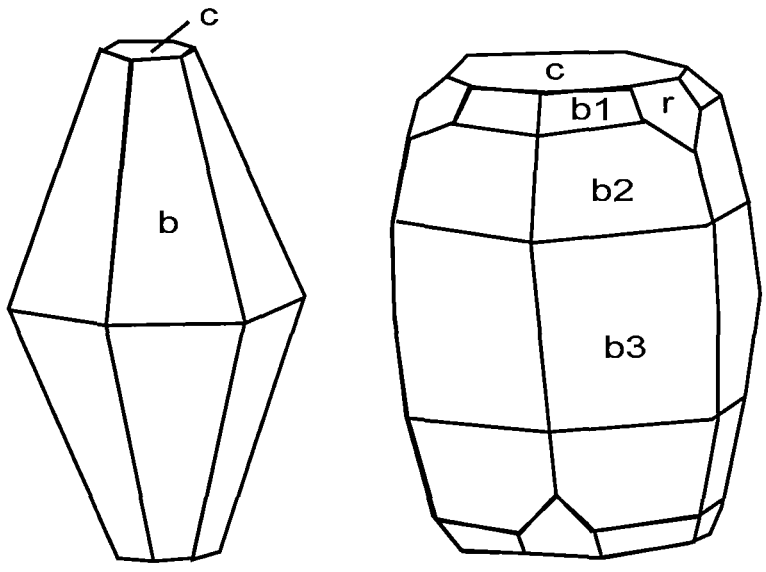

(b) Barrel-shaped

Figure 5.2 Crystal habit of corundum (a) metamorphic ruby dominated habit and (b) barrel-shaped habit; c = pinacoid, r = rhombohedron, a = prism, b = bipyramidal (modified from Guo, 1993)

sapphires colours range from very dark blue (almost black), blue, green to less common yellow (Klein and Hurlbut, 1993).

Recent comparative study of corundums from Barrington (Australia) and West Pailin (Cambodia) were assigned to two colour groups (Sutherland *et al.*, 1998b). Although the first group mainly ranges from blue-green-yellow (BGY) its colour extend to colourless, brown and dark grey to black. The second group ranges from blue, purple, and pink through red (ruby).

5.4.3 Nature of its inclusions

Inclusion studies (solid, fluid, and melt) are becoming more important in the field of geological sciences, especially with the continuing development of microanalytical techniques. These studies are of particular importance to investigate the origin of corundum as they provide invaluable data on the temperature, pressure and nature of corundum-forming solutions or melts. Inclusion data is therefore crucial in constraining meaningful genetic models for corundum.

Studies of fluid inclusion in sapphires from Eastern Australia and Thailand (Barrington and Anakie, Australia, and Bo Ploi, Thailand) reported multiple phases of CO_2 (L+V) and saline water (Stephenson, 1990; Sutherland, 1996; Srithai *et al.*, 1999). The mineral inclusions have the potential to carry useful information about their host rocks. Guo (1993) has reported a wide range of mineral inclusions in corundum derived from several basaltic fields (Eastern Australia and SE-Asia). These include mainly oxides, silicates, sulphides and phosphates. The mineral inclusions are briefly listed in Table 5.1 and are as follows: (i) oxides, the most abundant mineral inclusions in this group are Nb-Ta oxides, including columbite [(Fe, Mn) $(Nb, Ta)_2O_6$], ilmenorutile ($Nb\text{-}TiO_2$), pyrochlore [(Ca, Na, Ce) $(Nb, Ti, Ta)_2$ $(O, OH, F)_7$], samarskite and fersmite, followed by uraninite (UO_2), spinel (hercynite), hematite (Fe_2O_3) and baddeleyite (ZrO_2). (ii) silicates, zircon ($ZrSiO_4$) is the most abundant inclusion phases in corundum megacrysts, followed by albite ($NaAlSi_3O_8$), K-feldspar, mullite, sillimanite (Al_2SiO_5), (iii) sulphide, pyrrhotite (FeS) and (iv) phosphate, brockite (Ca, Th-dominant).

5.4.4 Mineral chemistry

Minor and trace element oxides in corundum, which derived from basaltic fields, have been used to classify corundum into "basaltic" and "metamorphic" suite. These were studied by Guo (1993) and Sutherland *et al.* (1998b) on corundums from eastern Australia and SE-Asia

Table 5.1 Category of mineral inclusions in corundum megacrysts (modified from Guo, 1993)

Group	Mineral inclusions	Formula	Crystallographic system	Colour
Oxides	columbite	(Fe, Mn) (Nb, Ta)$_2$O$_6$	orthorhombic	black to brownish black
	ilmenorutile (Nb-rutile)	Nb-TiO$_2$	tetragonal	variable
	pyrochlore	(Ca, Na, Ce) (Nb, Ti, Ta)$_2$ (O, OH, F)$_7$	isometric	brown or black
	uranopyrochlore/betafite	(Ca, Na, U)$_2$ (Nb, Ta)$_2$ O$_6$OH	isometric	brown or yellow
	spinel (hercynite)	FeAl$_2$O$_4$	isometric	variable
	spinel (gahnite)	ZnAl$_2$O$_4$	isometric	variable
	uraninite	UO$_2$	isometric	black
	hematite	Fe$_2$O$_3$	hexagonal	steel grey to red
	ilmenite	FeTiO$_3$	hexagonal	black or dark brown
	rutile	TiO$_2$	tetragonal	variable
	baddeleyite	ZrO$_2$	monoclinic	variable
Silicates	zircon	ZrSiO$_4$	tetragonal	colourless
	albite	NaAlSi$_3$O$_8$	triclinic	white
	calcic plagioclase	CaAl$_2$Si$_2$O$_8$	triclinic	white
	K-feldspars	(K,Na)(AlSi$_3$O$_8$)	monoclinic, triclinic	colourless or white
	mullite	3Al$_2$O$_3$.2SiO$_2$	orthorhombic	colourless or white
	thorite	ThSiO$_4$	isometric	black
	sillimanite	Al$_2$SiO$_5$	orthorhombic	variable
Sulphides	pyrrhotite	FeS	hexagonal	bronze-yellow to brown
	pentlandite	(Fe, Ni)$_9$S$_8$	isometric	light bronze-yellow
Phosphates	brockite	(Ca,Th)PO$_4$ H$_2$O	hexagonal	brown or black

suites. Trace elements present in significant amounts in most corundums are Fe, Ti, Cr and Ga. Other elements that may be present in corundum include V, Mn, Cu and Zn.

Sutherland *et al.* (1998b) established a quantitative empirical classification to distinguish corundum, discharged in basaltic fields, between "metamorphic-type" (including ruby) and "basaltic-type". The "metamorphic-type" corundums are characterised by low Ga_2O_3 (<0.01wt%) and high Cr_2O_3/Ga_2O_3 ratios (~10-100), whereas the "basaltic-type" corundums show higher Ga_2O_3 and Cr_2O_3/Ga_2O_3 ratios mostly below 1.

Sapphire samples in this study were analysed using a CAMECA SX-50 electron microprobe, described in Section 5.2.1. Sample preparation is explained in Section 5.3. Although it is noted that rubies have been reported in the study area, no rubies were detected in the samples included in this study. The minor and trace element concentrations obtained using the electron microprobe are listed in Table 5.2 and give the following abundances: Fe_2O_3 (0.32-1.98wt%), TiO_2 (0.01-0.23wt%), Cr_2O_3 (< 0.01wt%), Ga_2O_3 (0.01-0.03wt%) and V_2O_5 (<0.03wt%).

Titanium (Ti)

The abundance of titanium is variable, ranging from 0.01 to 0.23wt%. No absolute distinction can be seen among different colours. The blue sapphires generally contain the highest TiO_2, while the yellowish green sapphires contain titanium values close to the detection limit.

Chromium (Cr)

The Cr_2O_3 content of ruby is commonly greater than 0.1wt%. However, all the blue, greenish blue and yellowish green varieties of sapphires available to this study are poor in Cr, typically below 0.006wt%, and mostly below the detection limit of the EMP.

Iron (Fe)

Fe is commonly detected in corundum of various origins, showing variation over a wide range. The sapphires studied here range from 0.3 to ~2wt% with a yellowish green sapphire (Sample MS004) contains the highest value (1.98wt%).

Vanadium (V)

The detection limit for vanadium in this study is around 0.007wt%. The highest vanadium content detected is 0.029wt% in a blue sapphire (Sample MS001). The other sapphires studied were mostly 0.015-0.025wt% values.

Table 5.2 Minor and trace element oxides (wt%) of the Denchai sapphires

Sample	Colour	Al_2O_3	TiO_2	Cr_2O_3	Fe_2O_3	V_2O_5	Ga_2O_3
BK003	blue	98 07	0 03	0.0007	0 58	0 023	0 02
BK001	blue	98 15	0 02	0 0010	1.12	0 020	0.03
BK003	blue	99 40	0.03	0.0002	0.56	0 002	0.02
BK003	blue	99.64	0 23	0.0002	0.53	0.009	0 03
BK003	blue	99.77	0.06	0 0002	0.51	0 005	0.02
BK003	blue	99 77	0 06	0 0002	0 53	nd	0 02
BK003	blue	99.91	0 04	0 0002	0 49	nd	0 01
BK003	blue	99.95	0.08	0.0002	0.54	0 003	0.02
BK003	blue	99 97	0 09	0.0002	0 57	nd	0.04
BK003	blue	100.02	0.05	0.0003	0.56	0 012	0 02
BK003	blue	100.07	0.07	0 0002	0.54	0.001	0 02
BK003	blue	100.12	0.08	0.0017	0.54	0.002	0.02
BK007	greenish blue	97.18	0.01	0 0054	0 87	0.015	0.02
BK007	greenish blue	97.72	0 02	0 0002	1.20	0.025	0.01
BK006	yellowish green	98 30	0 42	nd	0 39	0 015	0.02
BK006	yellowish green	98 42	0.13	nd	0 45	0 021	0.02
MS001	blue	96.57	0 02	0.0042	0.32	0.029	0 02
MS001	blue	97 56	0 08	0.0004	1.53	0 017	0 02
MS002	blue	98.23	0.02	0.0001	0.64	0 017	0.02
MS002	greenish blue	96.86	0.15	nd	1.25	0 013	0 01
MS003	greenish blue	96.80	0.02	nd	1.95	0.014	0 01
MS004	yellowish green	96 93	0.01	0.0024	1 98	0.016	0 02
detection limit (wt%)			0 01	0 004	0 02	0.007	0 01

nd = not detected

Gallium (Ga)

All different colours of the studied sapphires contain a narrow range of gallium (0.01-0.04wt%). The gallium contents detected in all the studied sapphires are close to the detection limit.

5.4.5 Oxygen isotope

Although it is now generally agreed that corundums are xenocrysts in alkali basalts (e.g., Aspen *et al.*, 1990; Guo *et al.*, 1996a; Sutherland *et al.*, 1998a) consensus on the exact genetic process for their formation has not yet been reached. It has been suggested that corundums in alkali basalts are a primary product of a high-pressure phase crystallised from felsic melts at mantle depths (e.g., Irving, 1986). However, it is not known if this mechanism may be involved in the formation of gem sapphires. One critical issue is whether mantle-derived magmas within the upper mantle can evolve to a composition peraluminous enough to crystallise significant amounts of peraluminous minerals such as corundum without contamination by Al-rich crustal rocks. Oxygen (O) isotopes are potentially useful to address this problem because mantle and crustal rocks usually exhibit distinctively different O-isotope compositions. Corundum is a refractory mineral difficult to analyse for O-isotope composition by the conventional method. However, recent development of the laser fluorination method provides a way to analyse O-isotope compositions of such refractory minerals (e.g., Sharp, 1990).

Oxygen isotope ratios in this study were measured for the Denchai sapphires at the Institute of Earth Science, Academia Sinica, Taipei, Taiwan. The analyses were performed by the CO_2 laser-fluorination method (Sharp, 1990). A Finnigan MAT 252 mass spectrometer was employed to analyse the CO_2 gas. All subhedral sapphire crystals were cleaned overnight to remove surface contaminants and then crushed for isotopic analysis. Two hexagonal-prism sapphire crystals with diameter (~5 mm) were sectioned to have thick slabs (~6 mm) parallel to {0001}, then slabs were broken to test the O-isotope homogeneity. In addition to sapphires, four representatives Denchai basalts were crushed, and mineral separates of olivine crystals were produced. These were analysed by conventional procedures for O-isotope analysis. The analysed sample weight ranges from 1.8 to 2.9 mg. Analyses were normalised to a value of $\delta^{18}O = 5.8$ for UWG-2 garnet standard (Valley *et al.*, 1995). The average analytical precision is ±0.1‰ (Yui, 2000). Values of $\delta^{18}O$ are reported in the standard per mil notation relative to Standard Mean Ocean Water (SMOW).

Analytical results

The O-isotope compositions of sixteen Denchai sapphires are shown in Table 5.3, and the O-isotope compositional variations of slabs of two sapphire crystals parallel to {0001} plane are illustrated in Figure 5.3. Most sapphires have $\delta^{18}O$ values in the range of +4.7 to +6.1‰ with one sample (BK2-b) show value of +8.4‰. This particular sample does not show any abnormal features and was analysed three times, with different batch of samples. As shown in Table 5.3 and Figure 5.4, sapphires with different colours (dark blue, blue and blue-green-yellow) do not show distinct $\delta^{18}O$ compositional ranges. Recent O-isotope compositions of corundum megacrysts from basaltic fields in Scotland are in the range +4.6 to +5.2‰ (Upton *et al.*, 1999).

Table 5.3 Oxygen isotope compositions of the Denchai sapphires

Sample	Colour	Weight (mg)	$\delta^{18}O$(‰)
BK1-a	dark blue	10.72	4.7
BK1-b	dark blue	20.46	4.7
BK1-c	dark blue	42.89	5.1
BK1-d	dark blue	88.12	5.1
BK1-e	dark blue	107.87	5.1
MS1-a	dark blue	33.55	5.5
MS1-b	dark blue	52.90	4.8
BK2-a	blue	20.35	4.9
BK2-b	blue	7.78	8.4
BK2-c	blue	15.19	6.1
MS2-a	blue	11.97	4.7
MS2-b	blue	27.96	6.1
BK3-a	blue-green-yellow	17.15	5.9
MS3-a	blue-green-yellow	30.36	5.1
MS3-b	blue-green-yellow	135.33	5.3
MS3-c	blue-green-yellow	140.12	5.7

Although the two ranges are comparable, the Denchai sapphires show a wider O-isotope compositional range and extend to higher $\delta^{18}O$ values. In contrast, O-isotope compositions of olivines from four representative Denchai basalts fall within a very narrow range of $\delta^{18}O$ values from +4.9 to +5.1‰ (Table 5.4).

Primary $\delta^{18}O$ values of olivine

The O-isotope compositions of olivines ($\delta^{18}O$ = +4.9 to +5.1‰) from four representative Denchai basalts are in good agreement with those reported for olivines from Ocean Island

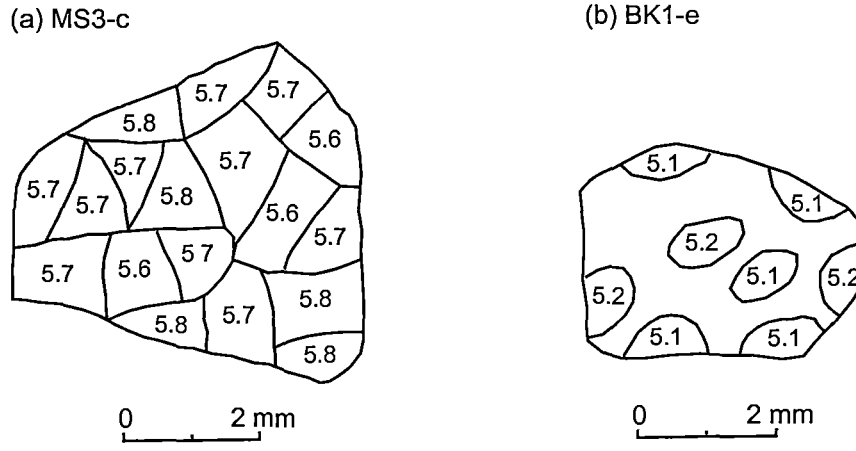

Figure 5.3 O-isotope variations of thin slab sapphires parallel to (0001) plane, (a) Sample MS3-c and (b) Sample BK1-e,
Analytical errors of O-isotope compositions across the slab is +0.1 per mil

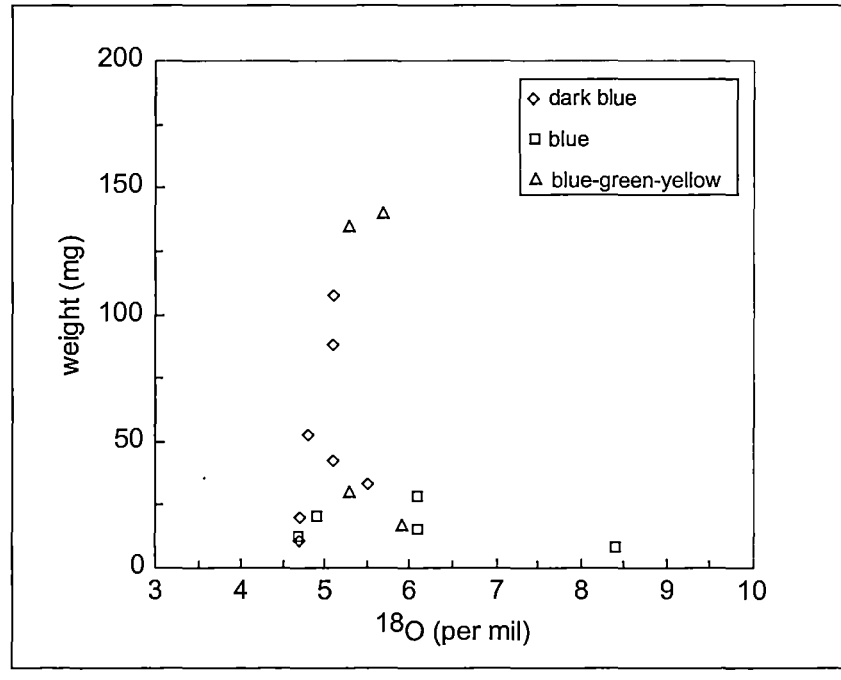

Figure 5.4 Variation diagram between O-isotope values versus sample weights of the Denchai sapphires

Basalt (OIB; $\delta^{18}O$ = +5.0 to +5.4‰; Eiler *et al.*, 1997; Harris *et al.*, 2000). Mantle olivines, whether from hydrous or anhydrous mantle, all have similar O-isotope compositions in the range from +4.8 to +5.5‰ (Mattey *et al.*, 1994), and basaltic magmas derived from such mantle sources would presumably have homogeneous and similar $\delta^{18}O$ values. Therefore, the $\delta^{18}O$ values of olivines from representative Denchai basalts are compatible with a strictly mantle origin for the basalts.

Table 5.4 Oxygen isotope compositions of olivine from the Denchai basalts

Sample	$\delta^{18}O$(‰)
DC28	5.1
DC40	5.1
DC45	5.1
DC61	4.9

Under temperature conditions of 1000-1300°C of basaltic magma, the equilibrium O-isotope fractionation between olivine and corundum would be in the range from +0.38 to +1.35‰ (Zheng, 1991, 1993), although theoretically olivine and corundum are not compatible minerals in basaltic systems (Liu and Presnall, 1990, 2000). Six samples out of sixteen Denchai sapphires have $\delta^{18}O$ values (> +5.4‰; Table 5.3) higher than expected for mantle O-isotope compositions, and one grain has $\delta^{18}O$ values beyond the maximum possible range (+5.4 to +6.8‰).

Primary $\delta^{18}O$ signature of sapphire

The O-isotope composition of the Denchai sapphires range from +4.7 to +8.4‰ (Table 5.3). The previous section has shown that some of the sapphire oxygen isotope variations are too large to be in equilibrium with the mantle $\delta^{18}O$ values (5.7 ± 0.3‰; Hoefs, 1987). Baker *et al.* (2000) reported that fractional crystallisation of the observed mineral phases (ol + cpx) in the Yemen flood basalts cannot generate the range in mineral $\delta^{18}O$ values more than +1‰. Clearly, some processes other than fractional crystallisation was involved during the genesis of sapphire. Upton *et al.* (1999) suggested that a carbonatitic melt was responsible for the peraluminous nature of the fractionated upper-mantle melts required to form corundum. However, this mechanism would lower, not increase, the O-isotope composition. Assimilation of continental crust could be the reason for elevated $\delta^{18}O$ values, at least for those Denchai sapphires with $\delta^{18}O$ values higher than +5.5‰. With increasing $\delta^{18}O$ values, sapphires could have originated from melts assimilating, most likely, crustal basement rocks (e.g., granulite and granitic rocks). Granulite rocks have quite low $\delta^{18}O$ values between +6

and +8‰ (Hoefs, 1987), and $\delta^{18}O$ values +7 to +10‰ are typical for most granitic rocks (Taylor, 1978). In particular, Sample BK-2-b ($\delta^{18}O$ value of +8.4‰) has a crustal O-isotope signature. The Denchai sapphires with variable O-isotope compositions may be products of melts with lower crust interaction that were picked up and carry to the surface via subsequent basaltic eruptions. The most important result is the variability of Denchai sapphires $\delta^{18}O$ isotope compositions that is interpreted here as evidence of mixing between two sources (i.e., crust and mantle).

5.5 Fluid/melt inclusion characteristics

Microthermometric measurements of fluid inclusions in the Denchai sapphires can provide important information on the prevailing physicochemical conditions of fluids associated with sapphire formation. Insights can be gained into the thermal history and chemical composition of distinct fluids that were present during growth of sapphires.

Classification criteria for fluid, solid and melt inclusion studies employed here are from Roedder (1984). There are four types of inclusions: fluid inclusion (FI), solid inclusion (SI), melt inclusion (MI) and composite inclusions (V ± L ± S), which can be classified into primary, pseudosecondary and secondary. Primary inclusions form during crystal growth and thus record conditions at which enclosing crystal forms. The primary inclusions in the Denchai sapphires occur within coloured growth bands. Pseudosecondary inclusions form during the growth of a crystal but along healed microfractures that do not dissect grain boundaries. Secondary inclusions form later, and are usually trapped as a result of the re-healing of fractures after crystal growth (Roedder, 1979, 1984). Primary and/or pseudosecondary inclusions can provide a valuable insight into the nature and origin of ancient mineral-forming fluids. Secondary inclusions have not been investigated in this study.

Forty-nine doubly polished thick sections (or wafers) of sapphires were prepared for fluid inclusion petrography and microthermometry. Most of the inclusions in the Denchai sapphires selected for analyses either have negative crystal or rounded shapes and are about 10-100 μm in diameter. Inclusions of less than 2 μm in size are abundant, but their small size precludes analysis. Based on optical studies, three types of primary fluid/melt inclusions can be distinguished: CO_2-rich inclusions (Type-I), polyphase (V+L+S) inclusions (Type-II) and silicate-melt inclusions (Type-III). These are shown in Figure 5.5.

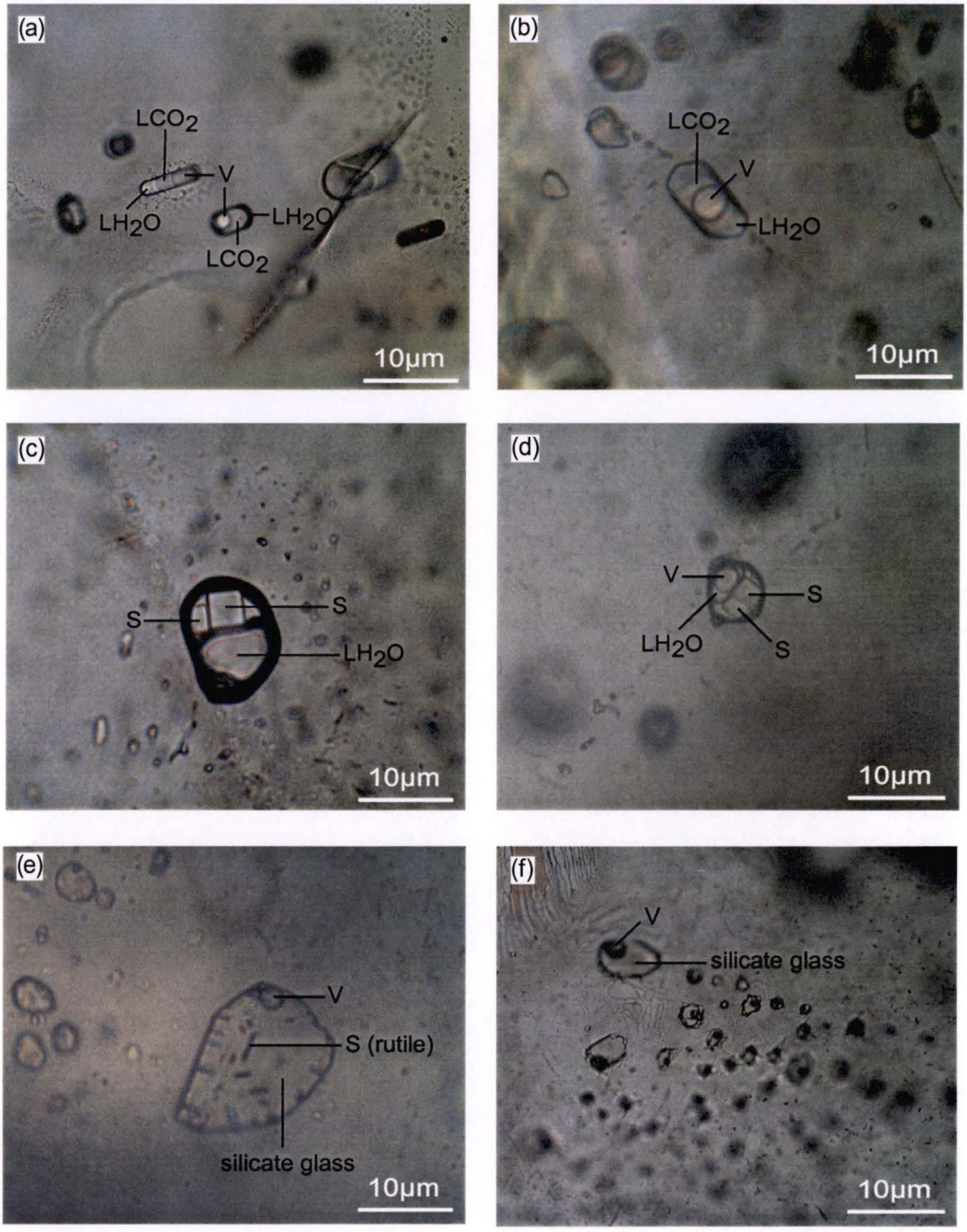

Figure 5.5 Photomicrographs of three types of inclusions in the Denchai sapphires.
(a), (b) CO_2-rich inclusions (Type-I); LH_2O = liquid H_2O, LCO_2 = liquid CO_2, V = Vapour,
(c), (d) polyphase (V+L+S) inclusion (Type-II); V = vapour, LH_2O = liquid H_2O, S = halite and sylvite,
and (e), (f) silicate-melt inclusions (Type-III) containing vapour bubble (V), silicate glass and
the solid phases (S). The needle-like solid mineral is rutile.

5.5.1 Microthermometric results

Microthermometry was carried out on both USGS and Linkam MDS600 heating/freezing stages. Heating and freezing experiments were conducted on the primary fluid inclusions of Type-I and Type-II. All fluid inclusion results are tabulated in Appendix E. Salinity was determined as NaCl equivalent weight percent (wt% NaCl equiv.). For those inclusions that contained undersaturated solutions of H_2O-NaCl, salinity was calculated as wt% NaCl equiv. using the method described by Shepherd *et al.* (1985).

Fluid inclusion microthermometry experiments have revealed that the two fluid inclusion types can be categorised into low salinity inclusions (Type-I) and high salinity inclusions (> 58 wt% NaCl equiv.; Type-II).

Type-I CO_2-rich inclusions

Type-I CO_2-bearing inclusions range in size between less than 5 μm and 30 μm. They contain three phases (LH_2O+LCO_2+V) with the vapour phase comprising less than ~10-15vol% (Figs.5.5a, b). During freezing experiments, all inclusions were frozen to aggregates of solid CO_2 by cooling the Type-I inclusions down to temperatures of about -170°C. No phase transitions were observed in this temperature range, implying that N_2 and CH_4 must either be not present or only be present in minor quantities (Touret, 1982; Kerkhof and Olsen, 1990). The melting temperatures (Tm) of CO_2 solid range between –55.6 to –57.7°C (n = 50), indicating pure CO_2 (Fig.5.6). Laser Raman Spectroscopic (LRS) analysis has confirmed the presence of CO_2 (see Section 5.5.2). Melting temperatures below -56.6°C may indicate the presence of additional components (e.g., N_2, CH_4). On heating, the homogenisation temperature of CO_2 into liquid ranges from +11.2 to +31.0°C (n = 41) and their density ranges between 0.87 to 0.46g/cm^3. The homogenisation temperature of CO_2 into vapour ranges from +24.6 to +30.4°C (n = 29; Fig.5.7) corresponding to densities in the range of 0.24 to 0.46g/cm^3, using the phase relation data from Shepherd *et al.* (1985). Some inclusions homogenise close to +31.1°C showing critical phenomenon.

Results from microthermometry and LRS analysis show that only minor amounts of volatile components other than CO_2 and H_2O are present in the Type-I inclusions. The volumetric properties of the inclusion fluids are therefore closely approximated by volumetric data for pure CO_2 (Holloway, 1981). As CO_2 was visible during all of the freezing measurements, the CO_2 concentrations in the fluid inclusions must be more than 4.4wt% (Roedder, 1984).

Many phase equilibria data for the binary H_2O-CO_2 system have been reported and the immiscibility field in the H_2O-CO_2 system at high *P-T* has been delimited experimentally (e.g., Bowers and Helgeson, 1983; Sterner and Bodnar, 1991; Duan *et al.*, 1995).

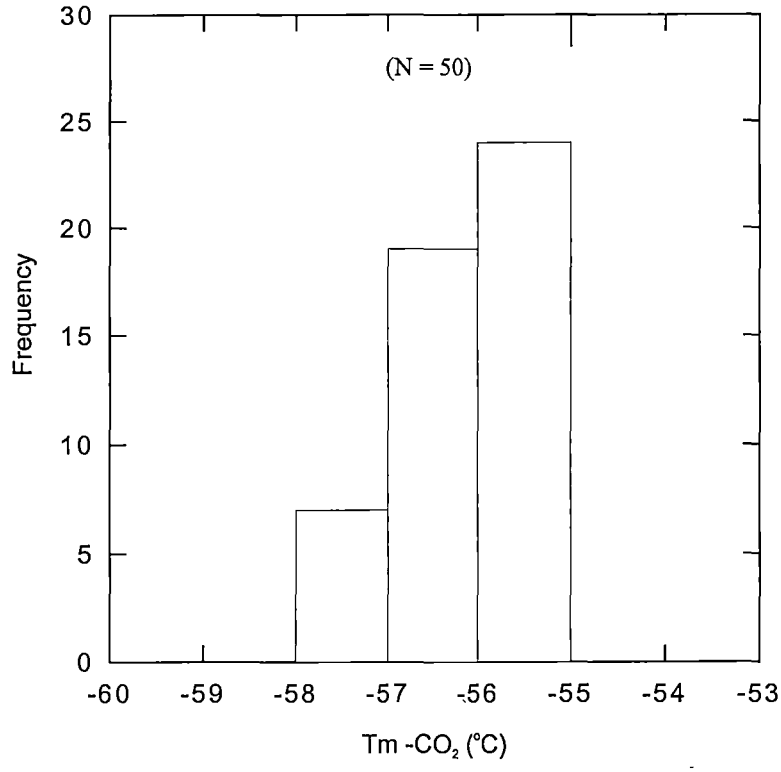

Figure 5.6 Histogram of melting temperature (Tm -Co_2) for CO_2-rich inclusions (Type-I) in the Denchai sapphires

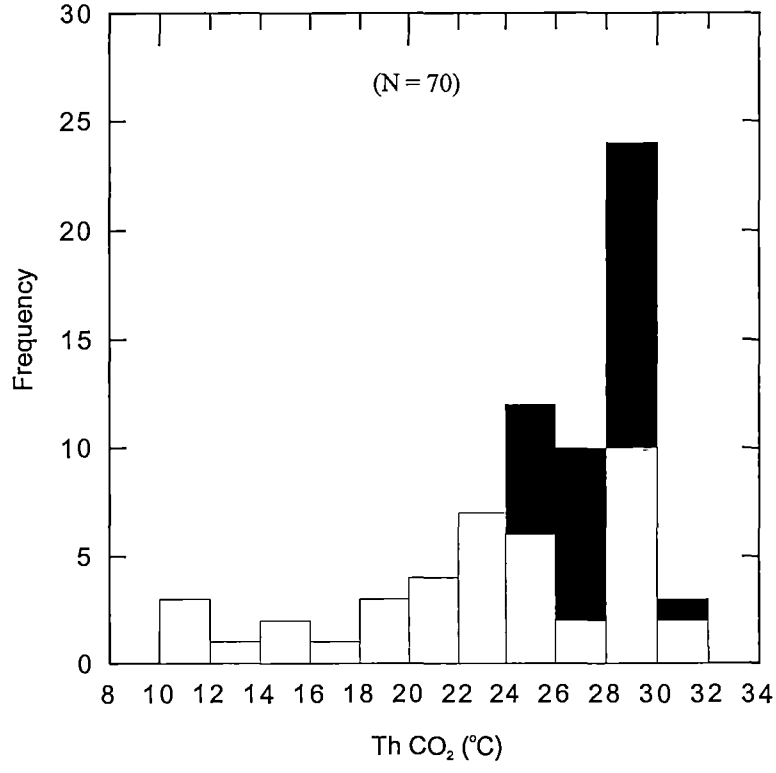

Figure 5.7 Histogram of homogenisation temperature (Th) of CO_2-rich inclusions (Type-I) in the Denchai sapphires
(a) Homogenisation to liquid (Th_L; grey) and
(b) Homogenisation to vapour (Th_V; black)

Helgeson *et al.* (1978) demonstrate that the H_2O-CO_2 immiscibility field can expand for a constant pressure if NaCl is added and the H_2O-CO_2 immiscibility field can exist well above 4 kbars and 300°C. An estimated trapping pressure of the Type-I inclusions was performed using a computer program MacFlincor (v.0.84) written by Brown and Hagemann (1994). The calculations have been performed using the Equation of State for H_2O-CO_2-NaCl fluids at high *P-T* (Bowers and Helgeson, 1983). The estimated trapping pressures of H_2O-CO_2 system (Type-I) range between 3.3 and 8.6 kbars at 800°C. In addition, the experimental results (Joyce and Holloway, 1993) suggested that H_2O-CO_2 immiscibility field occur at 2 kbars, 750°C and 4 kbars, 650°C. These results are in good agreement with the predictions of Kerrick and Jacobs (1981) equation at high temperatures (> 550°C). The probable trapping temperatures of Type-I inclusions are > 550°C with a minimum pressure of 4 kbars.

Type-II Polyphase inclusions

Type-II polyphase inclusions are small, ranging in size from less than 5 to 20 μm. They contain a vapour bubble, which occupies about 20-30vol% of the inclusion, an aqueous phase which occupies 10-15vol% of the inclusion and translucent cubic-shaped crystals (Figs.5.5c, d). Recognition of solid phases within inclusions using their optical properties (cubic and isotropic) indicates that they are probably halite (higher relief) and/or sylvite (lower relief). The dissolution temperatures of large daughter minerals (halite) are between 480°C and 510°C (n = 2) with lower dissolution temperatures less than 400°C of small daughter minerals (sylvite). Based on dissolution temperatures of halite these Type-II inclusions contain solutions with salinity between 58 and 64 wt% NaCl equiv. (Shepherd *et al.*, 1985). Total homogenisation of Type-II inclusions was not achieved as a vapour bubble still remained even when the inclusions was held at 600°C (the maximum temperature of both USGS and Linkam MDS600 heating/freezing stage) for half an hour.

Bodnar *et al.* (1985) suggested that hypersaline inclusions imply formation in shallow magmatic-hydrothermal system, as the high salinity inclusions (Type-II) could not coexist with the CO_2-rich inclusions (Type-I) at high confining pressure. However, adding NaCl to the H_2O-CO_2 system dramatically increases the *T-P* range of immiscibility field. The experimental prediction of immiscibility boundary for NaCl-H_2O-CO_2 system at 900°C and 7 kbars (Johnson, 1991) indicates that both CO_2-rich (Type-I) and high salinity (Type-II) inclusions could coexist within the sapphire at least up to the limits of the experiments at 7 kbars.

5.5.2 The LRS results

LRS analysis is widely used in the study of natural gemstones because it provides a non-destructive method for identifying small quantities of some molecular components (CO_2, O_2, N_2, H_2S and CH_4) in the vapour phase of individual inclusions as well as identification of both host gemstones and their mineral inclusions. However, the host sapphires need to be transparent so the beam can be focused directly onto the inclusions. Rough surfaces are not recommended because of inaccuracy in focusing of the laser beam as well as difficulties of finding the inclusions. The best results are obtained when they are very close to the surface but it is possible down to a depth of 5 mm. Then spectra for the unknown inclusions are compared with the reference database spectra in order to match the peaks and identify the molecular species.

In this study, sapphire samples were initially studied using grain mounts and doubly polished sections less than 0.3 mm thick. Primary fluid, solid, melt and composite inclusions were partly analysed by Laser Raman Spectroscope (LRS) using a Dilor® SuperLabram spectrometer housed at the Australian Geological Survey Organisation, Canberra. This analytical technique is described in Section 5.2.3. Some of the Raman analyses was done by Mananya (2000) using a Renishaw System 1000 Confocal Raman System, with a 514.5 μm argon ion laser as the excitation source housed at the Analytical Division, Department of Mineral Resources (DMR), Bangkok, Thailand.

The presence of composite (V ± L ± S) inclusions suggests volatile saturation of the melt. LRS was used to scan for CO_2 and CH_4 fluid species in the fluid bubble of Type-I and in the shrinkage bubble of Type-III inclusions (Fig.5.5). CO_2 was present in the bubbles of both types of inclusions, whereas CH_4 was not detected in any of the inclusions. The LRS results suggest that the Denchai sapphires coexisted with CO_2-bearing fluids early in its evolution. The LRS analysis also identified the presence of feldspar and zircon as mineral inclusions in sapphires. Anhydrite ($CaSO_4$) was also identified within the high salinity inclusions (Type-II). In addition, within the Type-III melt inclusions, accidentally trapped minerals were found adjacent to a shrinkage bubble and are close enough to the surface for quantitative Raman analysis. The LRS analysis confirmed the presence of rutile (TiO_2), magnetite (Fe_3O_4) and hematite (Fe_2O_3). Raman spectra of CO_2 and mineral inclusions are shown in Figure 5.8 and the mineral inclusions in the Denchai sapphires are described in Section 5.7.

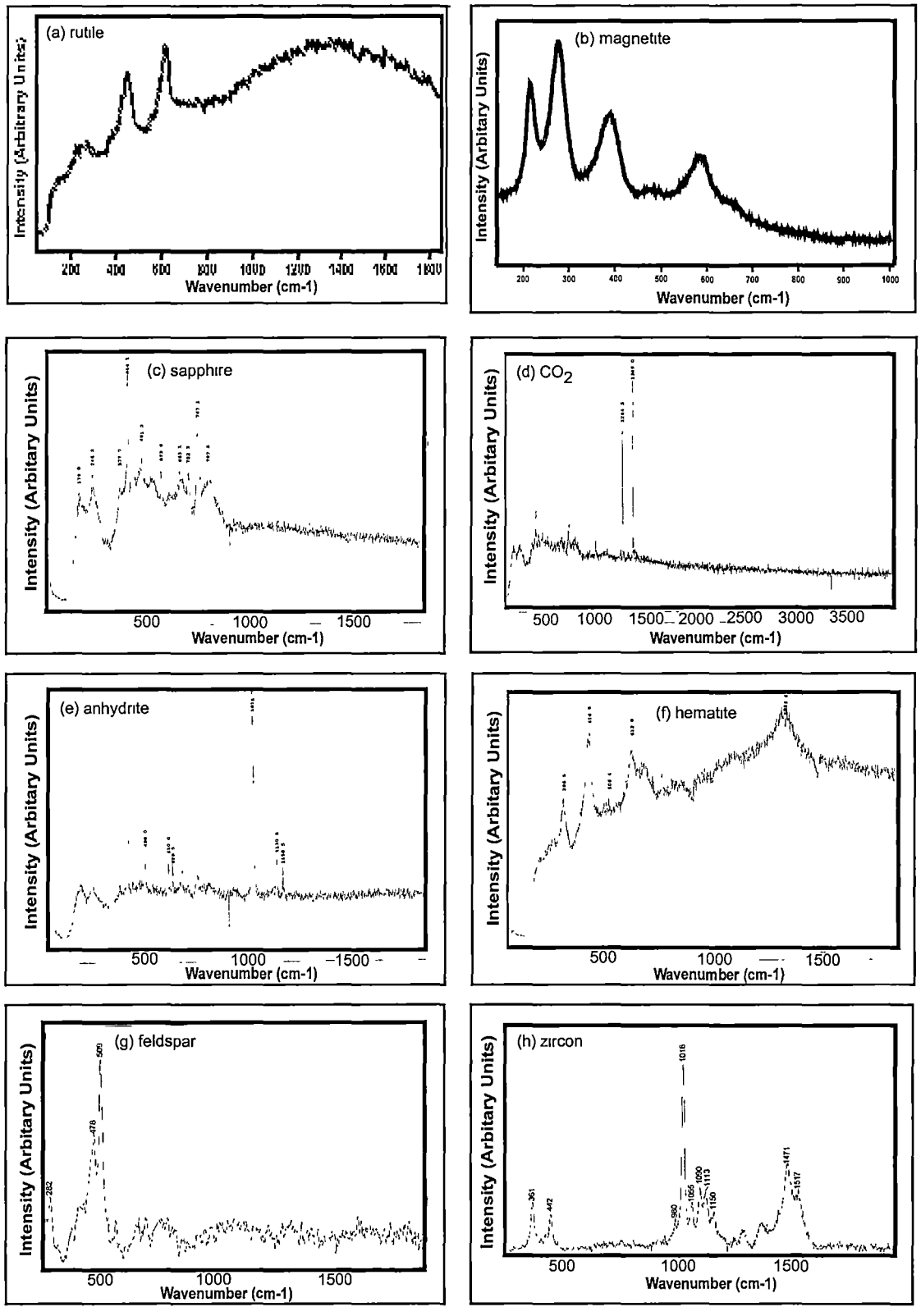

Figure 5.8 Laser Raman Spectra;
(a) rutile, (b) magnetite, (c) host sapphire, (d) CO_2, (e) anhydrite, (f) hematite, (g) feldspar and (h) zircon

5.5.3 The PIXE results

In the early stage of this study, three silicate-melt inclusions (Type-III) from two different sapphire grains were analysed by Proton Induced X-ray Emission (PIXE) using the CSIRO-GEMOC Nuclear Microprobe described in Section 5.2.4. These three inclusions generally contain silicate glass, a shrinkage bubble and solid phases (e.g., rutile and magnetite? or hematite?; Limtrakun *et al.*, 2001). The PIXE results of elemental concentrations are presented in Table 5.5 with PIXE spectra illustrated in Figure 5.9 and element distribution images are shown in Figure 5.10 for the following elements: Al, Ca, Cl, Cr, Fe, Ga, K, Mn, Rb, Sr, Ti, V, Zn and Zr.

Sample Sapp-1-1-1

The results of the PIXE analyses suggest that the chemical content of the melt inclusions (Table 5.5 and Fig.5.9a) include 2.0wt% Fe, 2.0wt% K, 0.8wt% Ti, 0.4wt% Ca, 0.3wt% Cl and 209ppm Zr contents. Element distribution images have been reproduced in Figure 5.10a. The diffuse patterns of K and Cl implies the melt inclusion contain alkali- and chlorine-rich solutions, whereas the concentrated distribution patterns Fe and Ti are more likely to be from trapped minerals (probably rutile and magnetite) but this would not explain the high Fe contents (Fe > Ti). A small opaque trapped mineral (Fe-Mn bearing mineral) can be seen attached with the bubble (Fig.5.10a).

Table 5.5 Results of PIXE analyses

Sample	Type	Cl	K	Ca	Ti	Fe	V	Cr	Mn	Ga	Zn	Br	Zr	Rb	Pb
		(wt%)					(ppm)								
Sapp-1-1-1	III	0 33	1.96	0 36	0.8	2.02	261	<8	379	437	15	<23	209	47	<34
Sapp-1-1-2	III	0 54	3.98	0 56	1.13	2 7	308	8	455	598	30	<36	242	70	64
Sapp-3-3-6	III	2.85	0.78	0.13	0.78	3 5	532	nd	365	889	45	36	<193	<203	91

nd = not detected

Sample Sapp-1-1-2

The melt inclusion measured contains 2.7wt% Fe, 4.0wt% K, 1.1wt% Ti, 0.6wt% Ca, 0.5wt% Cl and 242ppm Zr values (Table 5.5 and Fig.5.9b). Elemental concentrations (e.g., Al, Br, Cr, Sr and Zn) were detected but quantitative analysis was not possible. Elevated concentrations can be seen in the element distribution images (Fig.5.10b). The diffuse pattern of potassium implies the glass is alkali-rich, whereas the concentrated distribution patterns Fe, Ti and Mn are from the needle-like trapped minerals (rutile). A small opaque trapped mineral (magnetite?) can be seen attached to the bubble (Fig.5.10b).

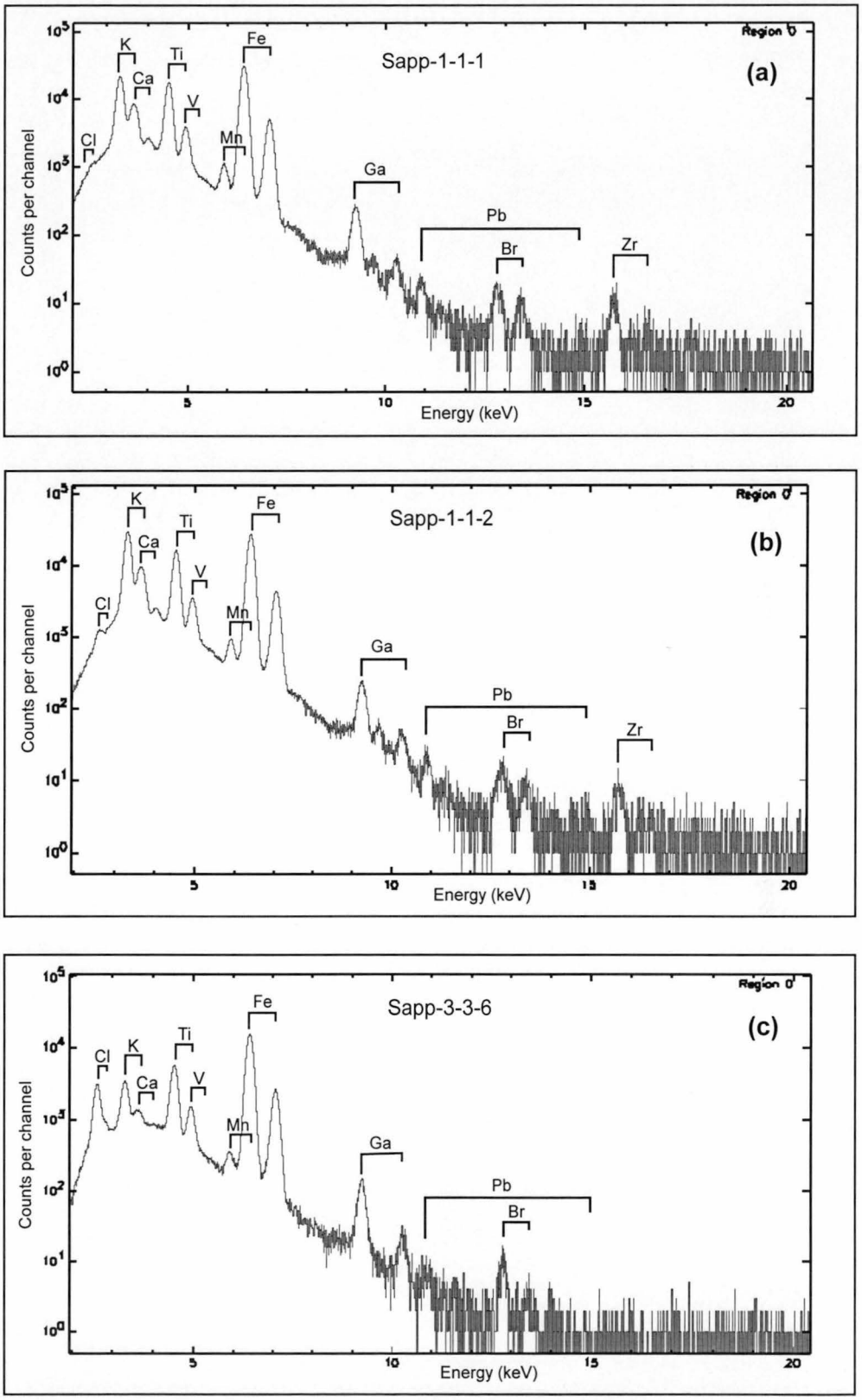

Figure 5.9 PIXE analytical spectra of silicate melt inclusions; (a) Sapp-1.1.1, (b) Sapp-1-1-2 and (c) Sapp-3-3-6

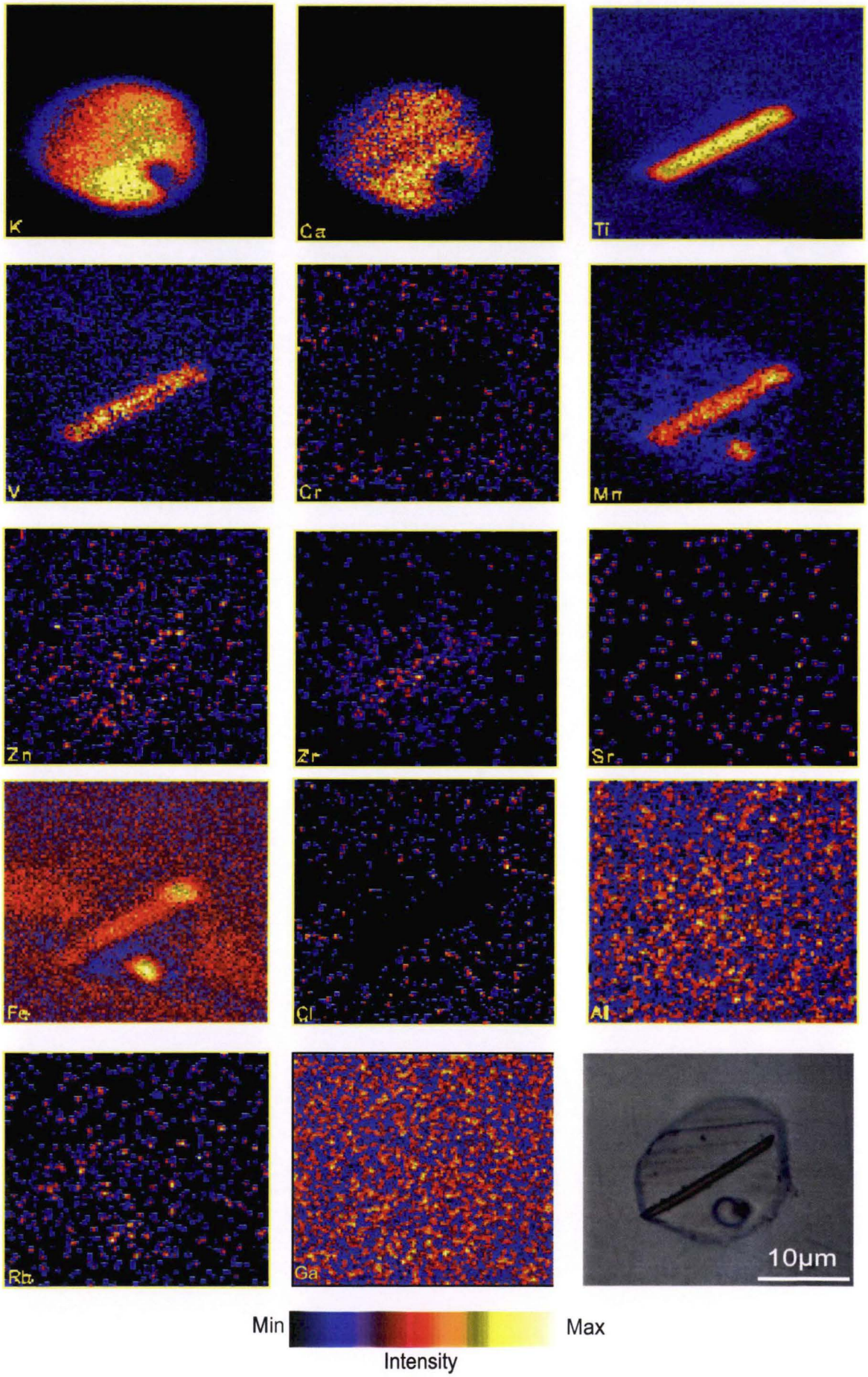

Figure 5.10a PIXE element distribution images of Sample Sapp-1-1-1,
The same intensity scale applies to all images. Scale bar is 10 microns for all images.
See text for discussion.

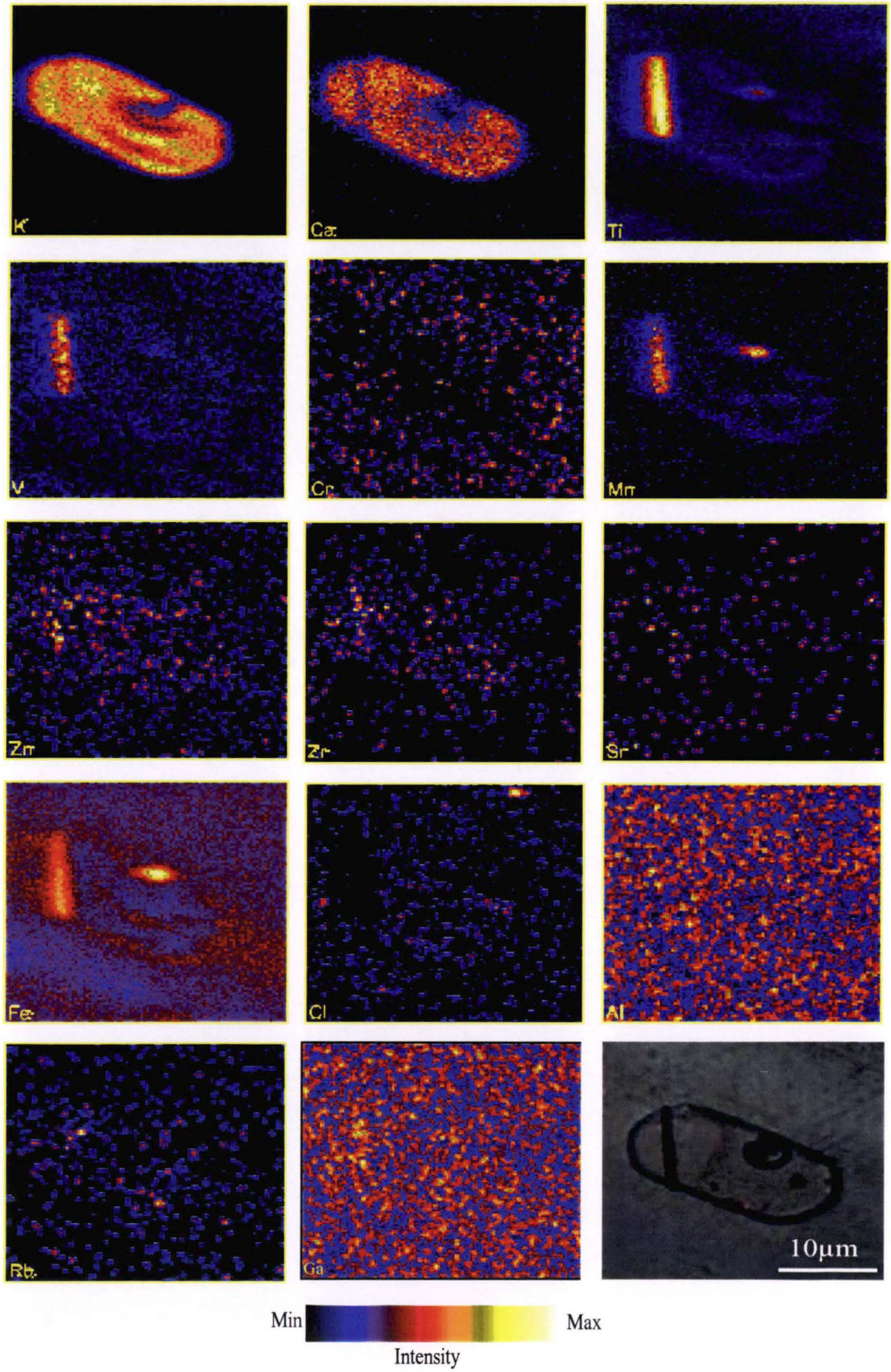

Figure 5.10b PIXE element distribution images of Sample Sapp-1.1-2,
The same intensity scale applies to all images. Scale bar is 10 microns for all images.
See text for discussion.

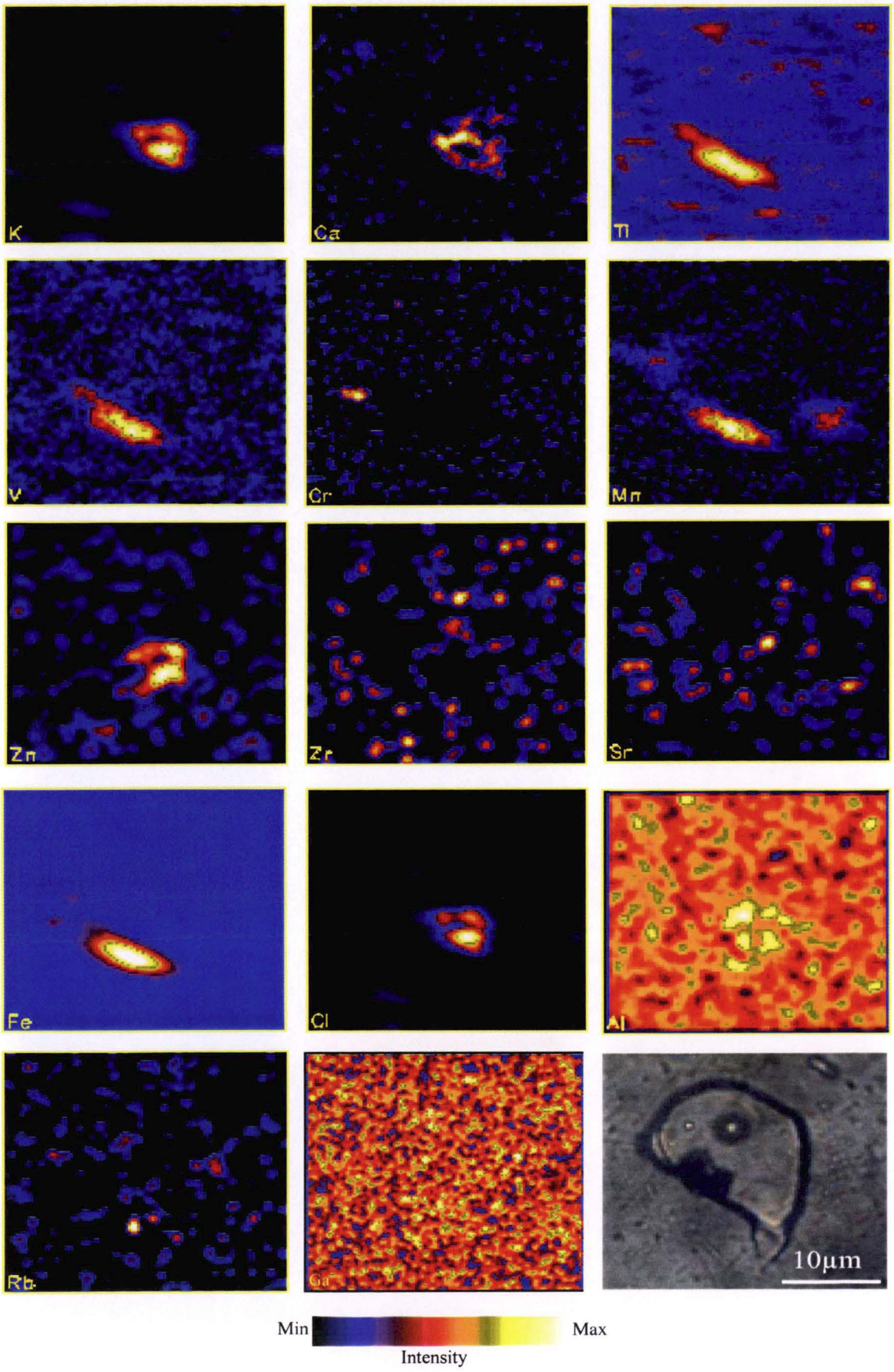

Figure 5.10c PIXE element distribution images of Sample Sapp-3-3-6,
The same intensity scale applies to all images. Scale bar is 10 microns for all images.
See text for discussion.

Sample Sapp-3-3-6

The results of the PIXE analyses show that the melt inclusion contains 3.5wt% Fe, 0.8wt% K and 2.8wt% Cl values (Table 5.5 and Fig.5.9c). This inclusion appears to have broken but elevated concentrations can still be seen in the element distribution images (Fig.5.10c). The diffuse pattern of elements such as K, Ca and Cl were detected, while Fe, Ti and Mn are from the trapped minerals (magnetite; Fig.5.10c).

In Sample Sapp-1-1-1 and Sample Sapp-1-1-2, the elements which could represent melt compositions are K, Ca and Cl, whereas Ti, Mn and V concentrations are possibly from trapped minerals (probably rutile and magnetite) within the inclusion. As iron and gallium are relatively enrich in sapphire (described in Section 5.4.4) their concentrations in the host could have affected the data presented. The Fe values could have been affected by both host and trapped minerals, whereas the high apparent Ga content of these two inclusions is probably due to contamination of the spectra by the host sapphire. These two melt inclusions also show low Al content compared to the Sample Sapp-3-3-6. This may indicate that the inclusion in Sample Sapp-3-3-6 is deeper than the other two examples.

In this technique, Al cannot be detected in the melt inclusions because of the Al-rich host (sapphire). A silicate melt without Al would be very unusual and no normal magmas are entirely devoid of Al. This problem can be solved by using electron microprobe analysis of exposed melt inclusions.

5.6 Magmatic inclusions

Studies of melt inclusions have been widely documented (Roedder, 1979; Clocchiatti and Massare, 1985; Sobolev *et al.*, 1991; Sisson and Layne, 1993), as it can provide a tool to explain the early stages of magma evolution. After the entrapment of melts, the crystallisation of host and several daughter phases continues within the melt inclusion and modifies the composition of the trapped melt. To approach this question, A Linkham-1600 melt inclusion heating stage at the School of Earth Sciences, University of Tasmania was used to redissolved daughter phases and the homogeneous melt quenched to a glass, then it can be prepared for electron microprobe analysis. This technique has been reported extensively by number of authors (Sigurdsson, 1994; Sobolev and Danyushevsky, 1994; Della-Pasqua, 1997) and is briefly described in the following section.

Ideally, the composition of homogenised melt inclusion glasses should resemble the original composition of the trapped melt. However in practice, the composition of these glasses may

differ from the original due to diffusion and re-equilibrium of the melt with the host, before eruption (Sobolev and Danyushevsky, 1994). Therefore, the interpretation of these bulk glass analyses in some cases may be ambiguous. Nevertheless, the ratios of incompatible major elements in these glasses are not changed and may be used to address primitive chemical compositions of the parental melt (Falloon and Green, 1986; Sullivan, 1991; Sigurdsson, 1994; Sobolev and Danyushevsky, 1994). In particular, melt inclusions in gem sapphires could be a direct tool to investigate the compositions of parental melts of gem sapphires. The rationale of this magmatic inclusion study is attempting to address what kind of parental melt compositions were involved in the crystallisation of the studied sapphires, i.e. carbonatitic/felsic melts or syenitic/pegmatitic/granitic melts (Guo *et al.*, 1996a; Upton, *et al.*, 1999).

Type-III silicate-melt inclusions

Classification used in this study for magmatic inclusions in the Denchai sapphires are described in Section 5.5. After entrapment, crystallisation of host continues on the wall of inclusion and with a continued decrease in temperature, several phases may form from the residual melt within the melt inclusion to produce a crystalline texture and is known as "crystalline melt inclusion" (Roedder, 1979, 1984; Sobolev *et al.*, 1991). Alternatively, after crystallisation of the host on the wall, the residual melt may be naturally quenched to have a glass texture due to relatively rapid cooling. These types of melt inclusions are known as "vitreous" melt inclusion (Sobolev *et al.*, 1989) or more commonly as "glassy" melt inclusion (Roedder, 1984). Cooling down of a melt inclusion after trapping also leads to the formation of a shrinkage bubble (vapour phase). A bubble forms due to a change in density, and thus volume, inside the inclusion as a result of the growth of daughter phases, which also leads to an increased volatile pressure within the melt inclusion. As a shrinkage bubble forms, volatile species dissolved in the trapped melt may partition into the shrinkage bubble, which may or may not approach a vacuum, depending on the original concentration of volatile in the melt (Roedder, 1984). Therefore, information can be obtained from (L+V) type primary inclusions on the volatile species that could have been dissolved in the parental melt (Bacon *et al.*, 1992; Tait, 1992). Alternatively, if the magma was volatile oversaturated, the immiscible fluid bubbles in the magma could either be accidentally trapped by a growing host to form (V±L) primary fluid inclusions, or attached to a pre-existing crystal (e.g., rutile) and later trapped by a growing host to form a composite (V + S ± L) type primary inclusion, as described in Figure 5.11. In the latter type of inclusions, the glass-bubble volume ratio will be random as opposed to the (V+L) inclusion type described above, where glass/bubble volume ratios are constant (Sisson and Layne, 1993).

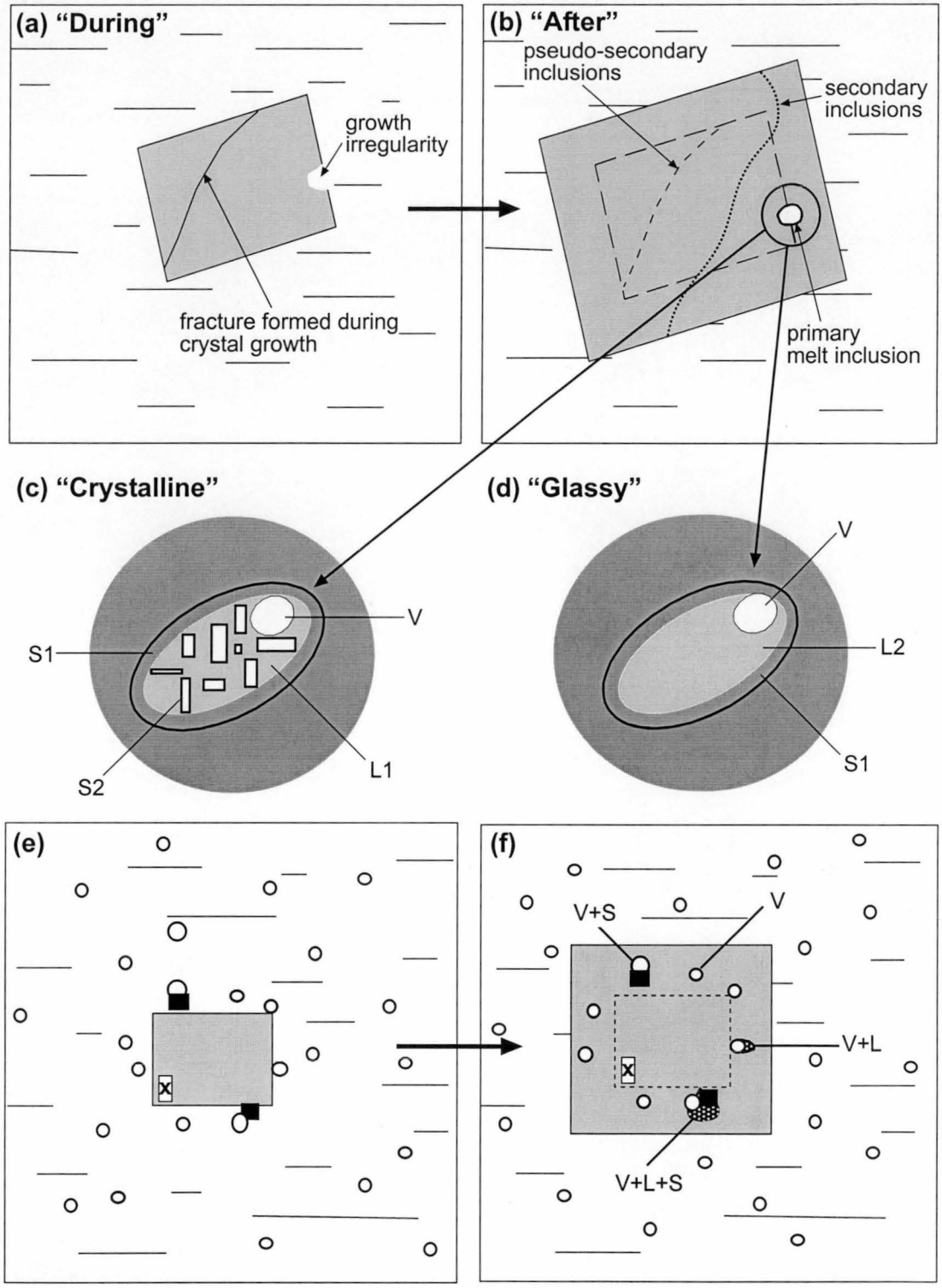

Figure 5.11 Illustration of the formation of trapped inlusions (modified from Roedder, 1979 and Della-Pasqua, 1997);
(a) "pseudo-secondary" inclusions trapped by the healing of fractures and "primary" melt inclusions trapped by growth irregularities synchronous with crystal growth. Both types are produced during crystal growth and become enclosed in the crystal as growth continues,
(b) "secondary" inclusions trapped by the healing of fractures produced after crystal growth,
(c) "crystalline" melt inclusion textures. After entrapment, crystallization of the host mineral continues on the wall (S1) and a shrinkage bubble forms (V). With continued decrease in temperature other phases may crystallize inside the inclusion to form daughter crystals (S2) and a residual glass (L1),
(d) "glassy" melt inclusion textures. Fast cooling rates after entrapment may naturally-quench the residual melt to a glass (L2) without the growth of daugther phases,
(e) and (f) Entrapment of a primary fluid inclusion (V), and "composite" primary inclusions (V+S, V+L, V+L+S) by a growing crystal.

Sample selected in this study

Melt inclusions within the Denchai sapphires include glassy and composite inclusions (Fig.5.12). The studied samples are listed in Table 5.6 and types of melt inclusions in the Denchai sapphires are described in Section 5.5. Primary melt inclusions vary from abundant to absent within a single grain from any sample. Melt inclusions are most commonly found in the dark blue to blue sapphires and less common in the blue-green-yellow sapphires. The sizes of melt inclusions range between ~10 to 30 μm and rarely exceeding 50 μm. Large melt inclusions contain a shrinkage bubble whereas smaller inclusions (< 10 μm) are glassy and lack a shrinkage bubble. Within crystalline melt inclusions, daughter phases (unidentified minerals) and a CO_2-rich vapour phase has been confirmed by the LRS study (Section 5.5.2). Composite inclusions consist typically of accidentally trapped minerals (i.e., rutile, hematite and magnetite) together with variable of proportions of melt, and an associated shrinkage bubble (V + L + S).

Table 5.6 The Denchai sapphire samples used for melt inclusion study

Sample	Location	Colour	Remarks
BK001	Ban Bo Kaeo	dark blue	transparent to opaque
BK002	Ban Bo Kaeo	dark blue	transparent to opaque
BK003	Ban Bo Kaeo	blue	transparent to opaque
BK004	Ban Bo Kaeo	blue	transparent to opaque
BK006	Ban Bo Kaeo	bluish green	transparent
BK007	Ban Bo Kaeo	yellowish green	transparent
BK010	Ban Bo Kaeo	blue-green-yellow	transparent
MS001	Ban Mae Sin	blue	transparent
MS002	Ban Mae Sin	blue	Transparent to semi-translucent
MS003	Ban Mae Sin	greenish blue	transparent
MS004	Ban Mae Sin	yellowish green	transparent
MS005	Ban Mae Sin	reddish blue	transparent
MS007	Ban Mae Sin	blue-green-yellow	transparent

5.6.1 Experimental methods

This study focuses on the compositions of silicate-melt inclusions from the Denchai sapphire samples. Sapphires with primary melt inclusions were selected for experimental work and extracted from their probe mounts for further study and homogenisation. Sample preparation procedures were described in Section 5.3.

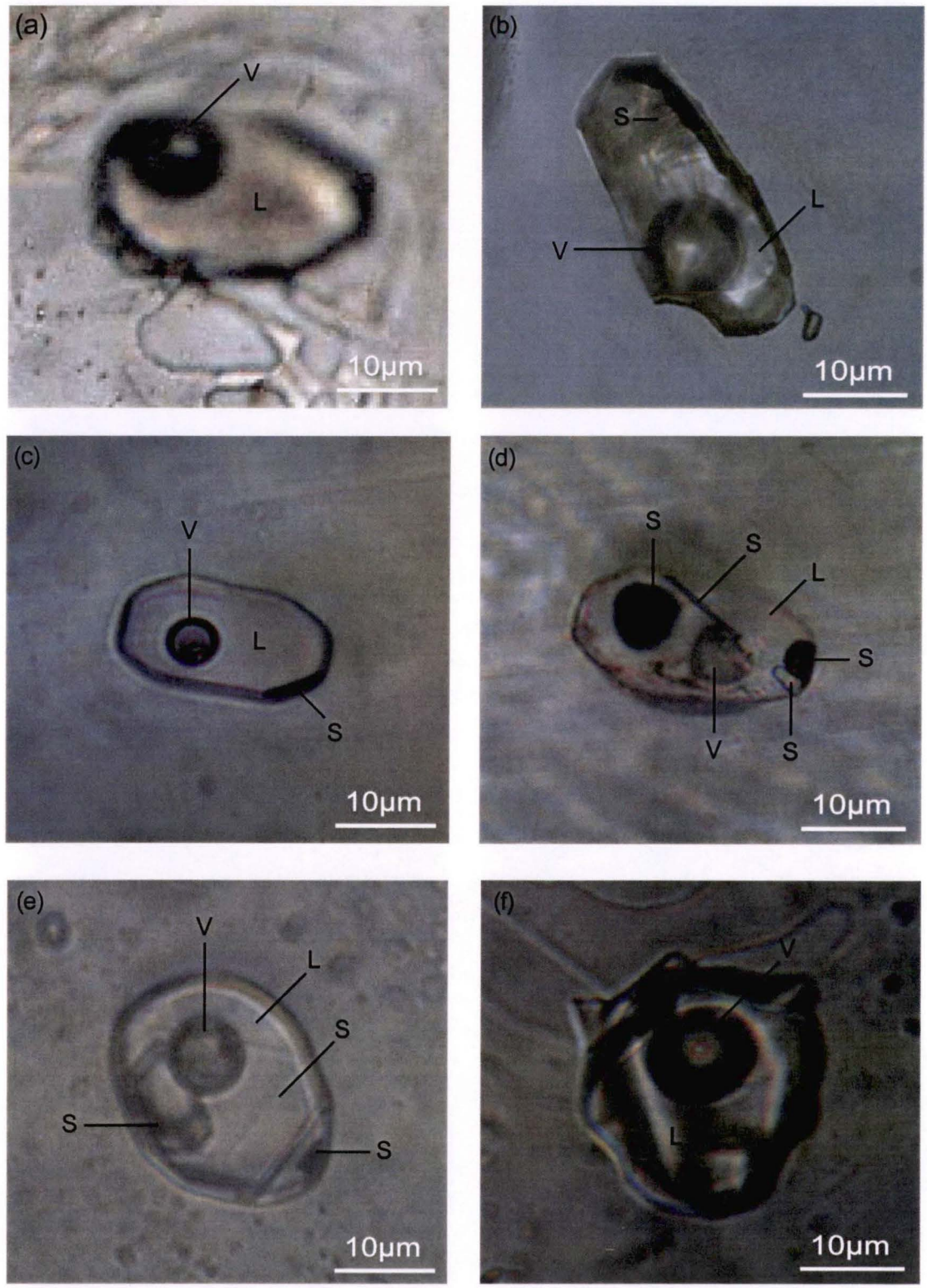

Figure 5.12 Photomicrographs of primary melt inclusions in the Denchai sapphires.
(a) "Glassy" melt inclusion; L = melt, V = shrinkage bubble, Sample BK007, plane polarised light (PPL), 100x,
(b) "Crystalline" melt inclusion; S = unidentified mineral, V = shrinkage bubble, Sample MS001, PPL, 50x,
(c) "Composite" melt inclusion; L = melt, S = rutile, V = shrinkage bubble, Sample MS003, PPL, 200x,
(d) "Composite" melt inclusion; L =melt, S = rutile, magnetite and K-feldspar? (colourless),
V = shrinkage bubble, Sample MS003, PPL, 200x,
(e) "Composite" melt inclusion; L = melt, S = magnetite and K-feldspars? (colourless),
V = shrinkage bubble, Sample BK001, PPL, 100x,
(f) optically homogenised ("heated") melt inclusion, Sample BK007, Tq = 1250^{o}C, PPL, 100x.

Homogenisation technique

Experimental work was carried out using a Vernadsky Institute heating stage set up at the School of Earth Sciences, University of Tasmania, as designed by Sobolev *et al.* (1980) which allows visual monitoring and manual control of temperature during heating. Homogenisation experiments with recrystallised melt inclusions were performed at 1 atm and the maximum homogenisation temperature of the melt inclusion heating stage is 1700°C. Each-inclusion-bearing grain is progressively heated in an ultra-pure He atmosphere while melting behaviour of the inclusion is observed and the temperature at which the various phases disappeared is recorded. This technique is most appropriate for fluid-saturated melts because it relies on fluid bubble disappearance to dictate the homogenisation point. After trapping, crystallisation on to the walls of inclusion leads to a decrease in pressure that causes this bubble to nucleate. During a homogenisation experiment, pressure inside the inclusion increases as daughter phases dissolve, and the bubble will disappear when the pressure inside the inclusion is equal to the pressure at the moment of trapping. At this moment all daughter phases that formed during cooling are molten and the composition of the melt theoretically corresponds to the composition of the trapped melt. At this stage the melt inclusion is "homogenised" and it can be quenched to a glass for electron microprobe analysis. However, in the sapphire melt inclusions studied, complete homogenisation was not achieved and bubbles remained as a separate phase even after considerable overheating (1250°C). This suggests kinetic effects may play a significant role in preventing complete homogenisation of the melt inclusion (Danyushevsky *et al.*, 1992; Gurenko *et al.*, 1992). This problem can compromise the use of standard homogenisation techniques that depend on the bubble disappearance as an indicator of complete homogenisation known as "optical homogenisation".

Optical homogenisation technique

In this technique melt inclusions are heated up to temperature at which the last daughter crystals are observed to melt, therefore melt inclusions become optically homogeneous (Sobolev *et al.*, 1990; Hansteen, 1991; Gurenko *et al.*, 1992). After optical homogenisation of the melt inclusions has been achieved, the host grains are quickly cooled and the molten melt inclusions quenched to homogeneous glass. Then the host grains are mounted in epoxy and individually cut and polished until the homogenised melt inclusions were exposed for electron microprobe investigation. However, incomplete remelting of the host on the wall or the melting of the host and trapped-minerals may modify the optically homogenised glass composition, therefore the homogenisation temperature at which these melt inclusions were quenched, does not necessarily represent the trapping temperatures. The implications of this result are discussed in Section 5.6.2.

Electron microprobe

Both homogenised and non-homogenised inclusions as well as host grains were analysed using a CAMECA SX-50 electron microprobe at the University of Tasmania, under analytical conditions described in Appendix C. The beam size used on the melt inclusion glasses was restricted by the size of the inclusions, occasionally 50 μm but average 10 to 20 μm in diameter. The risk is that the excited volume of the electron beam might interact with the host sapphire. When small melt inclusions were being analysed, a focused beam in the centre of the inclusion was used to reduce this effect. Analysis points were chosen to be more than 5 μm away from the edge based on the results of microprobe traverses across melt inclusions by Roedder (1979) and Sullivan (1991). The melt inclusions which are relatively large (> 10μm) are simple to analyse. However, melt inclusions with diameters less than ~10 μm were also analysed due to lack of primary melt inclusions in the studied sapphires, therefore the smallest beam size used on the exposed glasses was 1 μm. Each analysis was done manually and checked for the correct positioning of analytical points in order to prevent any likely interaction of the electron beam with the host sapphire. Volatilisation under these beam conditions was assessed following methods described by Falloon and Green (1987), Sisson and Layne (1993) and Spray and Rae (1995) in which spot and broad area analyses of a glass standard are compared with its known bulk composition. Analyses of glass standard VG-A99 (USNM113498/1) by Jarosewich *et al.* (1980), using 1, 4 and 10 μm beam sizes are shown in Table 5.7. With a 4 μm beam size, Na_2O and K_2O contents are only lower than the standard by 0.1wt%. With a beam size of 1 μm, Na_2O values are ~0.2wt% lower than the standard value (Table 5.7). Analytical conditions for glasses in this study may cause some loss of alkalis but this loss is not sufficient to invalidate the conclusions reached. These analytical conditions reduce the edge effects introduced by a defocused beam on small melt inclusions. Compositional homogeneity of the glass was confirmed wherever possible by analysing the centre and rim of melt inclusions.

5.6.2 Experimental result assessment

The main experimental uncertainty encountered in determinations of the composition of the melts that were originally trapped in the sapphires is related to the "optical homogenisation" technique modified in this study. This uncertainty results because the host continues to crystallise within the melt inclusions during post-entrapment cooling. Within melt inclusions hosted by sapphires for instance, trapped minerals are deposited on the walls of the melt inclusion. Some of the trapped minerals are difficult to identify optically from the primary

host sapphire. With the optical homogenisation technique employed in this study (Section 5.6.1), all of the trapped minerals might not be remelted during heating experiments. Alternatively, some of the host mineral might be melted into the inclusion due to overheating. Hence the melt inclusions compositions from heated inclusions may still be contaminated and their compositions might not be directly representative of trapped melt. Several tests were performed on the analytical data (Appendix C) and confirm that this problem has occurred.

If at the moment of melt-entrapment, the growing crystals are at chemical equilibrium with the surrounding melt in the magma, then the composition of the successfully homogenised melt inclusions should also be at equilibrium with their hosts. This equilibrium for instance can be checked using the mineral-melt thermometer, which calculated the dry-liquidus temperature from the compositions of olivine-melt pairs (Ford *et al.*, 1983). However no such equilibria are available for a corundum host. Corundum stability in the measured glasses is discussed in Section 5.8.

Table 5.7 Microprobe analyses of basaltic glass standard VG-A99 at 1, 4 and 10μm beam size. Operating conditions: 15 kV accelerating voltage, 10 nA beam current, 20 seconds counting times except Na_2O (10 seconds), focussed beam

	1μm			4μm			10μm			VG-A99[1]	
	avg	**std**		**avg**	**std**		**avg**	**std**			
SiO_2	51.13	0.25	***51.53***	50.58	0.26	***51.57***	50.59	0.21	***51.56***	50.94	***51.38***
TiO_2	3.99	0.08	***4.02***	4.00	0.12	***4.08***	4.04	0.09	***4.12***	4.06	***4.09***
Al_2O_3	12.35	0.26	***12.45***	12.14	0.05	***12.38***	12.08	0.41	***12.31***	12.49	***12.59***
FeO*	13.34	0.63	***13.45***	13.38	0.59	***13.64***	13.22	0.38	***13.47***	13.30	***13.41***
MgO	5.08	0.55	***5.12***	4.79	0.35	***4.89***	5.01	0.13	***5.10***	5.08	***5.12***
CaO	9.47	0.58	***9.54***	9.25	0.24	***9.43***	9.25	0.08	***9.42***	9.30	***9.38***
MnO	0.26	0.03	***0.26***	0.24	0.05	***0.24***	0.25	0.04	***0.26***	0.15	***0.15***
Na_2O	2.44	0.15	***2.46***	2.53	0.05	***2.58***	2.57	0.12	***2.62***	2.66	***2.68***
K_2O	0.73	0.08	***0.74***	0.76	0.04	***0.77***	0.78	0.04	***0.80***	0.82	***0.83***
P_2O_5	0.43	0.02	***0.44***	0.41	0.03	***0.42***	0.34	0.18	***0.35***	0.38	***0.38***
Total	99.21			98.07			98.12			99.18	

FeO* = total iron as FeO, avg = average of 10 analyses, std = standard deviation. Numbers in Italics are averages summed to 100%. (1) Standard glass USNM113498/1 (Jarosewich *et al.*, 1980)

5.6.3 Compositions of melt inclusions

The crucial aim of this chapter is to discover whether the melt inclusions trapped in the Denchai sapphires have compositions of basaltic affinities. Electron microprobe analyses were performed on exposed melt inclusions in the sapphires (described in Section 5.6.1). The analytical condition details are described in Appendix C and the complete set of analytical data is given in Appendix F. Compositions of glassy (naturally quenched), heated and mostly non-heated melt inclusions in the Denchai sapphires, with Al_2O_3 values < 30wt% are listed in Table 5.8. They are described below as the compositions of glassy (naturally quench) melt inclusions, the compositions of heated (optically homogenised) melt inclusions and the compositions of non-heated melt inclusions.

Glassy (naturally quenched) melt inclusions

Naturally quenched melt inclusions in the Denchai sapphires were analysed (analyses 3-8; Table 5.8) using electron microprobe analysis. One analysis has the highest Al_2O_3 value (~30wt%) with relatively low SiO_2 content (~52wt%). These glasses contain 24.0-29.6wt% of Al_2O_3 content and the SiO_2 value ranges from 52.2-59.4wt% with a maximum Na_2O/K_2O ratio value of 0.94.

Heated melt inclusions

Five composite melt inclusions were selected and heated using Vernadsky heating stage but the complete homogenisation of these melt inclusions was failed and bubbles remained as a separate phase even after considerable heating at ~1250°C. The first optical property change was observed at 770°C (n = 1). All melt inclusions became clearer and the bubbles moved from the edge into the centre with no significant change in their size at ~1200-1250°C. Neither did the bubbles grow after quenching. Given these changes to the optical properties within the melt inclusions, the minimum homogenisation temperature of melt inclusions is 770°C. For additional data, the heated melt inclusions in sapphires were exposed onto the surface and analysed. Because of sapphire melting of the inclusion walls, the composition of those inclusions could not be used directly as entrapped melt compositions. These representative heated melt inclusions, analysed after heating and optical homogenisation, having 60wt% SiO_2, 25wt% Al_2O_3 and Na_2O/K_2O ratio value about 0.6 (analyses 1-2; Table 5.8).

Non-heated melt inclusions

Most of the melt inclusion compositions in this study were analysed without a heating experiment. The selected melt compositions from non-heated inclusions were critically

Table 5.8 Electron microprobe analyses of melt inclusion compositions in the Denchai sapphires

Sample	SiO_2	Ti_2O	Al_2O_3	FeO	MnO	MgO	CaO	Na_2O	K_2O	P_2O_5	Total	Remarks
BK007/1	60 01	0 72	24 88	1.56	0.44	0 15	1 66	2 87	4 42	0.31	97.01	heated
BK007/1	60 84	0 65	25.25	1 66	0 42	0 14	1 74	2 58	4.40	0.36	98 04	heated
BK007/2	59.44	0 19	23 96	1 36	0 36	0.13	1 38	1.73	5.19	0 32	94 06	non-heated[1]
BK007/2	57 00	0.74	24.64	1 65	0.30	0.10	1.66	3.10	5.32	0 23	94 74	non-heated[1]
BK007/2	57.29	0.65	24.65	1.50	0.44	0 11	1.75	3 91	5 33	0.29	95.90	non-heated[1]
BK007/2	56.89	0 69	24.87	1.65	0.43	0 12	1 80	2 81	5.36	0.34	94.96	non-heated[1]
BK007/2	57.61	0 70	25 27	1.74	0 35	0.11	1.77	2 32	5 31	0.27	95.44	non-heated[1]
BK007/2	52 16	0.61	29.65	1 53	0 44	0 10	1.54	4.70	5.01	0 33	96 09	non-heated[1]
BK001/1	65 05	0.01	16.87	0.09	nd	nd	0 48	4.74	4.59	0 08	91 91	non-heated[2]
MS002/1	65 01	0 31	16.45	0.64	0 19	0.20	0 85	3 30	5.94	0 08	92.95	non-heated[2]
MS003/1	64 92	nd	17.39	0.06	0.11	0 01	0 43	4 27	6 66	0.06	93 92	non-heated[2]
BK002/1	64.39	0.02	17.51	0 01	nd	nd	0.39	5.46	4 36	0 04	92 17	non-heated[2]
BK001/1	64 29	0 07	18.36	0 35	0 17	0 01	2.84	1.81	4.91	0 22	93 03	non-heated[2]
BK002/1	66 53	0 06	18 51	0.10	0.21	0.01	0.55	2.56	5 10	0.09	93.73	non-heated[2]
MS001/1	67 50	0 56	18 59	0.47	0.01	0 20	1 01	0 88	4 83	0.06	94.12	non-heated[2]
BK001/1	63 32	0.06	18.68	0 04	0 05	nd	0 45	4.46	4 42	0 04	91.51	non-heated[2]
BK003	65 51	0 03	18.85	0.03	0 05	nd	0 48	2.63	3.90	0 06	91 54	non-heated[2]
MS002/2	62 87	0.74	19.18	0 61	0.37	0.10	0.83	2.70	5.37	0.07	92 84	non-heated[2]
MS002/2	62 22	0.79	19 21	0 66	0 47	0 09	0.83	4.58	6 20	0 02	95 06	non-heated[2]
BK003	68 63	0 03	19 67	0.03	0.09	nd	0.87	2.76	1.92	0 07	94.07	non-heated[2]
MS007	65 37	0.06	19.78	0 13	0 04	0 02	4.57	3 43	3 19	0 08	96 68	non-heated[2]
MS002/3	64 12	0 79	20.03	0.69	0.49	0.09	0.85	1 91	5 18	0 06	94 20	non-heated[2]
MS002/3	63 77	0.72	20.08	0.63	0 41	0.10	0 79	2.25	5 49	0.06	94 31	non-heated[2]
BK003	67 63	0.01	20.12	0 05	0 18	nd	0 95	2 89	2.02	0 08	93 93	non-heated[2]
MS003/1	63.10	nd	20.14	0.06	0.04	nd	0.45	6 36	4 38	0 02	94.55	non-heated[2]
BK006/1	62 97	0.28	20.77	0 67	0.12	0 15	0 80	2.81	5.69	0 07	94 32	non-heated[2]
MS002/4	58.64	0.78	20.94	1.66	0.81	0.15	1 28	6 48	5 39	0.09	96 23	non-heated[2]
MS002/5	63.80	0 54	21 11	0 82	0.39	0.06	0 64	2 50	5.67	0.04	95.58	non-heated[2]
BK004/1	63 05	0 02	21 22	0 08	0.07	0.01	0 40	2 10	4.18	0.07	91.20	non-heated[2]
MS002/5	64.28	0 53	21 27	0.69	0.06	0.05	0.57	3 48	5 54	0 10	96.56	non-heated[2]
BK001/1	64.67	nd	21.73	nd	0.02	0.03	0.41	2 63	3 89	0.02	93 38	non-heated[2]
MS005/1	57.94	0 89	21 85	1.60	0 86	0.14	1.23	6.52	5.38	0 07	96 47	non-heated[2]
BK005	55 41	0 16	22 07	0.14	0.05	0 01	0 48	6.03	6.60	0 10	91 05	non-heated[2]
MS001/2	58 23	0.84	22.31	2 13	0 09	0 20	0 85	3 25	5 64	0.04	93 58	non-heated[2]
BK006/2	55.64	0.15	22.31	0 13	0 01	nd	0.45	5 76	6.66	0 06	91.18	non-heated[2]
MS003/2	60 22	0 40	22 42	0.64	0.55	0 01	0 78	3.88	5 20	0 17	94.26	non-heated[2]
MS004	64 54	0 49	22 47	1.24	0.18	0 25	0 84	3.09	6.29	0 02	99.42	non-heated[2]
MS005/2	59 79	0.99	22.77	1 65	0.82	0.14	1 25	3.94	5 33	0.01	96.69	non-heated[2]
MS003/2	62.94	0.01	22 88	0 07	0.01	nd	0 46	3.66	4 24	0.04	94.31	non-heated[2]
MS005/2	59.95	0 82	22 95	1 63	0.78	0.14	1.14	3 60	5.18	nd	96.18	non-heated[2]
BK002/2	58 94	0 32	22.97	0 67	0 50	0 02	0 78	6.06	5 65	0.05	95 95	non-heated[2]

Note 1 = 'glassy' melt inclusions, 2 = 'composite' melt inclusions, nd = not detected

Table 5.8 (Continued)

Sample	SiO_2	Ti_2O	Al_2O_3	FeO	MnO	MgO	CaO	Na_2O	K_2O	P_2O_5	Total	Remarks
MS005/2	59 95	0.91	23.10	1.80	0 80	0 16	1 21	3.79	5 23	0.03	96.99	non-heated[2]
MS003/3	58 30	0.41	23.20	1.08	0 08	0 11	0 39	4.30	6 50	nd	94.38	non-heated[2]
BK006/3	59.84	0.44	23.39	0.66	0 64	nd	0.74	4.08	5.20	0.06	95.06	non-heated[2]
BK008	58 09	0.13	23.48	0 13	0 04	0 01	0.46	3.65	5 65	0.08	91.71	non-heated[2]
MS002/6	60 43	0 48	23.73	0 73	0.10	0.17	0 93	2 42	5 17	0.06	94.23	non-heated[2]
BK010	59 12	0.24	23 83	0 17	0.03	nd	0 41	3.66	5 52	0.12	93.11	non-heated[2]
BK007	57 09	0 15	23 92	0.08	0 04	nd	0.48	3 49	6.09	0.06	91 40	non-heated[2]
BK001/2	58.41	0 04	23 93	0.53	0 04	0 03	0.50	5 26	4.21	0 03	92 99	non-heated[2]
MS003/3	58.50	0 40	23 95	1.29	0 06	0 14	0.40	3 63	6.43	0 07	94 87	non-heated[2]
MS003/3	58.81	0.40	24.19	1 26	nd	0.15	0.39	4.75	6.79	0.03	96.77	non-heated[2]
BK004/1	61.97	0.34	24.38	0 67	0 54	0.09	0.70	4.71	5.42	0 11	98.92	non-heated[2]
BK001/2	59.43	0.04	24.92	0 33	0 07	0.01	2.26	3.22	4.83	0.14	95.27	non-heated[2]
BK001/2	58.73	nd	24.98	0 45	0.03	0 01	0.22	3.91	4.38	0 04	92 75	non-heated[2]
BK006/3	59.84	0 37	25.10	0 76	0 55	0.01	0.75	4.18	5 29	0 11	96 94	non-heated[2]
BK001/2	59.30	0 06	25.34	0 06	nd	nd	0 40	4.71	2 20	0 04	92 11	non-heated[2]
MS001/2	57 53	0 21	25 65	0.42	0 09	0 02	0 23	3 98	5.44	0 04	93.61	non-heated[2]
BK001/2	58 59	0.03	25.94	0 23	0.05	0.03	0 27	3.38	4 39	0.01	92 91	non-heated[2]
BK002/3	55 08	0.19	26.11	0 89	0.06	0 01	0 22	4.79	5.47	0.22	93.04	non-heated[2]
BK002/3	56.57	0.19	26 26	0 74	0.05	nd	0.20	5.04	5.23	0.08	94.37	non-heated[2]
BK001/3	56.03	0.04	26 28	0.84	0.22	0.02	0.17	1.76	5.93	0.04	91.32	non-heated[2]
BK001/3	55 24	0.02	26 51	2 72	0.03	0 19	0.19	1.59	4.64	0.07	91.20	non-heated[2]
MS001/3	59 69	0.15	26.54	0 95	0.02	0 02	0.23	4.94	5 55	0.15	98 24	non-heated[2]
MS001/3	59.76	0.17	26.69	0 91	0.08	0 01	0.21	4.69	5 50	0.04	98 06	non-heated[2]
MS001/4	58 16	0.16	26.86	0 61	0.06	0 02	0 19	4.55	5 94	0 11	96 67	non-heated[2]
BK001/4	60 05	0 01	26 92	0.12	0 02	0 01	0 37	4.49	3 71	0 06	95.75	non-heated[2]
BK009	58.33	0 12	27 06	0 16	0 04	nd	0 40	3 47	5 35	0.14	95 07	non-heated[2]
MS003/3	59 14	0.12	27 10	0 83	0.34	0 04	0 20	2 33	4.78	0 09	94.96	non-heated[2]
BK002/4	51.47	0.24	27 57	1 03	0.02	nd	0.17	5 04	5 68	0.14	91.36	non-heated[2]
BK004/2	53 08	0.16	27.62	0 41	0.07	0.03	0.48	6 20	6.20	0.07	94 31	non-heated[2]
BK006/4	54.74	0.48	27.95	0 60	0 56	0.03	0 74	4.70	4 54	0.01	94 36	non-heated[2]
MS001/4	57 31	0.25	28.08	0 72	nd	nd	0 20	4.79	5 59	0 11	97.05	non-heated[2]
BK006/4	56.23	0 44	28.20	0.72	0 60	0 06	0 76	3.57	4 45	0 12	95 14	non-heated[2]
BK006/4	55 62	0 47	28 57	0.70	0 52	0 04	0 75	5 34	4 71	0.11	96 83	non-heated[2]

Note: 1 = 'glassy' melt inclusions, 2 = 'composite' melt inclusions, nd = not detected

considered, and are in good agreement with the other two melt inclusion compositions (glassy and heated). The non-heated melt compositions contain 51.5-68.6wt% SiO_2 and 16.4-29.6wt% Al_2O_3 with Na_2O/K_2O ratio value ranges between 0.2 to 2.1 (Table 5.8). The large variability in Na/K in the composite inclusions probably reflects the presence of quench feldspars.

All analyses are combined together in the discussion below. The analyses (Table 5.8) have a very large range in compositions. Compositions from 15 samples, 41 different grains (74 analyses in total) are in the ranges of 51.5-68.6wt% SiO_2, 16.4-29.6wt% Al_2O_3, 1.9-6.8wt% K_2O, 0.01-0.25wt% MgO and 1.7-4.6wt% CaO contents. The majority of the silicate melt compositions fall within the trachy-andesite and trachyte fields on the basis of SiO_2 versus total alkalis classification diagram (Le Bas *et al.*, 1986; Fig.5.13). Plots of the Al_2O_3 content versus the other major elements are also illustrated in Figure 5.13. With increasing Al_2O_3, the SiO_2 contents increased while all other major elements show no or little variations.

Major elements

Variations in silicate melt compositions within individual sapphire grains are generally small compared with the measured total variation in the entire suite (Table 5.8). The major element compositions show a wide range of Al_2O_3 contents (~16-30wt%) but most other elements are relatively consistent. The TiO_2 and MnO contents are mostly below 0.6wt%. Higher values are probably due to analyse of some part of accidentally trapped minerals (i.e., rutile and hematite) that are present within melt inclusions. Their total alkali contents range between 8-10wt% with an averaged K_2O content about 5wt% whereas the Na_2O contents vary from 1-7wt%. The Na_2O could have been affected by analytical conditions for glasses with a small beam size, as described in Section 5.6.1. The P_2O_5 contents range from 0.01 to 0.36wt% with the majority analyse contents less than 0.1wt%. The CaO contents are also very low (<1wt%) with a few analyses with 1-3wt% CaO and one analysis has 4.5wt%. The melt inclusions also have extremely low MgO contents (0.01-0.25wt%). They contain low FeO contents, ranging from 0.01 to 2.7wt%. Again the analyses with more than 1wt% FeO value could be contaminated by trapped minerals (hematite) below the surface. The association of the melts with hematite (LRS study) suggests most of this FeO will be present in the melt as Fe^{3+}.

The large ranges in Al_2O_3 content from 16-30wt% suggest these analyses may be affected by edge effects. Most melt inclusions that contain over 25wt% Al are small and may include a component of Al_2O_3 from the host sapphires. In order to validate the Al_2O_3 value in the melt compositions, detailed "traverse sections" across some of larger and smaller melt inclusions

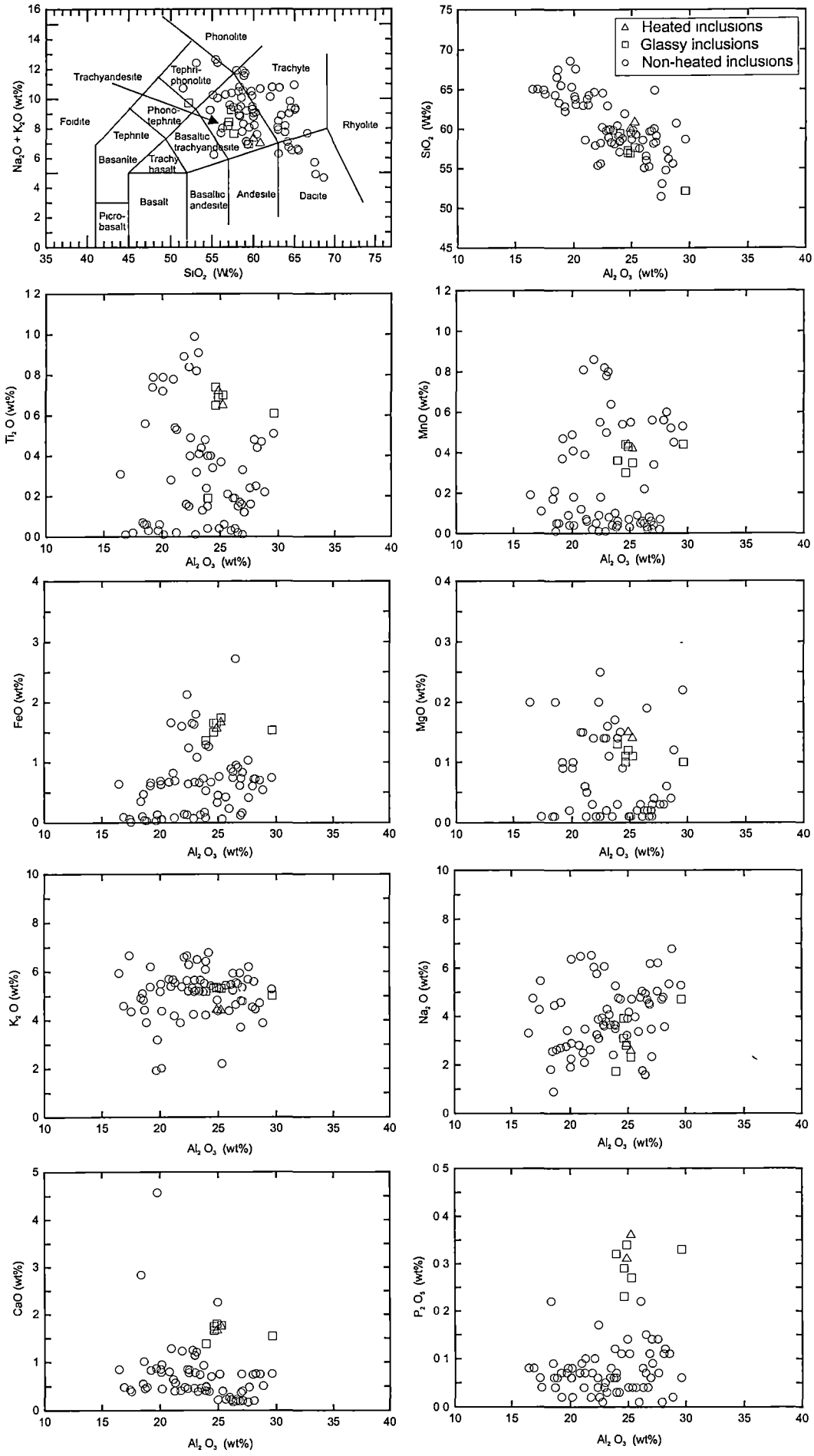

Figure 5.13 Major element variation diagrams of glass inclusions in the Denchai sapphires

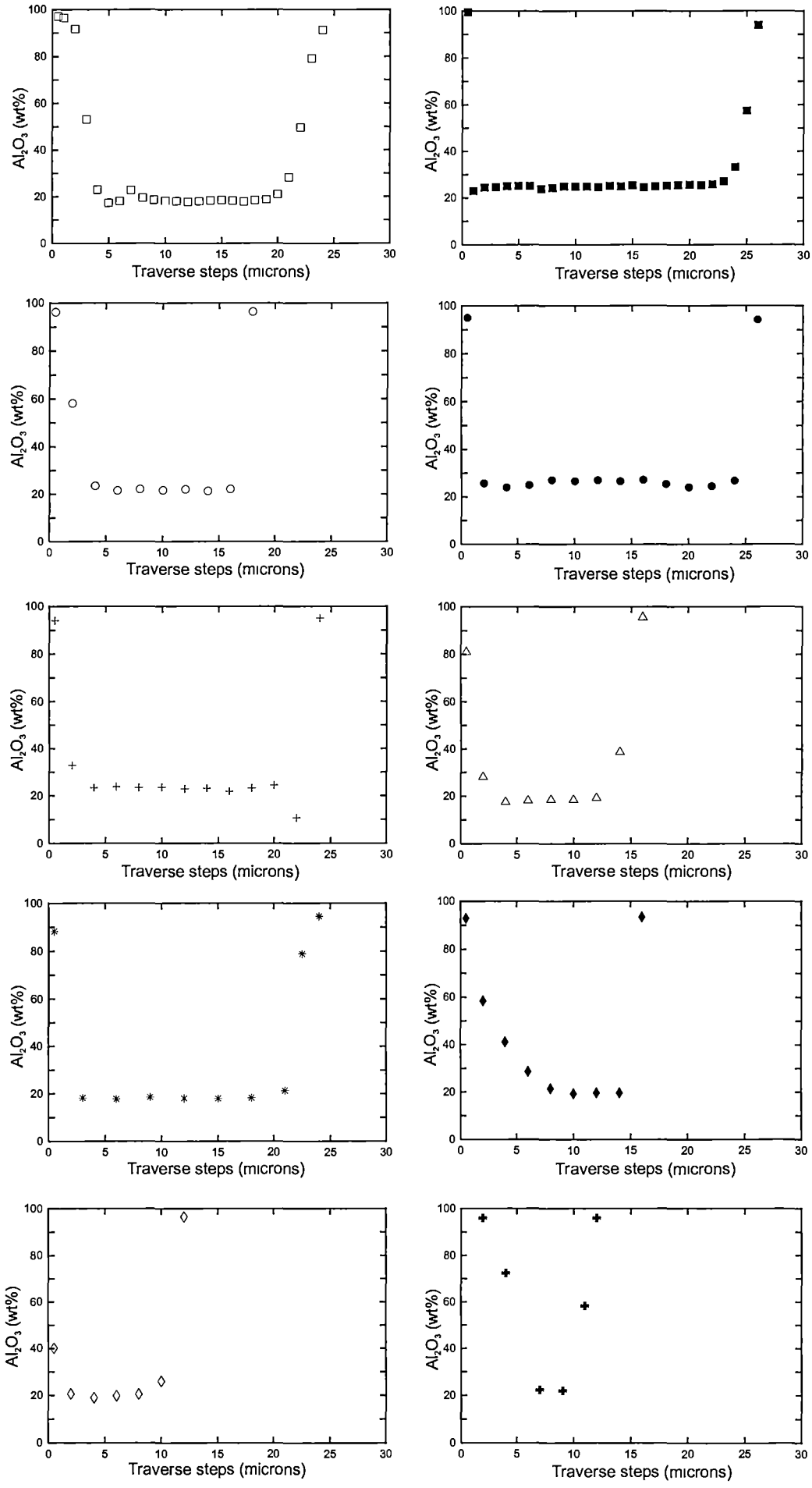

Figure 5.14 The detailed traverse sections across the different sizes of melt inclusions

were tested (Fig.5.14) and indicate that at least some of the glass compositions have real Al_2O_3 of 25wt%. While these glasses have not been heated in the laboratory, the process that brought them to the surface is similar. All sapphires were carried to the surface in basalts at about 1000°C. Thus there is the potential to overheat these melt inclusions after trapping. The high Al_2O_3 content in these melt inclusions may not reflect the trapped liquid compositions (see Section 5.8).

Volatile components

The presence of anhydrite (LRS study) within the high salinity inclusions implies SO_2 may be important in the genesis of sapphire. Volatile components, chlorine, sulphur and fluorine (Cl, S and F) in glass inclusions was measured using the EMP at 15 kV, 25nA and a 5 μm diameter of electron beam size with extended counting times. Some of larger melt inclusions were chosen for analysis in order to avoid edge effects. The analytical detection limit for Cl is 0.003wt%, 0.005wt% for S and 0.1wt% for F (Table 5.9). Significant Cl was detected in the glass inclusions, ranging from 0.01 to ~1wt% with a mean value of 0.39wt%. The glass inclusions have detectable S content (0.01-0.41wt%) with an average 0.06wt%. Given the oxidised nature of the high salinity inclusions it is assumed that this will be dissolved in the glass as sulphate. The glass inclusions contain up to 0.12wt% F content but are mostly below the detection limit (0.1wt%) of the EMP. With increasing melt evolution, as expressed by increasing $Na_2O + K_2O$ contents, there is slight increase in S contents of glasses (Fig.5.15). When compared to glass inclusions in volcanic rocks, the average volatile contents (S and Cl) in the Denchai glasses are similar to those of glass inclusions in clinopyroxene from volcanic rocks at Mt. Somma-Vesuvius, Italy (Webster *et al.*, 2001). In contrast, the Denchai glasses have higher S and Cl contents than the glasses reported from volcanic rocks of the Minoan eruption, Santorini, Greece (Michaud *et al.*, 2000).

Estimated H_2O content

Water is the major volatile dissolved in natural magmatic system and strongly influences the chemical and physical properties of magmas such as phase relationships and density. Natural melts can be generated at different water activities (e.g., Thompson, 1982; Holtz and Johannes, 1994). The knowledge of the minimum and maximum water contents that can be dissolved in natural melts at given *P-T* and water activity is of particular importance. Recent studies to determine water solubility in granitic melts generated in the crust (Holtz *et al.*, 2001) concluded that melts generated in the crust at contain up to 20% water content at 800-900°C and 3-7 kbars. Assuming no other minor and volatile components, the Denchai glass inclusions have an averaged total of about 94-95wt% (Table 5.8). Since F, Cl and S are low the remaining component of the glasses is probably water (~5-6wt%).

Table 5.9 Volatile components (wt%) in melt inclusions

Sample	BK001	BK001	BK001	BK001	BK001	BK002	BK002	BK002	BK002	BK002
S	nd	0.03	0.04	0.07	0.07	0.02	0 02	0.03	nd	0 41
Cl	0.08	0 03	0.17	0 23	0 06	0.09	0.20	0.31	0.06	0.25
F	0.03	nd	0.12	0.10	0 04	0 09	nd	0.05	0.03	0.06

Sample	BK003	BK003	BK003	BK003	BK003	BK006	BK006	BK007	BK007	MS001	MS001
S	0.02	0.15	nd	0.01	0.14	0.08	nd	nd	0 03	0.04	0.02
Cl	0.44	0 01	0.44	0.51	0.07	0.41	0.64	nd	0.47	0 01	0 62
F	nd	0.01	0.08	0.01	0.03	0.03	0 09	0.05	0 03	0.07	0.04

Sample	MS001	MS001	MS002	MS002	MS002	MS002	MS002	MS003	MS003	MS005
S	0.02	0 06	0.04	0 04	0.01	0.05	0.05	0.16	0.04	0.04
Cl	0 58	0.68	0 45	0.57	1.08	0.52	0.63	0.73	0.59	0.80
F	0.11	0.08	nd	0.06	0.04	0.10	0.05	0.02	0.08	0.09

Note: detection limit for S (0.005 wt%), for Cl (0 003 wt%) and for F (0.1 wt%), nd = not detected

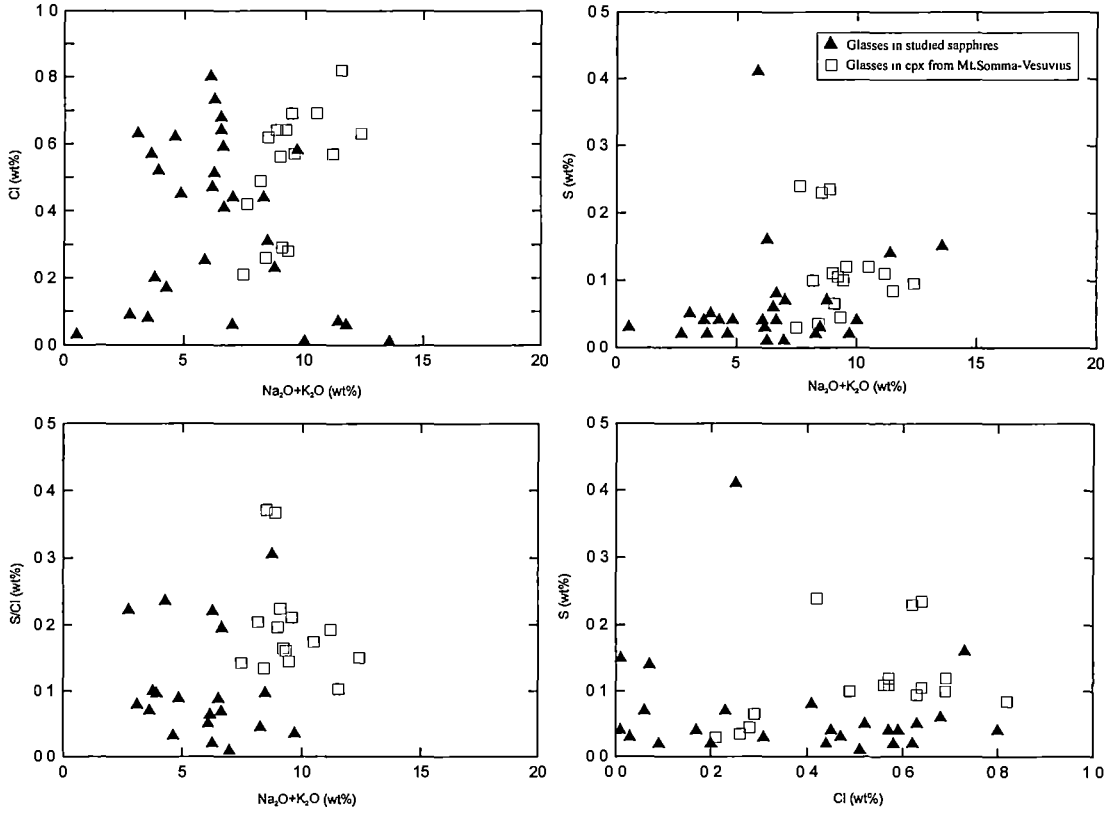

Figure 5.15 Plots of concentrations of volatile components (S and Cl) within melt inclusions in the Denchai sapphires

5.7 Mineral inclusions

Mineral inclusions may provide crucial information concerning the past history of their hosts. This information provides information about the original source region and the various processes involved in the generation of gem-quality corundum. Recently, identified mineral inclusions in corundum megacrysts from basaltic fields (Guo *et al.*, 1996a; Sutherland *et al.*, 1998a; Table 5.1) have led into the discussion of the corundum genesis. Mineral inclusions in sapphires in this study were identified and are shown in Table 5.10.

Table 5.10 Mineral inclusions in the Denchai sapphires

Sample	Mineral inclusions	Hosted by	Identification techniques
BK001 & BK003	feldspar	sapphire	EMP & LRS
MS001	zircon	sapphire	EMP & LRS
BK004/1	muscovite	sapphire	EMP
BK003	nepheline	sapphire	EMP
BK001	rutile	melt inclusion	LRS & PIXE
BK002	hematite	melt inclusion	LRS
MS002	magnetite	melt inclusion	LRS
MS001	anhydrite	fluid inclusion	LRS

Note: EMP = Electron Microprobe, LRS = Laser Raman Spectroscopy,
PIXE = Proton Induced X-ray Emission

In this section, sapphire samples containing mineral inclusions which are not close enough to the surface for the LRS analysis were first examined under a petrographic microscope to locate mineral inclusions and then photographed (Fig.5.16). Then they were exposed at the surface for investigation using a CAMECA SX-50 electron microprobe analysis. Analytical techniques are described in Section 5.2 and sample preparation is described in Section 5.3. Several mineral inclusions in the Denchai sapphires have been identified; these include a suite of minerals trapped during the sapphire growth (feldspar, muscovite, nepheline and zircon), and another suite is of accidentally trapped minerals hosted by melt inclusions within sapphires, including rutile, hematite and magnetite.

5.7.1 Feldspar

Several elongate feldspar inclusions were identified by the EMP in dark blue sapphires from Ban Bo Kaeo (Samples BK001, BK003). They are mostly forms as single crystal, euhedral and transparent grains (Fig.5.16a). Their compositions are K-rich and Ca-free and have a composition of 63.8-64.8wt% SiO_2, 1.4-3.9wt% Na_2O and 11.0-14.3wt% K_2O contents with an average composition of $Ab_{40.7}$-$Or_{58.0}$ (Table 5.11).

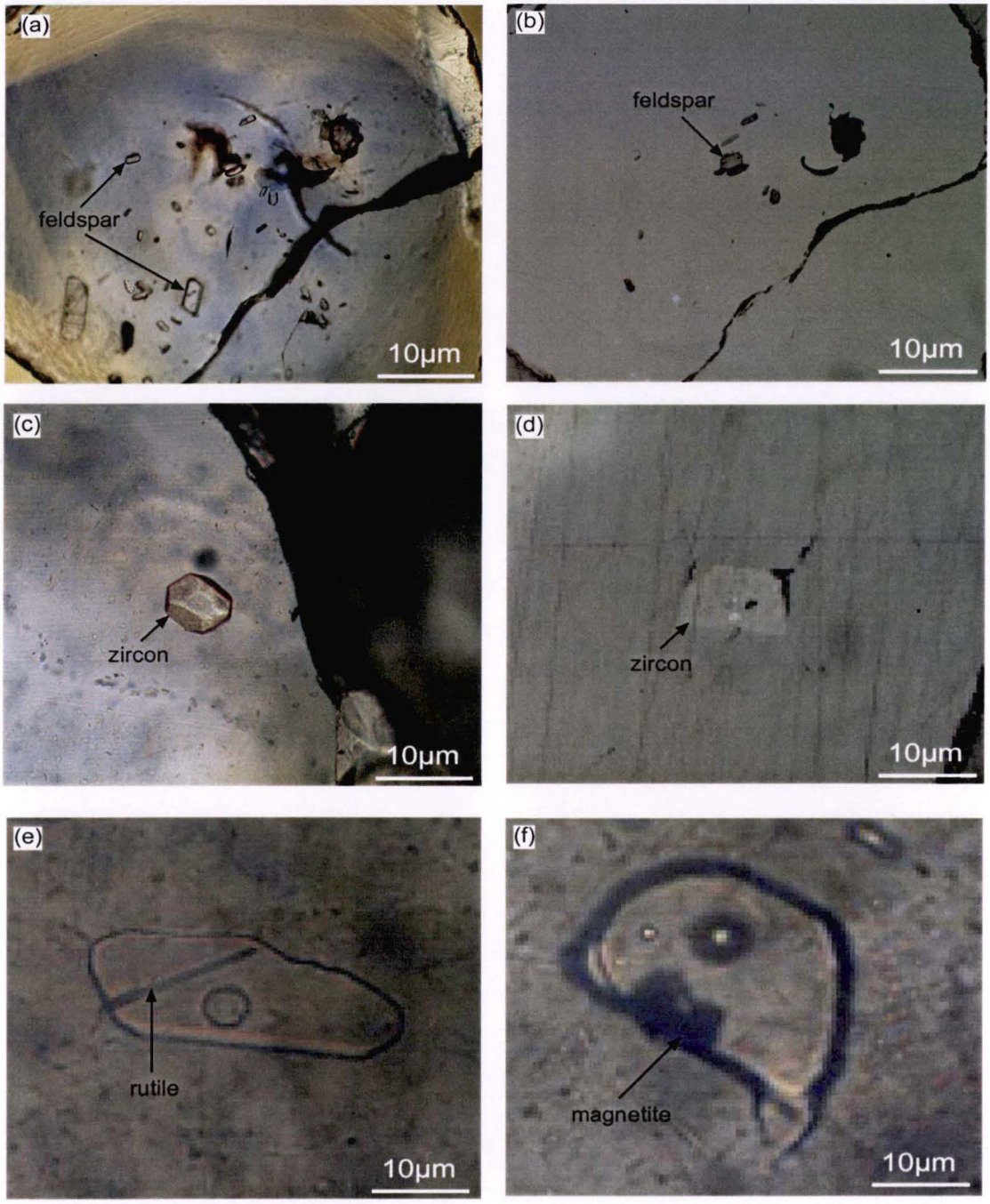

Figure 5.16 Photomicrographs of mineral inclusions in the Denchai sapphires.
(a) feldspar, transmitted light (TL), (b) feldspar, reflected light (RL), (c) zircon (TL), (d) zircon (RL), (e) rutile (TL) and (f) magnetite (TL)

Table 5.11 Electron microprobe analyses of mineral inclusions in the Denchai sapphires

Sample	BK003	BK001	BK001	BK001	BK004/1	BK004/1	BK003	BK003	BK003	MS001	MS001
Mineral	fsp	fsp	fsp	fsp	mu	mu	ne	ne	ne	zr	zr
SiO_2	63.75	64.73	64.82	64.84	48.18	48 75	42.94	43.03	43.38	31.16	30 82
TiO_2	0.03	0 01	0.04	0 00	0 24	0.34	0.11	0 11	0 07	NA	NA
Al_2O_3	20.21	19.61	19.57	19 60	33.88	31.98	34.13	34 85	35 36	NA	NA
Fe_2O_3	0 14	0.06	0 01	0.03	0.00	0 00	0.17	0.17	0 18	NA	NA
FeO	0.00	0.00	0.00	0.00	2.67	3.89	0.00	0.00	0.00	NA	NA
MnO	0.02	0 00	0.00	0.03	0.11	0 19	0.00	0.00	0.04	NA	NA
MgO	0.01	0.00	0.01	0.00	0.30	0.70	0.00	0.00	0.00	NA	NA
CaO	0.08	0.28	0.26	0.29	0.04	0.06	0.37	0.37	0 39	0 00	0.00
Na_2O	1.37	3.87	3.88	3.83	1.23	1.19	15.72	15.80	14.21	NA	NA
K_2O	14.33	11.16	10 97	11.14	9.21	9 16	5.75	5.84	5.98	NA	NA
P_2O_5	NA	NA	NA	NA	NA	NA	NA	NA	NA	0.08	0.08
ZrO_2	NA	NA	NA	NA	NA	NA	NA	NA	NA	65.21	64.83
HfO_2	NA	NA	NA	NA	NA	NA	NA	NA	NA	0.98	0.95
Y_2O_3	NA	NA	NA	NA	NA	NA	NA	NA	NA	0.48	0.42
Yb_2O_3	NA	NA	NA	NA	NA	NA	NA	NA	NA	0.08	0 19
UO_2	NA	NA	NA	NA	NA	NA	NA	NA	NA	0.05	0.10
Total	99.96	99.73	99.57	99.77	95.87	96.27	99.19	100.17	99.61	98.69	97.63
Oxygen	8	8	8	8	11	11	8	8	8	16	16
Si	2.930	2.952	2.957	2 955	3 183	3 229	2.071	2.055	2 070	3 910	3.910
Ti	0.001	0.000	0.001	0.000	0.012	0.017	0.004	0.004	0.003	NA	NA
Al	1.095	1.054	1.052	1.053	2.638	2.497	1.940	1.962	1.989	NA	NA
Fe^{3+}	0.005	0.002	0.000	0.001	0.000	0.000	0.006	0.006	0.006	NA	NA
Fe^{2+}	0.000	0.000	0.000	0.000	0.148	0.215	0.000	0.000	0.000	NA	NA
Mn^{2+}	0.001	0 000	0.000	0 001	0 006	0.011	0.000	0.000	0.002	NA	NA
Mg	0.001	0.000	0.001	0.000	0.030	0.069	0.000	0.000	0.000	NA	NA
Ca	0 004	0.014	0.013	0.014	0.003	0.004	0.019	0.019	0.020	0.000	0.000
Na	0.122	0.342	0.343	0 338	0.158	0.153	1.470	1.463	1 315	NA	NA
K	0.841	0.650	0.639	0.648	0.777	0.775	0.354	0.356	0.364	NA	NA
P	NA	NA	NA	NA	NA	NA	NA	NA	NA	0.010	0.010
Zr	NA	NA	NA	NA	NA	NA	NA	NA	NA	3.990	4 010
Hf	NA	NA	NA	NA	NA	NA	NA	NA	NA	0 040	0.030
Y	NA	NA	NA	NA	NA	NA	NA	NA	NA	0.030	0.030
Yb	NA	NA	NA	NA	NA	NA	NA	NA	NA	0.000	0.010
U	NA	NA	NA	NA	NA	NA	NA	NA	NA	0.000	0.000
Sum Ca#	5	5	5	5	7	7	6	6	6	8	8

Note: fsp = feldspar, mu = muscovite, ne = nepheline, zr = zircon, NA = not analysed

Alkali feldspar has been reported as an inclusion in corundum megacrysts from King Plains, New South Wales of Australia and Mingxi area, Fujian Province of China (Guo *et al.*, 1996a). The presence of feldspar inclusions is common in basalt-related corundum. Compositions of feldspar inclusions trapped in the Denchai sapphires are similar to those feldspar inclusions from Eastern Australia reported by Guo *et al.* (1996a) and Sutherland *et al.* (1998a).

5.7.2 Muscovite

Muscovite occurs over a wide range of low- to high-grade metamorphic rocks and Si- and Al-rich plutonic igneous rocks (pegmatite and granite). It is frequently accompanied by biotite (Deer *et al.*, 1992). Two muscovite grains were identified by the EMP in dark blue and blue sapphires from Ban Bo Kaeo (Sample BK004/1). Their compositions are 48wt% SiO_2, 32-34wt% Al_2O_3, 1.2wt% Na_2O and 9.2wt% K_2O (Table 5.11). The preservation of muscovite is unexpected in xenolithic conditions.

5.7.3 Nepheline

Nepheline ($NaAlSiO_4$) is a characteristic mineral of the alkali igneous rocks, occurring as a primary phase in many plutonic and volcanic rocks. It commonly occurs in textural intergrowths with alkali feldspar, and less often with plagioclase (Deer *et al.*, 1992). Three nepheline inclusions were identified by the EMP in a blue sapphire from Ban Bo Kaeo (Sample BK003). Their compositions have 42.9-43.4wt% SiO_2, 34-35wt% Al_2O_3, 14.2-15.8wt% Na_2O and 5.8-6.0wt% K_2O contents (Table 5.11).

5.7.4 Zircon

A colourless zircon inclusion was identified in a light blue sapphire from Ban Mae Sin (Sample MS001). It is perfectly euhedral, showing distinct {110} prism and its tetragonal form (Fig.5.16b). It contains 31wt% SiO_2, 65wt% ZrO_2, < 0.1wt% P_2O_5, 0.45wt% Y_2O_3, 1wt% HfO_2 and < 0.1wt% UO_2 contents (Table 5.11). Zircon has been reported as inclusions in Australian-Asian BGY corundums (Guo *et al.*, 1996a; Sutherland *et al.*, 1998a). In most zircon inclusions the {110} prism dominates over the {100} prism and such prism developments have been related to high U (Th), Y and P contents of the parental medium (Benisek and Finger, 1993; Guo *et al.*, 1996a, b; Sutherland *et al.*, 1998a). However, the zircon inclusion here contains lower U (< 0.1wt%) and Hf (< 1wt%) contents than recorded for those of zircon inclusions in Australian-Asian BGY corundums (Guo *et al.*, 1996a; Sutherland *et al.*, 1998a).

5.8 Significant of melts and minerals trapped in the Denchai sapphires

In this section, phase equilibrium calculations are used to place constraints on the *P-T* conditions of sapphire crystallisation. Significant melt and mineral assemblages trapped within the sapphires are compared with predictions based on the thermodynamic modelling.

The melts trapped in the sapphires are compositionally very close to NKASH system (muscovite + feldspar + quartz + sillimanite + corundum + liquid + H_2O), and the phase relationships will be considered in this simple system. The phase relationships are considered here using a model for haplogranitic melts (Holland and Power, 2001 and references therein).

The detected mineral inclusions within these sapphires include feldspar, nepheline and muscovite (Section 5.7). The relationship of these mineral inclusions to the melt can be investigated in the NKASH system. A *P-T* projection for NKASH system (medium solid lines) from Holland and Powell (2001) is shown in Figure 5.17. The KASH system is also shown in dashed lines as this explains many of the high temperature terminations of NKASH univariant lines (Holland and Powell 2001). Addition of nepheline to the system calculations (nepheline was identified as an inclusion in the sapphires) resulted in a third invariant point (Fig.5.17).

Of particular interest on Figure 5.17 is the univariant line of end-member plagioclase (pl) + corundum (cor) + H_2O to liquid (liq) + nepheline (ne) + K-feldspar (ksp). This curve is drawn above the feldspar solvus (heavy solid line) assuming feldspar composition of $Ab_{50}Or_{50}$. Consequently, all the phases in the reaction above the feldspar solvus region are found as inclusions within the sapphires (feldspar, nepheline, liquid, H_2O plus the corundum as an including phase; Fig.5.17).

This diagram is drawn assuming H_2O is a pure phase. The phase relationships are highly sensitive to water activity. As the water-rich inclusions are hypersaline, the water activity in this system will be depressed. Thus, the water activity of the coexisting hypersaline inclusions was estimated using the H_2O activity relationship in concentrated NaCl solutions at high pressures and temperatures. 60wt% NaCl in Type-II inclusions is equivalent to xH_2O of 0.68 which using the model of Aranovich and Newton (1996) gives an aH_2O of about 0.5 (xH_2O ~0.68). The relevant univariant line (liq + ne to fsp + cor + H_2O; Fig.5.17) moves rapidly to higher temperature when water activity drops. As it does this, the (Sill, q) invariant point also migrates very rapidly to higher pressure along the H_2O absent reaction: plagioclase (pl) + muscovite (mu) to liquid (liq) + K-feldspar (ksp) + corundum (cor) + nepheline (ne).

The univariant reaction has been used to predict the water content in the liquid (glass). The importance of water activity can be seen in Figure 5.18, in which the water activity (aH_2O) of the vapour phase in equilibrium with the silicate melts runs from 1 to 0.5.

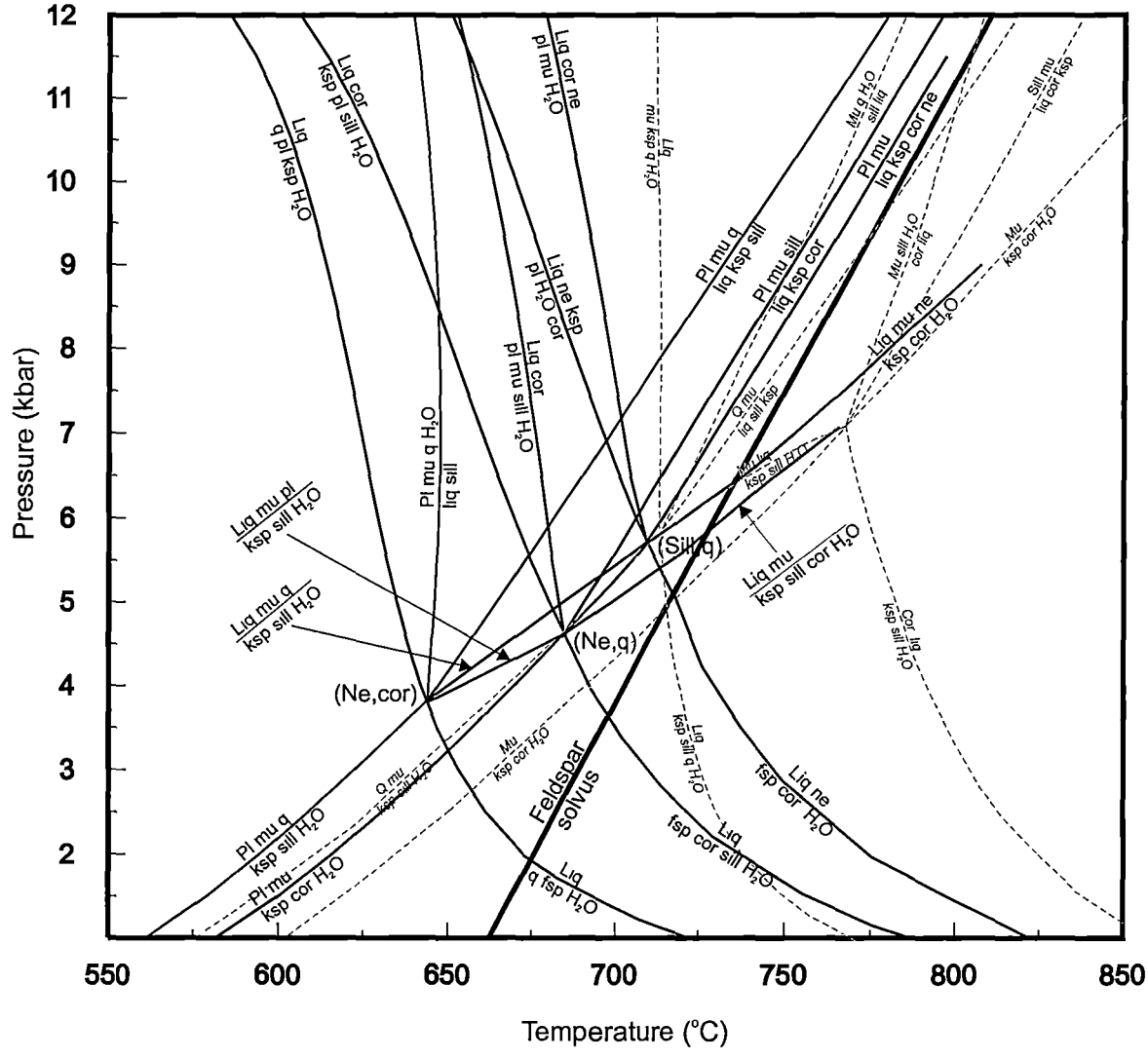

Figure 5.17 A *P-T* projection for NKASH (medium solid lines), showing the relationship to KASH equilibria (dashed lines) and feldspar solvus (heavy solid line); (modified from Holland and Powell, 2001)

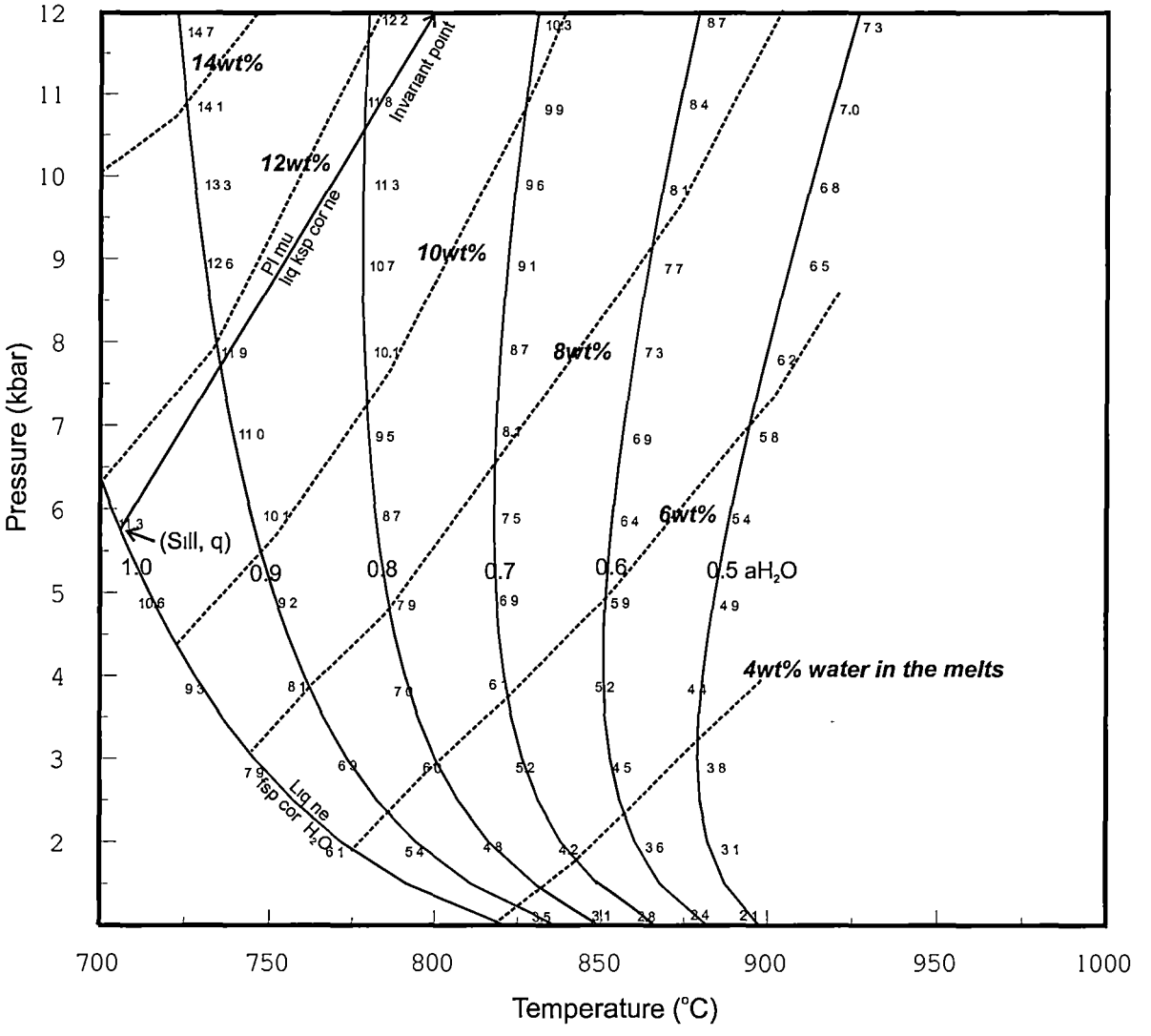

Figure 5.18 Contour map of water contents (dashed lines) in the equilibrium silicate melts, showing the univariant lines (Liq + ne to fsp + cor + H_2O, feldspar $Ab_{50}Or_{50}$ above the feldspar solvus) for a range of water activities (aH_2O; solid lines)

Figure 5.18 shows the position of the relevant univariant line for a range of water activity. This water content is contoured on Figure 5.18. As the average glass inclusion has a total of 94.6wt% (Table 5.8), the actual liquid composition should lie near the 6wt% contour on Figure 5.18. This matches the low aH_2O estimated from the Type-II inclusions.

An alternative way to progress is to model the phase relationships of the actual glass compositions. The highest Al_2O_3 in glass inclusion that has been demonstrated using microprobe profiles is 24.6wt% (Fig.5.14). The very high Al_2O_3 content of some inclusion analyses is probably due to edge effects during the analysis. Therefore, for the purposes here all the inclusions with Al_2O_3 between 24 and 26wt% were averaged. The composition was projected into NKASH system by ignoring the minor amounts of other elements. The phase relationships of this composition were calculated using THERMOCALC computer program (Holland and Powell, 1998; Powell *et al.*, 1998). The results are shown on Figure 5.19. This liquid is stable above 1100°C at 4 kbars and the liquidus phase is corundum. At 800°C feldspar comes onto the liquidus. The Al_2O_3 of the melt is also shown on the Figure 5.19. For K-feldspar (ksp) stability this is about 14.5wt% which is very close to the lowest Al_2O_3 content measured in any of the glasses (Table 5.8).

The assumptions in this modelling approach are significant, especially assuming that the NKASH system is a close match to the glasses and ignoring other volatiles (Cl, SO_4 and F in melt) and all minor elements. The melt model in the THERMOCALC program (Holland and Powell, 2001) was based on experimental data far from the compositions calculated here.

Despite these problems:

- The phase relationships predicted by the model are compatible with the observations in this study.
- These relationships require that the melt compositions at trapping were close to the lowest Al_2O_3 glasses surviving in the sapphire crystals.
- High Al_2O_3 glasses (up to 25wt% Al_2O_3) are consistent with glasses reacting with corundum walls as the sapphires are transported to the surface as xenocrysts within basalts at about 1100°C.
- The possible field for formation of the original trapped melts and their associated mineral inclusions lies somewhere along a field from 800°C at 5 kbars to 1000°C at 15 kbars. The water content of the trapped glasses is most consistent with conditions near the high-pressure end of this range.

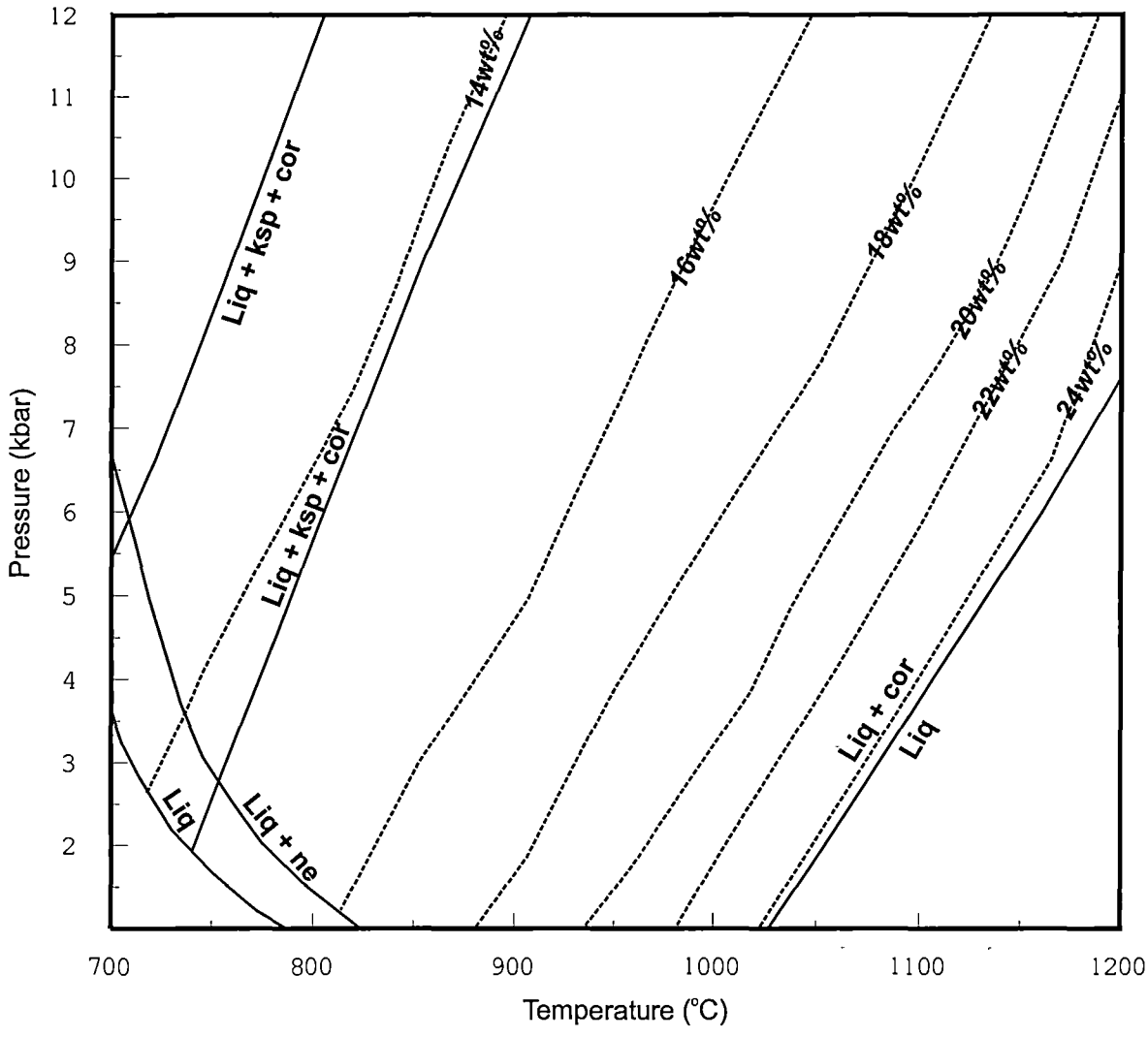

Figure 5.19 Calculated phase relationships of the Denchai glass inclusion compositions, liquidus curves (NKASH; solid lines) and the Al contents (wt%) of melts (dashed lines)

5.9 Collected associated alluvial minerals

Besides the sapphires that were collected from the Denchai gem field, other associated heavy minerals were found during sample preparation and gem identification. The detrital heavy minerals in the Denchai gem fields were previously studied and reported by Vichit (1992) and Tonthongchai *et al.* (1996). They reported a suite of heavy minerals of spinel (hercynite), ilmenite, garnet (pyrope), zircon, black pyroxene, quartz (rock crystal and milky) and olivine (peridot). However, in this study the associated minerals collected were mainly spinel and zircon, and less commonly magnetite, ilmenite and quartz (Fig.5.20).

5.9.1 Spinel

Black spinels are commonly found together with sapphires in the Denchai gem fields. They range in size between 0.5 to 5 cm and show octahedral crystal-shaped (Fig.5.20a). Most of them are in spinel-hercynite series but one grain is a picotite (Al > Cr). The spinel (*sensu stricto*) grains have 62-64wt% Al_2O_3 and 0.2-1.3wt% Cr_2O_3. They have a relatively narrow range of $100Cr/(Cr+Al+Fe^{3+})$; $Cr\#_{Sp}$ from 0.2 to 1.4 and the $Mg\#_{Sp}$ values range from 69.8 to 73.5. Spinel is a common high-temperature mineral in metamorphic rocks and in Al-rich xenoliths however these grains have unusually high Mg#. The picotite grain has a composition of 38wt% Al_2O_3 and 28wt% Cr_2O_3 values with a Mg# of 70.6 and Cr# of 31.9 (Table 5.12). In comparison the spinels in mantle xenoliths (Chapter 3) have Al_2O_3 (49.6-60.5wt%) and Cr_2O_3 (8.3 to 19.7wt%). The alluvial spinels have crystallised in a different (low Cr) environment from spinels in mantle xenoliths. The high calculated Fe^{3+} contents of spinel suggest oxidising conditions.

5.9.2 Zircon

Zircon has been reported intergrown with sapphire and magnetite at Ban Khao Wua in the western zone of Chanthaburi-Trat gem deposits (Coenraads *et al.*, 1995) and as inclusions in blue and yellow sapphires from basaltic terrains in Eastern Australia and Eastern China (Guo *et al.*, 1996a). The chemistry of the latter inclusions shows high contents of Hf, U, Th, Y and REEs similar to values in zircons intergrown with corundum from Scotland (Aspen *et al.*, 1990). They interpreted the unusually high contents of these elements as consistent with crystallisation of zircon from highly evolved silicic melts, which had undergone extensive fractional crystallisation (Guo *et al.*, 1996a). In this study alluvial zircon were collected from both Ban Bo Kaeo and Ban Mae Sin (Fig.5.20b). The HfO_2 contents are very consistent at

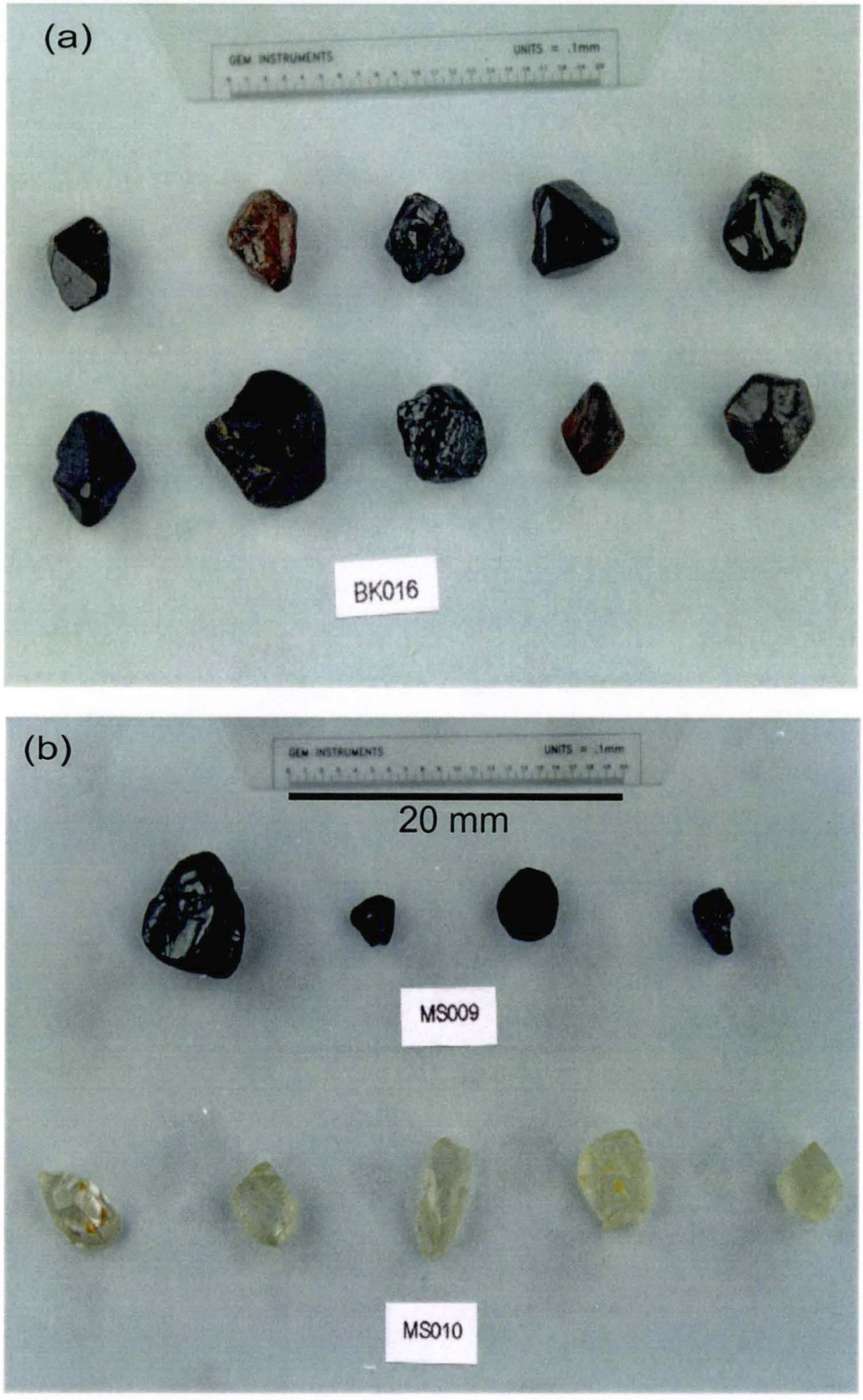

Figure 5.20 Photographs of the alluvium minerals collected in the Denchai area; BK = Ban Bo Kaeo and MS = Ban Mae Sin.
(a) zircon (BK016) and (b) magnetite (MS009) and quartz (MS010)

Table 5.12 Electron microprobe analyses of detrital spinel in the Denchai gem fields

Sample	One	One	One	One	One	One	One	One	Two	Three
Grain	12	13	14	15	16	17	18	19	11	8
SiO_2	0.07	0.15	0.14	0.13	0.13	0.16	0.11	0.13	0.15	0.15
Al_2O_3	38 20	62.34	62 87	61.95	62.13	64.27	61.40	62 91	63 50	62.59
Cr_2O_3	28 42	1.34	0.52	0.47	0.25	0.54	0.18	0.58	0.41	1 25
Fe_2O_3	3.75	3.98	4.18	5.73	5.15	3.03	6.12	4.43	3.91	3.77
FeO	12.62	12 74	12.71	13.62	14 00	12.12	14.18	12.68	12.60	12.76
MnO	0 07	0.10	0.14	0.15	0 12	0 12	0.17	0.15	0.08	0 12
MgO	16.94	19.30	19.31	18.81	18 56	19 84	18.38	19.37	19.54	19.23
NiO	0.32	0.25	0 13	0.29	0.17	0.24	0.18	0 30	0 21	0 24
Total	101.24	100.99	100.69	101.98	101.30	100.75	101 47	101.21	101.10	100.70
Si	0.002	0.004	0 004	0.003	0.003	0.004	0.003	0.003	0.004	0.004
Ti	0.012	0 009	0.008	0.010	0.010	0.005	0.010	0.009	0.008	0.007
Al VI	1.261	1 868	1.885	1.852	1.867	1.910	1.850	1.878	1.892	1.878
Cr	0.629	0 027	0.010	0.009	0.005	0.011	0 004	0 012	0.008	0.025
Fe^{3+}	0 079	0.076	0.080	0.109	0.099	0.058	0.118	0 084	0 074	0 072
Fe^{2+}	0 295	0 271	0.270	0.289	0.299	0.256	0.303	0.269	0.266	0.272
Mn^{2+}	0.002	0.002	0.003	0 003	0 003	0 003	0 004	0.003	0.002	0 003
Mg	0.707	0.731	0.732	0.711	0.706	0.746	0.700	0 731	0 736	0 730
Ni	0 007	0.005	0 003	0.006	0 003	0 005	0.004	0.006	0.004	0.005
Sum Ca#	3.000	3.000	3 000	3 000	3.000	3.000	3.000	3.000	3.000	3.000
Mg#	70 6	73.0	73.1	71.1	70.2	74.5	69.8	73.1	73.5	72.9
Cr#	31 9	1.4	0.5	0.5	0.3	0.6	0.2	0.6	0.4	1.3

Table 5.13 Electron microprobe analyses of detrital zircon in the Denchai gem fields

Sample	One	One	Two	Two	Three	Three	Four	Four
Grain	3	10	6	8	5	6	3	8
SiO_2	31.66	31.90	32.05	31.47	31.69	31.52	31.62	31.42
ZrO_2	66.29	65 74	65 90	65.74	65.90	65.26	65.72	65.90
FeO	nd	0.02	0.01	0.02	nd	nd	nd	0.01
P_2O_5	0.08	0.08	0 08	0 08	0 07	0.08	0.08	0.08
Y_2O_3	0.08	0 07	0 12	0 10	0 10	0.35	0.26	0 35
HfO_2	0.72	0.82	0.61	0 77	0.80	0.66	0 65	0.60
Yb_2O_3	0 02	nd	0.04	0.02	0.03	0.10	0 08	0.10
ThO_2	nd	0 01	nd	0.02	0.01	0.45	0 03	0.06
UO_2	0 02	0 01	0.02	0.04	0.03	0.16	0.06	0.06
Total	98 88	98 69	98.89	98.32	98.67	98 69	98.58	98.67
Si	0.985	0 992	0 993	0 985	0.987	0.986	0 987	0 981
Zr	1.005	0 997	0.996	1.003	1.001	0.995	1 000	1.004
Fe^{2+}	nd	0.001	0.001	0 001	nd	nd	nd	0.001
P	0 002	0.002	0.002	0.002	0.002	0.002	0.002	0.002
Y	0.001	0.001	0 002	0 002	0 002	0.006	0.004	0.006
Hf	0.006	0.007	0.005	0 007	0 007	0 006	0.006	0.005
Yb	nd	nd	nd	nd	nd	0 001	0.001	0.001
Th	nd	nd	nd	nd	nd	0 003	nd	nd
U	nd	nd	nd	nd	nd	0.001	nd	nd
Sum Cat#	2	2	2	2	2	2	2	2

nd = not detected

0.6-1.0wt% (Table 5.13) and this is much lower than typical HfO_2 reported for zircon inclusions in BGY corundums by Sutherland *et al.* (1998a). The associated alluvial zircons here are compositionally similar to the zircon inclusions identified in the studied sapphires (Table 5.11). This may indicate that both detrital zircons and zircon inclusions in the studied sapphires have crystallised in different environment from zircon inclusions in Eastern Australian corundum (Guo *et al.*, 1996a; Sutherland *et al.*, 1998a).

5.10 Discussion and conclusion

The Denchai gem deposits are in close spatial association with the Denchai basalts, which are Cenozoic in age. Occurrences of these gem-quality corundums are considered to be related to the Denchai basalts. Gem-quality corundums are mostly found as alluvial materials and have not been observed within the basaltic rocks.

Chemical compositions of the Denchai sapphires studied here are similar in the minor and trace element concentrations (Fe, Ti, Cr and Ga) to other sapphires reported from the SE-Asian suites (Thailand, Burma, Laos, Cambodia and Vietnam; Intasopa *et al.*, 1998; Pisutha-Arnond *et al.*, 1998; Tin Tin Win *et al.*, 1998), however the Denchai sapphires have very low Cr_2O_3 contents.

Oxygen isotope compositions for the Denchai sapphires are in the range of +4.7 to +8.4‰. In contrast, olivine from representative Denchai basalts are in the range of $\delta^{18}O$ values from +4.9 to +5.1‰ which are compatible with a strictly mantle origin for the basalts. Most Denchai sapphires have $\delta^{18}O$ values compatible with formation in uncontaminated mantle. However, a third of the sapphire analyses require some crustal contamination. The variability of Denchai sapphires $\delta^{18}O$ isotope compositions suggest mixing between two sources (i.e., crust and mantle).

A study of inclusion within the Denchai sapphires has distinguished the three compositional types of primary fluid/melt inclusions: CO_2-rich inclusions (Type-I), polyphase (V+L+S) inclusions (Type-II) and silicate-melt inclusions (Type-III). Solid inclusions (feldspar, muscovite, nepheline and zircon were also identified within the sapphires by both LRS and EMP analyses. The presence of Type-I suggests that the sapphire formation was saturated in CO_2-bearing fluids early in its evolution. Estimated trapping temperature of CO_2-rich inclusions is > 550°C with minimum pressure of 4 kbars. High salinity fluid inclusions (Type-II) trapped in the sapphires are evidence for the existence and involvement of

hypersaline fluids during the crystallisation of sapphire. Anhydrite was also identified within Type-II inclusions by the LRS. The trapping temperature of Type-II inclusions is > 600°C based on their homogenisation temperature.

Analyses of melt inclusions (Type-III) have demonstrated compositions ranging from trachyandesite to trachyte (Fig.5.13). The LRS study has confirmed the presence of rutile, hematite and magnetite as trapped minerals within melt inclusions, suggesting oxidised condition during the sapphire crystallisation. This is also consistent with the presence of anhydrite and the total dominance of CO_2 over CH_4 in Type-I and II inclusions. Furthermore, the high Fe^{3+} contents of the associated alluvial spinels suggest an oxidised condition.

To constraint *P-T* conditions of sapphire crystallisation, the glass compositions were projected into the NKASH system (Holland and Powell, 2001). Using this simple system, many of the phase relations inferred from the mineral, glass and Type-II inclusions were modelled (Fig.5.17). The (Sill, q) invariant point at 710°C and ~6 kbars has all the phases recognised as inclusions. However, this invariant point predicts melt compositions which contain 12wt% water, far more than estimated from the glass compositions. The invariant point migrates to higher pressure and temperature in systems where $aH_2O < 1.0$ (Fig.5.18). Using the H_2O activity relationship in concentrated NaCl solutions (Aranovich and Newton, 1996), the hypersaline Type-II inclusions have a water activity (aH_2O) of about 0.5. At this aH_2O the "invariant" point is at very high pressure (> 15 kbars). The associated basalts fractionated at pressures ~15 kbars and for this pressure the "invariant" point is at > 850°C.
The modelling of actual glass compositions (Fig.5.19) suggest that the trapped melt compositions is close to 15wt% Al_2O_3 and most melt inclusions have been "overheated" during the ascent to surface within a basaltic magma.

In summary, the melt compositions are compatible with a medium to high-pressure origin (> 6 kbars) at 700-900°C. The Type-I inclusions indicate > 4 kbars with CO_2 saturation and the Type-II inclusions are most consistent with temperature > 600°C. The four types of inclusions (low density Type-I, high salinity Type-II, glass Type-III and mineral) are consistent with a silica undersaturated and highly oxidised (H-M buffer) environment. The high salinity requires a source for Cl. The O-isotope compositions are best explained by variable contamination of mantle source material. The contaminant has crustal O-isotopes, high NaCl, and was probably very oxidised. The O-isotope data are best explained by mixing between a mantle and crustal source with the mantle source being volumetrically dominant. In this scenario the crustal component should include high H_2O, high NaCl and be very oxidised.

Chapter 6

Synthesis

Work on gem-quality corundum (sapphires and rubies) has long recognised a spatial link with alkali intraplate basalts. This is particularly well illustrated by the occurrence of gem-quality corundum in association with the alkali intraplate basalts provinces of eastern Australia and southeast Asia (e.g., Barr and Mcdonald, 1978, 1981; Vichit, 1987, 1992; Coenraads *et al.*, 1995; Guo *et al.*, 1996a; Sutherland, 1996; Sutherland *et al.*, 1998a, 1998b; Sutthirat *et al.*, 2001). Such associations have lead to the recognition of intraplate basalts as among the best sources of commercial gem-quality corundum.

Several occurrences of late Cenozoic alkali basalts in Thailand are a major source of gem-quality corundum, and most are mined from nearby alluvial placer deposits. However, in spite of this straightforward association, a petrogenetic link between gem-quality corundum and the associated basalts remains to be shown. And moreover, a longstanding controversy is driven by the fact that although gem-corundum is found as a product of nearby weathered basalts, they are rarely found hosted within them.

This thesis has focused on evidence obtained from inclusion studies of sapphires from Denchai area, with the aim at constraining the interpretation of current models. Conclusion from each chapter are drawn together in the sections below and briefly summarised in Section 6.3

6.1 Late Cenozoic volcanism in SE-Asia

Late Cenozoic volcanic activity in Southeast Asia began at least 25 Ma ago and has randomly continued throughout the Southeast Asian continent until the present times, without any apparent space-time relationship. Southeast Asia nonetheless is a region of complex tectonics. Several major tectonic events such as the opening of the South China Sea (Ben-Avraham and Uyeda, 1973), the opening of the Andaman Sea (Lawver *et al.*, 1976) and the collision between Indian and Eurasia (Tapponnier *et al.*, 1986) may have influenced the distribution and occurrence of volcanic activity throughout the region. The late Cenozoic basalts in mainland Southeast Asia represent a surface expression of regional "escape"

tectonic events related to the collision between India and Asia. Escape tectonics may be genetically related to the occurrence of gem areas in Southeast Asia.

6.2 The Denchai basalts

The Denchai basalts are located in Phrae Province, Northern Thailand, in an area of northeast-trending hilly terrain. These basalts are medium to dark grey in colour, and are fine to medium grained. Their overlying weathered red soils tend to form flat plains covering a total area of about 70 km^2. Xenoliths are common within the basalts and range in size up to 5 cm across. Vesicles and fractures are also present in the basalts, and are infilled mainly by carbonate, zeolite and iron oxide/hydroxide minerals.

Olivine, clinopyroxene and plagioclase occur in variable amounts as phenocrysts as well as microphenocrysts. Olivine is the dominant phase, followed by clinopyroxene and plagioclase. Groundmasses are holocrystalline to hypocrystalline texture, and composed of plagioclase, olivine, clinopyroxene, Ti-magnetite and devitrified brown glass. Xenoliths and disaggregated nodule materials are also abundant within the basalts. The associated xenoliths are rounded or sub-angularly-shaped, medium to coarse-grained and are granoblastic in texture. The majority of these xenoliths are mantle-derived (spinel-lherzolites). Crustal-derived xenoliths, as well as a quartz xenocryst, are also present but minor. *P-T* estimates from spinel-lherzolite xenoliths indicate temperatures of around 1030°C and pressures in the range 8-20 kbars. Assuming a temperature of approximately 700°C, the coexisting phase assemblages (clinopyroxene-plagioclase-quartz) of the crustal xenoliths indicate an equilibration pressure of about 8 kbars.

On the basis of their petrographic character and chemical compositions, the Denchai basalts were subdivided into four groups (Groups A, B, C and D). All four groups have identical chondrite-normalised HREE but are variable in LREE enrichments. All Denchai basalts also show near identical multi-element patterns with significant enrichments in K relative to Nb, U, Th and LREE. The REE and spidergram patterns are comparable to the North Queensland and SE-China intraplate basalts. The Denchai basalts also show features of high pressure (> 10 kbars) fractionation, with no evidence for low-pressure crystal fractionation.

Radiogenic isotope (Sr, Nd and Pb) compositions of the Denchai basalts lie well above the Northern Hemisphere Reference Line (NHRL) line. They are comparable to those of Indian Ocean MORB in terms of Pb-Pb isotopic ratios, but are more enriched in Sr and less in Nd than Indian Ocean MORB. An EM-2 mantle component was not detected in the Denchai

basalts, their isotopic compositions also indicate a less depleted parental source than that for Indian Ocean MORB and the North Queensland intraplate basalts. Isotopic data suggest that most of the Denchai basalts have not experienced crustal contamination. Their compositions are best modelled by the mixing of three mantle end-member components as illustrated in Figure 4.12. End-member 1: an "A" end-member consisting of a mixture of a depleted Mantle HIMU component and a component lying between DM and HIMU line, End-member 2: "A"-EM1 mix end-member, and End-member 3: EM2-enriched subcontinental lithospheric mantle. Group C lavas are the most enriched in radiogenic Sr and have early crystallised magnetite suggesting a more oxidised composition.

6.3 The Denchai sapphires

The Denchai gem fields are located in the Denchai district (Phrae Province), northern Thailand. They are in close spatial association with Cenozoic Denchai basalts. Sapphires from these gem fields range in size up to 0.9 cm across, and are found as alluvial materials with an *in situ* sapphire crystal has been found within the the Denchai basalts (Vichit, 1992). The majority (~90%) of these sapphires are blue in colour and vary in shade from light to dark blue. Blue-green-yellow sapphires are also present but theses are less common. Spinel and zircon are the most common alluvial minerals associated with sapphires in these gem fields.

Minor and trace compositions of the Denchai sapphires are characterised by low Cr contents but mostly have higher Ti/Ga ratios compared to those of typical blue-green-yellow (BGY) sapphires of eastern Australia (Section 5.4.4). The chemical characteristics of the Denchai sapphires are comparable in terms of their genetic features (colour and mineral chemistry) to sapphires derived from other alkali basaltic provinces (e.g., eastern Australia and eastern China; Guo *et al.*, 1996a; Sutherland *et al.*, 1998a).

The Denchai sapphires have $\delta^{18}O$ values in the range of +4.7 to +8.4‰. Olivine crystals separated from the Denchai basalts have $\delta^{18}O$ values varying from +4.9 to +5.1‰ which are compatible with a strictly mantle origin for the basalts. Some sapphires match the host basalts with "mantle" $\delta^{18}O$ values, while the other sapphires indicate mixing between crust and mantle components. The variability of $\delta^{18}O$ values in the Denchai sapphires suggest that they originated from a source that underwent some interaction between crust and mantle components prior to sapphire crystallisation. Unlike the Denchai sapphires, the Loch Roag corundums from Scotland have a strictly mantle O-isotope signature (+4.6‰ to +5.2‰) and

megacrysts of Nb-Ta rich oxides (e.g., columbite and ilmenorutile) also occur in the alkali basaltic hosts (Aspen *et al.*, 1990; Hinton and Upton, 1991; Upton *et al.*, 1999). The consistency of $\delta^{18}O$ value of the Loch Roag corundums is very similar to $\delta^{18}O$ value in the sub-continental mantle of Scotland, and it rules out any significant crustal contamination.

Four types of inclusions are identified within Denchai sapphires: CO_2-rich inclusions (Type-I), polyphase (V+L+S) inclusions (Type-II), silicate-melt inclusions (Type-III) and mineral inclusions (feldspar, muscovite, nepheline and zircon). LRS studies confirmed the presence of CO_2, rutile, hematite, magnetite and anhydrite. PIXE suggests reasonable amounts of K, Ca and Cl within melt inclusions. Type-I inclusions were trapped at temperature > 550°C with a minimum pressure of 4 kbars (Section 5.5.1). Type-II inclusions are hypersaline with homogenisation temperatures, indicating trapping T > 600°C. Glass compositions of Type-III inclusions have 52-69wt% SiO_2, 16-30wt% Al_2O_3, ~10wt% K_2O + Na_2O and relatively low (< 1wt%) FeO, MgO, CaO, P_2O_5 values. Thermodynamic modelling (Figs.5.17-5.19) in the NKASH system suggests that the original glass inclusions were trapped at pressure > 6 kbars and temperature range between 700-900°C. The preferred condition is at ≥ 15 kbars and 800-900°C. Fluid/melt inclusion characteristics provide evidence for the existence of at least three compositionally distinct fluids (CO_2, high salinity water and silicate melt), all of which must appear at some stage during the primary growth stage of the Denchai sapphires. All the inclusions present (Type-I, Type-II, Type-III and mineral inclusions), the O-isotope data and the highly oxidised NaCl-bearing source rocks must be explained by any model for the formation of the Denchai sapphires.

6.4 Implication for corundum genesis

Corundums are generally found in metamorphic and magmatic environments. Metamorphic corundum is the most common and forms locally in Al-rich and Si-poor host rocks. Magmatic corundums involve plutonic crystallisation, and require a highly aluminous, volatile and trace element-rich alkali parental magma. However, petrogenetic models by which such parental magma can form remain controversial. There is a diversity of corundum genesis models. Despite the controversy however, there is currently a general consensus that corundum genesis must involve at least two main stages. An early stage where corundum is formed as a magmatic or metamorphic phase at upper mantle or lower crustal depths, and a second stage where corundum is incorporated and transported to the surface via a magmatic event (e.g., Guo *et al.*, 1996a; Sutherland *et al.*, 1998b).

This thesis aims to generate petrological and geochemical constraints to discriminate amongst current models of corundum formation. The results are outlined, compared and discussed below.

6.4.1 Role of carbonatite melts association

The role of carbonatitic melts in the genesis of corundum has been investigated by several authors (e.g., Guo *et al.*, 1996a; Upton *et al.*, 1999). However if carbonatite melts were involved in the crystallisation of the Denchai sapphires, the overwhelming concentration of Ca into the melt would lead to a relatively high Ca content in the silicate melts. The low CaO contents in both feldspar inclusions and glass inclusions of the Denchai sapphires is therefore inconsistent with a carbonatite association. Carbonatite melts also contain highly incompatible trace elements (Nb, Ta, Zr and REE; Sokolov, 2002), enhancing these trace elements in the silicate-oxide phases. Hf is taken into the silicate melts in preference to Zr (Fielding, 1992; Upton *et al.*, 1999) resulting in high Hf content in zircon. Instead, both zircon inclusions and associated alluvial zircon presented here have lower Hf contents than typical values in zircon inclusions in sapphires reported by Guo *et al.* (1996a) and Upton, *et al.* (1999). The sum of evidence is against a contribution from carbonatite in the genesis of the Denchai sapphires. Further to this, in contrast to those sapphires from eastern Australia, eastern China and Scotland (Guo *et al.*, 1996a; Sutherland *et al.*, 1998a; Upton, *et al.*, 1999), the lack of Nb-Ta oxide inclusions, together with a trend towards crustal $\delta^{18}O$ values, is not consistent with an involvement of carbonatitic melts during crystallisation of the Denchai sapphires.

6.4.2 Oxidation state in sapphire forming environment

Solid inclusions coexisting with glass inclusions within Denchai sapphires (rutile, hematite and magnetite) suggest a distinctively oxidised environment for sapphire crystallisation. This is consistent with the absence of ilmenite and sulphide inclusions in Denchai sapphires, unlike most sapphires from eastern Australia (Guo *et al.*, 1996a; Sutherland *et al.*, 1998a). Furthermore, the common alluvial minerals associated with the Denchai sapphires collected in this study include spinel and zircon. The spinels have $Mg\#_{sp} > 70$, which are higher that those reported by Sutherland *et al.* (1998a) with $Mg\#_{sp}$ of 30. Both associated alluvial zircons and zircon inclusions contain low Hf contents (< 1wt%), and contrast with zircon inclusions in Eastern Australian, Eastern China and Scottish corundums (Guo *et al.*, 1996a; Sutherland *et al.*, 1998a; Upton *et al.*, 1999) where Hf values are > 1.5wt%. In addition, one of the gem-

related Denchai basalt groups is more oxidised which may indicate an oxidised contaminating material in the mantle.

6.4.3 Low Si activity system

Mineral inclusions in Denchai sapphires include feldspar, muscovite, nepheline and zircon. Nb-Ta enriched inclusions (e.g., columbite and ilmenorutile) are absent in Denchai sapphires despite being very common in the Eastern Australian sapphires (Guo *et al.*, 1996a; Sutherland *et al.*, 1998a). Nepheline, also present as mineral inclusions in Denchai sapphires has not previously been reported elsewhere. This finding is highly significant as it testifies for the presence of low silica activity environment during sapphire formation.

6.4.4 Candidate source rocks for the Denchai sapphire formation

A continental crustal source rock

Suprasolidus decompression-dehydration reactions (SDDRs) involving muscovite with K-feldspar (KASH) for assemblages without quartz can produce corundum (Thompson, 2001). Thompson (2001) reported that the corundum-bearing invariant point could reach near 9.5 kbars at 850°C and at this condition muscovite still remains in the absence of quartz. This is consistent with the presence of muscovite, K-feldspar and nepheline inclusions in the Denchai sapphires. The model demonstrates that direct melting of pelitic crustal rocks at high temperatures and under conditions of silica-undersaturation, could lead to the crystallisation of corundum. Melting of crustal source rock can form corundum, but in this model the O-isotope composition of sapphires should have strictly crustal O-isotope signature. Instead the O-isotope compositions of the Denchai sapphires (+4.7 to +8.4‰) indicate $\delta^{18}O$ values dominated by mantle compositions with only minor crustal contamination. On this basis the model that the Denchai sapphires were formed by melting of crustal source rock is rejected.

A mafic composition source rock

Recent inclusion studies on alluvial corundums from the Chanthaburi-Trat gem deposits, southeastern Thailand have reported a suite of Fe-Mg-rich silicate mineral inclusions (clinopyroxene, pyropic garnet and sapphirine; Sutthirat *et al.*, 2001). The study reported that the clinopyroxene inclusions in alluvial corundums have very similar composition to the corundum-bearing clinopyroxene xenocryst, indicating the same origin of these two types of clinopyroxene. A mafic composition (i.e., corundum-garnet-pyriclastite and/or corundum-garnet-clinopyroxenite), which contains coexisting garnet + clinopyroxene + sapphirine +

corundum was proposed as a source rock of the clinopyroxene + corundum assemblages crystallising at *T* (800-1100°C) and *P* (10-25 kbars). However, these inclusions suggest higher Ca (as indicated by clinopyroxene) and Fe-Mg (as indicated by garnet + sapphirine) contents in parental composition, than that of the Denchai sapphires (low Ca, Fe and Mg). Such a mafic composition (Sutthirat *et al.*, 2001) as a source rock for the sapphire from Denchai is unlikely. While the suite of silicate inclusions in Thai corundums is similar to those reported from Eastern Australian corundums, they still lack Nb-Ta oxide inclusions. This could reflect different source rock compositions for these two settings (i.e., eastern Australia and Thailand).

Some authors have suggested that sapphires are formed when corundum crystallises by plutonic crystallisation of intraplate magmas (nephelinites, basanites) or syenitic melts of mantle origin (see section 1.1.1). These models assume that alkali melts can evolve to extreme compositions under closed system fractionation. There is no direct experimental evidence to support the claims that these compositions can evolve to corundum saturation at high pressure, but it is impossible to disprove this model based on theoretical and experimental grounds since there are a very large range of possible fractionation environments to be considered.

There are some indirect indicators that suggest this model is unlikely as an explanation for the particular sapphires included in this study. The melt inclusion compositions found in the Denchai sapphires do not match any published evolved syenite or trachyte compositions currently documented in the literature. For a SiO_2 content of 63 to 68wt%, Al_2O_3 of 16 to 20wt% and MgO content < 0.2wt%, trachytes and syenites always have a higher FeO (2wt% rather than 0.25wt%) and lower H_2O (2wt% rather than 6wt%). The Cl/K ratio of the Denchai glasses is ~ 0.1 and much higher than the 0.04wt% typical of uncontaminated mantle melts (Lassiter *et al.* 2002). The evidence from O isotopes supports contamination of the mantle source, as does the highly oxidised nature of environment demonstrated by the associated hematite inclusions. For these reasons this model is not considered applicable to the Denchai sapphires.

Partial melting of mantle source rocks

Studies of glass inclusions in minerals in mantle xenoliths have demonstrated silica-rich glass compositions and its role in mantle processes. The origin of silica-rich melts in mantle rocks however is still debated (e.g., Francis, 1987; Schiano and Clocchiatti, 1994; Schiano *et al.*, 1995; Chazot *et al.*, 1996). In general, glasses in mantle xenoliths have variable compositions (52-68wt% SiO_2, 18-23wt% Al_2O_3, 3-10wt% Na_2O and 0.3-2.3wt% K_2O) and are proposed to

have a diverse origin. For example, Eiler *et al.* (1993) and Schiano *et al.* (1994a) concluded that they represent small amounts of metasomatic melts, originated at depth as part of an exotic migrating phase within the lithosphere. A two-stage model to account for the Si-Al-alkali-rich melts corresponding to mantle xenolith glasses also proposed by Draper and Green (1997). When compared to the Denchai glasses, glass compositions in typical mantle xenoliths (c.f., Yaxley *et al.*, 1997) contain much higher Ca, Fe and Mg contents than the glasses from Denchai.

In comparison to melt glasses in mantle xenoliths from intraplate continental and oceanic regions worldwide, the study of melt inclusions in olivine, orthopyroxene and clinopyroxene in ultramafic peridotites (spinel-lherzolites and harzburgites; Schiano and Clocchiatti, 1994) suggest similarity in major element chemistry to the Denchai glass compositions in terms of Si, Al, Ti, Mn and P contents. The silica-rich melts from continental and oceanic intraplate settings, and from the Denchai sapphires both contain CO_2 in shrinkage bubbles within melt inclusions. The fact that CO_2 bubbles did not disappear during heating experiments, suggests a CO_2 oversaturation within glass inclusions from intraplate mantle xenoliths (Schiano *et al.*, 1994b) and from the Denchai sapphires (this study). The crystallising mineral phases (e.g., kaersutite, diopside, rutile, ilmenite and magnesite) identified in glass inclusions in minerals from intraplate mantle xenoliths are different from the rutile, hematite and magnetite trapped in the Denchai glass inclusions. However, the main difference is that these glasses in sub-continental and sub-oceanic mantle environments are much higher in Ca, Fe and Mg contents than the Denchai glass compositions. Further to this, the volatile contents (Cl and S) in intraplate mantle melt glasses contain lower Cl (~2000 ppm) and S (< 500 ppm) than the volatile content of the Denchai glasses (Cl ~5000 ppm and S ~600 ppm). The glass compositions from intraplate mantle melts also indicate more anhydrous condition (H_2O < 2wt%) of trapped melts than the Denchai glass inclusions (H_2O ~5wt%). On the basis of chemical compositions and higher volatile components within the Denchai glasses, they are unlikely to have been generated by migrating metasomatic melts within the lithosphere. The highly volatile components in melt inclusions also suggest that volatiles played an important role during melt generation.

The preserved glass compositions in mantle xenoliths from Phillippine arc lavas (Schiano *et al.*, 1995) are silica-rich (53-62wt% SiO_2), hydrous (~5wt% H_2O) and volatile-rich melts (~5000 ppm Cl and ~500 ppm S). These glasses are very similar in H_2O and other volatiles to the Denchai glasses. Glasses from "slab melts" also demonstrate high Mg# (81) Al-rich spinel within them, which is similar to the high Mg# (~72) Al-rich spinels associated with the Denchai sapphires. Although the Cl, S and H_2O contents in glasses from sub-arc sources are

similar to the Denchai glass compositions, the CaO, FeO and MgO contents are still relatively higher than the Denchai glass compositions. Thus, metasomatic melt in sub-arc mantle is not a perfect candidate source rock for the Denchai sapphire formation.

On example of low Ca glass from an arc environment was described by McInnes and Cameron (1994). They argued the low Ca content in glass compositions, was explained by crystallising mineral phases (calcite and anhydrite) and produced a model for Sulfate-Carbonate-H_2O-Alkali-rich Melt (SCHARM). They suggested that SCHARM is highly oxidised and contains substantial Cl, F, Sr and Ba, and proposed that SCHARM was derived by melting of a subducted slab containing seawater-altered basalts. The SCHARM hypothesis was constrained from preliminary experimental results on melting of altered oceanic crust, and showed that melting occurs at 875°C at 10 kbars and 975°C at 20 kbars to produce a carbonated, nepheline-normative melt with major element and dissolved CO_2 contents similar to SCHARM, but more enriched in Fe and Mg contents (McInnes and Wyllie, 1992). Although the SCHARM glasses have very similar compositions to the Denchai glasses, the higher CO_2 content of and presence of a crystallising phase (e.g., carbonate) in the SCHARM glass inclusions contrasts with the Denchai sapphires.

A more likely origin of the Denchai sapphire formation is a melting of a highly weathered subducted slab component. The much lower Ca and Mg in the Denchai glasses can be explained by extreme seafloor weathering. Hekinian (1982) pointed out that seafloor weathering (rather than alteration) caused rapid depletion in Ca and Mg, enrichment in K and oxidation. The highly weathered subducted slab component was probably trapped in the subcontinental lithosphere during late Triassic collision between the Shan-Thai and Indochina Terranes in Southeast Asia (e.g., Panjasawatwong and Yaowanoiyothin, 1993; Singharajwarapan and Berry, 2000). The cold subducted slab was heated either during post collisional granite formation or by an asthenosphere upwelling, resulting in sapphire crystallisation. The sapphires were then incorporated into, and transported to the surface via, late Cenozoic alkali magmatism.

Although there is no perfect model explaining where the Denchai sapphire source rock can be formed, the results demonstrate that crustal melting cannot produce the sapphires. Instead, it requires some contamination of a rock with mantle signature. The contaminant is highly oxidised, NaCl-rich, increases CO_2 and decreases Ca, Mg and Fe contents in the system. The alkali basalts provide a heat source, a low $aSiO_2$ buffer to react with an aluminous contaminant, and a method for rapid transport to the surface.

6.5 Concluding remarks

This inclusion-based study emphasises the large variability in the sources of corundums. There are at least four critical features of corundum source rocks from four source regions (Eastern Australia, Eastern China, Scotland and Thailand) relevant to the genesis of corundum formation. One end-member requires alkali basaltic rocks for the transportation of earlier formed corundum to the Earth's surface. The other end-member may be a range of potential contaminants. These contaminants may be (1) Nb-Ta rich, (2) highly oxidised (3) Ca-poor and/or (4) have a crustal O-isotope signature.

The Eastern Australian and Eastern China suites represent Nb-Ta rich and reduced (ilmenite and sulphides) contaminants interpreted as carbonatite melts (Guo *et al.*, 1996a), while the other authors interpreted the contaminants as a volatile-rich felsic rocks derived from metasomatised mantle (Sutherland *et al.*, 1998a). The Loch Roag corundums from Scotland have Nb-Ta enrichment with strictly mantle O-isotope signature features in association with carbonatite melts (Aspen *et al.*, 1990; Upton *et al.*, 1999). The Thai settings (Denchai and Chanthaburi-Trat) lack Nb-Ta enrichments. They are oxidised (hematite and sulphate stable) and contaminated by crustal O-isotope features. They range from Ca-poor (Denchai sapphires) and Ca-normal (Chanthaburi-Trat; Sutthirat *et al.*, 2001) parental melts.

Although this study has established a framework for the genesis of corundum, there are several aspects requiring further study.
These include:

- Sulphur (S) isotopic studies of gem-quality corundums to define crystallisation environments (i.e., oxidation and reducing) and possibly source of S.
- Chlorine (Cl) isotopic studies of gem-quality corundums, as a means of identifying the source of Cl.
- Inclusion studies of alluvial minerals associated with gem-quality corundums in order to constrain and compare their parental source with associated gem-quality corundums.

This detailed study of the Denchai sapphires demonstrates that there is a range of possible source compositions for sapphires. Further work is required to define the extent of this range.

References

Aranovich, L. Y. and Newton, R. C., 1996, H_2O activity in concentrated NaCl solutions at high pressures and temperatures measured by the brucite-periclase equilibrium. *Contributions to Mineralogy and Petrology*, **125**: 200-212.

Aranyakanon, P., Sampatavanija, S. and Ruengsuwan, J., 1970, *Report on gem deposit at Si Sa Ket.* Economic Geology Division, Department of Mineral Resources, Bangkok, Thailand, 12 pp (in Thai).

Arndt, N. T. and Christensen, U., 1992, The role of lithosphere mantle in continental flood volcanism: thermal and geochemical constraints. *Journal of Geophysical Research*, **97**: 10967-10981.

Aspen, P., Upton, B. G. J. and Dicken, A. P., 1990, Anorthoclase, sanidine and associated megacrysts in Scottish alkali basalts: high pressure syenitic debris from upper mantle sources? *European Journal of Mineralogy*, **2**: 503-517.

Atkinson, D. and Kothavala, R. Z., 1983, Kashmir sapphire. *Gems and Gemology*, **19**: 64-76.

Bacon, C. R., Newman, S. and Stolper, E., 1992, Water, CO_2, Cl and F in melt inclusions in phenocrysts from three Holocene explosive eruptions, Crater Lake, Oregon. *American Mineralogist*, **77**: 1021-1031.

Baker, J. A., Macpherson, C. G., Menzies, M. A., Thirlwall, M. F., Al-kadasi, M. and Mattey, D. P., 2000, Resolving crustal and mantle contributions to continental flood volcanism, Yemen: Constraints from mineral oxygen isotope data. *Journal of Petrology*, **41(12)**: 1805-1820.

Ballhuas, C., Berry, R. F. and Green, D. H., 1991, High pressure experimental calibration of the olivine-orthopyroxene-spinel oxygen geobarometer: implications for the oxidation state of the upper mantle. *Contributions to Mineralogy and Petrology*, **107**: 27-40.

Barr, S. M. and Dostal, J., 1986, Petrochemistry and origin on megacrysts in Upper Cenozoic basalts, Thailand. *Journal of Southeast Asian Earth Sciences,* **1**: 107-116.

Barr, S. M. and MacDonald, A. S., 1978, Geochemistry and Petrogenesis of Late Cenozoic Alkaline Basalts of Thailand. *Geological Society of Malaysia Bulletin,* **10**: 25-52.

Barr, S. M. and MacDonald, A. S., 1979, Palaeomagnetism, Age and Geochemistry of the Denchai Basalt, Northern Thailand. *Earth and Planetary Science Letters,* **46**: 113-124.

Barr, S. M. and MacDonald, A. S., 1981, Geochemistry and geochronology of Late Cenozoic basalts of Southeast Asia – part II. *Geological Society of American Bulletin,* **92**: 1069-1142.

Barr, S. M., MacDonald, A. S., Haile, N. S. and Raynolds, P. H., 1976, Paleomagnetism and age of the Lampang basalt (northern Thailand) and age of the underlying pebble tools. *Journal of Geological Society of Thailand*, **2**: 1-10.

Barron, L. M., Lishmund, S. R., Oakes, G. M., Barron, B. J. and Sutherland, F. L., 1996, Subduction model for the origin of some diamonds in the Phanerozoic of eastern New South Wales. *Australian Journal of Earth Sciences*, **43**: 257-267.

Ben-Avraham, Z. and Uyeda, S., 1973, Evolution of the China Basin and the Mesozoic palaeogeography of Borneo. *Earth and Planetary Science Letters*, **18**: 365-376.

Bender, F., 1983, *Geology of Burma*, Gebruder Borntraeger, Berlin-Stuttgar, 43-49.

Benisek, A. and Finger, F., 1983, Factors controlling the development of prism faces in granite zircons: a microscope study. *Contributions to Mineralogy and Petrology*, **114**: 441-451.

Bertrand, P. and Mercier, J. C. C., 1985, The mutual solubility of coexisting ortho- and clinopyroxene: toward an absolute geothermometer for the natural system. *Earth and Planetary Science Letters*, **76**: 109-122.

Bignell, J. D. and Snelling, N. J., 1977, K-Ar ages on some basic igneous rocks from peninsula Malaysia and Thailand. *Bulletin of Geological Society of Malaysia*, **8**: 93-98.

Binns, R. A., 1969, High-pressure megacrysts in basanitic lava near Armidale, New South Wales. *American Journal of Science*, **267A**: 33-49.

Binns, R. A., Duggan, M. B. and Wilkinson, J. F. G., 1970, High pressure megacrysts in alkaline lavas from northeastern New South Wales. *American Journal of Science*, **269**: 132-168.

Bodnar, R. J., Burnham, C. W. and Sterner, S. M., 1985, Synthetic fluid inclusions in natural quartz, III. Determination of phase equilibrium properties in the system H_2O-NaCl to 100oC and 1500 bars. *Geochimica et Cosmochimica Acta*, **49**: 1861-1873.

Boonsoong, A., 1997, Geochemistry and petrology of Mae Tha Basalts, Changwat Lampang. *Unpublished MSc. thesis,* Chiang Mai University, Thailand, 124 pp.

Boonsoong, A., 2001, The characterisation of corundum gems and petrogenesis of basalts in the Chanthaburi-Trat gem fields, Thailand. *Unpublished PhD. thesis,* The University of Birmingham, UK, 431 pp.

Bowersox, G. W., 1985, A status report on gemstones from Afghanistan. *Gems and Gemology*, **21**: 192-204.

Bowers, T. S. and Helgeson, H. C., 1983, Calculations of the thermodynamic and geochemical consequences of nonideal mixing in the system H_2O-CO_2-NaCl on phase relations in geologic systems: Equation of state for H_2O-CO_2-NaCl fluids at high pressures and temperatures. *Geochimica et Cosmochimica Acta*, **47**: 1247-1275.

Brey, G. P. and Kohler, T., 1990, Geothermobarometry in Four-phase Lherzolites II. New Thermobarometers, and Practical Assessment of Existing Thermobarometers. *Journal of Petrology*, **31(6)**: 1353-1378.

Brown, G. M., Pinsent, R. H. and Coisy, P., 1980, The petrology of spinel-peridotite xenoliths from the Massif Central, France. *American Journal of Science*, **280-A**: 471-498.

Brown, P. E. and Hagemann, S. G., 1994, MacFlincor: A computer program for fluid inclusion data reduction and manipulation. *In Fluid inclusions in minerals: Methods and applications*, (B. Devivo and M.L.Frezzotti, eds.), Virginia Tech Publishing, USA, 231-250.

Brownlow, A. H. and Komorowski, J. C., 1988, Geology and origin of the Yoko sapphire deposit, Montana. *Economic Geology*, **83**: 875-880.

Bunopas, S. and Bunjitadulya, S., 1975, Geology of Amphoe Bo Ploi, North Kanchanaburi with special notes on the "Kanchanaburi Series". *Journal of Geological Society of Thailand*, **1**: 51-67.

Carbonnel, J. P., Selo, M. and Poupeau, G., 1973, Fission-track age of the gem deposit of Pailin, Cambodia and the recent tectonics in the Indochina. *Modern Geology*, **14**: 61-64.

Carlson, H. D., 1957, Origin of the corundum deposits of Renfrew Country, Ontario, Canada. *Bulletin of Geological Society of America*, **68**: 1605.

Chakraborty, K. R., 1977, Olivine nephelinite and limburgite from Kuantan, Pahang. *Geological Society of Malaysia Newsletter*, **3**: 1-5.

Charaljavanaphet, J., 1951, Gem deposits at Bo Na Wong, Tok-Phrom, Bo-Rai in Chanthaburi and Trat Provinces and Bo Phloi in Kanchanaburi Province in geologic reconnaissance of the mineral deposits of Thailand. *U.S. Geological Survey Bulletin,* **984**: 148-150.

Charoenprawat, A., Phuanda, J. and Maneenai, D., 1987, *Geologic Map of Ban Bo Kaeo (1:50,000, Sheet 4944 I).* Geological Survey Division, Department of Mineral Resources, Bangkok, Thailand.

Charusiri, P., 1989, Lithophile Metallogenic Epochs of Thailand: A Geological and Geochronological Investigation. *Unpublished PhD. thesis,* Queen's University, Ontario, Canada, 819 pp.

Charusiri, P., Plathong, C. and Pongsapich, W., 1995, Geology and petrochemistry of basaltic rocks at Khao Kradong, Burirum, NE Thailand – Implications for rock wool and tectonic setting. *Eighth Regional Conference on Geology, Minerals, and Energy Resources of Southeast Asia,* Manila, Philippines, Abstract, 1.

Chatterjee, N. D. and Terhart, L., 1985, Thermodynamic calculation of peridotite phase relations in the system MgO-Al_2O_3-SiO_2-Cr_2O_3, with some geological applications. *Contributions to Mineralogy and Petrology*, **89**: 273-284.

Chazot, G., Menzies, M. and Harte, B., 1996, Silicate glasses in spinel lherzolites from Yemen: origin and chemical composition. *Chemical Geology (Isotope Geoscience)*, **134**: 159-179.

Chhibber, H. L., 1934, *The Geology of Burma*. MacMillan, London.

Chuaviroj, S., Charoenprawat, A., Hinthong, C. and Chonglakmanee, C., 1992, *Geologic Map of Ban Bo Kaeo (1:50,000, Sheet 4944 I).* Geological Survey Division, Department of Mineral Resources, Bangkok, Thailand.

Chung, S. L. and Sun, S. S., 1992, A new model for the East Taiwan ophiolite and its implications for Dupal domains in the Northern Hemisphere. *Earth and Planetary Science Letters*, **190(1-2)**: 133-145.

Chung, S. L., Wang, K. L., Crawford, A. J., Kamenetsky, V. S., Chen, C. H., Lan, C. Y. and Chen, C. H., 2001, High-Mg potassic rocks from Taiwan; implications for the genesis of orogenic potassic lavas. *Lithos*, **59(4)**: 153-170.

Clabaugh, S. E., 1952, Corundum deposits of Montana. *U.S. Geological Survey Bulletin*, No. 983.

Clocchiatti, R. and Massare, D., 1985, Experimental crystal growth in glass inclusions: the possibilities and limits of the method. *Contributions to Mineralogy and Petrology*, **89**: 193-204.

Coenraads, R. R., 1992, Sapphires and rubies associated with volcanic provinces: Inclusions and surface features shed light on their origin. *Australian Gemmologist,* **18(3)**: 70-78.

Coenraads, R. R. and Van Der Graaf, 1991, An occurrence of gem garnets from Horse Gully in the New England gemfields, New South Wales. *Australian Gemmologist,* **17**: 412-415.

Coenraads, R. R., Vichit, P. and Sutherland, F. L., 1995, An unusual sapphire-zircon-magnetite xenolith from Chanthaburi Gem Province, Thailand. *Mineralogical Magazine,* **59**: 465-479.

Coetzee, C. B., 1940, Sillimanite-corundum rock: A metamorphosed bauxite in Namaqualand. *Transactions Royal Society of South Africa*, **28**: 199.

Coldham, T., 1985, Sapphires from Australia. *Gems and Gemology*, **21**: 130-146.

Cooray, P. G. and Kumarapeli, P. S., 1960, Corundum in biotite-sillimanite gneiss from near Polgahawela, Ceylon. *Geological Magazine*, **97**: 480-487.

Cousens, B. L., Allan, J. F. and Gorton, M. P., 1994, Subduction-modified pelagic sediments as the enriched component in back-arc from the Japan Sea; Ocean Drilling Program Sites 797-794. *Contributions to Mineralogy and Petrology*, **117(4)**: 421-434.

Danyushevsky, L. V., 2001, The effect of small amounts of H_2O on crystallisation of mid-oceanic ridge and backarc basin magmas. *Journal of Volcanology and Geothermal Research*, **110**: 265-280.

Danyushevsky, L. V., Sobolev, A. V. and Kononkova, N. N., 1992, Methods of studying melt inclusions in minerals during investigations on water-bearing primitive mantle melts (Tonga Trench boninites). *Geochemical International*, **29(7)**: 48-62.

Danyushevsky, L. V., Sobolev, A. V. and Dimitriev, L. V., 1996, Estimation of the pressure of crystallisation and H_2O content of MORB and BABB glasses: calibration of an empirical technique. *Mineralogy and Petrology*, **57**: 185-204.

Dawson, J. B., 1980, *Kimberlites and Their Xenoliths*. Springer-Verlag Heidelberg, New York, 252 pp.

Deer, W. A., Howie, R. A. and Zussman, J., 1992, *An Introduction to the Rock-Forming Minerals*. 2nd edition, Longman, Hong Kong, 696 pp.

Della-Pasqua, F., 1997, Primitive ankaramitic melts in island arcs: evidence from melt inclusions. *Unpublished PhD. thesis*, University of Tasmania, Australia, 233 pp.

Douglass, J. and Schilling, J. G., 2000, Systematics of three-component, pseudo-binary mixing lines in 2D isotope ratio space representations and implications for mantle plume-ridge interaction. *Chemical Geology*, **163(1-4)**: 1-23.

Draper, D. S. and Green, T. H., 1997, P-T phase relations of silicic, alkaline, aluminous xenolith glasses under anhydrous and C-O-H fluid-saturated conditions. *Journal of Petrology*, **38**: 1187-1224.

Du Toit, A. L., 1918, Plumasite (corundum-aplite) and magnetite rocks from Natal. *Transactions Geological Society of South Africa,* **21**: 53-73.

Duan, Z., Moller, N. and Weare, J. H., 1995, Equation of state for the $NaCl-H_2O-CO_2$ system: Prediction of phase equilibria and volumetric properties. *Geochimica et Cosmochimica Acta*, **59(14)**: 2869-2882.

Duggan, N. T., 1972, Tertiary volcanic rocks of the Inverell area. *Unpublished B.Sc. thesis,* University of New England, Armidale, Australia.

Dunning, G. R., MacDonald, A. S. and Barr, S. M., 1995, Zircon and monazite U-Pb dating of the Doi Inthanon core complex, northern Thailand: implications for extension within the Indosinian orogen. *Tectonophysics*, **251(1-4)**: 197-213.

Eiler, J. M., Valley, J. W. and Baumgartner, L. P., 1993, A new look at stable isotope thermometry. *Geochimica et Cosmochimica Acta*, **57**: 2571-2583.

Eiler, J. M., Farley, K. A., Valley, J. W., Hauri, E., Craig, H., Hart, S.R. and Stolper, E. M., 1997, Oxygen isotope variations in ocean island basalt phenocrysts. *Geochimica et Cosmochimica Acta*, **61**: 2281-2293.

Ellis, D. J., 1980, Osumilite-Sapphirine-Quartz Granulites from Enderby Land, Antarctica: P-T conditions of metamorphism, implications for garnet-cordierite equilibria and the evolution of the deep crust. *Contributions to Mineralogy and Petrology*, **74**: 201-210.

Evans, B. W., 1964, Fractionation of elements in the pelitic hornfelses of Cashel-Lough Wheelaun intrusion, Connemara, Eire. *Geochimica et Cosmochimica Acta*, **28**: 127-156.

Exley, R. A., Smith, J. V. and Dawson, J. B., 1983, Alkremite, garnetite and eclogite xenoliths from Bellsbank and Jagersfontein, South Africa. *American Mineralogist*, **68**: 512-516.

Fabries, J., Figueroa, O. and Lorand, J. P., 1987, Petrology and thermal history of highly deformed mantle xenoliths from the Montferrier basanites, Languedoc, southern France: A comparison with ultramafic complexes from the North Pyrenean Zone. *Journal of Petrology*, **28(5)**: 887-919.

Falloon, T. J. and Green, D. H., 1986, Glass inclusions in magnesian olivine phenocrysts from Tonga: evidence for high refractory parental magmas in the Tonga Arc. *Earth and Planetary Science Letters*, **81**: 95-103.

Falloon, T. J. and Green, D. H., 1987, Anhydrous partial melting of MORB pyrolite and other peridotite compositions at 10 kbar: implications for the origin of primitive MORB glasses. *Mineralogy and Petrology*, **37**: 181-219.

Falloon, T. J. and Green, D. H., 1988, Anhydrous partial melting of peridotite from 8 to 35 kbar and the petrogenesis of MORB. *Journal of Petrology, Special Lithosphere Issue*, 379-414.

Fan, Q. and Hooper, P., 1989, The Mineral chemistry of ultramafic xenoliths of Eastern China: Implications for upper mantle composition and the paleogeotherms. *Journal of Petrology*, **30(5)**: 1117-1158.

Fan, Q. and Hooper, P., 1991, The Cenozoic basaltic rocks of Eastern China: Petrology and chemical composition. *Journal of Petrology*, **32**: 765-810.

Ferguson, C. C. and Al-Ameen, S. I., 1985, Muscovite breakdown and corundum growth at anomalously low fH_2O: A study of contact metamorphism and convective fluid movement around the Omey granite, Connemara, Ireland. *Mineralogical Magazine*, **49**: 505-514.

Fielding, K., 1992, Element partitioning between coexisting carbonate and silicate liquids. *Unpublished PhD. thesis*, University of Edinburgh, Scotland.

Fitch, F. H., 1952, The geology and mineral resources of the neighbourhood of Kuantan, Pahang. *Federation of Malaya Geological Survey Department Memoir*, **6**: 143 pp.

Flower, M. F. J., Zhang, M., Chen, C. Y., Tu, K. and Xie, G. H., 1992, Magmatism in the South China basin, 2, Post-spreading Quaternary basalts from Hainan Island, South China. *Chemical Geology*, **97(1-2)**: 65-87.

Flower, M. F. J., Tamaki, K. and Hoang, N., 1998, Mantle extrusion: a model for dispersed volcanism and DUPAL-like asthenosphere in East Asia and the Western Pacific. *In Mantle Dynamics and Plate Interactions in East Asia*, (M.F.J. Flower, S.L. Chung, C.H. Lo and T.Y. Lee, eds.), *American Geophysical Union, Geodynamics*, **27**: 67-88.

Flower, M. F. J., Ma, Z., Mocanu, V., Russo, R., Nguyen, T. Y., Cung, T. C., Nguyen, Q. C., Deng, J., Dilek, Y., Dinu, C., Liu, F., Liu, M., Nguyen, H., Robinson, P., Mo, X., Punongbayan, R., Wenzel, F., Yumul, G. and Widom, E., 2000, Project targets mantle dynamics and Tethyan hazard mitigation. *Transactions American Geophysical Union (EOS)*, **81(49)**: 593, 600-601.

Ford, C. E., Russel, D. G., Craven, J. A. and Fisk, M. R., 1983, Olivine-liquid equilibria: temperature, pressure and composition dependence of the crystal/liquid cation partition coefficients for Mg, Fe^{2+}, Ca and Mn. *Journal of Petrology*, **24**: 256-265.

Francis, D. M., 1987, Mantle-melt interaction recorded in spinel lherzolites from the Alligator Lake Volcanic Complex. *Journal of Petrology*, **28**: 569-597.

Frey, F. A. and Green, D. H., 1974, The mineralogy, geochemistry, and origin of lherzolite inclusions in Victorian basanites. *Geochimica et Cosmochimica Acta*, **38**: 1023-1059.

Frey, F. A. and Prinz, M., 1978, Ultramafic inclusions from San Carlos, Arizona: petrologic and geochemical data bearing on their petrogenesis. *Earth and Planetary Science Letters*, **38**: 129-176.

Gasparik, T., 1984, Two-pyroxene thermobarometry with new experimental data in the system CaO-MgO-Al_2O_3-SiO_2. *Contributions to Mineralogy and Petrology*, **87**: 87-97.

Golani, P. R., 1989, Sillimanite-corundum deposits of Sonapahar, Meghalaya, India: A metamorphosed Precambrian paleosoil. *Precambrian Research*, **43**: 175-189.

Green, D. H., 1989, Experimental Petrology. *In Intraplate Volcanism in Eastern Australia and New Zealand*, (R.W. Johnson, ed.), Cambridge University Press, Singapore, 321-324.

Green, D. H. and Hibberson, W., 1970, Experimental duplication of conditions of precipitation of high pressure phenocrysts in a basaltic magma. *Physics Earth Planetary International*, **3**: 247-254.

Green, D. H. and Ringwood, A. E., 1970, Mineralogy of peridotite compositions under upper mantle conditions. *Physics Earth Planetary International*, **3**: 359-371.

Green, D. H. and Falloon, T. J., 1998, Pyrolite: A Ringwood concept and its current expression. *In The Earth's Mantle: Composition, Structure and Evolution*, (I.N.S. Jackson, ed.), Cambridge University Press, 311-380.

Green, D. H., Trevor, T. J. and Taylor, W. R., 1987, Mantle-derived magma-roles of variable source peridotite and variable C-H-O fluid compositions. *In Magmatic Processes: Physiochemical Principles*, (B.O. Mysen, ed.), *The Geochemical Society, Special Publication*, **1**: 139-154.

Gubelin, E. J., 1982, Gemstones from Pakistan: Emerald, ruby and spinel. *Gems and Gemology*, **18**: 123-139.

Guo, J. F., 1993, Origin and distribution of corundum from basaltic terrains. *Unpublished PhD. thesis,* Macquarie University, Sydney, Australia, 326 pp.

Guo, J. F., O'Reilly, S. Y. and Griffin, W. L., 1996a, Corundum from basaltic terrains: a mineral inclusion approach to the enigma. *Contributions to Mineralogy and Petrology*, **122**: 368-386.

Guo, J. F., O'Reilly, S. Y. and Griffin, W. L., 1996b, Zircon inclusions in corundum megacrysts: I. Trace element geochemistry and clues to the origin of corundum megacrysts in alkali basalts. *Geochimica et Cosmochimica Acta*, **60**: 2347-2363.

Gurenko, A. A., Sobolev, A. V. and Kononkova, N. N., 1992, New petrological data on Icelandic rift alkali basalts. *Geochemical International*, **29(4)**: 41-53.

Hall, A. L. and Nel, L. T., 1926, On an occurrence of corundum-sillimanite rock in the norite of the Bushveld igneous complex west of Lydenburg. *Transactions Geological Society of South Africa*, **29**: 1.

Hamid, G., Kelly, S. M. B. and Brown, G., 1996, Ruby from Tunduru-Songea, East Africa: Some basic observations. *Australian Gemmologist,* **20**: 326-330.

Hansteen, T. H., 1991, Multi-stage evolution of the Picritic Maelifell rocks, SW Iceland: constraints from mineralogy and inclusions of glass and fluid in olivine. *Contributions to Mineralogy and Petrology*, **109**: 225-239.

Harris, C., Smith, H. S. and Le Roex, A. P., 2000, Oxygen isotope composition of phenocrysts from Tristan da Cunha and Gough Island lavas: variation with fractional

crystallisation and evidence for assimilation. *Contributions to Mineralogy and Petrology*, **138**: 164-175.

Hart, S. R., 1984, A large scale isotope anomaly in the Southern Hemisphere mantle. *Nature*, **309**: 753-757.

Hekinian, R., 1982, *Petrology of the Ocean Floor*. Elsevier Oceanography Series No. 33, Elsevier Scientific Publishing Company Inc., New York, 393 pp.

Helgeson, H. C., Delaney, J. M., Nesbit, H. W. and Bird, D. K., 1978, Summary and critiqu of the thermodynamic properties of the rock-forming minerals. *American Journal of Science*, **278A**: 1-228.

Herzberg, C. T., 1978, Pyroxene geothermometry and geobarometry: experimental and thermodynamic evaluation of some subsolidus phase relations involvings pyroxenes in the system CaO-MgO-Al_2O_3-SiO_2. *Geochimica et Cosmochimica Acta*, **42**: 945-957.

Herzberg, C. T. and Chapman, N. A., 1976, Clinopyroxene geothermometry of spinel-lherzolite. *American Mineralogist*, **61**: 626-637.

Hickey-Vargas, R., Hergt, J. M. and Spadea, P., 1995, The Indian Ocean-type isotopic signature in western Pacific marginal basins: origin and significance. *In Active Margins and Marginal Basins of the Western Pacific*, (D. Taylor and J. Natland, eds.), *Geophysical Monograph, American Geophysical Union*, **88**: 175-197.

Hill, D. V. and Haggerty, S. E., 1989, Petrochemistry of eclogites from the Koidu Kimberlite Complex, Sierra Leone. *Contributions to Mineralogy and Petrology*, **103**: 397-422.

Hinton, R. W. and Upton, B. G. J., 1991, The chemistry of zircons and coexisting phases from alkali basalt xenoliths and a syenite. *Geochimica et Cosmochimica Acta*, **55**: 3287-3302.

Hoang, N. and Han, N. X., 1990, Petrochemistry of Quaternary basalts of Xuan Loc area (South Vietnam). *Geology of Cambodia, Laos and Vietnam*, **2**: 77-88.

Hoang, N. and Flower, M., 1998, Petrogenesis of Cenozoic Basalts from Vietnam: Implication for Origins of a "Diffuse Igneous Province". *Journal of Petrology*, **39(3)**: 369-395.

Hoang, N., Flower, M. F. J. and Carlson, R. W., 1996, major, trace element, and isotopic compositions of Vietnamese basalts: Interaction of hydrous EM1-rich asthenosphere with thinned Eurasian lithosphere. *Geochimica et Cosmochimica Acta*, **60(22)**: 4329-4351.

Hoefs, J., 1987, *Stable Isotope Geochemistry*, 3rd edition, Springer-Verlag, New York, 241 pp.

Hoffet, J. H., 1933, Etude geologique sur le centre de I'Indochine entre tourane et le Makhong (Annam central et Bas-Laos). *Bulletin Du Service Geologique De I'Indochine*. **20**: 154 pp.

Hoftmann, A. W., 1997, Mantle geochemistry: the message from oceanic volcanism. *Nature*, **385**: 219-229.

Holland, T. J. B. and Powell, R., 1998, An internally-consistent thermodynamic data set for phases of petrological interest. *Journal of Metamorphic Geology*, **16**: 309-343.

Holland, T. J. B. and Powell, R., 2001, Calculation of phase relations involving haplogranitic melts using an internally consistent thermodynamic dataset. *Contributions to Mineralogy and Petrology*, **42(4)**: 673-683.

Holloway, J. R., 1981, Compositions and volumes of supercritical fluids in the Earth's crust. *In Short course in fluid inclusions: applications to petrology*, (L.S. Hollister and M.L. Crawford, eds.), *Mineral Association of Canada, Short course handbook*, **6**: 13-38.

Holtz, F. and Johannes, W., 1994, Maximum and minimum water contents of granitic melts: implications for chemical and physical properties of ascending magmas. *Lithos*, **32**: 149-159.

Holtz, F., Johannes, W., Tamic, N. and Behrens, H., 2001, Maximum and minimum water contents of granitic melts generated in the crust: a reevaluation and implications. *Lithos*, **56**: 1-14.

Hughes, R. W., 1997, *Ruby and Sapphire*. RWH Publishing Boulder Co., USA, 511 pp.

Hutchison, C. S., 1973, Geology of the Malaya Peninsula: West Malaysia and Singapore. *In VolcanicActivity*, (D.J. Gobbet and C.S. Hutchison, eds.), Wiley Interscience, 177-214.

Intasopa, S., 1993, Petrology and geochronology of the volcanic rocks of the central Thailand volcanic belt. *Unpublished PhD. thesis,* University of New Brunswick, Canada, 242 pp.

Intasopa, S., Atichat, W. and Pisutha-Arnond, V., 1998, A comparative study on corundums from Southeast Asia: their application to origin determination. *Proceedings of Ninth Regional Congress on Geology, Mineral Energy Resources of Southeast Asia,* Kuala Lumpur, Malaysia, 220-222.

Irving, A. J., 1974, Megacrysts from the Newer Basalts and other basaltic rocks of Southeastern Australia. *Geological Society American Bulletin*, **85**: 1503-1514.

Irving, A. J., 1980, Petrology and geochemistry of composite ultramafic xenoliths in alkalic baslts and implications for magmatic processes within the mantle. *American Journal of Science*, **280-A**: 389-426.

Irving, A. J., 1986, Polybaric mixing in alkalic basalts and kimberlites: Evidence from corundum, zircon and ilmenite megacrysts. *Geological Society of Australia,* Abstract, **16**: 262-264.

Jarosewich, E., Nelen, J. A. and Norberg, J. A., 1980, Reference samples for electron microprobe analysis. *Geostandards Newsletter*, **4**: 43-47.

Johnson, E. L., 1991, Experimentally determined limits of H_2O-CO_2-NaCl immiscibility in granulites. *Geology*, **19**: 925-928.

Joyce, D. B. and Holloway, J. R., 1993, An experimental determination of the thermodynamic properties of H_2O-CO_2-NaCl fluids at high pressures and temperatures. *Geochimica et Cosmochimica Acta*, **57**: 733-746.

Jungyusuk, N., 1971, *Geologic Map of Ban Bo Kaeo (1:50,000, Sheet 4944 I).* Geological Survey Division, Department of Mineral Resources, Bangkok, Thailand.

Jungyusuk, N. and Khositanont, S., 1992, Volcanic rocks and associated mineralization in Thailand. *Proceedings of Conference on Geology and Mineral Resources of Thailand,* Bangkok, Thailand, 1-9.

Kamenetsky, V. S., Everard, J. L, Crawford, A. J., Varne, R., Eggins, S. M. and Lanyon, R., 2000, Enriched end-member of primitive MORB melts: Petrology and geochemistry of glasses from Macquarie Island (SW Pacific). *Journal of Petrology*, **41**: 411-430.

Kamenetsky, V. S., Maas, R., Sushchevskaya, N. M., Norman, M. D., Cartwright, I. and Peyve, A. A., 2001, Remnants of Gondwana continental lithosphere in oceanic upper mantle: evidence from the South Atlantic Ridge. *Geology*, **29**: 243-246.

Keller, P. C., 1983, The ruby of Burma: A review of the Mogok Stone Tract. *Gems and Gemology*, **19**: 209-219.

Keller, P. C., Koivula, J. I. and Jara, G., 1985, Sapphires from the Mercaderes-Rio Mayo Area, Cauca, Colombia. *Gems and Gemology*, **2**: 20-25.

Kerkhof, A. M. V. and Olsen, S. N., 1990, A natural example of superdense CO_2 inclusions: microthermometry and Raman analysis. *Geochimica et Cosmochimica Acta*, **54**: 895-901.

Kerr, P. F., 1977, *Optical Mineralogy*. McGraw-hill, USA, 225 pp.

Kerrick, D. M. and Jacobs, G. K., 1981, A modified Redlich-Kwong equation for H_2O, CO_2, and H_2O-CO_2 mixtures at elevated pressures and temperatures. *American Journal of Science*, **281**: 735-767.

Klein, C. and Hurlbut, C. S. Jr., 1993, *Manual of Mineralogy*. The 21st edition, John Wiley and Sons Inc., New York, 681 pp.

Kornprobst, J., Piboule, M., Boudeulle, M. and Roux, L., 1982, Corundum-bearing garnet pyroxenites at Beni Bousera (Morocco): An exceptionally Al-rich clinopyroxene from "grospydites" associated with ultramafic rocks. *Terra Cognita*, **2**: 257-259.

Larsen, E. S., 1928, A hydrothermal origin of corundum and albite bodies. *Economic Geology*, **23**: 398.

Lassiter, J. C., Hauri, E. H., Nikogosian, I. K. and Barsczus, H. G., 2002, Chlorine-potassium variations in melt inclusions from Raivavae and Rapa, Austral Islands: constraints on chlorine recycling in the mantle and evidence for brine-induce melting of oceanic crust. *Earth and Planetary Science Letters*, **202**, 525-540.

Lawrence, R. W., James, P. R. and Oliver, R. L., 1987, Relative timing of folding and metamorphism in the ruby mine area of Harts Range, central Australia. *Australian Journal of Earth Sciences*, **34**: 293-309.

Lawson, A. C., 1904, Plumasite, an oligoclase-corundum rock near Spanish Peak, California. *University of California Published Bulletin, Department of Geology*, **3**: 219-229.

Lawver, L. A., Curry, J. R. and Moore, D. G., 1976, Tectonic evolution of the Andaman Sea. *American Geophysical Union Transections (EOS)*, **75**: 333.

Lee, T. Y., Lo, C. H., Chung, S. L., Chen, C. Y., Wang, P. L., Lin, W. P., Hoang, N., Chi, C. T. and Yem, N. T., 1998, ^{40}Ar-^{39}Ar dating result of Neogene basalts in Vietnam and its tectonic implications. *In Mantle Dynamics and Plate Interactions in East Asia*, (M.F.J. Flower, S.L. Chung, C.H. Lo and T.Y. Lee, eds.), *American Geophysical Union, Geodynamics*, **27**: 317-330.

Le Bas, M. J., Le Maitre, R. W., Streckeisen, A. and Zanettin, B., 1986, *A Classification of Igneous Rocks and Glossary of Terms*. Blackwell, Oxford.

Le Maitre, R. W., 1993, MinPet computer program (v.1.02): a petrological package.

Levinson, A. A. and Cook, F. A., 1994, Gem corundum in alkali basalt: origin and occurrence. *Gems and Gemology*, **30**: 253-262.

Limtrakun, P., Khin Zaw, Ryan, C. G. and Mernagh, T. P., 2001, Formation of the Denchai gem sapphires, northern Thailand: Evidence from mineral chemistry and fluid/melt inclusion characteristics. *Mineralogical Magazine*, **65(6)**: 725-735.

Liu, C. Q., Masuda, A. and Xie, G. H., 1994, Major and trace-element compositions of Cenozoic basalts in eastern China: Petrogenesis and mantle source. *Chemical Geology*, **114**: 19-42.

Liu, T. C. and Presnall, D. C., 1990, Liquidus phase relationships on the join anorthite-forsterite-quartz at 20 kbar with applications to basalt petrogenesis and igneous sapphirine. *Contributions to Mineralogy and Petrology*, **104**: 735-742.

Liu, T. C. and Presnall, D. C., 2000, Liquidus phase relations in the system CaO-MgO-Al_2O_3-SiO_2 at 2.0 GPa: Applications to basalt fractionation, eclogites, and igneous sapphirine. *Journal of Petrology*, **41**: 3-20.

MacNevin, A. A., 1972, Sapphires in the New England district, New South Wales. *New South Wales Geological Survey Record*, **14**: 19-35.

Mahoney, J. J., Natland, J. H., White, W. M., Poreda, R., Bloomer, S. H., Fisher, R. L. and Baxter, A. N., 1989, Isotopic and geochemical provinces of the Western Indian Ocean Spreading. *Journal of Geophysical Research*, **94**: 4033-4052.

Mahoney, J. J., Le Roex, A. P., Peng, Z., Fisher, R. L. and Natland, J. H., 1992, Southwestern limits of Indian Ocean ridge mantle and the origin of low $^{206}Pb/^{207}Pb$ Mid Ocean ridge basalts: Isotope systematics of the Central Southwest Indian Ridge (17°-50°E). *Journal of Geophysical Research*, **97**: 19771-19790.

Malinkova, P., 1999, Origin of sapphires from Jizerska Louka alluvial deposit in North Bohemia, Czech Republic. *Australian Gemmologist*, **20**: 202-206.

Mananya, S., 2000, Characteristics of the Denchai gem sapphires, Phrae Province, Northern Thailand. *Unpublished BSc.thesis,* Chiang Mai University, Thailand, 109 pp (in Thai).

Mattey, D., Lowry, D. and Macpherson, C., 1994, Oxygen isotope composition of mantle peridotite. *Earth and Planetary Science Letters*, **128**: 231-241.

McClenaghan, M. P., Turner, N. J., Baillie, P. W., Brown, A. V., Williams, P. R. and Moore, W. R., 1982, Geology of the Ringarooma-Boobyalla Area. *Geological Survey Bulletin,* Tasmania Department of Mines, **61**.

McInnes, B. I. A. and Wyllie, P. J., 1992, Scapolite formation and the production of nephelinitic melts during the subduction of carbonated basalt. *Transactions American Geophysical Union (EOS)*, **73(43)**: 637.

McInnes, B. I. A. and Cameron, E. M., 1994, Carbonated, alkaline hybridizing melts from a sub-arc environment: Mantle wedge samples from the Tabar-Lihir-Tanga-Feni arc, Papua New Guinea. *Earth and Planetary Science Letters*, **122**: 125-141.

McKenzie, D., 1989, Some remarks on the movement of small melt fractions in the mantle. *In Continental Mantle*, (M.A. Menzies, ed.), Oxford, Clarendon Press, 31-54.

Meyer, H. O. and Mitchell, R. H., 1988, Sapphire-bearing ultramafic lamprophyre from Yogo, Montana: an ouachitite. *Canadian Mineralogist*, **26**: 81-88.

Michaud, V., Clocchiatti, R. and Sbrana, S., 2000, The Minoan and post-Minoan eruptions, Santorini (Greece), in the light of melt inclusions: chlorine and sulphur behaviour. *Journal of Volcanology and Geothermal Research*, **99**: 195-214.

Milisenda, C. C. and Henn, U., 1996, Compositional characteristics of sapphires from a new find in Madagascar. *Journal of Gemmology*, **25(3)**: 177-184.

Mitchell, A. H. G., 1993, Cretaceous-Cenozoic tectonic events in the Western Myanmar (Burma)-Assam region. *Journal of Geological Society of London*, **150**: 1089-1102.

Morley, C. K., Woganan, N., Sankumarn, N., Hoon, T. B., Alief, A. and Simmon, M., 2001, Late Oligocene-Recent stress evolution in rift basins of northern and central Thailand: implications for escape tectonics. *Tectonophysics*, **334(2)**: 115-150.

Moromito, N., 1989, Nomenclature of pyroxenes. *Canadian Mineralogist*, **27**: 143-156.

Mottana, A., Crespi, R. and Liborio, G., 1978, *Simon and Schuster'sGuide to Rocks and Minerals*. Simon & Schuster Inc., New York, 607 pp.

Mukasa, S. M., Fischer, G. M. and Barr, M. S., 1996, The character of the Subcontinental Mantle in southeast Asia: Evidence from isotopic and elemental composition of extension-related Cenozoic basalts in Thailand. *Geophysical Monograph*, **95**: 233-252.

Murdoch, J. and Webb, R. W., 1942, Notes on some minerals from southern California III. *American Mineralogist*, **27**: 323.

Mychaluk, K. A., 1995, The Yoko sapphire deposit. *Gems and Gemology*, **31**: 28-41.

Nakornsri, N., 1981, *Geology and Mineral Resources of Amphoe Ban Mi (Sheet ND 47-4).* Geological Survey Report, Department of Mineral Resources, Bangkok, Thailand, **3**: 36 pp.

Nassau, K., 1983, *The Physics and Chemistry of Color: the fifteen causes of color.* John Wiley and Son, New York, 454 pp.

Oakes, G. M., Barron, L. M. and Lishmund, S. R., 1996, Alkali Basalts and associated volcaniclastic rocks as a source of sapphire in Eastern Australia. *Australian Journal of Earth Sciences*, **43**: 289-298.

Oftedahl, C., 1963, Contributions to the mineralogy of Norway, No.19 Red corundum of Froland at Arendal. *Norsk Geografisk Tidssk*, **43**: 433-440.

Okrusch, M., Bunch, T. E. and Blank, H., 1976, Paragenesis and petrogenesis of a corundum-bearing marble at Hunza (Kashmir). *Mineralium Deposita*, **11**: 278-297.

O'Neill, H. St. C., 1981, The transition between spinel lherzolite and garnet lherzolite, and its use as a geobarometer. *Contributions to Mineralogy and Petrology*, **77**: 185-194.

O'Reilly, S. Y. and Zhang, M., 1995, Geochemical characteristics of lava-field basalts from eastern Australia and inferred sources: connections with the subcontinental lithospheric mantle? *Contributions to Mineralogy and Petrology*, **121**: 148-170.

O'Reilly, S. Y., Nicholls, I. A. and Griffin, W. L., 1989, Xenoliths and megacrysts of eastern Australia. *In Intraplate Volcanism in Eastern Australia and New Zealand*, (R.W. Johnson, ed.), Cambridge University Press, Singapore, 249-288.

Panjasawatwong, Y., 1995, Late Cenozoic basalts from Khao Phanom Sawai, northeastern Thailand – Petrography and geochemistry. *Eighth Regional Conference on Geology, Minerals, and Energy Resources of Southeast Asia,* Manila, Philippines, Abstract, 2.

Panjasawatwong, Y. and Yaowanoiyothin, W., 1993, Petrochemical study of Post-Triassic basalts from the Nan Suture, northern Thailand. *Journal of Southeast Asian Earth Sciences,* **8**: 147-158.

Panjasawatwong, Y. and Youngsanong, M., 1996, Chiang Khong corundum-bearing basalts, Amphoe Chiang Khong, Changwat Chiang Rai. *Journal of Science Faculty, Chiang Mai University,* **23(1)**: 39-52.

Petrussenko, S., 1981, Andalusite, corundum and tourmaline from the Markova Trapeza pegmatite deposit, District of Samokov. *Geochimica et Cosmochimica Acta,* **14**: 73-82 (in Russian).

Pisutha-Arnond, V., Wathanakul, P., Intasopa, S. and Griffin, W. L., 1998, Corsilzirspite, a corundum-sillimanite-zircon-hercynite rock: New eveidence on the origin of Kanchanaburi sapphire, Thailand. *Proceedings of Ninth Regional Congress on Geology, Mineral Energy Resources of Southeast Asia*, Kuala Lumpur, Malaysia, 95-96.

Piyasin, S., 1975, *Geology of Uttaradit, Sheet NE 47-11, Report of Investigation,* Department of Mineral Resources, Bangkok, Thailand, **15**: 68 pp.

Powell, R. and Holland, T. J. B., 1988, An internally consistent thermodynamic dataset with uncertainties and correlations: 3. Application methods, worked examples and a computer program. *Journal of Metamorphic Geology*, **6**: 173-204.

Powell, R., Holland, T. J. B. and Worley, B., 1998, Calculating phase diagrams with THERMOCALC: methods and examples. *Journal of Metamorphic Geology*, **16**: 577-588.

Press, S., Witt, G., Seck, H. A., Eonov, D. and Kovalenko, V. I., 1986, Spinel peridotite xenoliths from the Tariat Depression, Mongolia I: Major element and mineralogy of a primitive mantle xenolith suite. *Geochimica et Cosmochimica Acta*, **50**: 2587-2599.

Promprated, P., Taylor, L. A. and Snyder, G. A., 1999, Petrochemistry of the Mantle beneath Thailand: Evidence from Peridotite Xenoliths. *International Geology Review*, **41**: 506-530.

Qu-Qi, Lawrence, T. A. and Xinmin Zhou, 1995, Petrology and Geochemistry of Mantle Peridotite Xenoliths from SE China. *Journal of Petrology*, **36(1)**: 55-79.

Read, H. H., 1931, On corundum-spinel xenoliths in the gabbro of Haddo House, Aberdeenshire. *Geological Magazine*, **68**: 446-453.

Roedder, E., 1979, Origin and significance of magmatic inclusion. *Bulletin of Mineralogy*, **102**: 487-510.

Roedder, E., 1984, *Fluid Inclusions: Reviews in Mineralogy*, v.12, Mineralogical Society of America, Washington D.C., 644 pp.

Rose, R. L., 1957, Andalusite and corundum-bearing pegmatites in Yosemite National Park, California. *American Mineralogist*, **42**: 635.

Rudnick, R. L., McDonough, W. F., McCulloch, M. T. and Taylor, S. R., 1986, Lower crustal xenoliths from Queensland, Australia: Evidence for deep crustal assimilation and fractionation of continental basalts. *Geochimica et Cosmochimica Acta*, **50**: 1099-1115.

Ryan, C.G., Heinrich, C.A., Van Achterbergh, E., Ballhaus, C. and Mernagh, T.P., 1995, Microanalysis of Ore-forming Fluids using the Scanning Proton Microprobe, *Nuclear Instrument Method,* **B104**, 182-190.

Ryan, C.G., Jamieson, D.N., Griffin, W.L., Cripps, G. and Szymanski, R., 2001, The New CSIRO-GEMOC Nuclear Microprobe: First Results, Performance and Recent Applications, *Nuclear Instrument Method*, **181**: 12-19.

Salyaphongse, S. and Jungyusuk, N., 1983, *Geological Map of Thailand (1: 500,000), Central and Eastern sheet.* Geological Survey Division, Department of Mineral Resources, Bangkok, Thailand.

Sasada, M., Ratanasathien, B. and Soponpongpipat, P., 1987, New K-Ar ages from the Lampang basalts, northern Thailand. *Bulletin of Geological Survey Japan*, **38**: 13-20.

Sato, J. I., 1993, PTMAFIC: software for thermobarometry and activity calculations with mafic and ultramafic assemblages. *American Mineralogist*, **78(7/8)**: 840-844.

Sato, J. I. and Sato, V. M., 1995, PTMAFIC: software package for thermometry, barometry, and activity calculations in mafic rocks using and IBM-compatible computer. *Computers and Geosciences*, **21(5)**: 619-652.

Schiano, P. and Clocchiatti, R., 1994, Worldwide occurrence of silica-rich melts in sub-continental and sub-oceanic mantle minerals. *Nature*, **368**: 621-624.

Schiano, P., Clocchiatti, R. and Shimizu, N., 1994a, Melt inclusion trapped in mantle minerals: a clue to identifying metasomatic agents in the upper mantle beneath continental and oceanic intraplate regions. *Mineralogical Magazine (V.M. Goldschmidt Conference)*, **58A**: 807-808.

Schiano, P., Clocchiatti, R., Shimizu, N., Weis, D. and Mattielli, N., 1994b, Cogenetic silica-rich and carbonate-rich melts trapped in mantle minerals in Kerguelen ultramafic xenoliths: implications for metasomatism in the oceanic upper mantle. *Earth and Planetary Science Letters*, **123(1-4)**: 167-178.

Schiano, P., Clocchiatti, R., Shimizu, N., Maury, R. C., Jochum, K. P. and Hoftmann, A. W., 1995, Hydrous, silica-rich melts in the sub-arc mantle and their relationship with erupted arc lavas. *Nature*: **377**: 595-600.

Schmetzer, K., 1999, Ruby and variously coloured sapphires from Ilakaka, Madagascar. *Australian Gemmologist*, **20**: 282-284.

Schmetzer, K. and Bank, H., 1980, Explanations of the absorption spectra of natural and synthetic Fe- and Ti-containing corundums. *Neues Jahrbuch für Mineralogie, Abhandlungen*, **139**: 216-225.

Schwartz, M. O., 1982, The porphyry copper deposit at La Granja, Peru. *Economic Geology*, **77**: 482-488.

Sharp, Z. D., 1990, A laser-based microanalytical method for the in situ determination of oxygen isotope ratios of silicates and oxides. *Geochimica et Cosmochimica Acta*, **54**: 1353-1357.

Shepherd, T., Rankin, A. H. and Alderton, D. H. M., 1985, *A Practical Guide to Fluid Inclusion Studies*. Blackie, Glasgow, 235 pp.

Shida, J., 2002, Gemmological study of corundum from Madagascar. *Australian Gemmologist*, **21**: 247-252.

Sigurdsson, I. A., 1994, Primitive magmas in convergent margins and at oceanic spreading ridges: evidence from early formed phenocryst phases and their melt inclusions. *Unpublished PhD. thesis*, University of Tasmania, Australia, 243 pp.

Silva, K. K. M. W. and Siriwardena, C. H. E. R., 1988, Geology and the origin of the corundum-bearing skarn at Bakamuna, Sri Lanka. *Mineralium Deposita*, **23**: 186-190.

Singharajwarapan, S. and Berry, R. F., 2000, Tectonic implications of the Nan Suture Zone and its relationship to the Sukhothai Fold Belt, Northern Thailand. *Journal of Asian Earth Sciences*, **18**: 663-673.

Sisson, T. W. and Layne, G. D., 1993, H_2O in basalt and basaltic andesite glass inclusions from four subduction-related volcanoes. *Earth and planetary Science Letters*, **117**: 619-635.

Sivabovorn, V., Paichitprapaporn, V. and Tansatein, S., 1976, *Geology of Phratabong–Chanthaburi (Sheet ND 48-9, ND 48-13)*. Geological Survey Division, Department of Mineral Resources, Bangkok, Thailand, 51 pp (in Thai).

Smith, C. P., Kammerling, R. C., Keller, A. S., Peretti, A., Scarratt, K. V., Khoa, N. D. and Repetto, S., 1995, Sapphires from southern Vietnam. *Gems and Gemmology*, **31(3)**: 168-186.

Smith, D. G. W., 1965, The chemistry and mineralogy of some emery-like rocks from Sithean Sluaigh, Strachur, Argyllshire. *American Mineralogist*, **50**: 1982-2002.

Sobolev, A. V. and Danyushevsky, L. V., 1994, Petrology and geochemistry of the high-Ca boninite primary magmas: evidence from the North Tonga trench. *Journal of Petrology*, **35**: 1183-1211.

Sobolev, A. V., Dmitriev, L. V., Baruskov, V. L., Nevsorov, V. N. and Slutsky, A. B., 1980, The formation conditions of the high-magnesium olivines from the monomineralic fraction of Luna 24 regolith. *Proceedings of the 11th Lunar Science Conference*, 105-116.

Sobolev, A. V., Kamenetsky, V. S. and Kononkova, N. N., 1989, New data on the petrology and geochemistry of the ultramafic volcanites of Valayinskiy Tange, eastern Kamchatka. *Geokhimiya*, **12**: 1694-1709 (in Russian).

Sobolev, A. V., Kamenetsky, V. S., Metrich, N., Clocchiatti, N. N., Devirts, A. L. and Ustinow, V. I., 1990, Volatile regime and crystallisation conditions in Etna Hawaiite lavas. *Geochemical International*, **28**: 53-65.

Sobolev, A. V., Dmitriev, L. V., Tsameryan, O. P., Kononkova, N. N. and Robinson, P. T., 1991, A possible primary melt compositions for ultramafic lavas on the Margi Area, Troodos Ophiolite. *In Cyprus crustal study project: Initial report, Holes CY-I and IA*, (I.L. Gibson, J. Malpas, P.T. Robinson and C. Xenophontos, eds.), *Geological Survey Canadian Paper*, **90-20**: 203-218.

Sobolov, N. V. Jr., Kuznetsova, I. K. and Zyuzin, N. I., 1968, The petrology of grospydite xenoliths from the Zagadochnaya kimberlite pipe in Yakutia. *Journal of Petrology*, **9**: 253-280.

Sokolov, G. A., 1931, The corundum plagioclastites of kaslinskaia dacha in the Urals. *Trasactions of the United Geological and Prospecting Service of USSR*, **56**: 3.

Sokolov, S., 2002, Melt inclusions as indicators of the magmatic origin of carbonatite rare metal and rare earth minerals. *Chemical Geology*, **183**: 373-378.

Solesbury, F. W., 1967, Gem corundum pegmatites in NE Tanganyka. *Economic Geology*, **62**: 983-991.

Spray, J. G. and Rae, D. A., 1995, Quantitative electron-microprobe analysis of alkali silicate glasses: A review and user guide. *Canadian Mineralogist*, **33**: 323-332.

Sriprasert, B., 1997, Geochemistry and petrology of Thoeng basalts, Changwat Chiang Rai. *Unpublished MSc. thesis,* Chiang Mai University, Thailand, 124 pp.

Srithai, B., Rankin, A. N., Price, G. D. and Jones, A. P., 1999, Fluid inclusion characteristic of gem sapphires from Bo Ploi, Kanchanaburi, Thailand. *Terra Nostra, ECROFI XV,* **99/6**: 296-299.

Steefel, C. I. and Atkinson, W. W., 1984, Hydrothermal andalusite and corundum in the Elkhorn district, Montana. *Economic Geology,* **79**: 573-579.

Stephenson, D. and Marshall, T. R., 1984, The petrology and mineralogy of Mt. Popa Volcano and the nature of the late-Cenozoic Burma Volcanic Arc. *Journal of the Geological Society of London*, **141**: 747-762.

Stephenson, P. J., 1976, Sapphire and zircon in some basaltic rocks from Queensland, Australia. *The 25th International Geological Congress,* Sydney, **2**: 602-603.

Stephenson, P. J., 1990, The geological context of sapphire occurrences in the Anakie region, Central Queensland. *The 10th Australia Geological Convention*, Hobart, 232-233.

Stephenson, P. J., Griffin, T. J. and Sutherland, F. L., 1980, Cainozoic volcanism in northeastern Australia. *In The Geology and Geophysics of Northeast Australia*, (R.A. Henderson and P.J. Stephenson, eds.), Geological Society of Australia Queensland Division, 349-374.

Stephenson, P. J., Sutherland, F. L., Robertson, A. D. and Hollis, J. D., 1989, Northern Queensland-Hoy. *In Intraplate Volcanism in Eastern Australia and New Zealand*, (R.W. Johnson, ed.), Cambridge University Press, Singapore, 101-103.

Sterner, S. M. and Bodnar, R. J., 1991, Synthetic inclusions, X: experimental determination of P-V-T-X properties in the CO_2-H_2O system to 6 kbar and 700°C. *American Journal of Scienece*, **291**: 1-54.

Sukvattananunt, P. and Assavapatchara, S., 1989, Geology of Amphoe Chiang Khong and Ban Sri Don Chai. *Geological Survey Report,* **0119(1)**: 61 pp (in Thai).

Sullivan, G. E., 1991, Chemical evolution of basalts from 23°N along the mid-Atlantic ridge: evidence from melt inclusions. *Contributions to Mineralogy and Petrology,* **106**: 296-308.

Sun, S.S. and McDonough, W. F., 1989, Magmatisms in the Ocean Basins. *Geological Society of London, Special Publication*, **42**: 313-345.

Sutherland, F. L., 1996, Alkaline rocks and Gemstones, Australia: a review and synthesis. *Australian Journal of Earth Sciences*, **43**: 323-343.

Sutherland, F. L. and Coenraads, R. R., 1996, An unusual ruby-sapphire-sapphirine-spinel assemblage from the Tertiary Barrington volcanic province, New South Wales, Australia. *Mineralogical Magazine*, **60**: 623-638.

Sutherland, F. L. and Fanning, C. M., 1996, Magmatism below Barrington volcano, NSW: Based on basalt and zircon megacryst dating. *Journal of Geological Society of Australia*, Abstract, **41**: 426.

Sutherland, F. L. and Schwarz, D., 2001, Origin of gem corundums from basaltic fields. *Australian Gemmologist*, **21**: 30-33.

Sutherland, F. L., Hoskin, P. W. O., Fanning, C. M. and Coenraads, R. R., 1998a, Models of corundum origin from alkali basaltic terrains: A reappraisal. *Contributions to Mineralogy and Petrology,* **133**: 356-372.

Sutherland, F. L., Schwarz, D., Jobbins, E. A., Coenraads, R. R. and Webb, G., 1998b, Distinctive gem corundum suites from discrete basalt fields: a comparative study of Barrington, Australia, and West Pailin, Cambodia, gemfields. *Journal of Gemmology*, **26(2)**: 65-85.

Sutthirat, C., 1995, Petrochemistry of basalts in Amphoe Sop Prab and Amphoe Ko Kha, Changwat Lampamg. *Unpublished MSc. thesis,* Chulalongkorn University, Thailand, 158 pp.

Sutthirat, C., Charusiri, P., Farrar, E. and Clark, A. H., 1994, New $^{40}Ar/^{39}Ar$ geochronology and characteristics of some Cenozoic basalts in Thailand. *Proceedings of International Symposium on Stratigraphic Correlation of Southeast Asia*, Bangkok, Thailand, 306-320.

Sutthirat, C., Charusiri, P., Pongsapich, W., Farrar, E. and Landgridge, R., 1995, A late Pliocene Ko Kha–Sop Prap and nam Cho basaltic eruption, Northern Thailand:

Evidences from geology and $^{40}Ar/^{39}Ar$ geochronology. *Proceedings of International Conference on Geology, Geotechnology and Mineral Resources of Indochina*, Khon Kaen, Thailand, 247-253.

Sutthirat, C, Saminpanya, S., Droop, G. T. R., Henderson, C. M. B. and Manning, D. A. C., 2001, Clinopyroxene-corundum assemblage from alkali basalt and alluvium, eastern Thailand: constraints on the origin of Thai rubies. *Mineralogical Magazine*, **65(2)**, 277-295.

Tait, S., 1992, Selective preservation of melt inclusions in igneous phenocryst. *American Mineralogist*, **77**: 146-155.

Tapponnier, P., Peltzer, G. and Armiro, R., 1986, On the mechanics of the collision between India and Asia. *In Collision Tectonics*, (M.P. Coward and A.C. Ries, eds.), *Geological Society of London, Special Publication*, **19**: 115-157.

Taylor, H. P., 1978, Oxygen and hydrogen isotope studies of plutonic granitic rocks. *Earth and Planetary Science Letters*, **38**: 177-210.

Thomas, H. H., 1922, On certain xenolithic Tertiary minor intrusions in the Island of Mull (Argyllshire). *Quaternary Journal of Geological Society*, **78**: 229.

Thompson, A. B., 1982, Dehydration melting of pelitic rocks and the generation of H_2O-undersaturated granitic liquids. *American Journal of Science*, **282**: 1567-1595.

Thompson, A. B., 2001, Clockwise P-T paths for crustal melting and H_2O recycling in granite source regions and migmatite terrains. *Lithos*, **56**: 33-45.

Tin Tin Win, Wanathanakul, P., French, D. H., Intasopa, S. and Pisutha-Arnond, V., 1998, Preliminary study on trace element geochemistry of corundums from South East Asia. *Proceedings of Ninth Regional Congress on Geology, Mineral Energy Resources of Southeast Asia,* Kuala Lumpur, Malaysia, 99-101.

Todt, W., Cliff, R. A., Hanser, A. and Hofmann, A. W., 1984, $^{202}Pb + ^{205}Pb$ double spike for lead isotope analyses. *Terra Cognita*, **4**: 209.

Tomlinson, W. H., 1939, Corundum in a dyke at Glen Riddle, Pensylvania. *American Mineralogist*, **24**: 339.

Tonthongchai, K., Munjai, D. and Hongvisest, S., 1996, *Geology of Mae Sin gem deposits, Si Sat Chanalai District, Sukhothai Province and Wangchin District, Phrae Province.* Economic Division, Department of Mineral Sciences of Thailand, 39 pp (in Thai).

Touret, J. L. R., 1982, An empirical phase diagram for a part of the N_2-CO_2 system at low temperature. *Chemical Geology*, **37**: 49-58.

Tu, K., Flower, M. F. J., Carlson, R. W., Guangdong, X., Yung, C. C. and Zhang, M., 1992, Magmatism in the South China Basin, 1, Isotopic and trace-element evidence for an endogeneous Dupal mantle component. *Chemical Geology*, **97(1-2)**: 47-63.

Upton, B. G. J., Aspen, P. and Chapman, N. A., 1983, The upper mantle and deep crust beneath the British Isles: Evidence from inclusions in volcanic rocks. *Journal of Geological Society of London,* **140**: 105-121.

Upton, B. G. J., Hinton, R. W., Aspen, P., Finch, A. and Valley, J. W., 1999, Megacrysts and associated xenoliths: Evidence for migration of geochemically enriched melts in the upper mantle beneath Scotland. *Journal of Petrology*, **40(6)**, 935-956.

Valley, J. W., Kitchen, N., Kohn, M. J., Niendorf, C. R. and Spicuzza, M. J., 1995, UWG-2, a garnet standard for oxygen isotope ratios: strategies for high precision and accuracy with laser heating. *Geochimica et Cosmochimica Acta*, **59**: 5223-5231.

Vichit, P., 1987, Gemstones in Thailand. *Journal of Geological Society of Thailand,* **9**: 108-133.

Vichit, P., 1992, Gemstones in Thailand. *Proceedings of National Conference on Geologic Resources of Thailand: Potential for Future Development*, Department of Mineral Resources, Bangkok, Thailand, 124-150.

Vichit, P., Vudhichativanich, S. and Hansawek, R., 1978, The distribution and some characteristics of corundum-bearing basalts in Thailand. *Journal of Geological Society of Thailand,* **3**: M4-M38.

Vichit, P., Udompornvirat, S., Tritra-ngan, A. and Jariyawat, P., 1988, *A report on gem deposits in Wichian Buri area, Phetchabun Province.* Economic Geology Report, Economic Geology Division, Department of Mineral Resources, Bangkok, Thailand, **61/198**: 145 pp (in Thai).

Wass, S. Y. and Irving, A. J., 1976, *XENMEG: A catalogue of occurrences of xenoliths and megacrysts in basic volcanic rocks of eastern Australia.* The Australian Museum, Sydney, Australia, 455 pp.

Webster, J. D., Raia, F., De Vivo, D. and Rolandi, G., 2001, The behavior of chlorine and sulfur during differentiation of the Mt.Somma-Vesuvius magmatic system. *Mineralogy and Petrology*, **73**: 177-200.

Weis, D., Ingle, S., Damasceno, D., Frey, F. A., Nicolaysen, K. and Barling, J., 2001, Origin of continental components in Indian Ocean basalts: Evidence from Elan Bank (Kerguelen Plateau, ODP Leg 183, Site 1137). *Geology*, **29(2)**: 147-150.

Wells, A. J., 1956, Corundum from Ceylon. *Geological Magazine*, **92**: 25-31.

Werre, R. W., Bodnar, R. J., Bethke, P. M. and Barton, P. B., 1979, A novel gas-flow fluid inclusion heating/freezing stage. *Geological Society of America,* Abstract, **11**: 540.

White, R. and McKenzie, D., 1989, Magmatism at rift zone: the generation of volcanic continental margins and flood basalts. *Journal of Geophysical Research*, **94**: 7685-7729.

Wickham, B. F. and Flower, M. F. J., 1994, $^{18}O/^{16}O$ in corundum and zircon megacrysts from mantle-derived magmas: a laser fluorination study. *Transactions American Geophysical Union (EOS)*, **75**: 371.

Wilkinson, J. F. G., 1966, Residual glasses from some alkalic basaltic lavas from New South Wales. *Mineralogical Magazine*, **35**: 847-860.

Wilkinson, J. F. G., 1969, Mesozoic and Cenozoic igneous rocks B, Northeastern New South Wales. *Journal of Geological Society of Australia*, **16**: 530-541.

Wilkinson, J. F. G., 1974, Garnet Clinopyroxenite Inclusions from Diatremes in the Gloucester Area, New South Wales, Australia. *Contributions to Mineralogy and Petrology*, **46**: 275-299.

Wilkinson, J. F. G. and Binns, R. A., 1977, Relatively Iron-Rich Lherzolite Xenoliths of the Cr-Diopside Suite: A Guide to the Primary Nature of Anorogenic Tholeiitic Andesite Magmas. *Contributions to Mineralogy and Petrology*, **65**: 199-212.

Wilkinson, J. F. G. and Hensel, H. D., 1991, An analcime mugearite-megacryst association from north-eastern New South Wales: implications for high-pressure amphibole-dominated fractionation of alkaline magmas. *Contributions to Mineralogy and Petrology*, **109**: 240-251.

Wilshire, H. G. and Shervais, J. W., 1975, Al-augite and Cr-diopside ultramafic xenoliths in basaltic rocks from the western United States. *Physics and Chemistry of the Earth*, **9**: 252-272.

Witt-Eickschen, G. and Seck, H. A., 1991, Solubility of Ca and Al in orthopyroxene from spinel peridotite: An improved version of an empirical geothermometer. *Contributions to Mineralogy and Petrology*, **106**: 431-439.

Wojdak, P. J. and Sinclair, A. J., 1984, Equite silver-copper-gold deposit: Alteration and fluid inclusion studies. *Economic Geology*, **79**: 969-990.

Wood, B. J. and Banno, S., 1973, Garnet-Orthopyroxene and Orthopyroxene-Clinopyroxene Relationships in Simple and Complex Systems. *Contributions to Mineralogy and Petrology*, **42**: 109-124.

Wood, T. L., Bethke, P. M., Bodnar, R. J. and Werre, R. W., 1981, Supplementary components and operation of the U.S.G.S. Geological Survey gas-flow heating/freezing stage. *U.S.G.S. Open File Report*, **81-954**: 12 pp.

Woodhead, J. D., Volker, F. and McCulloch, M. T., 1995, Routine Pb isotope determination using a ^{207}Pb-^{208}Pb double-spike: a long-term assessment of analytical precision and accuracy. *Analyst*, **120**: 35-39.

Wu, L., 1984, *Mesozoic and Cenozoic Volcanic Rocks in Eastern China*. Beijing Science Publishing House, 287 pp (in Chinese).

Yaemniyom, N., 1982, The petrochemical study of corundum-bearing basalts at Bo Ploi District, Kanchanaburi. *Unpublished MSc. thesis,* Chulalongkorn University, Thailand, 100 pp.

Yamamoto, M., 1991, Occurrences and petrochemistry of the Lampang and Sop Prap basalts, Northern Thailand. *Report of Research Institute of natural Resources,* Mining College, Akita University, Japan, **56**: 85-94.

Yaxley, G. M., Kamenetsky, V., Green, D. H. and Falloon, T. J., 1997, Glasses in mantle xenoliths from western Victoria, Australia, and their relevance to mantle processes. *Earth and Planetary Science Letters*, **148**: 433-446.

Yim, W. W. S., 1990, Heavy mineral provenance and the genesis of stanniferous placer in northeastern Tasmania. *Unpublished PhD. thesis*, University of Tasmania, Australia, 303 pp.

Yui, T. F., 2000, Preliminary results on CO_2 laser-fluorination system for O-isotope microanalysis of silicate/oxide grain separates. *Journal of Geological Society of China*, **43**: 237-246.

Zhang, M., Stephenson, P. J., O'Rielly, S. Y., McCulloch, M. T. and Norman, M., 2001, Petrogenesis and Geodynamic Implications of Late Cenozoic Basalts in North Queensland, Australia: Trace elements and Sr-Nd-Pb Isotopic Evidence. *Journal of Petrology*, **42(4)**: 685-719.

Zhang, R. and Cong, B., 1987, Cenozoic volcanic rocks and ultramafic xenoliths from southeastern China. *In The Cenozoic Basalts and Xenoliths from Eastern China*, (M. Er and D. Zhao, eds.), Beijing Science Publishing House, 349-476 (in Chinese).

Zheng, Y. F., 1991, Calculation of oxygen isotope fractionation in metal oxides. *Geochimica et Cosmochimica Acta*, **55**: 2299-2307.

Zheng, Y. F., 1993, Calculation of oxygen isotope fractionation in anhydrous silicate minerals. *Geochimica et Cosmochimica Acta*, **57**: 1079-1091.

Zhou, P. and Mukasa, S. B., 1997, Nd-Sr-Pb isotopic and major- and trace-element geochemistry of Cenozoic lavas from the Khorat Plateau, Thailand: sources and petrogenesis. *Chemical Geology*, **137**: 175-193.

Zindler, A. and Hart, S. R., 1986, Chemical geodynamics. *Annual Review of Earth and Planetary Sciencs*, **14**: 493-571.

Zou, H., Zindler, A., Xu, X. and Qu Qi, 2000, Major, trace element, and Nd, Sr and Pb isotope studies of Cenozoic basalts in SE China: mantle sources, regional variations, and tectonic significance. *Chemical Geology*, **171**: 33-47.

Appendix A

Sample locations, occurrences and lithologies of the Denchai basalts,
Topographic map referred to is 1:50000 (Series L7017, Sheet 4944 I, BAN BO KAEO),
Royal Thai Army Survey Map

Sample	Grid Reference	Occurrence and Lithology
DC1-2	999850	Two flows outcrop at a roadcut on Highway 11; upper and lower flows are respectively 1 and > 3 m in thickness, samples of both flows are grey and fine to medium-grained.
DC3-4	017849	Outcrop at a roadcut on Highway 11 shows folding of platy and columnar joint sets. Fresh samples are dark grey and fine to medium-grained.
DC5	948807	Columnar jointing occurs at an outcrop in a stream close to the Highway 101; dark grey, fine-grained and contains xenoliths (1x1x2 cm)
DC6	001837	Sample from an outcrop at a roadcut on Highway 101; dark grey and fine to medium-grained, carbonate minerals occur along fractures.
DC7	992824	Sample from an outcrop at a roadcut on Highway 101; dark grey and fine to medium-grained, carbonate and iron oxides occur along fractures. (altered)
DC8	944795	Sample from an outcrop at a roadcut on Highway 101; dark grey and fine to medium-grained
DC10	943791	Outcrop on the top of Doi Pailin (close to Highway 101); grey and fine to medium-grained
DC11	934780	Road cut outcrop on Highway 101; dark grey, fine to medium-grained and partly amygdaloidal, vesicles are partly infilled by carbonate minerals.
DC12	930776	Road cut outcrop on Highway 101; dark grey, fine to medium-grained and amygdaloidal, pipe vesicles infilled by carbonate minerals, indicating flow direction to the north. This unit is underlained by Triassic sedimentary rocks.
DC13	929771	Road cut outcrop on Highway 101; dark grey, very fine-grained and contains xenoliths (2x1x1 cm)
DC14	929768	Road cut outcrop on Highway 101; grey, fine-grained and contains xenoliths (2x3x2 cm)
DC15	921716	Road cut outcrop on Highway 101; dark grey and fine to medium-grained

DC16	920703	Road cut outcrop on Highway 101; grey, fine to medium-grained and partly amygdaloidal, vesicles are partly infilled by carbonate minerals.
DC17	926700	Outcrop sample; dark grey, fine-grained and xenolithic, carbonate minerals occur along fractures.
DC18	931717	Float rock from the hilltop; dark grey and fine to medium-grained (altered)
DC19	933769	Float rock from Huai Mae Khanung; dark grey, fine-grained and xenolithic, carbonate minerals occur along fractures.
DC20	926747	Float rock; dark grey and medium-grained
DC21	919746	Float rock; dark grey, fine to medium-grained and partly amygdaloidal, vesicles are partly infilled by carbonate and zeolite.
DC22	914744	Outcrop sample: dark grey and fine to medium-grained, vesicles are partly infilled by carbonate minerals.
DC23	907744	Float rock; dark grey, fine-grained and contains xenoliths, vesicles are partly infilled by carbonate minerals.
DC24	903741	Float rock; dark grey, fine-grained and xenolithic (altered)
DC25	900738	Float rock; dark grey and fine-grained
DC26	896740	Float rock from the hillside; dark grey to black and fine to medium-grained, vesicles and fracture surfaces are partly infilled by carbonate minerals. (altered)
DC27	924766	Outcrop sample from the Three Brothers Garden, close to Highway 101; dark grey, fine-grained and xenolithic, carbonate and iron oxides occur along fractures.
DC28	906752	Float rock; dark grey and fine to medium-grained
DC29	905758	Float rock; grey and fine to medium-grained
DC30	909765	Float rock; dark grey and fine to medium-grained, fractures are infilled by carbonate minerals. This unit is underlained by Triassic sedimentary rocks.
DC31	933757	Float rock at Ban I Go Dong Yang School; grey and fine to medium-grained, carbonate minerals occur along fractures.
DC32	922771	Float rock; dark grey, fine-grained and contains xenoliths, carbonate minerals occur as veinlets occupying fractures.
DC33	932741	Float rock; dark grey and fine to medium-grained
DC34	936739	Float rock from the Sak Tree Hill; dark grey and fine to medium-grained, carbonate minerals occur along fractures.
DC35	938730	Float rock; dark grey, fine to medium-grained and partly amygdaloidal, vesicles are partly infilled by carbonate minerals.

DC36	950730	Float rock; dark grey and fine to medium-grained, carbonate minerals occur along fractures.
DC37	934724	Float rock; dark grey, fine to medium-grained and partly amygdaloidal, vesicles are partly infilled by carbonate and zeolite.
DC38	943724	Float rock; dark-grey, fine to medium-grained and partly amygdaloidal, carbonate minerals occur both along fractures and partially infilling vesicles.
DC39	940712	Float rock; dark grey and fine to medium-grained, carbonate minerals occur along fractures.
DC40	950792	Float rock; dark grey, fine to medium-grained and partly amygdaloidal, vesicles are partly infilled by carbonate and zeolite.
DC41	952800	Outcrop sample from the flat area close to the reservoir; dark grey and fine to medium-grained, carbonate minerals occur along fractures.
DC42	971796	Outcrop sample from close to the reservoir; dark grey, fine-grained and contains xenoliths (2x2x2 cm). Vesicles are partly infilled by carbonate minerals.
DC43	968803	Float rock excavated during pool construction; dark grey and fine-grained
DC44	952813	Columnar jointing is shown in an outcrop at a small waterfall; dark grey and fine-grained
DC45	962818	Float rock from the flood plain area; dark grey, fine to medium-grained and partly amygdaloidal, carbonate minerals occur along fractures and partially infilling vesicles.
DC46	955818	Float rock from the flood plain area; dark grey and fine to medium-grained, carbonate minerals occur along fractures and in vesicles.
DC47	981821	Float rock from the Fruit garden; dark grey and medium-grained
DC48	974840	Float rock from close to the bridge at Ban Pa Pai; dark grey, fine to medium-grained and partly amygdaloidal, carbonate minerals occur along fractures and partially infilling vesicles.
DC49	036859	Outcrop sample from the hilltop; dark grey, fine to medium-grained and partly amygdaloidal, vesicles are partly infilled by carbonate minerals.
DC50	037854	Float rock from the bottom of the hill, close to Highway 101; dark grey and fine to medium-grained
DC51	022845	Outcrop sample from the hilltop close to the Pa Mae Pan

		Office; dark grey and fine to medium-grained
DC52	010845	Float rock excavated during dam construction; grey and fine to medium-grained
DC53	985809	Float rock; dark-grey and fine to medium-grained
DC54	997813	Float rock from Ban Nam Pao; dark grey and fine to medium-grained
DC55	003810	In situ float on the hilltop; dark grey, fine to medium-grained and partly amygdaloidal, vesicles are partly infilled by carbonate and zeolite.
DC56	918700	Float rock; dark grey and fine to medium-grained
DC57	919709	Outcrop sample located opposite to Chao Mae Nang Kaew; dark grey, fine-grained and partly amygdaloidal, vesicles are sparsely infilled by carbonate minerals.
DC58	910713	Sample from an outcrop at a roadcut on Highway 101; dark grey and fine-grained
DC59	921716	Float rock; grey, fine-grained and contains xenoliths, vesicles are partly infilled by carbonate minerals.
DC60	926738	Sample from an outcrop at a roadcut on Highway 101; dark grey and fine-grained, carbonate minerals occur along fractures.
DC61	929767	Road cut outcrop on Highway 101;grey, fine-grained and contains xenoliths
DC62	929771	Road cut outcrop on Highway 101; dark grey, fine-grained and contains xenoliths
DC63	935780	Road cut outcrop on Highway 101; dark grey, fine-grained and partly amygdaloidal; vesicles are infilled by carbonate minerals. (altered)
DC64	944793	Float rock; dark grey and fine to medium-grained, carbonate minerals occur along fractures.
DC65	945796	Float rock close to Doi Pai Lin; dark grey and fine to medium-grained
DC66	945803	Float rock; dark grey, fine to medium-grained and partly amygdaloidal, carbonate minerals occur along fractures and partially infilling vesicles.

Appendix B

Summarised petrographic features of the Denchai basalts

Sample	Phenocrysts/Microphenocrysts	Groundmass	Remarks
DC1 Ol 3% Plag 1% Cpx < 0.5%	Olivine + Plagioclase ± Clinopyroxene Microphyric, Olivine is the most abundant phenocrysts/microphenocrysts while plagioclase and clinopyroxene occur as microphenocrysts. They form as isolated crystals and a few as plagioclase-clinopyroxene glomerocrysts. Olivine: anhedral to sparsely euhedral with sizes up to 0.8 mm across Plagioclase: anhedral to subhedral with sizes up to 0.3 mm across. Clinopyroxene: anhedral to subhedral with sizes up to 0.45 mm across	Fine-grained holocrystalline, consisted mainly of anhedral to subhedral felted plagioclase laths with subordinate anhedral to subhedral olivine, anhedral to subhedral pink clinopyroxene and anhedral to subhedral Fe-Ti oxides	Vesicles and fractures partly infilled with carbonate, zeolite and iron oxide minerals. Olivine moderately replaced by iddingsite, chlorite/serpentine and iron oxide minerals. Plagioclase slightly replaced by sericite and clay minerals. Clinopyroxene slightly replaced by chlorite.
DC2 Ol 3% Plag 1% Cpx < 0.5%	Olivine + Plagioclase ± Clinopyroxene Microphyric, Olivine is the most abundant phenocrysts/microphenocrysts while plagioclase and clinopyroxene occur as microphenocrysts. They form as isolated crystals and a few as olivine glomerocrysts and olivine-plagioclase-clinopyroxene glomerocrysts. Olivine: anhedral to subhedral with sizes up to 0.7 mm across Plagioclase: anhedral to subhedral with sizes up to 0.25 mm across Clinopyroxene: anhedral to subhedral with sizes up to 0.3 mm across	Holocrystalline, made up of mainly anhedral to subhedral felted plagioclase laths with subordinate anhedral olivine, anhedral to subhedral pink clinopyroxene and anhedral Fe-Ti oxides	Vesicles and fractures partly infilled with carbonate, zeolite and iron oxide minerals. Olivine highly replaced by chlorite/serpentine, iddingsite and iron oxide minerals. Plagioclase slightly replaced by sericite and clay minerals. Clinopyroxene slightly replaced by chlorite.
DC3 Ol 1%	Olivine Aphyric, Olivine is the most abundant microphenocrysts.	Highly weathered hypocrystalline, trachytic texture, made	Xenolithic, Vesicles and fractures partly infilled with

	They form as isolated crystals. Olivine: anhedral to subhedral with sizes up to 0.33 mm across	up of mainly reddish brown glass with anhedral to subhedral felted plagioclase laths, anhedral olivine, anhedral clinopyroxene and anhedral Fe-Ti oxides Plagioclase laths show preferred orientation.	carbonate, zeolite and iron oxide minerals. Olivine moderately replaced by chlorite/serpentine, iddingsite and iron oxide minerals. Plagioclase moderately replaced by sericite and clay minerals.
DC4 Ol 3% Plag 0.5% Cpx < 0.5%	Olivine + Plagioclase ± Clinopyroxene Aphyric, Olivine is the most abundant phenocrysts/microphenocrysts, following by plagioclase and clinopyroxene. They form as isolated crystals. Olivine: anhedral to sparsely euhedral with sizes up to 0.66 mm across and shows corroded outlined Plagioclase: anhedral to subhedral with sizes up to 0.2 mm across Clinopyroxene: anhedral to subhedral with sizes up to 0.45 mm across	Moderately weathered holocrystalline, composed of largely anhedral to subhedral felted plagioclase laths with subordinate anhedral to subhedral olivine, anhedral to subhedral clinopyroxene and anhedral to subhedral Fe-Ti oxides	Vesicles and fractures partly infilled with carbonate, zeolite and iron oxide minerals. Olivine moderately replaced by chlorite/serpentine, iddingsite and iron oxide minerals. Plagioclase moderately replaced by sericite and clay minerals. Clinopyroxene slightly replaced by chlorite.
DC5 Ol 3% Cpx 1%	Olivine + Clinopyroxene Aphyric, Olivine is the most abundant microphenocrysts, including clinopyroxene. They form as isolated crystals. Olivine: anhedral to subhedral with sizes up to 0.4 mm across Clinopyroxene: anhedral to subhedral with sizes up to 0.2 mm across	Fine-grained hypocrystalline, trachytic texture, consisted of anhedral to subhedral felted plagioclase laths with subordinate anhedral to subhedral olivine, anhedral clinopyroxene, dark brown glass and anhedral Fe-Ti oxides Plagioclase laths show preferred orientation.	Xenolithic (ol+px+sp), Vesicles and fractures partly infilled with carbonate, zeolite and iron oxide minerals. Olivine moderately replaced by iddingsite, chlorite/serpentine and iron oxide minerals.
DC6 Ol 2%	Olivine + Plagioclase + Clinopyroxene Aphyric,	Moderately weathered holocrystalline,	Vesicles and fractures partly infilled with

Plag 1% Cpx < 0.5%	Olivine is the most abundant phenocrysts/microphenocrysts, including plagioclase and clinopyroxene. They form as isolated crystals, some as olivine-plagioclase-clinopyroxene glomerocrysts. Olivine: anhedral to sparsely euhedral with sizes up to 1 mm across Plagioclase: anhedral to subhedral with sizes up to 0.3 mm across Clinopyroxene: anhedral to subhedral with sizes up to 0.33 mm across	trachytic texture, consisted of anhedral to subhedral felted plagioclase laths with subordinate anhedral to subhedral olivine, anhedral to subhedral clinopyroxene and anhedral to subhedral Fe-Ti oxides. Plagioclase laths show preferred orientation.	carbonate, zeolite and iron oxide minerals. Olivine moderately replaced by iddingsite, chlorite/serpentine and iron oxide minerals. Plagioclase slightly replaced by sericite and clay minerals. Clinopyroxene slightly replaced by chlorite.
DC7 Ol 2% Plag 0.5% Cpx < 0.5%	Olivine ± Plagioclase ± Clinopyroxene Aphyric, Olivine is the most abundant phenocrysts/microphenocrysts while plagioclase and clinopyroxene occur as microphenocrysts. They form as isolated crystals. Olivine: anhedral to subhedral with sizes up to 0.85 mm across Plagioclase: anhedral to subhedral with sizes up to 0.2 mm across Clinopyroxene: anhedral to subhedral with sizes up to 0.8 mm across	Moderately weathered holocrystalline, consisted of anhedral to subhedral felted plagioclase laths with subordinate anhedral to subhedral olivine, anhedral to subhedral clinopyroxene and anhedral to subhedral Fe-Ti oxides	Vesicles and fractures partly infilled with carbonate, zeolite and iron oxide minerals. Olivine highly replaced by iddingsite, chlorite/serpentine and iron oxide minerals. Plagioclase moderately replaced by sericite and clay minerals. Clinopyroxene moderately replaced by chlorite.
DC8 Ol 3% Plag 2% Cpx < 0.5%	Olivine + Plagioclase ± Clinopyroxene Aphyric, Olivine is the most abundant phenocrysts/microphenocrysts while plagioclase and clinopyroxene occur as microphenocrysts. They form as isolated crystals and a few as olivine-plagioclase-clinopyroxene glomerocrysts. Olivine: anhedral to sparsely euhedral with sizes up to 1.2 mm across Plagioclase: anhedral to subhedral with sizes up to 0.3 mm across	Fine-grained holocrystalline, trachytic texture, consisted of anhedral to subhedral felted plagioclase laths with subordinate anhedral to subhedral olivine, anhedral to subhedral pink clinopyroxene and anhedral to subhedral Fe-Ti oxides. Plagioclase laths show	Vesicles infilled with carbonate, zeolite and iron oxide minerals. Olivine moderately replaced by iddingsite, chlorite/serpentine and iron oxide minerals. Plagioclase slightly replaced by sericite and clay minerals. Clinopyroxene slightly replaced by chlorite.

	Clinopyroxene: anhedral to subhedral with sizes up to 0.35 mm across	preferred orientation.	
DC10 Ol 3% Plag < 0.5%	Olivine + Plagioclase Aphyric, Olivine is the most abundant phenocrysts/microphenocrysts while plagioclase occurs as microphenocrysts. They form as isolated crystals. Olivine: anhedral to sparsely euhedral with sizes up to 1.8 mm across Plagioclase: anhedral to subhedral with sizes up to 0.4 mm across	Hypocrystalline, consisted of anhedral to subhedral felted plagioclase laths with subordinate anhedral to subhedral olivine, anhedral to subhedral Fe-Ti oxides, anhedral to subhedral clinopyroxene and dark brown glass	Vesicles infilled with carbonate, zeolite and iron oxide minerals. Olivine moderately replaced by iddingsite, chlorite/serpentine and iron oxide minerals. Plagioclase slightly replaced by sericite and clay minerals.
DC11 Ol 2% Plag 1%	Olivine + Plagioclase Aphyric, Olivine is the most abundant phenocrysts/microphenocrysts, following by plagioclase. They form as isolated crystals. Olivine: anhedral to subhedral with sizes up to 0.65 mm across and shows corroded outlined Plagioclase: anhedral to subhedral with sizes up to 0.3 mm across	Holocrystalline, consisted of anhedral to subhedral felted plagioclase laths with subordinate anhedral to subhedral olivine, anhedral to subhedral clinopyroxene and anhedral to subhedral Fe-Ti oxides	Vesicles infilled with carbonate, zeolite and iron oxide minerals. Olivine moderately replaced by iddingsite, chlorite/serpentine and iron oxide minerals. Plagioclase slightly replaced by sericite and clay minerals.
DC12 Ol 3% Plag < 0.5%	Olivine + Plagioclase Aphyric, Olivine is the most abundant phenocrysts/microphenocrysts while plagioclase sparsely occurs as microphenocrysts. They form as isolated crystals. Olivine: anhedral to sparsely euhedral with sizes up to 0.66 mm across Plagioclase: anhedral to subhedral with sizes up to 0.2 mm across	Hypocrystalline, composed of anhedral to subhedral felted plagioclase laths with subordinate anhedral to subhedral olivine, anhedral to subhedral Fe-Ti oxides, anhedral to subhedral pink clinopyroxene and dark brown glass	Vesicles infilled with carbonate and zeolite. Olivine moderately replaced by iddingsite and iron oxides. Plagioclase slightly replaced by sericite and clay minerals.
DC13 Ol 2% Cpx 0.5%	Olivine ± Clinopyroxene Aphyric, Olivine is the most abundant phenocrysts/microphenocrysts, including clinopyroxene. They form as isolated crystals. Olivine: anhedral to subhedral with	Hypocrystalline, made up largely of devitrified reddish brown glass with anhedral to subhedral felted plagioclase laths,	Xenolith (ol+opx+cpx+sp), Vesicles and fractures infilled with carbonate and zeolite. Olivine slightly replaced by

	sizes up to 0.8 mm across Clinopyroxene: anhedral to subhedral with sizes up to 0.1 mm across	anhedral to subhedral olivine, anhedral to subhedral clinopyroxene and anhedral to subhedral Fe-Ti oxides	iddingsite and iron oxides. Plagioclase slightly replaced by sericite and clay minerals. Clinopyroxene slightly replaced by chlorite.
DC14 Ol 1%	Olivine Aphyric	Hypocrystalline, trachytic texture, made up of dark brown glass with anhedral felted plagioclase laths, anhedral olivine and anhedral Fe-Ti oxides Plagioclase laths show preferred orientation.	Xenolith (ol+px+sp)
DC15 Ol 3% Plag 1% Cpx < 0.5%	Olivine + Plagioclase + Clinopyroxene Microphyric, Olivine is the most abundant phenocrysts/microphenocrysts, following by plagioclase and clinopyroxene They form as isolated crystals and a few as olivine-plagioclase glomerocrysts Olivine: anhedral to subhedral with sizes up to 1 mm across Plagioclase: anhedral to subhedral with sizes up to 0.3 mm across Clinopyroxene: anhedral to subhedral with sizes up to 0.9 mm across	Holocrystalline, consisted of anhedral to subhedral felted plagioclase laths with subordinate anhedral to subhedral olivine, anhedral to subhedral clinopyroxene and anhedral to subhedral Fe-Ti oxides	Quartz xenocryst, Vesicles infilled with carbonate and iron oxide minerals. Olivine highly replaced by iddingsite and iron oxides. Plagioclase very slightly replaced by sericite and clay minerals.
DC16 Ol 3% Plag 1% Cpx 1%	Olivine + Plagioclase + Clinopyroxene Microphyric, Olivine is the most abundant microphenocrysts, following by plagioclase and clinopyroxene They form as isolated crystals. Olivine: anhedral to subhedral with sizes up to 1.2 mm across Plagioclase: anhedral to subhedral with	Holocrystalline, composed of fine-grained anhedral to subhedral felted plagioclase laths with subordinate anhedral to subhedral olivine, anhedral to subhedral pink clinopyroxene and	Crustal-derived xenolith (cpx+plag), Vesicles infilled with carbonate, zeolite and iron oxide minerals. Olivine slightly replaced by iddingsite and iron oxides. Plagioclase moderately

	sizes up to 0.2 mm across Clinopyroxene: anhedral to subhedral with sizes up to 0.2 mm across	anhedral to subhedral Fe-Ti oxides	replaced by sericite and clay minerals. Clinopyroxene slightly replaced by chlorite.
DC17 Ol 3% Plag 1%	Olivine + Plagioclase Aphyric, Olivine is the most abundant phenocrysts/microphenocrysts, following by plagioclase. They form as isolated crystals and as olivine-plagioclase glomerocrysts. Olivine: anhedral to subhedral with sizes up to 1.5 mm across Plagioclase: anhedral to subhedral with sizes up to 0.45 mm across	Moderately weathered fine-grained holocrystalline, consisted of anhedral to subhedral felted plagioclase laths with subordinate anhedral to subhedral olivine, anhedral to subhedral clinopyroxene and anhedral to subhedral Fe-Ti oxides	Xenolithic, Vesicles infilled with carbonate, zeolite and iron oxide minerals. Olivine moderately replaced by iddingsite and iron oxides. Plagioclase moderately replaced by sericite and clay minerals.
DC18 Ol 2% Plag 1% Cpx < 0.5%	Olivine + Plagioclase + Clinopyroxene Aphyric, Olivine is the most abundant phenocrysts/microphenocrysts, following by plagioclase and sparsely clinopyroxene. They form as isolated crystals and a few as olivine-plagioclase glomerocrysts. Olivine: anhedral to subhedral with sizes up to 0.8 mm across Plagioclase: anhedral to subhedral with sizes up to 0.6 mm across Clinopyroxene: anhedral to subhedral with sizes up to 0.6 mm across	Highly weathered holocrystalline, consisted of anhedral to subhedral felted plagioclase laths with subordinate anhedral to subhedral olivine, anhedral to subhedral pink clinopyroxene and anhedral to subhedral Fe-Ti oxides	Vesicles infilled with carbonate, zeolite and iron oxide minerals. Olivine slightly replaced by iddingsite and iron oxide/hydroxide minerals Plagioclase slightly replaced by sericite and clay minerals. Clinopyroxene moderately replaced by chlorite.
DC19 Ol 2% Cpx 0.5%	Olivine + Clinopyroxene Aphyric, Olivine is the most abundant phenocrysts/microphenocrysts, following by clinopyroxene. They form as isolated crystals. Olivine: anhedral to subhedral and with sizes up to 0.45 mm across Clinopyroxene: anhedral to subhedral with sizes up to 0.25 mm across	Fine-grained holocrystalline, consisted of anhedral to subhedral felted plagioclase laths with subordinate anhedral to subhedral olivine, anhedral to subhedral pink clinopyroxene and	xenolith (ol+sp), Vesicles infilled with iron oxides, carbonate and zeolite. Olivine moderately replaced by iddingsite and iron oxides. Plagioclase slightly replaced by sericite

		anhedral to subhedral Fe-Ti oxides	and clay minerals. Clinopyroxene moderately replaced by chlorite.
DC20 Ol 3% Plag 1% Cpx 1%	Olivine + Plagioclase + Clinopyroxene Microphyric, Olivine is the most abundant microphenocrysts, following by plagioclase and clinopyroxene. They form as isolated crystals, olivine-plagioclse-clinopyroxene glomerocrysts. Olivine: anhedral to subhedral and with sizes up to 0.6 mm across Plagioclase: anhedral to subhedral with sizes up to 0.2 mm across Clinopyroxene: anhedral to subhedral with sizes up to 0.15 mm across	Coarse-grained holocrystalline, composed of anhedral to subhedral felted plagioclase laths with subordinate anhedral to subhedral olivine, anhedral to subhedral pink clinopyroxene and anhedral to subhedral Fe-Ti oxides	Vesicles infilled with iron oxide minerals. Olivine slightly replaced by iddingsite and iron oxides. Plagioclase slightly replaced by sericite and clay minerals. Clinopyroxene slightly replaced by chlorite.
DC21 Ol 3% Plag 1% Cpx 1%	Olivine + Plagioclase + Clinopyroxene Microphyric, Olivine is the most abundant phenocrysts/microphenocrysts, following by plagioclase and clinopyroxene. They form as isolated crystals. Olivine: anhedral to subhedral with sizes up to 0.7 mm across Plagioclase: anhedral to subhedral with sizes up to 0.2 mm across Clinopyroxene: anhedral to subhedral with sizes up to 0.2 mm across	Holocrystalline, consisted of anhedral to subhedral felted plagioclase laths with subordinate anhedral to subhedral olivine, anhedral to subhedral pink clinopyroxene and anhedral to subhedral Fe-Ti oxides	Xenolithic, Vesicles infilled with carbonate, zeolite and iron oxide minerals. Olivine is slightly replaced by iddingsite and iron oxides. Plagioclase slightly replaced by sericite and clay minerals. Clinopyroxene slightly replaced by chlorite.
DC22 Ol 3% Plag 1%	Olivine + Plagioclase Microphyric, Olivine is the most abundant phenocrysts/microphenocrysts, following by plagioclase. They form as isolated crystals and a few as olivine-plagioclase glomerocrysts. Olivine: anhedral to subhedral with sizes up to 0.4 mm across	Coarse grained hypocrystalline, made up of anhedral to subhedral felted plagioclase laths with subordinate anhedral to subhedral olivine, anhedral to subhedral clinopyroxene,	Xenolith (ol+sp), Vesicles and fractures infilled with carbonate, zeolitic and iron oxide/hydroxide minerals. Olivine moderately replaced by iddingsite, chlorite/serpentine and

	Plagioclase: anhedral to subhedral with sizes up to 0.2 mm across	devitrified brown glass and anhedral to subhedral Fe-Ti oxides	iron oxide/hydroxide minerals. Plagioclase slightly replaced by sericite and clay minerals.
DC23 Ol 2% Cpx 1%	Olivine ± Clinopyroxene Aphyric, Olivine is the most abundant phenocrysts/microphenocrysts while clinopyroxene occurs as microphenocrysts. They form as isolated crystals and a few as olivine-clinopyroxene glomerocrysts. Olivine: anhedral to subhedral with sizes up to 0.6 mm across Clinopyroxene: anhedral to subhedral with sizes up to 0.4 mm across and sparsely shows stellate fashion	Holocrystalline, consisted of anhedral to subhedral felted plagioclase laths with subordinate anhedral to subhedral olivine, anhedral to subhedral pink clinopyroxene and anhedral to subhedral Fe-Ti oxides	Xenolith (ol+sp), Vesicles infilled with carbonate, zeolite and iron oxide minerals. Olivine moderately replaced by iddingsite and iron oxides. Plagioclase slightly replaced by sericite and clay minerals.
DC24 Ol 2%	Highly Altered Olivine Aphyric, Olivine is the most abundant phenocrysts/microphenocrysts. Olivine traces: size up to 1 mm across	Highly weathered groundmass, composed of anhedral felted plagioclase laths, olivine and Fe-Ti oxides	Highly weathered xenolith (ol+plag+cpx), Vesicles and fractures infilled with iron oxide, carbonate and zeolite. Olivine highly replaced by iddingsite, chlorite and iron oxide/hydroxide minerals. Plagioclase highly replaced by sericite and clay minerals.
DC25 Ol 2% Cpx < 0.5%	Olivine ± Clinopyroxene Phyric, Olivine is the most abundant phenocrysts/microphenocrysts while clinopyroxene sparsely occurs as microphenocrysts. They form as isolated crystals and a few as olivine cumulocrysts.	Holocrystalline, trachytic texture, consisted of anhedral to subhedral felted plagioclase laths with subordinate anhedral to subhedral olivine,	Vesicles and fractures infilled with carbonate and iron oxides. Olivine moderately replaced by iddingsite, chlorite/serpentine and iron oxide minerals.

	Olivine: anhedral to subhedral, with sizes up to 1.5 mm across and shows corroded outlined Clinopyroxene: anhedral to subhedral with sizes up to 1.2 mm across	anhedral to subhedral pink clinopyroxene and anhedral to subhedral Fe-Ti oxides Plagioclase laths show preferred orientation.	Plagioclase moderately replaced by sericite and clay minerals. Clinopyroxene moderately replaced by chlorite.
DC26 Ol 2% Cpx 1% Plag 1%	Olivine + Clinopyroxene + Plagioclase Aphyric, Olivine is the most abundant phenocrysts/microphenocrysts, following by clinopyroxene and plagioclase. They form as isolated crystals. Olivine: anhedral to subhedral, with sizes up to 0.8 mm across Clinopyroxene: anhedral to subhedral with sizes up to 0.8 mm across Plagioclase: anhedral to subhedral with sizes up to 0.6 mm across	Highly weathered holocrystalline, trachytic texture, composed of anhedral to subhedral felted plagioclase laths with subordinate anhedral to subhedral olivine, anhedral to subhedral pink clinopyroxene and anhedral to subhedral Fe-Ti oxides Plagioclase laths show preferred orientation.	Vesicles and fractures infilled with carbonate, iron oxide and zeolite. Olivine moderately replaced by iddingsite, chlorite/serpentine and iron oxides. Clinopyroxene moderately replaced by chlorite. Plagioclase slightly replaced by sericite and clay minerals.
DC27 Ol 2%	Olivine Aphyric, Olivine is the most abundant microphenocrysts. They form as isolated crystals. Olivine: anhedral to subhedral, with sizes up to 0.25 mm across and shows corroded outlined	Hypocrystalline, consisted of anhedral to subhedral felted plagioclase laths with subordinate anhedral to subhedral olivine, anhedral to subhedral clinopyroxene, anhedral to subhedral Fe-Ti oxides and dark brown glass	Xenolith (ol+px+sp), Vesicles and fractures infilled with carbonate. Olivine is moderately replaced by iddingsite and chloriteserpentine. Plagioclase slightly replaced by sericite and clay minerals.
DC28 Ol 2% Cpx 0.5%	Olivine + Clinopyroxene Phyric, Olivine is the most abundant phenocrysts/microphenocrysts while clinopyroxene sparsely occurs as microphenocrysts. They form as isolated crystals and a few as olivine-clinopyroxene glomerocrysts. Olivine: anhedral to subhedral, with sizes up to 2.1 mm across and shows	Hypocrystalline, consisted largely of anhedral to subhedral felted plagioclase laths with subordinate anhedral to subhedral olivine, anhedral to subhedral pink clinopyroxene,	Vesicles and fractures infilled with carbonate and iron oxides. Olivine moderately replaced by iddingsite, chlorite/serpentine and iron oxide minerals. Plagioclase moderately replaced by sericite

	corroded outlined Clinopyroxene: anhedral to subhedral with sizes up to 2.4 mm across	anhedral to subhedral Fe-Ti oxides and devitrified dark brown glass	and clay minerals. Clinopyroxene moderately replaced by chlorite.
DC29 Ol 3% Plag 1% Cpx 1%	Olivine + Plagioclase + Clinopyroxene Microphyric, Olivine is the most abundant phenocrysts/microphenocrysts, following by plagioclase and clinopyroxene. They form as isolated crystals. Olivine: anhedral to subhedral, with sizes up to 0.5 mm across and shows corroded outlined Plagioclase: anhedral to subhedral with sizes up to 0.5 mm across and shows zoning Clinopyroxene: anhedral to subhedral with sizes up to 0.2 mm across	Holocrystalline, consisted of anhedral to subhedral felted plagioclase laths with subordinate anhedral to subhedral olivine, anhedral to subhedral clinopyroxene and anhedral to subhedral Fe-Ti oxides	Crustal-derived xenolith (cpx+plag), Vesicles and fractures infilled with carbonate, iron oxide and zeolite. Olivine slightly replaced by iddingsite, chlorite/serpentine and iron oxide minerals. Plagioclase slightly replaced by sericite and clay minerals. Clinopyroxene slightly replaced by chlorite.
DC30 Ol 3% Plag 2% Cpx < 0.5%	Olivine + Plagioclase ± Clinopyroxene Microphyric, Olivine is the most abundant phenocrysts/microphenocrysts, following by plagioclase and clinopyroxene. They form as isolated crystals and a few as olivine-plagioclase glomerocrysts. Olivine: anhedral to subhedral, with sizes up to 0.6 mm across and shows corroded outlined Plagioclase: anhedral to subhedral with sizes up to 0.6 mm across and shows zoning Clinopyroxene: anhedral to subhedral with sizes up to 1 mm across	Holocrystalline, composed of anhedral to subhedral felted plagioclase laths with subordinate anhedral to subhedral olivine, anhedral to subhedral clinopyroxene and anhedral to subhedral Fe-Ti oxides	Weathered xenolith, Vesicles and fractures infilled with carbonate, iron oxide and zeolite. Olivine moderately replaced by iddingsite, chlorite/serpentine and iron oxide minerals. Plagioclase slightly replaced by sericite and clay minerals. Clinopyroxene slightly replaced by chlorite.
DC31 Ol 2% Plag 1%	Olivine + Plagioclase Aphyric, Olivine is the most abundant phenocrysts/microphenocrysts, following by plagioclase.	Weathered holocrystalline, composed of anhedral to subhedral felted	Xenolithic, Vesicles and fractures infilled with carbonate, iron oxide and zeolite.

	They form as isolated crystals. Olivine: anhedral to subhedral, with sizes up to 0.75 mm across and shows corroded outlined Plagioclase: anhedral to subhedral with sizes up to 0.2 mm across	plagioclase laths with subordinate anhedral to subhedral olivine, anhedral to subhedral clinopyroxene and anhedral to subhedral Fe-Ti oxides	Olivine highly replaced by iddingsite, chlorite/serpentine and iron oxide minerals. Plagioclase highly replaced by sericite and clay minerals. Clinopyroxene highly replaced by chlorite.
DC32 Ol 2% Cpx 0.5%	Olivine ± Clinopyroxene Aphyric, The most abundant phenocrysts/microphenocrysts is olivine, following by clinopyroxene. They form as isolated crystals. Olivine: anhedral to subhedral with sizes up to 1.2 mm across Clinopyroxene: anhedral to subhedral with sizes up to 0.3 mm across	Holocrystalline, consisted of anhedral to subhedral felted plagioclase laths with subordinate anhedral to subhedral olivine, anhedral to subhedral clinopyroxene and anhedral to subhedral Fe-Ti oxides	Xenolith (ol++plag+cpx+sp), Vesicles and fractures partly infilled with carbonate, zeolite and iron oxide minerals. Olivine moderately replaced by chlorite/serpentine, iddingsite and iron oxide minerals. Plagioclase slightly replaced by sericite and clay minerals.
DC33 Ol 3% Plag 1%	Olivine ± Plagioclase Aphyric, The most abundant phenocrysts/microphenocrysts is olivine while plagioclase sparsely occurs as microphenocrysts. They form as isolated crystals. Olivine: anhedral to subhedral with sizes up to 0.6 mm across Plagioclase: anhedral to subhedral with sizes up to 0.2 mm across	Weathered holocrystalline, composed of anhedral to subhedral felted plagioclase laths with subordinate anhedral to subhedral olivine, anhedral to subhedral clinopyroxene and anhedral to subhedral Fe-Ti oxides	Vesicles and fractures partly infilled with carbonate, zeolite and iron oxide minerals. Olivine moderately replaced by chlorite/serpentine, iddingsite and iron oxide minerals. Plagioclase moderately replaced by sericite and clay minerals.
DC34 Ol 3%	Olivine Aphyric, Olivine occurs as microphenocrysts. They form as isolated crystals. Olivine: anhedral to subhedral with sizes up to 0.5 mm across	Highly weathered holocrystalline, consisted of anhedral to subhedral felted plagioclase laths with	Weathered xenolith, Vesicles and fractures partly infilled with carbonate, zeolite and iron oxide minerals.

		subordinate anhedral to subhedral olivine, anhedral to subhedral clinopyroxene and anhedral to subhedral Fe-Ti oxides	Olivine moderately replaced by chlorite/serpentine, iddingsite and iron oxide minerals. Plagioclase highly replaced by sericite and clay minerals. Clinopyroxene is highly replaced by chlorite.
DC35 Ol 3%	Olivine Aphyric, Olivine occurs as phenocrysts/microphenocrysts. They form as isolated crystals. Olivine: anhedral to subhedral with sizes up to 0.7 mm across and shows corroded outlined	Holocrystalline, consisted of anhedral to subhedral felted plagioclase laths with subordinate anhedral to subhedral olivine, anhedral to subhedral clinopyroxene and anhedral to subhedral Fe-Ti oxides	Vesicles and fractures partly infilled with carbonate, zeolite and iron oxide minerals. Olivine moderately replaced by chlorite/serpentine, iddingsite and iron oxide minerals. Plagioclase moderately replaced by sericite and clay minerals. Clinopyroxene moderately replaced by chlorite.
DC36 Ol 2% Plag 1% Cpx 1%	Olivine + Plagioclase + Clinopyroxene Aphyric, The most abundant phenocrysts/microphenocrysts is olivine, following by plagioclase and clinopyroxene. They form as isolated crystals and a few as olivine-clinopyroxene glomerocrysts. Olivine: anhedral to subhedral with sizes up to 0.8 mm across.Plagioclase: anhedral to subhedral with sizes up to 0.38 mm across Clinopyroxene: anhedral to subhedral	Coarse-grained holocrystalline, composed of anhedral to subhedral felted plagioclase laths with subordinate anhedral to subhedral olivine, anhedral to subhedral pink clinopyroxene and anhedral to subhedral Fe-Ti oxides	Vesicles partly infilled with carbonate, zeolite and iron oxides. Olivine moderately replaced by chlorite/serpentine, iddingsite and iron oxide minerals. Plagioclase moderately replaced by sericite and clay minerals. Clinopyroxene moderately replaced by chlorite.

	with sizes up to 3 mm across		
DC37 Ol 3% Plag 1%	Olivine + Plagioclase Aphyric, The most abundant phenocrysts/microphenocrysts is olivine while plagioclase sparsely occurs as microphenocrysts. They form as isolated crystals. Olivine: anhedral to subhedral with sizes up to 1.2 mm across Plagioclase: anhedral to subhedral with sizes up to 0.15 mm across	Holocrystalline, consisted of anhedral to subhedral felted plagioclase laths with subordinate anhedral to subhedral olivine, anhedral to subhedral clinopyroxene and anhedral to subhedral Fe-Ti oxides	Vesicles and fractures partly infilled with carbonate, zeolite and iron oxide minerals. Olivine moderately replaced by chlorite/serpentine, iddingsite and iron oxide minerals. Plagioclase slightly replaced by sericite and clay minerals.
DC38 Ol 2% Plag 1% Cpx 0.5%	Olivine + Plagioclase + Clinopyroxene Aphyric, The most abundant phenocrysts/microphenocrysts is olivine, following by plagioclase and clinopyroxene. They form as isolated crystals. Olivine: anhedral to subhedral with sizes up to 1.2 mm across. Plagioclase: anhedral to subhedral with sizes up to 0.4 mm across Clinopyroxene: anhedral to subhedral with sizes up to 2.5 mm across	Moderately weathered holocrystalline, composed of anhedral to subhedral felted plagioclase laths with subordinate anhedral to subhedral olivine, anhedral to subhedral pink clinopyroxene and anhedral to subhedral Fe-Ti oxides	Vesicles and fractures partly infilled with carbonate, zeolite and iron oxide minerals. Olivine slightly replaced by chlorite/serpentine, iddingsite and iron oxide minerals. Plagioclase slightly replaced by sericite and clay minerals. Clinopyroxene slightly replaced by chlorite.
DC39 Ol 2% Plag 1% Cpx 1%	Olivine + Plagioclase + Clinopyroxene Aphyric, The most abundant phenocrysts/microphenocrysts is olivine, following by plagioclase and plagioclase. They form as isolated crystals and a few as olivine-clinopyroxene glomerocrysts. Olivine: anhedral to subhedral with sizes up to 0.9 mm across. Plagioclase: anhedral to subhedral with sizes up to 0.3 mm across	Moderately weathered holocrystalline, composed of anhedral to subhedral felted plagioclase laths with subordinate anhedral to subhedral olivine, anhedral to subhedral pink clinopyroxene and anhedral to subhedral Fe-Ti oxides	Vesicles and fractures partly infilled with carbonate, zeolite and iron oxide minerals. Olivine moderately replaced by chlorite/serpentine, iddingsite and iron oxide minerals. Plagioclase moderately replaced by sericite and clay minerals. Clinopyroxene

	Clinopyroxene: anhedral to subhedral with sizes up to 1.8 mm across		moderately replaced by chlorite.
DC40 Ol 3% Plag 1% Cpx < 0.5%	Olivine + Plagioclase ± Clinopyroxene Microphyric, The most abundant phenocrysts/microphenocrysts is olivine, including plagioclase and sparsely clinopyroxene. They form as isolated crystals and a few as olivine-plagioclase glomerocrysts. Olivine: anhedral to subhedral with sizes up to 1 mm across. Plagioclase: anhedral to subhedral with sizes up to 0.6 mm across Clinopyroxene: anhedral to subhedral with sizes up to 0.3 mm across	Holocrystalline, composed of anhedral to subhedral felted plagioclase laths with subordinate anhedral to subhedral olivine, anhedral to subhedral pink clinopyroxene and anhedral to subhedral Fe-Ti oxides	Vesicles and fractures partly infilled with carbonate, zeolite and iron oxide minerals. Olivine moderately replaced by chlorite/serpentine, iddingsite and iron oxide minerals. Plagioclase slightly replaced by sericite and clay minerals. Clinopyroxene slightly replaced by chlorite.
DC41 Ol 2% Plag 0.5%	Olivine + Plagioclase Aphyric, The most abundant phenocrysts/microphenocrysts is olivine, following by plagioclase. They form as isolated crystals. Olivine: anhedral to subhedral with sizes up to 0.66 mm across Plagioclase: anhedral to subhedral with sizes up to 0.5 mm across	Moderately weathered holocrystalline, composed of anhedral to subhedral felted plagioclase laths with subordinate anhedral to subhedral olivine, anhedral to subhedral Clinopyroxene and anhedral to subhedral Fe-Ti oxides	Vesicles and fractures partly infilled with carbonate, zeolite and iron oxide minerals. Olivine moderately replaced by chlorite/serpentine, iddingsite and iron oxide minerals. Plagioclase moderately replaced by sericite and clay minerals. Clinopyroxene highly replaced by chlorite.
DC42 Ol 2% Cpx 0.5%	Olivine + Clinopyroxene Phyric, Olivine is the most abundant phenocrysts/microphenocrysts. Plagioclase and clinopyroxene occur as microphenocrysts. They form as isolated crystals and a few as olivine-plagioclase-clinopyroxene glomerocrysts. Olivine: anhedral to subhedral with	Holocrystalline, composed of anhedral to subhedral felted plagioclase laths with subordinate anhedral to subhedral olivine, anhedral to subhedral pink clinopyroxene and anhedral to subhedral	Crustal-derived xenolith (qtz+plag+cpx), Vesicles and fractures partly infilled with carbonate, zeolite and iron oxide minerals. Olivine slightly replaced by

	sizes up to 1.4 mm across Clinopyroxene: anhedral to subhedral with sizes up to 0.2 mm across	Fe-Ti oxides	chlorite/serpentine, iddingsite and iron oxide minerals. Plagioclase slightly replaced by sericite and clay minerals. Clinopyroxene slightly replaced by chlorite.
DC43 Ol 2% Cpx < 0.5%	Olivine ± Clinopyroxene Aphyric, Olivine is the most abundant phenocrysts/microphenocrysts. Clinopyroxene sparsely occurs as microphenocrysts. They form as isolated crystals. Olivine: anhedral to subhedral with sizes up to 0.6 mm across and shows corroded outlined Clinopyroxene: anhedral to subhedral with sizes up to 0.2 mm across	Holocrystalline, trachytic texture, consisted of anhedral to subhedral felted plagioclase laths with subordinate anhedral to subhedral olivine, anhedral to subhedral pink clinopyroxene and anhedral to subhedral Fe-Ti oxides Plagioclse laths shows preferred orientation.	Xenolith (ol+px+sp), Vesicles and fractures partly infilled with carbonate, zeolite and iron oxide minerals. Olivine moderately replaced by chlorite/serpentine, iddingsite and iron oxide minerals. Plagioclase moderately replaced by sericite and clay minerals. Clinopyroxene moderately replaced by chlorite.
DC44 Ol 3% Plag 1%	Olivine + Plagioclase Microphyric, Olivine is the most abundant phenocrysts/microphenocrysts, following by plagioclase. They form as isolated crystals and a few as olivine-plagioclase glomerocrysts. Olivine: anhedral to euhedral with sizes up to 0.6 mm across and shows corroded outlined and sieve texture Plagioclase: anhedral to subhedral with sizes up to 0.3 mm across	Holocrystalline, composed of anhedral to subhedral felted plagioclase laths with subordinate anhedral to subhedral olivine, anhedral to subhedral clinopyroxene and anhedral to subhedral Fe-Ti oxides	Vesicles and fractures infilled with carbonate, zeolite and iron oxides. Olivine slightly replaced by chlorite/serpentine, iddingsite and iron oxide minerals. Plagioclase slightly replaced by sericite and clay minerals.
DC45 Ol 2% Plag 1%	Olivine + Plagioclase Aphyric, Olivine is the most abundant phenocrysts/microphenocrysts, following by plagioclase.	Holocrystalline, composed of anhedral to subhedral felted plagioclase laths with	Vesicles and fractures infilled with carbonate, zeolite and iron oxides. Olivine moderately

	They form as isolated crystals and a few as olivine-plagioclase glomerocrysts. Olivine: anhedral to sparsely euhedral with sizes up to 0.7 mm across and shows corroded outlined Plagioclase: anhedral to subhedral with sizes up to 0.35 mm across	subordinate anhedral to subhedral olivine, anhedral to subhedral clinopyroxene and anhedral to subhedral Fe-Ti oxides	replaced by chlorite/serpentine, iddingsite and iron oxide minerals. Plagioclase slightly replaced by sericite and clay minerals.
DC46 Ol 3% Plag 1%	Olivine + Plagioclase Aphyric, Olivine is the most abundant phenocrysts/microphenocrysts, following by plagioclase. They form as isolated crystals. Olivine: anhedral to sparsely euhedral with sizes up to 0.66 mm across. Plagioclase: anhedral to subhedral with sizes up to 0.35 mm across	Holocrystalline, consisted of anhedral to subhedral felted plagioclase laths with subordinate anhedral to subhedral olivine, anhedral to subhedral pink clinopyroxene and anhedral to subhedral Fe-Ti oxides	Vesicles and fractures infilled with carbonate, zeolite and iron oxide minerals. Olivine moderately replaced by chlorite/serpentine, iddingsite and iron oxide minerals. Plagioclase slightly replaced by sericite and clay minerals.
DC47 Ol 3% Plag 1%	Olivine + Plagioclase Microphyric, Olivine is the most abundant phenocrysts/microphenocrysts, following by plagioclase. They form as isolated crystals. Olivine: anhedral to sparsely euhedral with sizes up to 0.7 mm across Plagioclase: anhedral to subhedral with sizes up to 0.4 mm across	Weathered holocrystalline, trachytic texture, composed of anhedral to subhedral felted plagioclase laths with subordinate anhedral to subhedral olivine, anhedral to subhedral clinopyroxene and anhedral to subhedral Fe-Ti oxides Plagioclase laths show preferred orientation.	Vesicles and fractures infilled with carbonate, zeolite and iron oxides. Olivine moderately replaced by chlorite/serpentine, iddingsite and iron oxide minerals. Plagioclase slightly replaced by sericite and clay minerals. Clinopyroxene moderately replaced by chlorite.
DC48 Ol 3% Plag 1% Cpx < 0.5%	Olivine + Plagioclase ± Clinopyroxene Microphyric, Olivine is the most abundant phenocrysts/microphenocrysts, following by plagioclase and clinopyroxene.	Moderately weathered holocrystalline, consisted of anhedral to subhedral felted plagioclase laths with subordinate anhedral to	Vesicles and fractures infilled with carbonate, zeolite and iron oxides. Olivine moderately replaced by chlorite/serpentine,

	They form as isolated crystals and a few as olivine-plagioclase clinopyroxene glomerocrysts. Olivine: anhedral to euhedral with sizes up to 0.7 mm across Plagioclasc: anhedral to subhedral with sizes up to 0.5 mm across Clinopyroxene: anhedral to subhedral with sizes up to 0.3 mm across	subhedral olivine, anhedral to subhedral pink clinopyroxene, anhedral to subhedral Fe-Ti oxides and devitrified brown glass	iddingsite and iron oxide minerals. Plagioclase slightly replaced by sericite and clay minerals. Clinopyroxene slightly replaced by chlorite.
DC49 Ol 2% Plag < 0.5% Cpx < 0.5%	Olivine ± Plagioclase ± Clinopyroxene Aphyric, Olivine is the most abundant phenocrysts/microphenocrysts, following by plagioclase and clinopyroxene. They form as isolated crystals. Olivine: anhedral to subhedral with sizes up to 0.8 mm across Plagioclase: anhedral to subhedral with sizes up to 0.15 mm across Clinopyroxene: anhedral to subhedral with sizes up to 0.33 mm across	Highly weathered holocrystalline, trachytic texture, consisted of anhedral to subhedral felted plagioclase laths with subordinate anhedral to subhedral olivine, anhedral to subhedral Clinopyroxene and anhedral to subhedral Fe-Ti oxides Plagioclase laths show preferred orientation.	Vesicles and fractures infilled with carbonate and zeolite. Olivine moderately replaced by chlorite/serpentine, iddingsite and iron oxide minerals. Plagioclase highly replaced by sericite and clay minerals. Clinopyroxene slightly replaced by chlorite.
DC50 Ol 3% Plag 1% Cpx < 0.5%	Olivine + Plagioclase ± Clinopyroxene Aphyric, Olivine is the most abundant phenocrysts/microphenocrysts, following by plagioclase and clinopyroxene. They form as isolated crystals and a few as olivine-plagioclase-clinopyroxene glomerocrysts. Olivine: anhedral to subhedral with sizes up to 0.7 mm across Plagioclase: anhedral to subhedral with sizes up to 0.2 mm across Clinopyroxene: anhedral to subhedral with sizes up to 0.33 mm across	Moderately weathered holocrystalline, composed of anhedral to subhedral felted plagioclase laths with subordinate anhedral to subhedral olivine, anhedral to subhedral clinopyroxene and anhedral to subhedral Fe-Ti oxides	Vesicles and fractures infilled with carbonate, zeolite and iron oxides. Olivine moderately replaced by chlorite/serpentine, iddingsite and iron oxide minerals. Plagioclase moderately replaced by sericite and clay minerals. Clinopyroxene slightly replaced by chlorite.
DC51 Ol 2%	Olivine + Plagioclase ± Clinopyroxene Aphyric,	Moderately weathered holocrystalline,	Vesicles and fractures occasionally presented.

Plag 1% Cpx < 0.5%	Olivine is the most abundant phenocrysts/microphenocrysts, following by plagioclase and clinopyroxene. They form as isolated crystals and a few as plagioclase-clinopyroxene glomerocrysts. Olivine: anhedral to subhedral with sizes up to 0.66 mm across Plagioclase: anhedral to subhedral with sizes up to 0.4 mm across Clinopyroxene: anhedral to subhedral with sizes up to 0.33 mm across	trachytic texture, consisted of anhedral to subhedral felted plagioclase laths with subordinate anhedral to subhedral olivine, anhedral to subhedral clinopyroxene and anhedral to subhedral Fe-Ti oxides Plagioclase laths show preferred orientation.	Olivine moderately replaced by chlorite/serpentine, iddingsite and iron oxide minerals. Plagioclase moderately replaced by sericite and clay minerals. Clinopyroxene moderately replaced by chlorite.
DC52 Ol 2% Plag 1% Cpx 0.5%	Olivine + Plagioclase ± Clinopyroxene Aphyric, Olivine is the most abundant phenocrysts/microphenocrysts, following by plagioclase and clinopyroxene. They form as isolated crystals and a few as olivine-plagioclase-clinopyroxene glomerocrysts. Olivine: anhedral to euhedral with sizes up to 0.7 mm across Plagioclase: anhedral to subhedral with sizes up to 0.25 mm across Clinopyroxene: anhedral to subhedral with sizes up to 0.3 mm across	Moderately weathered holocrystalline, trachytic texture, consisted of anhedral to subhedral felted plagioclase laths with subordinate anhedral to subhedral olivine, anhedral to subhedral clinopyroxene and anhedral to subhedral Fe-Ti oxides Plagioclase laths show preferred orientation.	Vesicles and fractures occasionally presented. Olivine moderately replaced by chlorite/serpentine, iddingsite and iron oxide minerals. Plagioclase slightly replaced by sericite and clay minerals. Clinopyroxene slightly replaced by chlorite.
DC53 Ol 2% Plag 1%	Olivine + Plagioclase Aphyric, Olivine is the most abundant phenocrysts/microphenocrysts, following by plagioclase. They form as isolated crystals. Olivine: anhedral to subhedral with sizes up to 0.66 mm across and shows corroded outlined Plagioclase: anhedral to subhedral with sizes up to 0.33 mm across	Highly weathered holocrystalline, trachytic texture, composed of anhedral to subhedral felted plagioclase laths with subordinate anhedral to subhedral olivine, anhedral to subhedral pink clinopyroxene and anhedral to subhedral Fe-Ti oxides	Vesicles and fractures infilled with carbonate, zeolite and iron oxides. Olivine moderately replaced by chlorite/serpentine, iddingsite and iron oxide minerals. Plagioclase moderately replaced by sericite and clay minerals.

		Plagioclase laths show preferred orientation.	
DC54 Ol 3% Plag 1% Cpx < 0.5%	Olivine + Plagioclase ± Clinopyroxene Microphyric, Olivine is the most abundant phenocrysts/microphenocrysts, following by plagioclase and clinopyroxene. They form as isolated crystals. Olivine: anhedral to sparsely euhedral with sizes up to 0.7 mm across and shows corroded outlined Plagioclase: anhedral to subhedral with sizes up to 0.33 mm across Clinopyroxene: anhedral to subhedral with sizes up to 0.35 mm across	Moderately weathered holocrystalline, trachytic texture, consisted of anhedral to subhedral felted plagioclase laths with subordinate anhedral to subhedral olivine, anhedral to subhedral clinopyroxene and anhedral to subhedral Fe-Ti oxides Plagioclase laths show preferred orientation.	Vesicles and fractures infilled with carbonate, zeolite and iron oxides. Olivine moderately replaced by chlorite/serpentine, iddingsite and iron oxide minerals. Plagioclase slightly replaced by sericite and clay minerals. Clinopyroxene slightly replaced by chlorite.
DC55 Ol 2%	Olivine Aphyric, Olivine occurs as microphenocrysts. They form as isolated crystals. Olivine: anhedral to subhedral with sizes up to 0.3 mm across	Highly weathered holocrystalline, consisted of anhedral to subhedral felted plagioclase laths with subordinate anhedral to subhedral olivine, anhedral to subhedral clinopyroxene and anhedral to subhedral Fe-Ti oxides	Xenolith (ol+sp), Vesicles and fractures infilled with carbonate, zeolite and iron oxide minerals. Olivine moderately replaced by chlorite/serpentine, iddingsite and iron oxide minerals. Plagioclase highly replaced by sericite and clay minerals.
DC56 Ol 3% Cpx < 0.5%	Olivine ± Clinopyroxene Aphyric, Olivine is the most abundant phenocrysts/microphenocrysts, following by plagioclase and clinopyroxene. They form as isolated crystals. Olivine: anhedral to subhedral with sizes up to 0.7 mm across Clinopyroxene: anhedral to subhedral with sizes up to 0.25 mm across	Fine-grained hypocrystalline, consisted of anhedral to subhedral felted plagioclase laths with subordinate anhedral to subhedral olivine, anhedral to subhedral clinopyroxene, anhedral to subhedral Fe-Ti oxides and pale	Vesicles and fractures infilled with carbonate, zeolite and iron oxides. Olivine moderately replaced by chlorite/serpentine, iddingsite and iron oxide minerals. Plagioclase slightly replaced by sericite and clay minerals.

		brown glass	Clinopyroxene slightly replaced by chlorite.
DC57 Ol 3% Plag 1% Cpx < 0.5%	Olivine + Plagioclase ± Clinopyroxene Aphyric, Olivine is the most abundant phenocrysts/microphenocrysts, following by plagioclase and clinopyroxene. They form as isolated crystals and a few as olivine-plagioclase glomerocrysts. Olivine: anhedral to euhedral with sizes up to 0.75 mm across Plagioclase: anhedral to subhedral with sizes up to 0.35 mm across Clinopyroxene: anhedral to subhedral with sizes up to 0.5 mm across	Moderately weathered holocrystalline, trachytic texture, consisted of anhedral to subhedral felted plagioclase laths with subordinate anhedral to subhedral olivine, anhedral to subhedral pink clinopyroxene and anhedral to subhedral Fe-Ti oxides Plagioclase laths show preferred orientation.	Vesicles and fractures infilled with carbonate, zeolite and iron oxides. Olivine moderately replaced by chlorite/serpentine, iddingsite and iron oxide minerals. Plagioclase slightly replaced by sericite and clay minerals. Clinopyroxene moderately replaced by chlorite.
DC58 Ol 3% Plag 1% Cpx < 0.5%	Olivine + Plagioclase ± Clinopyroxene Aphyric, Olivine is the most abundant phenocrysts/microphenocrysts, following by plagioclase and clinopyroxene. They form as isolated crystals and a few as olivine-plagioclase glomerocrysts. Olivine: anhedral to euhedral with sizes up to 0.7 mm across Plagioclase: anhedral to subhedral with sizes up to 0.35 mm across Clinopyroxene: anhedral to subhedral with sizes up to 0.33 mm across	Moderately weathered holocrystalline, trachytic texture, consisted of anhedral to subhedral felted plagioclase laths with subordinate anhedral to subhedral olivine, anhedral to subhedral pink clinopyroxene and anhedral to subhedral Fe-Ti oxides Plagioclase laths show preferred orientation.	Vesicles and fractures infilled with carbonate, zeolite and iron oxides. Olivine moderately replaced by chlorite/serpentine, iddingsite and iron oxide minerals. Plagioclase moderately replaced by sericite and clay minerals. Clinopyroxene slightly replaced by chlorite.
DC59 Ol 3% Plag 1% Cpx 0.5%	Olivine + Plagioclase ± Clinopyroxene Microphyric, Olivine is the most abundant phenocrysts/microphenocrysts, following by plagioclase and clinopyroxene. They form as isolated crystals and a few as olivine-plagioclase	Moderately weathered holocrystalline, trachytic texture, consisted of anhedral to subhedral felted plagioclase laths with subordinate anhedral to subhedral olivine,	Vesicles and fractures infilled with carbonate, zeolite and iron oxides. Olivine moderately replaced by chlorite/serpentine, iddingsite and iron oxide minerals.

	glomerocrysts. Olivine: anhedral to sparsely euhedral with sizes up to 1 mm across Plagioclase: anhedral to subhedral with sizes up to 0.33 mm across Clinopyroxene: anhedral to subhedral with sizes up to 0.52 mm across	anhedral to subhedral pink clinopyroxene and anhedral to subhedral Fe-Ti oxides. Plagioclase laths show preferred orientation.	Plagioclase slightly replaced by sericite and clay minerals. Clinopyroxene slightly replaced by chlorite.
DC60 Ol 3% Plag 1% Cpx 0.5%	Olivine + Plagioclase ± Clinopyroxene Microphyric, Olivine is the most abundant phenocrysts/microphenocrysts, following by plagioclase and clinopyroxene. They form as isolated crystals and a few as olivine-plagioclase glomerocrysts. Olivine: anhedral to euhedral with sizes up to 0.99 mm across Plagioclase: anhedral to subhedral with sizes up to 0.48 mm across Clinopyroxene: anhedral to subhedral with sizes up to 0.6 mm across	Moderately weathered holocrystalline, trachytic texture, consisted of anhedral to subhedral felted plagioclase laths with subordinate anhedral to subhedral olivine, anhedral to subhedral pink clinopyroxene and anhedral to subhedral Fe-Ti oxides Plagioclase laths show preferred orientation.	Vesicles and fractures infilled with carbonate, zeolite and iron oxides. Olivine moderately replaced by chlorite/serpentine, iddingsite and iron oxide minerals. Plagioclase slightly replaced by sericite and clay minerals. Clinopyroxene slightly replaced by chlorite.
DC61 Ol 3%	Olivine Aphyric, Olivine is the most abundant phenocrysts/microphenocrysts, following by plagioclase. They form as isolated crystals. Olivine: anhedral to sparsely euhedral with sizes up to 0.9 mm across	Hypocrystalline, composed of anhedral to subhedral felted plagioclase laths with subordinate anhedral to subhedral olivine, anhedral to subhedral clinopyroxene, pale brown glass and anhedral to subhedral Fe-Ti oxides	Vesicles and fractures infilled with carbonate, zeolite and iron oxides. Olivine slightly replaced by chlorite/serpentine, iddingsite and iron oxide minerals. Plagioclase slightly replaced by sericite and clay minerals.
DC62 Ol 3%	Olivine Microphyric, Olivine is the most abundant microphenocrysts, following by plagioclase. They form as isolated crystals. Olivine: anhedral to euhedral with sizes up to 0.48 mm across	Hypocrystalline, composed of anhedral to subhedral felted plagioclase laths with subordinate anhedral to subhedral olivine, anhedral to subhedral	Vesicles and fractures infilled with carbonate, zeolite and iron oxides. Olivine moderately replaced by chlorite/serpentine, iddingsite and iron

		clinopyroxene, brown glass and anhedral to subhedral Fe-Ti oxides	oxide minerals. Plagioclase slightly replaced by sericite and clay minerals.
DC63 Ol 1% Cpx < 0.5%	Olivine ± Clinopyroxene Aphyric, Olivine is the most abundant microphenocrysts, following by clinopyroxene. They form as isolated crystals. Olivine: anhedral to subhedral with sizes up to 0.66 mm across Clinopyroxene: anhedral to subhedral with sizes up to 0.54 mm across and sparsely shows stellate fashion	Moderately weathered holocrystalline, consisted of anhedral to subhedral felted plagioclase laths with subordinate anhedral to subhedral olivine, anhedral to subhedral pink clinopyroxene and anhedral to subhedral Fe-Ti oxides	Vesicles infilled with carbonate, zeolite and iron oxide minerals. Olivine moderately replaced by iddingsite and iron oxides. Plagioclase moderately replaced by sericite and clay minerals.
DC64 Ol 3% Plag 1%	Olivine + Plagioclase Aphyric, The most abundant phenocrysts/microphenocrysts is olivine, following by plagioclase. They form as isolated crystals. Olivine: anhedral to subhedral with sizes up to 1.5 mm across Plagioclase: anhedral to subhedral with sizes up to 0.78 mm across	Holocrystalline, composed of anhedral to subhedral felted plagioclase laths with subordinate anhedral to subhedral olivine, anhedral to subhedral Clinopyroxene and anhedral to subhedral Fe-Ti oxides	Vesicles and fractures partly infilled with carbonate, zeolite and iron oxide minerals. Olivine moderately replaced by chlorite/serpentine, iddingsite and iron oxide minerals. Plagioclase moderately replaced by sericite and clay minerals.
DC65 Ol 3% Plag 1% Cpx < 0.5%	Olivine + Plagioclase ± Clinopyroxene Microphyric, Olivine is the most abundant phenocrysts/microphenocrysts, following by plagioclase and clinopyroxene. They form as isolated crystals and a few as olivine-plagioclase glomerocrysts. Olivine: anhedral to euhedral with sizes up to 0.97 mm across Plagioclase: anhedral to subhedral with sizes up to 0.54 mm across	Slightly weathered hypocrystalline, consisted of anhedral to subhedral felted plagioclase laths with subordinate anhedral to subhedral olivine, anhedral to subhedral pink clinopyroxene, brown glass and anhedral to subhedral Fe-Ti oxides	Vesicles and fractures infilled with carbonate, zeolite and iron oxides. Olivine moderatelym replaced by chlorite/serpentine, iddingsite and iron oxide minerals. Plagioclase slightly replaced by sericite and clay minerals. Clinopyroxene slightly replaced by chlorite.

	Clinopyroxene: anhedral to subhedral with sizes up to 0.3 mm across		
DC66 Ol 3% Plag 2% Cpx < 0.5%	Olivine + Plagioclase ± Clinopyroxene Microphyric, Olivine is the most abundant phenocrysts/microphenocrysts, following by plagioclase and clinopyroxene. They form as isolated crystals and a few as olivine-plagioclase glomerocrysts. Olivine: anhedral to euhedral with sizes up to 0.78 mm across Plagioclase: anhedral to subhedral with sizes up to 0.33 mm across Clinopyroxene: anhedral to subhedral with sizes up to 0.33 mm across	Slightly weathered hypocrystalline, consisted of anhedral to subhedral felted plagioclase laths with subordinate anhedral to subhedral olivine, anhedral to subhedral pink clinopyroxene, brown glass and anhedral to subhedral Fe-Ti oxides	Vesicles and fractures infilled with carbonate, zeolite and iron oxides. Olivine slightly replaced by chlorite/serpentine, iddingsite and iron oxide minerals. Plagioclase slightly replaced by sericite and clay minerals. Clinopyroxene slightly replaced by chlorite.

Appendix C

1. Electron microprobe analysis

All analyses were performed from epoxy grain mounts using a CAMECA SX-50 electron microprobe at Central Science Laboratory (CSL), University of Tasmania calibrated with natural glass and mineral standards listed in Table C-1 (Jarosewich *et al.*, 1980). Concentrations were calculated from relative peak intensities using the PAP matrix correction procedure that is in incorporated into the Cameca software.

Table C-1 Natural standards

Olivine, San Carlos		USNM 111312/444
Fayalite, Rock Port		USNM 85276
Basaltic glass, Makaopuhi Lava Lake	VG-A99	USNM 113498/1
Basaltic glass, Juan de Fuca Ridge	VG-2	USNM 111249/52
Plagioclase, Lake Country		USNM 115900
Augite, Kakanui, NZ.		USNM 122142
Chromite, Tiebaghi Mine, NC.		USNM 117075

Routine analytical labels used for most microprobe analyses are often tested on the standard samples (OLIVINE & KSPCOLTR for olivine, LEOPYR for pyroxene, UVSPLEO for spinel and GLASSLEO for glass) together with their corresponding analytical conditions and counting times. A multi-purpose analytical label (MISCELLAN) was also used in which all elements were analysed at 20 seconds on the peak and 10 seconds on the background except for Si and Na that were analysed at 10 and 15 seconds.

Analytical conditions for the analyses of olivine, clinopyroxene and plagioclase phenocryst and microphenocryst phases were 15 kV accelerating voltage, 25 nA beam current, and 5 μm beam size. Mineral and melt inclusions in sapphires were analysed were 15 kV accelerating voltage and 10-20 nA beam current. For melt inclusion glasses, beam size was varied between 1-5 μm depending on the size of the melt inclusion.

2. Rare earth elements

Rock samples were crushed in a steel-jaw crusher and the pea-sized fragment hand picked and recrushed in a Chrome-Steel mill. Rare earth elements (REE) were obtained from a HP4500 Inductively Couple Plasma Mass Spectrometer (ICP-MS), housed at the School of Earth Sciences, University of Tasmania. Detection limits of ICP-MS analysis are listed in Table C-2.

Table C-2 ICP-MS detection limits

Elements	Dectection limits (ppm)
La	0.00174
Ce	0.00137
Pr	0.00034
Nd	0.00131
Sm	0.00128
Eu	0.00055
Gd	0.00144
Tb	0.00021
Dy	0.00058
Ho	0.00022
Er	0.00044
Tm	0.00019
Yb	0.00071

Appendix D-1

Electron microprobe analyses of olivine phenocrysts/microphenocrysts of the Denchai basalts

Group A

Sample	dc25	dc25	dc25	dc28	dc28	dc28	dc42	dc42	dc42	dc42	dc42	dc42
SiO_2	38 41	39.12	39 42	38.24	38 85	39.20	37.94	38.02	38.45	38 63	38.64	38.66
TiO_2	0 01	0.01	nd	0.04	0.01	0.02	0.02	0 04	0.02	0 06	0.05	nd
Al_2O_3	0 02	0.03	0 05	0.02	0.05	0 09	0.11	0 05	0 05	0 05	0.05	0.06
Cr_2O_3	0 06	0.01	0 07	0.04	nd	nd	0.03	0 04	nd	nd	nd	nd
FeO	21 59	18 29	17 79	21 23	19 62	17 72	23.67	22 58	22 91	23.35	23.76	23.15
MnO	0.38	0 21	0 21	0 32	0.32	0.21	0 47	0.32	0 27	0 43	0 34	0.39
MgO	39 75	42.56	42 90	39 87	41.11	42 76	37.44	38 58	38 83	38.56	38.67	38.52
CaO	0.12	0.24	0 24	0 26	0.20	0.25	0.35	0 29	0.21	0 26	0.25	0 21
NiO	0 15	0 16	0 22	0 14	0.24	0.15	0.16	0 09	nd	0 10	0.01	0 03
Total	100 49	100.63	100.90	100 17	100.39	100.38	100.20	100.01	100 74	101.43	101 77	101 03
Si	0 992	0.993	0 995	0 990	0.995	0.994	0 994	0.992	0 995	0.996	0 994	0 999
Ti	nd	nd	nd	nd	nd	nd	nd	0.001	nd	0.001	0 001	nd
Al/Al IV	nd	0 001	0 001	0.001	0.002	0 003	0 004	0.002	0 002	0.001	0 002	0.002
Cr	0.001	nd	0.001	0 001	nd	nd	0 001	0.001	nd	nd	nd	nd
Fe^{2+}	0 467	0.388	0 376	0 460	0.420	0 376	0 519	0.493	0.496	0 503	0 511	0 500
Mn^{2+}	0.008	0.005	0.004	0 007	0 007	0 005	0.010	0.007	0 006	0.009	0 007	0.009
Mg	1 531	1.610	1.614	1 539	1 569	1.617	1.462	1 501	1 498	1 482	1.483	1 484
Ca	0 003	0.007	0.007	0 007	0.006	0.007	0.010	0.008	0.006	0 007	0.007	0 006
Ni	0 003	0.003	0 004	0 003	0.005	0.003	0.003	0.002	nd	0 002	nd	0.001
Sum Cat#	3 006	3.007	3.003	3.008	3.004	3.004	3.003	3.006	3 003	3 002	3.004	3.000
Fa	0.23	0 19	0.19	0.23	0 21	0.19	0.26	0 25	0 25	0.25	0.26	0.25
Fo	0 77	0 81	0.81	0 77	0 79	0.81	0.74	0 75	0 75	0.75	0.74	0.75

Group A

Sample	dc42	dc42	dc42	dc42	dc42	dc42	dc42	dc42	dc42	dc42	dc42	dc42
SiO_2	38 69	38 69	38 90	39.12	39 30	39 94	40 29	40 43	40.49	40 58	40 72	40 81
TiO_2	0.04	0.04	0 05	0 03	0 02	0.01	0 01	nd	0 02	0.01	0 03	0 02
Al_2O_3	0.08	0.06	0 05	0.06	0.05	0 05	0 02	0.08	0.06	0 05	0 04	0.06
Cr_2O_3	nd	nd	nd	nd	nd	nd	0 07	0.02	0.12	0 04	0 09	0.01
FeO	23.63	22.90	22 26	17 17	15.73	13 37	15.22	13.67	14.50	14 13	13.66	13.90
MnO	0.33	0.33	0 43	0 29	0.20	0.20	0 23	0 22	0.22	0.21	0.12	0.13
MgO	38 67	39.15	39.50	43 10	44.55	46.28	45.32	46.21	45.68	45.71	46.19	45.77
CaO	0.23	0.24	0.26	0.23	0.28	0.23	0.22	0.23	0 23	0 20	0.21	0.21
NiO	nd	0.07	0.15	nd	0.22	0.33	0.21	0.23	0.25	0 22	0.32	0.27
Total	101 66	101 48	101.59	100 01	100 36	100 40	101 59	101.08	101.57	101.16	101 38	101 19
Si	0.995	0.994	0 996	0.994	0.989	0.993	0 997	0.999	0 999	1.003	1.002	1 007
Ti	0 001	0 001	0.001	0.001	nd	nd	nd	nd	nd	nd	0.001	nd
Al/Al IV	0.002	0.002	0 002	0 002	0.002	0.001	0 001	0.002	0.002	0.002	0.001	0.002
Cr	nd	nd	nd	nd	nd	nd	0 001	nd	0.002	0.001	0 002	nd
Fe^{2+}	0.508	0 492	0.477	0.365	0.331	0 278	0.315	0 282	0 299	0 292	0.281	0 287
Mn^{2+}	0.007	0 007	0 009	0.006	0.004	0 004	0 005	0.005	0.005	0.004	0 002	0 003
Mg	1.483	1 500	1.507	1.631	1.671	1 716	1.672	1.701	1 680	1 684	1.694	1 683
Ca	0.006	0.007	0 007	0 006	0.007	0 006	0.006	0 006	0 006	0 005	0 006	0.005
Ni	nd	0.001	0.003	nd	0 004	0.007	0.004	0 005	0.005	0 004	0 006	0.005
Sum Cat#	3 003	3.004	3.002	3 005	3 010	3.006	3.001	3.000	2.999	2.996	2 996	2.992
Fa	0.26	0.25	0.24	0.18	0.17	0 14	0 16	0.14	0.15	0 15	0 14	0.15
Fo	0 75	0 75	0.76	0 82	0 84	0.86	0.84	0.86	0 85	0 85	0.86	0.85

nd = not detected

Appendix D-1 (Continued)

Group B

Sample	dc5	dc5	dc5	dc5	dc5	dc5	dc19	dc19	dc19	dc19	dc19	dc23
SiO_2	40 41	40 60	40.99	41 02	41 02	41.28	38.96	39 65	39.74	40.47	40.48	39.02
TiO_2	nd	0 03	nd	0 01	0 01	nd	0.02	0 02	0.03	0 01	0 03	0.02
Al_2O_3	0 03	0 02	0 04	0.01	0.04	0 02	0.04	0 07	0.06	0.03	0.03	0 05
Cr_2O_3	0 01	nd	0 03	nd	0 03	0.03	0 08	0 04	0.04	0 02	0 03	0.05
FeO	9 76	10 43	10.32	9 81	10 70	8 88	17 44	13.87	14.01	10.31	10 27	17 02
MnO	0 20	0.15	0 19	0 19	0 11	0.11	0 32	0.24	0.22	0 16	0 10	0 25
MgO	48.76	48.57	48.72	48.64	48 55	49 97	42 43	45 31	45 38	48 78	48 87	43 35
CaO	0.08	0.08	0.07	0.06	0.11	0 10	0.30	0.20	0 21	0.10	0 08	0.20
NiO	0 34	0.40	0 45	0 38	0 30	0.43	0.19	0.21	0 21	0.36	0 37	0.22
Total	99 60	100 27	100.81	100 13	100 87	100.83	99.77	99.62	99.89	100.23	100.24	100.18
Si	0 996	0.997	1 000	1.005	1.001	1 000	0.995	0.996	0 996	0 994	0.994	0.990
Ti	nd	0.001	nd	nd	nd	nd	nd	nd	nd	nd	0.001	nd
Al/Al IV	0 001	0.001	0 001	0 000	0.001	0 001	0 001	0.002	0.002	0 001	0.001	0.002
Cr	nd	nd	0 001	nd	0.001	0 001	0 002	0.001	0.001	nd	0.001	0.001
Fe^{2+}	0 201	0.214	0.211	0 201	0 218	0 180	0 372	0.291	0 294	0 212	0 211	0 361
Mn^{2+}	0 004	0.003	0 004	0 004	0.002	0 002	0.007	0 005	0 005	0 003	0 002	0 005
Mg	1.792	1 777	1 772	1 776	1 766	1.805	1.614	1 696	1 695	1.785	1 788	1.639
Ca	0 002	0.002	0 002	0.002	0 003	0 003	0.008	0 005	0 006	0.003	0.002	0.005
Ni	0 007	0 008	0.009	0 008	0.006	0 008	0.004	0.004	0 004	0 007	0 007	0 004
Sum Cat#	3 003	3 002	2.999	2 995	2.998	2.999	3.003	3.002	3 002	3.005	3.005	3 008
Fa	0 10	0 11	0.11	0 10	0.11	0.09	0.19	0.15	0.15	0.11	0.11	0 18
Fo	0 90	0.89	0.89	0 90	0.89	0 91	0.81	0 85	0 85	0.89	0 90	0 82

Group B

Sample	dc23	dc23	dc23	dc23	dc27	dc27	dc27	dc27	dc27	dc55	dc55	dc55
SiO_2	40 17	40 61	40.84	40.87	38.34	39.34	39 60	40.37	40 52	40.74	38 10	39 06
TiO_2	0 02	0 01	nd	0 03	0 04	0.01	0.01	0 02	0 01	0 02	nd	0 03
Al_2O_3	0.04	nd	0 01	0 02	0 06	0.06	0.05	0.03	0 03	0 03	0 07	0 04
Cr_2O_3	0.06	0 03	nd	nd	0 04	nd	nd	0 04	0 01	0 01	nd	nd
FeO	10.27	9.73	9 24	10 58	20 52	16 59	15.13	10 50	10.31	8 64	22 04	17.77
MnO	0 18	0.19	0 12	0 09	0.22	0 27	0.20	0.20	0.12	0.15	0 45	0.41
MgO	48 67	49.51	49 64	48.15	40 53	43 67	44.61	48 49	48.41	49.85	39.08	42 62
CaO	0 08	0 05	0.07	0.03	0 21	0.19	0 20	0.17	0 08	0.08	0.41	0 26
NiO	0 40	0 41	0.55	0 40	0 11	0.19	0 18	0 39	0 43	0 41	0 13	0.31
Total	99.89	100.54	100.47	100.18	100.07	100.33	99.97	100.21	99.92	99.91	100 28	100.49
Si	0 991	0.992	0 996	1.004	0.990	0.994	0 996	0.993	0.998	0 996	0 990	0 992
Ti	nd	nd	nd	0 001	0 001	nd	nd	nd	nd	nd	nd	0.001
Al/Al IV	0 001	nd	nd	0.001	0 002	0 002	0 002	0.001	0 001	0.001	0 002	0.001
Cr	0 001	0.001	nd	nd	0.001	nd	nd	0 001	nd	nd	nd	nd
Fe^{2+}	0.212	0 199	0.188	0.217	0 443	0 350	0.318	0.216	0 212	0 177	0 479	0 377
Mn^{2+}	0 004	0.004	0 003	0 002	0.005	0 006	0.004	0.004	0.003	0 003	0 010	0.009
Mg	1 789	1.802	1.804	1 763	1.559	1 644	1.673	1.778	1.777	1 816	1 514	1 614
Ca	0.002	0.001	0.002	0 001	0.006	0.005	0 005	0.004	0.002	0.002	0.011	0 007
Ni	0.008	0 008	0 011	0.008	0 002	0 004	0 004	0 008	0.008	0.008	0 003	0.006
Sum Cat#	3 008	3.007	3.004	2 995	3.008	3 005	3 003	3.006	3.001	3.003	3.009	3.007
Fa	0.11	0.10	0.10	0 11	0 22	0.18	0.16	0.11	0 11	0 09	0 24	0.19
Fo	0.89	0.90	0 91	0 89	0 78	0.82	0.84	0.89	0 89	0 91	0 76	0.81

nd = not detected

Appendix D-1 (Continued)

Group B

Sample	dc55	dc55	dc55	dc55	dc61	dc61	dc61	dc61	dc61	dc61	dc61	dc61
SiO_2	39.85	40 09	40.12	40.74	39 30	39.52	40 06	40.13	40.22	40 49	40 68	40 75
TiO_2	nd	0.02	0.03	0 02	0 04	nd	0.01	0 03	0.01	nd	0 01	0.04
Al_2O_3	0 02	0.05	0 04	0 03	0.04	0.02	0 07	0 07	0.04	0 01	0 08	0.32
Cr_2O_3	nd	0.05	0 06	0 01	0.01	nd	0 03	nd	0 03	0 02	nd	0.01
FeO	13 83	11.40	12.54	8.64	18 72	16.76	14.12	14.90	14.29	11 63	12 25	12.31
MnO	0 20	0 15	0 22	0 15	0.36	0.34	0.25	0.25	0.19	0.14	0.16	0.25
MgO	45.71	47.50	47.10	49.85	41.72	43 45	45 47	45.35	45 18	47.65	46.86	46 29
CaO	0 15	0.12	0 10	0 08	0.31	0.09	0.24	0.24	0.25	0.09	0.16	0.23
NiO	0.36	0 35	0 32	0.41	0.22	0.31	0.41	0.24	0.26	0.44	0.39	0 32
Total	100 14	99.74	100.54	99 91	100 73	100 50	100.66	101.22	100 48	100.47	100.59	100 52
Si	0.996	0 995	0 993	0.996	0 999	0.997	0.997	0.996	1.002	0.998	1.003	1.005
Ti	nd	nd	0.001	nd	0 001	nd	nd	0.001	nd	nd	nd	0.001
Al/Al IV	0 001	0.001	0 001	0 001	0.001	0.001	0.002	0.002	0 001	0.000	0.002	0 009
Cr	nd	0 001	0 001	nd	nd	nd	0.001	nd	0 001	nd	nd	nd
Fe^{2+}	0.289	0.236	0 259	0 177	0.398	0.354	0 294	0.309	0 298	0.240	0 253	0 254
Mn^{2+}	0.004	0.003	0.005	0 003	0 008	0 007	0.005	0 005	0.004	0.003	0 003	0 005
Mg	1 703	1.756	1.737	1.816	1.580	1 634	1 687	1 678	1.678	1.750	1.722	1.702
Ca	0.004	0.003	0.003	0.002	0.008	0 003	0 006	0 006	0.007	0 002	0 004	0.006
Ni	0.007	0.007	0 006	0.008	0.005	0 006	0 008	0 005	0.005	0.009	0 008	0 006
Sum Cat#	3.004	3.004	3.006	3.003	3 000	3 002	3 001	3 002	2.997	3.002	2 996	2.989
Fa	0.15	0 12	0 13	0.09	0.20	0 18	0.15	0 16	0.15	0.12	0 13	0.13
Fo	0 86	0.88	0.87	0.91	0 80	0 82	0.85	0.84	0 85	0 88	0.87	0.87

Group B

Sample	dc61	dc61	dc61	dc62	dc62	dc62	dc62	dc62	dc62	dc62	dc62	dc62
SiO_2	40.90	41.17	41 19	39.37	39.85	40 42	40 63	40 75	40.90	40.93	40.97	41.05
TiO_2	0.05	0 02	nd	nd	nd	nd	0 04	0.02	0.01	0.01	nd	nd
Al_2O_3	0.03	0 01	0.02	0.04	0 01	0.02	nd	0.03	0.03	nd	0.05	0 02
Cr_2O_3	nd	0 02	nd	nd	0 02	0.01	nd	0 01	0.03	0.03	nd	0 03
FeO	11 54	10.43	10.56	17 46	14 82	10 28	11.01	9 72	10 26	9.03	9 68	9 07
MnO	0.25	0.14	0.11	0 25	0 25	0.15	0 16	0.13	0 17	0 09	0 10	0 16
MgO	47.43	48.83	48 52	42.18	44.42	48.19	47.93	48.83	48.64	49 75	48 66	49.46
CaO	0.19	0 08	0.07	0.26	0.15	0 13	0 11	0.07	0.11	0 08	0 10	0.11
NiO	0 31	0.39	0.37	0 15	0 38	0 36	0 34	0.42	0 36	0.37	0.34	0 33
Total	100.70	101.09	100 85	99.72	99 91	99 56	100.23	100.00	100.50	100 29	99 90	100 24
Si	1 004	1 001	1.004	1 004	1.002	0 999	1 000	1.000	1.000	0 998	1.005	1 001
Ti	0 001	nd	nd	nd	nd	nd	0 001	nd	nd	nd	nd	nd
Al/Al IV	0.001	nd	0 001	0.001	nd	0.001	nd	0.001	0.001	nd	0 001	0 001
Cr	nd	nd	nd	nd	nd	nd	nd	nd	0.001	0.001	nd	0 001
Fe^{2+}	0.237	0.212	0 215	0 372	0 312	0.212	0.227	0 200	0.210	0.184	0 198	0.185
Mn^{2+}	0.005	0.003	0 002	0.005	0.005	0.003	0.003	0 003	0.004	0.002	0.002	0.003
Mg	1.735	1.771	1.763	1 603	1 665	1 775	1.759	1 786	1 773	1 808	1.779	1.798
Ca	0 005	0.002	0.002	0 007	0 004	0.003	0 003	0 002	0.003	0.002	0 003	0 003
Ni	0.006	0.008	0.007	0 003	0 008	0.007	0 007	0.008	0.007	0.007	0 007	0 006
Sum Cat#	2.995	2.998	2.995	2.996	2 997	3.001	2 999	2.999	2.999	3.002	2 995	2 998
Fa	0.12	0.11	0 11	0 19	0 16	0 11	0.11	0.10	0.11	0 09	0 10	0 09
Fo	0.88	0 89	0 89	0 81	0 84	0.89	0.89	0 90	0 89	0 91	0.90	0.91

nd = not detected

Appendix D-1 (Continued)

Group C

Sample	dc15	dc15	dc15	dc16	dc16	dc16	dc16	dc16	dc16	dc16	dc16	dc16
SiO_2	39.03	39 15	40 18	37 80	38 37	39 23	39.70	40 12	40 37	40 47	40 53	40.82
TiO_2	0.01	0.02	nd	0.03	0 01	0 03	nd	0 02	nd	0 04	nd	nd
Al_2O_3	0.04	0 06	0.07	0.01	0 03	0 02	0 05	0.04	0.02	0.04	0 01	0.01
Cr_2O_3	nd	0 04	0.05	0.06	0 04	nd	0.04	nd	nd	0.04	nd	nd
FeO	17 00	17.51	14.47	27.00	19.76	19.94	18 27	12.46	13 23	11.18	13 34	13.43
MnO	0.25	0 26	0 13	0.46	0 33	0.34	0 30	0.12	0.17	0.17	0 18	0 16
MgO	43.33	42 74	45.65	35 21	41.05	40 99	42.82	46.99	46 92	47.62	46.99	46 59
CaO	0 25	0.20	0 23	0.33	0 29	0.26	0 24	0.10	0.08	0.11	0 08	0.09
NiO	0.19	0 19	0 26	0 08	0.17	0 14	0 22	0.40	0 33	0.38	0 29	0 24
Total	100 09	100 17	101.04	100 97	100.05	100 94	101.65	100 25	101.12	100.04	101 42	101 34
Si	0 991	0.995	0 997	0 997	0 988	0 999	0.997	0.995	0.995	0.999	0 996	1 003
Ti	nd	nd	nd	0 001	nd	0 001	nd	nd	nd	0.001	nd	nd
Al/Al IV	0 001	0 002	0.002	nd	0.001	0 001	0.002	0 001	0 001	0.001	nd	nd
Cr	nd	0.001	0 001	0 001	0 001	0 000	0.001	nd	nd	0.001	nd	nd
Fe^{2+}	0 361	0.372	0 300	0.596	0 426	0.425	0 384	0 258	0.273	0.231	0.274	0 276
Mn^{2+}	0 005	0.006	0.003	0 010	0.007	0 007	0 006	0 003	0.004	0.003	0.004	0 003
Mg	1 639	1 619	1.688	1 385	1.576	1 557	1.602	1 737	1.724	1.753	1.722	1.707
Ca	0 007	0 006	0 006	0 009	0.008	0 007	0.006	0.003	0 002	0.003	0.002	0.002
Ni	0.004	0.004	0.005	0 002	0 004	0 003	0 004	0.008	0 007	0.007	0.006	0.005
Sum Cat#	3.008	3 004	3 002	3 001	3.011	3 000	3 002	3.004	3 005	2.999	3 004	2.997
Fa	0 18	0.19	0 15	0.30	0.21	0.21	0 19	0 13	0.14	0.12	0.14	0 14
Fo	0 82	0 81	0.85	0 70	0.79	0 79	0 81	0.87	0 86	0.88	0.86	0.86

Group C

Sample	dc17	dc17	dc17	dc17	dc17	dc17	dc30	dc30	dc36	dc36	dc36	dc36
SiO_2	38.79	39.44	39 50	39.55	39 79	40.23	38.99	39.98	37.83	37 92	38 32	38.53
TiO_2	0.05	0 02	nd	0.02	0 04	nd	0 03	nd	0.04	0 01	0.02	0 01
Al_2O_3	0 04	0 02	0.03	nd	0 03	0 04	0.03	0.05	0.03	0 03	0.01	0 05
Cr_2O_3	0.01	0 01	0.03	nd	0 01	0.04	0 05	0.01	nd	0 03	nd	nd
FeO	22.04	17 75	16.54	17 57	15.90	13 54	16 95	11.63	26.03	25 40	24.23	23.18
MnO	0.28	0 27	0.23	0 20	0.26	0 17	0 27	0.16	0.35	0 43	0.37	0.34
MgO	38 58	42.36	43.82	43 02	44 06	46.16	43 18	47.89	36 01	36 62	37.50	38 45
CaO	0.27	0.28	0 16	0.16	0.22	0 17	0.27	0 08	0.30	0 28	0.28	0.30
NiO	0.14	0 16	0 27	0.26	0.24	0.27	0.15	0 40	0 17	0.15	0 09	0.14
Total	100.20	100 29	100.58	100 77	100 55	100.62	99.91	100.20	100.76	100.86	100 83	101 00
Si	1.005	1.001	0 995	0.998	0.999	0.998	0.991	0.989	0.996	0 994	0 998	0.997
Ti	0.001	nd	nd	nd	0 001	nd	nd	nd	0 001	nd	nd	nd
Al/Al IV	0.001	nd	0 001	nd	0 001	0.001	0.001	0.002	0 001	0 001	nd	0 001
Cr	nd	nd	0 001	nd	nd	0.001	0 001	nd	nd	0 001	nd	nd
Fe^{2+}	0.478	0.377	0 348	0.371	0 334	0 281	0 360	0.241	0.573	0 557	0.528	0 502
Mn^{2+}	0.006	0.006	0 005	0.004	0.006	0 003	0 006	0.003	0.008	0 010	0.008	0.007
Mg	1.491	1 603	1.645	1.618	1 649	1 707	1.637	1.766	1.413	1.431	1 456	1 483
Ca	0 007	0.007	0.004	0.004	0 006	0 005	0.007	0.002	0 008	0.008	0 008	0 008
Ni	0 003	0.003	0.005	0.005	0 005	0.005	0.003	0.008	0 004	0.003	0.002	0 003
Sum Cat#	2 993	2.998	3 004	3 002	3.000	3 001	3.007	3.010	3 003	3 005	3.001	3 002
Fa	0 24	0.19	0 18	0.19	0 17	0.14	0.18	0.12	0 29	0.28	0 27	0 25
Fo	0.76	0.81	0.83	0 81	0 83	0 86	0.82	0 88	0.71	0 72	0 73	0 75

nd = not detected

Appendix D-1 (Continued)

Group C

Sample	dc36	dc59	dc59	dc59
SiO_2	38.64	39 07	39 10	39.19
TiO_2	0.02	0 02	0 03	0 03
Al_2O_3	0.03	0.04	0 04	0.02
Cr_2O_3	nd	0.06	0.01	nd
FeO	23.53	18.02	17.65	18 78
MnO	0.28	0.23	0 22	0.31
MgO	38.79	41.86	42.25	41 75
CaO	0.24	0 25	0.17	0 30
NiO	0.09	0.13	0 19	0 16
Total	101.61	99.69	99.67	100.53
Si	0 994	1.000	0.999	0 998
Ti	nd	nd	0.001	0 001
Al/Al IV	0 001	0 001	0 001	0 001
Cr	nd	0.001	nd	nd
Fe^{2+}	0.506	0 386	0.377	0.400
Mn^{2+}	0.006	0.005	0 005	0 007
Mg	1.488	1.596	1.609	1 584
Ca	0.007	0.007	0 005	0 008
Ni	0 002	0 003	0 004	0 003
Sum Cat#	3.005	2 999	3 000	3.001
Fa	0 25	0 20	0 19	0 20
Fo	0 75	0 81	0.81	0 80

Group D

Sample	dc11	dc11	dc11	dc13	dc53	dc53
SiO_2	38 92	39 22	39.39	41 15	38.76	39.13
TiO_2	0.03	0 04	0.02	nd	0 03	0 03
Al_2O_3	0.06	0 06	0 05	0.02	0.06	0 06
Cr_2O_3	0.05	0.03	0 02	0 03	0.06	0.02
FeO	16 47	16 61	16.06	10 22	20 28	18 76
MnO	0.21	0.18	0 20	0 15	0 25	0.23
MgO	43.18	43 94	43.82	48 87	40 55	42 35
CaO	0.29	0.23	0.25	0 08	0 27	0.20
NiO	0 15	0.27	0.24	0.36	0 21	0.16
Total	99 37	100 57	100 05	100.88	100 46	100.93
Si	0 993	0 989	0.995	1.002	0.995	0.992
Ti	0 001	0.001	nd	nd	0 001	nd
Al/Al IV	0 002	0.002	0.002	nd	0 002	0.002
Cr	0 001	0 001	nd	0 001	0.001	nd
Fe^{2+}	0.351	0.350	0.339	0.208	0 435	0.398
Mn^{2+}	0.005	0 004	0.004	0 003	0.005	0 005
Mg	1.642	1 651	1 651	1 774	1.552	1 600
Ca	0.008	0 006	0 007	0 002	0.007	0 005
Ni	0 003	0.005	0 005	0 007	0.004	0.003
Sum Cat#	3 005	3 009	3 003	2 997	3 003	3 006
Fa	0 18	0 18	0.17	0.11	0 22	0 20
Fo	0.82	0 83	0 83	0 90	0 78	0 80

Group D

Sample	dc53	dc63	dc63	dc63	dc63	dc63	dc63	dc63	dc63	dc66	dc66	dc66
SiO_2	39 42	37.68	38 34	39 17	39.51	39 80	40.02	40.17	40.22	38.21	38.46	38.98
TiO_2	0.03	0.05	0 02	0 01	0.01	0.01	0.03	0.04	0.03	0.09	0 02	nd
Al_2O_3	0 05	0 09	0.05	0.04	0.04	0.06	0 07	0 05	0.05	0.06	0 05	0 06
Cr_2O_3	0.03	nd	nd	nd	0.01	0 01	nd	nd	0 02	0 01	0 02	0 04
FeO	15.59	27 16	23 40	20 19	17 67	17.05	15 47	14 32	14.07	23 35	20 36	18 27
MnO	0 28	0 38	0 34	0 35	0.28	0 21	0.25	0.22	0.20	0.36	0 30	0.22
MgO	43 97	35.47	38 07	41 24	42 72	43.38	44 44	45 40	45 53	37 36	40 48	41 57
CaO	0 21	0 16	0.13	0.26	0.16	0.12	0 21	0.17	0.06	0.29	0 27	0.22
NiO	0 30	0.10	0.08	0 13	0 16	0 14	0 14	0.21	0.30	0.14	0.13	0 19
Total	99.87	101.09	100 43	101 40	100 57	100 79	100 64	100 58	100.49	99.86	100 07	99 56
Si	0.996	0.993	0.998	0.995	0.999	1.001	1.001	1.000	1.001	1 001	0.992	1.000
Ti	0.001	0.001	nd	nd	nd	nd	0.001	0 001	nd	0 002	nd	nd
Al/Al IV	0 002	0.003	0.002	0.001	0 001	0 002	0.002	0 001	0 002	0.002	0.001	0 002
Cr	0.001	nd	nd	nd	nd	nd	nd	nd	nd	nd	nd	0 001
Fe^{2+}	0.329	0.599	0.510	0 429	0 374	0 359	0.324	0 298	0 293	0 512	0.439	0 392
Mn^{2+}	0.006	0 009	0 007	0 008	0.006	0.005	0.005	0 005	0.004	0.008	0.007	0.005
Mg	1.656	1 394	1 478	1 562	1 611	1.626	1 657	1 685	1 689	1 460	1.556	1.589
Ca	0.006	0 005	0 004	0 007	0 004	0 003	0.006	0.005	0 002	0.008	0.007	0.006
Ni	0 006	0 002	0.002	0 003	0 003	0 003	0.003	0.004	0.006	0.003	0.003	0.004
Sum Cat#	3 002	3 005	3.000	3.004	3 000	2.998	2 998	2 998	2.997	2.996	3.007	2.999
Fa	0 17	0 30	0.26	0.22	0.19	0.18	0 16	0.15	0 15	0.26	0.22	0.20
Fo	0 83	0 70	0.74	0.78	0.81	0.82	0.84	0 85	0 85	0 74	0.78	0.80

nd = not detected

Appendix D-1 (Continued)

Group D

Sample	dc66	dc66	dc66	dc66
SiO_2	39 04	39 12	39.14	39.14
TiO_2	0 03	0.03	nd	nd
Al_2O_3	0 05	0.05	0.05	0.06
Cr_2O_3	0 05	0.03	0.02	0.04
FeO	19.12	19.22	17.56	16 80
MnO	0.23	0 18	0.22	0.23
MgO	41.40	41 51	43.22	42.87
CaO	0.28	0.20	0 22	0.19
NiO	0 15	0 24	0 26	0 25
Total	100.35	100 60	100 69	99.57
Si	0.997	0 997	0 990	0.997
Ti	0 001	0 001	nd	nd
Al/Al IV	0 002	0.002	0.001	0 002
Cr	0 001	0.001	nd	0 001
Fe^{2+}	0 409	0.410	0.372	0 358
Mn^{2+}	0.005	0.004	0.005	0 005
Mg	1.576	1.577	1 630	1 628
Ca	0.008	0.006	0 006	0 005
Ni	0 003	0.005	0 005	0.005
Sum Cat#	3.001	3 001	3.009	3 001
Fa	0 21	0.21	0 19	0.18
Fo	0 79	0 79	0 81	0.82

nd = not detected

Appendix D-2

Electron microprobe analyses of clinopyroxene phenocrysts/microphenocrysts of the Denchai basalts

Group A

Sample	dc25	dc25	dc25	dc28	dc28	dc28	dc42	dc42	dc42	dc42	dc42
SiO_2	46 88	48 29	48.33	47 36	47.98	49 35	49.08	49 61	50 19	50 30	50.38
TiO_2	1 96	1.43	1.95	1.47	1 10	1.05	1 69	1.58	1.32	1 30	1 51
Al_2O_3	8.87	7 20	4.61	8 02	7 22	5.92	4.44	5.16	4.00	3 98	3.80
Cr_2O_3	0 60	0 24	0 52	0 49	0 83	0.49	0 22	0.54	0.39	0 38	0 26
FeO*	6.52	6 56	6 69	6.32	6.10	6.06	6 46	6.05	5.89	6.11	7.01
MnO	0 15	0 09	0.15	0.18	0.20	0.15	0 15	0.09	0.13	0 18	0.09
MgO	13 72	14.24	13 73	14 28	14 98	15 23	14.73	14.46	14.89	14.77	14.89
CaO	21 25	21.10	23 21	20.92	20 22	20.58	22.33	22.66	22.65	22.75	22.00
Na_2O	0 65	0.70	0 43	0.68	0 69	0.70	0 34	0.43	0.41	0 36	0.36
Total	101 01	100.22	100 05	100.14	99 74	99 87	99.77	100.83	100 14	100 37	100.51
Si	1 715	1.775	1 797	1.742	1.768	1.814	1 820	1 819	1.850	1.852	1.856
Ti	0 054	0 039	0 055	0 041	0 030	0.029	0 047	0.044	0 037	0 036	0.042
Al/Al IV	0.285	0 225	0.202	0.258	0 232	0.186	0.180	0.181	0.150	0 148	0.144
Al VI	0.097	0 087	nd	0.090	0 081	0.071	0 015	0 042	0 024	0.025	0 020
Cr	0.017	0 007	0.015	0 014	0 024	0.014	0.007	0 016	0 011	0 011	0 008
Fe^{3+}	0.109	0 102	0 112	0 121	0 116	0.093	0 089	0 068	0 071	0.066	0 058
Fe^{2+}	0 091	0 100	0 096	0.073	0 073	0 093	0 112	0 118	0.111	0 123	0 158
Mn^{2+}	0.005	0.003	0 005	0 006	0 006	0.005	0.005	0.003	0 004	0 006	0.003
Mg	0.748	0 780	0.761	0 783	0 822	0 834	0 814	0.790	0 818	0 811	0 818
Ca	0.833	0 831	0.925	0 824	0.798	0 811	0.887	0.890	0 895	0 898	0 868
Na	0.046	0 050	0.031	0 048	0.049	0 050	0.025	0 030	0 029	0.026	0 025
Sum Cat#	4.000	4.000	4 000	4.000	4 000	4.000	4.000	4 000	4.000	4 000	4.000
Mg#	78 9	79.4	78 5	80.1	81.3	81 8	80 2	80 9	81.8	81.1	79.1
Ca#	46.6	45 8	48.7	45 6	44.0	44.2	46 5	47.6	47 1	47.2	45 6
Wo	46 6	45.8	48 7	45.6	44.0	44 2	46.5	47 6	47 1	47 2	45 6
En	41 9	43.0	40.1	43 3	45.3	45 4	42 7	42.3	43 1	42.6	42 9
Fs	11 5	11.3	11.2	11 1	10.7	10 4	10 8	10.1	9.8	10.2	11.5

Group A

Sample	dc42	dc42	dc42	dc42	dc42
SiO_2	52.65	52 69	52 95	53.05	53 24
TiO_2	0.55	0.60	0 56	0 28	0.49
Al_2O_3	2 75	2 42	2 58	1 60	2.17
Cr_2O_3	0.56	0.16	0.27	0.16	0 32
FeO*	5.71	7.45	6.69	6 64	6 13
MnO	0.15	0.20	0 19	0.18	0.13
MgO	15 53	15 49	15.85	15 92	15 57
CaO	22 42	21.48	21.61	22 05	22 40
Na_2O	0 45	0 38	0.40	0 34	0 39
Total	100 89	101 01	101 21	100 38	100.91
Si	1.920	1 927	1.926	1.947	1.942
Ti	0 015	0.017	0.015	0 008	0.014
Al/Al IV	0.080	0.073	0 074	0 053	0.058
Al VI	0.038	0.031	0 037	0.016	0.036
Cr	0.016	0.005	0.008	0.005	0 009
Fe^{3+}	0.028	0.032	0 027	0.042	0.013
Fe^{2+}	0 146	0 196	0 176	0.162	0.174
Mn^{2+}	0 005	0.006	0.006	0 006	0.004
Mg	0 844	0.844	0 860	0 871	0.847
Ca	0.876	0 842	0.842	0.867	0 876
Na	0 032	0 027	0 029	0 025	0 028
Sum Cat#	4 000	4.000	4.000	4 000	4.000
Mg#	82.9	78 7	80 9	81.0	81.9
Ca#	46.1	43.9	44 1	44 5	45.8
Wo	46 1	43.9	44.1	44 5	45 8
En	44.4	44 0	45.0	44.7	44 3
Fs	9 4	12.2	10 9	10 8	10.0

Group B

Sample	dc61
SiO_2	46.63
TiO_2	2 96
Al_2O_3	6 67
Cr_2O_3	0.00
FeO*	7.40
MnO	0.13
MgO	12.80
CaO	23 18
Na_2O	0 46
Total	100 65
Si	1 730
Ti	0 083
Al/Al IV	0 270
Al VI	0 022
Cr	nd
Fe^{3+}	0.116
Fe^{2+}	0 113
Mn^{2+}	0.004
Mg	0 708
Ca	0 921
Na	0 033
Sum Cat#	4 000
Mg#	75.6
Ca#	49 5
Wo	49.5
En	38 0
Fs	12.5

nd = not detected; total Fe as FeO*

Appendix D-2 (Continued)

Group C

Sample	dc15	dc15	dc15	dc29	dc29	dc29	dc29	dc29	dc29	dc29	dc29
SiO_2	47.82	48 00	50 44	48 69	49 68	50 17	50.66	50.88	51 24	51 97	52.81
TiO_2	1.82	1 65	1 16	2.60	1 95	1 90	1 42	1.30	1.36	1.04	0.74
Al_2O_3	6.80	7.07	3 84	4 33	3 61	4 06	3 36	3.00	3 13	2 54	1 38
Cr_2O_3	0.67	0 64	0 26	0.09	0 09	0.29	0 47	0.23	0 51	0 07	0 09
FeO*	5.92	5.89	6 39	9 08	7 41	7.39	6.78	7.04	7.28	7 26	7 84
MnO	0.14	0 15	0.18	0 14	0 15	0 19	0 07	0.16	0.19	0.24	0.19
MgO	13.88	14 22	15 67	12.98	13 62	13.90	14 60	14.69	14 61	14.54	14.48
CaO	22.41	21.58	21 41	22 44	22 54	22.66	22.67	22 57	22 92	22 85	23 35
Na_2O	0.51	0 60	0.41	0 49	0 42	0 41	0.35	0.33	0 38	0 31	0 26
Total	100.33	100.14	100 01	101.16	99 65	101.17	100 55	100.40	101 86	100.95	101.28
Si	1 763	1 767	1 858	1 805	1.856	1 845	1 867	1 879	1 869	1.910	1.940
Ti	0 050	0.046	0 032	0.072	0 055	0.053	0.039	0 036	0.037	0 029	0 020
Al/Al IV	0.237	0 233	0.142	0 189	0.144	0 155	0 133	0.121	0 131	0.090	0.060
Al VI	0 058	0.074	0 024	nd	0 015	0.021	0 013	0 010	0.003	0 020	nd
Cr	0.020	0 019	0.008	0 002	0.003	0 008	0.014	0.007	0 015	0 002	0 002
Fe^{3+}	0.096	0 092	0 076	0 088	0.048	0 050	0 052	0.056	0 066	0.033	0.036
Fe^{2+}	0 086	0 089	0 121	0 194	0 184	0 178	0.157	0.161	0 156	0 189	0.204
Mn^{2+}	0 004	0.005	0 006	0 004	0 005	0.006	0 002	0.005	0 006	0 007	0 006
Mg	0 763	0.781	0.860	0 717	0.758	0 762	0.802	0.809	0.794	0 797	0 793
Ca	0.885	0 851	0.845	0 891	0.902	0 893	0.895	0.893	0 896	0 900	0 919
Na	0 037	0 043	0.029	0 035	0 030	0 029	0 025	0 023	0.027	0 022	0 019
Sum Cat#	4 000	4 000	4 000	4.000	4 000	4.000	4 000	4.000	4 000	4 000	4.000
Mg#	80 7	81.2	81 4	71 8	76 6	77 0	79 3	78.8	78 1	78 2	76 8
Ca#	48 3	46.8	44 3	47.0	47 5	47.3	46 9	46 4	46 7	46 7	46 9
Wo	48 3	46 8	44 3	47.0	47 5	47 3	46 9	46 4	46.7	46 7	46.9
En	41 6	43.0	45 1	37.9	40 0	40.3	42 0	42.0	41 4	41 4	40.5
Fs	10.1	10 2	10.6	15 1	12.5	12 4	11.1	11 5	11.9	11 9	12.6

Group C

Sample	dc36	dc36	dc36	dc36	dc36	dc36	dc36	dc36	dc59	dc59	dc59
SiO_2	49.22	49 61	49 83	49 89	49 92	50 05	50 47	51.05	48 88	50.12	50.36
TiO_2	1.60	1.55	1 42	1.90	1 65	1.38	1.31	1.06	1.61	1.17	1.08
Al_2O_3	5.73	4.90	5 72	3.63	4 77	4.68	4.59	4.55	5.72	5 06	4.55
Cr_2O_3	0.47	0 47	0 48	0.27	0 39	0.58	0.41	0 21	0 63	0.33	0 35
FeO*	6.03	6.00	6 37	7.21	5 78	6 11	6.01	6 03	6 03	6.01	5 71
MnO	0 09	0.11	0.09	0 16	0.14	0.06	0 16	0.19	0 07	0.12	0.11
MgO	14.58	14.53	14 61	14.27	14.67	15.06	15.13	15 79	14.27	15 04	15 49
CaO	22 19	22.89	21.53	22 58	22 75	22.34	22.24	21.03	22 10	21 45	21.40
Na_2O	0 50	0 46	0.60	0.43	0 39	0 43	0.49	0.56	0 47	0.59	0 47
Total	100.71	100.84	100 89	100 63	100.69	100 96	101.08	100.70	100.03	100.17	99.71
Si	1 804	1 819	1 821	1 843	1.831	1.830	1.840	1 860	1 805	1.840	1 855
Ti	0 044	0 043	0 039	0 053	0.046	0.038	0 036	0 029	0 045	0.032	0 030
Al/Al IV	0.196	0 181	0 179	0.157	0 169	0 170	0.160	0.140	0 195	0 160	0 145
Al VI	0.051	0.030	0 068	0.001	0 037	0.031	0 038	0.056	0.055	0 059	0.053
Cr	0 014	0.014	0 014	0 008	0 011	0.017	0 012	0.006	0.019	0.010	0.010
Fe^{3+}	0 079	0 085	0.062	0 075	0 058	0.077	0 074	0 060	0.066	0 068	0 056
Fe^{2+}	0 106	0 099	0.132	0 148	0.119	0.110	0.110	0 124	0 120	0.116	0 120
Mn^{2+}	0.003	0 004	0.003	0 005	0.004	0 002	0.005	0.006	0.002	0.004	0 003
Mg	0.796	0 794	0.796	0 786	0.802	0 820	0 822	0.858	0 786	0.823	0 850
Ca	0.871	0 899	0.843	0.893	0.894	0 875	0 869	0.821	0 874	0.844	0 844
Na	0.036	0 033	0 043	0.031	0 028	0 030	0 035	0.040	0 034	0 042	0.033
Sum Cat#	4.000	4 000	4.000	4 000	4 000	4.000	4 000	4.000	4 000	4.000	4.000
Mg#	81.1	81 2	80.4	77 9	81.9	81.4	81.7	82.3	80.9	81.7	82 8
Ca#	47 0	47.8	45.9	46.8	47 6	46.4	46.2	43.9	47.3	45 5	45.1
Wo	47 0	47 8	45.9	46.8	47.6	46.4	46 2	43.9	47 3	45.5	45.1
En	42 9	42.2	43 4	41.2	42 7	43 5	43 7	45 9	42 5	44.4	45 4
Fs	10.1	10 0	10.7	12 0	9.6	10 0	10 1	10.2	10.2	10 1	9 6

nd = not detected, total Fe as FeO*

Appendix D-2 (Continued)

Group C			*Group D*			
Sample	dc59	dc59	Sample	dc7	dc7	dc66
SiO_2	50.47	51 57	SiO_2	48.06	50.16	48.28
TiO_2	1 06	0 92	TiO_2	1.73	1.16	1 93
Al_2O_3	4 89	3.39	Al_2O_3	6.36	3 86	5 96
Cr_2O_3	0 45	0.58	Cr_2O_3	0.86	0.45	0.50
FeO*	5.51	5.29	FeO*	5.91	6.04	6 93
MnO	0 12	0.15	MnO	0.11	0.10	0.12
MgO	15.17	15.61	MgO	13 70	15.05	13 57
CaO	21 36	21.26	CaO	23.31	22 99	22.25
Na_2O	0.56	0.70	Na_2O	0 44	0.34	0 42
Total	99.76	100.06	Total	100.85	100 52	100.22
Si	1 857	1.892	Si	1.766	1.844	1 789
Ti	0 029	0.025	Ti	0.048	0.032	0 054
Al/Al IV	0.143	0.108	Al/Al IV	0.234	0.156	0 211
Al VI	0.069	0 039	Al VI	0 042	0.011	0 049
Cr	0.013	0 017	Cr	0 025	0.013	0 015
Fe^{3+}	0.042	0 051	Fe^{3+}	0 102	0 093	0 071
Fe^{2+}	0 128	0.124	Fe^{2+}	0 079	0.093	0 144
Mn^{2+}	0.004	0 005	Mn^{2+}	0.004	0 003	0 004
Mg	0 832	0.854	Mg	0 751	0 825	0 749
Ca	0.842	0 836	Ca	0.918	0 906	0 883
Na	0 040	0.050	Na	0 031	0.024	0 031
Sum Cat#	4.000	4 000	Sum Cat#	4 000	4 000	4 000
Mg#	83.0	82 9	Mg#	80 6	81 6	77.7
Ca#	45.6	46.9	Ca#	49 5	47.2	47 7
Wo	45.6	44 7	Wo	49.5	47 2	47.7
En	45.0	45.7	En	40.5	43.0	40.5
Fs	9.4	9 6	Fs	10.0	9.8	11 8

nd = not detected; total Fe as FeO*

Appendix D-3

Electron microprobe analyses of plagioclase microphenocrysts of the Denchai basalts

Group A		
Sample	dc61	dc62
SiO_2	50.85	52.43
TiO_2	0 14	0.21
Al_2O_3	31.34	30 05
Fe_2O_3	0 59	0 69
MnO	0 02	nd
MgO	0.07	0 09
CaO	14 08	12 36
Na_2O	3 29	3.99
K_2O	0 46	0.81
Total	100 84	100 73
Si	2 303	2.371
Ti	0.005	0.007
Al/Al IV	1.672	1 602
Fe^{3+}	0.020	0 023
Mn^{2+}	0.001	nd
Mg	0.005	0.006
Ca	0.683	0 599
Na	0.289	0.350
K	0.026	0.047
Sum Cat#	5 004	5 007
Ab	28.9	35.1
An	68.4	60 1
Or	2 6	4.7

Group C								
Sample	dc15	dc15	dc15	dc15	dc15	dc15	dc15	dc15
SiO_2	50 67	50 72	50 78	50.82	50 98	51.00	51.05	52.53
TiO_2	0 11	0.06	0 05	0 11	0 06	0.11	0 11	0 12
Al_2O_3	31.35	31 04	31 31	31.03	31 07	31.27	30 58	29 87
Fe_2O_3	0 42	0 43	0.41	0 48	0.47	0 43	0 55	0.45
MnO	0.01	0 02	nd	nd	nd	nd	0 01	0 02
MgO	0.12	0 12	0 09	0.10	0.11	0 10	0.16	0 10
CaO	14 02	13 91	13.82	13.82	13.62	13 66	13 56	12.35
Na_2O	3.54	3.43	3 44	3 54	3 67	3.71	3.53	4.12
K_2O	0.34	0 36	0 38	0 38	0.41	0.37	0 40	0.44
Total	100.78	100.18	100 38	100 33	100.63	100 78	99 95	100.12
Si	2 298	2 309	2 308	2.312	2.313	2 310	2 328	2.381
Ti	0 004	0 002	0.002	0.004	0 002	0 004	0.004	0.004
Al/Al IV	1.676	1.666	1.677	1.664	1 661	1.669	1.644	1 596
Fe^{3+}	0 014	0 015	0 014	0.017	0 016	0.015	0.019	0 015
Mn^{2+}	nd	nd	nd	nd	nd	nd	nd	0 001
Mg	0.008	0 008	0.006	0.006	0.007	0.007	0 011	0.006
Ca	0 681	0 678	0 673	0.674	0.662	0.663	0 663	0.600
Na	0 311	0.303	0 304	0 312	0.323	0 326	0 312	0.362
K	0 020	0 021	0.022	0.022	0 024	0.021	0 023	0 025
Sum Cat#	5 018	5 006	5.008	5.011	5.015	5 017	5 004	4 996
Ab	30 6	30 2	30 3	30 9	31 8	32.2	31 3	36 7
An	67 0	67 7	67 3	66 8	65.4	65.4	66 4	60.7
Or	1.9	2 1	2 2	2 2	2 4	2 1	2 3	2.6

Group C												
Sample	dc16	dc16	dc16	dc16	dc16	dc16	dc16	dc16	dc16	dc16	dc16	dc16
SiO_2	50.79	50.88	51.21	51.26	51.95	52 34	52.91	53.11	53.16	53.25	54 94	55.82
TiO_2	0 08	0 07	0.09	0 09	0.14	0 13	0 13	0.16	0.11	0 14	0 20	0.12
Al_2O_3	31 56	31.57	31 55	30.56	30 30	30.63	29 93	29 88	29 99	30 10	28 01	27 09
Fe_2O_3	0.44	0.55	0 45	0.48	0.44	0 47	0 31	0 45	0.50	0 61	0 72	0 64
MnO	nd	0.02	nd	nd	nd	nd	0 05	nd	0 05	nd	nd	nd
MgO	0.08	0.15	0 09	0.12	0.13	0 13	0 10	0 13	0.05	0 09	0 10	0.05
CaO	14 65	14 52	14 23	13 19	12 86	13.33	12.49	12 72	12 72	12 75	10 71	8.84
Na_2O	3 29	3.23	3 38	3.90	4.16	3 90	4.21	4.17	4.23	4 25	5 22	5.98
K_2O	0 27	0 32	0.29	0.36	0 42	0.35	0.47	0.43	0.46	0 48	0 71	0.88
Total	101 25	101 34	101 38	100 03	100 58	101.30	100 66	101 12	101.31	101.69	100 71	99.48
Si	2.292	2.294	2.305	2.336	2.354	2 352	2 388	2 387	2 385	2 382	2 472	2.532
Ti	0.003	0.002	0.003	0.003	0.005	0.004	0.004	0.006	0 004	0.005	0 007	0.004
Al/Al IV	1.678	1.677	1.673	1.641	1.618	1.622	1.592	1.583	1.586	1.587	1.486	1.448
Fe^{3+}	0.015	0.018	0.015	0.016	0.015	0.016	0.011	0.015	0.017	0 020	0.024	0.022
Mn^{2+}	nd	nd	nd	nd	nd	nd	0.002	nd	0.002	nd	nd	nd
Mg	0.006	0.010	0.006	0.008	0 009	0.009	0 007	0.009	0.004	0.006	0.007	0 003
Ca	0 708	0 701	0.686	0.644	0 625	0 642	0 604	0.612	0.611	0 611	0.517	0 430
Na	0.288	0 283	0.295	0.345	0 365	0 340	0 369	0.363	0.368	0.368	0 456	0.526
K	0.015	0 019	0.016	0.021	0.024	0 020	0.027	0.025	0.026	0 027	0 041	0.051
Sum Cat#	5.008	5.006	5.002	5.015	5 019	5 004	5 004	5.001	5 004	5 007	5 012	5.017
Ab	28 4	28 2	29 5	34 1	35.9	33 9	36 9	36 3	36.6	36 6	45 0	52.2
An	70 0	69.9	68.7	63.7	61.3	64 1	60 4	61 2	60 8	60 7	51 0	42.6
Or	1.5	1 9	1 6	2.1	2 4	2 0	2 7	2.5	2 6	2 7	4 0	5 0

nd = not detected

Appendix D-3 (Continued)

Group C

Sample	dc17	dc17	dc29	dc29	dc29	dc29	dc29	dc29	dc30	dc30	dc30	dc36
SiO_2	51 10	51.57	52 65	52 65	53.03	52 47	53.05	55 10	50.02	50.69	51 05	52 64
TiO_2	0.08	0 08	0 14	0 13	0 12	0 10	0.11	0.19	0 05	0 11	0.07	0.07
Al_2O_3	31.64	30 88	29.94	30 23	30 15	30.31	29.42	28 59	31 78	31.10	31.16	30.29
Fe_2O_3	0.45	0.46	0.59	0 54	0 50	0.61	0.53	0.52	0 47	0.38	0.36	0.49
MnO	nd	nd	nd	0.03	0 03	nd	0.02	0.04	nd	0.01	nd	nd
MgO	0.13	0 09	0 16	0.09	0.10	0 07	0.08	0.07	0 12	0.10	0 09	0.05
CaO	14.33	13.65	12.57	12 78	12 53	12.88	12.11	10.76	14.18	13 58	13.59	12.56
Na_2O	3 30	3.72	3 77	4 11	4 22	4 00	4.46	5.12	3 49	3.77	3.77	4.21
K_2O	0 35	0.36	0 63	0.44	0 47	0 44	0.52	0.65	0.27	0.37	0 37	0.38
Total	101.41	100.81	100.54	100.99	101 18	100.91	100.31	101.08	100 54	100.21	100.61	100 75
Si	2 300	2.331	2 381	2 371	2.382	2 365	2.402	2.466	2.276	2 309	2 314	2 373
Ti	0 003	0 003	0 005	0.004	0 004	0.003	0.004	0.006	0 002	0 004	0 002	0 002
Al/Al IV	1 678	1.645	1.596	1 604	1 596	1.610	1 570	1.508	1 704	1 670	1.665	1 609
Fe^{3+}	0.015	0.016	0.020	0 018	0.017	0.021	0 018	0.018	0 016	0.013	0 012	0.017
Mn^{2+}	nd	nd	nd	0 001	0 001	nd	0 001	0.001	nd	nd	nd	nd
Mg	0.009	0 006	0 011	0 006	0 007	0.005	0 006	0.005	0 008	0 007	0 006	0 003
Ca	0.691	0.661	0.609	0.617	0 603	0 622	0.588	0.516	0 691	0 663	0.660	0 607
Na	0.288	0.326	0.330	0 359	0 367	0.350	0 392	0.445	0 308	0.333	0 332	0 368
K	0.020	0.021	0.036	0 025	0.027	0.025	0 030	0 037	0.016	0.022	0 022	0.022
Sum Cat#	5 004	5.008	4.990	5.006	5 004	5.002	5.010	5 004	5.024	5.023	5 018	5.004
Ab	28 8	32.3	33.8	35 9	36 8	35.1	38.8	44 6	30 2	32.6	32.7	36.9
An	69 2	65 6	62.3	61 6	60 5	62.4	58 2	51 7	67.9	65.0	65.0	60.9
Or	2 0	2 1	3 7	2 5	2 7	2 5	3 0	3 7	1.5	2 1	2 1	2 2

Group C

Sample	dc36	dc59	dc59	dc59	dc59
SiO_2	53.40	50.98	51 35	51 49	52 38
TiO_2	0.06	0 10	0.11	0 09	0 11
Al_2O_3	30 15	31.08	31.03	30 66	30 28
Fe_2O_3	0.60	0.43	0 46	0 56	0 39
MnO	0 05	0 02	nd	0 01	0 02
MgO	0.09	0 13	0.10	0 11	0 11
CaO	12 28	13 84	13 58	13 31	12 83
Na_2O	4.29	3 51	3.64	3 69	4 02
K_2O	0 47	0 36	0.40	0.41	0.47
Total	101.47	100.51	100.76	100 36	100 72
Si	2 390	2.314	2 322	2.337	2.367
Ti	0 002	0.003	0.004	0.003	0 004
Al/Al IV	1.590	1 663	1 653	1.640	1 612
Fe^{3+}	0 020	0 015	0.016	0.019	0.013
Mn^{2+}	0.002	0 001	nd	0.001	0 001
Mg	0.006	0.009	0.007	0 007	0 007
Ca	0.589	0 673	0.658	0.647	0.621
Na	0.372	0 309	0.319	0 325	0.352
K	0.027	0.021	0 023	0.023	0.027
Sum Cat#	5.001	5.009	5 005	5.004	5.006
Ab	37 6	30 8	31 9	32.6	35.1
An	59.5	67.0	65 8	65.0	62.0
Or	2 7	2 1	2 3	2.4	2.7

Group D

Sample	dc7	dc7	dc7	dc11	dc11
SiO_2	50 31	50.50	50 60	49 95	50 12
TiO_2	0.09	0 08	0 07	0 08	0.10
Al_2O_3	31 45	31 61	31 83	32.08	31 78
Fe_2O_3	0 56	0 46	0 39	0.55	0.51
MnO	nd	0 01	0 05	0.01	nd
MgO	0.10	0.08	0 12	0 21	0.12
CaO	14 37	14.38	14.43	15 04	14 63
Na_2O	3 43	3.46	3 41	3.08	3 28
K_2O	0 34	0 34	0 37	0.27	0 33
Total	100.80	101.14	101 34	101.43	101.00
Si	2 284	2 285	2.283	2 257	2 272
Ti	0.003	0 003	0.002	0.003	0.003
Al/Al IV	1.683	1 686	1.692	1 708	1 698
Fe^{3+}	0 019	0 016	0.013	0.019	0 018
Mn^{2+}	nd	nd	0.002	nd	nd
Mg	0 007	0.006	0.008	0.014	0 008
Ca	0 699	0.697	0 697	0.728	0.711
Na	0.302	0.303	0.298	0.270	0.289
K	0 020	0 019	0 021	0 016	0 019
Sum Cat#	5 020	5 021	5 020	5 019	5 021
Ab	29 5	29 6	29.3	26 5	28.2
An	68.3	68.0	68.5	71 6	69 6
Or	1.9	1 9	2.1	1 6	1 9

nd = not detected

Appendix D-3 (Continued)

Group D

Sample	dc53	dc53	dc53	dc63	dc66	dc66	dc66	dc66	dc66	dc66	dc66	dc66
SiO_2	49 55	49.89	50 23	55.84	50 82	50.83	50 91	51.06	51 07	51.13	51 38	51 72
TiO_2	0 11	0.16	0 10	0.00	0 12	0.07	0 09	0 11	0 09	0.09	0 06	0 07
Al_2O_3	31.93	32.03	31 54	28 73	31.14	31.11	31.01	30.81	31 03	31.06	30.90	30 77
Fe_2O_3	0.47	0 36	0 46	0 08	0 41	0.40	0.38	0.42	0 53	0.44	0.42	0 47
MnO	0.01	nd	0.03	0.05	nd	nd	0.03	0.03	0 01	0 01	0.01	0 02
MgO	0.06	0 09	0.11	0 01	0.09	0 12	0.10	0.12	0 16	0.10	0.10	0 10
CaO	14 91	14.78	14 43	10 54	14.08	13 88	14.00	13.54	13.73	13.74	13.36	13 28
Na_2O	3.21	3 22	3 36	5 26	3 43	3 51	3.47	3.61	3 51	3.57	3.59	3.76
K_2O	0 29	0.29	0 30	0 56	0 32	0.33	0.29	0 30	0.36	0 31	0.31	0 32
Total	100 78	101.15	100.69	101 14	100 52	100 27	100.29	100.05	100 52	100.46	100.17	100.60
Si	2 255	2.261	2 282	2.488	2 307	2.312	2.315	2.325	2.317	2 319	2 333	2 341
Ti	0 004	0.005	0.003	0 000	0 004	0 002	0.003	0 004	0 003	0 003	0 002	0.002
Al/Al IV	1 713	1.711	1 689	1 509	1.667	1.668	1.662	1 653	1 659	1.661	1 654	1.641
Fe^{3+}	0 016	0.012	0.016	0 003	0 014	0 014	0 013	0.015	0.018	0 015	0 014	0.016
Mn^{2+}	0 001	nd	0.001	0.002	nd	nd	0.001	0 001	nd	nd	nd	0 001
Mg	0.004	0 006	0 007	0.001	0 006	0 008	0.007	0 008	0 011	0.007	0.007	0.007
Ca	0 727	0 718	0.702	0.503	0 685	0.676	0.682	0 661	0 667	0.668	0.650	0 644
Na	0 284	0.283	0 296	0.454	0.302	0 309	0.306	0.319	0 309	0.314	0.316	0 330
K	0.017	0.017	0 018	0.032	0 018	0 019	0.017	0 018	0 021	0.018	0 018	0 019
Sum Cat#	5.026	5 021	5.018	4 994	5 006	5.009	5.005	5 004	5.005	5.006	4.996	5 002
Ab	27.5	27.6	29.0	45 9	30.0	30 8	30.4	32.0	31 0	31.4	32.1	33 2
An	70.4	70.0	68 9	50.9	68.0	67.3	67 9	66.2	66 9	66.8	66.0	64.8
Or	1.6	1.7	1 7	3.2	1.8	1.9	1 6	1.8	2 1	1.8	1 8	1.9

nd = not detected

Appendix D-4

Electron microprobe analyses of olivine in mantle xenoliths within the Denchai basalts

Group B

Sample	dc5	dc5	dc5	dc5	dc5	dc5	dc5	dc13	dc13	dc14	dc14	dc19
SiO_2	40.73	40 78	40 83	40.87	40.95	41.04	41.13	41 24	41.36	40 49	40 67	40 76
TiO_2	0 02	nd	nd	0.02	0.02	nd	nd	0 02	nd	0 01	nd	nd
Al_2O_3	0 04	0 01	0 02	0.06	0.04	0 02	0.02	nd	0 01	0 03	0 03	nd
Cr_2O_3	nd	0.01	0 02	0.03	nd	0 05	0.01	0 06	0.02	0 01	0 05	0.02
FeO	9.43	10.54	10.52	9 80	9.79	9 55	9.67	9 68	9 87	10 55	10.74	10.42
MnO	0.12	0.15	0.18	0.16	0.15	0.15	0 17	0.11	0 12	0 11	0 15	0 16
MgO	48.95	47.85	48.13	49.21	49.35	48.82	48 90	49.12	48 77	47.51	47 75	48 08
CaO	0.08	0.08	0 06	0.10	0 09	0.07	0 09	0.06	0.07	0 07	0 07	0.08
NiO	0 49	0.33	0 34	0.37	0 41	0 37	0 41	0.45	0.39	0.33	0 36	0.42
Total	99 86	99 75	100.10	100 63	100.81	100 07	100.41	100.73	100.60	99 13	99 82	99.95
Si	1 000	1.006	1 003	0.997	0 997	1.005	1.004	1.003	1 008	1.005	1.004	1.003
Ti	nd	nd	nd	nd	nd	nd	nd	nd	nd	nd	nd	nd
Al/Al IV	0.001	nd	0.001	0.002	0.001	nd	0.001	nd	nd	0.001	0 001	nd
Cr	nd	nd	nd	0.001	nd	0 001	nd	0.001	nd	nd	0 001	nd
Fe^{2+}	0.194	0.217	0 216	0.200	0 199	0.196	0 197	0 197	0 201	0 219	0.222	0 214
Mn^{2+}	0 003	0 003	0 004	0 003	0.003	0.003	0 004	0 002	0.003	0 002	0 003	0 003
Mg	1 791	1.759	1 763	1.789	1 791	1.781	1 779	1.781	1 771	1 758	1.756	1 764
Ca	0.002	0.002	0 001	0.003	0 002	0 002	0 002	0.001	0.002	0.002	0.002	0 002
Ni	0 010	0 006	0.007	0 007	0.008	0 007	0.008	0 009	0.008	0.007	0.007	0 008
Sum Cat#	3 000	2 994	2 996	3 002	3 002	2 995	2.996	2.996	2.992	2.994	2 995	2.996
Fa	0.10	0.11	0.11	0.10	0.10	0 10	0 10	0 10	0.10	0 11	0 11	0.11
Fo	0.90	0.89	0.89	0.90	0.90	0.90	0.90	0 90	0 90	0.89	0 89	0.89

Group B

Sample	dc19	dc19	dc27	dc27	dc27	dc27	dc27	dc27	dc27	dc27	dc43	dc43
SiO_2	40.83	40.93	38 73	40.45	40 45	40.48	40 74	40.74	40.81	40.81	40.19	40 25
TiO_2	0.03	0 01	0.06	0.02	0.01	nd	nd	nd	0 01	nd	nd	nd
Al_2O_3	0.01	0.01	0.03	0.03	0 03	0.01	nd	0 03	0 03	0.03	0 02	0.04
Cr_2O_3	nd	nd	0.03	0.01	0 03	nd	0.02	0 01	0.05	0 06	0 03	0.03
FeO	10.30	10.24	19.54	10.39	10 26	9.37	9.59	9 49	9.52	9 68	11 48	11 94
MnO	0.18	0.12	0.40	0.08	0 09	0.14	0.11	0 15	0 13	0.16	0.14	0 18
MgO	48 71	48.33	40 59	48 03	48 22	49.06	49.25	48 55	48.94	49.09	47 29	47 24
CaO	0 06	0.08	0.38	0 08	0.07	0.08	0 08	0.09	0.11	0.11	0 07	0 06
NiO	0 40	0.43	0.17	0 35	0.31	0 41	0.40	0 42	0.42	0.37	0 41	0.26
Total	100 54	100.15	99.93	99.45	99 47	99 56	100 20	99 48	100.02	100.31	99.63	99.99
Si	0.999	1.004	0 997	1 000	1.000	0.997	0 997	1.003	1 000	0.998	0 998	0 997
Ti	0 001	nd	0 001	nd	nd	nd	nd	nd	nd	nd	nd	nd
Al/Al IV	nd	nd	0.001	0.001	0 001	nd	nd	0.001	0.001	0.001	0.001	0.001
Cr	nd	nd	0.001	nd	0 001	nd	nd	nd	0.001	0.001	0.001	0.001
Fe^{2+}	0.211	0.210	0.421	0.215	0 212	0.193	0 196	0 195	0.195	0.198	0.238	0 247
Mn^{2+}	0.004	0 002	0.009	0 002	0.002	0 003	0.002	0.003	0 003	0.003	0 003	0 004
Mg	1.776	1.768	1 558	1.771	1.776	1.800	1 796	1 782	1.788	1.789	1 751	1 745
Ca	0.002	0 002	0.010	0 002	0.002	0.002	0.002	0.002	0.003	0.003	0.002	0 002
Ni	0.008	0.008	0 004	0.007	0.006	0 008	0.008	0 008	0.008	0 007	0.008	0 005
Sum Cat#	3 000	2.995	3 001	2.999	2 999	3.003	3 003	2 996	2 999	3 001	3.001	3 002
Fa	0.11	0 11	0 21	0 11	0 11	0.10	0 10	0 10	0.10	0.10	0 12	0 12
Fo	0 89	0.89	0 79	0 89	0.89	0.90	0 90	0.90	0 90	0.90	0 88	0.88

nd = not detected

Appendix D-4 (Continued)

Group B

Sample	dc43	dc55	dc55	dc55	dc55
SiO_2	40.40	40.83	40.88	40.99	41 00
TiO_2	nd	nd	nd	0.01	nd
Al_2O_3	0 03	nd	0 02	nd	0.01
Cr_2O_3	0 01	0.03	0 04	nd	0.00
FeO	11.70	8.65	9 09	8 65	8.76
MnO	0 12	0.17	0 15	0.18	0.16
MgO	46 93	49 69	49 73	49 92	49.29
CaO	0 09	0.11	0 07	0.09	0 08
NiO	0.40	0 38	0.34	0.37	0.48
Total	99 69	99 86	100.32	100.22	99.81
Si	1.003	0.999	0.997	0.999	1.003
Ti	nd	nd	nd	nd	nd
Al/Al IV	0.001	nd	nd	nd	nd
Cr	nd	0 001	0.001	nd	nd
Fe^{2+}	0.243	0 177	0.185	0 176	0.179
Mn^{2+}	0 003	0.004	0 003	0 004	0.003
Mg	1 736	1 811	1 808	1 813	1.798
Ca	0.002	0.003	0 002	0.002	0.002
Ni	0.008	0.007	0 007	0.007	0 010
Sum Cat#	2 996	3.001	3 003	3.001	2.996
Fa	0.12	0 09	0.09	0.09	0 09
Fo	0.88	0.91	0.91	0.91	0.91

Group D

Sample	dc3	dc3	dc3	dc3	dc3
SiO_2	40 18	40.48	40.54	40.58	40.70
TiO_2	0.02	0 01	0 03	0 01	nd
Al_2O_3	0.05	0 05	0.02	0 04	0 04
Cr_2O_3	0 02	0.06	nd	0.02	0.02
FeO	9 89	9 73	10.02	9 84	9.84
MnO	0.12	0.22	0.17	0 15	0.13
MgO	49.11	48 79	48.84	48.52	48.98
CaO	0 07	0.10	0.10	0.09	0.11
NiO	0 31	0 45	0 44	0.42	0 35
Total	99.74	99 91	100.18	99 66	100.16
Si	0 990	0.995	0.995	1.000	0.997
Ti	nd	nd	0.001	nd	nd
Al/Al IV	0.001	0.002	0 001	0.001	0 001
Cr	nd	0 001	nd	nd	nd
Fe^{2+}	0 204	0.200	0 206	0.203	0 202
Mn^{2+}	0.002	0.005	0.004	0 003	0.003
Mg	1 803	1.788	1 787	1.782	1 789
Ca	0.002	0 003	0.003	0.002	0.003
Ni	0.006	0.009	0.009	0.008	0 007
Sum Cat#	3.009	3 003	3.004	2.999	3 002
Fa	0.10	0 10	0 10	0.10	0.10
Fo	0.90	0.90	0.90	0 90	0 90

nd = not detected

Appendix D-5

Electron microprobe analyses of clinopyroxene in mantle xenoliths within the Denchai basalts

Group B

Sample	dc5	dc5	dc5	dc5	dc5	dc5	dc5	dc5	dc5	dc5	dc5
SiO_2	51.03	52.44	52.44	51 98	52.54	52 90	51 33	51.53	52 40	52 24	52 42
TiO_2	0.61	0.35	0.32	0.36	0.36	0 36	0.38	0 42	0 43	0 43	0 39
Al_2O_3	7.99	3.83	3.84	4.68	5 74	4.83	4.87	4 79	3 90	4 71	3 29
Cr_2O_3	0.84	1 35	1 07	1.25	1 20	1 35	1.40	1 28	1.43	1.47	1 38
FeO*	3.03	2.78	3.11	3.03	3.14	3 07	3.30	3 12	3 13	2 83	2.99
MnO	0.09	0 04	0.06	0.09	0 04	0.09	0.11	0 00	0 12	0 09	0 02
MgO	14.92	16.34	16 26	15.87	15 47	16.07	15.44	15.75	16 42	15 85	17 63
CaO	19 06	22.86	24 12	24.11	22 44	24.21	24.47	24.00	24 07	22 95	22 24
Na_2O	1.65	0.66	0 46	0.48	1 08	0.52	0 49	0.48	0.42	0 69	0.53
Total	99 30	100 80	101 94	102.09	102 17	103 57	102 12	101.61	102 58	101 26	100.89
Si	1 854	1 893	1.878	1 860	1.870	1 865	1 841	1.853	1.867	1 877	1.920
Ti	0.017	0.010	0.009	0.010	0 010	0.009	0 010	0.011	0 012	0.012	0.010
Al/Al IV	0 146	0.107	0 122	0 140	0 130	0 135	0.159	0 147	0 133	0 123	0.080
Al VI	0.196	0.056	0.040	0 057	0.111	0 066	0.047	0 056	0.031	0 077	0 057
Cr	0.024	0.039	0 030	0.035	0 034	0.038	0 040	0.036	0 040	0.042	0 039
Fe^{3+}	0 010	0.039	0 066	0 062	0 041	0 049	0 085	0.066	0 068	0 030	0.002
Fe^{2+}	0.082	0.045	0 027	0 028	0.052	0.042	0 014	0 028	0 026	0.056	0 087
Mn^{2+}	0.003	0.001	0 002	0 003	0.001	0 003	0 003	nd	0.004	0 003	0 001
Mg	0.808	0.879	0 868	0 846	0 821	0 844	0 826	0.844	0 872	0 849	0.927
Ca	0.742	0.885	0 926	0.924	0 856	0.914	0.941	0.925	0 919	0.884	0 841
Na	0.116	0.046	0 032	0 033	0 075	0.036	0.034	0.034	0 029	0 048	0.036
Sum Cat#	4.000	4.000	4 000	4.000	4.000	4 000	4 000	4.000	4 000	4.000	4.000
Mg#	89.8	91 3	90.3	90.4	89 8	90 3	89 3	90.0	90.3	90 8	91.2
Ca#	45.1	47 9	49.0	49.6	48.3	49 4	50.3	49.7	48.7	48.5	45.3
Wo	45 1	47.9	49 0	49.6	48 3	49.4	50.3	49.7	48.7	48.5	45 3
En	49.1	47 5	46.0	45.4	46.4	45.6	44.2	45 3	46.2	46 6	49 9
Fs	5 8	4.6	5.0	5 0	5 3	5.1	5 5	5.0	5 2	4.9	4.8

Group B

Sample	dc5	dc13	dc13	dc13	dc13	dc13	dc13	dc13	dc14	dc14	dc14
SiO_2	52.12	51.81	51.99	52 28	52 40	51 87	52.47	53.02	50.63	51 20	51.23
TiO_2	0.44	0.45	0 43	0 48	0.48	0 43	0.51	0 51	0.65	0 61	0 63
Al_2O_3	4.47	7.16	7 08	7.08	7.05	6 88	7.00	8.24	5.31	4 99	5 27
Cr_2O_3	1.26	1.09	1 09	1 04	1.04	1 07	0.94	0.92	0 99	0.81	0.90
FeO*	3.07	2 79	2 69	2 71	3.01	2.83	2.90	2.87	3 06	3 03	2.95
MnO	0.05	0 04	0 06	0.12	0.10	0.09	0 05	0.04	0 09	0 08	0.13
MgO	16 51	15.08	15.15	15.33	15 10	14.97	15 28	14 50	16.00	16.68	16 32
CaO	22.84	20 36	20.21	20.31	20.25	19 94	20 15	19.33	21.75	21 28	21.46
Na_2O	0.49	1 67	1.66	1.68	1.68	1 69	1.66	1.99	0.58	0.54	0.51
Total	101 41	100.61	100 46	101.16	101.22	99 87	101.03	101 57	99 20	99.30	99 43
Si	1 872	1.861	1 869	1.866	1.872	1 876	1.876	1.880	1 856	1 871	1 871
Ti	0.012	0.012	0.011	0 013	0 013	0.012	0.014	0.014	0.018	0 017	0.017
Al/Al IV	0.128	0 139	0.131	0 134	0 128	0.124	0.124	0.120	0.144	0.129	0.129
Al VI	0.061	0 164	0.169	0 164	0 168	0.170	0 170	0.224	0.086	0.086	0.098
Cr	0 036	0 031	0.031	0.029	0.029	0 031	0.026	0 026	0.029	0.023	0 026
Fe^{3+}	0 041	0 037	0 025	0.031	0 022	0 020	0.015	0.000	0.034	0.025	0 007
Fe^{2+}	0 052	0 048	0.056	0.050	0 068	0.065	0 072	0 085	0.060	0.067	0.083
Mn^{2+}	0 002	0.001	0 002	0.004	0.003	0 003	0 002	0.001	0.003	0.003	0 004
Mg	0.884	0 808	0 811	0.816	0 804	0.807	0 814	0 766	0.874	0 908	0.888
Ca	0 879	0.783	0.778	0 777	0.775	0 773	0.772	0.734	0 855	0.833	0.840
Na	0 034	0.116	0 116	0.116	0.116	0 119	0.115	0.137	0 041	0 038	0.036
Sum Cat#	4.000	4.000	4.000	4 000	4 000	4.000	4.000	3 994	4.000	4 000	4.000
Mg#	90 5	90 5	90.9	91 0	89.9	90 5	90 3	90.0	90 3	90.8	90 8
Ca#	47 3	46.7	46 5	46.3	46 4	46.3	46.1	46 3	46.8	45.4	46 1
Wo	47 3	46.7	46 5	46.3	46 4	46.3	46.1	46 3	46 8	45.4	46.1
En	47.6	48.2	48.5	48 6	48 1	48.4	48.6	48 3	47.9	49 5	48 7
Fs	5.1	5.1	5 0	5.1	5.6	5 3	5.3	5 4	5 3	5 2	5.2

nd = not detected, total Fe as FeO*

Appendix D-5 (Continued)

Group B

Sample	dc19	dc19	dc19	dc23	dc27	dc27	dc27	dc27	dc27	dc43
SiO_2	51.11	51 15	51.29	52 05	50.77	51 46	51.54	51.83	51 91	51 11
TiO_2	0 68	0 61	0.62	0.47	0.64	0.56	0 18	0.16	0 21	0 68
Al_2O_3	7.72	7.82	7 83	6.92	5.07	4 88	5.24	5 05	5.33	5.38
Cr_2O_3	0 75	0 71	0.82	1.02	1 02	0 82	0 97	0 96	0 94	0.92
FeO*	3.11	2 91	2.91	2 58	3 30	2 98	2.96	2.85	2 82	3 48
MnO	0.07	0.09	0 14	0 06	0.14	0.04	0.08	0.07	0 08	0.05
MgO	14.90	14.93	14 76	15 14	16.26	16 89	16 54	16.56	16.60	16.13
CaO	19.83	19.75	19 90	20 71	21.48	21.36	21 81	21.53	21.58	21.87
Na_2O	1 70	1.73	1 77	1 68	0.59	0.40	0 66	0 65	0 67	0.46
Total	100 06	99.86	100 19	100.79	99.45	99 41	100.17	99.77	100.24	100.15
Si	1 846	1 849	1 849	1 865	1.857	1.878	1 866	1.883	1 876	1.859
Ti	0 018	0 017	0.017	0.013	0.018	0.015	0 005	0.004	0.006	0 018
Al/Al IV	0.154	0 151	0.151	0.135	0.143	0.122	0.134	0.117	0.124	0 141
Al VI	0 174	0 182	0.182	0.158	0.076	0 087	0.090	0.099	0 103	0.089
Cr	0 021	0.020	0.023	0 029	0.030	0 024	0 028	0.028	0 027	0 026
Fe^{3+}	0.041	0 038	0.036	0.039	0 044	0.009	0.052	0.028	0 030	0 022
Fe^{2+}	0 053	0 050	0 052	0 038	0.057	0 082	0 037	0.058	0 056	0 084
Mn^{2+}	0.002	0 003	0.004	0.002	0 004	0 001	0.002	0.002	0 002	0 001
Mg	0.802	0.804	0 793	0 809	0 887	0.918	0 893	0.897	0 894	0 874
Ca	0 767	0 765	0.769	0.795	0 842	0 835	0 846	0 838	0.835	0.852
Na	0.119	0.121	0 123	0.117	0.042	0.028	0.046	0 046	0 047	0.033
Sum Cat#	4.000	4 000	4.000	4.000	4 000	4 000	4.000	4 000	4.000	4.000
Mg#	89.5	90 1	90 0	91.3	89 8	91 0	90.9	91.3	91.2	89.2
Ca#	46.1	46 1	46 5	47 2	45.9	45 3	46 2	46.0	46 0	46.5
Wo	46 1	46 1	46 5	47.24	45.9	45 3	46 2	46.0	46 0	46 5
En	48.2	48 4	47 9	48.07	48 4	49 8	48 8	49.2	49 2	47.7
Fs	5.8	5 5	5 6	4.69	5.7	5 0	5 0	4.8	4 8	5.8

Group D

Sample	dc3
SiO_2	52 05
TiO_2	0.16
Al_2O_3	4.63
Cr_2O_3	1 15
FeO*	2 97
MnO	0 07
MgO	16 86
CaO	20.57
Na_2O	0.73
Total	99.23
Si	1.899
Ti	0.004
Al/Al IV	0.101
Al VI	0.097
Cr	0.033
Fe^{3+}	0.014
Fe^{2+}	0.077
Mn^{2+}	0 002
Mg	0.917
Ca	0 804
Na	0.051
Sum Cat#	4 000
Mg#	91.0
Ca#	44.3
Wo	44.3
En	50 6
Fs	5.1

nd = not detected, total Fe as FeO*

Appendix D-6

Electron microprobe analyses of orthopyroxene in mantle xenoliths within the Denchai basalts

Group B

Sample	dc5	dc5	dc5	dc5	dc5	dc5	dc5	dc5	dc5	dc5	dc5	dc5
SiO_2	55 32	55.55	55.55	55 65	55 70	55.74	55.82	55.98	55 64	56 06	56.04	55.83
TiO_2	0 11	0.06	0.08	0.07	0 11	0 06	0.08	0 07	0.09	0 09	0.07	0.11
Al_2O_3	4.10	4 30	4.14	4.04	4 08	4.10	4 07	4.02	4 01	4.11	4 08	4 13
Cr_2O_3	0 51	0.50	0.53	0.52	0.41	0 50	0 60	0 50	0 36	0.46	0.42	0 59
FeO*	6.70	6 26	6.43	6.21	6 34	6.48	6.41	6 59	6 35	6.43	6 32	6 40
MnO	0 11	0.22	0.17	0.17	0.18	0 15	0.19	0.16	0 14	0.13	0 14	0 20
MgO	33 00	32 84	32 98	32.87	32 95	33 00	32 58	32 92	32.59	32.70	32 78	32.58
CaO	0 83	0.83	0.82	0.74	0.78	0 79	0.80	0.82	0 78	0.81	0 79	0 77
Total	100.90	100 71	100 89	100.38	100.75	100.97	100.67	101 14	100.08	100 89	100.76	100 73
Si	1 897	1.906	1.904	1.915	1.911	1.909	1.917	1.914	1 920	1.919	1 920	1 916
Ti	0.003	0 002	0.002	0.002	0 003	0.002	0 002	0.002	0 002	0.002	0.002	0 003
Al/Al IV	0 103	0.094	0.096	0.085	0 089	0 091	0.083	0.086	0 080	0.081	0 080	0.084
Al VI	0 063	0.080	0.071	0.078	0.076	0 074	0.081	0.077	0.083	0 085	0 085	0 083
Cr	0.014	0 013	0 014	0.014	0 011	0.014	0.016	0.013	0 010	0.013	0.011	0 016
Fe^{3+}	0 028	0.005	0.015	nd	0.007	0 008	nd	nd	nd	nd	nd	nd
Fe^{2+}	0.164	0.175	0.170	0.179	0.175	0 178	0.184	0.188	0.183	0 184	0 181	0 184
Mn^{2+}	0 003	0.006	0.005	0 005	0.005	0 004	0.006	0.004	0 004	0.004	0 004	0 006
Mg	1 687	1.680	1.685	1 686	1 685	1.684	1 668	1.678	1 676	1.669	1.674	1 666
Ca	0 030	0.031	0.030	0 027	0 029	0 029	0.029	0.030	0 029	0 030	0.029	0 028
Sum Cat#	4 000	4.000	4.000	3 998	4 000	4.000	3.995	3 999	3 996	3 993	3.994	3 994
Mg#	89 8	90.3	90.1	90.4	90 3	90 1	90.1	89 9	90.2	90 1	90 2	90.1
Ca#	1 6	1.6	1 6	1.4	1 5	1 5	1.6	1.6	1.5	1 6	1.5	1 5
Cr#	4.5	4.5	4.7	5.0	3 9	4 8	5.7	4.5	3 7	4.7	4 0	5.6
Wo	1 6	1 6	1.6	1 4	1 5	1.5	1.6	1.6	1.5	1 6	1.5	1 5
En	89.7	89.1	89 4	89.1	89.2	89 1	88.7	88 5	88.8	88.6	88 9	88.7
Fs	8 7	9.3	9.0	9 4	9.3	9 4	9 8	9.9	9.7	9 8	9.6	9 8

Group B

Sample	dc13	dc13	dc13	dc13	dc13	dc13	dc13	dc13	dc13	dc13	dc13
SiO_2	55 16	55.72	55.82	55 42	55.78	55 88	55 46	55 39	55.65	55 76	55 59
TiO_2	0 12	0.10	0 14	0 12	0.12	0.14	0 11	0.09	0.12	0 11	0 09
Al_2O_3	4.89	4.76	4 80	4 83	4.79	4 70	4.61	4.77	4.63	4 58	4 59
Cr_2O_3	0 40	0.48	0.42	0 49	0.46	0.40	0.48	0 43	0.44	0 45	0 43
FeO*	6 28	6.00	6 12	6 18	6 06	6 11	6.02	6 19	6.21	6.28	6.15
MnO	0.27	0.14	0.12	0 08	0.14	0.16	0.14	0.18	0 12	0.15	0.11
MgO	32.88	32.76	32 74	32.82	32.81	32.72	32.56	33.01	32 90	32.81	32.94
CaO	0.85	0 81	0.83	0.84	0.85	0.83	0.87	0 82	0 79	0.84	0.81
Total	101.04	100.90	101.13	100 89	101.13	101.08	100 39	101 07	100.99	101 11	100 82
Si	1 887	1.905	1 904	1 897	1.903	1.907	1 906	1.893	1.903	1.905	1.903
Ti	0 003	0 003	0.004	0 003	0 003	0.004	0.003	0.002	0.003	0.003	0 002
Al/Al IV	0 113	0 095	0.096	0 103	0 097	0 093	0.094	0 107	0.097	0 095	0.097
Al VI	0 084	0 096	0.097	0 092	0 096	0 097	0 093	0 085	0 089	0 089	0 088
Cr	0 011	0.013	0.011	0 013	0 012	0 011	0.013	0.012	0 012	0 012	0.012
Fe^{3+}	0 020	nd	nd	nd	nd	nd	nd	0 015	nd	nd	nd
Fe^{2+}	0.160	0.172	0.175	0.177	0.173	0.174	0.173	0.162	0 178	0 180	0 176
Mn^{2+}	0.008	0.004	0.003	0.002	0.004	0 005	0 004	0.005	0.004	0.004	0 003
Mg	1.676	1 669	1.665	1.674	1 668	1 665	1.668	1.681	1.677	1.671	1.681
Ca	0.031	0.030	0 030	0.031	0.031	0.030	0 032	0.030	0.029	0 031	0 030
Sum Cat#	4.000	3 994	3.995	4.000	3 995	3 993	3.995	4.000	3.999	3 998	4.000
Mg#	90.3	90.7	90.5	90 4	90 6	90.5	90 6	90 5	90 4	90.3	90 5
Ca#	1 7	1 6	1 6	1.6	1 7	1 6	1.7	1 6	1.5	1.6	1.6
Cr#	2.8	3.5	2 9	3 4	3.2	2.9	3 5	3 1	3.2	3 2	3.2
Wo	1 7	1.6	1.6	1.6	1 7	1 6	1.7	1 6	1.5	1 6	1 6
En	89 8	89 2	89.0	89 0	89 1	89 0	89 0	89.7	89.0	88 8	89 1
Fs	8.6	9 2	9 3	9.4	9 2	9 3	9.2	8.7	9.4	9 5	9 3

nd = not detected; total Fe as FeO*

Appendix D-7

Electron microprobe analyses of spinel in mantle xenoliths within the Denchai basalts

Group B

Sample	dc5	dc5	dc5	dc5	dc5	dc5	dc5	dc5	dc5	dc5	dc13	dc13
Al_2O_3	40.45	49 62	51 94	51 95	52 11	52 20	52 35	57.01	58.28	59 67	56.13	56.31
Cr_2O_3	29.02	19.67	17.52	16.95	17 01	17.46	17 10	11 71	11 41	9.54	12.97	12 36
Fe_2O_3	1.31	1 27	1.41	1.57	1 37	0.21	1 06	1 09	0.00	0.49	1.10	1 48
FeO	13 73	10 60	10 42	10 14	10.39	10.93	10.52	9.30	10 64	10.38	9 51	8.91
MnO	0.17	0 03	0 06	0 13	0 03	0 12	0.18	0.12	0.04	0 05	0 03	0 06
MgO	16.12	19 27	19 60	19 62	19 51	19 20	19 36	20 65	19.93	20.36	20 50	20 73
NiO	0 30	0 27	0 41	0.36	0.40	0 28	0.38	0 32	0 37	0 38	0.36	0.41
Total	101 49	101.00	101.66	101.09	101.28	100.80	101 40	100.54	100.88	101.06	100 91	100 58
Si	0.001	0.002	0 001	0.001	0 001	0.002	0 001	0.001	0.001	0 001	0 001	0 001
Ti	0.001	0.002	0.002	0.002	0 002	0.002	0 002	0 002	0 002	0 002	0 002	0 001
Al VI	1.327	1.552	1.601	1.608	1.611	1 621	1.617	1.731	1 763	1.791	1.706	1.713
Cr	0 639	0 413	0 362	0.352	0.353	0 364	0.354	0.239	0 232	0.192	0.265	0.252
Fe^{3+}	0 027	0 025	0 028	0 031	0.027	0 004	0 021	0 021	nd	0.009	0 021	0.029
Fe^{2+}	0 320	0 235	0 228	0 223	0.228	0.241	0 230	0 200	0.228	0.221	0.205	0 192
Mn^{2+}	0 004	0.001	0 001	0 003	0.001	0.003	0 004	0 003	0.001	0.001	0 001	0 001
Mg	0.668	0.763	0 764	0 768	0.763	0.754	0 756	0 793	0 763	0.773	0 788	0 798
Ni	0.007	0 006	0 009	0 008	0 008	0 006	0 008	0 007	nd	nd	0 007	0 009
Sum Cat#	3 000	3 000	3 000	3 000	3 000	3 000	3 000	3 000	2 999	3 000	3 000	3 000
Mg#	65 8	74 6	74 9	75.1	75 0	75.5	75.1	78 2	77 0	77 1	77.7	78.3
Cr#	32.1	20.8	18.2	17.7	17 7	18 3	17 8	12 0	11 6	9 6	13 3	12 6

Group B

Sample	dc13	dc13	dc13	dc14	dc14	dc19	dc19	dc19	dc19	dc27	dc27	dc43
Al_2O_3	56 55	56.59	56 71	59 51	59.69	59.95	59 99	60 04	60 49	58 96	59.08	58.67
Cr_2O_3	12.42	12.55	12.46	9.11	9.32	8.63	8 51	8.49	8 26	9.68	10.00	10 01
Fe_2O_3	1 19	1 01	1 01	0 31	0.66	0 92	0 56	0.65	0.82	0.43	0.14	0 61
FeO	9.36	9.50	9.45	10.71	10.33	9 66	9 43	9 88	9 60	10.14	10.60	10 87
MnO	0.12	0 11	0 09	0 10	0 15	0 05	0.05	0.09	0.09	0.07	0 11	0.11
MgO	20.53	20 51	20.47	19 90	20 20	20.71	20 79	20 48	20 92	20.16	19 99	19.87
NiO	0 33	0 41	0 41	0 12	0 22	0 45	0.37	0 36	0 34	0 42	0 39	0 33
Total	100.89	101.04	100.98	100 36	101 16	100 69	99 91	100.22	100.80	100.22	100 79	100.79
Si	0 001	0 002	0 001	0 002	0 001	0.002	0.001	0.001	0.002	0 001	0 002	0 001
Ti	0 002	0 002	0.001	0 002	0 002	0.002	0.002	0.002	0 002	0 003	0 003	0.003
Al VI	1.717	1.716	1.720	1.801	1.793	1.800	1 809	1.810	1 809	1 787	1.784	1.776
Cr	0 253	0 255	0.254	0.185	0.188	0.174	0 172	0.172	0.166	0.197	0.203	0 203
Fe^{3+}	0.023	0 020	0.020	0.006	0.013	0.018	0 011	0.013	0.016	0 008	0.003	0 012
Fe^{2+}	0.202	0 204	0.203	0.230	0 220	0.206	0.202	0 211	0 204	0 218	0.227	0 233
Mn^{2+}	0.003	0 002	0.002	0.002	0 003	0.001	0 001	0.002	0 002	0 002	0.002	0 002
Mg	0.788	0 786	0 785	0.762	0 767	0.786	0.793	0.781	0.791	0 773	0.763	0 760
Ni	0.007	0.009	0.008	0.008	0.009	0 009	0 008	0.007	0.007	0.009	0.008	0 007
Sum Cat#	3.000	3.000	3.000	3.000	3.000	3.000	3 000	3.000	3 000	3.000	3.000	3 000
Mg#	77 8	77.8	77 9	76 4	76 7	77 8	78.8	77.7	78 2	77.4	76.8	75 6
Cr#	12.7	12.8	12.7	9.3	9.4	8.7	8.6	8 6	8 3	9 9	10 2	10.2

nd = not detected

Appendix D-7 (Continued)

Group B

Sample	dc43	dc43	dc43	dc62
Al_2O_3	58 83	59.41	60 15	56 00
Cr_2O_3	10.44	9 58	8 42	8 87
Fe_2O_3	0 40	0 52	0 68	3.33
FeO	10.14	11.00	11.18	13.87
MnO	0.12	0 12	0.05	0.19
MgO	20.35	19.93	19.80	17 44
NiO	0 41	0 36	0 40	0.33
Total	100.99	101 13	101 06	100 49
Si	0 002	0.001	0 001	0.002
Ti	0 002	0 003	0.003	0.004
Al VI	1 772	1 788	1 809	1 738
Cr	0 211	0 193	0 170	0 185
Fe^{3+}	0 008	0 010	0.013	0.066
Fe^{2+}	0.217	0 235	0 239	0 305
Mn^{2+}	0.003	0.003	0 001	0 004
Mg	0.775	0.759	0.753	0 685
Ni	0 008	0.007	0.008	0.007
Sum Cat#	3 000	3.000	3 000	3.000
Mg#	77 5	75 6	74 9	64.9
Cr#	10 6	9 7	8.5	9.3

nd = not detected

Appendix D-8

Electron microprobe analyses of clinopyroxene in crustal xenoliths within the Denchai basalts

Group A					
Sample	dc42	dc42	dc42	dc42	dc42
SiO_2	52.42	52 19	52.18	51 95	52 15
TiO_2	0 22	0.17	0 17	0 14	0 21
Al_2O_3	1 20	1 21	1 20	1.20	1 22
Cr_2O_3	nd	0 05	0.02	0 02	nd
FeO*	12 59	12.35	12.28	12.48	12.06
MnO	0 47	0.40	0.33	0 38	0.36
MgO	12 32	12.35	12.33	12.38	12.41
CaO	21 38	21.33	21.77	21.36	21.46
Na_2O	0.34	0 35	0 33	0.37	0 33
Total	101.05	100.56	100 80	100.46	100 31
Si	1 962	1.961	1.957	1.955	1.963
Ti	0 006	0.005	0.005	0.004	0.006
Al/Al IV	0 038	0.039	0.043	0 045	0.037
Al VI	0.016	0.015	0.010	0 008	0.017
Cr	nd	0.002	0 001	0 001	nd
Fe^{3+}	0.034	0.038	0 047	0 055	0.032
Fe^{2+}	0.360	0.350	0 339	0 338	0.347
Mn^{2+}	0.015	0.013	0 011	0.012	0.012
Mg	0.687	0.692	0.689	0.695	0.696
Ca	0 857	0.859	0 875	0 861	0 866
Na	0.025	0 026	0.024	0.027	0.024
Sum Cat#	4 000	4.000	4 000	4.000	4.000
Mg#	63.6	64.1	64 1	63.9	64 7
Ca#	43.9	44.0	44 6	43 9	44 3
Wo	43 9	44.0	44 6	43.9	44 3
En	35 2	35.5	35 1	35.4	35 6
Fs	20 9	20.5	20 2	20.7	20 0

Group C			
Sample	dc16	dc16	dc16
SiO_2	47 57	50.22	50.52
TiO_2	2.64	0.11	0 07
Al_2O_3	4.50	1.06	0 92
Cr_2O_3	0.07	0.05	nd
FeO*	10 06	15.99	16 56
MnO	0.13	0 26	0 35
MgO	12.19	8 63	8 79
CaO	21 59	22 52	22.55
Na_2O	0.47	0.23	0.20
Total	99.50	99 23	100.20
Si	1.801	1.957	1.953
Ti	0.075	0 003	0 002
Al/Al IV	0.199	0 043	0.042
Al VI	0.002	0 006	nd
Cr	0.002	0.002	nd
Fe^{3+}	0.080	0 046	0 063
Fe^{2+}	0.238	0 476	0 472
Mn^{2+}	0.004	0.008	0 012
Mg	0.688	0 501	0 507
Ca	0 876	0 940	0 934
Na	0.035	0 017	0 015
Sum Cat#	4.000	4.000	4 000
Mg#	68.4	49 0	48.7
Ca#	46.4	47 7	47.0
Wo	46 4	47.7	47.0
En	36 5	25.4	25.5
Fs	17.1	26 9	27.5

Group C										
Sample	dc16	dc16	dc16	dc16	dc16	dc16	dc16	dc16	dc16	dc16
SiO_2	50.61	51.05	51.18	51 20	51.21	51.30	51 41	51 42	51.43	51.54
TiO_2	0 09	0.37	0.09	0.09	0 16	0 08	0.11	0 34	0.10	0.06
Al_2O_3	0.92	1 36	0 82	0 88	1.14	0.86	0 93	1.27	0.86	0.83
Cr_2O_3	0.03	0.03	0.03	nd	0 04	0.05	0.03	0 05	0.01	nd
FeO*	16.49	14 05	15.59	16 17	15 90	15 92	16 44	12.77	15 72	15.85
MnO	0.43	0.34	0 36	0 37	0 47	0.32	0.43	0.24	0.31	0 33
MgO	8.41	10.35	9 19	8 82	9 30	9 08	8.59	11 35	9 11	9 12
CaO	22 20	23.22	23 53	23 51	23.03	23 51	22.80	23 30	23 40	23 34
Na_2O	0 22	0 27	0 21	0 21	0.29	0 21	0 22	0.30	0 19	0 20
Total	99 51	101 30	101 24	101 48	101.85	101.58	101 07	101.37	101.32	101.47
Si	1 971	1.930	1.952	1.953	1.941	1 951	1.970	1 930	1.960	1.961
Ti	0.003	0.010	0.002	0 003	0 005	0.002	0 003	0.010	0 003	0.002
Al/Al IV	0.029	0.061	0 037	0.039	0.051	0.039	0.030	0 056	0 038	0 037
Al VI	0.013	nd	nd	nd	nd	nd	0.012	nd	nd	nd
Cr	0 001	0 001	0 001	nd	0 001	0.001	0.001	0 002	nd	nd
Fe^{3+}	0 027	0.077	0 070	0.066	0 080	0 069	0.028	0.087	0 050	0 051
Fe^{2+}	0 509	0 367	0 427	0 450	0 424	0.438	0 499	0.314	0 451	0 453
Mn^{2+}	0.014	0 011	0.012	0 012	0.015	0 010	0 014	0.008	0 010	0 011
Mg	0 488	0.583	0 522	0 502	0 526	0 515	0.491	0.635	0 517	0 517
Ca	0.926	0 940	0.961	0 961	0 935	0 958	0 936	0.937	0 955	0.952
Na	0 017	0.020	0 015	0 016	0 021	0.016	0 016	0.022	0 014	0 015
Sum Cat#	4 000	4 000	4 000	4 000	4 000	4 000	4.000	4 000	4.000	4.000
Mg#	47.7	56 8	51.2	49.3	51.1	50.4	48.2	61 3	50.8	50.6
Ca#	47.1	47.5	48.2	48.3	47.2	48.1	47.6	47.3	48.2	48.0
Wo	47.1	47 5	48 2	48.3	47 2	48 1	47.6	47 3	48.2	48 0
En	24 8	29 5	26 2	25.2	26 6	25 9	24.9	32.1	26 1	26 1
Fs	28 0	23.0	25 6	26.5	26 2	26.0	27.5	20 6	25.8	26 0

nd = not detected, total Fe as FeO*

Appendix D-8 (Continued)

Group C

Sample	dc16	dc16	dc16	dc16	dc16	dc29	dc29	dc29	dc29	dc29	dc29
SiO_2	51 63	51.75	51 86	52 15	52.28	50 66	51.17	51 48	51.61	51.65	51.84
TiO_2	0.19	0.25	0.25	0 19	0 33	0.06	0.09	0.18	0 11	1.07	0.22
Al_2O_3	0 90	0.90	0.90	0 96	1 07	0.70	1.07	0.78	1 02	4.41	0.91
Cr_2O_3	0 08	nd	0.02	0 09	0.04	nd	0.05	0.01	0.04	0.11	nd
FeO*	14 08	13.74	12 73	13 71	12 27	14.43	14.29	11.10	13 78	9.88	11 42
MnO	0 29	0.40	0.34	0 48	0.30	0.22	0.21	0.22	0 43	0.20	0.31
MgO	10 58	10 73	11 59	10.96	11 93	9.89	9.82	12.36	10 63	10 74	12.04
CaO	23.22	23 32	23 14	22.78	22 97	23.60	23.33	22.90	23 18	20 41	22 92
Na_2O	0.27	0 28	0.30	0 31	0 30	0.17	0.22	0.30	0 23	0 69	0.29
Total	101 51	101 63	101.43	101 85	101 74	100.03	100.45	99 58	101 28	100 00	100 13
Si	1 947	1.946	1.944	1.955	1.948	1 946	1.954	1 951	1 948	1.933	1.957
Ti	0 005	0 007	0 007	0.005	0 009	0 002	0.003	0.005	0 003	0 030	0 006
Al/Al IV	0.040	0 040	0.040	0 042	0.047	0.032	0 046	0 035	0 046	0.067	0.041
Al VI	nd	nd	nd	nd	nd	nd	0 002	nd	nd	0 127	nd
Cr	0.002	nd	nd	0 003	0.001	nd	0.001	nd	0.001	0 003	nd
Fe^{3+}	0.074	0.074	0 080	0.057	0 060	0 086	0 054	0 075	0 067	nd	0.054
Fe^{2+}	0.370	0 358	0 319	0 373	0 323	0.378	0 403	0 277	0 368	0 309	0.307
Mn^{2+}	0.009	0 013	0.011	0 015	0.010	0 007	0.007	0 007	0 014	0.006	0 010
Mg	0.595	0.602	0 648	0 612	0 662	0 566	0 559	0 698	0.598	0 599	0 678
Ca	0.938	0 940	0 929	0.915	0 917	0.971	0 955	0.930	0.938	0 818	0.927
Na	0.020	0 020	0.022	0 022	0.021	0 013	0.017	0 022	0.017	0.050	0 021
Sum Cat#	4.000	4.000	4 000	4.000	4 000	4.000	4 000	4 000	4.000	3.983	4.000
Mg#	57 3	58.2	61 9	58 7	63.3	55 0	55.0	66.5	57.9	66.0	65.3
Ca#	47 2	47.3	46 8	46.4	46 5	48.4	48 3	46.8	47 3	47.2	46.9
Wo	47 2	47.3	46 8	46 4	46.5	48 4	48.3	46.8	47.3	47.2	46 9
En	30 0	30.3	32 6	31 0	33 6	28 2	28.3	35.1	30 1	34.6	34.3
Fs	22 8	22 4	20.6	22 6	19.9	23.5	23 5	18.1	22 6	18 2	18.8

Group C

Sample	dc29	dc29	dc29	dc29	dc29	dc29	dc29	dc29	dc29	dc29
SiO2	51.99	52 06	52 11	52.19	52 19	52 33	52 46	52 55	52 72	53 26
TiO2	0.08	0 05	0 16	0.45	0 13	0 12	0 23	0.14	0.37	0 20
Al2O3	1 33	1.35	2 06	1.38	2 01	1 67	0 83	2.04	1 24	0.46
Cr2O3	0.07	0 03	0.04	0.11	0 02	0 04	0.06	nd	0.01	0 03
FeO*	11.57	10 73	8 51	9.69	9 17	8.91	11 49	8.72	8 65	9 47
MnO	0 30	0.38	0 33	0 23	0.31	0 35	0.26	0 30	0 27	0.22
MgO	11 85	12.15	13.67	13.54	13 12	13.24	12 48	13 42	14.24	13.79
CaO	23.69	23.90	23.92	22 98	23.45	23.90	23.51	23.86	22 95	23 25
Na2O	0.12	0.11	0 12	0 32	0.15	0.13	0.32	0.14	0.31	0.25
Total	101.22	100 93	101.15	101 16	100.68	100 87	101.95	101.31	100 97	101.11
Si	1 945	1.947	1 924	1.933	1 940	1 942	1 944	1.938	1.946	1 972
Ti	0.002	0 001	0 004	0.012	0 004	0 003	0.006	0.004	0 010	0 005
Al/Al IV	0.055	0 053	0.076	0.060	0.060	0 058	0 036	0.062	0 054	0.020
Al VI	0 004	0 007	0.014	nd	0.029	0 015	nd	0 027	nd	nd
Cr	0 002	0.001	0 001	0.003	nd	0.001	0.002	nd	nd	0 001
Fe3+	0.055	0 050	0.061	0 069	0.035	0 046	0 083	0.037	0 055	0 043
Fe2+	0 307	0 286	0.201	0 231	0 250	0 231	0 273	0.232	0 212	0 250
Mn2+	0.009	0.012	0 010	0 007	0.010	0.011	0.008	0.009	0 009	0 007
Mg	0.661	0.678	0 752	0 747	0.727	0.732	0.690	0 738	0.784	0 761
Ca	0 950	0 958	0.946	0 912	0.934	0.950	0.934	0 943	0 908	0.922
Na	0.009	0 008	0 009	0.023	0 011	0 010	0 023	0.010	0 022	0 018
Sum Cat#	4.000	4 000	4.000	4.000	4 000	4 000	4 000	4.000	4 000	4 000
Mg#	64 6	66 9	74.2	71.3	71 8	72 5	66.0	73 3	74.6	72 2
Ca#	47.9	48.3	48.0	46 4	47.8	48.2	47.0	48 1	46.1	46.5
Wo	47.9	48.3	48 0	46.4	47 8	48.2	47.0	48.1	46.1	46 5
En	33.4	34 2	38 2	38.0	37.2	37.2	34 7	37.7	39 8	38.4
Fs	18 7	17 5	13 8	15.6	15 1	14 6	18 3	14.2	14 0	15 1

nd = not detected, total Fe as FeO*

Appendix D-9

Electron microprobe analyses of plagioclase in crustal xenoliths within the Denchai basalts

Group A

Sample	dc42	dc42	dc42	dc42	dc42	dc42
SiO_2	58 23	58.42	58.45	58.52	58 73	58 98
TiO_2	nd	nd	0.01	nd	nd	0 04
Al_2O_3	26 24	26 24	26.17	26.34	26 20	26 79
Fe_2O_3	0.09	0.29	0.15	0.23	0.12	0.10
MnO	nd	nd	nd	nd	nd	0.01
MgO	0.00	0.01	nd	nd	0 01	nd
CaO	7.67	7.68	7 69	7.78	7 55	7 77
Na_2O	6 19	6 24	6.25	6.32	6.34	6.27
K_2O	0 77	0 83	1.00	0.76	0.79	0.80
Total	99.38	99 76	99 84	100.08	99.80	100.83
Si	2.621	2.619	2 621	2 617	2 629	2 613
Ti	nd	nd	nd	nd	nd	0.001
Al/Al IV	1 392	1 386	1.384	1.388	1.382	1.399
Fe^{3+}	0 003	0 010	0.005	0.008	0.004	0 003
Mn^{2+}	nd	nd	nd	nd	nd	nd
Mg	nd	0.001	nd	nd	0 001	nd
Ca	0.370	0.369	0.370	0 373	0.362	0.369
Na	0.540	0.543	0 544	0 548	0 550	0 539
K	0.044	0.048	0.057	0 043	0 045	0 045
Sum Cat#	4 974	4 977	4 984	4 980	4 975	4 972
Ab	56.4	56.6	55.9	56.7	57.4	56.5
An	38.6	38.5	38.0	38.5	37.8	38.7
Or	4.6	5.0	5 9	4 5	4 7	4 8

Group C

Sample	dc16	dc16	dc16	dc16
SiO_2	52.83	52 95	53 06	53 43
TiO_2	0 02	nd	0.03	0.01
Al_2O_3	31 11	30.99	30 26	30.49
Fe_2O_3	0 07	0 07	0.25	0 18
MnO	nd	nd	0 02	0 01
MgO	nd	0 01	0 03	nd
CaO	13.15	12 94	12.01	12 63
Na_2O	4.06	4.13	4.38	4.36
K_2O	0 29	0.27	0.34	0.34
Total	101 60	101.47	100 46	101.50
Si	2 361	2 368	2 393	2.388
Ti	0.001	nd	0 001	nd
Al/Al IV	1.639	1 633	1 609	1 606
Fe^{3+}	0.002	0 002	0.009	0 006
Mn^{2+}	nd	nd	0 001	0 001
Mg	nd	0.001	0.002	nd
Ca	0.629	0.620	0 580	0 605
Na	0 352	0.358	0.383	0 377
K	0.016	0 015	0 019	0 019
Sum Cat#	5 002	5 000	4.998	5.004
Ab	35.2	36.0	38.9	37.6
An	63.0	62.3	59.0	60.3
Or	1 6	1.5	2.0	1 9

Group C

Sample	dc16	dc16	dc16	dc16	dc16	dc16	dc16	dc16	dc16	dc16	dc16	dc16
SiO_2	53 60	53 62	53 79	53 97	54.01	54 10	54 15	54 46	54.56	55 38	55.38	55.49
TiO_2	nd	nd	nd	nd	0 01	0.10	0.01	0.02	0.09	nd	0.02	nd
Al_2O_3	29 66	30 23	30 37	29 94	29 83	29 66	29 81	29 72	29.22	28.18	28.99	28 93
Fe_2O_3	0.08	0.13	0.11	0.26	0.22	0 35	0 11	0 08	0.39	0 13	0.07	0.03
MnO	0.03	nd	nd	0.02	nd	nd	nd	0.01	0 01	nd	0.01	nd
MgO	0.02	0.02	0.02	0 03	nd	0 04	nd	0 02	0.11	0.02	0.01	nd
CaO	11.48	12.40	12.29	12.11	12.15	11.92	12.00	11.60	11 72	9 90	10 88	10.83
Na_2O	4.52	4.56	4.46	4.63	4.67	4.68	4.66	4.71	4 80	5.45	5.25	5.29
K_2O	0 50	0.29	0.39	0.33	0 39	0 52	0 37	0.40	0.42	0.52	0.44	0.50
Total	99 94	101 30	101.47	101.40	101 33	101.38	101.18	101.03	101.37	99.57	101.06	101.09
Si	2.424	2.400	2.401	2.412	2 416	2.419	2.423	2.436	2.437	2.504	2.472	2 477
Ti	nd	nd	nd	nd	nd	0.003	nd	0.001	0 003	nd	0.001	nd
Al/Al IV	1 581	1.594	1 597	1.577	1.572	1 563	1 572	1 566	1.538	1.501	1.525	1 522
Fe^{3+}	0 003	0.004	0.004	0 009	0.008	0 012	0 004	0 003	0 013	0.004	0.002	0.001
Mn^{2+}	0 001	nd	nd	0 001	nd	nd	nd	nd	nd	nd	0.001	nd
Mg	0.001	0.001	0 001	0.002	nd	0.002	nd	0.002	0 007	0.001	0.001	nd
Ca	0.556	0 594	0 588	0.580	0.582	0.571	0 575	0.556	0 561	0.480	0 520	0 518
Na	0.396	0 395	0 386	0 401	0.405	0 405	0.405	0.408	0 416	0.477	0 455	0.458
K	0.029	0 017	0 022	0.019	0.022	0 030	0.021	0.023	0.024	0.030	0 025	0 029
Sum Cat#	4.994	5.007	5.000	5.003	5.007	5.007	5.002	4.994	5.002	4.997	5 003	5 005
Ab	40 4	39.3	38.8	40.1	40 1	40.3	40.4	41 4	41.5	48.4	45.5	45.6
An	56 7	59.0	59.0	57.9	57 6	56.8	57.4	56.3	56.0	48.6	52.0	51.6
Or	2.9	1.6	2.2	1.9	2.2	2.9	2.1	2.3	2 4	3.1	2 5	2.9

nd = not detected

Appendix D-9 (Continued)

Group C

Sample	dc16	dc16	dc16	dc16	dc16	dc29	dc29	dc29	dc29	dc29	dc29	dc29
SiO_2	55.54	55 58	55 95	55.97	56 38	46 71	46 90	46.99	47 19	47 24	47.28	47 40
TiO_2	nd	0.01	0 03	0 03	nd	0 01	nd	0 02	nd	0.03	0 01	0 01
Al_2O_3	28.79	28 78	28 21	28 78	28.31	34.29	34 20	34 19	34.21	34 36	34.11	34 19
Fe_2O_3	0.29	0 15	0 17	0 17	0.14	0.09	0 14	0.15	0.12	0.11	0.15	0.16
MnO	nd	0.02	0.03	nd	nd	0 05	0.06	nd	nd	nd	nd	nd
MgO	0 01	0 02	0 02	0.02	0.04	0 03	0 01	0.00	0.02	0.01	0.03	0.03
CaO	10 87	10.75	10.50	10 78	10 14	17 31	17.23	17.29	17 10	17.35	17.26	17.15
Na_2O	5.40	5.23	5 58	5 36	5.57	1.87	1 91	1.81	1.86	1.86	1 96	2.01
K_2O	0 46	0.52	0.48	0.55	0 60	0.09	0.13	0.10	0 11	0 09	0 10	0 14
Total	101.39	101.09	101.06	101.69	101 24	100 47	100.61	100 59	100.73	101 09	100.97	101.10
Si	2 475	2 481	2.499	2.484	2.510	2 139	2.145	2.148	2 153	2 149	2.154	2 156
Ti	nd	nd	0.001	0.001	nd	nd	nd	0.001	nd	0 001	nd	nd
Al/Al IV	1 512	1 514	1.485	1.506	1.486	1 851	1 843	1 842	1.839	1.842	1.832	1 832
Fe^{3+}	0 010	0.005	0.006	0.006	0 005	0 003	0.005	0.005	0 004	0 004	0.005	0 006
Mn^{2+}	nd	0 001	0.001	nd	nd	0 002	0.002	nd	nd	nd	nd	nd
Mg	0.001	0.002	0.001	0 001	0 003	0 002	0 001	nd	0.001	0 001	0.002	0.002
Ca	0.519	0 514	0.503	0.513	0.484	0 849	0 844	0 847	0.836	0.845	0.842	0.836
Na	0 466	0 452	0.483	0.461	0.480	0.166	0.170	0.161	0.164	0.164	0.173	0.177
K	0 026	0 029	0 027	0.031	0 034	0.005	0.008	0.006	0 006	0 005	0.006	0.008
Sum Cat#	5 010	4.999	5 008	5 004	5.002	5.019	5.018	5.010	5 008	5.012	5.016	5.017
Ab	46 1	45.4	47.6	45.9	48.1	16 3	16 6	15.8	16 3	16 2	16.9	17 4
An	51.3	51.6	49 6	51.0	48 4	83 2	82 6	83.6	82.9	83 3	82 4	81 9
Or	2.6	3.0	2.7	3.1	3 4	0 5	0 8	0 6	0 6	0.5	0.6	0 8

Group C

Sample	dc29	dc29	dc29	dc29	dc29	dc29	dc29	dc29	dc29	dc29	dc29	dc29
SiO_2	47 46	47.46	47 47	47 57	47 64	47 75	48.02	48.31	45 36	45.54	45 76	46 04
TiO_2	nd	nd	0.01	nd	nd	nd	nd	nd	0.02	nd	0 02	nd
Al_2O_3	33 91	34.20	34.35	33.79	34 13	34.13	33 84	33.24	35.99	35.64	35 80	35.50
Fe_2O_3	0.23	0 25	0.17	0.24	0.10	0 19	0 11	0.26	0 23	0 17	0 08	0 09
MnO	0.05	0.05	nd	nd	0 02	0 02	nd	nd	nd	0 01	nd	nd
MgO	0.01	0.03	nd	0 03	nd	0.05	0 03	0.01	0.03	0.02	0 02	0 01
CaO	16 99	17.13	17.18	16 34	17 14	17.10	16 16	16.53	18.94	18.83	18.54	18 79
Na_2O	1.99	2.01	1 93	2.20	2.07	2.00	2.33	2.28	1.03	1.13	1.19	1.17
K_2O	0.15	0.17	0.09	0 18	0 11	0 10	0 15	0.17	0 07	0.07	0 08	0 07
Total	100.81	101 31	101 24	100 40	101 32	101 42	100.69	100 83	101 77	101.42	101 52	101 69
Si	2.164	2.155	2.155	2.174	2.160	2.163	2.186	2.199	2.060	2.074	2.079	2.089
Ti	nd	nd	nd	nd	nd	nd	nd	nd	nd	nd	nd	nd
Al/Al IV	1.822	1 830	1 838	1.820	1.824	1.822	1 816	1 783	1.926	1 913	1 917	1.898
Fe^{3+}	0.008	0 008	0 006	0 008	0.003	0.007	0 004	0 009	0 008	0 006	0 003	0 003
Mn^{2+}	0 002	0 002	nd	nd	0.001	0.001	nd	nd	nd	nd	nd	nd
Mg	0.001	0.002	nd	0 002	nd	0.003	0.002	0 001	0.002	0.001	0.001	0 001
Ca	0.830	0 834	0 835	0 800	0.833	0 830	0 788	0 806	0 921	0 919	0 903	0 914
Na	0.176	0.177	0.170	0.195	0 182	0.176	0 206	0 201	0 091	0 100	0 105	0 103
K	0.008	0.010	0.005	0.010	0 006	0.006	0 009	0 010	0 004	0 004	0 004	0 004
Sum Cat#	5.012	5.018	5 010	5 013	5 014	5.010	5 011	5 010	5 017	5 017	5 014	5 013
Ab	17 3	17 3	16.8	19.4	17.9	17.4	20.5	19.8	9 0	9 7	10.4	10 1
An	81.8	81.7	82.6	79.5	81.5	82 0	78.5	79 2	90 6	89 9	89 1	89.5
Or	0 8	0 9	0.5	1.0	0.6	0.6	0 9	1 0	0 4	0 4	0 4	0 4

nd = not detected

Appendix E

Fluid inclusion data

Sample	Type	Size (microns)	Population	Tm -CO2	Th (V)	Th (L)	Tdissolv.
MS001	I	9	2	-55 8			
MS001	I	10	2	-55 8			
MS001	I	30	1	-55 8			
MS001	I	6	2	-55.9			
MS001	I	9	1	-55 9			
MS001	I	10	2	-55.9			
MS001	I	15	1	-55.9			
MS001	I	10	4	-56.3		19 9	
MS001	I	7	1	-56.7			
MS001	I	5	1	-56 9			
MS001	I	5	1	-56.2			
MS001	I	4	3	-56 3			
MS001	I	6	1	-57.2			
MS001	I	12	1	-57 2			
MS001	I	3	1	-57.0			
MS001	I	15	1	-57 0			
MS001	I	7	1	-56.9			
MS001	I	3	1	-56.5			
MS001	I	9	5	-57 2			
MS001	I	27	1	-57.7			
MS001	I	15	1	-57.0			
MS001	I	6	2	-57.1			
MS001	I	12	1	-57.1			
MS001	I	8	4	-57.1	25.5		
MS002	I	9	3	-56.1			
MS002	I	24	1	-55 6			
MS002	I	9	2	-56 3			
MS002	I	5	2	-56 0			
MS002	I	6	1	-56.0			
MS002	I	12	1	-56.0			
MS005	I	10	1		24.6		
MS005	I	7	1	-55 7		13.9	
MS005	I	6	4			14.2	
MS005	II	13	1				480-510
MS005	II	15	1				480-510
BK003	I	15	2	-56.4			
BK003	I	9	2	-56 5			
BK003	I	9	1	-56 0			
BK003	I	9	1		24.9		
BK003	I	10	1		26.6		
BK003	I	15	1		28.8		
BK003	I	9	1	-56.1			
BK003	I	5	4	-56 1			
BK003	I	5	2	-56 0			
BK003	I	10	5	-56 3			
BK003	I	5	2	-56 3			
BK001	I	9	1	-55.9			
BK001	I	5	1	-55.8			
BK001	I	7	1	-55.7			
BK009	I	9	1	-56 4			
BK009	I	12	1	-55 6			
BK009	I	5	1		28.2		
BK017	I	5	1		29.7		
BK017	I	6	1		28.9		
BK017	I	11	1		29 6		
BK019	I	9	1			11.2	
BK019	I	9	1		29.6		
BK019	I	7	1		28 4		
BK003	I	6	1	-55.6			

Note. Tm = melting temperature, Th = homogenisation temperature, Tdissolv. = dissoved temperature

Appendix E (Continued)

Sample	Type	Size (microns)	Population	Tm -CO2	Th (V)	Th (L)	Tdissolv.
BK001	I	10	1			28.1	
BK001	I	7	1			20 6	
BK001	I	5	1	-55 6			
BK001	I	9	1	-55 7			
BK001	I	5	1		29 5		
BK006	I	7	1			29 9	
BK006	I	7	1			19 3	
BK006	I	11	1			29 5	
BK006	I	12	1			20 7	
BK006	I	7	1			29 8	
BK006	I	5	1			20 2	
MS002	I	6	1			29.9	
MS002	I	6	1			29 6	
MS002	I	10	1			19 7	
MS002	I	6	1			29 8	
MS002	I	9	1			20 7	
MS002	I	6	1			29 4	
MS002	I	7	1			23.5	
MS004	I	10	1		26.8		
MS004	I	5	1		27.5		
MS004	I	6	1			22.7	
MS004	I	12	1		27 7		
MS004	I	5	1		24 6		
MS004	I	5	1			22 9	
BK003	I	9	1		29 3		
BK003	I	9	1		29 2		
BK003	I	7	1			23 4	
BK003	I	9	1		24 6		
BK003	I	9	1			16 2	
BK003	I	12	1			30.6	
BK003	I	12	1			31	
BK003	I	10	1			28 3	
BK003	I	12	1			23 7	
BK003	I	9	1			11.6	
BK003	I	12	1			29.1	
BK003	I	6	1		27.5		
BK003	I	12	1		29.7		
BK003	I	9	1		25.7		
BK003	I	7	1		30.4		
BK003	I	5	1		26.4		
BK003	I	7	1		29.9		
BK003	I	12	1			24.2	
BK003	I	5	1	-55 6			
BK003	I	6	1	-55.7			
BK003	I	7	1			25.5	
BK003	I	9	1			22.9	
BK003	I	7	1		26.4		
BK003	I	11	1		28 8		
BK003	I	10	1			24 3	
BK003	I	12	1			26 6	
BK003	I	10	1			24 5	
BK003	I	6	1		26.0		
BK003	I	5	1		28.6		
BK003	I	12	1			24.4	
BK003	I	5	1			23.1	
BK003	I	7	1	-55 7			
BK003	I	5	1			25.3	
BK003	I	10	1			14.4	
BK003	I	5	1			26.6	
BK003	I	7	1			11 6	

Note. Tm = melting temperature, Th = homogenisation temperature, Tdissolv = dissoved temperature

Appendix F

Electron microprobe analyses of melt inclusion compositions in the Denchai sapphires

Label	SiO_2	Ti_2O	Al_2O_3	FeO	MnO	MgO	CaO	Na_2O	K_2O	P_2O_5	Cr_2O_3	NiO	ZnO	Total	Remarks
melt1	57 00	2.41	27.30	2 54	0 52	0 14	1.48	1.90	3.14	0.13	nd	0 06	0.09	96.70	glass + rutile
melt2a	60.01	0.72	24.88	1.56	0 44	0.15	1.66	2.87	4 42	0 31	0.03	nd	0 01	97.05	glass + hydrous
melt2b	60 84	0.65	25.25	1 66	0.42	0 14	1.74	2 58	4 40	0.36	nd	0 01	nd	98.05	glass + hydrous
M2-1a-incl	59 76	0.17	26.69	0.91	0 08	0 01	0.21	4.69	5 50	0.04	0 05	0 01	nd	98.12	glass + hydrous
M2-1b-incl	59.69	0.15	26 54	0 95	0.02	0.02	0.23	4 94	5.55	0.15	nd	0 04	nd	98 28	glass + hydrous
M2-1c-incl	58 16	0.16	26 86	0 61	0 06	0.02	0 19	4.55	5.94	0.11	nd	0 07	0.01	96 75	glass + hydrous
M2-1d-incl	57.53	0 21	25 65	0 42	0 09	0.02	0 23	3 98	5.44	0.04	nd	0.04	0.24	93 89	glass + hydrous
M2-2a-incl	57.31	0 25	28 08	0.72	nd	nd	0 20	4 79	5.59	0.11	nd	0.07	0.03	97 15	glass + hydrous
M3-1a-incl	67.63	0 01	20 12	0 05	0.18	nd	0 95	2 89	2 02	0 08	0 01	0.01	0.02	93 96	glass + hydrous
M3-1b-incl	68.63	0 03	19.67	0 03	0 09	nd	0 87	2 76	1 92	0 07	0 01	0.02	0 04	94 14	glass + hydrous
M3-1d-incl	63.75	0 03	20 21	0 13	0 02	0.01	0 08	1.37	14.33	0.06	0.04	0 07	0 10	100.20	K-feldspar
M3-1e-incl	54.56	0 04	19.44	0.61	0.05	0.08	0 02	0.76	14.67	0 02	0.01	0 04	0 10	90.41	K-feldspar
M4-2a-incl	48.75	0.34	31.98	3.89	0 19	0 70	0.06	1.19	9 16	nd	nd	nd	0.02	96.28	muscovite
M4-2b-incl	48.18	0.24	33.88	2.67	0 11	0 30	0.04	1.23	9.21	nd	0 01	nd	0.19	96 06	muscovite
M4-2e-incl	63.05	0 02	21.22	0 08	0 07	0 01	0.40	2.10	4.18	0 07	nd	nd	0 05	91.25	glass + hydrous
M6-1e-incl	61.97	0 34	24.38	0 67	0 54	0.09	0.70	4.71	5 42	0.11	0 01	nd	0 15	99 09	glass + hydrous
M6-2d-incl	58.67	0 51	29.61	0.74	0 53	0 22	0.76	5.28	5.28	0.06	0 04	nd	0 31	102.00	glass + hydrous
1	52 16	0.61	29.65	1.53	0 44	0.10	1.54	4.70	5.01	0.33	nd	nd	0.07	96.16	glass + hydrous
3	52 52	0 16	32.35	1.35	0 34	0.11	1.17	4.39	5.18	0 33	nd	nd	0 15	98.07	glass + hydrous
8	49 21	11.37	21 83	4 22	1 14	0.01	0.46	4.00	4.06	0 07	nd	nd	0 34	96.70	glass + rutile
A_7_1_q	64 39	0.02	17.51	0.01	nd	nd	0 39	5 46	4.36	0.04	nd	nd	nd	92.17	glass + hydrous
A_7_2_q	54 45	0.13	21.96	0.88	0 05	0 03	0 10	1.20	11 62	0 03	nd	0 01	0 35	90.81	K-feldspar
A_8_1_q	58 94	0.32	22 97	0.67	0 50	0 02	0.78	6.06	5.65	0 05	0 01	nd	nd	95 96	glass + hydrous
B_5_1_q	62.22	0 79	19 21	0 66	0.47	0 09	0 83	4 58	6 20	0 02	0 03	0.01	0.07	95 16	glass + hydrous
B_5_2_q	53.81	0.88	32 94	1 26	1.11	0.07	0.76	4.03	4 90	0.02	0 03	nd	0.10	99.90	glass + hydrous
B_7_1_p	57 94	0.89	21 85	1.60	0.86	0.14	1.23	6.52	5.38	0.07	0 01	nd	nd	96 48	glass + hydrous
B_8_1_q	53.27	1.17	32 32	1 44	0.79	0.13	0.97	4.86	4 99	0.02	nd	nd	0.10	100.07	glass + hydrous
C_3_12_q	63 32	0.06	18 68	0 04	0.05	nd	0.45	4.46	4 42	0.04	nd	nd	0.23	91.74	glass + hydrous
C_4_2_s	59.43	0 04	24 92	0 33	0.07	0.01	2.26	3.22	4.83	0 14	0 04	nd	1.06	96 36	glass + hydrous
C_5_1_s	58.59	0 03	25 94	0 23	0 05	0 03	0 27	3.38	4.39	0 01	0 01	nd	0.13	93.05	glass + hydrous
C_6_4_s	56 03	0.04	26.28	0 84	0.22	0 02	0 17	1 76	5.93	0 04	0 02	nd	0.60	91.94	glass + hydrous
C_7_3_s	53 85	0.01	25.04	0.04	nd	nd	0.39	8 43	2 26	nd	nd	0.05	0 42	90 49	glass + hydrous

nd = not detected

Appendix F (Continued)

Label	SiO_2	Ti_2O	Al_2O_3	FeO	MnO	MgO	CaO	Na_2O	K_2O	P_2O_5	Cr_2O_3	NiO	ZnO	Total	Remarks
E_3_1_p	64.84	nd	19 60	0 03	0.03	nd	0 29	3 83	11.14	nd	0 02	nd	0.20	99.97	K/Na felspar
E_4_3_s	40 52	1 13	35.77	1 01	0 08	0.05	0.02	1.84	8 42	0.03	0 02	nd	2.11	91.01	muscovite
E_4_4_s	42.94	0 11	34.13	0.15	nd	nd	0.37	15 72	5 75	nd	nd	nd	0.35	99 52	nepheline
E_5_1_s	55.41	0 16	22.07	0.14	0 05	0.01	0.48	6.03	6.60	0.10	nd	nd	0 01	91.06	glass + hydrous
E_5_2_s	53.08	0.16	27.62	0 41	0 07	0.03	0.48	6.20	6 20	0.07	nd	0.07	0.02	94.40	glass + hydrous
E_5_3_s	55.64	0 15	22.31	0 13	0 01	nd	0.45	5 76	6 66	0 06	nd	nd	0.14	91 31	glass + hydrous
E_7_1_q	50.09	0 18	32.80	0.29	nd	0 01	0 28	5.33	4 73	0 03	nd	nd	0 09	93 83	glass + hydrous
E_8_2_s	49 64	0.78	27 23	0 21	0 04	nd	0 11	3.77	9 53	nd	0 01	nd	0 07	91 41	glass + hydrous
E_8_3_s	49 68	1 16	31 50	0.23	0 10	nd	0 11	5 22	4 51	0 03	nd	0 04	0.17	92.74	glass + hydrous
F_1_1_p	58 23	0.84	22 31	2.13	0.09	0 20	0 85	3 25	5.64	0 04	0.01	0 03	0.05	93.66	glass + hydrous
F_4_1_q	49 59	0.41	27.03	3 18	0.26	0 22	0 70	3 01	5.48	nd	0.01	0 05	0.42	90.35	glass + hydrous
N1_1_1	56 89	0 69	24.87	1 65	0.43	0.12	1.80	2.81	5 36	0.34	0.04	nd	0 01	95 01	glass + hydrous
N1_1_1a	57 00	0.74	24.64	1 65	0 30	0.10	1.66	3 10	5 32	0.23	0.01	0.02	nd	94 77	glass + hydrous
N1_1_1b	57.61	0 70	25.27	1 74	0 35	0.11	1.77	2 32	5 31	0.27	nd	0.06	0 10	95 61	glass + hydrous
N1_2_1	57 05	2.73	25 19	2 95	0.66	0.14	1 63	0.49	3 65	0 34	0.02	0.06	0 04	94 94	glass + rutile
N1_2_1a	55.59	2 62	23.97	3 01	0 61	0.15	1.61	1.67	4.82	0 31	0 01	nd	nd	94 38	glass + rutile
N1_3_1	59.44	0 19	23.96	1.36	0 36	0 13	1 38	1.73	5.19	0.32	nd	nd	0.03	94.09	glass + hydrous
N2_1_1a	65 49	0 03	19.26	0 03	0 11	nd	0 93	2 40	1 94	0 08	0 02	0 01	0.04	90.35	glass + hydrous
N3_1_1	55 08	0 19	26.11	0 89	0 06	0 01	0 22	4.79	5.47	0.22	nd	0 02	0.02	93.08	glass + hydrous
N3_1_1a	56 57	0 19	26.26	0.74	0 05	nd	0 20	5 04	5.23	0.08	0.01	0 06	nd	94 44	glass + hydrous
N3_2_1	51.47	0.24	27 57	1.03	0.02	nd	0.17	5 04	5.68	0 14	nd	nd	nd	91.36	glass + hydrous
N7_1_1	65 51	0 03	18.85	0.03	0 05	nd	0.48	2 63	3 90	0 06	nd	nd	nd	91.54	glass + hydrous
N7_2_1	62.38	0 03	18.08	0.05	nd	nd	0.05	0 90	14 49	nd	0 01	nd	0 04	96 03	K-feldspar
N8_1_1	59.84	0 37	25.10	0.76	0.55	0 01	0.75	4 18	5 29	0.11	nd	0 01	0.18	97.13	glass + hydrous
N8_1_1a	59.84	0.44	23 39	0.66	0.64	nd	0 74	4.08	5 20	0 06	0.06	0.01	0.01	95.14	glass + hydrous
N8_2_1	54 74	0.48	27 95	0.60	0.56	0.03	0 74	4.70	4 54	0 01	nd	nd	nd	94 36	glass + hydrous
N8_2_1a	55.62	0 47	28.57	0 70	0.52	0.04	0.75	5.34	4.71	0.11	0.02	nd	nd	96.86	glass + hydrous
N8_2_1b	56 23	0.44	28 20	0 72	0 60	0.06	0 76	3 57	4 45	0 12	nd	nd	nd	95 14	glass + hydrous
H1_1_1	58.50	0.40	23.95	1 29	0 06	0.14	0 40	3 63	6.43	0.07	nd	nd	0.01	94 88	glass + hydrous
H1_2_1	64.73	0 05	20.59	0.04	0 04	0 01	0 68	5 73	7.85	0.06	0 02	0 01	0 01	99.83	glass + hydrous
H1_2_1a	64.70	0.04	20.44	0 02	nd	nd	0.65	5.89	7 71	0.11	0 04	0.06	nd	99.65	glass + hydrous
H1_1_1a	58.81	0 40	24.19	1 26	nd	0 15	0.39	4.75	6.79	0 03	nd	0 01	0 04	96 82	glass + hydrous
H2_2_1a	62.44	0 26	22.15	0.13	0 01	0 01	0.27	3.42	10.10	0 01	0 01	0 04	0.05	98.91	K/Na feldspar
H4_1_1	63.80	0 54	21 11	0 82	0 39	0.06	0.64	2.50	5 67	0 04	nd	nd	0.23	95.80	glass + hydrous

nd = not detected

Appendix F (Continued)

Label	SiO_2	Ti_2O	Al_2O_3	FeO	MnO	MgO	CaO	Na_2O	K_2O	P_2O_5	Cr_2O_3	NiO	ZnO	Total	Remarks
H4_2_1	64.28	0 53	21.27	0 69	0.06	0 05	0 57	3 48	5.54	0.10	nd	0.04	0.08	96.68	glass + hydrous
H5_2_1	63 77	0 72	20.08	0 63	0 41	0 10	0 79	2.25	5 49	0.06	0.01	0.03	0.03	94.38	glass + hydrous
H5_2_1a	64.12	0.79	20 03	0.69	0 49	0 09	0.85	1.91	5.18	0.06	nd	0.07	nd	94.27	glass + hydrous
H5_3_1	62.98	2.00	19 84	0.92	1 30	0 08	0.98	2.77	5.73	0.01	0 01	nd	0 05	96.67	glass + rutile
H7_1_1	59.79	0.99	22.77	1.65	0 82	0 14	1.25	3 94	5.33	0.01	0 04	0 03	nd	96.75	glass + hydrous
H7_1_1a	59.95	0.91	23.10	1.80	0 80	0 16	1 21	3.79	5 23	0 03	nd	0.01	0.04	97.04	glass + hydrous
H7_1_1b	59.95	0 82	22 95	1.63	0.78	0 14	1 14	3.60	5.18	nd	nd	0.07	0 04	96 30	glass + hydrous
H7_2_1	64 15	2.04	19 74	1.57	0.40	0.06	1.18	3.60	5 76	0.07	0.01	0.02	nd	98 60	glass + rutile
H7_3_1	64 39	1.92	19.51	2.22	0 49	0.07	1.05	3 17	5.63	0 07	nd	0 06	0.04	98.62	glass + rutile
H7_4_1	68.32	2.08	20 01	1 60	0 50	0 08	1 26	0 55	2.81	0 05	nd	nd	0.01	97.29	glass + rutile
H7_6_1	57.14	2 86	21.07	4.54	1.06	0 06	0 94	4.82	5.38	0 10	nd	nd	0.03	98.01	glass + rutile
H8_2_1	60.08	1 27	26.62	1.30	0 88	0.12	1 03	1.94	5.16	0.07	0 01	0.01	0.01	98 50	glass + hydrous
H8_2_1a	60 05	1 44	23.79	1 31	0 76	0 12	1.14	3 91	5 60	0.03	0 04	nd	nd	98 18	glass + hydrous
U3_1_1	64.67	nd	21.73	nd	0 02	0.03	0.41	2 63	3 89	0.02	0 02	nd	0 17	93 57	glass + hydrous
U4_3_1	64.29	0.07	18 36	0.35	0 17	0 01	2.84	1 81	4.91	0.22	nd	nd	0.49	93 52	glass + hydrous
U5_2_1	61 80	2.17	19 58	1.24	0 11	0.21	0.29	2.07	4 39	0 12	0 02	0 02	0.01	92.04	glass + rutile
U6_1_1	47.20	0.06	35 02	1.39	0 14	0.02	0 04	0.62	9 37	0 03	0.02	nd	0.28	94.18	glass + hydrous
U6_2_1	44 96	0 36	36.15	0 48	0.03	0.05	1.76	1.66	10 17	0 01	0.02	0.06	0 15	95 85	muscovite
U7_1_1	59.30	0 06	25.34	0 06	nd	nd	0 40	4.71	2.20	0 04	nd	0.05	0.34	92.50	glass + hydrous
M1_1_1	65.37	0 06	19 78	0.13	0 04	0.02	4.57	3 43	3 19	0.08	nd	0.07	0 22	96 97	glass + hydrous
M4_2_1	66 53	0 06	18 51	0.10	0 21	0.01	0.55	2 56	5 10	0 09	0 04	0.04	1.38	95.18	glass + hydrous
G3_1_1	64.82	0.04	19.57	0.01	nd	0 01	0 26	3 88	10.97	nd	nd	nd	0.16	99 72	K/Na feldspar
G3_1_1a	64.73	0.01	19.61	0 05	nd	nd	0 28	3.87	11 16	0 01	0.02	0.01	0.02	99.77	K/Na feldspar
G4_2_1	51 15	0.14	24.55	1 16	0 08	0.24	0 40	2 20	10.85	0.05	0 01	0 09	1 39	92.31	K/Na feldspar
G4_3_1	40 45	0 65	36.27	1.33	0 18	0.07	nd	1 35	8 34	nd	0 03	nd	1 67	90.35	glass + hydrous
G4_4_1	43 03	0.11	34.85	0 15	nd	nd	0.37	15 80	5.84	0 03	0 03	nd	0 15	100.34	nepheline
G4_4_1a	43.38	0 07	35 36	0.16	0 04	nd	0.39	14 21	5.98	0 07	nd	0.03	0.21	99 89	nepheline
G4_5_1	39.55	0 04	37 80	0.47	0 01	0 04	0 05	1.51	8.75	0 06	0.01	nd	2.32	90 63	glass + hydrous
G5_1_1	58 09	0.13	23 48	0.13	0 04	0 01	0 46	3.65	5.65	0.08	0 06	0.02	nd	91.79	glass + hydrous
G5_2_1	58.33	0.12	27 06	0.16	0.04	nd	0 40	3.47	5 35	0.14	0 03	nd	0.11	95.21	glass + hydrous
G5_3_1	57 09	0 15	23 92	0.08	0 04	nd	0.48	3 49	6 09	0 06	0 01	0 03	0 17	91 62	glass + hydrous
G5_4_1	59 12	0.24	23.83	0 17	0.03	nd	0 41	3 66	5.52	0.12	nd	nd	0.10	93 21	glass + hydrous
G8_1_1	57 84	1 21	24 21	0.66	0 30	nd	0 13	3.15	3 78	0.00	nd	nd	0 08	91.38	glass + hydrous
L1_1_1	67 50	0 56	18 59	0.47	0 01	0 20	1.01	0.88	4 83	0 06	nd	nd	0 07	94 19	glass + hydrous

nd = not detected

Appendix F (Continued)

Label	SiO_2	Ti_2O	Al_2O_3	FeO	MnO	MgO	CaO	Na_2O	K_2O	P_2O_5	Cr_2O_3	NiO	ZnO	Total	Remarks
L1_2_1	65 01	0.31	16 45	0.64	0 19	0.20	0 85	3.30	5.94	0 08	nd	nd	0.13	93.09	glass + hydrous
L3_1_1	59.14	0 12	27.10	0 83	0 34	0.04	0 20	2 33	4 78	0.09	nd	nd	0.05	95.01	glass + hydrous
L4_1_1	64 54	0.49	22.47	1 24	0 18	0.25	0.84	3 09	6.29	0.02	nd	nd	0 34	99.76	glass + hydrous
R1_1_1	63.10	nd	20.14	0 06	0 04	nd	0.45	6.36	4 38	0 02	nd	nd	0 10	94 65	glass + hydrous
R1_1_1a	62.94	0.01	22 88	0.07	0.01	nd	0 46	3.66	4.24	0 04	nd	nd	0 01	94.32	glass + hydrous
R1_1_2	64.92	nd	17.39	0.06	0.11	0 01	0 43	4 27	6.66	0 06	nd	0.01	0.06	93.99	glass + hydrous
R1_1_2a	62.14	0 07	18.69	0.31	nd	0.05	0.05	1.16	14 82	0 04	0.01	0.03	0 20	97.56	K-feldspar
R1_4_1	48 81	0 59	33.94	0 23	0 02	0.01	0.22	5 89	3.43	0.02	nd	0 05	0.12	93 33	glass + hydrous
R3_1_1a	48 42	1.22	29.51	1 90	0 17	0.11	0.25	1.94	3.91	0.06	nd	0 03	3 02	90.54	glass + rutile
R3_2_1	52.83	0.01	32 96	0 14	nd	0 01	0 40	4.64	3 01	0 03	nd	0 02	0 06	94.09	glass + hydrous
R3_3_1	56 11	2 69	22.62	3 43	0 55	0.16	0.33	3.83	4 81	nd	nd	nd	0.10	94.62	glass + rutile
R3_3_1a	53 34	0 08	37 00	0.40	0 06	0.02	0 32	1 46	3 34	0 04	nd	nd	0.10	96.15	glass + hydrous
R3_3_3	65 05	0.01	16.87	0 09	nd	nd	0.48	4 74	4 59	0.08	nd	nd	0 05	91 96	glass + hydrous
R3_3_3a	65 47	0.03	17 93	0 03	0 01	0 01	0 55	2.06	3.97	0 06	0 01	nd	0 11	90.25	glass + hydrous
R3_3_6	60.05	0.01	26.92	0 12	0.02	0 01	0 37	4 49	3 71	0.06	0.01	nd	0.00	95.76	glass + hydrous
R3_4_2	58 73	nd	24 98	0.45	0.03	0.01	0 22	3 91	4.38	0 04	0 01	0 01	0 84	93 61	glass + hydrous
R3_4_2a	55.24	0 02	26 51	2.72	0 03	0.19	0.19	1 59	4.64	0 07	nd	nd	0 68	91 88	glass + hydrous
R5_1_1	55.07	0 05	34.57	0.08	nd	nd	1.41	7.79	1.13	0 03	0.02	0 04	0 07	100.28	glass + hydrous
R5_2_1	59 79	0 15	21.61	0.31	nd	nd	0.24	4.19	8.89	0 03	0 02	nd	0.17	95.41	glass + hydrous
R5_2_1a	60.15	0.09	21.53	0.38	nd	0.01	0 25	3.25	8 65	0.02	0 05	0 06	0.18	94 63	glass + hydrous
R5_3_1	49.32	0.63	35 63	0.27	0 03	0.01	0 11	5 14	4.00	nd	nd	0 01	0 13	95 27	glass + hydrous
R5_3_2	46.71	0.45	33 47	0.22	0.03	0 03	0.10	5.54	4 14	0 01	nd	nd	0 18	90.88	glass + hydrous
R5_3_3	44 23	0 97	40.54	0 37	0 06	0.01	0.13	5 30	3.98	nd	nd	0 01	0.12	95.73	glass + hydrous
R5_4_1	46.35	0 19	40 94	0 68	0 17	0 02	0 40	4.83	5.11	0 09	nd	0.02	0.05	98.85	glass + hydrous
R5_6_1	58 41	0.04	23.93	0 53	0 04	0 03	0 50	5.26	4.21	0.03	nd	0.02	0.02	93.03	glass + hydrous
R5_7_1	62.97	0.28	20 77	0.67	0 12	0.15	0 80	2.81	5 69	0.07	nd	0 03	0 15	94 51	glass + hydrous
R4_1_1	47.41	0 19	45.07	0 30	nd	nd	0 17	2.56	7.51	0 05	0.04	nd	0 06	103.35	glass + hydrous
R4_2_1	54.19	0 20	23 93	0.63	0 12	0.02	0.23	8.85	5.63	0 10	nd	0 04	0.02	93.96	glass + hydrous
R4_2_1a	54 45	0.20	23.68	0 72	0.07	0.01	0 20	8.86	5 77	0.08	0.01	nd	0 02	94 07	glass + hydrous
R4_2_2	48 50	0 25	31.05	0 67	0 04	0.01	0.18	8 26	5 08	0.06	0.05	nd	0 10	94.27	glass + hydrous
R4_3_2	51.22	0 21	35.96	0 39	0 04	0 05	0 81	2 80	7.85	0.02	nd	nd	0 25	99.60	glass + hydrous
R4_7_1	48 10	0.57	38 25	1.56	0.44	0 10	0.85	6 18	4.27	0 03	nd	nd	0.03	100 37	glass + hydrous
R4_7_2	54 60	0.92	30 21	2 08	0.77	0.20	1.08	5.43	4.90	0.06	nd	nd	0.09	100 34	glass + hydrous
R2_6_1	58 30	0.41	23 20	1.08	0.08	0 11	0 39	4.30	6 50	nd	nd	nd	0.01	94 39	glass + hydrous

nd = not detected

Appendix F (Continued)

Label	SiO_2	Ti_2O	Al_2O_3	FeO	MnO	MgO	CaO	Na_2O	K_2O	P_2O_5	Cr_2O_3	NiO	ZnO	Total	Remarks
R2_7_1	60 22	0 40	22 42	0.64	0 55	0 01	0.78	3 88	5 20	0 17	nd	0.01	0 05	94 32	glass + hydrous
R2_7_2	52.83	0.45	25.57	0 67	0 49	0.06	0.75	7.11	4.72	0.03	nd	nd	0.07	92.73	glass + hydrous
R2_8_1	57.29	0.65	24.65	1.50	0.44	0.11	1.75	3.91	5.33	0 29	0.02	0 05	0.06	96.03	glass + hydrous
R2_8_3	53.27	0 19	33 11	1.29	0.36	0 12	1 21	2 54	4 71	0 23	nd	nd	0.12	97.16	glass + hydrous
R6_1_1	58.64	0.78	20 94	1.66	0.81	0 15	1 28	6 48	5 39	0 09	0.04	nd	0.10	96.37	glass + hydrous
R6_2_1	62.87	0.74	19 18	0.61	0.37	0.10	0 83	2.70	5 37	0.07	nd	nd	nd	92 84	glass + hydrous
R6_2_2	59 82	1.11	21.38	1 03	1.16	0.08	1.04	3.38	5 41	0.08	nd	0.06	0.05	94 61	glass + rutile
R6_3_1	47.54	5 40	29 38	8.99	0 99	0 18	0.79	2.99	4 06	0 02	0.04	nd	0.01	100 38	glass + rutile
R6_5_1	60 43	0 48	23 73	0.73	0 10	0 17	0.93	2.42	5.17	0 06	nd	nd	0 05	94 28	glass + hydrous
R6_6_1	43 72	0.13	33 03	0.20	nd	0 01	0 36	14 16	5.88	0.05	0.02	nd	0.39	97.94	glass + hydrous
R6_7_1	64.06	0.00	19 23	nd	nd	0 01	0 28	3 90	10.69	0.05	0.01	0 09	0 15	98.46	glass + hydrous

nd = not detected

Appendix G

Mineralogical Magazine, December 2001, Vol. 65(6), pp. 725–735

Formation of the Denchai gem sapphires, northern Thailand: evidence from mineral chemistry and fluid/melt inclusion characteristics

P. LIMTRAKUN[1]*, KHIN ZAW[2], C. G. RYAN[3] AND T. P. MERNAGH[4]

[1] School of Earth Sciences, University of Tasmania, GPO Box 252-79, Hobart, TAS 7001, Australia
[2] Centre for Ore Deposit Research, University of Tasmania, GPO Box 252-79, Hobart, TAS 7001, Australia
[3] CSIRO Exploration and Mining, PO Box 136, North Ryde, NSW 2113, Australia
[4] Australian Geological Survey Organisation, Canberra, ACT 2601, Australia

ABSTRACT

The Denchai gem sapphire deposits in Phrae Province, northern Thailand are closely associated with late Cenozoic alkaline basaltic rocks. The sapphires occur in alluvial placer deposits in palaeo-channels at shallow depths. Electron microprobe analysis of minor and trace element contents (Fe, Ti, Cr, Ga and V) of the sapphires indicate the following oxide abundances: Fe_2O_3 (0.32–1.98 wt.%), TiO_2 (0.01–0.23 wt.%), Cr_2O_3 (<0.01 wt.%), Ga_2O_3 (0.01–0.03 wt.%) and V_2O_5 (<0.03 wt.%). Optical studies of sapphires revealed three types of primary fluid/melt inclusions. CO_2-rich inclusions (Type I) contain three phases (LH_2O + LCO_2 + V) with the vapour phase comprising <10–15 vol.%. The presence of CO_2 was confirmed by microthermometry and laser Raman analysis. Polyphase inclusions (Type II) (vapour + liquid + solid) contain a fluid bubble (20–30 vol.%), an aqueous phase (10–15 vol.%) and several solid phases. Silicate-melt inclusions (Type III) comprise vapour bubbles, silicate glass and solid phases. Proton-induced X-ray emission (PIXE) analysis revealed high concentrations of K (~4 wt.%) as well as Ca (~0.5 wt.%), Ti (~1 wt.%), Fe (~2 wt.%), Mn (~0.1 wt.%), V (<0.03 wt.%), Rb (~70 ppm) and Zr (~200 ppm) in the silicate glass. The Ga_2O_3 abundances and Cr_2O_3/Ga_2O_3 values (<1) of the sapphires favour their formation by magmatic processes. The presence of CO_2-rich fluids and high K concentrations in the silicate melt inclusions link the origin of the Denchai gem sapphires to CO_2-rich alkaline magmatism.

KEYWORDS: sapphire, fluid and melt inclusions, alkaline magmatism, basalt, Thailand.

Introduction

GEM-quality corundums (sapphires and rubies) in Thailand are generally found as alluvial materials that form economic placer deposits. Sapphires and rubies occur in great abundance compared to other gemstones (e.g. garnet, zircon and spinel). The conventional view is that sapphires and rubies are found as weathered and eroded products of late Cenozoic alkali basalts which crop out nearby, though they are sometimes found hosted within fresh basalts (Vichit *et al.*, 1978; Vichit, 1992). Many workers have presented geochemical studies on Thai basalts over the last two decades (e.g. Barr and MacDonald, 1979, 1981; Vichit, 1987, 1992; Vichit *et al.*, 1978) to establish a genetic link between corundum occurrences and basalt geochemistry, though the corundum genesis remains uncertain.

The Denchai gem sapphire deposits are located in Phrae Province, northern Thailand, ~700 km north of Bangkok (Fig. 1). They are in close spatial association with late Cenozoic alkali basalts, known as 'Denchai Basalts', which unconformably overlie Permo-Triassic sedimentary and volcanic rocks. The Denchai basalts consist of seven flows with thicknesses varying from 1–5 m. The uppermost flow has a K-Ar

* E-mail: plimtrak@postoffice.utas ed u.au
DOI: 10.1180/0026461016560004

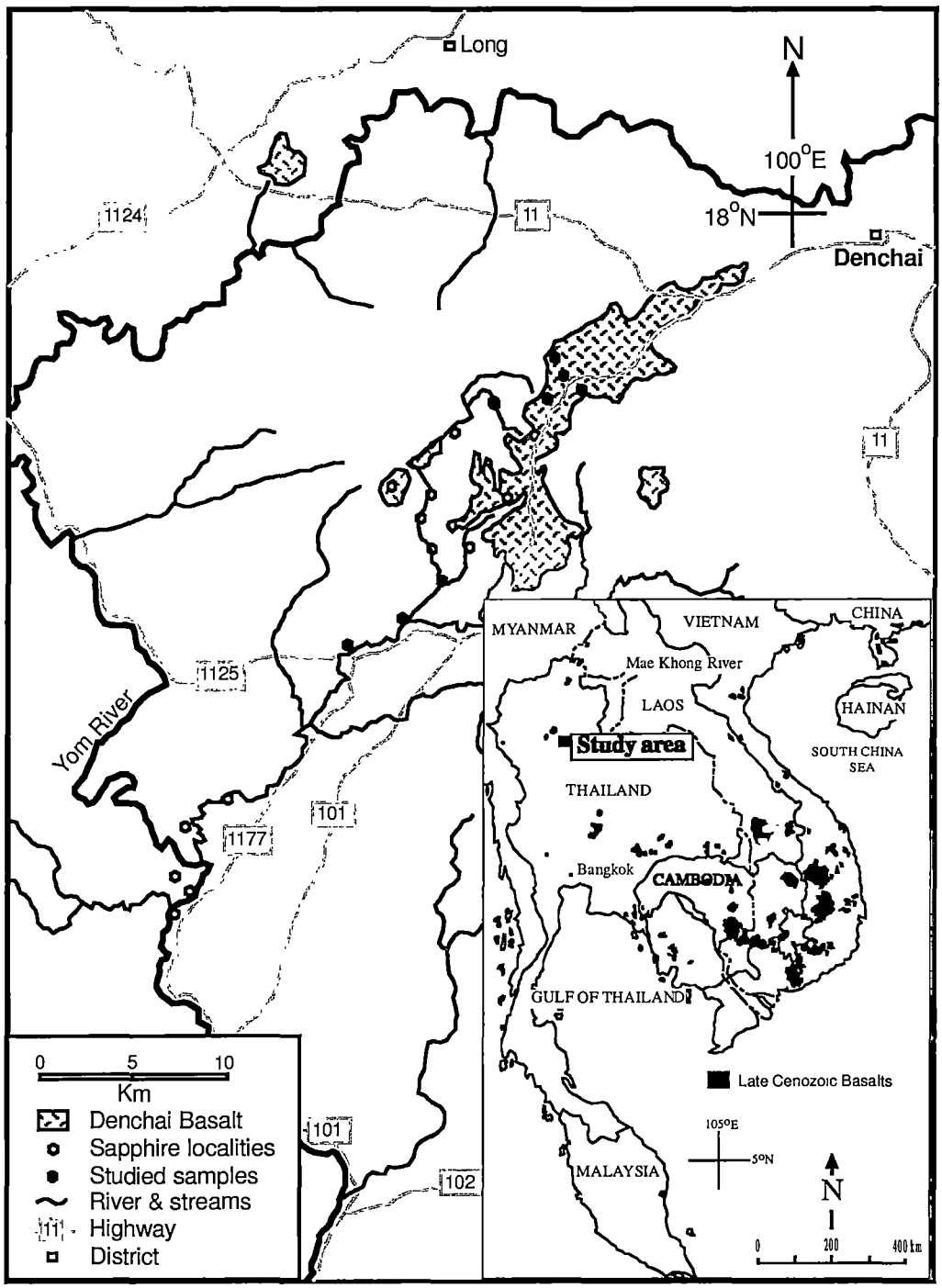

FIG. 1. Map showing the distribution of the basalt outcrops, drainage pattern and sapphire localities in the Denchai area, northern Thailand.

whole-rock age of 5.64 ± 0.28 Ma (Barr and MacDonald, 1979, 1981). These basalts range in composition from hawaiite to basanite with abundant mantle-derived xenoliths (Barr and MacDonald, 1979).

The sapphire samples used in this study are all alluvial sapphires, recovered from alluvial placer and palaeo-channel deposits at shallow depths (Fig. 1) but are probably equivalent to corundum megacrysts that occur in host basalts.

The aim of this paper is to present the more detailed results of mineral chemistry studies and fluid/melt characteristics of the gem sapphires to constrain the origin of the Denchai gem sapphire and to discuss a possible genetic link to the host basalts.

Review of models for corundum genesis

Several studies of corundum occurrences indicate an association with intra-plate alkaline basaltic volcanism, particularly in eastern Australia and southeast Asia (e.g. Barr and Mcdonald, 1978, 1981; Vichit, 1987, 1992; Coenraads *et al.*, 1995; Guo *et al.*, 1996; Sutherland, 1996; Sutherland *et al.*, 1998*a,b*; Sutthirat *et al.*, 2001). A better petrogenetic explanation of the association between gem-quality corundums and intraplate alkaline basaltic volcanism is needed. Current models are controversial, although there is consensus that corundum genesis involved at least two main stages: a first stage where corundum is produced as a magmatic or metamorphic phase at mantle/crustal depths, and a second stage where corundum is incorporated and transported to the surface via subsequent alkaline intra-plate magmatism (e.g. Guo *et al.*, 1996; Sutherland *et al.*, 1998*b*). The following is a brief description of currently postulated models for corundum genesis.

Plutonic crystallization of corundum at high pressures

Four models are currently proposed that involve plutonic crystallization for corundum: (1) from highly evolved alkaline melts derived by the crystallization of intraplate (e.g. nephelinite and basanite) magmas at mantle and lower crustal pressures (Irving, 1986); (2) from syenitic melts that crystallize at deep crustal level or in the upper mantle (Aspen *et al.*, 1990); (3) from alkaline melts produced by low to moderate degrees (6–14 wt.%) of partial melting of amphibole-metasomatized mantle, or even lower crustal amphibole-bearing assemblages (e.g. amphibole pyroxenite; Sutherland *et al.*, 1998*b*); and (4) from syenitic melts possibly originating from partial melting of metasomatized mantle, but with aluminous character developed by loss of alkalis and carbonatitic fractions (Upton *et al.*, 1999). The plutonic crystallization models of corundum genesis are all similar in that they require a highly aluminous volatile and trace element-rich alkaline parental magma. They only differ in how such a magmatic melt composition was produced.

Generation of corundum by magma mixing at mid-crustal levels

This model suggests that at least two melt components (carbonatitic and felsic melts) combine to produce the corundum. This model applied studies of mineral inclusions in corundum (Guo *et al.*, 1996) and suggested that at mid-crustal depth, the interaction between granitic lithology and intruding carbonatitic magma caused the Al-rich phase to crystallize in the hybrid zone. Then, subsequent basaltic magmatism rich in alkalis and volatiles, ascended rapidly to carry pre-formed corundums to the surface.

Generation of corundum by metamorphic recrystallization

Metamorphic corundum is considered as products of the recrystallization process of Al-rich and Si-poor host rocks by either ocean-floor subduction (Levinson and Cook, 1994) or contact metamorphism (Sutherland and Coenraads, 1996). Sutthirat *et al.* (2001) proposed that high-pressure metamorphism of Al-rich mafic rocks also crystallized corundum. The model proposed by Oakes *et al.* (1996) suggested corundum derived by reworking of clay-altered volcaniclastic host rocks. Barron *et al.* (1996) included corundum as an additional aspect of the subduction model for diamond.

Analytical techniques

The rough Denchai sapphires were examined optically under a petrographic microscope to locate and photograph all types of inclusions. For fluid-inclusion studies, these sapphires were prepared as doubly polished sections ~0.3 mm thick. Those containing solid and melt inclusions were mounted in epoxy and cut carefully using a fine diamond wheel. When the inclusions neared the surface, 6 μ and 3 μ diamond paste was used

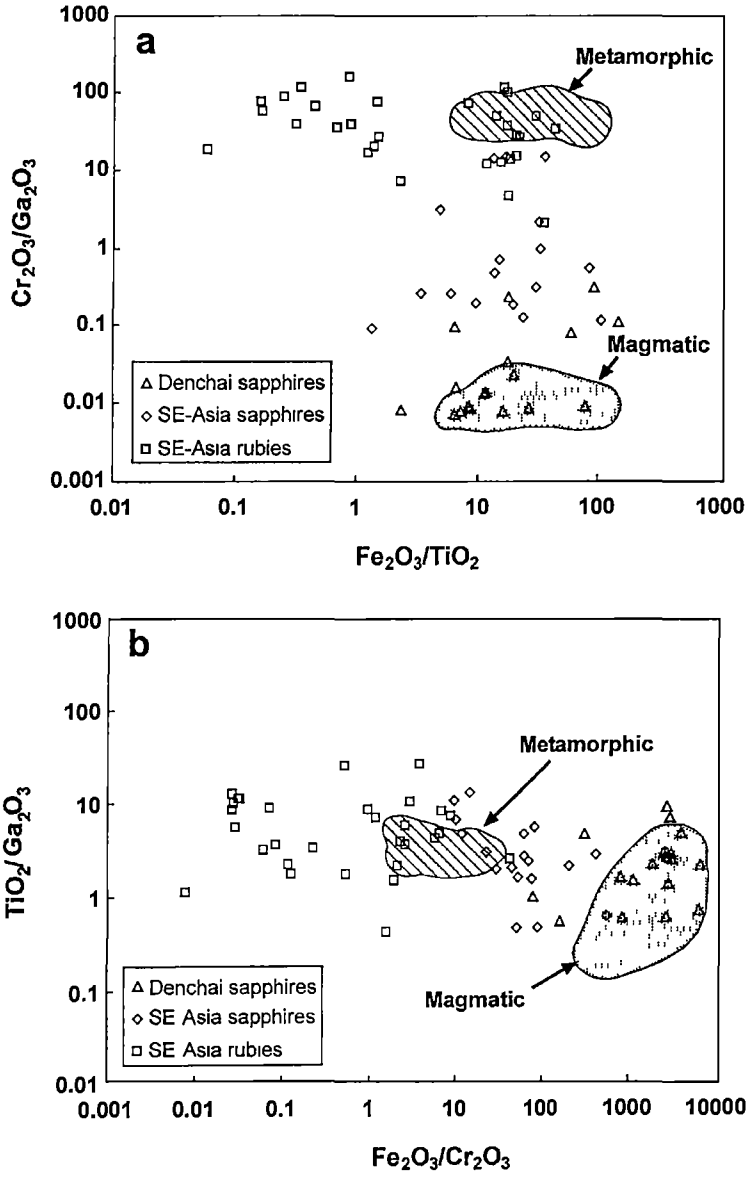

FIG. 2. Trace element distribution diagrams of the Denchai gem sapphires and SE Asia suites, magmatic and metamorphic fields are from Sutherland *et al.* (1998*a*). (*a*) Fe_2O_3/TiO_2 *vs.* Cr_2O_3/Ga_2O_3, and (*b*) Fe_2O_3/Cr_2O_3 *vs.* Cr_2O_3/Ga_2O_3

in grinding until they were exposed. Finally, the polished samples were coated with carbon for electron microprobe investigation.

A Cameca SX 50 electron microprobe with EDS attachment (Central Science Laboratory (CSL), University of Tasmania) was used for the trace element analysis of sapphires. An accelerating voltage of 15 kV was used with a stable beam current of 20 nA. In order to analyse the trace elements at lower levels, the counting time for background was extended to the same value at ~15 min per analysis.

Fluid/melt inclusions in the sapphires were analysed at the Centre for Ore Deposit Research,

University of Tasmania, using the FLUID INC-adapted U.S.G.S. gas-flow heating/freezing system. The fluid inclusion stage is mounted on a Nikon microscope fitted with a long-focus 32 × magnification lens. To avoid a fog covering the lens during the freezing examinations, N_2 gas was blown over the sample chamber. Homogenization experiments with recrystallized melt inclusions were performed at 1 atm using a Vernadsky Institute heating stage with optical control set up (School of Earth Sciences, University of Tasmania). The maximum homogenization temperature of the Vernadsky Institute heating stage is 1700°C.

Laser Raman microprobe analysis was undertaken at the Australian Geological Survey Organisation, Canberra, using a Dilor® SuperLabram spectrometer equipped with a holographic notch filter, 600 and 1800 g/mm gratings, and a liquid-N_2-cooled, 2000 × 450 pixel CCD detector. The inclusions were illuminated with 514.5 nm laser excitation from a Spectra Physics model 2017 argon ion laser, using 5 mW power at the samples, and a single 30 s accumulation. A 100 × Olympus microscope objective was used to focus the laser beam and collect the scattered light. The focused laser spot on the samples was ~1 μm in diameter. Wavenumbers are accurate to ± 1 cm^{-1} as determined by plasma and neon emission lines. For the analysis of CO_2, O_2, N_2, H_2S and CH_4 in the vapour phase, spectra were recorded from 1000 to 3800 cm^{-1} using a single 20 s integration time per spectrum. The detection limits are dependent upon the instrumental sensitivity, the partial pressure of each gas, and the optical quality of each fluid inclusion. Raman detection limits are estimated to be ~0.1 mol.% for CO_2, O_2 and N_2, and 0.03 mol.% for H_2S and CH_4, and errors in the calculated gas ratios are generally <1 mol.%.

The PIXE study was undertaken at the CSIRO Exploration and Mining, Sydney, Australia. Melt and fluid inclusions were imaged using a raster-scanned beam of 3 MeV protons, focused into a beam-spot of ~1.5 μm using the CSIRO-GEMOC Nuclear Microprobe (Ryan *et al.*, 2001). The predictable nature of MeV proton trajectories enables the generation of PIXE X-rays from the inclusion volume to be calculated, which leads to a standardless measure of inclusion composition (Ryan *et al.*, 1995). This approach was used to determine the composition of the original trapped fluid and to image inclusion content.

Mineral chemistry

The trace elements useful for studies of corundum genesis are Fe, Ti, Cr, Ga and V. Sutherland *et al.* (1998*a*) established a quantitative empirical classification to discriminate between corundum from 'metamorphic-type' (including ruby) and 'basaltic-type' (both magmatic and metamorphic corundums discharged in basaltic fields) origins The 'metamorphic-type' corundums are characterized by low Ga_2O_3 (<0.01 wt.%) and high Cr_2O_3/Ga_2O_3 (~10–100), whereas the 'basaltic-type' corundums display higher Ga_2O_3, and Cr_2O_3/Ga_2O_3 ratios mostly <1. The minor and trace element concentrations (as wt.% oxides) in the Denchai sapphires (Table 1) give the following abundances: Fe_2O_3 (0.32–1.98 wt.%),

TABLE 1. Representative electron microprobe analyses of trace element concentrations (wt.%) of the Denchai gem sapphires, northern Thailand.

Colour	Al_2O_3 (wt.%)	TiO_2 (wt.%)	Fe_2O_3 (wt.%)	Cr_2O_3 (wt.%)	V_2O_5 (wt.%)	Ga_2O_3 (wt.%)
Blue	99.91	0.0426	0.4938	0.0002	0.0004	0 0146
Blue	100 07	0 0746	0.5421	0 0002	0.0008	0.0252
Blue	100.02	0.0493	0.5582	0.0003	0.0118	0.0224
Blue	99.40	0.0344	0.5591	0 0002	0 0017	0.0246
Blue	99.77	0.0618	0 5127	0.0002	0.0049	0.0219
Blue	99 64	0.2256	0.5323	0.0002	0.0094	0.0243
Blue	98.23	0.0241	0.6374	0.0001	0.0168	0.0113
Blue	98.07	0.0325	0.5766	0.0007	0.0232	0.0204
Yellowish green	97.72	0.0153	1.2024	0.0002	0.0247	0 0213
Yellowish green	98.15	0.0186	1 1209	0.0010	0.0200	0.0126

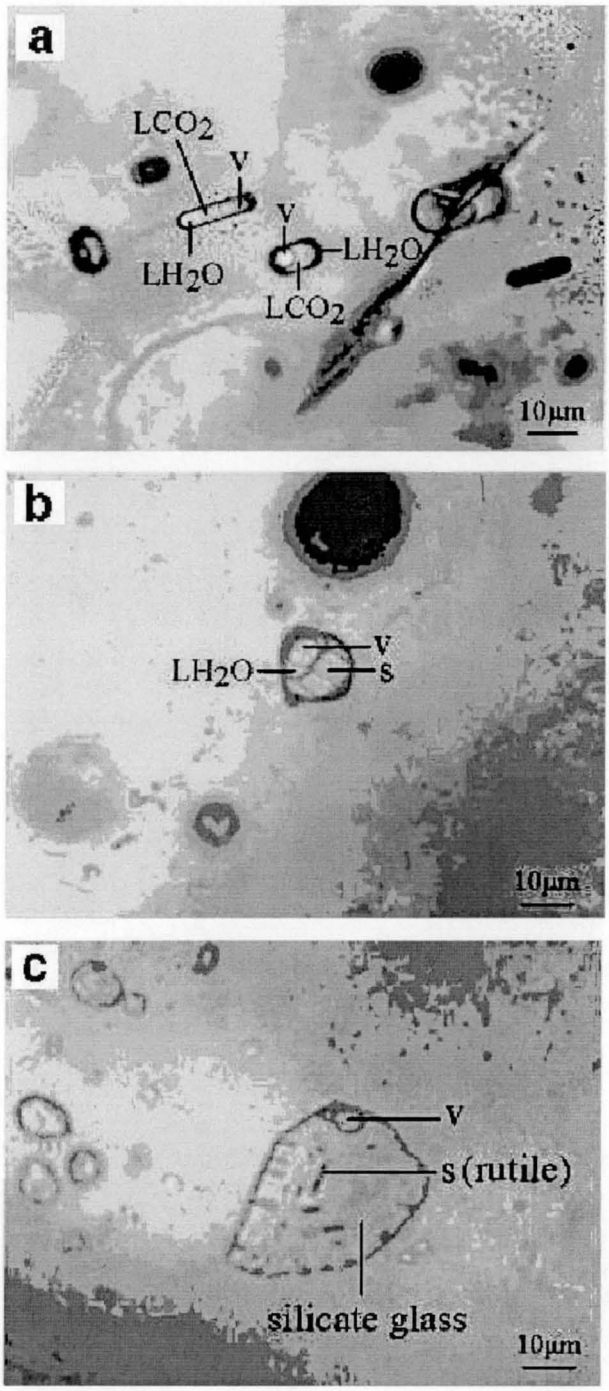

FIG. 3. Photomicrographs of three types of inclusions in the Denchai gem sapphires, northern Thailand. (*a*) CO_2-rich inclusions (Type I); LH_2O = liquid H_2O, LCO_2 = liquid CO_2, V = Vapour; (*b*) Polyphase (V + L + S) inclusion (Type II); S = solid (unidentified minerals); (*c*) Silicate-melt inclusions (Type III) containing vapour bubble (V), silicate glass and the solid phases (S). The needle-like solid mineral is rutile.

TiO_2 (0.01–0.23 wt.%), Cr_2O_3 (<0.01 wt.%), Ga_2O_3 (0.01–0.03 wt.%) and V_2O_5 (<0.03 wt.%).

Published data, for regional comparison purposes are the trace element data of sapphires and rubies from the other SE Asia suites (Thailand, Myanmar, Laos, Cambodia and Vietnam) (Intasopa *et al.*, 1998; Pisutha-Arnond *et al.*, 1998; Tin Tin Win *et al.*, 1998). The SE Asia rubies have higher Cr_2O_3/Ga_2O_3 and lower Fe_2O_3/Cr_2O_3 ratios than the SE Asia and Denchai sapphires (Fig. 2*a,b*). Most of the Denchai sapphires show smaller Cr_2O_3/Ga_2O_3 and greater Fe_2O_3/Cr_2O_3 ratios compared to the other SE Asia sapphires. The Denchai sapphires also lie close to or within magmatic 'basaltic-type' corundums field of Sutherland *et al.* (1998*a*) (Fig. 2*a,b*).

Fluid/melt inclusion characteristics

The majority of the fluid/melt inclusions present in the Denchai sapphires have either negative crystal or rounded shapes and are 10–100 μm in size. Primary inclusions occur within coloured growth bands, whereas inclusions that occur along healed fractures are either secondary or pseudo-secondary. Based on optical studies, three types of primary fluid/melt inclusions can be distinguished: CO_2-rich inclusions (Type I), polyphase (V + L + S) inclusions (Type II) and silicate-melt inclusions (Type III) and are shown in Fig. 3.

Microthermometric and analytical results

Type I CO_2-bearing inclusions contain three phases (LH_2O (liquid H_2O) + LCO_2 (liquid CO_2) + V (vapour)) with the vapour phase comprising <10–15 vol.%. Laser Raman spectroscopy (LRS) analysis confirmed the presence of the CO_2. Freezing and heating experiments were restricted to the primary fluid inclusions of Type I. The melting temperatures (T_m) of CO_2 solid are around −55.8 to −57.2°C (n = 58) (Fig. 4). The lower melting temperature may indicate the presence of N_2 and CH_4. The homogenization temperature of CO_2 liquid into vapour ranges from 24.3–31.1°C corresponding to densities in the range of 0.24 to 0.46 g/cm^3, using the phase relation data from Shepherd *et al* (1985).

Type II polyphase inclusions contain a fluid bubble, which occupies ~20–30 vol.% of the inclusion, an aqueous phase which occupies 10–15 vol.% of the inclusion and other unidentified cubic-shaped solid phases. Total homogenization of Type II inclusions was not achieved, even when the sample was held at 700°C (the maximum temperature of the U.S.G.S. heating/freezing stage) for 30 min.

Type III silicate-melt inclusions are more complex and are preserved as primary, pseudosecondary and secondary inclusions. They generally contain silicate glass, a shrinkage bubble and solid phases. The LRS studies of Type III inclusions indicate the presence of rutile and magnetite (Fig. 5). The presence of rutile was confirmed by petrographic, PIXE and LRS studies of the melt inclusions. The complete homogenization of Type III inclusions (n = 5) using the Vernadsky Institute heating stage failed and bubbles remained as a separate phase even after considerable heating at 1250°C, though the first optical property change was observed at 770°C (n = 1). All inclusions became clearer and the bubbles moved from the edge into the centre with no significant change in their size at ~1200–1250°C (n = 5). Neither did the bubbles grow after quenching. Given these changes to the optical properties within the inclusions, a possible homogenization temperature for Type III inclusions could range between 770 and 1200°C.

The PIXE analysis images of Type III inclusions (n = 3) are shown in Fig. 6 for the

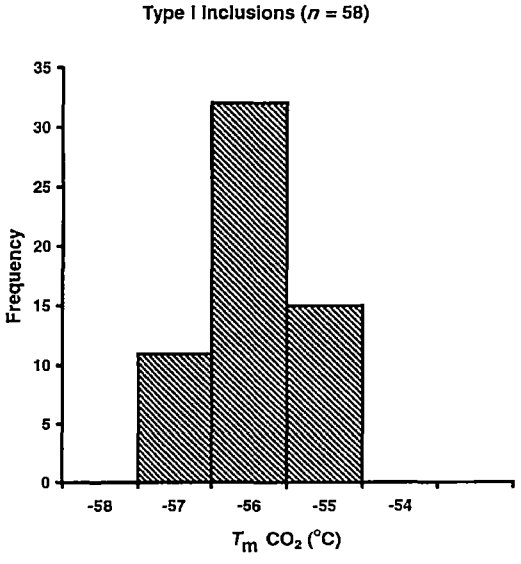

FIG. 4. Melting temperatures, T_m, of CO_2-rich inclusions (Type I) in the Denchai gem sapphires, northern Thailand.

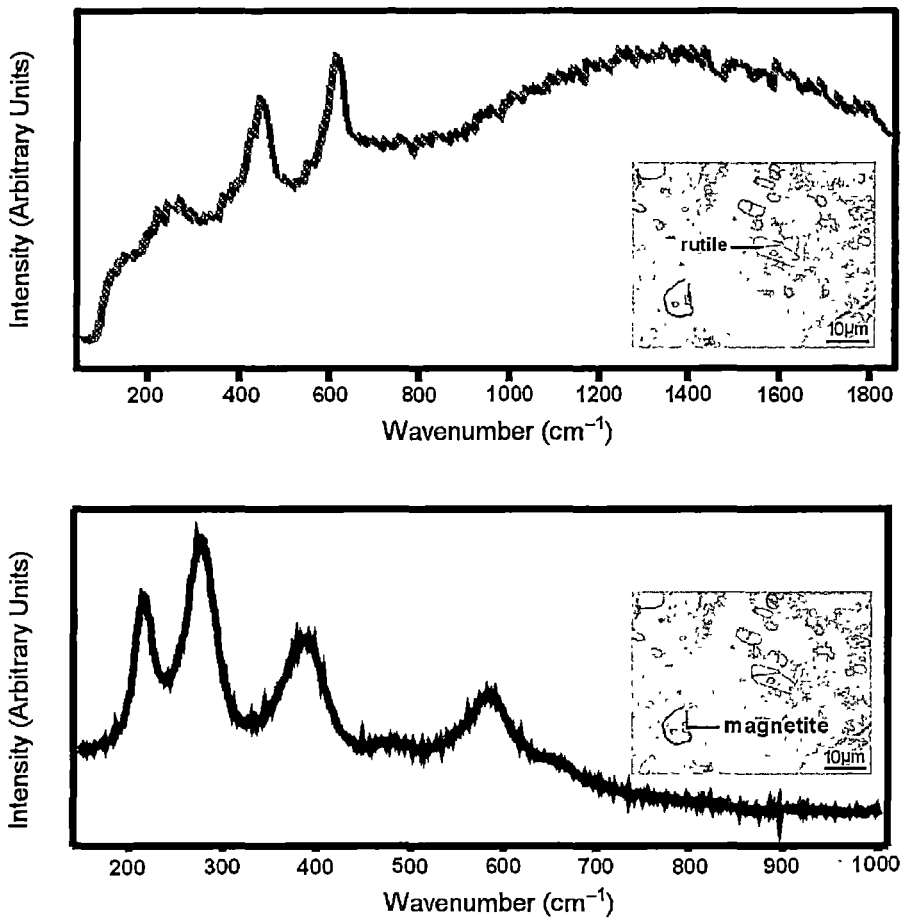

FIG. 5. Laser Raman spectrum of the solid phases (rutile and magnetite) in Type III silicate-melt inclusions in the Denchai gem sapphires, northern Thailand.

following elements: Al, As, Ba, Br, Ca, Cl, Cr, Fe, Ga, K, Mn, Rb, S, Sr, Ti, V, Zn and Zr. No detectable Al, As, Ba, Br, Cl, Cr, Ga, S, Sr and Zn were observed, whereas K (~4 wt.%), Ca (~0.5 wt.%), Ti (~1 wt.%), Fe (~2 wt.%), Mn (~0.1 wt.%), V (<0.03 wt.%), Rb (~70 ppm) and Zr (~200 ppm) were detected. We could not measure quantitatively the Al in the melt due to lack of PIXE sensitivity for Al within an Al-rich host. Other analytical techniques are required.

Discussion

Several models of corundum genesis have been proposed (e.g. Irving, 1986; Aspen *et al.*, 1990; Guo *et al.* 1996; Sutherland *et al.*, 1998*b*; Upton *et al.*, 1999; Sutthirat *et al.*, 2001) but the origin of corundum remains poorly understood. There is a consensus that corundum genesis involves at least two main stages. A prior stage where corundum formed as a magmatic or metamorphic phase at upper mantle or lower crustal depths and was followed by corundum incorporation and transport to the surface via a subsequent magmatic event.

The trace-element chemistry of the Denchai sapphires is considered to match values recorded for magmatic 'basaltic-type' corundums, as established by Sutherland *et al.* (1998*a*). The Denchai sapphires contain low Cr_2O_3/Ga_2O_3 and high Fe_2O_3/Cr_2O_3 ratios (Fig. 2*a,b*) in line with magmatic 'basaltic-type' corundums from eastern

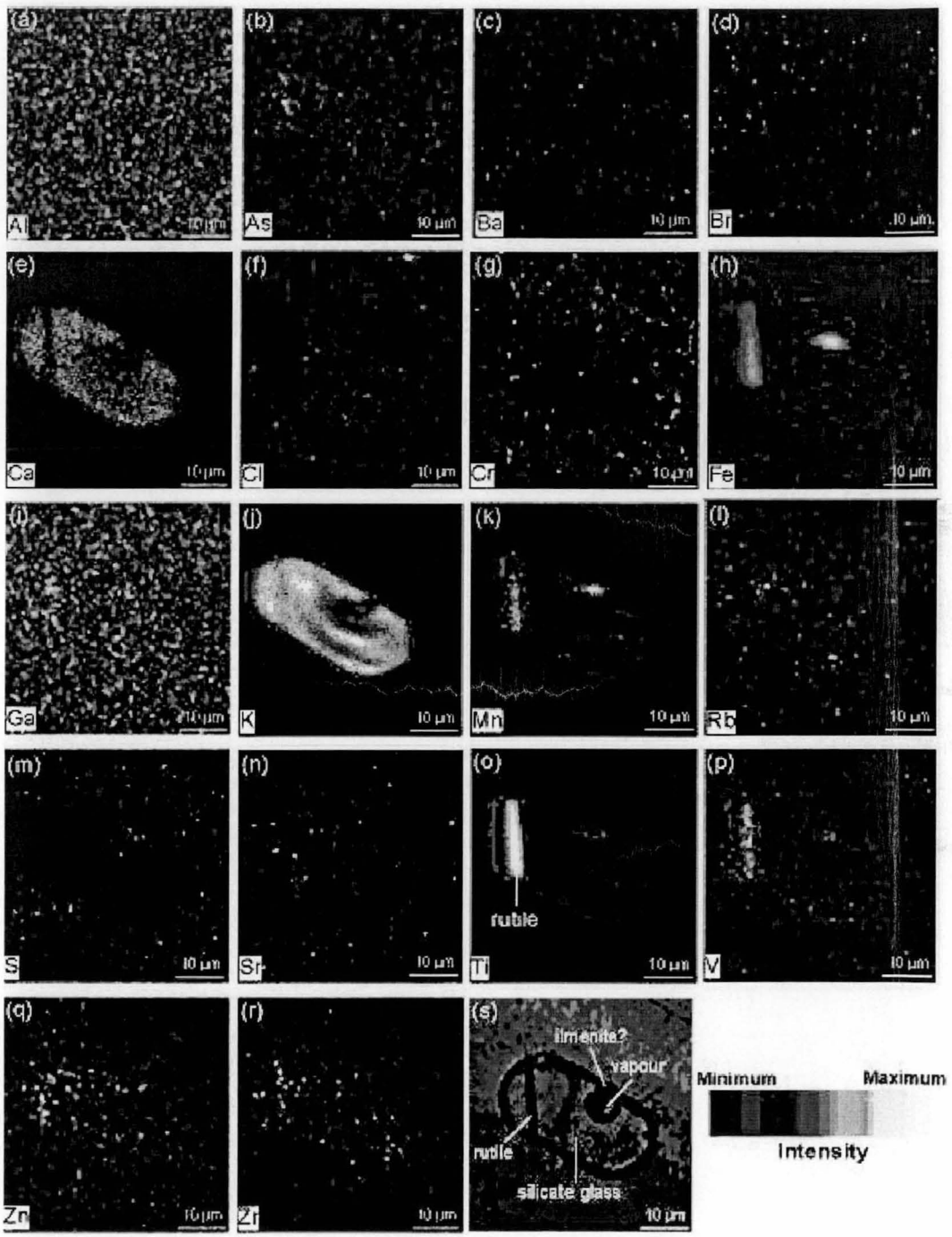

FIG. 6. PIXE images showing the elemental concentrations of a silicate melt inclusion(s) in the Denchai gem sapphires, northern Thailand. Note presence of a rutile inclusion in (part *o*) and an Fe-Mn-Ti-bearing inclusion (ilmenite?) in (parts *h*, *k* and *o*). Also, note the large concentration of K in (*j*) and of Ca in (*e*). The same intensity scale applies to all images.

Australia and west Pailin, Cambodia (Sutherland *et al.*, 1998*a*).

The presence of three types of fluid and melt inclusions in the Denchai sapphires provides some constraints on their origin. During primary growth of the sapphires, at least three distinct compositional fluids (LCO_2, LH_2O and silicate melt) appeared at some stage. The inferred trapping temperature to have crystallized corundum probably ranges 770–1200°C according to homogenization experiments of Type III inclusions.

The PIXE analysis of silicate-melt inclusions demonstrates the significance of K, Ca, Ti, Fe and Mn in the silicate glass (Fig. 6). However, the elemental concentrations from PIXE could not address what kind of melt compositions were involved, i.e. carbonatitic/felsic or syenitic/pegmatitic/granitic (Guo *et al.*, 1996; Upton *et al.*, 1999).

We have concluded that at least two main stages were involved in the formation of the Denchai gem sapphires, as they were produced at lower crustal or upper mantle depths and then ascended to the surface during the subsequent alkali-rich magmatic event. This conclusion is consistent with experimental investigation by Liu and Presnall (1990) that corundum is not a stable phase in a basaltic magma (see discussion in Guo *et al.*, 1996). The presence of Type I inclusions is also consistent with experimental evidence that the presence of CO_2-rich liquids in the silicate melt could reduce the Al_2O_3 solubility in magma (Green *et al.*, 1978), resulting in Al-oversaturation, and corundum may crystallize.

The mineral chemistry of the sapphires is in line with magmatic 'basaltic-type' corundums of empirical classification described by Sutherland *et al.* (1998*a*). The CO_2-rich fluids and high K in the silicate melt inclusions suggest that the Denchai gem-sapphire formation was related to CO_2-rich alkaline magmatism. The evidence clearly suggests magmatic involvement in the crystallization of corundum, as proposed by Guo *et al.* (1996) and Upton *et al.* (1999).

Summary

(1) The mineral chemistry of the Denchai gem sapphires is well correlated to magmatic 'basaltic-type' corundums from eastern Australia and west Pailin, Cambodia.

(2) Three compositional fluids were preserved during the primary growth of the Denchai sapphires.

(3) The Denchai sapphires formed at lower crustal or upper mantle depths before ascending to the surface during the subsequent alkali-rich magmatic event.

(4) The presence of Type III silicate-melt inclusions is evidence of magmatic involvement in the formation of the Denchai sapphires.

(5) Further detailed studies on silicate melt inclusion compositions might provide more information about the environment in which corundum crystallizes.

Acknowledgements

The authors are grateful to Dr David Steele of the Central Science Laboratory, University of Tasmania, for the electron microprobe analyses and to Drs Trevor Falloon, Ron Berry, Vadim Kamenetsky and Leonid Danyushevsky of the School of Earth Sciences, University of Tasmania for helful discussions. We also thank Dr Pornsawat Wathanakul and Ms Somruedee Sakkaravej of the Department of General Sciences, Faculty of Science, Kasetsart University, Bangkok, Thailand for providing some of the sapphire samples from Thailand. Thanks are also extended to Mr Weerapan Sricharn and Ms Mananya Suchaya of the Department of Geological Sciences, Faculty of Science, Chiang Mai University, Chiang Mai, Thailand, for their assistance during this study. This work was supported by an Internal Research Grant from the ARC-funded Centre for Ore Deposit Research, University of Tasmania and by a Royal Thai Government Scholarship. Two anonymous reviewers are thanked for their efforts to improve the manuscript.

References

Aspen, P., Upton, B.G.J. and Dicken, A.P. (1990) Anorthoclase, sanidine and associated megacrysts in Scottish alkali basalts: high pressure syenitic debris from upper mantle sources? *Eur. J. Mineral*, **2**, 503–17.

Barr, S.M. and MacDonald, A.S. (1978) Geochemistry and petrogenesis of Late Cenozoic alkaline basalts of Thailand. *Geol. Soc. Malaysia Bull.*, **10**, 21–48.

Barr, S.M. and MacDonald, A.S. (1979) Palaeomagnetism, age and geochemistry of the Denchai basalt, Northern Thailand. *Earth Planet Sci. Lett.*, **46**, 113–24.

Barr, S.M. and MacDonald, A.S. (1981) Geochemistry and geochronology of Late Cenozoic basalts of

Southeast Asia – part II. *Geol. Soc. Amer. Bull.*, **92**, 1069–142.

Barron, L.M., Lishmund, S.R., Oakes, G.M., Barron, B.J. and Sutherland, F.L. (1996) Subduction model for the origin of some diamonds in the Phanerozoic of eastern New South Wales. *Austral. J. Earth Sci.*, **43**, 257–67.

Coenraads, R.R., Vichit, P. and Sutherland, F.L. (1995) An unusual sapphire-zircon-magnetite xenolith from Chanthaburi Gem Province, Thailand. *Mineral Mag.*, **59**, 465–79.

Green, T.H., Wass, S.Y. and Ferguson, J. (1978) Experimental study of corundum stability in basalts (abstract). *Abstracts and Program for the 3rd Australian Geological Convention, Townsville*, p. 34.

Guo, J.F., O'Reilly, S.Y. and Griffin, W.L. (1996) Corundum from basaltic terrains: a mineral inclusion approach to the enigma. *Contrib. Mineral. Petrol.*, **122**, 368–86.

Intasopa, S., Atichat, W. and Pisutha-Arnond, V. (1998) A comparative study on corundums from southeast Asia: their application to origin determination. *Proceedings of the Ninth Regional Congress on Geology, Mineral Energy Resources of Southeast Asia, Kuala Lumpur, Malaysia*, pp. 220–2.

Irving, A.J. (1986) Polybaric mixing in alkalic basalts and kimberlites. Evidence from corundum, zircon and ilmenite megacrysts. *Geol. Soc. Austral. Abstracts*, **16**, 262–4.

Levinson, A.A. and Cook, F.A. (1994) Gem corundum in alkali basalt: origin and occurrence. *Gems Gemol.*, **30**, 253–62.

Liu, T.C and Presnall, D.C. (1990) Liquidus phase relationships on the join anorthite-forsterite-quartz at 20 kbar with applications to basalt petrogenesis and igneous sapphirine. *Contrib. Mineral. Petrol.*, **104**, 735–42.

Oakes, G.M., Barron, L.M. and Lishmond, S.R. (1996) Alkali basalts and associated volcaniclastic rocks as a source of sapphire in eastern Australia. *Austral. J. Earth Sci.*, **43**, 289–98.

Pisutha-Arnond, V., Wathanakul, P., Intasopa, S. and Griffin, W.L. (1998) Corsilzirspite, a corundum-sillimanite-zircon-hercynite rock: New eveidence on the origin of Kanchanaburi sapphire, Thailand. *Proceedings of the Ninth Regional Congress on Geology, Mineral Energy Resources of Southeast Asia, Kuala Lumpur, Malaysia*, pp 95–6.

Ryan, C.G., Heinrich, C.A., Van Achterbergh, E., Ballhaus, C and Mernagh, T.P. (1995) Microanalysis of Ore-forming Fluids using the Scanning Proton Microprobe. *Nuclear Instrument Method*, **B104**, 182–90.

Ryan, C.G., Jamieson, D.N., Griffin, W.L., Cripps, G. and Szymanski, R. (2001) The New CSIRO-GEMOC Nuclear Microprobe: First results, performance and recent applications. *Nuclear Instrument Method* (in press).

Shepherd, T., Rankin, A.H. and Alderton, D.H.M. (1985) *A Practical Guide to Fluid Inclusion Studies*. Blackie, Glasgow, UK.

Sutherland, F.L. (1996) Alkaline rocks and gemstones, Australia: a review and synthesis. *Austral. J. Earth Sci.*, **43**, 323–43.

Sutherland, F.L. and Coenraads, R.R. (1996) An unusual ruby-sapphire-sapphirine-spinel assemblage from the Tertiary Barrington volcanic province, New South Wales, Australia. *Mineral. Mag.*, **60**, 623–38.

Sutherland, F.L., Schwarrz, D., Jobbins, E.A., Coenraads, R.R. and Webb, G. (1998*a*) Distinctive gem corundum suites from discrete basalt fields: a comparative study of Barrington, Australia, and West Pailin, Cambodia, gemfields. *J. Gemmol.*, **26**, 65–85.

Sutherland, F.L., Hoskin, P.W.O., Fanning, C.M. and Coenraads, R.R. (1998*b*) Models of corundum origin from alkali basaltic terrains: A reappraisal. *Contrib Mineral. Petrol.*, **133**, 356–72.

Sutthirat, C., Saminpanya, S., Droop, G.T.R., Henderson, C.M.B. and Manning, D.A.C. (2001) Clinopyroxene-corundum assemblage from alkali basalt and alluvium, eastern Thailand: constraints on the origin of Thai rubies. *Mineral. Mag.*, **65**, 277–95.

Tin Tin Win, Wanathanakul, P., French, D.H., Intasopa, S. and Pisutha-Arnond, V. (1998) Preliminary study on trace element geochemistry of corundums from South East Asia. *Proceedings of the Ninth Regional Congress on Geology, Mineral Energy Resources of Southeast Asia, Kuala Lumpur, Malaysia*, pp. 99–101.

Upton, B.G.J., Hinton, R.W., Aspen, P., Finch, A. and Valley, J.W. (1999) Megacrysts and associated xenoliths. Evidence for migration of geochemically enriched melts in the upper mantle beneath Scotland. *J. Petrol.*, **40**, 935–56.

Vichit, P. (1987) Gemstones in Thailand. *J. Geol. Soc. Thailand*, **9**, 108–33.

Vichit, P. (1992) Gemstones in Thailand. *Proceedings of National Conference on Geologic Resources of Thailand: Potential for Future Development, Department of Mineral Resources, Bangkok, Thailand*, pp. 124–50.

Vichit, P., Vudhichativanich, S. and Hansawek, R. (1978) The distribution and some characteristics of corundum-bearing basalts in Thailand. *Journal of Geological Society of Thailand, Special Issue for III GEOSEA*, **3**, M4 1–38.

{*Manuscript received 8 May 2001: revised 12 September 2001*}

Appendix H

Sample catalogue

Catalog#	Field#	Rock Name	Latitude	Longitude	Mine Northing	Mine Easting	Area	State	Country	Lithostratigraphy	Preparation
150045	DC1	basalt	17°53'00"N	99°53'00"E	999	850	Denchai	Phrae	Thailand	Late Cenozoic	R, CR, PD
150046	DC2	basalt	17°53'00"N	99°53'00"E	999	850	Denchai	Phrae	Thailand	Late Cenozoic	R, CR, PD
150047	DC3	basalt	17°53'00"N	99°53'00"E	017	849	Denchai	Phrae	Thailand	Late Cenozoic	R, CR, PD
150048	DC4	basalt	17°53'00"N	99°53'00"E	017	849	Denchai	Phrae	Thailand	Late Cenozoic	R, CR, PD
150049	DC5	basalt	17°53'00"N	99°53'00"E	948	807	Denchai	Phrae	Thailand	Late Cenozoic	R, CR, PD
150050	DC6	basalt	17°53'00"N	99°53'00"E	001	837	Denchai	Phrae	Thailand	Late Cenozoic	R, CR, PD
150051	DC7	basalt	17°53'00"N	99°53'00"E	992	824	Denchai	Phrae	Thailand	Late Cenozoic	R, CR, PD
150052	DC8	basalt	17°53'00"N	99°53'00"E	944	795	Denchai	Phrae	Thailand	Late Cenozoic	R, CR, PD
150053	DC10	basalt	17°53'00"N	99°53'00"E	943	791	Denchai	Phrae	Thailand	Late Cenozoic	R, CR, PD
150054	DC11	basalt	17°53'00"N	99°53'00"E	934	780	Denchai	Phrae	Thailand	Late Cenozoic	R, CR, PD
150055	DC12	basalt	17°53'00"N	99°53'00"E	930	776	Denchai	Phrae	Thailand	Late Cenozoic	R, CR, PD
150056	DC13	basalt	17°53'00"N	99°53'00"E	929	771	Denchai	Phrae	Thailand	Late Cenozoic	R, CR, PD
150057	DC14	basalt	17°53'00"N	99°53'00"E	929	768	Denchai	Phrae	Thailand	Late Cenozoic	R, CR, PD
150058	DC15	basalt	17°53'00"N	99°53'00"E	921	716	Denchai	Phrae	Thailand	Late Cenozoic	R, CR, PD
150059	DC16	basalt	17°53'00"N	99°53'00"E	920	703	Denchai	Phrae	Thailand	Late Cenozoic	R, CR, PD
150060	DC17	basalt	17°53'00"N	99°53'00"E	926	700	Denchai	Phrae	Thailand	Late Cenozoic	R, CR, PD
150061	DC18	basalt	17°53'00"N	99°53'00"E	931	717	Denchai	Phrae	Thailand	Late Cenozoic	R
150062	DC19	basalt	17°53'00"N	99°53'00"E	933	769	Denchai	Phrae	Thailand	Late Cenozoic	R, CR, PD
150063	DC20	basalt	17°53'00"N	99°53'00"E	926	747	Denchai	Phrae	Thailand	Late Cenozoic	R, CR, PD
150064	DC21	basalt	17°53'00"N	99°53'00"E	919	746	Denchai	Phrae	Thailand	Late Cenozoic	R, CR, PD
150065	DC22	basalt	17°53'00"N	99°53'00"E	914	744	Denchai	Phrae	Thailand	Late Cenozoic	R, CR, PD
150066	DC23	basalt	17°53'00"N	99°53'00"E	907	744	Denchai	Phrae	Thailand	Late Cenozoic	R, CR, PD
150067	DC24	basalt	17°53'00"N	99°53'00"E	903	741	Denchai	Phrae	Thailand	Late Cenozoic	R
150068	DC25	basalt	17°53'00"N	99°53'00"E	900	738	Denchai	Phrae	Thailand	Late Cenozoic	R, CR, PD
150069	DC26	basalt	17°53'00"N	99°53'00"E	896	740	Denchai	Phrae	Thailand	Late Cenozoic	R
150070	DC27	basalt	17°53'00"N	99°53'00"E	924	766	Denchai	Phrae	Thailand	Late Cenozoic	R, CR, PD
150071	DC28	basalt	17°53'00"N	99°53'00"E	906	752	Denchai	Phrae	Thailand	Late Cenozoic	R, CR, PD
150072	DC29	basalt	17°53'00"N	99°53'00"E	905	758	Denchai	Phrae	Thailand	Late Cenozoic	R, CR, PD
150073	DC30	basalt	17°53'00"N	99°53'00"E	909	765	Denchai	Phrae	Thailand	Late Cenozoic	R, CR, PD
150074	DC31	basalt	17°53'00"N	99°53'00"E	933	757	Denchai	Phrae	Thailand	Late Cenozoic	R, CR, PD
150075	DC32	basalt	17°53'00"N	99°53'00"E	922	771	Denchai	Phrae	Thailand	Late Cenozoic	R, CR, PD
150076	DC33	basalt	17°53'00"N	99°53'00"E	932	741	Denchai	Phrae	Thailand	Late Cenozoic	R, CR, PD
150077	DC34	basalt	17°53'00"N	99°53'00"E	936	739	Denchai	Phrae	Thailand	Late Cenozoic	R, CR, PD
150078	DC35	basalt	17°53'00"N	99°53'00"E	938	730	Denchai	Phrae	Thailand	Late Cenozoic	R, CR, PD
150079	DC36	basalt	17°53'00"N	99°53'00"E	950	730	Denchai	Phrae	Thailand	Late Cenozoic	R, CR, PD
150080	DC37	basalt	17°53'00"N	99°53'00"E	934	724	Denchai	Phrae	Thailand	Late Cenozoic	R, CR, PD

Note. R = rock specimen, CR = crushed rock, PD = rock powder

Appendix H (Continued)

Catalog#	Field#	Rock Name	Latitude	Longitude	Mine Northing	Mine Easting	Area	State	Country	Lithostratigraphy	Preps
150081	DC38	basalt	17°53'00"N	99°53'00"E	943	724	Denchai	Phrae	Thailand	Late Cenozoic	R, CR, PD
150082	DC39	basalt	17°53'00"N	99°53'00"E	940	712	Denchai	Phrae	Thailand	Late Cenozoic	R, CR, PD
150083	DC40	basalt	17°53'00"N	99°53'00"E	950	792	Denchai	Phrae	Thailand	Late Cenozoic	R, CR, PD
150084	DC41	basalt	17°53'00"N	99°53'00"E	952	800	Denchai	Phrae	Thailand	Late Cenozoic	R, CR, PD
150085	DC42	basalt	17°53'00"N	99°53'00"E	971	796	Denchai	Phrae	Thailand	Late Cenozoic	R, CR, PD
150086	DC43	basalt	17°53'00"N	99°53'00"E	968	803	Denchai	Phrae	Thailand	Late Cenozoic	R, CR, PD
150087	DC44	basalt	17°53'00"N	99°53'00"E	952	813	Denchai	Phrae	Thailand	Late Cenozoic	R, CR, PD
150088	DC45	basalt	17°53'00"N	99°53'00"E	962	818	Denchai	Phrae	Thailand	Late Cenozoic	R, CR, PD
150089	DC46	basalt	17°53'00"N	99°53'00"E	955	818	Denchai	Phrae	Thailand	Late Cenozoic	R, CR, PD
150090	DC47	basalt	17°53'00"N	99°53'00"E	981	821	Denchai	Phrae	Thailand	Late Cenozoic	R, CR, PD
150091	DC48	basalt	17°53'00"N	99°53'00"E	974	840	Denchai	Phrae	Thailand	Late Cenozoic	R, CR, PD
150092	DC49	basalt	17°53'00"N	99°53'00"E	036	859	Denchai	Phrae	Thailand	Late Cenozoic	R, CR, PD
150093	DC50	basalt	17°53'00"N	99°53'00"E	037	854	Denchai	Phrae	Thailand	Late Cenozoic	R, CR, PD
150094	DC51	basalt	17°53'00"N	99°53'00"E	022	845	Denchai	Phrae	Thailand	Late Cenozoic	R, CR, PD
150095	DC52	basalt	17°53'00"N	99°53'00"E	010	845	Denchai	Phrae	Thailand	Late Cenozoic	R, CR, PD
150096	DC53	basalt	17°53'00"N	99°53'00"E	985	809	Denchai	Phrae	Thailand	Late Cenozoic	R, CR, PD
150097	DC54	basalt	17°53'00"N	99°53'00"E	997	813	Denchai	Phrae	Thailand	Late Cenozoic	R, CR, PD
150098	DC55	basalt	17°53'00"N	99°53'00"E	003	810	Denchai	Phrae	Thailand	Late Cenozoic	R, CR, PD
150099	DC56	basalt	17°53'00"N	99°53'00"E	918	700	Denchai	Phrae	Thailand	Late Cenozoic	R, CR, PD
150100	DC57	basalt	17°53'00"N	99°53'00"E	919	709	Denchai	Phrae	Thailand	Late Cenozoic	R, CR, PD
150101	DC58	basalt	17°53'00"N	99°53'00"E	910	713	Denchai	Phrae	Thailand	Late Cenozoic	R, CR, PD
150102	DC59	basalt	17°53'00"N	99°53'00"E	921	716	Denchai	Phrae	Thailand	Late Cenozoic	R, CR, PD
150103	DC60	basalt	17°53'00"N	99°53'00"E	926	738	Denchai	Phrae	Thailand	Late Cenozoic	R, CR, PD
150104	DC61	basalt	17°53'00"N	99°53'00"E	929	767	Denchai	Phrae	Thailand	Late Cenozoic	R, CR, PD
150105	DC62	basalt	17°53'00"N	99°53'00"E	929	771	Denchai	Phrae	Thailand	Late Cenozoic	R, CR, PD
150106	DC63	basalt	17°53'00"N	99°53'00"E	935	780	Denchai	Phrae	Thailand	Late Cenozoic	R, CR, PD
150107	DC64	basalt	17°53'00"N	99°53'00"E	944	793	Denchai	Phrae	Thailand	Late Cenozoic	R, CR, PD
150108	DC65	basalt	17°53'00"N	99°53'00"E	945	796	Denchai	Phrae	Thailand	Late Cenozoic	R, CR, PD
150109	DC66	basalt	17°53'00"N	99°53'00"E	945	803	Denchai	Phrae	Thailand	Late Cenozoic	R, CR, PD

Note R = rock specimen, CR = crushed rock, PD = rock powder